

AFML-TR-71-204

# METAL MATRIX COMPOSITE TECHNOLOGY

K. G. Kreider, L. Dardi, K. Prewo

United Aircraft Research Laboratories



UNITED AIRCRAFT CORPORATION

EAST HARTFORD, CONNECTICUT 06108

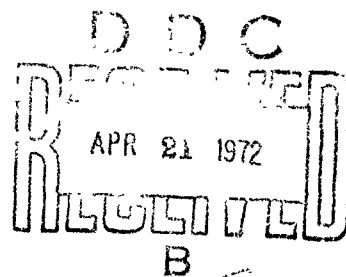
and

Pratt & Whitney Aircraft



DIVISION OF UNITED AIRCRAFT CORPORATION

EAST HARTFORD, CONNECTICUT 06108



TECHNICAL REPORT AFML-TR-71-204

DECEMBER 1971

AD 740584

## NOTICES

When Government drawings, specifications, or other data are used for any purpose other than in connection with a definitely related Government procurement operation, the United States Government thereby incurs no responsibility nor any obligation whatsoever; and the fact that the Government may have formulated, furnished, or in any way supplied the said drawings, specifications, or other data, is not to be regarded by implication or otherwise as in any manner licensing the holder or any other person or corporation, or conveying any rights or permission to manufacture, use, or sell any patented invention that may in any way be related thereto.

Copies of this report should not be returned unless return is required by security considerations, contractual obligations, or notice on a specific document.

ACCESSION (w)	
CPSTI	WHITE SECTION <input checked="" type="checkbox"/>
DDC	BUFF SECTION <input type="checkbox"/>
UNANNOUNCED	<input type="checkbox"/>
JUSTIFICATION	
BY	
SIGNATURE/APPROPRIATE CODE	
DATE	APPROVAL AND SIGNATURE
A	

METAL MATRIX COMPOSITE TECHNOLOGY

K. G. Kreider, L. Dardi, K. Prewo

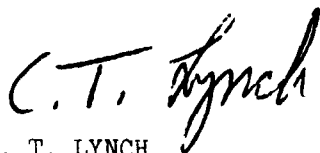
This document has been approved for public release and sale;  
its distribution is unlimited.

Details of illustrations in  
this document may be better  
studied on microfiche

## FOREWORD

This Technical Report covers all work performed on Contract F33615-69-C-1539 for the period July 1, 1969 to June 30, 1971. The work on this contract with United Aircraft Research Laboratories and Pratt and Whitney Division of United Aircraft Corporation of East Hartford, Connecticut is performed under the direction of the Metals and Ceramics Division of the Air Force Materials Laboratory with Captain D. Rice as program monitor.

This technical report has been reviewed and is approved.



C. T. LYNCH  
Chief, Advanced Metallurgical Studies  
Metals and Ceramics Division



## ABSTRACT

The goals of this program include a critical property evaluation of the best aluminum and titanium alloy matrix boron composite systems available today and improvement of the understanding of fracture in metal matrix composites. This program is intended to develop criteria for material selection and metallurgical processing and to generate data to guide the structural engineer in designing with metal matrix composites. Areas of concentrated studies include: environmental effects, transverse properties, off-axis properties, failure mechanisms of fatigue, notch bending fracture, and notched tensile fracture.

The effects of exposing boron aluminum composites to synthetic sea water was similar to that observed with the matrix alloys. High temperature air exposure indicated that BORSIC<sup>®</sup> was more resistant to attack than boron. Thermal cycling studies indicated that boron aluminum composites are durable under severe thermal fluctuations.

The transverse strength of boron aluminum composites was studied as a function of primary fabrication parameters, matrix and fiber types, secondary processing parameters, fiber content, specimen surface, condition and thermal history. It was found that the transverse strength of the 4 mil fiber severely limited composite transverse strength; whereas strengths of up to 48,000 psi were realized with the large diameter fiber. In these strong composites the aluminum fails in ductile shear. The elastic constants for boron aluminum were determined for boron aluminum composites and compare well with micro-mechanical predictions available in the literature. The strength as a function of angle between the loading and filament directions was found to follow the maximum distortional energy prediction.

Fatigue failure mechanisms were studied in boron aluminum for longitudinally and transversely reinforced specimens. Failure of the longitudinal specimens was related to nucleating zones of fiber failure. With notches present, plastic deformation and shear failure of the matrix blunted stress concentrations. In specimens fatigued with  $\pm 45^\circ$  fiber orientations high (10%) plastic strains to failure were observed.

Charpy impact and notched bend tests were used to study energy absorption mechanisms in the fracture of boron aluminum. The critical parameters were found to be the strength, diameter, and volume fraction of the fiber and the shear yield strength of the matrix.

Notch tensile tests were performed on longitudinally and transversely reinforced BORSIC aluminum and on BORSIC-titanium. The minimum strength modifying flaw size and the maximum flaw stress concentration effects were determined for two inch wide specimens. Transversely reinforced specimens had net section strengths unaffected by flaw size.

UNCLASSIFIED  
Security Classification

DOCUMENT CONTROL DATA - R&D

(Security classification of title, body of abstract and indexing annotation must be entered when the overall report is classified)

1 ORIGINATING ACTIVITY (Corporate author) United Aircraft Corporation Research Laboratories East Hartford, Connecticut		2a REPORT SECURITY CLASSIFICATION Unclassified	
		2b GROUP	
3 REPORT TITLE  Metal Matrix Composite Technology			
4 DESCRIPTIVE NOTES (Type of report and inclusive dates) Final Report 1 July 1969 - 30 June 1971			
5 AUTHOR(S) (Last name, first name, initial)  Kreider, Kenneth G., Dardi, L. E., and Prewo, K. M.			
6 REPORT DATE December 1971		7a TOTAL NO. OF PAGES 362	7b NO. OF REFS 120
8a CONTRACT OR GRANT NO. F33615-69-C-1539		8b ORIGINATOR'S REPORT NUMBER(S)  K910853-12	
b. PROJECT NO. 9M-574/7351			
c. Task No. 734107		9b OTHER REPORT NO(S) (Any other numbers that may be assigned this report)  AFML-TR-71-204	
10 A NOTE OF NOTICE: This document is subject to export controls and restrictions of the U.S. Government. It is to be controlled only by the U.S. Government and its authorized agencies. It is not to be distributed outside the U.S. without prior approval of the U.S. Government.			
11 SUPPLEMENTARY NOTES		12 SPONSORING MILITARY ACTIVITY Air Force Materials Laboratory Wright-Patterson Air Force Base, Ohio 45433	
13 ABSTRACT The goals of this program include a critical property evaluation of the best aluminum and titanium alloy matrix boron composite systems available today and improvement of the understanding of fracture in metal matrix composites. This program is intended to develop criteria for material selection and metallurgical processing and to generate data to guide the structural engineer in designing with metal matrix composites. Areas of concentrated studies include: environmental effects, including exposure to sea water, high temperatures, and thermal cycling; transverse properties; off-axis properties; failure mechanisms of fatigue; notch bending fracture; and notched tensile fracture.  The transverse strength of boron aluminum composites was studied as a function of primary fabrication parameters: matrix and fiber types, secondary processing parameters, fiber content, specimen surface condition and thermal history. It was found that the transverse strength of the 4 mil fiber severely limited composite transverse strength; whereas strengths of up to 48,000 psi were realized with the large diameter fiber. In these strong composites the aluminum fails in ductile shear. Charpy impact and notched bend tests were used to study energy absorption mechanisms in the fracture of boron aluminum. The critical parameters were found to be the strength, diameter, and volume fraction of the fiber and the shear yield strength of the matrix.  Notch tensile tests were performed on longitudinally and transversely reinforced BORSIC aluminum and on BORSIC-titanium. The minimum strength modifying flaw size and the maximum flaw stress concentration effects were determined for two inch wide specimens. Transversely reinforced specimens had net section strengths unaffected by flaw size.			

DD FORM 1473  
1 JAN 64

UNCLASSIFIED  
Security Classification

**UNCLASSIFIED**  
**Security Classification:**

14. KEY WORDS	LINK A		LINK B		LINK C	
	ROLE	WT	ROLE	WT	ROLE	WT
Boron Composites Aluminum Boron/Aluminum Titanium Mechanical Properties Fatigue Environmental Exposure Impact Notch Toughness Orthotropic Properties						

**INSTRUCTIONS**

**1. ORIGINATING ACTIVITY:** Enter the name and address of the contractor, subcontractor, grantee, Department of Defense activity or other organization (corporate author) issuing the report.

**2a. REPORT SECURITY CLASSIFICATION:** Enter the overall security classification of the report. Indicate whether "Restricted Data" is included. Marking is to be in accordance with appropriate security regulations.

**2b. GROUP:** Automatic downgrading is specified in DoD Directive 5200.10 and Armed Forces Industrial Manual. Enter the group number. Also, when applicable, show that optional markings have been used for Group 3 and Group 4 as authorized.

**3. REPORT TITLE:** Enter the complete report title in all capital letters. Titles in all cases should be unclassified. If a meaningful title cannot be selected without classification, show title classification in all capitals in parenthesis immediately following the title.

**4. DESCRIPTIVE NOTES:** If appropriate, enter the type of report, e.g., interim, progress, summary, annual, or final. Give the inclusive dates when a specific reporting period is covered.

**5. AUTHOR(S):** Enter the name(s) of author(s) as shown on or in the report. Enter last name, first name, middle initial. If military, show rank and branch of service. The name of the principal author is an absolute minimum requirement.

**6. REPORT DATE:** Enter the date of the report as day, month, year, or month, year. If more than one date appears on the report, use date of publication.

**7a. TOTAL NUMBER OF PAGES:** The total page count should follow normal pagination procedures, i.e., enter the number of pages containing information.

**7b. NUMBER OF REFERENCES:** Enter the total number of references cited in the report.

**8a. CONTRACT OR GRANT NUMBER:** If appropriate, enter the applicable number of the contract or grant under which the report was written.

**8b, 8c, & 8d. PROJECT NUMBER:** Enter the appropriate military department identification, such as project number, subproject number, system number, task number, etc.

**9a. ORIGINATOR'S REPORT NUMBER(S):** Enter the official report number by which the document will be identified and controlled by the originating activity. This number must be unique to this report.

**9b. OTHER REPORT NUMBER(S):** If the report has been assigned any other report numbers (either by the originator or by the sponsor), also enter this number(s).

**10. AVAILABILITY/LIMITATION NOTICES:** Enter any limitations on further dissemination of the report, other than those

imposed by security classification, using standard statements such as:

- (1) "Qualified requesters may obtain copies of this report from DDC."
- (2) "Foreign announcement and dissemination of this report by DDC is not authorized."
- (3) "U. S. Government agencies may obtain copies of this report directly from DDC. Other qualified DDC users shall request through \_\_\_\_\_."
- (4) "U. S. military agencies may obtain copies of this report directly from DDC. Other qualified users shall request through \_\_\_\_\_."
- (5) "All distribution of this report is controlled. Qualified DDC users shall request through \_\_\_\_\_."

If the report has been furnished to the Office of Technical Services, Department of Commerce, for sale to the public, indicate this fact and enter the price, if known.

**11. SUPPLEMENTARY NOTES:** Use for additional explanatory notes.

**12. SPONSORING MILITARY ACTIVITY:** Enter the name of the departmental project office or laboratory sponsoring (paying for) the research and development. Include address.

**13. ABSTRACT:** Enter an abstract giving a brief and factual summary of the document indicative of the report, even though it may also appear elsewhere in the body of the technical report. If additional space is required, a continuation sheet shall be attached.

It is highly desirable that the abstract of classified reports be unclassified. Each paragraph of the abstract shall end with an indication of the military security classification of the information in the paragraph, represented as (TS), (S), (C), or (U).

There is no limitation on the length of the abstract. However, the suggested length is from 150 to 225 words.

**14. KEY WORDS:** Key words are technically meaningful terms or short phrases that characterize a report and may be used as index entries for cataloging the report. Key words must be selected so that no security classification is required. Identifiers, such as equipment model designation, trade name, military project code name, geographic location, may be used as key words but will be followed by an indication of technical context. The assignment of links, rules, and weights is optional.

## TABLE OF CONTENTS

	<u>Page</u>
I. INTRODUCTION . . . . .	1
SECTION I - REFERENCES . . . . .	3
II. MATERIALS AND PROCESSING . . . . .	4
2.1 Materials . . . . .	4
2.1.1 Fiber . . . . .	4
2.1.2 Matrix Material . . . . .	4
2.1.3 5.6 Mil Boron Fiber Composites . . . . .	4
2.2 Processing . . . . .	5
SECTION II - REFERENCES . . . . .	7
FIGURES 2-1 - 2-8 . . . . .	8
TABLES II-I - II-IV . . . . .	16
ENVIRONMENTAL EFFECTS - SUMMARY . . . . .	23
III. ENVIRONMENTAL EFFECTS . . . . .	24
3.1 Salt Exposure . . . . .	24
3.2 High Temperature Exposure . . . . .	26
3.3 Thermal Cycling . . . . .	28
3.4 Conclusions . . . . .	32
SECTION III - REFERENCES . . . . .	34
FIGURES 3-1 - 3.27 . . . . .	35
TABLES III-I - III-II . . . . .	62
TRANSVERSE PROPERTIES - SUMMARY . . . . .	64
IV. TRANSVERSE PROPERTIES . . . . .	65
4.1 Matrix Properties . . . . .	65
4.2 Composite Transverse Elastic Modulus . . . . .	66
4.3 Transverse Tensile Strength of 4.2 Mil BORSIC-Aluminum . . . . .	69
4.3.1 The Effects of Processing Parameters and Heat Treatment . . . . .	69
4.3.2 Transverse Strength as a Function of Test Temperature and Matrix Strength . . . . .	72
4.3.3 Transverse Tensile Strength as a Function of Volume Fraction Fiber . . . . .	74
4.3.4 The Effects of Tensile Specimen Configuration and Edge Conditions on Transverse Strength. . . .	75

**Preceding page blank**

# TABLE OF CONTENTS (Cont'd)

	<u>Page</u>
4.3.5 Dispersion Hardened Aluminum 4.2 Mil BORSIC Composites . . . . .	79
4.3.6 Transverse Fiber Properties . . . . .	81
4.3.7 BORSIC-Aluminum-Stainless Steel Composites . . . . .	84
4.3.8 BORSIC-Aluminum-Titanium Composites . . . . .	85
4.4 Transverse Tensile Properties of 5.6 Mil Fiber Reinforced Composites . . . . .	86
4.5 Titanium Matrix Composites . . . . .	88
4.6 Conclusions . . . . .	90
SECTION IV - REFERENCES . . . . .	92
FIGURES 4-1 - 4-49 . . . . .	94
TABLES IV-I - IV-VII . . . . .	143
OFF-AXIS BEHAVIOR - SUMMARY . . . . .	150
V. OFF-AXIS BEHAVIOR . . . . .	151
5.1 Tensile Tests . . . . .	152
5.2 Sonic Velocity Measurements . . . . .	157
5.3 Conclusions . . . . .	159
SECTION V - REFERENCES . . . . .	161
FIGURES 5-1 - 5-29 . . . . .	163
TABLES V-I - V-IV . . . . .	192
FATIGUE FAILURE MECHANISMS - SUMMARY . . . . .	197
VI. FATIGUE FAILURE MECHANISMS . . . . .	198
6.1 Fatigue of Axially Reinforced Specimens . . . . .	198
6.2 Fatigue of Center Notched Specimens . . . . .	202
6.3 Transverse Tensile Fatigue . . . . .	204
6.4 Fatigue of Cross Ply Composites . . . . .	205
6.5 Conclusions . . . . .	209
SECTION VI - REFERENCES . . . . .	210
FIGURES 6-1 - 6-25 . . . . .	211
TABLES VI-I - VI-II . . . . .	236

# TABLE OF CONTENTS (Cont'd)

	<u>Page</u>
NOTCH BEND FRACTURE - SUMMARY . . . . .	238
VII. NOTCHED BEND FRACTURE . . . . .	239
7.1 Charpy Impact Tests . . . . .	239
7.2 Slow Bend Tests . . . . .	244
7.3 Notched Bend Analysis . . . . .	247
7.4 Conclusions . . . . .	251
SECTION VII - REFERENCES . . . . .	253
FIGURES 7-1 - 7-25 . . . . .	254
TABLES VII-I - VII-IV . . . . .	279
NOTCH TENSILE FRACTURE - SUMMARY . . . . .	284
VIII. NOTCH TENSILE FRACTURE . . . . .	285
8.1 Longitudinal Reinforcement . . . . .	285
8.1.1 BORSIC + Aluminum Composites . . . . .	286
8.1.2 BORSIC + Titanium Composites . . . . .	290
8.1.3 HMG-50 + BP 907 Composites . . . . .	290
8.2 Transverse Reinforcement . . . . .	291
8.3 Analysis . . . . .	292
8.3.1 Fracture Mechanics . . . . .	292
8.3.2 Flaw Stress Field . . . . .	293
8.3.3 Notch Blunting Indices . . . . .	294
8.3.4 System Comparisons . . . . .	295
8.4 Conclusions . . . . .	295
SECTION VIII - REFERENCES . . . . .	296
FIGURES 8-1 - 8-24 . . . . .	298
TABLES VIII-I - VIII-X . . . . .	322

## LIST OF ILLUSTRATIONS

### Figure

- 2-1      Axial Tensile Stress-Strain Curve for 64 v/o-5.6 Mil Boron 2024-T6 Composite Tested at 70°F
- 2-2      Composite Filament Winding Apparatus
- 2-3      Plasma Spray Apparatus
- 2-4      Diffusion Bonded 4.2 Mil BORSIC-Aluminum Composite Using Monolayer Plasma Sprayed Tapes
- 2-5      53 v/o Large Diameter BORSIC-6061 Aluminum Composite
- 2-6      4.2 Mil BORSIC-Aluminum-Titanium Composite
- 2-7      4.2 Mil BORSIC-Aluminum-AFC-77 Rocket Wire Composite
- 2-8      4.2 Mil BORSIC-Titanium 6 Al/4 V Matrix Composite
  
- 3-1      Three Point Bend Fixture Used for Salt Corrosion Tests
- 3-2      Stress Corrosion As a Function of Exposure in Synthetic Sea Salt Spray at 95°F
- 3-3      Edge Views of BORSIC + 6061-F (Top) and BORSIC + 2024-F (Bottom) Composite Bend Specimens After Exposure for One Week in Synthetic Sea Salt Spray at 95F and 100 KSI
- 3-4      Edge Views of BORSIC + 6061-F (Top) and BORSIC + 2024-F (Bottom) Composite Bend Specimens After Exposure for One Month in Synthetic Sea Salt Spray at 95F and 100 KSI
- 3-5      Transverse Sections of BORSIC + 2024-F (Top) and BORSIC + 2024-T6 (Bottom) Bend Specimens After Exposure for One Week in Synthetic Sea Salt Spray at 95F and 100 KSI
- 3-6      Edge Views of 4.2 Mil BORSIC + 6061-T6 (Top) and BORSIC + 2024-T6 (Bottom) Composite Bend Specimens After Exposure for One Month in Synthetic Sea Salt Spray at 95F and 100 KSI

## LIST OF ILLUSTRATIONS (Cont'd)

### Figure

- 3-7      Strength of 4.2 Mil BORSIC Fiber Removed from 2024 Aluminum Matrix Composites
- 3-8      Effect of Exposure Time in Synthetic Sea Salt Spray at 95°F and 100 KSI on the Flexural Strength of 4.2 Mil BORSIC + 6061 Aluminum and BORSIC + 2024 Aluminum Composite Materials
- 3-9      Room Temperature Longitudinal Strength and Modulus of 4-Mil Boron + 6061 Aluminum as a Function of Exposure Time in Air at 700°F
- 3-10     Room Temperature Transverse Strength and Modulus of 4-Mil Boron + 6061 Aluminum as a Function of Exposure Time in Air at 700°F
- 3-11     Taper Section of 4 Mil Boron + 6061-F Aluminum at 10,000X Along Fiber Axis and 500X in Transverse Direction
- 3-12     Room Temperature Longitudinal Strength and Modulus of 4.2 Mil BORSIC + 6061 Aluminum as a Function of Exposure Time in Air at 700°F
- 3-13     Room Temperature Transverse Strength and Modulus of 4.2 Mil BORSIC + 6061 Aluminum as a Function of Exposure Time in Air at 700°F
- 3-14     Transverse Tensile Strength as a Function of Percent Split Fibers on the Fracture Surface of 4.2-Mil BORSIC + 6061-F Thermal Exposure Specimens
- 3-15     Fracture Surfaces of 4.2 Mil BORSIC + 6061-F Transverse Tensile Specimens Showing Typical Appearance of High Strength Material (Left), Low Strength Material (Middle) and Intermediate Strength Material (Right)
- 3-16     Room Temperature Longitudinal Strength of 5.7 Mil BORSIC + 6061 Aluminum as a Function of Exposure Time in Air at 700°F
- 3-17     Room Temperature Transverse Strength and Modulus of 5.7 Mil BORSIC + 6061 Aluminum as a Function of Exposure Time in Air at 700°F
- 3-18     Edges of 4.2 Mil BORSIC + 6061-F Aluminum After Thermal Cycling from 70F to 670F
- 3-19     Effect of Thermal Cycling on Material Density



LIST OF ILLUSTRATIONS (Cont'd)

Figure

- 3-20 Flexural Strength of Unidirectional 4.2-Mil BORSIC + 6061-F Aluminum Composite Material as a Function of the Number of Thermal Cycle Exposures from 70°F to 670°F
- 3-21 Dynamic Flexural Modulus of 4.2-Mil BORSIC + 6061-F Aluminum Composite Laminates as a Function of the Number of Thermal Cycle Exposures from 70°F to 670°F
- 3-22 Longitudinal Microstructure of Unidirectional 4.2 Mil BORSIC + 6061-F Composite Material after Thermal Cycling
- 3-23 Longitudinal Microstructure of  $\pm 45^\circ$ ,  $0^\circ$ ,  $\pm 45^\circ$  Laminates of 4.2 Mil BORSIC + 6061-F Composite Material After Thermal Cycling
- 3-24 Fracture Surfaces of 4.2 Mil BORSIC + 6061-F Material After Thermal Cycling and Flexural Testing
- 3-25 4.2 Mil BORSIC + 6061-F Composite Specimen After Thermal Cycling Leached to Expose the Fibers (Mag: 56X)
- 3-26 Effect of Thermal Cycling on Time Interval for Extensional Wave Propagation in Longitudinal Direction
- 3-27 Effect of Thermal Cycling on Average Ultrasonic Attenuation Level
- 4-1 Aluminum-7% Si Plasma Sprayed and Foil Matrix Material
- 4-2 Aluminum Alloy Matrix Fracture Surface
- 4-3 Ultimate Tensile Strength of 6061 Matrix as a Function of Temperature
- 4-4 Ultimate Tensile Strength of 2024 Matrix as a Function of Temperature
- 4-5 Composite Transverse Elastic Modulus
- 4-6 Transverse Modulus as a Function of Temperature
- 4-7 Transverse Strength as a Function of Matrix Strength for 4.2 Mil BORSIC-Aluminum

## LIST OF ILLUSTRATIONS (Cont'd)

### Figure

- 4-8 Fracture Surface of a 50% Volume Fraction 4.2 Mil BORSIC-6061 Composite 90° Tensile Specimen
- 4-9 Transverse Tensile Fracture Surface of 4.2 Mil BORSIC-1100
- 4-10 46 v/o 4.2 Mil BORSIC-6061 Aluminum 90° Tensile Stress Strain Curves
- 4-11 Transverse Tensile Strength of 4.2 Mil BORSIC-6061 Aluminum as a Function of Test Temperature
- 4-12 Transverse Tensile Strength of 4.2 Mil BORSIC-2024 Aluminum as a Function of Test Temperature
- 4-13 Transverse Tensile Strength of 50% by Volume 4.2 Mil BORSIC-Aluminum
- 4-14 Transverse Tensile Strength of 50% by Volume 4.2 Mil BORSIC-Aluminum
- 4-15 Compressive Stress Strain Curves for Axial and 90° Fiber Reinforcement
- 4-16 Transverse Compression Specimen of BORSIC-6061 Aluminum after Completion of Test
- 4-17 Fracture Surface of a Transverse Compression Specimen
- 4-18 Transverse Tensile Strength as a Function of Volume Fraction 4.2 Mil BORSIC Fiber
- 4-19 4.2 Mil BORSIC Fibers Cut by a Diamond Abrasive Cutoff Wheel and Mat
- 4-20 Radiograph of Crack Tip in 4.2 Mil BORSIC-6061 Transverse Tensile Specimen
- 4-21 90° 4.2 Mil BORSIC-Al Tensile Specimen with Free Fiber Ends
- 4-22 Transverse Tensile Test 46 v/o 4.2 Mil BORSIC-2024 Al Alloy
- 4-23 Transverse Tensile Test 46 v/o 4.2 Mil BORSIC-5052/56 Al Alloy
- 4-24 Transverse Tensile Strength of 46 v/o 4.2 Mil BORSIC-Aluminum

## LIST OF ILLUSTRATIONS (Cont'd)

### Figure

- 4-25      Fracture Surfaces of Free Fiber End (Top) and Cut Edge (Bottom)  
          Specimens of 50 v/o-4.2 Mil BORSIC-5052/56
- 4-26      51 v/o 4.2 Mil BORSIC - S.A.P.
- 4-27      Transverse Tensile Strength of 51 v/o 4.2 Mil BORSIC - S.A.P.
- 4-28      Strength Distribution of 4.2 Mil BORSIC Fiber Tested in Diametral  
          Compression
- 4-29      Fragments of a BORSIC Fiber Fractured Under Diametral Compression
- 4-30      Fiber Fracture Using the Fiber Flaw Model
- 4-31      Strength Distribution of 5.6 Mil Boron Fiber Tested in Diametral  
          Compression
- 4-32      Strength Distribution of 5.7 Mil BORSIC Fiber Tested in Diametral  
          Compression
- 4-33      5.7 Mil Diameter BORSIC Fiber
- 4-34      Radiograph of 4.2 Mil BORSIC-6061-AFC-77 Tensile Specimen
- 4-35      Transverse 47%-4.2 Mil BORSIC-6061-Axial-6%-S.S. Tested in the Axial  
          Direction
- 4-36      Radiograph of 45 v/o 4.2 Mil BORSIC-35 v/o-6061-20%-Ti-6/4 Tensile  
          Specimen
- 4-37      Transverse Tensile Stress-Strain Curve for 55 v/o-5.6 Mil Boron  
          2024-T6 Composite Tested at 70°F
- 4-38      Composite Transverse Tension Fracture Surface
- 4-39      Transverse Tensile Strength as a Function of Test Temperature
- 4-40      Composite Transverse UTS as a Function of Matrix UTS
- 4-41      Transverse Tensile Fracture Surface of 56 v/o-5.7 Mil BORSIC-2024

## LIST OF ILLUSTRATIONS (Cont'd)

### Figure

- 4-42 Transverse Tensile Stress-Strain Curve for 52 v/o-5.7 Mil BORSIC 6061-T6 Composite Tested at 70°F
- 4-43 Transverse Tensile Stress-Strain Curve for 54 v/o-5.7 BORSIC-1100
- 4-44 Transverse Tensile Strength of 5.7 Mil BORSIC-6061
- 4-45 Transverse Tensile Elastic Modulus for 5.7 Mil BORSIC-6061 Aluminum Composites
- 4-46 Transverse Tensile Strength of 60 v/o-5.7 Mil BORSIC-6061
- 4-47 Composite Transverse UTS as a Function of Matrix UTS for 60 v/o-5.7 Mil BORSIC-6061
- 4-48 Transverse Tensile Strength of 2024 Aluminum Matrix Composites as a Function of Fiber Type (40-50% Fiber Content)
- 4-49 Dynamic Modulus,  $E_{11}$ , as a Function of Temperature for 50 Percent by Volume BORSIC + Beta III Titanium Composite Material
  
- 5-1 Off-Axis Specimen in Rotating Grids
- 5-2 Continuous Load-Strain Recording Instrumentation
- 5-3 Coordinate System for Off-Axis Uniaxial Tension Tests with Orthotropic Axes 1, 2 and Load Axes X, Y
- 5-4 Rosette Strain Gage Configurations Used in Off-Axis Tension Tests
- 5-5  $S_{11}$  of Unidirectional 4.2 Mil BORSIC + 6061-F Aluminum as a Function of Angle from the Filament Direction
- 5-6  $S_{12}$  of Unidirectional 4.2 Mil BORSIC + 6061-F Aluminum as a Function of Angle from the Filament Direction
- 5-7  $S_{16}$  of Unidirectional 4.2 Mil BORSIC + 6061-F Aluminum as a Function of Angle from the Filament Direction

## LIST OF ILLUSTRATIONS (Cont'd)

### Figure

- 5-8  $S_{11}$  of Unidirectional 5.7 Mil BORSIC + 6061-T6 Aluminum as a Function of Angle from the Filament Direction
- 5-9  $S_{12}$  of Unidirectional 5.7 Mil BORSIC + 6061-T6 Aluminum as a Function of Angle from the Filament Direction
- 5-10  $S_{16}$  of Unidirectional 5.7 Mil BORSIC + 6061-T6 Aluminum as a Function of Angle from the Filament Direction
- 5-11 Theoretical  $S_{11}$  Values for Unidirectional BORSIC + 6061-F Aluminum as a Function of Angle from the Filament Direction
- 5-12 Theoretical  $S_{12}$  Values for Unidirectional BORSIC + 6061-F Aluminum as a Function of Angle from the Filament Direction
- 5-13 Theoretical  $S_{16}$  Values for Unidirectional BORSIC + 6061-F Aluminum as a Function of Angle from the Filament Direction
- 5-14 Stress-Normal Strain Curves for 50 v/o 4.2 Mil BORSIC + 6061-F Aluminum
- 5-15 Stress-Shear Strain Curves for 50 v/o 4.2 Mil BORSIC + 6061-F Aluminum
- 5-16 Stress-Normal Strain Curves for 63 v/o 5.7 Mil BORSIC + 6061-T6 Aluminum
- 5-17 Stress-Shear Strain Curves for 63 v/o 5.7 Mil BORSIC + 6061-T6 Aluminum
- 5-18 Off-Axis Tensile Strength of 4.2 Mil BORSIC + 6061-F Aluminum
- 5-19 Off-Axis Tensile Strength of 5.7 Mil BORSIC + 6061-T6 Aluminum
- 5-20 End and Side Views of Fractured 0, 2, and 5 Degree Off-Axis 50 v/o 4.2 Mil BORSIC + 6061-F Aluminum Tensile Specimens
- 5-21 End and Side views of Fractured 10 and 30 Degree Off-Axis 4.2 Mil BORSIC + 6061-F Aluminum Tensile Specimens

## LIST OF ILLUSTRATIONS (Cont'd)

### Figure

- 5-22 End and Side Views of Fractured 45 Degree Off-Axis 4.2 Mil BORSIC + 6061-F Aluminum Tensile Specimens Tested in Rotating and Rigid Grips
- 5-23 End and Side Views of Fractured 60 and 80 Degree Off-Axis 4.2 Mil BORSIC + 6061-F Aluminum Tensile Specimens
- 5-24 End and Side Views of Fractured 90 Degree Off-Axis 4.2 Mil BORSIC + 6061-F Aluminum Tensile Specimen
- 5-25 End and Side Views of Fractured 10°, 30°, and 45° Off-Axis 63 v/o 5.7 Mil BORSIC + 6061-F Aluminum Tensile Specimens
- 5-26 Transverse Section of 5.7 Mil BORSIC + 6061-T6 Composite Material
- 5-27 Ultrasonic Velocity Measurement System
- 5-28 Density Times the Square of Sonic Velocity as a Function of Angle Relative to the Filament Orientation
- 5-29 Ratio of Density Times the Square of Sonic Velocity to Elastic Modulus as a Function of Angle Relative to the Filament Orientation
- 6-1 Experimental Method in Fatigue Testing
- 6-2 Axial Tension - Tension Low Cycle Fatigue of 4.2 Mil BORSIC-6061-F Aluminum
- 6-3 Region of Axial-50 v/o-4.2 BORSIC-6061 Fatigue Specimen
- 6-4 Axial 50 v/o-4.2 BORSIC-6061 Fatigue Specimen After Fatigue Testing
- 6-5 Radiograph Taken at the Fracture Surface of a 0°-50 v/o-4.2 Mil BORSIC-6061 Aluminum Composite Low Cycle Fatigue Specimen
- 6-6 56 v/o-5.7 BORSIC-6061 Tensile Specimens
- 6-7 Progressive Fiber Failure at the Edges of Notch in 30 v/o-5.7 Mil BORSIC-6061 Tensile Specimen Loaded to 96% of the Ultimate Fracture Load
- 6-8 Notch Edges After Tensile Failure for Same Specimen as Figure 6-7

## LIST OF ILLUSTRATIONS (Cont'd)

### Figure

- 6-9 Notch Tips of 56 v/o-5.7 Mil BORSIC-6061-Fatigue Specimen after 1347 Cycles
- 6-10 Fractured Center Notched Fatigue Specimen Net UTS = 186,000 psi. Same Specimen as Figure 6-9
- 6-11 Notch Region of Fractured Fatigue Specimen. Same Specimen as Figure 6-9
- 6-12 Fracture Surface of Center Notched Fatigue Specimen. Same Specimen as Figure 6-9
- 6-13 Fractured Specimens After Fatigue Cycling
- 6-14 Transverse Tension - Tension Low Cycle Fatigue of 4.2 Mil BORSIC-6061 Aluminum
- 6-15 Transverse Tension - Tension Low Cycle Fatigue of 58% 5.7 BORSIC-6061 Aluminum
- 6-16 Tension - Tension Low Cycle Fatigue of 4 v/o 4.2 Mil BORSIC-6061 Aluminum
- 6-17 Radiograph of Fatigued Cross Ply 4.2 Mil BORSIC-6061 Composite
- 6-18 Fracture Surface of  $\pm 45^\circ$ -4.2 Mil BORSIC-6061 Fatigue Specimen
- 6-19 Fracture Surface of  $0^\circ/90^\circ$  5.7 Mil BORSIC-6061 Fatigue Specimen
- 6-20 Tensile Stress Strain Curve for  $0^\circ/90^\circ$  57 v/o-5.7 BORSIC-6061
- 6-21 Tension - Tension Low Cycle Fatigue of  $0^\circ/90^\circ$  57 v/o-5.7 BORSIC-6061
- 6-22 Radiograph of Crack Tip in  $0^\circ/90^\circ$ -57 v/o-5.7 Mil BORSIC-6061
- 6-23 Tensile Stress Strain Curve for  $\pm 45^\circ$  5.7 BORSIC-6061
- 6-24 Fracture Surface of  $\pm 45^\circ$  5.7 BORSIC 6061 Fatigue Specimen
- 6-25 Fiber Fracture in a  $\pm 45^\circ$ -57 v/o 5.7 Mil BORSIC-6061 Fatigue Specimen

## LIST OF ILLUSTRATIONS (Cont'd)

### Figure

- 7-1 Microstructures of 4.2 Mil BORSIC + 6061-F Aluminum Composite Material
- 7-2 Impact Energy Per Unit Area for 4.2 Mil BORSIC + 6061-F Aluminum Full Size Charpy "V" Notch Specimens
- 7-3 Effect of Heat Treatment on the Impact Energy Per Unit Area for 50 v/o BORSIC + 6061 Aluminum (Full Size Charpy "V" Notch Specimens)
- 7-4 Effect of Width on the Impact Energy Per Unit Area for 4.2 Mil BORSIC 6061-F Aluminum Charpy "V" Notch Specimens
- 7-5 Effect of Thickness on the Impact Energy Per Unit Area for 4.2 Mil BORSIC + 6061-F Aluminum Charpy "V" Notch Specimens
- 7-6 Effect of Orientation on Impact Energy Per Unit Area for 4.2 Mil BORSIC + 6061-F Aluminum Full Size Charpy "V" Notch Specimens
- 7-7 Scanning Electron Fractograph of Type LT50 v/o 4.2 Mil BORSIC + 6061-F Aluminum Impact Specimen
- 7-8 Charpy Impact Fracture Surfaces of 4.2 Mil BORSIC + 6061-F Constant Width and Notch Depth - Variable Thickness
- 7-9 Charpy Impact Fracture Surfaces of 4.2 Mil BORSIC + 6061-F Constant Thickness and Notch Depth - Variable Width
- 7-10 Scanning Electron Fractograph of Type TL50 v/o 4.2 Mil BORSIC + 6061-F Aluminum Impact Specimen
- 7-11 Scanning Electron Fractograph of Type TT50 v/o 4.2 Mil BORSIC + 6061-F Aluminum Impact Specimen
- 7-12 Fractograph of Type LT63 v/o 8.0 Mil Boron + 6061-F Aluminum Impact Specimen
- 7-13 Scanning Electron Fractographs of 50 v/o 4.2 Mil BORSIC + 6061-F Aluminum +45 Degree Laminates
- 7-14 Charpy Impact Strength of Selected Materials



## LIST OF ILLUSTRATIONS (Cont'd)

### Figure

- 7-15 Typical Load-Deflection Curve for Type LT 4.2 Mil BORSIC + 6061 Al Slow Bend Test
- 7-16 Typical Load-Deflection Curve for Type TL and Type TT 4.2 Mil BORSIC + 6061 Al Slow Bend Test
- 7-17 Effect of Volume Percent Filament on the Notched Flexural Strength of 4.2 Mil BORSIC + 6061-F Aluminum
- 7-18 Variation of Impact and Slow Bend Fracture Energy with Volume Percent Fiber for Axially Reinforced 4.2 Mil BORSIC + 6061-F Aluminum Composites
- 7-19 Variation of Impact and Slow Bend Fracture Energy with Volume Percent Fiber for Transversely Reinforced 4.2 Mil BORSIC + 6061-F Aluminum Composites
- 7-20 Kahn Tear-Test Specimens and Representation of Load-Deformation Curves (Left) and Unit Propagation Energy vs. Tensile Yield Strength of 0.063 in. Aluminum Alloy Sheet (Right) (After Kaufman and Holt)
- 7-21 Photomicrographs of Interrupted Three Point Bend Test of Type LT41 v/o 4.2 Mil BORSIC + 6061-F Aluminum (Specimen Polished Prior to Test and Loaded to Point A in Figure 7-15)
- 7-22 Photomicrographs of Interrupted Three Point Bend Test of Type LT50 v/o 4.2 Mil BORSIC + 6061-F Aluminum (Specimen Polished Prior to Test and Loaded to Point B in Figure 7-15)
- 7-23 Photomicrographs of Interrupted Three Point Bend Test of Type TL41 v/o 4.2 Mil BORSIC + 6061-F Aluminum (Specimen Polished Prior to Test and Loaded to Point A in Figure 7-16)
- 7-24 Photomicrographs of Interrupted Three Point Bend Test of Type TT50 v/o 4.2 Mil BORSIC + 6061-F Aluminum (Specimen Polished Prior to Test and Loaded to Point A in Figure 7-16)
- 7-25 Variation of Impact Energy Per Unit Area with the Parameter  $\frac{V_f d_f (\sigma_{uf})^2}{24 \tau_{my}}$  for BORSIC + Aluminum and Boron + Aluminum Composites

## LIST OF ILLUSTRATIONS (Cont'd)

### Figure

- 8-1 Center-Notched Tensile Specimen in Loading Fixture
- 8-2 Net Fracture Strength of Center Notched 4.2 Mil BORSIC + Aluminum
- 8-3 Variation of Net Fracture Strength with Flaw Size as a Function of Specimen Thickness for 4.2 Mil BORSIC + 6061-F Aluminum Composites
- 8-4 Net Fracture Strength of 4.2 Mil BORSIC + 6061-F Aluminum with Center Circular Holes
- 8-5 Net Fracture Strength of Notched Heat Treated 4.2 Mil BORSIC + Aluminum
- 8-6 Typical Stress-Displacement Curve for 4.2 Mil BORSIC + 6061-F Aluminum Center Notch Specimen Under Uniaxial Tension
- 8-7 View of Stress-Coat Crack Pattern on an Axially Reinforced (Type LT) 50 v/o 4.2 Mil BORSIC + 2024-F Aluminum Center-Notched Tensile Specimen
- 8-8 Fracture Surface of 50 v/o 4.2 Mil BORSIC + 6061-F Aluminum Center-Notched Tensile Specimen
- 8-9 Side View of Fractured Axially Reinforced (Type LT) 4.2 Mil BORSIC + 2024-F Aluminum Alloy Center Notched Tensile Specimen (Left) and X-ray Radiograph of Region Near Original Crack Tip (Right)
- 8-10 Fractured 4.2 Mil BORSIC + 6061 Aluminum Center Notched Specimen
- 8-11 Cr Shadowed Replica Around Circular Hole in 4.2 Mil BORSIC + 6061-F Aluminum at 99 Percent of Fracture Stress
- 8-12 Fractured 4.2 Mil BORSIC + 6061-F Aluminum Specimen Containing a Circular Hole
- 8-13 Net Fracture Strength of Center Notched 4.2 Mil BORSIC + Titanium and Graphite + Epoxy
- 8-14 Fracture Surface of 50 v/o 4.2 Mil BORSIC + Beta III Titanium Center-Notched Tensile Specimen

## LIST OF ILLUSTRATIONS (Cont'd)

### Figure

- 8-15      Fractured 4.2 Mil BORSIC + Beta III Titanium Center Notched Specimen
- 8-16      View of Fractured Longitudinally Reinforced (Type LT) 50 v/o HMG-50 Graphite + BP-907 Epoxy Center Notched Tensile Specimen
- 8-17      Net Fracture Stress as a Function of Initial Flaw Length for BORSIC + 6061-F Aluminum Composite Material
- 8-18      Fracture Surface of a Typical Transversely Reinforced (Type TL) 50 v/o 4.2 Mil BORSIC + 6061-F Aluminum Center-Notched Tensile Specimen
- 8-19      Variation of Transverse Strength with Percent Split Fibers on the Fracture Surface of 50 v/o 4.2 Mil BORSIC + 6061-F Aluminum Composite Material
- 8-20      Gross Fracture Strength of Center Notched 4.2 Mil BORSIC + Aluminum
- 8-21      Elastic Longitudinal Stress Concentration Factor for 50 v/o 4.2 Mil BORSIC + 6061-F Aluminum Under Uniaxial Longitudinal Tension
- 8-22      Elastic Shear Stress Concentration Factor for 50 v/o 4.2 Mil BORSIC + 6061-F Aluminum Under Uniaxial Longitudinal Tension
- 8-23      Elastic Transverse Stress Concentration Factor for 50 v/o 4.2 Mil BORSIC + 6061-F Aluminum Under Uniaxial Longitudinal Tension
- 8-24      Variation of Gross Fracture Strength with Flaw Size for Selected Materials

## LIST OF TABLES

### Table No.

II-I	Axial Tensile Strength of 5.6 Mil B-Al
II-II	Axial Tensile Strength of 48 v/o 5.6 Mil B-6061
II-III	Axial Tensile Strength of 5.7 mil BORSIC-Al Composites
II-IV	Strength of 4.2 Mil BORSIC Fibers Extracted from Composite Tapes
III-I	Heat Treatments Given BORSIC-Aluminum Salt Exposure Specimens
III-II	High Temperature Air Exposure of 6061-F Composites
IV-I	Heat Treatment Procedures
IV-II	Experimentally Determined Properties of Plasma Sprayed Material with Foil
IV-III	Diffusion Bonding Conditions Capable of Producing Fully Consolidated 50% BORSIC-Matrix Composites
IV-IV	Transverse Tensile Properties of 5.6 mil B-Al
IV-V	Transverse Tensile Properties of 5.7 mil BORSIC-Al
IV-VI	4.2 Mil BORSIC-Titanium Composites
IV-VII	5.7 Mil BORSIC-Titanium Composites
V-I	Results of 4.2 Mil BORSIC + 6061-F Off-Axis Tests
V-II	Results of 5.7 Mil BORSIC + 6061-T6 Off-Axis Tests
V-III	Micromechanical Elastic Predictions for BORSIC + 6061 Aluminum
V-IV	Strength of 6061 Aluminum Alloy
VI-I	5.7 BORSIC-6061 Center Notched Specimen Tensile Test Results
VI-II	Tensile Properties of 57%-5.7 mil BORSIC-6061 Cross Ply Composites Tested at 45° to the Fiber Axes

# LIST OF TABLES (Cont'd)

## Table No.

VII-I	Impact Energy Per Unit Area for Plasma Sprayed BORSIC + Aluminum Composites
VII-II	Impact Energy Per Unit Area for Nominal 50 v/o 4.2 Mil BORSIC Fiber + Aluminum
VII-III	Slow Bend Fracture Work for Type LT BORSIC + 6061-F Specimens
VII-IV	Strength of Filaments in Impact Specimens
VIII-I	Fracture Strength of Longitudinally Reinforced Center Notched BORSIC + Aluminum Composites
VIII-II	Fracture Strength of Longitudinally Reinforced 4.2 Mil BORSIC + 6061-F Aluminum Composites with Center Circular Holes
VIII-III	Fracture Strength of Longitudinally Reinforced Heat Treated Center Notched 4.2 mil BORSIC + Aluminum Composites
VIII-IV	Fracture Strength of Longitudinally Reinforced Center Notched 4.2 mil BORSIC + Beta III Titanium Composites
VIII-V	Fracture Strength of Longitudinally Reinforced Center Notched HMG-50 Graphite + BP-907 Epoxy Composites
VIII-VI	Net Fracture Strength of Type LT BORSIC + Aluminum Composites
VIII-VII	Longitudinal Tensile Properties of 50 v/o 4.2 mil BORSIC + Beta III Titanium
VIII-VIII	Longitudinal Tensile Properties of HMG-50 Graphite + BP-907 Epoxy Composites
VIII-IX	Fracture Strength of Transversely Reinforced Center Notched BORSIC + 6061-F Aluminum Composites
VIII-X	Elastic Stress Concentration Factors for 0.100 inch Elliptical Flaws in Fiber Reinforced Composite Systems

## I. INTRODUCTION

The aluminum-boron metal matrix composite system has been studied with considerable intensity over the last few years. This system has been used to prove the feasibility of fabricating metal matrix composites (without serious degradation) and excellent properties have been obtained. Aerospace hardware shapes, such as gas turbine engine fan blades, have been produced, proving the feasibility of important applications of this system.

Considerable data has been gathered concerning the strong points of the system. In the reinforced direction, this system has a strength-to-density and modulus-to-density superior to any engineering alloy at temperatures up to 500°C. However, many other properties, also important in aerospace applications, are not nearly as well substantiated. These include the strength properties in nonreinforced directions, the effect of corrosive or erosive environment, the characteristics of multidirectionally reinforced composites, the strength of notched composites, and the fatigue behavior. These properties, along with others required in hardware development, must be evaluated if the aluminum-boron composites are to be certified for aerospace structural applications.

One advantage of the metal matrix systems, when compared to resin matrix systems, is that the matrix is less sensitive to elevated temperature effects, both chemical and mechanical. However, since aluminum matrix composites may be used in structural applications at temperatures above those used for aluminum alloys, the properties of composite systems must be evaluated carefully at high temperatures, particularly in the unreinforced directions. In addition, since the standard aluminum alloys were not developed for high strength in this temperature range (above 400°F), new heat treatments and alloys may be extremely useful. Titanium alloys in the matrix may also be very desirable for service at higher temperatures.

Early work on the theory of reinforcement, such as the "rule of mixtures" with its modifications for predicting strength, was useful but not entirely satisfactory with aluminum matrix alloys and has not been successful in predicting the strength with titanium alloys. It appears that an improved understanding of fracture in these materials is required. The prediction of strength properties in other axial directions is considerably less well developed. Here the relationship between composite failure and the failure of the isotropic constituents should be useful.

The goals of this program include a critical property evaluation of the best aluminum alloy boron composite systems available today in areas which are significant with respect to aerospace hardware development and a better understanding of fracture in metal matrix composites. This program is intended to develop criteria for material selection and metallurgical processing and to develop data to guide the structural engineer in design.

Previous work conducted at the research Laboratories has included work on Air Force-funded contracts; AF 33615-3209 entitled, "Services and Materials Necessary to Develop a Process to Produce Fibrous Reinforced Metal Composite Materials", 1966 (Ref. 1.1), and Contract AF 33615-67-C-1655 entitled, "Investigation of Plasma Sprayed Metal Matrix Reinforced Composites" (Ref. 1.2). In the initial metal matrix program, the plasma-sprayed process was developed and the first boron-aluminum composites were achieved which exhibited substantial strengthening. During this program, composites were produced using both commercially pure aluminum and 2024 aluminum alloy matrix material. In addition, studies were initiated to prepare titanium matrix composites. Under the second metal matrix program, the plasma-spray process was refined and BORSIC<sup>®</sup> (silicon carbide coated boron filament) was introduced. Newer matrix alloys such as 6061 and brazing alloys were introduced, and the composite tensile strengths were increased to over 180,000 psi with fiber contents of 45-50% by volume. Multidirectional layups were also produced and the materials were characterized with respect to fatigue characteristics, off-axis properties, moduli, and Poisson's ratio.

In complementary programs, United Aircraft Corporation-sponsored work has included the development of BORSIC fiber and further investigation of composite behavior. An interesting example of a parallel program includes the development of 5.6 mil boron and 5.7 mil BORSIC which was concurrent with this program. The availability of these fibers actually altered the direction of the present program in that a major change was effected on the transverse properties in the aluminum boron system. Due to the introduction of the new fiber a second class of aluminum-boron composites was studied. These composites have transverse tensile strengths of up to 50,000 psi and improved axial strength and lower cost. This work together with other related work has been published or presented recently (Refs. 1.3-14).

The emphasis in this program has been to carefully analyze those properties which are characterized by significant interaction between the constituents rather than those which can be fairly well predicted knowing the properties of the constituents. For example, the elastic moduli, the axial composite strength, and shear yielding properties of the matrix (especially at elevated temperatures) are well predicted knowing the fiber and matrix elastic properties, the fiber strength, and the metal matrix stress-strain curve; whereas the transverse strength, effect of thermal cycling, impact properties, and the effect of notches and stress concentrations are not as easily predicted and reflect more complex phase interactions.

This Technical Report is addressed to the work performed in Contract F33615-69-C-1539. Included are a discussion on the materials and processing and reports on studies in the areas of transverse properties, environmental effects and thermal cycling, fatigue, and fracture of composites. Also included in these reports are discussions on the relationship of this primary empirical study to more analytical composite studies and a discussion of the technological impact of the program.

## SECTION I - REFERENCES

1. K. Kreider and G. R. Leverant, "Boron Fiber Metal Matrix Composites", AFML-TR-66-219, July 1966.
2. K. G. Kreider, R. D. Schile, E. M. Breinan, and M. A. Marciano, "Plasma Sprayed Metal Matrix Fiber Reinforced Composites", AFML-TR-68-119, July 1968.
3. K. G. Kreider and M. A. Marciano, "Mechanical Properties of Boron Aluminum Composite", Trans. AIME, June 1969.
4. "Mechanical Testing of Metal Matrix Composites", Composite Materials: Testing and Design, STP 490 ASTM, Philadelphia, 1969.
5. E. M. Breinan and K. G. Kreider, "Braze Bonding and Joining of BORSIC Aluminum Composites", Metal Engineering Quarterly, November 1969.
6. E. R. Thompson and K. G. Kreider, "Composite Materials", McGraw Hill Yearbook of Science and Technology, 1970.
7. E. M. Breinan and K. G. Kreider, "Materials Technology for BORSIC Aluminum Rotating Structural Aircraft Parts", Metals Progress, May 1970.
8. K. Kreider, "Metal Matrix Composite Mechanical Testing", Conference on Testing Fibrous Composites for Mechanical Properties, July 15, 1970, Teddington, Middlesex, England.
9. K. Kreider, "High Modulus Composites in the United States", Presented at U. S. Department of Commerce Symposium on High Performance Materials, London, U. K., April 27, 1971.
10. K. G. Kreider and V. M. Patarini, "Thermal Expansion of Boron Fiber-Aluminum Composites", Metallurgical Trans., Vol. 1, December 1970.
11. K. Kreider and K. Prewo, "Transverse Strength of Boron Fibers", Presented at Second Conference on Composite Materials: Testing and Design, Anaheim, Calif., April 1971.
12. K. Kreider and K. Prewo, "The Transverse Strength and Elastic Modulus of Boron-Aluminum Composites", Presented at TMS-AIME in Las Vegas, Nevada, May 1970; To be published in Met. Trans.
13. E. Breinan and K. Kreider, "Transverse Creep and Fracture of BORSIC-Aluminum Composites", Presented at TMS Spring Meeting, May 1970.
14. K. Kreider, "BORSIC Titanium Aluminum Composites", Presented at TMS Spring Meeting, May 14, 1970.



## II. MATERIALS AND PROCESSING

### 2.1 Materials

#### 2.1.1 Fiber

Fiber composites were fabricated using primarily boron or BORSIC fiber. Four mil fiber ( $0.004 \pm 0.0001$  in. in diameter) has an axial modulus of  $56-57 \times 10^8$  psi and typically has an ultimate tensile strength of 450,000 psi with a mean deviation of less than 80,000 psi. The BORSIC 4.2 mil fiber has a coating of silicon carbide approximately 0.001 in. thick which permits fabrication at higher temperatures in aluminum and titanium and has far superior oxidation resistance (Refs. 2.1,2). Although the oxidation resistance of boron is poor above 400°C, BORSIC has excellent oxidation resistance up to 1000°C. In addition, the reaction between boron and aluminum limits the maximum time-temperature exposure product (without significant fiber degradation) to approximately 1/2 hr at 500°C. This generally forces the diffusion bonding step to be performed at 4000 psi or higher which is often inconvenient in large, or complex shaped parts particularly if they are cross-plyed. BORSIC, in both 4 mil and 5.6 mil fiber diameters, has ultimate tensile strengths of approximately 10% lower than the uncoated boron fiber as it is currently being produced. This lower strength is also observed in the BORSIC-aluminum composites. However, the large diameter boron fiber has a 10% higher average strength compared to 4 mil or 500,000 psi. These differences are evident in the composites described in Table II-I. The boron fiber used in this program was supplied by the Air Force Materials Laboratory.

#### 2.1.2 Matrix Material

The matrix alloys employed included both foil and plasma spray deposits from prealloyed powder. Commercial foils of 2024, 6061, 5052, SAP, 713 (Al + 7%Si), and 1145 were used with the corresponding aluminum alloy powders. Also, aluminum-iron and 8001 powders were employed separately. The titanium matrix composites were made with commercial Ti 6/4 (Ti + 6Al + 4V) and  $\beta_{III}$  (Ti + 11.5Mo + 6Zr + 4.5Sn) foils. The specific properties of these matrix materials is treated in Section IV-Transverse Properties, particularly as they apply to composite properties.

#### 2.1.3 5.6 Mil Boron Fiber Composites

Composites made from the 5.6 mil boron fiber have somewhat superior axial properties compared to those fabricated with 4 mil fiber. Since information on their strength values is not in the open literature, a discussion of the axial properties of 5.6 mil boron composites is given below. These properties are determined at United Aircraft Research Laboratories under Corporate funds.

The results of the axial tensile tests performed at room temperature on the boron reinforced composites are presented in Table II-I. The data in Table II-I indicate that composite tensile strength increases with increasing

volume fraction fiber and through the use of the T6 heat treatment. The composite elastic modulus data are in approximate agreement with a rule-of-mixtures calculation. Figure 2.1 presents the axial tension stress-strain curve for a 2024 alloy matrix composite containing 64% by volume of 5.6 mil diameter boron fiber. The composite was heat treated prior to testing to produce a modified T-6 condition. The composite ultimate tensile strength was 279,000 psi.

Tensile tests at elevated temperature were performed on composites containing approximately 50% by volume 5.6 mil boron in the 6061 alloy matrix. Table II-II includes the results of the elevated temperature tensile results. In each case, the specimen was held at temperature for approximately 30 minutes prior to testing. At 900°C, these composites still exhibited 60% of their room temperature tensile strength.

Axially reinforced composites of 5.7 mil BORSIC-aluminum were also tensile tested at room temperature. The results for 6061 aluminum matrix specimens tested in the as-fabricated and heat treated conditions are presented in Table II-III. For comparison it may be pointed out that composites containing 58% by volume 4.2 mil BORSIC fiber in 6061 matrix failed at approximately 185,000 psi. The data in Table II-III indicate that a strength level of 200-220,000 psi is typical of the large diameter BORSIC composites for the same volume fraction fiber. This higher axial tensile strength is directly due to the superior performance of the large diameter fiber. Transverse strength of these composites is discussed in Section III.

## 2.2 Processing

The composites were fabricated by hot press diffusion bonding of either plasma-sprayed or polystyrene-bonded monolayer tapes. The filament winding operation is performed on a modified engine lathe, using a screw-thread auger to control the fiber spacing (Fig. 2.2). The aluminum foil wrapped mandrel which receives the winding is spring loaded to allow for thermal expansion mismatch between the aluminum foil substrate and the fiber. Plasma-spray fabrication was done in argon (Fig. 2.3). The cylindrical mandrel covered with a layer of aligned filament is rotated and traversed before a plasma arc to deposit an even layer of matrix alloy. Aluminum alloy powder is then injected into the hot gas of the plasma arc and melted in the exothermic or recombination zone. The molten aluminum droplets are impacted on the foil and fiber and quickly solidified bonding the monolayer tape together.

The hot press diffusion bonding step is discussed also in the transverse property section, particularly as to how the various parameters affect the properties. Best results are obtained by hot pressing within 100°F of the solidus temperature at greater than 5000 psi in a nonoxidizing atmosphere. Plastic deformation, which is very important in the diffusion of aluminum, is accomplished by compressing the porosity of the plasma-spray layer and deforming the foil. This composite fabrication technique was used in order to fabricate the composite containing 6061 aluminum alloy matrix and 50% volume fraction BORSIC depicted in Fig. 2.4. Similar photomicrographs are given for composites made with 5.7 mil BORSIC fiber (Fig. 2.5), and triplex composites boron-aluminum-titanium (Fig. 2.6) and boron-aluminum-rocket wire (Fig. 2.7).

After plasma spraying the monolayer tape, the fibers were removed by dissolving the aluminum in 10% hydrochloric acid and tensile tested. No filament degradation was evident and typical values of the measured strength are given in Table II-IV.

Titanium matrix composites and some aluminum matrix composites were fabricated using the foil plus fiber with a fugitive binder polystyrene. The laminate is heated to 450°C in vacuum to outgas the binder and subsequently hot pressed (typically at 800°C and 10,000 psi for titanium composites) for diffusion bonding. Both alloys, Ti 6/4 and  $\beta_{III}$ , were used with BORSIC fibers and a typical microstructure is given in Fig. 2.8.

## SECTION II - REFERENCES

1. M. Basche, R. Fanti, and F. Galasso, "Preparation and Properties of Silicon Carbide Coated Boron Filaments", Int. Fiber Sci. and Tech., Vol. 1, 1968.
2. M. Basche, "Interfacial Stability of Silicon Carbide Coated Boron Filament Reinforced Metals" from "Interfaces in Composites, ASTM-STP 452, Am. Soc. Testing and Material, p. 130, 1969.

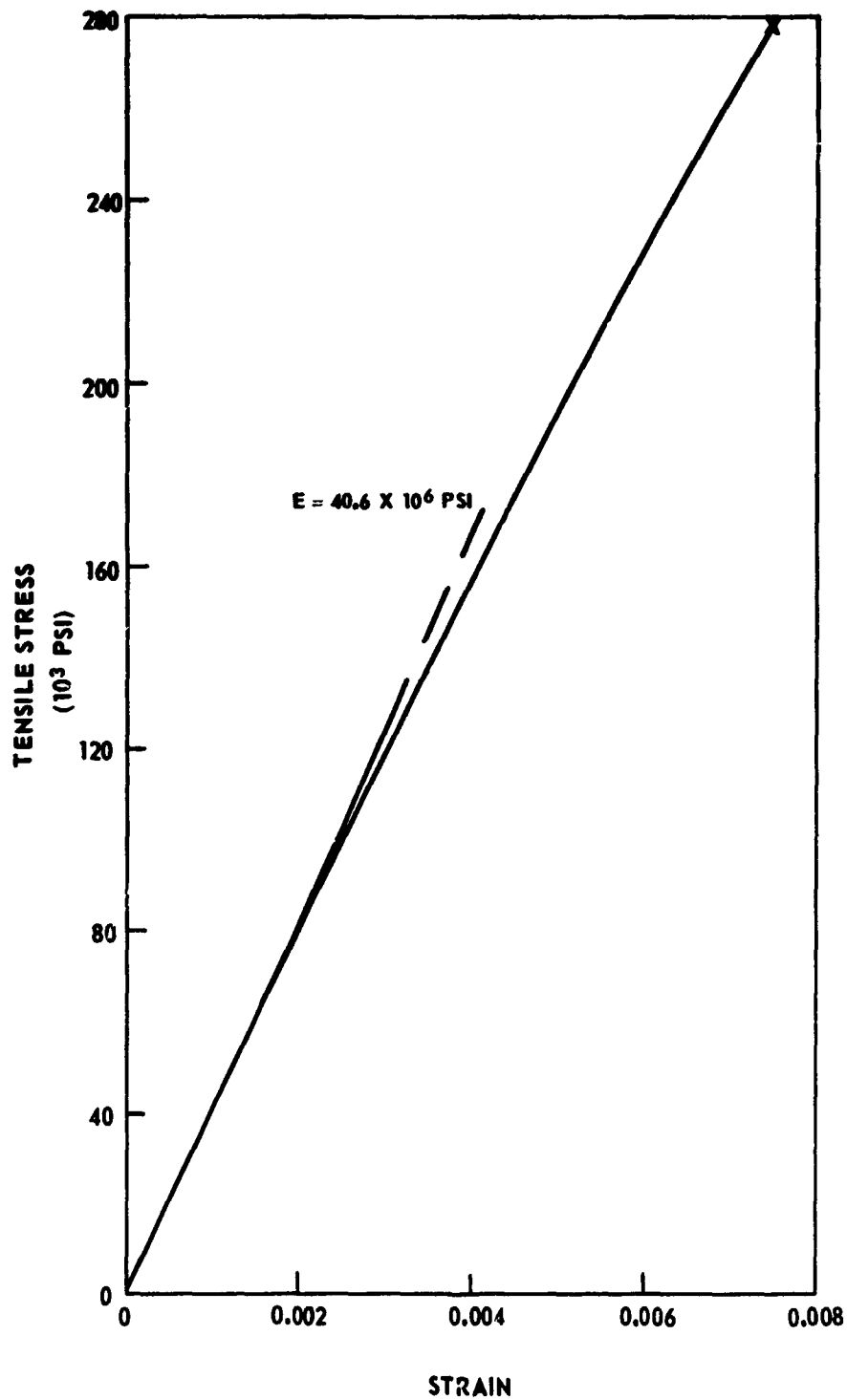
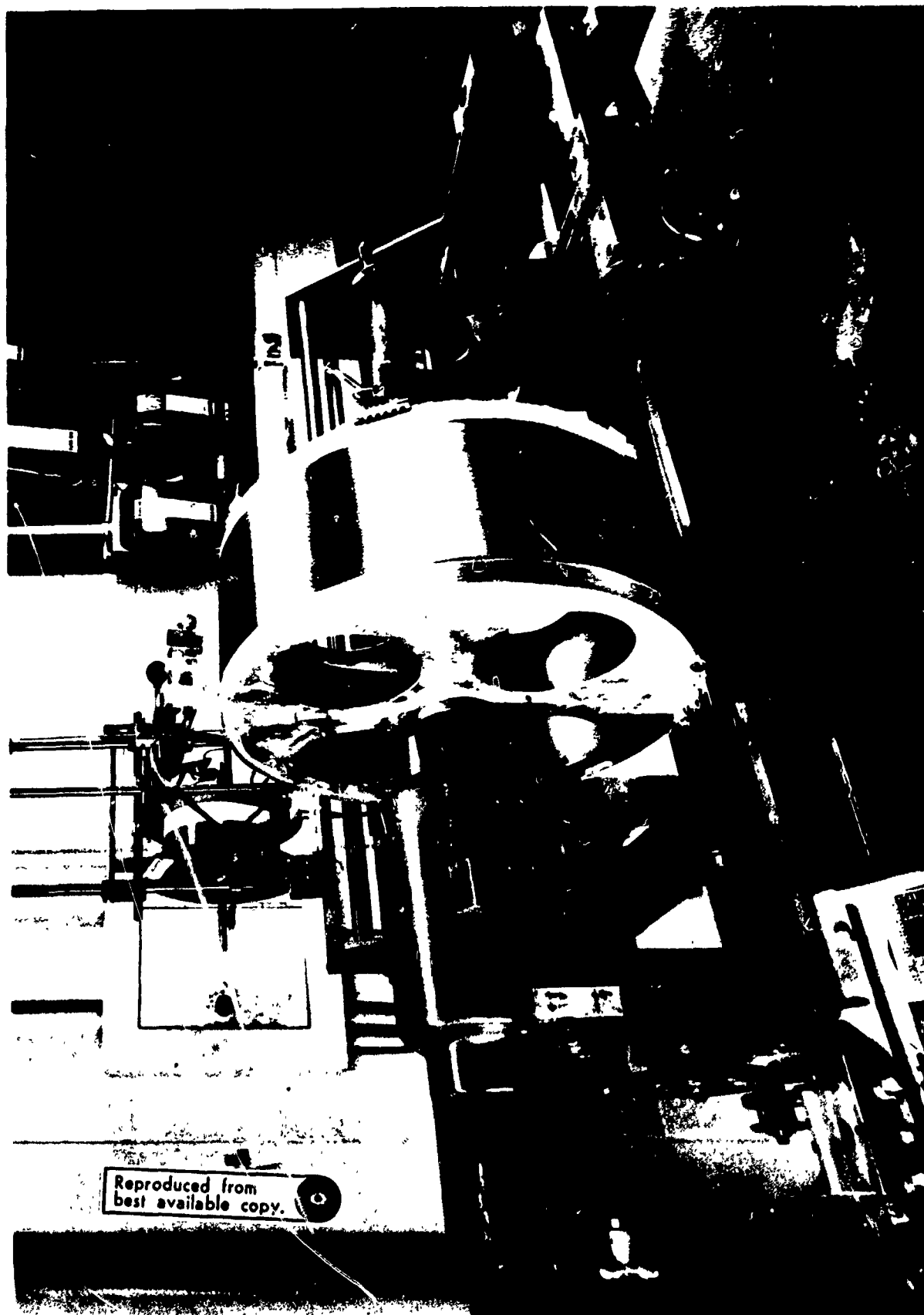


FIGURE 2-1. AXIAL TENSILE STRESS-STRAIN CURVE FOR 64 v/o-5.6 MIL  
BORON 2024-T6 COMPOSITE TESTED AT 70°F



Reproduced from  
best available copy.

FIGURE 2-2. COMPOSITE FILAMENT WINDING APPARATUS



FIGURE 2-3. PLASMA SPRAY APPARATUS

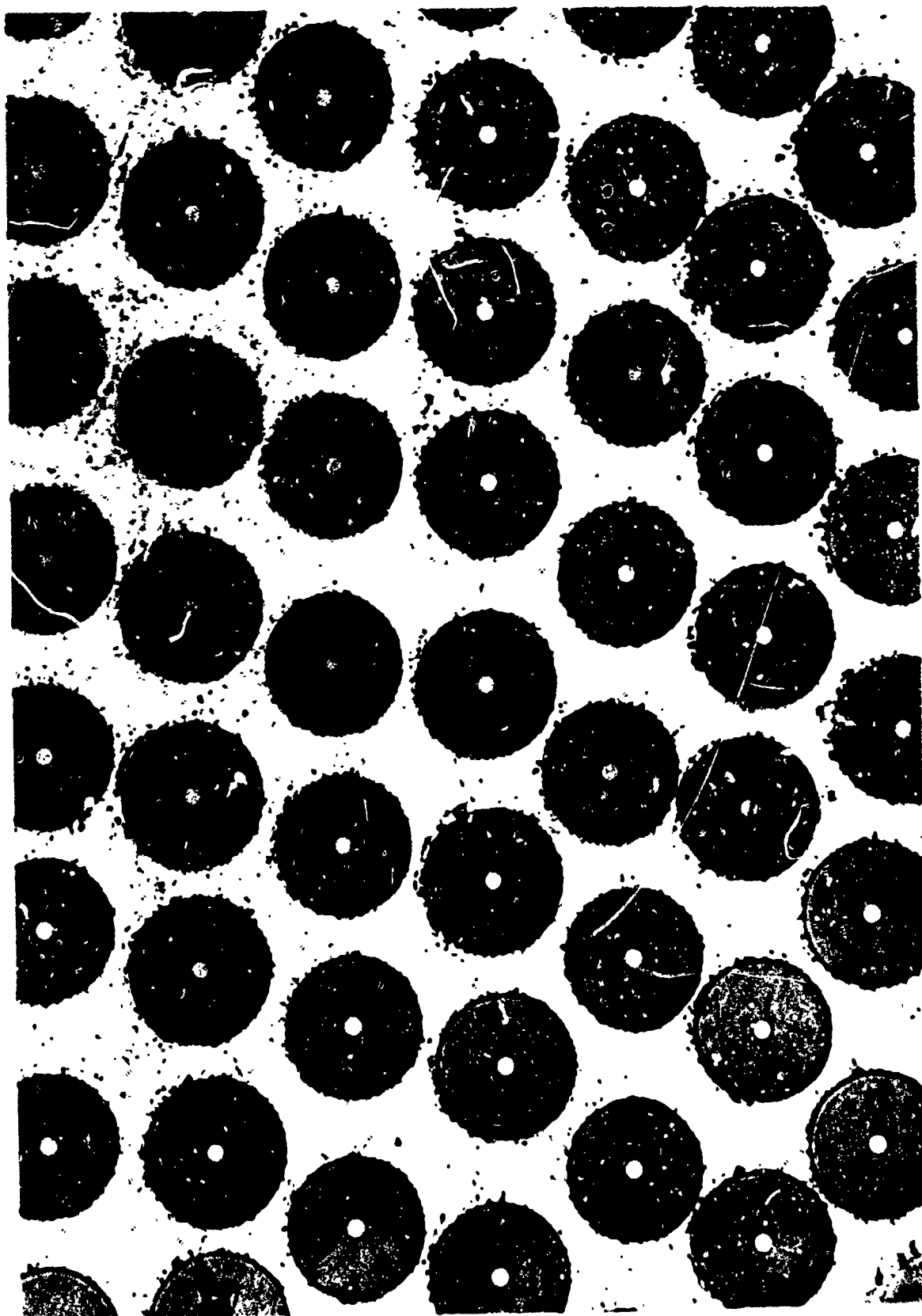
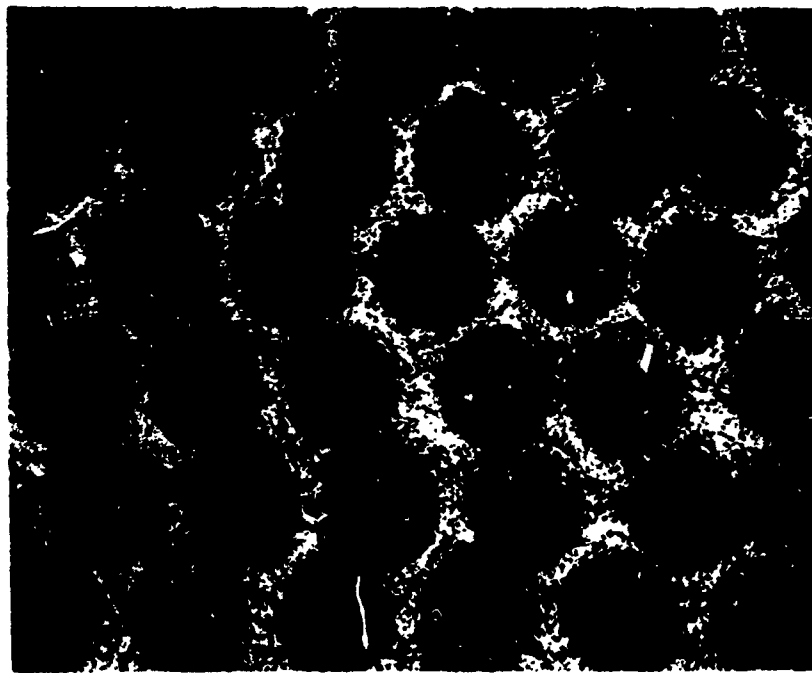


FIGURE 2-4. DIFFUSION BONDED 4.2 MIL BORSIC-ALUMINUM COMPOSITE USING MONOLAYER PLASMA SPRAYED TAPES

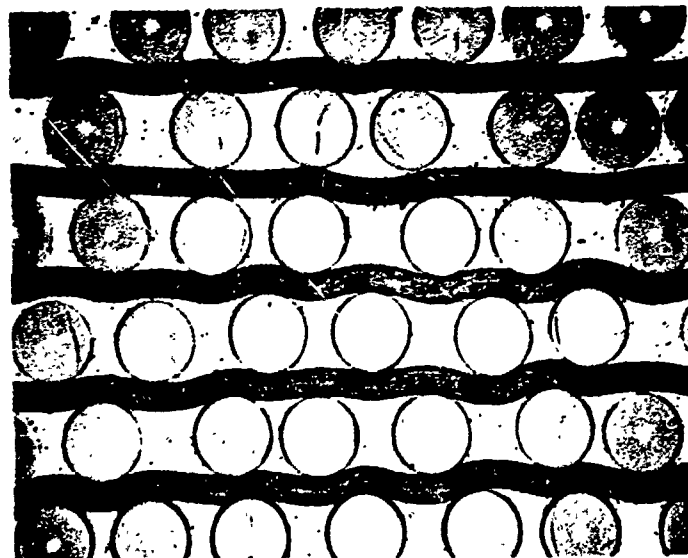




Reproduced from  
best available copy.

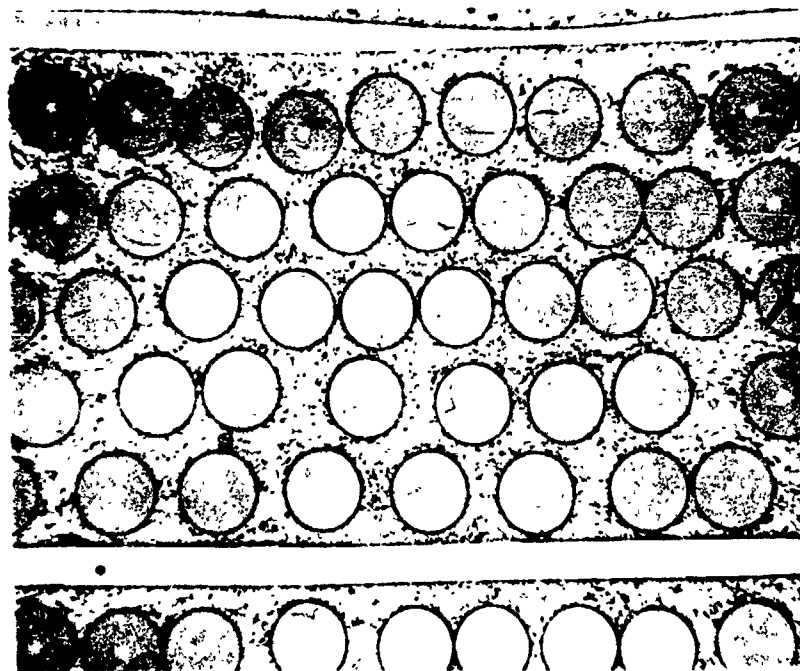
100X

FIGURE 2-5. 53 v/o LARGE DIAMETER BORSIC-6061 ALUMINUM COMPOSITE



┌  
100  $\mu$

FIGURE 2-6. 4.2 MIL BORSIC - ALUMINUM - TITANIUM COMPOSITE



Reproduced from  
best available copy.

100  $\mu$

FIGURE 2-7. 42 MIL BORSIC - ALUMINUM - AFC - 77 ROCKET WIRE COMPOSITE

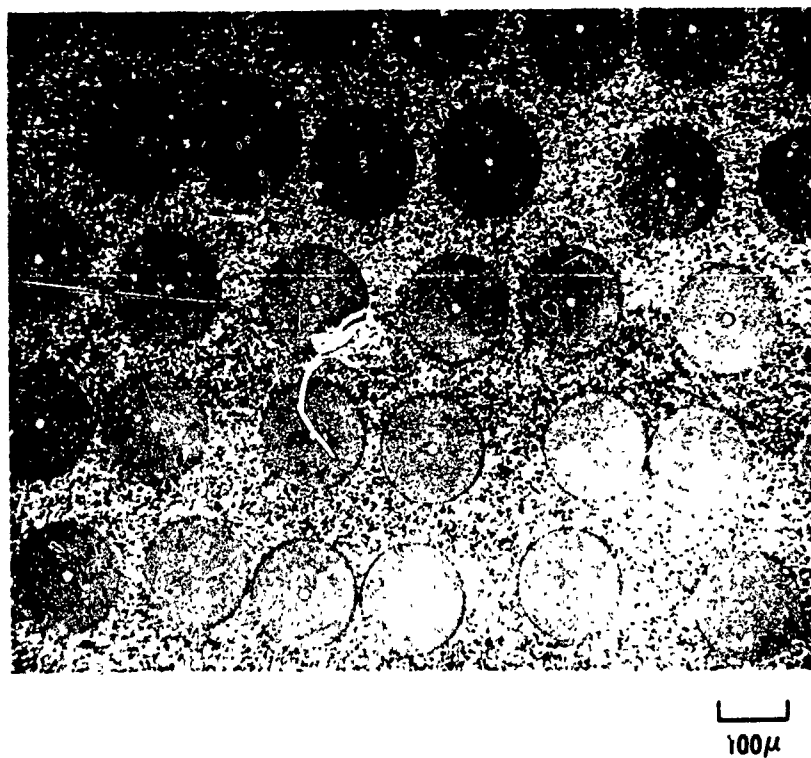


FIGURE 2-8. 4.2 MIL BORSIC - TITANIUM 6 Al / 4 V MATRIX COMPOSITE

Table II-I

## Axial Tensile Strength of 5.6 Mil B-A1

<u>Matrix</u>	<u>v/o Boron (%)</u>	<u>Ultimate Tensile Strength (10<sup>3</sup> psi)</u>	<u>Elastic Modulus (10<sup>3</sup> psi)</u>	<u>Strain to Fracture (%)</u>
2024F	45	185.7	30.4	0.765
	45	197.5	27.5	0.835
	44	177.0	30.0	0.725
	47	212.0	32.0	0.825
	47	212.0	32.6	0.820
	49	194.0	32.0	0.740
2024-T6	46	202.5	32.8	0.75
	46	213.6	31.6	0.81
	47	217.0	32.3	0.830
	48	213.0	31.3	0.845
	64	279.0	40.0	0.755
2024F	70	279.5	-	-
	66	253.0	-	-
	67	250.2	-	-
6061F	48	196.3	31.8	0.710
	48	171.0	28.2	0.590
	50	204.0	33.8	0.72
	50	208.0	32.0	0.76
6061-T6	52	216.5	33.8	0.78
	51	197.0	33.4	0.69
	50	203.0	-	-

Table II-II

Axial Tensile Strength of 48 v/o 5.6 Mil B-6061

<u>Test Temperature</u> (°F)	<u>UTS</u> (10 <sup>3</sup> psi)
70	196.3
70	171.0
500	177.0
500	135.2
900	143.8
900	137.3

Table II-III

## Axial Tensile Strength of 5.7 mil BORSIC-Al Composites

<u>Matrix</u>	<u>% BORSIC (%)</u>	<u>Ultimate Tensile Strength (10<sup>3</sup> psi)</u>	<u>Elastic Modulus (10<sup>6</sup> psi)</u>	<u>Strain to Fracture (%)</u>
6061-F	30	115.0 113.3	17.6 18.9	0.71 0.71
6061-T6	30	156.2 152.4		
6061-F	54	203.4 181.5 199.0	36.6 36.0 36.1	0.675 0.630 0.655
6061-F	56	214.0 212.0		
6061-F	57	228.0 222.0		
6061-F	58	227.0 219.0 216.0 222.0		
6061-F	61	199.1 207.6	39.4	0.57
2024-F	58	211.5 221.0		
2024-T6	61	235.0 210.0		
5052/56	59	177.6 182.0	37.7	0.54
1100/1145	57	158.2 175.5		

Table II-IV  
Strength of 4.2 Mil BORSIC Fibers Extracted  
from Composite Tapes

Tape No.	Individual Fiber Tests UTS x 10 <sup>3</sup> psi						Ave UTS 10 <sup>3</sup> psi
	#1	#2	#3	#4	#5	#6	
783 A	535	478	528	505	---	---	509
B	205	270	400	332	375	380	327
C	372	375	370	370	---	---	372
D	310	365	338	220	375	275	314
E	275	375	450	220	450	205	329
F	210	380	340	375	210	295	302
G	348	250	420	360	300	400	346
H	400	370	230	380	425	---	361
I	305	332	413	365	---	---	354
J	375	432	428	282	430	---	389
K	375	400	450	355	405	---	397
L	385	450	405	360	---	---	400
M	530	325	245	310	455	470	356
N	405	455	500	400	300	---	371
O	230	328	382	360	---	---	350
P	230	350	235	180	230	195	237
Q	375	345	360	408	335	455	373
R	385	395	450	525	465	375	433
S	340	395	325	370	352	415	366
T	382	530	415	385	432	355	417
U	390	382	345	415	375	380	381
V	365	300	355	525	338	330	369
W	394	305	275	300	315	338	321
809 A	482	466	436	310	365	295	392
B	340	445	360	420	370	425	395
C	482	418	425	465	460	475	454
D	462	420	440	380	330	440	412
E	450	398	392	466	460	294	410
603 Q	423	427	386	390	---	---	407
579 E	438	423	450	---	---	410	430
586 T	376	386	363	391	---	---	379
586 W	406	532	476	471	---	---	471
586 X	411	487	437	497	---	---	458
682	393	294	405	399	408	415	386
653	505	512	518	474	506	482	500
730 A	375	312	354	252	439	378	352
B	526	380	---	508	442	515	474
733	500	495	485	506	586	578	525
734 D	464	493	400	419	433	440	441
H	408	410	482	472	425	490	448



Table II-IV (Cont'd)

Tape No.	Individual Fiber Tests						Ave UTS 10 <sup>3</sup> psi
	UTS x 10 <sup>3</sup> psi						
	#1	#2	#3	#4	#5	#6	
738	350	347	374	311	327	267	329
739	510	430	570	480	360	540	482
740	465	465	462	468	448	260	428
741 A	525	442	400	468	432	465	455
746	408	375	424	417	360	478	414
753 A	75	408	418	---	---	---	300
754 A	90	540	90	555	420	90	297
B	425	440	422	450	435	---	434
C	520	575	455	445	445	---	468
D	448	445	470	390	320	470	424
760	485	558	500	445	486	540	502
764 B	510	512	410	370	405	485	449
C	505	225	480	472	110	465	376
766	335	365	420	400	365	380	378
771	470	432	390	442	415	390	423
771 D	345	420	520	280	400	560	421
E	478	488	450	340	495	---	450
F	340	462	478	478	385	---	429
784	398	406	435	365	---	---	401
792	400	402	412	398	415	335	394
793	375	340	300	340	370	430	359
804	355	385	345	325	310	385	351

## Strength of Boron Fibers Extracted from Composite Tapes

785 A	250	325	345	425	425	405	363
B	305	325	350	270	---	---	313

Table II-IV (Cont'd)

## Strength of 5.7 mil BORSIC Extracted from Composite Tapes

Tape No.	C/No.	Material	Individual Fiber Tests UTS x 10 <sup>3</sup> psi						Ave UTS 10 <sup>3</sup> psi
			#1	#2	#3	#4	#5	#6	
894	--	6061/6061	445	425	495	500	460	360	448
899	929	"	525	480	395	490	505	480	479
902	931	"	400	485	365	555	565	460	472
914 D	--	"	480	385	475	435	550	435	460
914 E	--	"	535	440	470	550	392	515	484
914 F	1018	"	525	470	482	470	545	540	505
914 C	--	"	445	460	310	440	375	445	413
914 B	--	"	498	485	585	550	545	535	533
914 G	--	"	465	460	515	485	530	480	489
914 H	--	"	528	460	465	445	500	435	472
914 I	--	"	425	475	382	500	475	470	455
914 J	--	"	400	440	455	435	385	412	421
914 A	--	"	425	295	435	335	385	245	353
914 K	--	"	508	382	475	485	465	505	470
914 L	--	"	425	540	468	430	480	470	469
914 M	--	"	480	420	380	408	470	225	397
914 N	--	"	390	515	500	455	460	435	459
914 O	--	"	440	505	495	500	465	405	467
914 P	--	"	292	310	340	305	398	---	274
914 Q	--	"	324	309	390	229	236	230	286
914 R	--	"	381	262	348	322	341	400	342
914 S	--	"	333	283	362	405	365	382	355
935	1042	"	460	540	460	425	485	470	467.5
			465	485	450	435			
939	1241	2024/2024	340	375	375	525	515	520	450
			470	495	495	390			
943	1140	6061/6061	500	440	490	445	530	500	456.5
			415	370	460	415			
949	1163	"	415	450	425	415	450	435	433
			445	415	425	455			
970	1123	7/3/528	479	510	421	531	497	509	483
			530	453	471	432			
994-1	--	6061/6061	370	500	525	385	495	---	455
994-2	--	"	445	420	440	435	405	---	429
997	1273	2024/2024	500	500	335	420	505	---	452
992	--		490	525	565	520	433	525	503
			575	485	445	480			
980	--		485	445	485	440	495	460	471
			465	455	460	525			

Table II-IV (Cont'd)

Tape No.	C/No.	Material	Individual Fiber Tests						Ave UTS 10 <sup>3</sup> psi
			UTS x 10 <sup>3</sup> psi						
			#1	#2	#3	#4	#5	#6	
980-1	--		524	461	454	455	421	437	455
			438	459	455	445			
980-2	--		488	463	455	434	440	403	436
			449	415	466	349			
998	1286	1145/1100	420	376	468	456	439	---	432
1001-1	1266	6061/6061	455	400	445	380	465	375	422
			445	415	380	45	565		
1001-2	1265	"	485	450	465	385	455	455	441
			450	435	420	415			
1001-3	1268	"	390	90	420	405	425	400	376
			400	415	390	425			
1001-4	1271	"	400	450	350	375	420	435	414
			415	420	460	415			
1006-1	1275	"	430	400	235	450	440	340	394
			435	365	430	415			
1006-2	1285	"	445	450	545	485	440	380	445
			450	455	385	400			
1000	--		403	455	380	422	438	---	424

## ENVIRONMENTAL EFFECTS

### SUMMARY

Matrix corrosion in 2024 alloy composites resulted in decreased mechanical properties after salt spray exposures. Longitudinal strengths of BORSIC filaments were not affected by the salt spray environment.

Exposure of 2024 and 6061 matrix BORSIC + aluminum composites to synthetic sea salt spray at 95°F and 100 ksi bending stress results in matrix corrosion that is most severe with 2024 matrix material in the as-fabricated condition. 6061-F and 6061-T6 matrix composites exhibit general corrosion without preference for regions of high stress whereas 2024-F and 2024-T6 matrix composites display depths of attack that are approximately 1.9 times greater on the tensile surfaces than on those in compression without indications of intergranular stress corrosion cracking. The flexural strengths of 6061-F and 6061-T6 matrix composites are unaffected by exposure for periods up to one month. The strength of BORSIC + 2024-F and BORSIC + 2024-T6 matrix composites can be reduced by as much as 100% and 14% respectively after one month as a result of matrix attack. The longitudinal strength of BORSIC filament is not degraded as a result of exposure to the humid salt environment.

The exposure of 50 v/o 4.2 mil diameter BORSIC + 6061-F aluminum composites to 700°F in air for periods up to 1000 hours has no significant effect on longitudinal properties ( $\sigma_L = 166 \times 10^3$  psi). The transverse strength and modulus of exceptional material ( $\sigma_T = 18.6 \times 10^3$  psi) were degraded after 1000 hours to levels usually exhibited by 4.2 mil BORSIC + 6061-F aluminum ( $\sigma_T = 13.4 \times 10^3$  psi,  $E_{22} = 18.9 \times 10^6$  psi). The strength degradation arises from reduced in situ transverse fiber strength.

The longitudinal strength of 61 v/o 5.7 mil BORSIC + 6061-F was degraded 11% ( $209 \times 10^3$  psi to  $186 \times 10^3$  psi) after 1000 hours at 700°F. Transverse properties were unaffected. Uncoated 4.0 mil boron + 6061-F material exhibited a 12% decrease in longitudinal strength ( $175 \times 10^3$  psi to  $154 \times 10^3$  psi, with the same exposure conditions. The transverse strength of this material was fundamentally unchanged ( $16.9 \times 10^3$  psi to  $16.4 \times 10^3$  psi).

Thermal cycling of 50 v/o 4.2 mil BORSIC + 6061-F aluminum matrix composites between 70°F and 670°F can cause void formation within the matrix of both unidirectional and complex laminate materials as a result of plastic strains caused by differences in thermal expansion coefficient among the constituents. These voids result in decreased density and reduced flexural moduli in complex (+45°, 0°, +45°) laminates (20% after 5000 cycles). The flexural strength of unidirectional material decreases by approximately 13% after 5000 cycles. Cyclic life can be calculated approximately using a form of the Manson-Coffin law.

### III. ENVIRONMENTAL EFFECTS

An effective composite matrix must not only transfer stress between filaments and serve as a barrier to crack propagation, it must also possess environmental stability and be chemically compatible with the reinforcing phase under service conditions. Since the filaments provide the bulk of the composite's load carrying capability and stiffness, the temperature range of useful filament properties may generally define the desired range of composite application. Thus, conventional alloys that find service as composite material matrices may well encounter environments outside their normal application domain.

The two phase structure of a composite introduces potential sources of environmental degradation beyond those expected with the constituents alone. For example, although the composite system allows a choice of aluminum matrix alloys to minimize the problem, residual stresses and electrochemical effects resulting from the contact of two dissimilar materials must now be considered. In addition, interdiffusion between fiber and matrix can result in degradation either during fabrication or subsequent elevated temperature exposure. Finally, thermally induced stresses can arise within unidirectional composite material, even in the absence of thermal gradients, as a result of differing coefficients of expansion between fiber and matrix. In laminated systems, thermal stresses can develop from the variation of thermal expansion coefficient with ply angle. In unbalanced layups these stresses can lead to warpage; in balanced ply configurations they are internally balanced but can lead to plastic deformation and cracking.

Three kinds of environmental effects have been investigated: low temperature humid salt, static elevated temperature, and cyclic temperature. Hot press diffusion bonded plasma sprayed monolayer tape material was used in all cases.

#### 3.1 Salt Exposure

##### Experimental Method

In the first study 20 layer unidirectional 50% by volume BORSIC fiber plus 2024 aluminum alloy composites and BORSIC fiber plus 6061 aluminum matrix composites were placed in an environmental test chamber and exposed to synthetic sea salt spray at 95°F and high relative humidity. The straight-sided 4 in. x 0.5 in. x 0.1 in. specimens were stressed in three point bend fixtures as shown in Fig. 3.1. To prevent direct contact with metal fixture, the specimen ends were coated with wax and a bakelite block was used as the mid-span fulcrum. A maximum bending stress of 100 ksi along the axis of the beam was applied to all specimens using one-sixteenth inch longitudinal strain gage instrumentation.

Specimens were exposed for periods of one week and one month in both the as-fabricated (6061-F, 2024-F) and precipitation hardened conditions (6061-T6, 2024-T6). A list of the specimen heat treatments is given in Table III-I.

Samples of the matrix alloys (as mill products) were also evaluated for comparative purposes. These samples were stressed to 8 ksi and 11 ksi respectively in the case of 6061-F and 2024-F and to 30 ksi in the case of the 6061-T6 and 2024-T6 materials.

Methods for determining the effect of exposure on the composite specimens included visual appearance, metallographic examination, and three-point flexural testing. The flexural test specimens were oriented with their tensile and compressive surfaces in the same sense that existed during the exposure. In addition, filament samples taken from corroded composite material were tensile tested at 70°F to determine if they had been degraded.

### Results and Discussion

The extent of corrosion for both the composite and matrix alloy specimens was determined metallographically; the results for these single specimen tests are given in Fig. 3.2. The 6061 matrix composite specimens exhibited general corrosion over their entire surfaces without preference for regions of high stress, whereas the 2024 matrix composites displayed depths of attack that were approximately 1.9 times greater on the tensile surfaces than on those in compression. The extent of corrosion per side given in Fig. 3.2 represents an average material loss for the combined effect.

Greatest attack was observed with 2024-F matrix composite material. Edge views of 2024-F and 6061-F matrix composites after one week and one month exposure periods are compared in Figs. 3.3 and 3.4. The higher corrosion rate of the 2024-F material is more evident after the longer exposure; the matrix is almost totally consumed, leaving a bundle of filaments in the fixture. Attack of the 6061-F matrix material after one month was extensive but far less severe than in the case of the 2024-F matrix material. The 6061-F matrix composite material exhibited exposed filaments along the edges and at the ends of the specimen but still supported a bending load. This ranking would be expected on the basis of monolithic alloy performance (Ref. 3.1).

Transverse sections of BORSIC plus 2024-F and 2024-T6 bend specimens after exposure for one week are shown in Fig. 3.5. Filaments in surface layers are exposed as a result of matrix corrosive attack; in the case of the 2024-F material, several fibers have fallen from the specimen. No evidence of intergranular stress corrosion cracking is apparent. It should be noted that the damage to the surface fibers is due to mounting and polishing rather than corrosion during exposure.

Additional testing is needed to confidently establish differences among the other materials, however, it appears that the composite specimens exhibit more corrosion than do the mill products matrices tested alone. There were two other significant differences between composite and mill product: first the surface oxide was different and this can considerably lengthen the incubation period (see Fig. 3.2); second a major part of the composite matrix is plasma sprayed which has a different microstructure. Both the 6061-T6 and 2024-T6 matrix composites incur less corrosion when tested with unprepared surfaces

(oxidized from solution treatment) than when they are polished prior to salt exposure. The lower corrosion rate of the 2024-T6 matrix composite material is illustrated in Fig. 3.6. It is interesting to note that with 2024-T6 the plasma sprayed composite is clearly superior.

To determine if BORSIC filament is degraded by salt exposure, fiber samples taken from the nearly consumed 2024-F matrix sample shown in Fig. 3.4 were tested at 70°F.

The results of these tests are given in Fig. 3.7. The filaments exhibited an average strength,  $\bar{X}$ , of 460 ksi with a standard deviation,  $\sigma$ , of 38.7 ksi. Also given in Fig. 3.7 are the strengths of both as-fabricated filament ( $\bar{X}$  = 474 ksi,  $\sigma$  = 58.0 ksi) and filament extracted from consolidated composite material ( $\bar{X}$  = 456 ksi,  $\sigma$  = 36.5 ksi). Thus, the longitudinal strength of BORSIC filament is not affected by exposure to the humid salt environment and composite property degradation arises from attack of the matrix material.

Residual composite strength was studied by flexural testing. The results of the three-point flexural tests are given in Fig. 3.8. The strengths of the 6061-F and 6061-T6 matrix materials were unaffected by exposure for periods up to one month (approximately 225 ksi and 280 ksi, respectively). However, significant degradation in the flexural strength of 2024 matrix specimens was observed. Material with 2024-F matrix alloy exhibited a 10% decrease in strength after an exposure of one week (221 ksi to 200 ksi); after exposure for one month, the matrix was almost entirely consumed and the material could no longer support any load. Samples with 2024-T6 alloy matrices exhibited an 11% decrease in strength after one week (285 ksi to 254 ksi) and a 14% decrease after one month (285 ksi to 245 ksi).

### 3.2 High Temperature Exposure

Three composite materials were exposed at 700°F in air for 500 hrs and 1000 hrs:

- 1) 50 v/o, 8 layer, 4.0 mil boron + 6061-F
- 2) 50 v/o, 10 layer, 4.2 mil BORSIC + 6061-F
- 3) 61 v/o, 6 layer, 5.7 mil BORSIC + 6061-F.

All were fabricated from plasma sprayed monolayer tapes. The BORSIC fiber systems were vacuum hot pressed at 1025°F/5 ksi/1 hr whereas the boron fiber system was consolidated at 900°F/10 ksi/1 hr.

After exposure, longitudinal and transverse tensile specimens were prepared using electrodischarge machining (EDM). The transverse tensile specimen used a straight-sided 3 in. long by 3/8 in. wide sample with a 1 in. gage length. The longitudinal specimen was 4 in. in overall length and 1/2 in. wide at the grips; it contained a 1 in. long reduced gage section of 0.150 in. width. Both specimens were loaded through 1 in. long epoxy bonded aluminum doublers; special fixtures were employed to ensure proper alignment. Testing was conducted using a 60,000 lb capacity Baldwin hydraulic tensile machine. Longitudinal 1/16 in. strain gages were mounted on both sides of the specimens and monitored separately during test to detect any bending and to allow modulus determinations.

## Results and Discussion

The effect of 700°F air exposure on the room temperature tensile properties of the boron + aluminum material is given in Figs. 3.9 and 3.10. After 1000 hrs the longitudinal tensile strength decreased approximately 12% ( $175 \times 10^3$  psi to  $154 \times 10^3$  psi) and the longitudinal modulus,  $E_{11}$ , was nearly unchanged ( $30.5 \times 10^6$  psi to  $30.8 \times 10^6$  psi). The fracture surface features of exposed and unexposed material observed at low magnification (50X) were similar.

The transverse tensile strength and modulus,  $E_{22}$ , of the boron + 6061-F material were fundamentally unchanged ( $16.9 \times 10^3$  psi to  $16.4 \times 10^3$  psi and  $16.3 \times 10^6$  psi to  $15.2 \times 10^6$  psi, respectively) after 1000 hrs. The transverse fracture surfaces were characterized by regions of ruptured aluminum matrix and boron fibers split largely along diametral planes.

The specimen exhibiting the lowest longitudinal strength after 1000 hrs (134 ksi) was examined metallographically using a tapered section, Fig. 3.11. Despite the use of a combined optical and mechanical magnification of 10,000X, no interfacial reaction layer or attack was observed. The decrease in strength is much less than that observed by Basche, et al (Ref. 3.2) (30% after 24 hrs) on bare fibers. This indicates that the aluminum matrix affords fairly good protection against the oxidation attack of the fiber at 700°F.

The effect of 700°F air exposure on the room temperature tensile properties of 50 v/o 4.2 mil BORSIC + 6061-F composites is given in Figs. 3.12 and 3.13. Longitudinal strength and modulus were unchanged after 1000 hrs of exposure.

Transverse strength and transverse modulus decreased approximately 28% and 10% respectively after 1000 hrs. However, the composite material used for the transverse property stability investigation proved to be of excellent quality. Transverse strength in the unexposed condition ranged from 18.1 to 19.7 ksi and averaged 18.6 ksi (5 tests). More typical strengths exhibited by as-fabricated BORSIC + 6061 aluminum, generated both in this program and elsewhere (Refs. 3.3, 3.4), range from approximately 12.5 to 15.5 ksi. The transverse strength exhibited by present material after exposure at 700°F for 1000 hrs ranged from 12.3 to 14.0 ksi and averaged 13.4 ksi (5 tests). Thus, the strength after exposure of the material used in this work is similar to the strength usually exhibited by 4.2 mil BORSIC + 6061 aluminum in the as-fabricated condition.

Exposure at 700°F has apparently lowered the in situ transverse fiber strength and thereby the composite tensile strength. This could have resulted from changes in the microstructure, defect character or residual stress pattern within the fiber itself, or may be a result of the oxygen attack on the split ends of the fibers.

The transverse fracture surfaces were examined optically at high magnification. The failures were characterized by split filaments and ruptured aluminum matrix. No regions of fiber-matrix interfacial failure were observed. There were large differences among the specimens in the number of split fibers



that appeared. A measure of the amount of splitting was determined from the ratio of the split fiber area observed to the maximum possible split area of the fibers. This permits correlation between composite strength and the area of split fibers in the fracture surface. Figure 3.14 illustrates this correlation and indicates that the split fibers were not contributing to the ultimate tensile strength since the line extrapolates to approximately the matrix strength (at zero splitting) and to very low strength (at total area splitting). The fact that increasing times lead to lower strengths and proportionately high fiber splitting ties the degradation to the fibers.

The correlation in Fig. 3.14 provides insight into the mechanism of failure. Apparently the 6061 aluminum matrix has no crack sensitivity (Ref. 3.5) and the transverse strength model proposed by Liu is appropriate. These properties will be discussed more fully in Section VI - Transverse Strength.

Typical 4.2 mil BORSIC + 6061 fracture surfaces are shown in Fig. 3.15. The photomicrographs on the left and center exhibit bright areas of aluminum matrix and dark bands of split fibers; most specimens are of this type. The fracture surface on the right is comparatively darker and somewhat mottled. Obtaining accurate measurements of the percent split fiber in these samples necessitated the use of a higher magnification (200X) than required for the other specimens (20X); underestimates were reported in the previous annual report TR-70-193.

The results of 700°F air exposure on the room temperature properties of 61 v/o 5.7 mil BORSIC + 6061 aluminum material is given in Figs. 3.16 and 3.17. A longitudinal strength decrease of approximately 11% after 1000 hrs was measured (duplicate tests).

The transverse properties were fundamentally unchanged by 700°F exposure. The measurement of transverse strength decreased by 3% and  $E_{22}$  increased by 6%. These changes are not considered significant. Examination of the fracture surfaces using optical microscopy revealed only slight fiber splitting near machined edges.

A summary of measured property changes for all three systems is given in Table III-II.

### 3.3 Thermal Cycling

#### Experimental Method

Material response to thermal cycling was investigated using 20-layer, 50% by volume BORSIC + 6061-F aluminum matrix composites. Two ply configurations were considered: unidirectional material, and a  $+45^\circ$ ,  $0^\circ$ ,  $+45^\circ$  (4,12,4) mid-plane symmetric laminate. Rectangular specimens of both configurations measuring 4 in. x 0.5 in. x 0.1 in. were gripped at one end and cycled between 70°F and 670°F. This was accomplished by alternate immersion in hot and cold air/sand fluidized beds. A complete cycle of heating from 70°F to 670°F and cooling to room temperature required approximately two minutes and included

a 50 second exposure to temperatures above 620°F and a 50 second exposure to temperatures below 120°F. Specimens were removed from the apparatus after exposures of 500, 1000, 2000, 3000, 4000, and 5000 cycles.

Sample conditions both prior to test and after exposure were measured in several ways; these included linear dimensions, density, ultrasonic attenuation level, and time for the propagation of an extensional wave in the longitudinal direction. The ultrasonic attenuation measurements were made using a 5 MHz 1/4 in. diameter lithium sulfate flat transducer and a metal plate beneath the sample (pulse-echo method). A measure of attenuation was obtained by passing energy through the specimen and measuring the reflected signal amplitude using an oscilloscope. The procedures used in determining extensional wave propagation times are essentially the same as those described in the Off-Axis section for ultrasonic velocity measurements. These nondestructive tests were of particular interest since they find utility in the inspection of composite material hardware.

In addition, small straight-sided specimens, measuring 3 in. x 0.1 in. x 0.1 in. were electrodischarge machined from each sample. The strength of exposed unidirectional material was determined using three-point flexural tests since composite material behavior in bending is important in many applications including fan and compressor blades. The flexural moduli of both the unidirectional material and the  $\pm 45^\circ$ ,  $0^\circ$ ,  $\pm 45^\circ$  laminates were obtained from first mode resonant frequency measurements of samples vibrating in free-free bending.

## Results and Discussion

### Characterization

Thermal cycling 4.2 mil BORSIC + 6061-F composite material from 70°F to 670°F resulted in dimensional changes. Measurements accurate to the nearest 0.0002 in. revealed the following:

1. The length (fiber direction) of all specimens remained unchanged as a result of filament constraint.
2. The width of unidirectional material increased by as much as 4.1% after 5000 cycles and thickness remained constant.
3. The width and thickness of the complex laminate increased by 2.6% and 6.0% respectively after 5000 cycles.

Extensive surface deformation and protrusions accompanied this growth, Fig. 3.18. Resulting density changes with cycling are given in Fig. 3.19. The reduced density suggests that voids or cracks have opened in the matrix.

The results of the three-point flexural tests of unidirectional material are given in Fig. 3.20. A decreased flexural strength results from cycling. The strength loss is approximately 13% after 5000 cycles and is

small considering the severity of the test. The specimens accumulated less than 100 hrs exposure above 600°F which would not have in itself caused degradation to BORSIC + 6061 aluminum, Fig. 3.2.

Flexural modulus determinations are given in Fig. 3.21. The stiffness of the unidirectional material remained unchanged while that of the  $\pm 45^\circ$ ,  $0^\circ$ ,  $\pm 45^\circ$  laminate decreased by approximately 20% after 5000 cycles. The modulus of the unidirectional material is not a sensitive indicator of matrix degradation and remains nearly constant despite matrix void formation. It is primarily determined by the volume fraction and modulus of the filaments as demonstrated by rule-of-mixtures calculations.

The stiffness of the laminated beam, however, is strongly weighted by the modulus of the  $\pm 45^\circ$  layers since they are the furthest from the neutral plane. Composite deformation is not strain limited by the filaments at angles other than  $0^\circ$  to the reinforcement direction and as a result, the influence of matrix behavior is significant in determining the properties of  $\pm 45^\circ$  material.

#### Metallography

Metallographic examination confirmed that voids had formed in the matrix as a result of thermal cycling, Figs. 3.22, 3.23. Their area fraction increased with the number of cycles exposure. The voids were elongated in the direction of the fibers and were often concentrated in regions of close fiber spacing. Void fraction in the  $\pm 45^\circ$ ,  $0^\circ$ ,  $\pm 45^\circ$  laminates was higher than in unidirectional material after the same number of cycles. No delamination or fiber-matrix interfacial failure was observed in either configuration. SEM photographs of several flexural fracture surfaces are given in Fig. 3.24. The increased matrix void size with cycling is evident in these views.

Fibers in exposed samples were examined by dissolving away the matrix alloy. Longitudinally oriented filaments in both the laminate core and in the unidirectional specimens were always unbroken. Several regions of transverse fiber splitting were evident in complex laminates exposed to 3000 or more cycles, Fig. 3.25. However, these could have been present prior to cycling.

#### Analysis

Void formation in the composite matrix apparently reflects fatigue damage arising from the cyclic plastic strain that occurs with each temperature cycle. The extent of damage is of the same magnitude in both types of laminates, though it is somewhat more severe in the  $\pm 45^\circ$ ,  $0^\circ$ ,  $\pm 45^\circ$  system. This observation confirms the results of separate studies (Ref. 3.6) which indicate that the strain amplitude arising from a 600°F temperature change in 50% BORSIC plus aluminum due to the difference in thermal expansion coefficient between fiber and matrix is approximately an order of magnitude greater than the strain arising from the ply orientation effect. The analysis of Halpin and Pagano (Ref. 3.7) was used for the latter calculation.

The matrix strain accompanying a temperature change in a one dimensional composite system where the matrix is perfectly plastic and the fibers are infinitely stiff relative to the matrix can be written:

$$\epsilon = (\alpha_M - \alpha_F) \Delta T \quad (3.1)$$

where  $\epsilon$  = matrix strain  
 $\alpha_M$  = matrix thermal expansion coefficient  
 $\alpha_F$  = fiber thermal expansion coefficient  
 $\Delta T$  = temperature change

In addition, for many metals the fatigue life can be approximately related to the cyclic plastic strain range by the Manson-Coffin law (Ref. 3.8):

$$\Delta \epsilon_{pl} = (N/D)^{-0.6} \quad (3.2)$$

where  $\Delta \epsilon_{pl}$  = cyclic plastic strain  
 $N$  = cycles to failure  
 $D = \ln(1/1-RA)$ , a ductility parameter  
 $RA$  = fractional reduction of area in a tensile test

Combining (3.1) and (3.2), noting that for a complete temperature reversal  $\Delta \epsilon_{pl} = 2\epsilon$ ,

$$N = \frac{\ln(1/1-RA)}{[2(\alpha_M - \alpha_F)\Delta T]^{1.6}} \quad (3.3)$$

This expression indicates that cyclic life will increase with increased matrix ductility, a closer match of expansion coefficient, and a decreased temperature range.

In the present case,  $\Delta T = 600^\circ\text{F}$  and  $\alpha_M - \alpha_F$  is approximately  $9.6 \times 10^{-6}$  in./in./ $^\circ\text{F}$  (Ref. 3.9). It is expected that the  $RA$  of plasma sprayed 6061-F alloy would be somewhat less than that of mill product 6061-0 aluminum but significantly higher than that of SAP alloy, 50% and 11% respectively (Ref. 3.10).

$N \approx 1000$  cycles for 50% reduction in area  
 $N \approx 500$  cycles for 30% reduction in area

The results in Fig. 3.18 indicate slight damage near 500 cycles and accelerated void/crack opening near 3000 cycles. Thus, the agreement with experiment is reasonable. A significant difference between the responses of the two configurations arises because the  $\pm 45^\circ$ ,  $0^\circ$ ,  $\pm 45^\circ$  laminate contains components of transverse stress.

This calculation does not allow for recovery effects or elastic strain components and assumes that failure will occur at the condition of maximum thermal stress and minimum ductility,  $70^\circ\text{F}$ . However, the actual cyclic strains could be somewhat higher than assumed by the one dimensional model as a result of transverse restraint. The behavior of this system contrasts sharply with that of many

multidirectional reinforced polymeric matrix systems of high glass transition temperature, where cracking can arise simply on cooling from the fabrication temperature.

### Nondestructive Inspection

Exposed material was examined using two nondestructive inspection techniques since the present samples represented a convenient vehicle for evaluating their potential usefulness in structural applications. Measured extensional wave propagation times are given in Fig. 3.26. The recorded times are approximately inversely proportional to the square root of Young's modulus and directly proportional to the square root of density. The measurements indicate no fundamental change in the stiffness of unidirectional material in the stiffness of unidirectional material in agreement with the dynamic modulus measurements (Fig. 3.21), and approximately a 15% decrease in the longitudinal stiffness of the  $\pm 45^\circ$ ,  $0^\circ$ ,  $\pm 45^\circ$  laminates (1/11.1 to 1/13.2).

The apparent bending modulus,  $E_B$ , exhibited by the complex laminate can be estimated using laminated beam theory:

$$E_B = 0.78 E(\pm 45^\circ) + 0.22 E(0^\circ) \quad (3.4)$$

In uniaxial tension the modulus,  $E_T$ , is:

$$E_T = 0.40 E(\pm 45^\circ) + 0.60 E(0^\circ) \quad (3.5)$$

Taking  $E(0^\circ) = 38 \times 10^6$  psi and  $E(\pm 45^\circ) = 18 \times 10^6$  psi from Eq. (3.4),  $E_B = 21 \times 10^6$  psi in fair agreement with the dynamic results in Fig. 3.21. The NDI indication that  $E_T$  decreases by 15% implies from Eq. (3.5) that  $E(\pm 45^\circ)$  in the laminate decreases by approximately 44% ( $18.0 \times 10^6$  to  $10 \times 10^6$  psi) after 5000 cycles. This would indicate a 27% decrease in bending modulus ( $22 \times 10^6$  psi to  $16 \times 10^6$  psi) which is reasonably consistent to the 20% decrease actually observed, Fig. 3.21.

The effect of thermal cycling on ultrasonic signal attenuation is given in Fig. 3.27. These measurements correlate in a general way with observed changes in density, Fig. 3.19, due to void formation: 1) the effect of cycling is slight in unidirectional material up to 3000 cycles and more extensive thereafter, 2) the complex laminate incurs somewhat greater damage below 3000 cycles than does unidirectional material, and displays a greater degree of voiding above 3000 cycles.

### 3.4 Conclusions

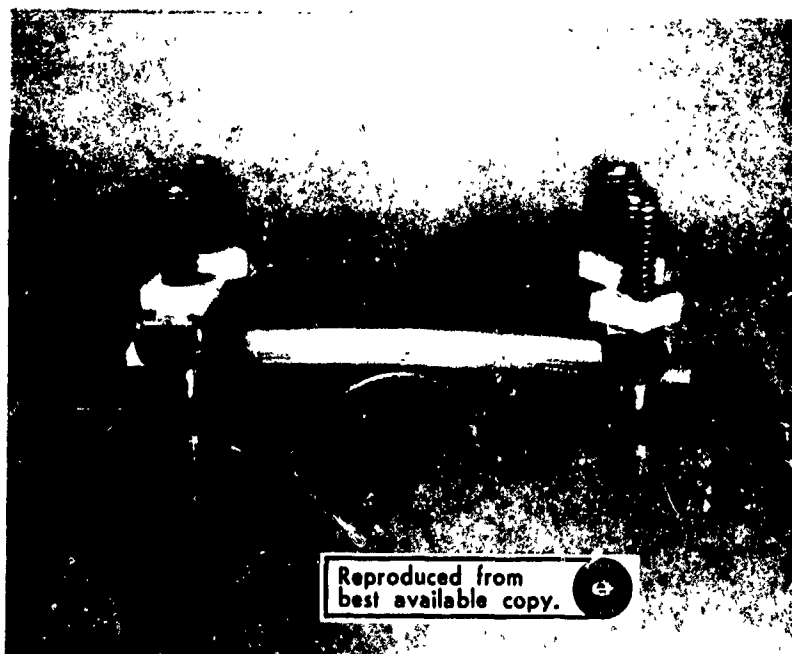
1. BORSIC + aluminum composites exhibit general corrosion when exposed to a humid sea salt environment as a result of matrix attack. Composites with 6061 alloy matrices have superior corrosion resistance to those with 2024 alloy matrices. The longitudinal strength of BORSIC filament is unaffected by humid salt environments.

2. The short time tensile properties of BORSIC + 6061-F composites are not significantly degraded by air exposure at 700°F for periods of up to 1000 hrs which points to their usefulness as elevated temperature structural materials.

3. Thermal cycling of 50 v/o 4.2 mil BORSIC + 6061-F aluminum matrix composites between 70°F and 670°F can cause void formation within the matrix of both unidirectional and complex laminates. These voids are the result of plastic strains caused by differences in thermal expansion coefficient between the constituents. However, less than one percent voids are observed after 1000 cycles and the problem is not nearly as severe as the behavior of multidirectionally reinforced polymeric matrix systems such as graphite and polyimide which can exhibit cracks on cooling from the fabrication temperature.

### SECTION III - REFERENCES

1. K. R. Van Horn, ed., Aluminum, Vol., Properties, Physical Metallurgy and Phase Diagrams, American Society for Metals, Metals Park, Ohio, 1967.
2. M. Basche, F. Galasso, and R. Fanti, "Preparation and Properties of Silicon Carbide Coated Fibers", Fiber Science and Technology, Vol. 1, p. 19, 1968.
3. J. Forest and J. Christian, "Development and Application of High Matrix Strength Al-B", Metals Eng. Quart., Feb. 1, 1970.
4. J. Long, et al, "The Evaluation of the Mechanical Behavior of Metal Matrix Composites Reinforced with SiC Coated B Fibers", AFML-TR-69-291, Nov. 1969.
5. J. L. Christian and J. F. Watson, "Mechanical Properties of Several 2000 and 6000 Series Aluminum Alloys", in Advances in Cryogenic Engineering, Vol. 10.
6. L. E. Dardi and J. L. Preston, Jr., Pratt & Whitney Aircraft, Unpublished work.
7. J. C. Halpin and N. J. Pagano, "Consequences of Environmentally Induced Dilation in Solids", Technical Report AFML-TR-68-395.
8. A. S. Tetelman and A. J. McLvily, Jr., Fracture of Structural Materials, John Wiley and Sons, 1967.
9. K. G. Kreider, V. M. Patarini, "Thermal Expansion of Boron Fiber-Aluminum Composites", Met. Trans., Vol. 1, No. 12, pp. 3431-3460, Dec. 1970.
10. L. E. Dardi, Pratt & Whitney Aircraft, Unpublished work.



Reproduced from  
best available copy.

MAG: 3/4X

FIGURE 3-1

THREE POINT BEND FIXTURE USED FOR SALT CORROSION TESTS



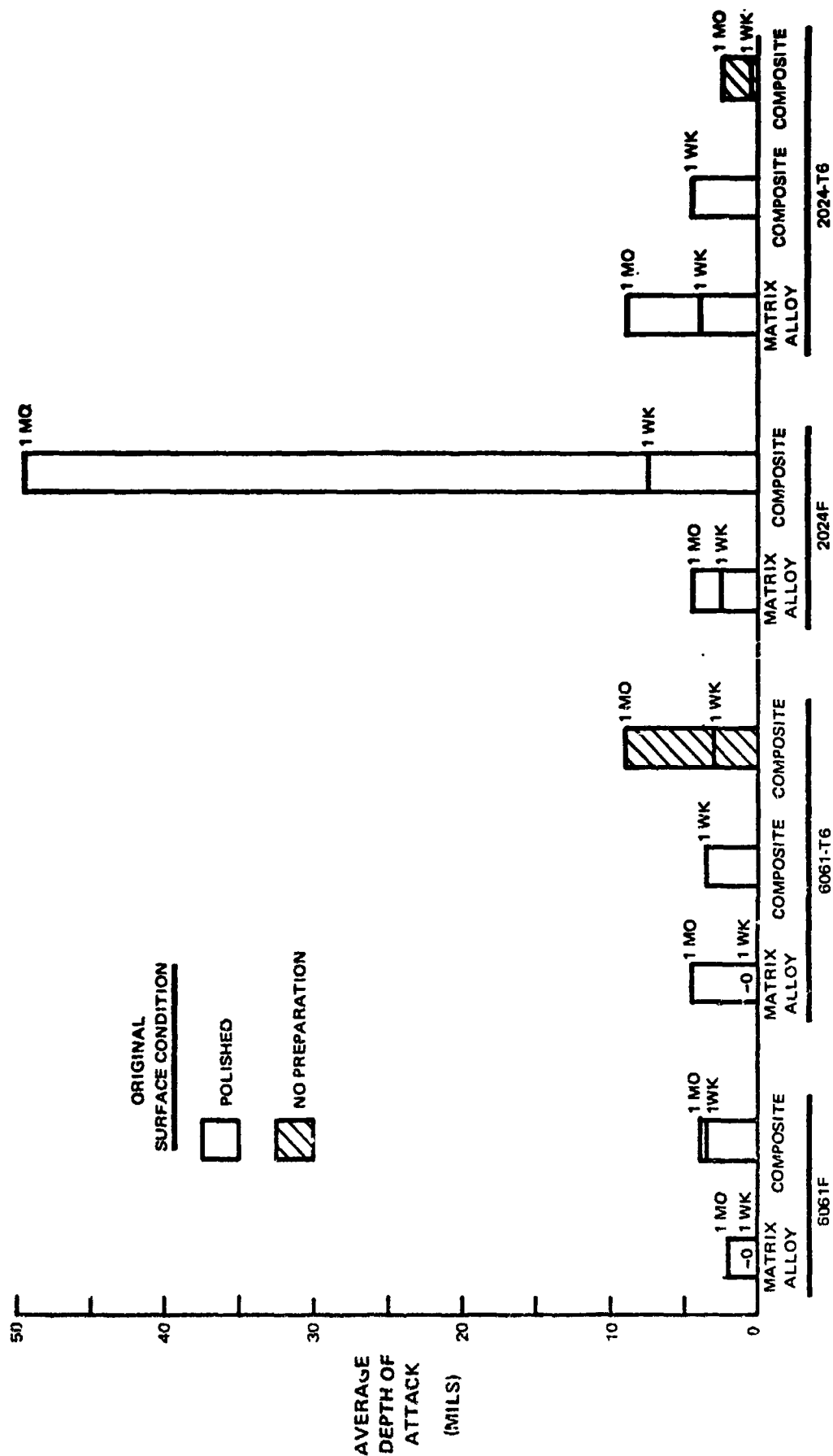
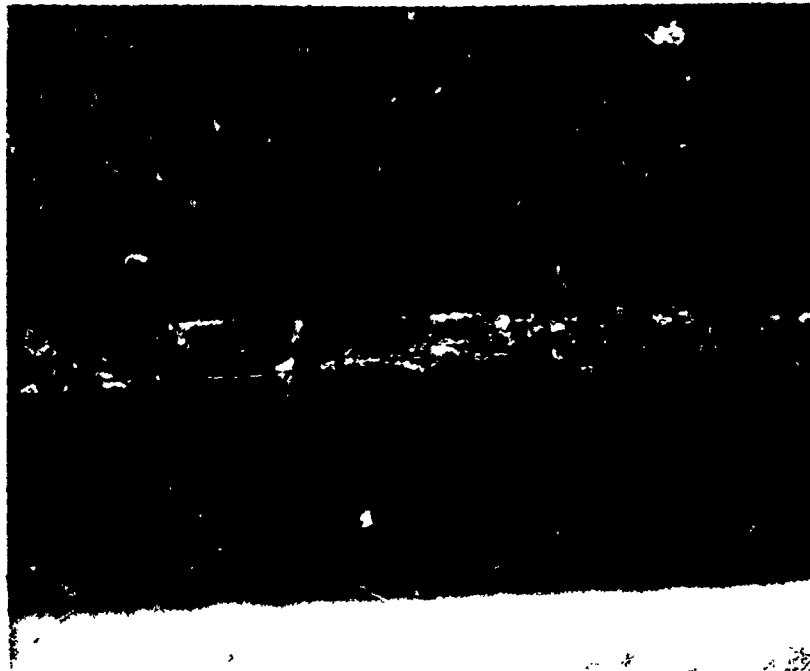


**FIGURE 3-2**  
**STRESS CORROSION AS A FUNCTION OF EXPOSURE IN SYNTHETIC SEA SALT SPRAY AT 95°F**



Reproduced from  
best available copy.



MAG: 1½ X

FIGURE 3-3

EDGE VIEWS OF 4.2 MIL BORSIC + 6061-F (TOP) AND BORSIC + 2024-F (BOTTOM)  
COMPOSITE BEND SPECIMENS AFTER EXPOSURE FOR ONE WEEK IN SYNTHETIC  
SEA SALT SPRAY AT 95F AND 100 KSI



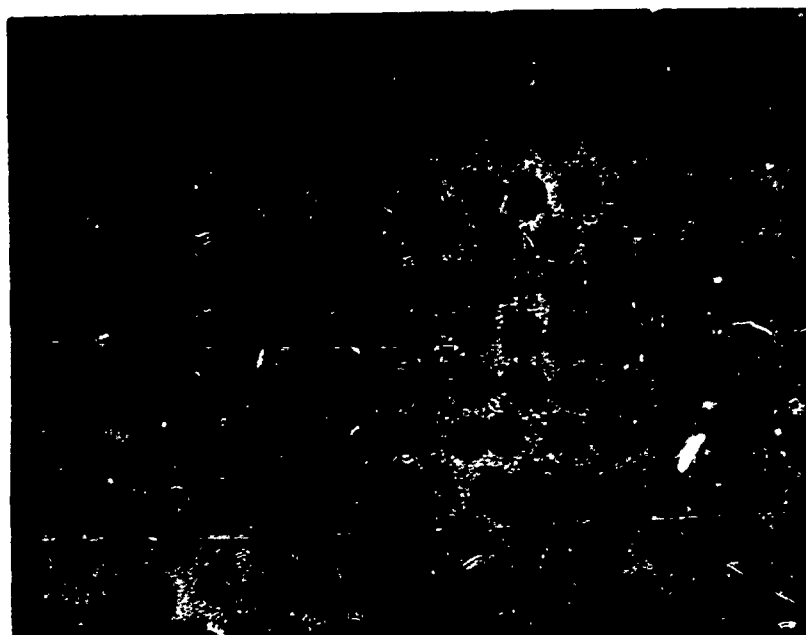
Reproduced from  
best available copy.



MAG: 4X

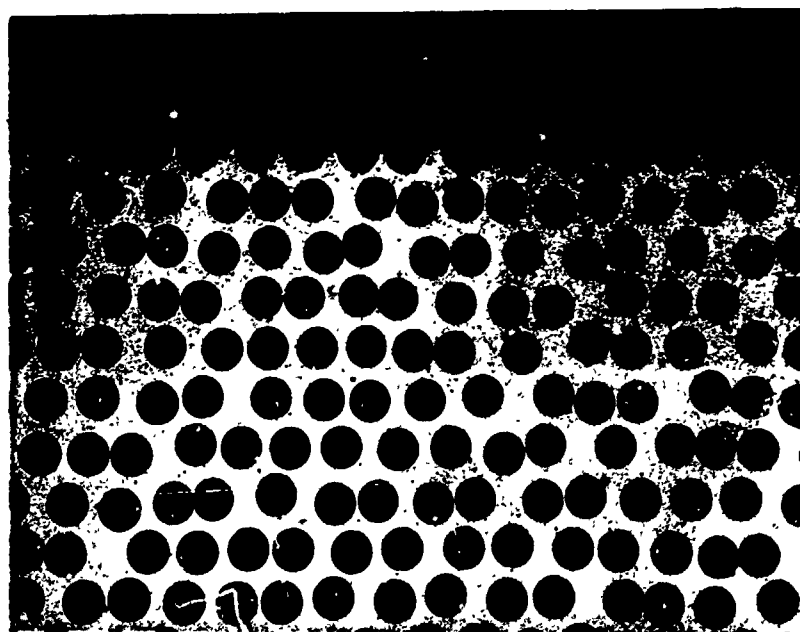
FIGURE 3-4

EDGE VIEWS OF 4.2 MIL BORSIC + 6061-F (TOP) AND BORSIC + 2024-F (BOTTOM)  
COMPOSITE BEND SPECIMENS AFTER EXPOSURE FOR ONE MONTH IN  
SYNTHETIC SEA SALT SPRAY AT 95F AND 100 KSI



ORIGINAL  
SURFACE

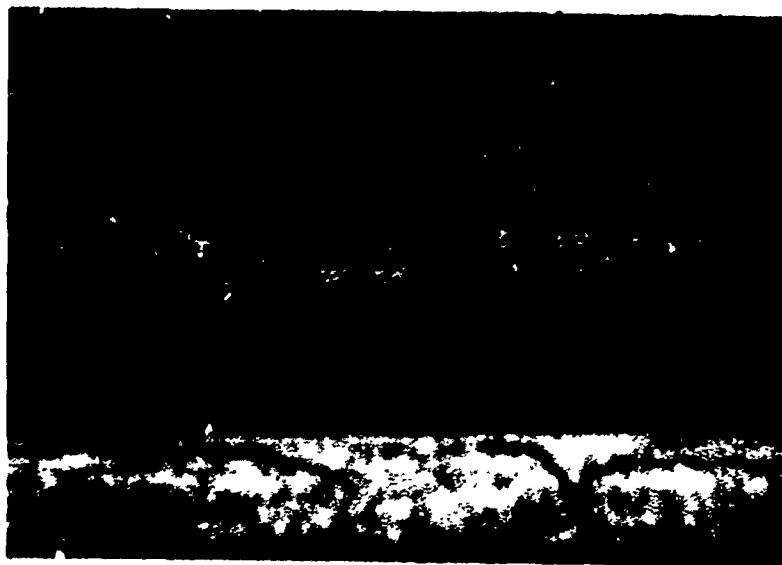
Reproduced from  
best available copy.



ORIGINAL  
SURFACE

MAG: 50X

FIGURE 3-5  
TRANSVERSE SECTIONS OF 4.2 MIL BORSIC + 2024-F (TOP) AND BORSIC  
+ 2024-T6 (BOTTOM) BEND SPECIMENS AFTER EXPOSURE FOR ONE  
WEEK IN SYNTHETIC SEA SALT SPRAY AT 95F AND 100 KSI



Reproduced from  
best available copy.



MAG: 3.5X

FIGURE 3-6  
EDGE VIEWS OF 4.2 MIL BORSIC + 6061-T6 (TOP) AND BORSIC  
+ 2024-T6 (BOTTOM) COMPOSITE BEND SPECIMENS AFTER  
EXPOSURE FOR ONE MONTH IN SYNTHETIC SEA SALT SPRAY  
AT 95F AND 100 KSI

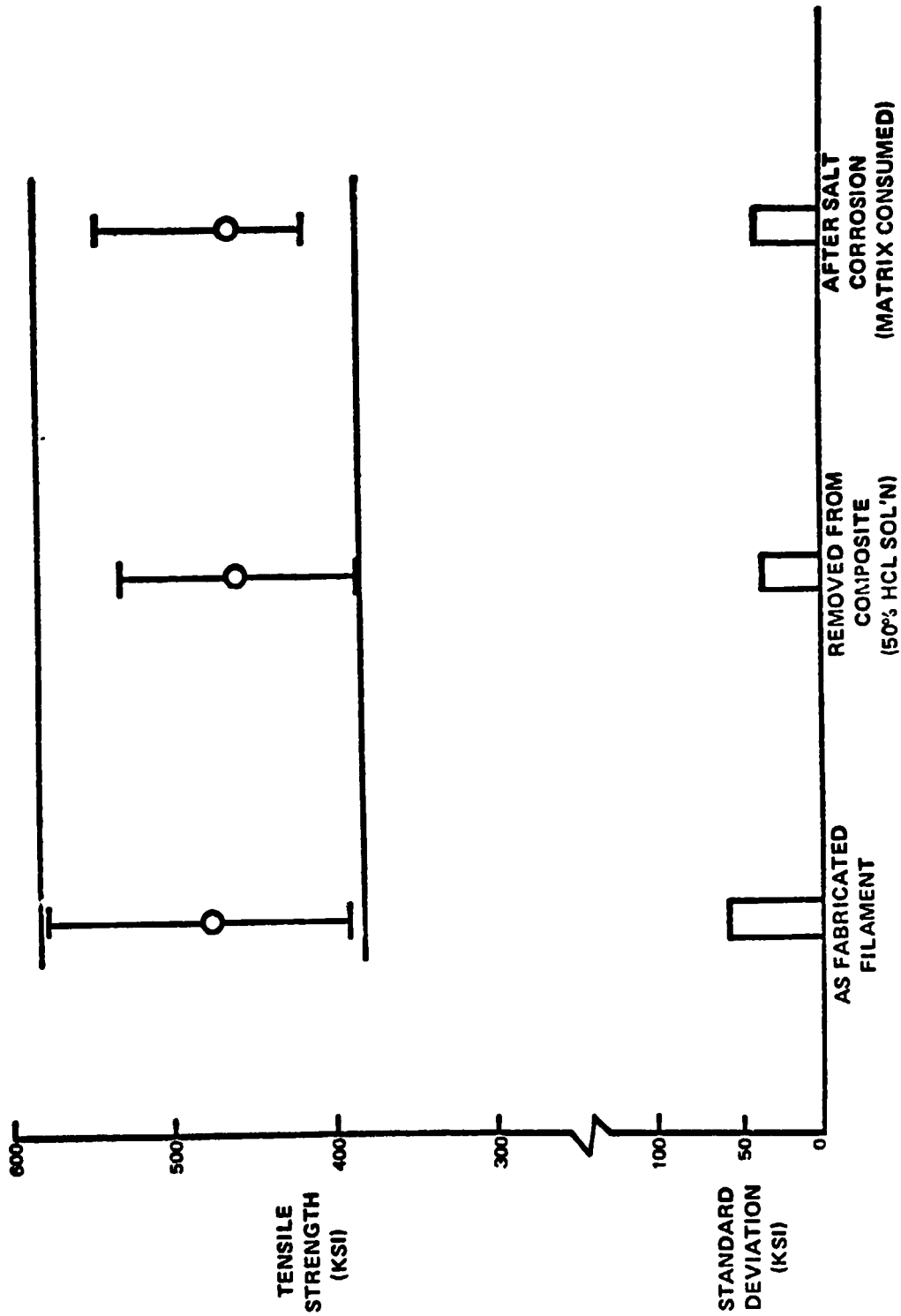
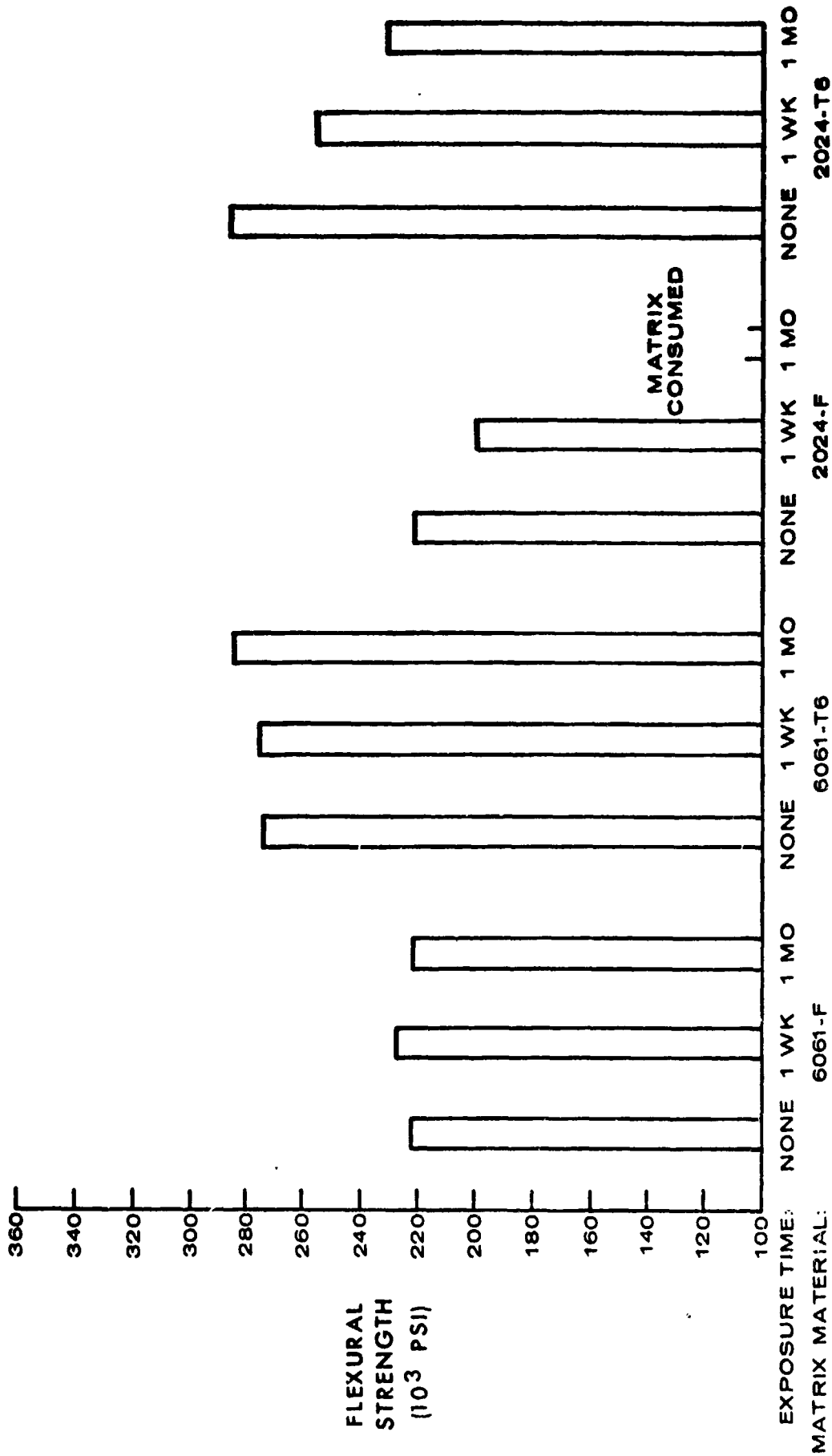


FIGURE 3-7  
STRENGTH OF 4.2 MIL BORSIC FIBER REMOVED FROM 2024 ALUMINUM MATRIX COMPOSITES



**FIGURE 3-8**  
**EFFECT OF EXPOSURE TIME IN SYNTHETIC SEA SALT SPRAY AT 95°F AND 100 KSI**  
**ON THE FLEXURAL STRENGTH OF 4.2 MIL BORSIC + 6061 ALUMINUM**  
**AND BORSIC + 2024 ALUMINUM COMPOSITE MATERIALS**

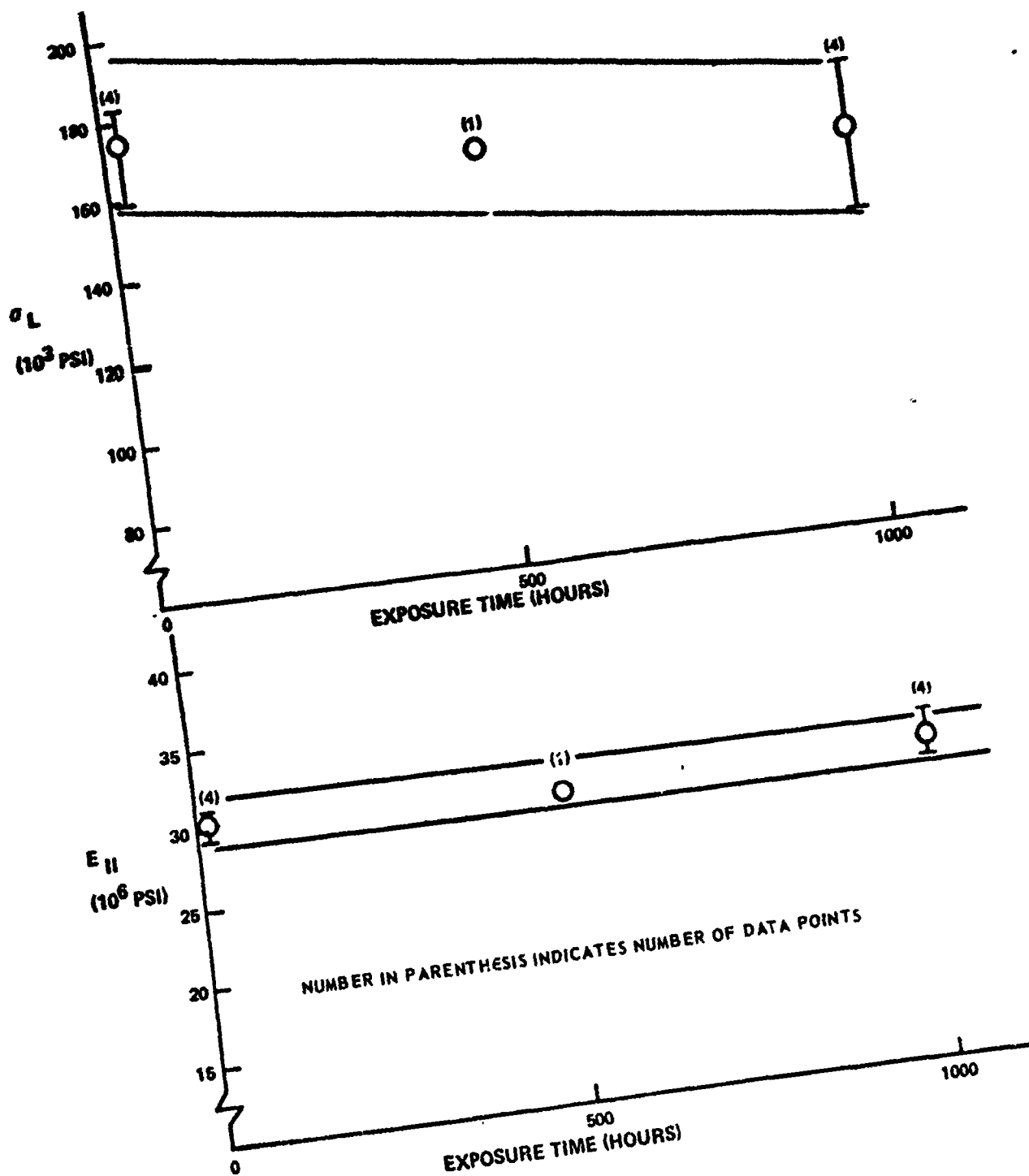


FIGURE 3-9  
ROOM TEMPERATURE LONGITUDINAL STRENGTH AND MODULUS OF  
4-MIL BORON + 6061 ALUMINUM AS A FUNCTION OF EXPOSURE TIME IN AIR  
AT 700 °F



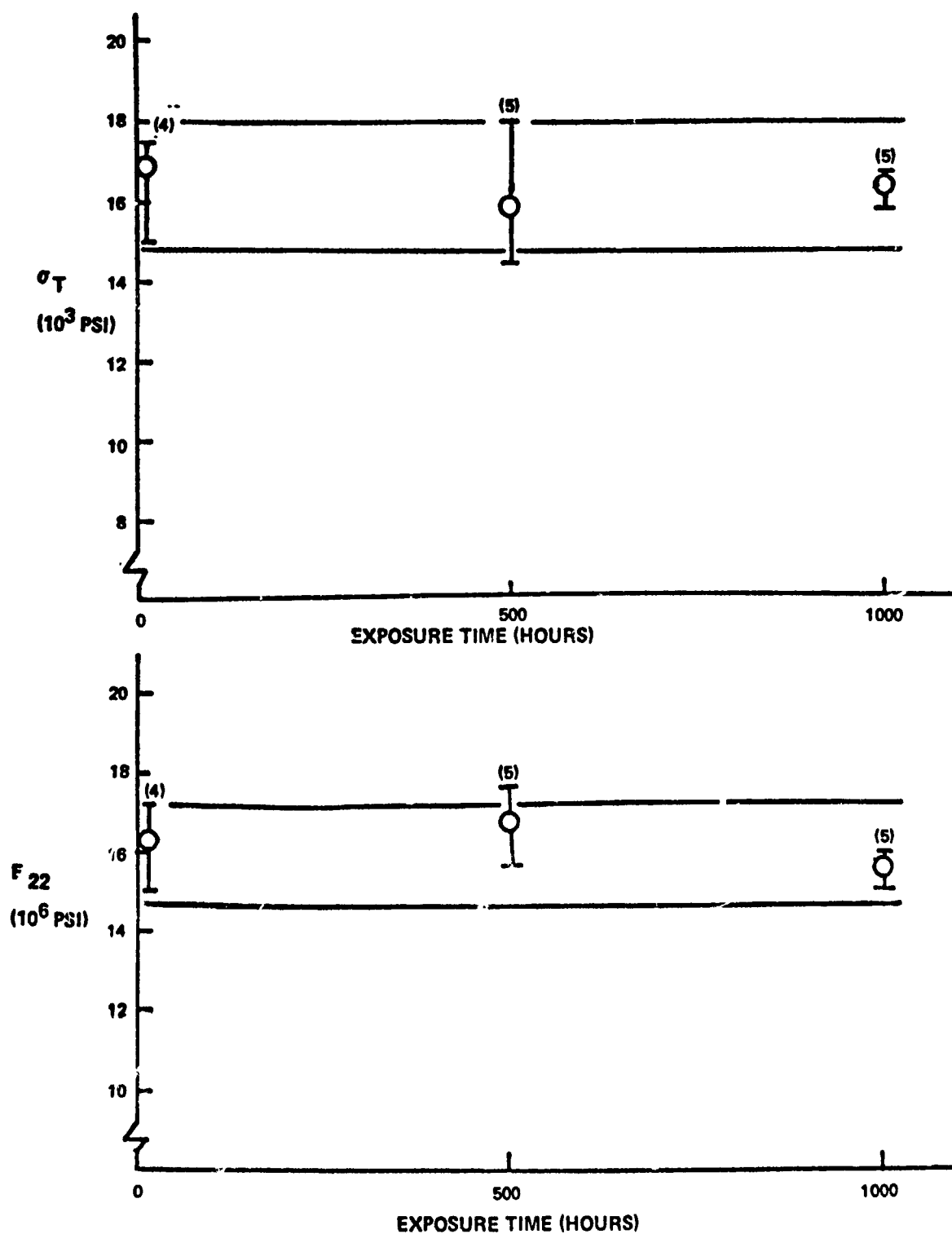
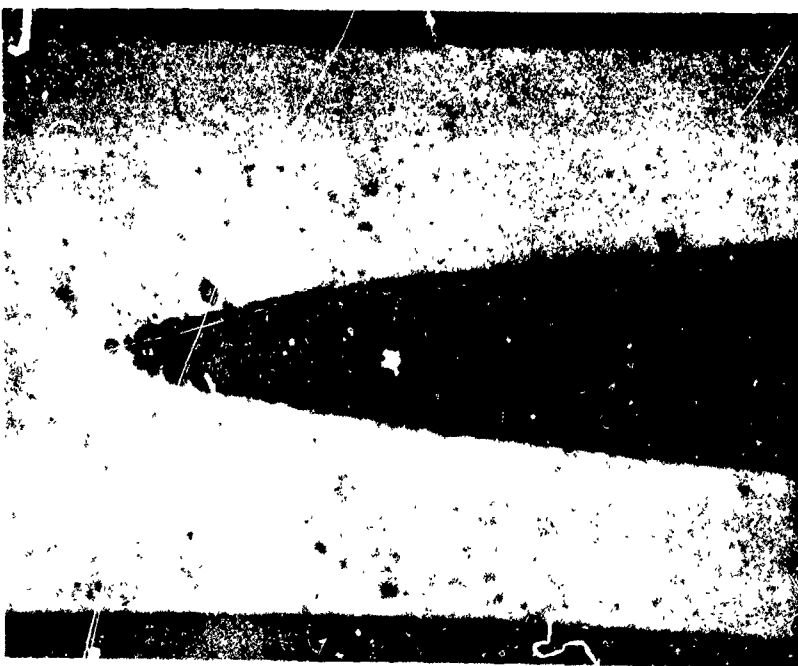
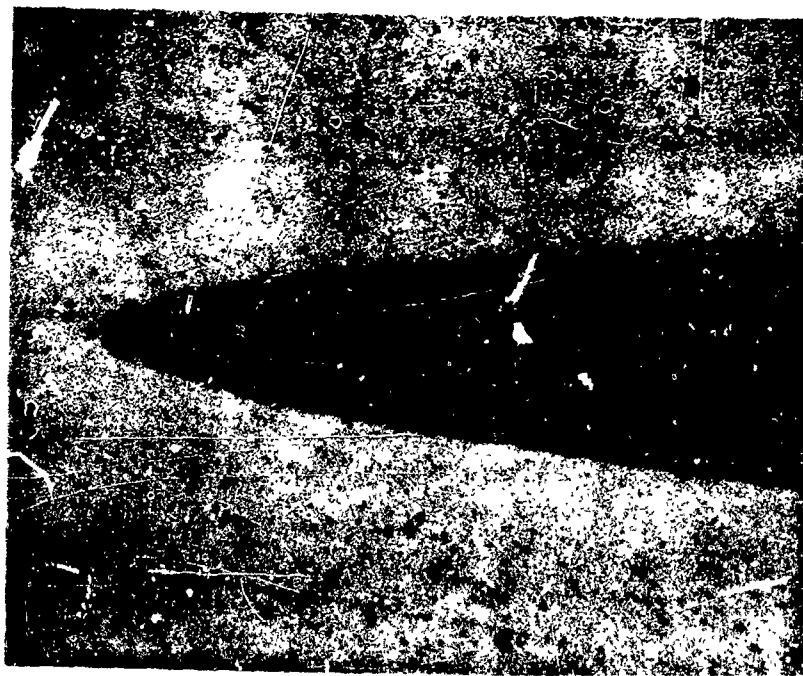


FIGURE 3-10  
ROOM TEMPERATURE TRANSVERSE STRENGTH AND MODULUS OF  
4-MIL BORON + 6061 ALUMINUM AS A FUNCTION OF EXPOSURE  
TIME IN AIR AT 700 °F



AS FABRICATED



700F/1000 HRS.

Reproduced from  
best available copy.

FIGURE 3-11  
TAPER SECTION OF 4 MIL BCRON + 6061-F ALUMINUM AT 10,000 X ALONG FIBER  
AXIS AND 500 X IN TRANSVERSE DIRECTION

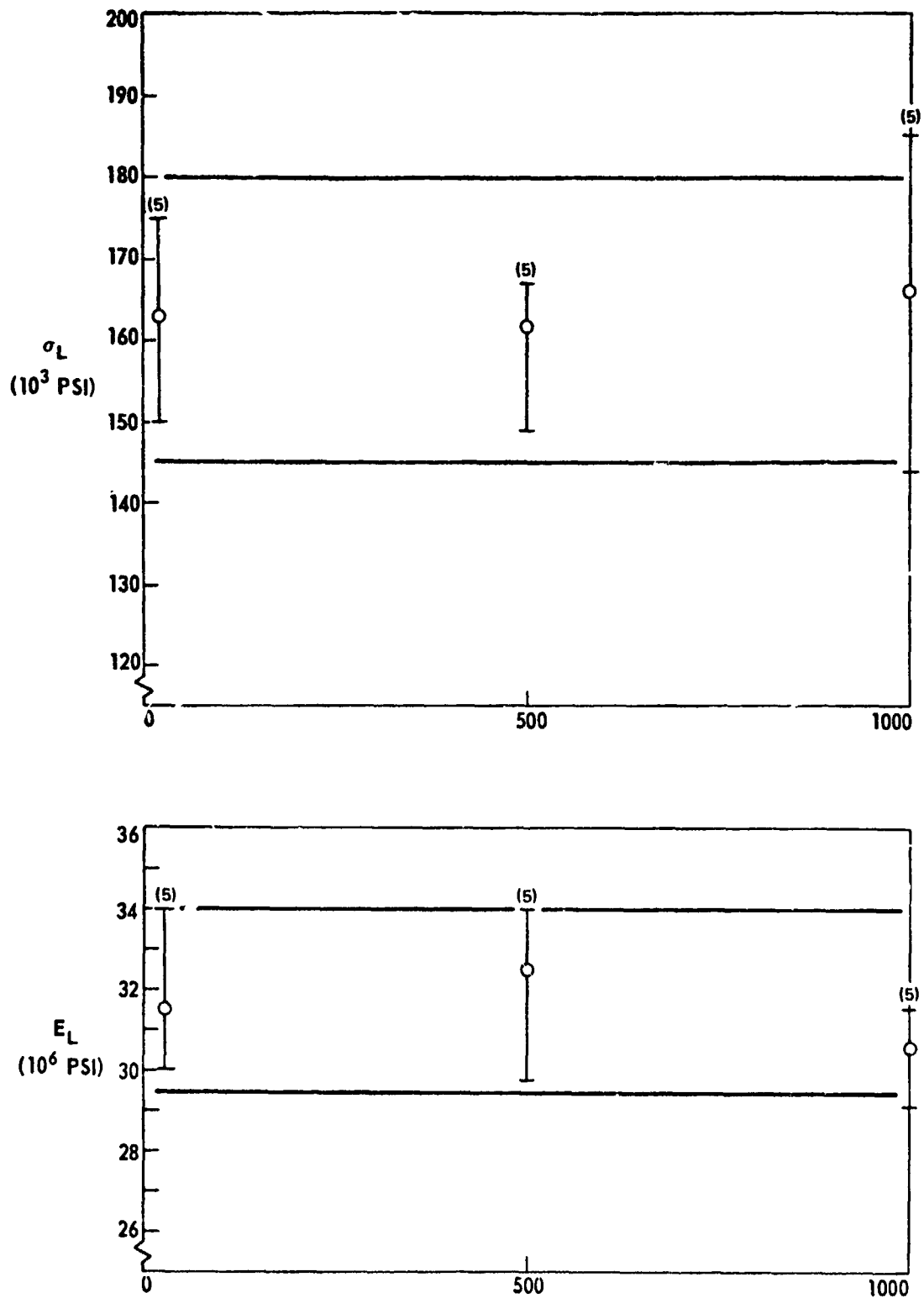


FIGURE 3-12  
ROOM TEMPERATURE LONGITUDINAL STRENGTH AND MODULUS  
OF 4.2 MIL BORSIC +6061 ALUMINUM AS A  
FUNCTION OF EXPOSURE TIME IN AIR AT 700°F

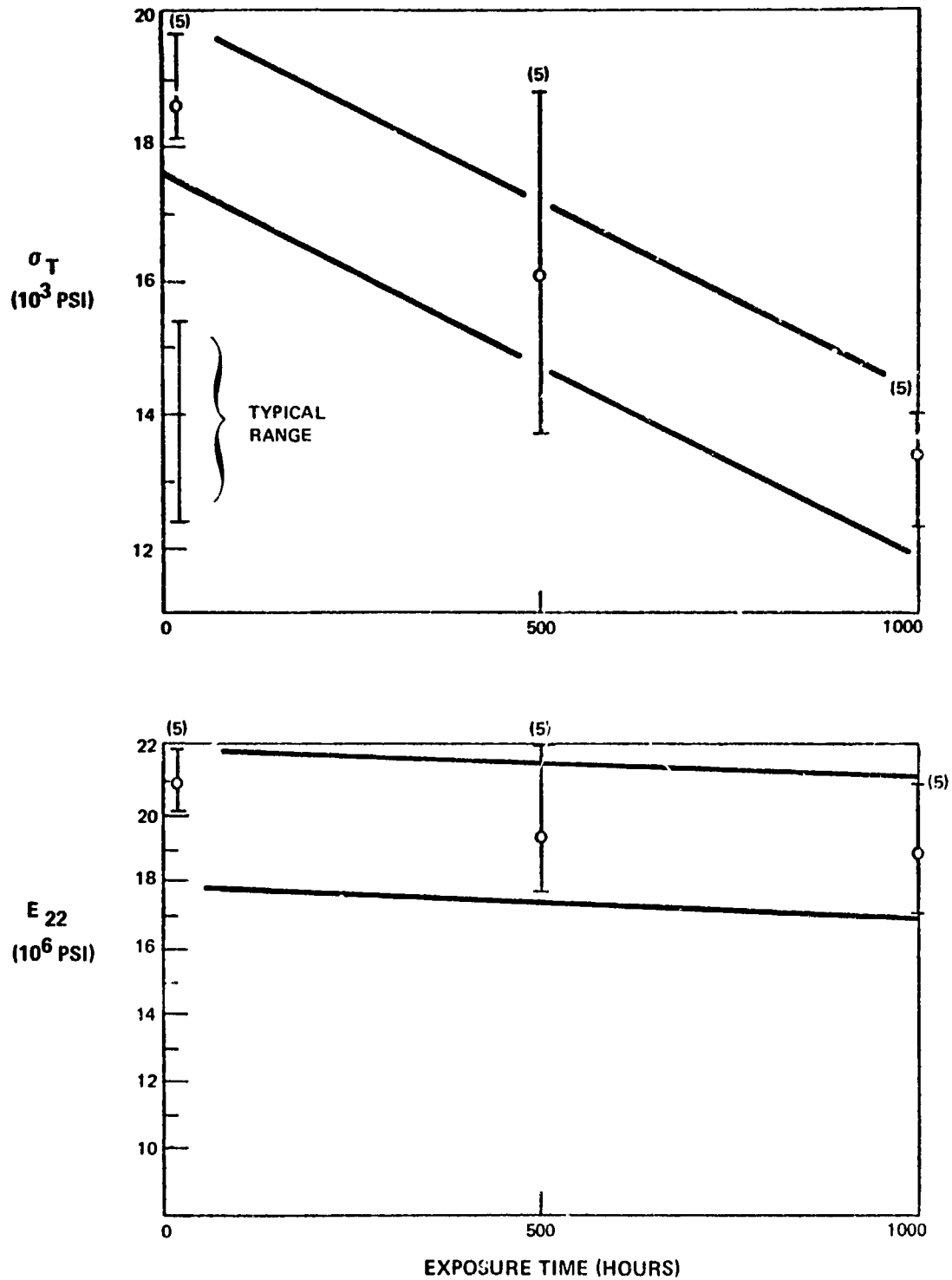


FIGURE 3-13  
 ROOM TEMPERATURE TRANSVERSE STRENGTH  
 AND MODULUS OF 4.2 MIL BORSIC + 6061  
 ALUMINUM AS A FUNCTION OF EXPOSURE TIME IN AIR AT 700°F

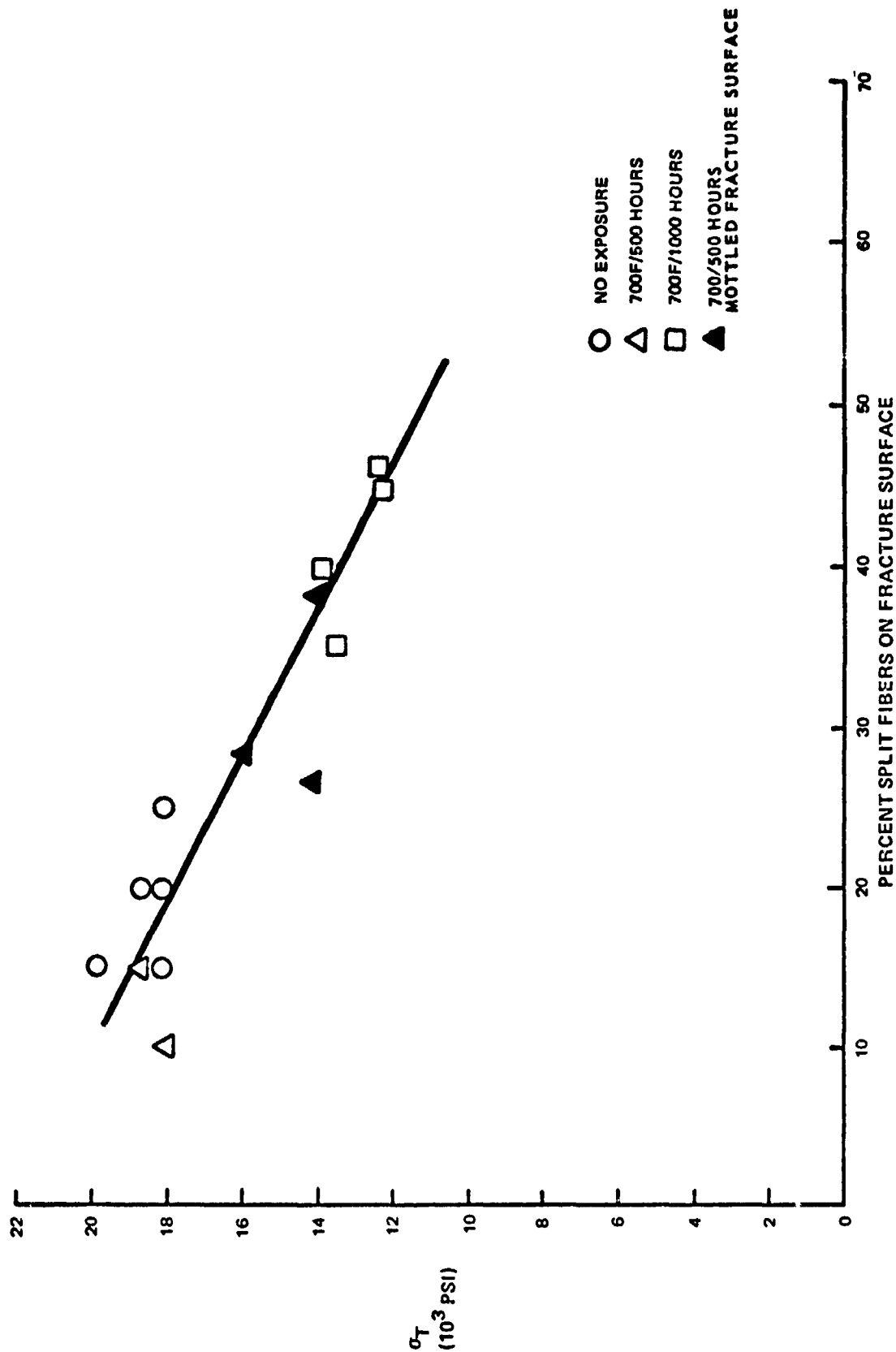


FIGURE 3-14  
 TRANSVERSE TENSILE STRENGTH AS A FUNCTION OF PERCENT SPLIT FIBERS ON THE  
 FRACTURE SURFACE OF 4.2-MIL 7,0RSIC + 6061-F THERMAL EXPOSURE SPECIMENS



MAG: 10X

FIGURE 3-15  
FRACTURE SURFACES OF 4.2 MIL BORSIC + 6061-F TRANSVERSE TENSILE SPECIMENS  
SHOWING TYPICAL APPEARANCE OF HIGH STRENGTH MATERIAL (LEFT), LOW  
STRENGTH MATERIAL (MIDDLE) AND INTERMEDIATE STRENGTH MATERIAL (RIGHT)

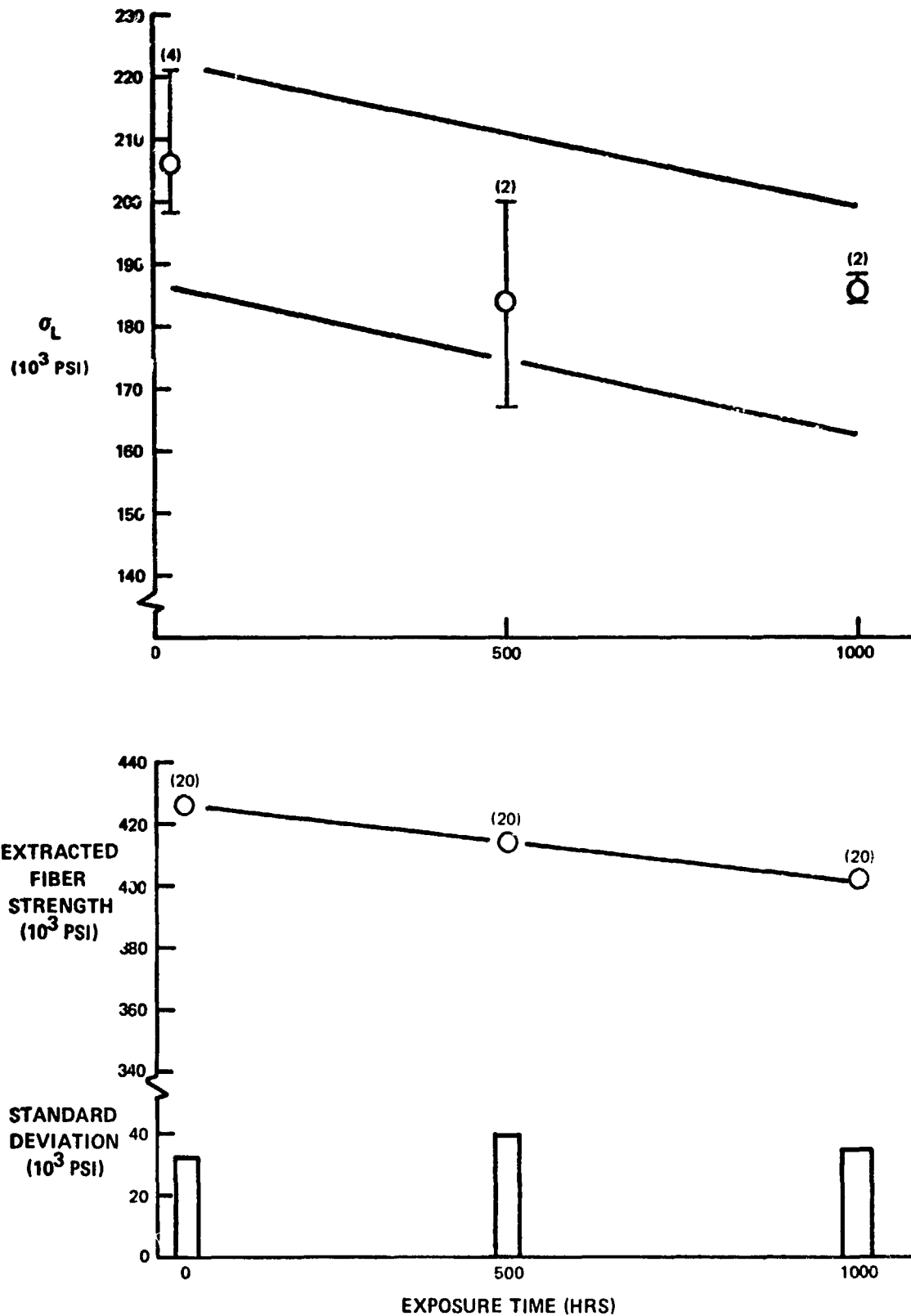


FIGURE 3-16  
ROOM TEMPERATURE LONGITUDINAL STRENGTH OF 5.7 MIL BORSIC +6061  
ALUMINUM AS A FUNCTION OF EXPOSURE TIME IN AIR AT 700°F

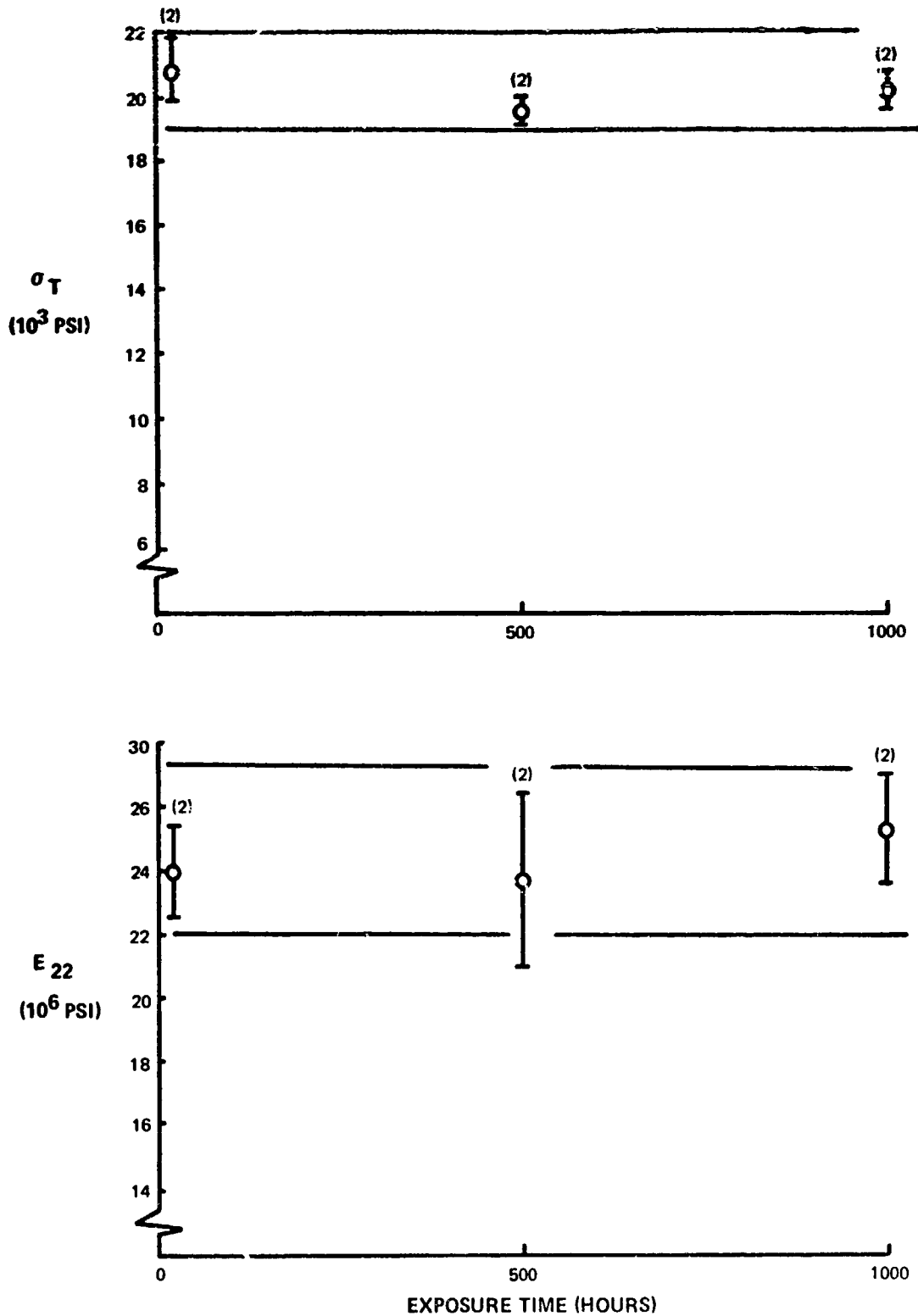
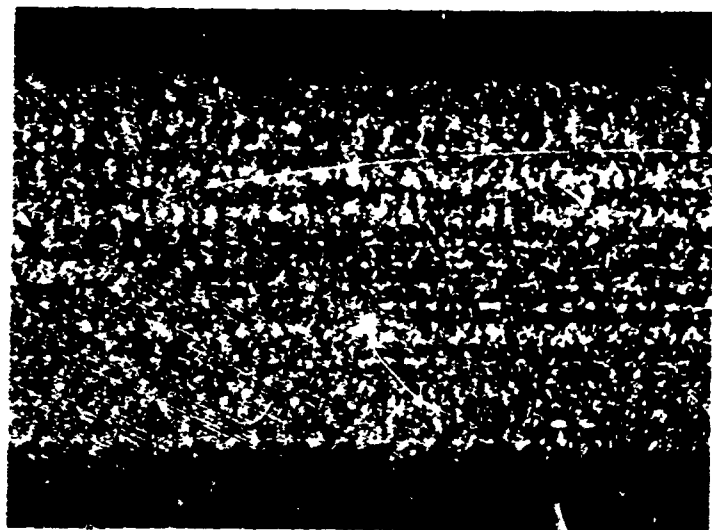


FIGURE 3-17  
 ROOM TEMPERATURE TRANSVERSE STRENGTH AND MODULUS  
 OF 5.7 MIL BORSIC + 6061 ALUMINUM  
 AS A FUNCTION OF EXPOSURE TIME IN AIR AT 700°F





5000 CYCLES

Reproduced from  
best available copy.

MA 3 20X



500 CYCLES

FIGURE 3-18  
EDGES OF 4.2 MIL 80R3IC® + 6061-F ALUMINUM AFTER  
THERMAL CYCLING FROM 70F TO 670F

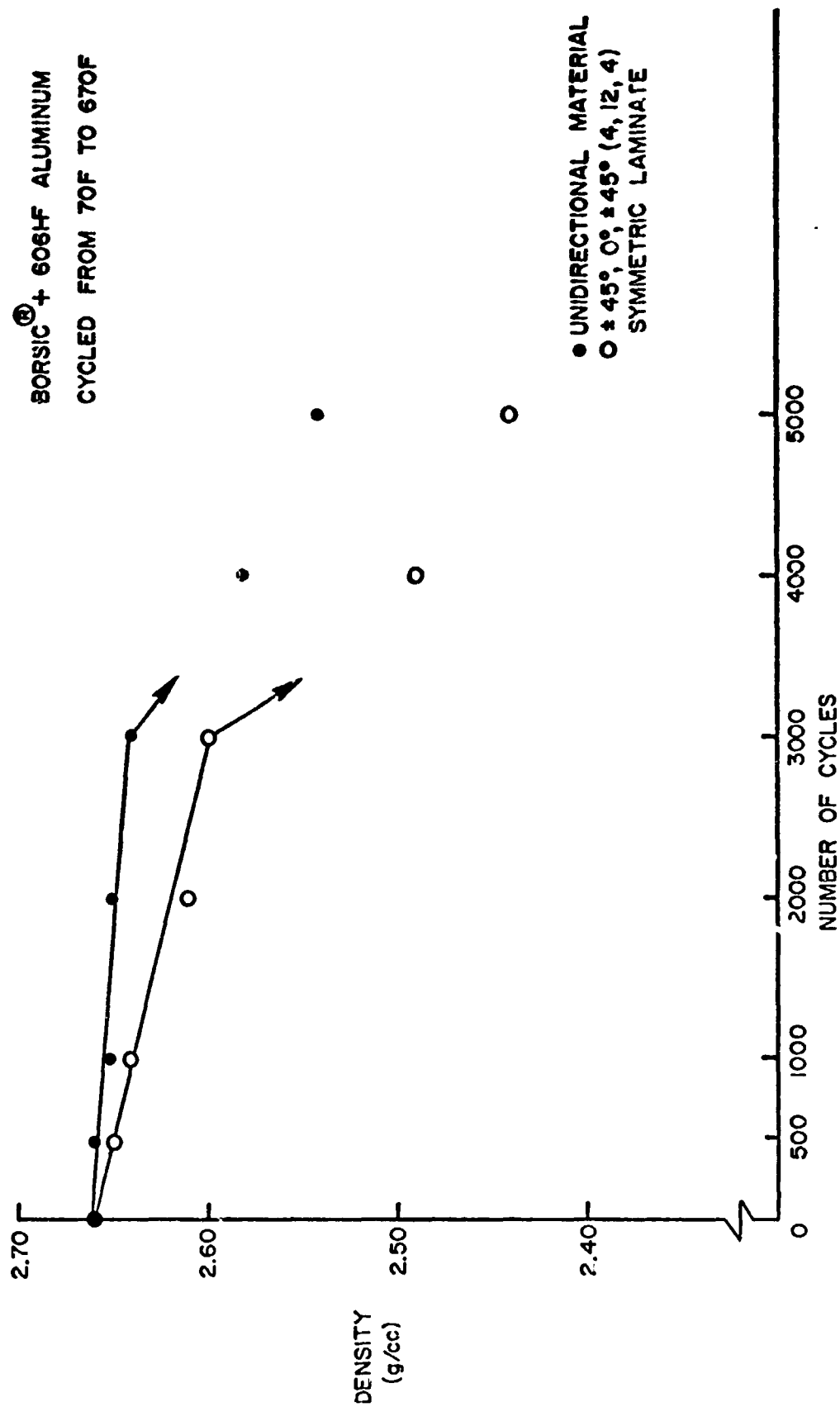
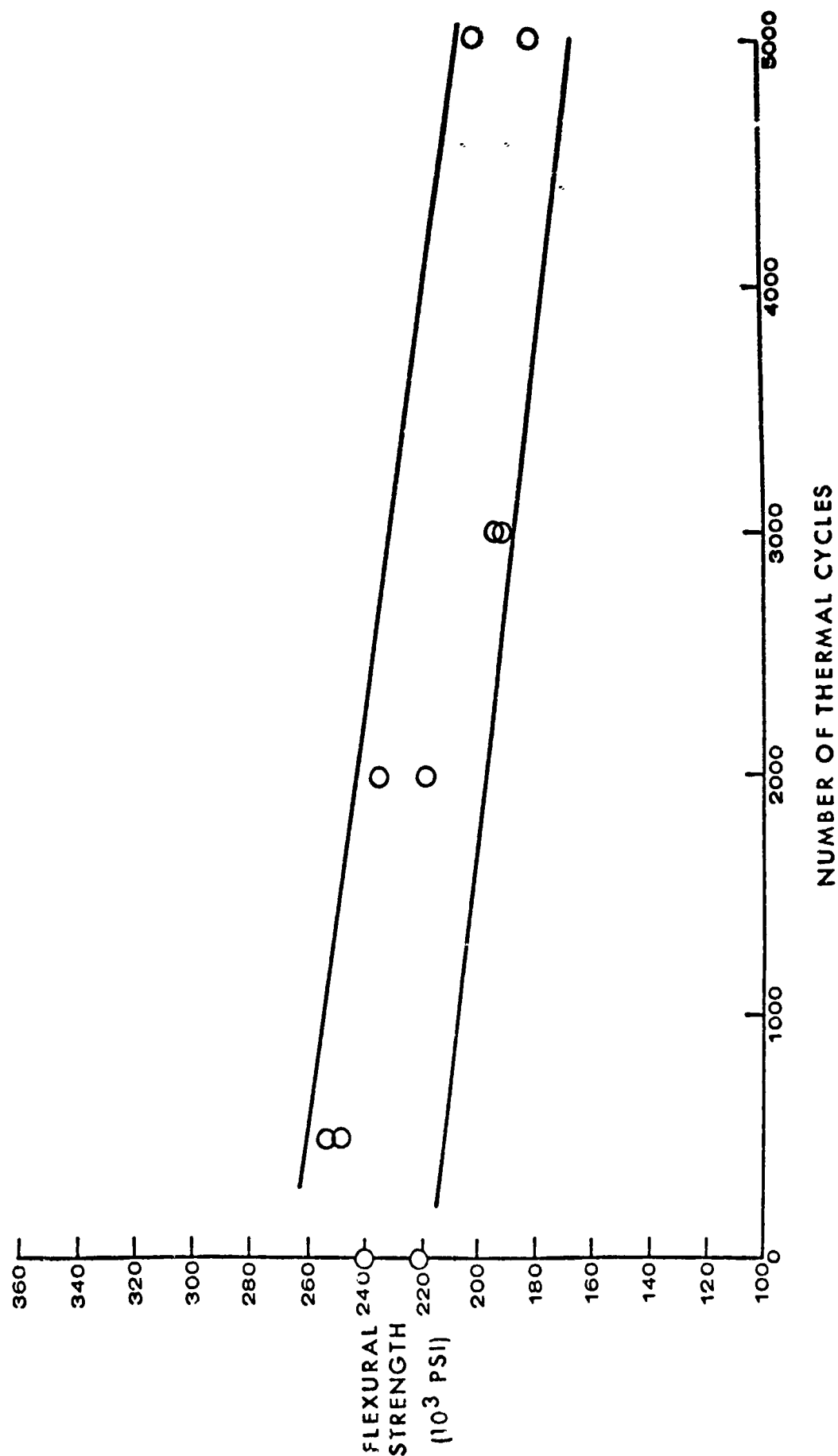


**FIGURE 3-19**  
**EFFECT OF THERMAL CYCLING ON MATERIAL DENSITY**



NUMBER OF THERMAL CYCLES

FIGURE 3-20

FLEXURAL STRENGTH OF UNIDIRECTIONAL 4.2-MIL BORSIC + 6061F ALUMINUM COMPOSITE MATERIAL AS A FUNCTION OF THE NUMBER OF THERMAL CYCLE EXPOSURES FROM 70° F TO 670° F

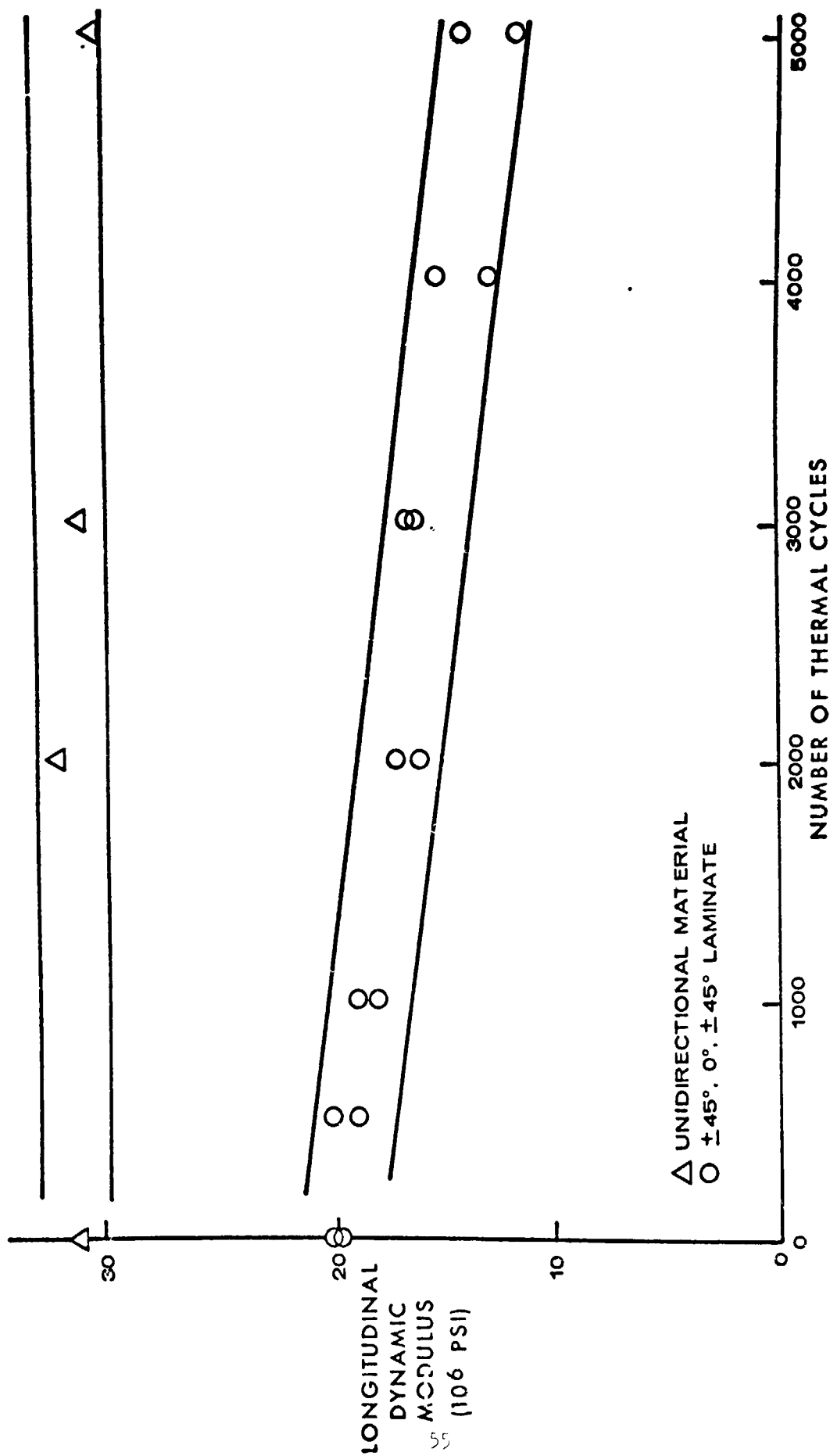


FIGURE 3-21

DYNAMIC FLEXURAL MODULUS OF 4.2-MIL BORSIC, 6061F ALUMINUM COMPOSITE LAMINATES  
 AS A FUNCTION OF THE NUMBER OF THERMAL CYCLE EXPOSURES FROM  $70^\circ\text{F}$  TO  $670^\circ\text{F}$

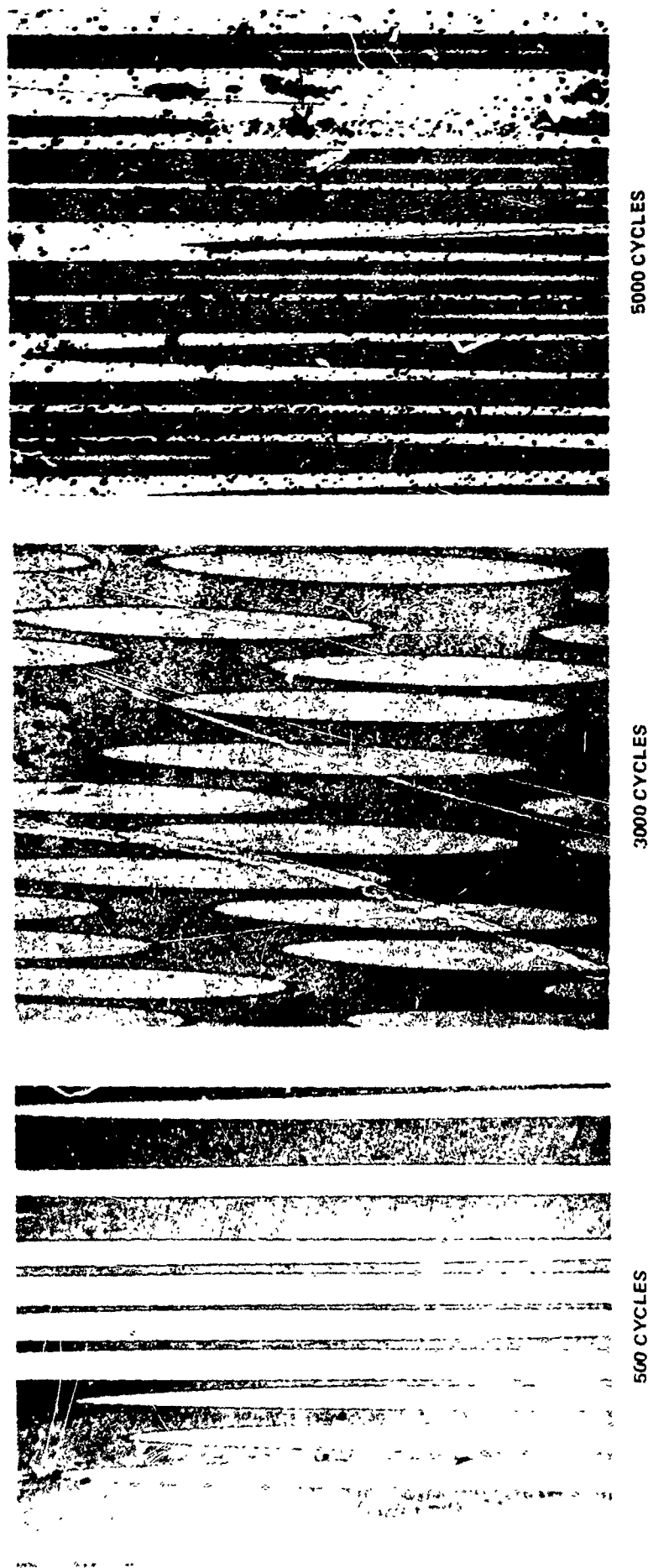


FIGURE 3-22  
LONGITUDINAL MICROSTRUCTURE OF UNIDIRECTIONAL 4.2 MIL BOPSIC + 6061-F  
COMPOSITE MATERIAL AFTER THERMAL CYCLING



FIGURE 3-23  
LONGITUDINAL MICROSTRUCTURE OF  $\pm 45^\circ$ ,  $0^\circ$ ,  $\mp 45^\circ$  LAMINATES OF 4.2 MIL  
BORSIC® + 6061-F COMPOSITE MATERIAL AFTER THERMAL CYCLING.



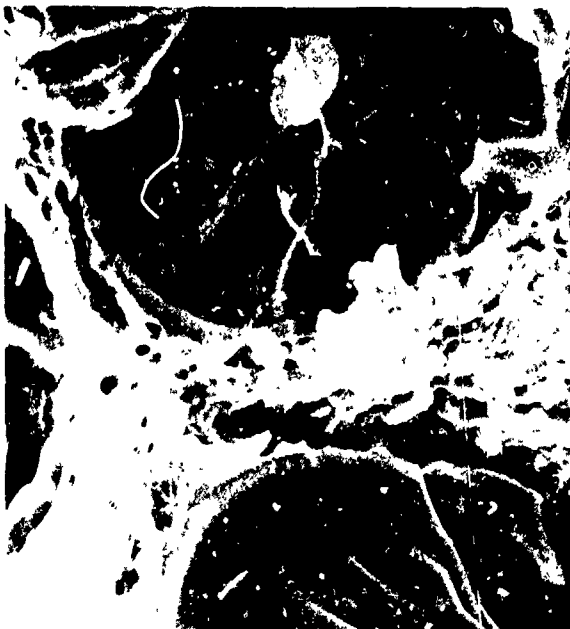
550X

AS FABRICATED



600X

500 CYCLES



620X

3000 CYCLES

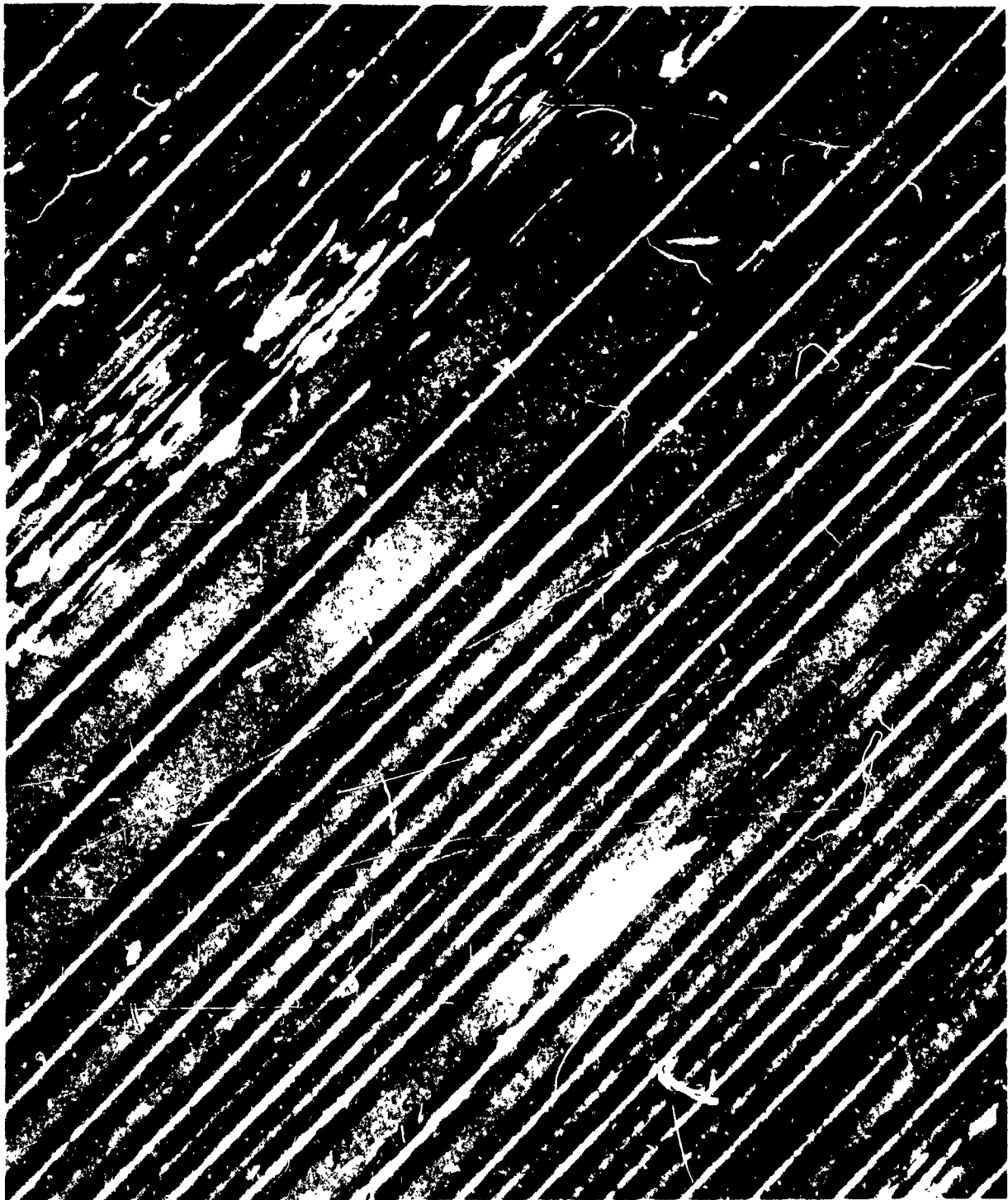


630X

5000 CYCLES

FIGURE 3-24

FRACTURE SURFACES OF 4.2 MIL BORSIC + 6061F MATERIAL AFTER THERMAL CYCLING AND FLEXURAL TESTING



Reproduced from  
best available copy.



4000 CYCLES

FIGURE 3-25

4.2 MIL BORSIC / 6061-F COMPOSITE SPECIMEN AFTER THERMAL CYCLING  
LEACHED TO EXPOSE THE FIBERS (MAG: 56X)



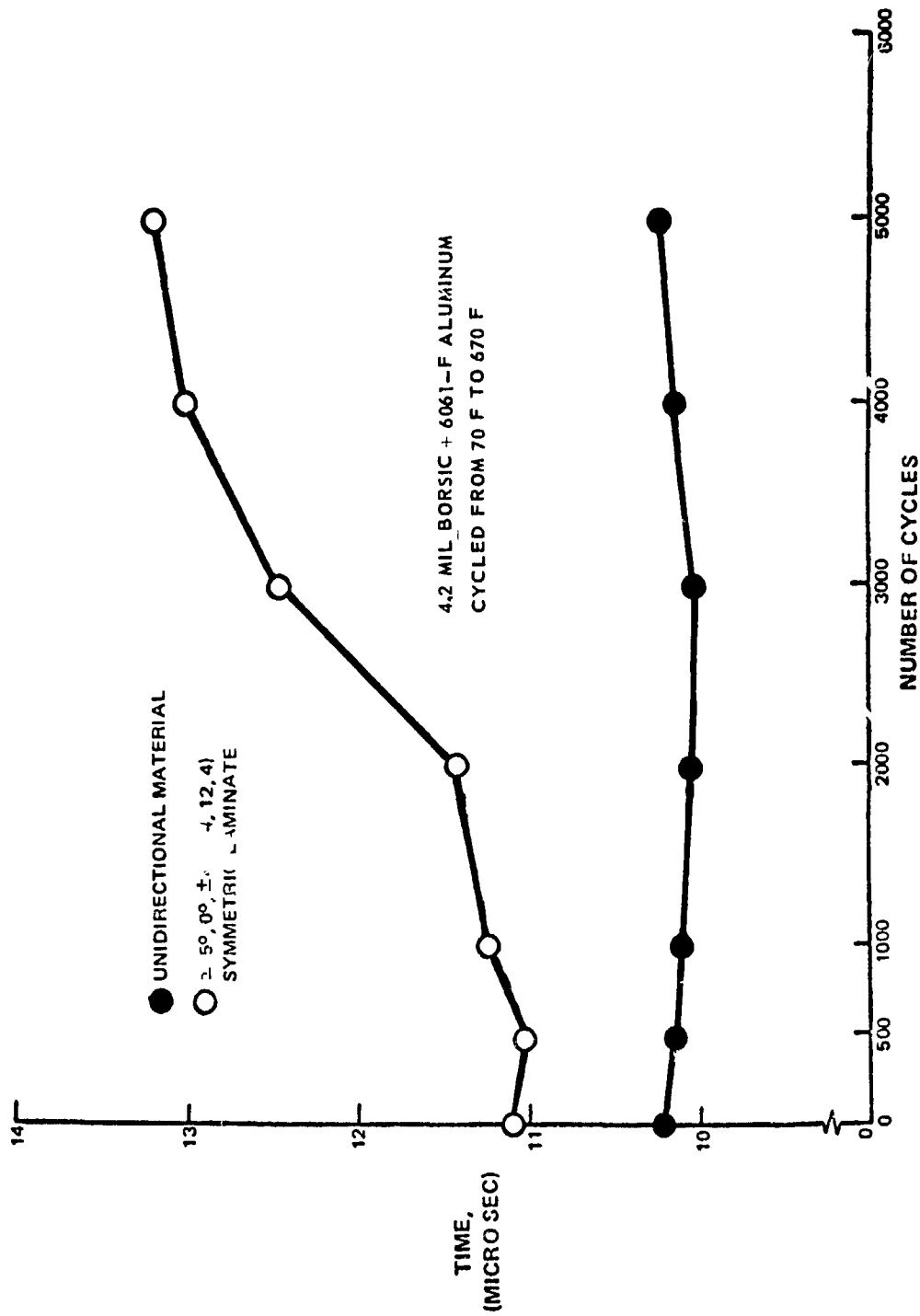


FIGURE 3-26  
EFFECT OF THERMAL CYCLING ON TIME INTERVAL FOR EXTENSIONAL WAVE  
PROPAGATION IN LONGITUDINAL DIRECTION

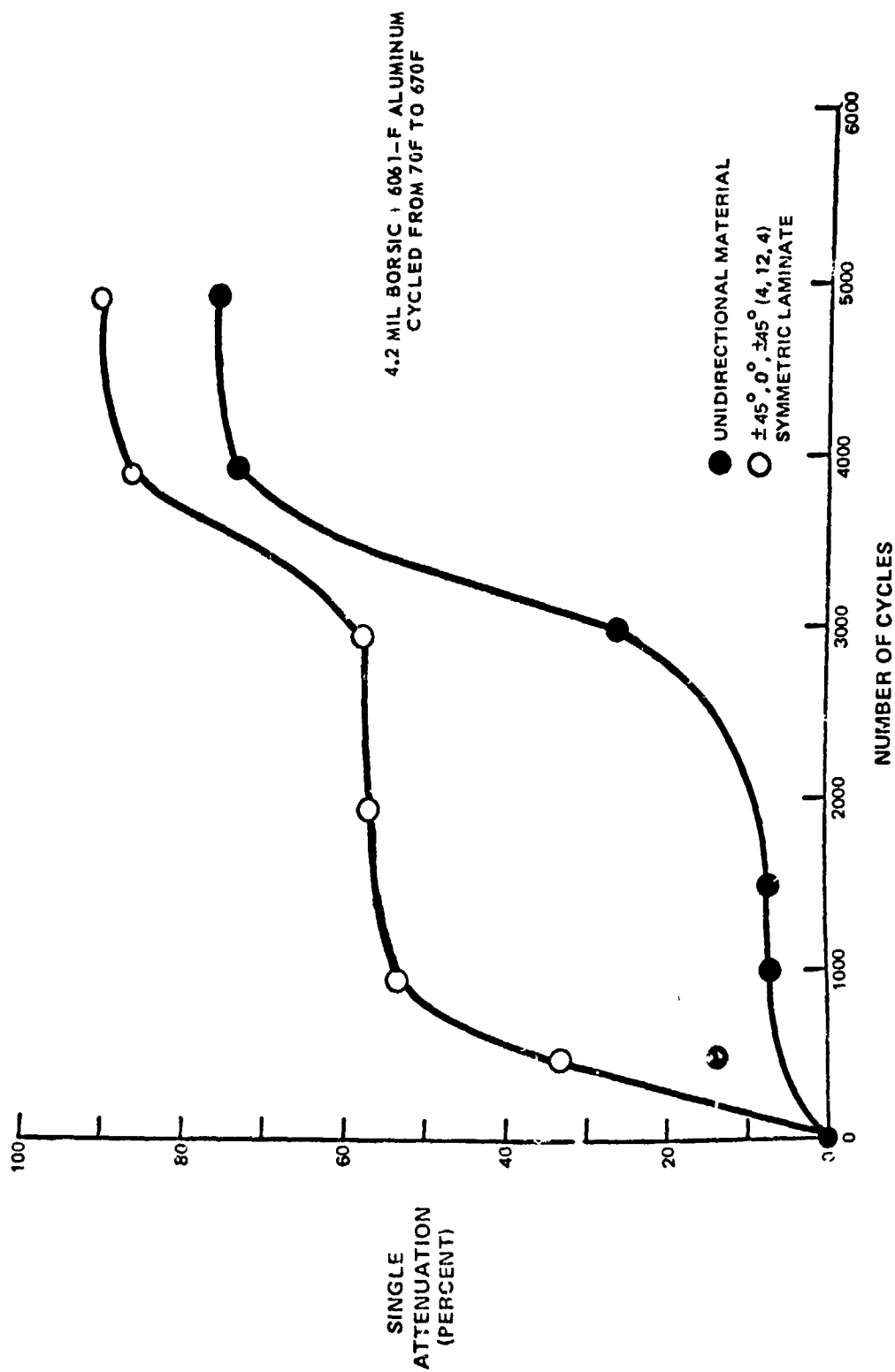


FIGURE 3-27

EFFECT OF THERMAL CYCLING ON AVERAGE ULTRASONIC ATTENUATION LEVEL

Table III-I

Heat Treatments Given BORSIC-Aluminum  
Salt Exposure Specimens

<u>Matrix</u>	<u>Temper</u>	<u>Treatment</u>
6061	F	As fabricated <sup>1</sup>
	T6	986°F/40 min/quench <sup>2</sup> + 320°F/18 hr/air cool
2024	F	As fabricated <sup>1</sup>
	T6	923°F/40 min/quench <sup>2</sup> + 374°F/16 hr/air cool

<sup>1</sup>slow cool under vacuum

<sup>2</sup>quenched in 30 percent solution of a commercial organic additive to eliminate distortion (Ucon A, Union Carbide)

Table III-II

## High Temperature Air Exposure of 6061-F Composites

Property (at 70°F)	Condition	Composite System		
		50 v/o- 4.0 mil Boron/6061	50 v/o- 4.2 mil BORSIC/6061	61 v/o- 5.7 mil BOPSIC/6061
$\sigma_L$ , long. strength	As-fabricated	175 ksi	163 ksi	209 ksi
	<u>700°F/1000 hr</u> change	<u>154 ksi</u> -12%	<u>166 ksi</u> +2%	<u>186 ksi</u> -11%
$E_{11}$ , long. modulus	As-fabricated	30.5x10 <sup>6</sup> psi	31.5x10 <sup>6</sup> psi	--
	<u>700°F/1000 hr</u> change	<u>30.8x10<sup>6</sup>psi</u> ~0	<u>30.5x10<sup>6</sup>psi</u> -3%	--
$\sigma_T$ , trans. strength	As-fabricated	16.9 ksi	18.6 ksi	20.8 ksi
	<u>700°F/1000 hr</u> change	<u>16.4 ksi</u> ~0	<u>13.4 ksi</u> -28%*	<u>20.2 ksi</u> -3%
$E_{22}$ , trans. modulus	As-fabricated	16.3x10 <sup>6</sup> psi	20.9x10 <sup>6</sup> psi	23.9x10 <sup>6</sup> psi
	<u>700°F/1000 hr</u> change	<u>15.2x10<sup>6</sup>psi</u> -7%	<u>18.9x10<sup>6</sup>psi</u> -10%	<u>25.3x10<sup>6</sup>psi</u> +6%

\*Anomalous result, material of unusually high quality prior to exposure

## TRANSVERSE PROPERTIES

### SUMMARY

The transverse properties of BORSIC fiber reinforced aluminum have been determined as a function of primary fabrication parameters. matrix and fiber types, secondary processing procedures, fiber content, specimen geometry, specimen surface condition and thermal environment. Matrices investigated include 2024, 6061, 5052, 5056, 2219, 1100, 1145, 8001, S.A.P., Al-7% Si, and aluminum containing several percentages of iron. The fibers investigated include 4.0 mil boron, 4.2 mil BORSIC, R. F. boron, 5.6 mil boron, 5.7 mil BORSIC, and 4.0 mil silicon carbide. It was shown that the composite transverse tensile strength is affected by all of these variables and that transverse strengths of up to 48,000 psi can be achieved by the choice of the proper combination of matrix, fiber type and fabrication procedures. The composite system of 5.7 mil BORSIC-2024 was demonstrated to be one of the materials capable of exhibiting this strength while 5.7 mil BORSIC-6061 has achieved strengths of up to 40,000 psi. These strength levels are approximately a factor of two greater than the strength of boron or BORSIC aluminum composites available at the outset of this research program and have mitigated one of the major impediments to the application of BORSIC-aluminum composites for aerospace applications. Composite transverse tensile strains in excess of 0.5% have also been achieved during this program.

Composite transverse tensile strength was shown to be related to both the matrix and fiber strengths. This latter quantity varies substantially with fiber type and illustrates the considerable anisotropy of boron fibers. Composite fracture mode, either predominantly matrix failure or fiber splitting, is dependent upon the magnitude of transverse fiber strength relative to matrix strength and controls the functional dependence of composite strength on composite fiber content.

The use of transverse reinforcements of stainless steel wires and titanium foils is shown to significantly increase composite strength. In addition, in the case of 4.2 mil BORSIC reinforced specimens, transverse strength is increased by minimizing the effects of fiber edge damage.

Two of the experimental procedures used in this program are indicated to be of significance in the determination of composite integrity and perfection. The measurement of the transverse modulus is sensitive to the degree of matrix consolidation and composite bonding while the use of radiographic techniques reveals the condition of the reinforcing fibers. The latter technique is a high resolution technique capable of discerning the condition of individual fibers.

## IV. TRANSVERSE PROPERTIES

### 4.1 Matrix Properties

In any attempt at understanding the transverse properties of composite systems it is important that the properties of the individual components of the composite be understood. For the composites studied in this investigation, the components are BORSIC fiber and a metal matrix composed of foil and plasma sprayed material. For a typical 50% by volume BORSIC composite the fraction of the metal matrix in the plasma sprayed form is approximately 60%. Thus, it is not clear that the properties of the matrix material can be defined in terms of the properties of commercially available wrought material. For this reason a number of specimens were hot press bonded containing only plasma sprayed material and foil.

#### Experimental Method

The aluminum alloys studied were 1100, 6061, 2024, 2219, 5052/56 (made by plasma spraying 5056 powder onto 5052 foil) and an Al-7% Si alloy prepared by spraying LSA 528 powder onto 713 foil. These materials were prepared by plasma spraying alloy powder onto 0.001 in. thick foil to produce metal tapes. Layers of these tapes were then hot press diffusion bonded under conditions of temperature and pressure equal to those used to produce the fiber reinforced composites to be discussed later in this report. The resultant specimens were approximately 20 layers thick and composed of approximately 65% to 75% plasma sprayed material. The single exception to this was the 2219 material which was made of only plasma sprayed alloy. Tensile specimens were machined to have a 1.25 in. long gage length and were tested at a crosshead velocity of 0.01 in. per minute using a Tinius-Olsen tensile tester.

The effects of several heat treatment procedures on the mechanical properties of these specimens was also determined. Standard T-6 heat treatments for both the 2024 and 6061 alloys were used. In addition, a heat treatment that would provide longer time stability of strength at elevated testing temperatures was investigated. The procedures for this heat treatment, designated T-4-600, as well as those of the T-6 heat treatments are described in Table IV-I.

#### Results and Discussion

The results of tensile tests performed on the plasma sprayed plus foil matrix alloys are given in Table IV-II. The alloys studied were 6061, 2024, 1100-1145, Al-7%Si (4343), 2219 and a combination of 5052-5056 alloys. In all cases the final processing step for these materials was a slow cool in the hot press dies from the pressing temperature. For this reason the data reported can best be compared with the properties of wrought materials of similar composition in the fully annealed (o) condition. Such a comparison reveals that the elastic moduli of the composite matrix materials are approximately equal to those of wrought material. This equality is evidence that the specimens tested were fully consolidated by the diffusion bonding procedures used. Elastic modulus is a sensitive function of void content of materials and even small percentages of voids

present would have caused the measured moduli to be considerably less than those measured (Refs. 4.1,2). The comparison of strengths reveals that the yield and ultimate tensile strengths of the composite matrices are greater than those of the wrought material. The greatest difference exists for the 2024 alloy which exhibits a yield strength of  $18.6 \times 10^3$  psi and an ultimate tensile strength of  $35 \times 10^3$  as compared with  $11 \times 10^3$  psi and  $27 \times 10^3$  psi for the wrought material. The strains to fracture are 30% to 40% less than those of wrought material. This higher strength and lower ductility can be related to the very fine dispersions of precipitate produced by annealing the plasma sprayed structure. Oxides present on the powder used in the plasma spray process will also contribute to this increase in strength. Polished sections of these alloys display the precipitate and oxide dispersions. The microstructural features of the plasma sprayed material are considerably finer than those of the adjacent foils as shown in Fig. 4.1. In this figure the structure of the aluminum-7% silicon plasma sprayed plus foil matrix material is shown. The thinner layers are the 0.001 in. foils used. They contain larger Si particles than the neighboring plasma sprayed layers. Examination of the fracture surfaces of the tested tensile specimens revealed fracture details similar to those typical of wrought aluminum alloys. Figure 4.2 illustrates the fracture surface details of the plasma sprayed plus foil matrix specimens. Large amounts of local plasticity are evident. A comparison between plasma spray behavior and foil fracture can be made in Fig. 4.2b where foil fracture is observed in the left portion of the photo and plasma spray failure is illustrated on the right.

Tensile tests at 400°F and 600°F also have been performed on these matrix materials. The data obtained for the 2024 and 6061 aluminum alloys are presented in Figs. 4.3, 4.4. In all cases the specimens were held at the test temperature for 30 minutes prior to testing. The effect of heat treatment on matrix strength is also shown in these figures. For both the 6061 and 2024 alloys, a standard T-6 heat treatment increased the room temperature tensile strength substantially above the levels of the as-fabricated material. This difference became smaller at the elevated temperatures due to rapid overaging of the alloys. Comparison of the data in the two figures indicates that the 2024 matrix material is capable of higher strengths than the 6061 material over the entire temperature range of testing.

#### 4.2 Composite Transverse Elastic Modulus

The transverse elastic modulus ( $E_{22}$ ) of 4.2 mil BORSIC-aluminum is of major concern in applications. Since these applications can occur at temperatures higher than 70°F and not only in tensile but also compressive stress states, investigations have been performed to determine  $E_{22}$  under these conditions as well as under the more usual room temperature tensile configuration. In addition, the transverse elastic modulus was selected as the parameter to be used in evaluating composite bonding procedures to establish those best capable of providing well bonded, fully consolidated composites. The transverse modulus is especially suited to this task. This is in contrast to longitudinal composite properties that are determined primarily by the volume fraction of fiber reinforcement present, degradation of fibers if any, and to a lesser extent processing variables.

### Experimental Method

Monolayer 4.2 mil BORSIC-aluminum alloy tapes were hot pressed in argon to form 6 layer composites. The parameters of pressure, temperature and time of hot pressing were varied to produce composites for mechanical properties evaluation to indicate the optimum hot pressing conditions. The composite systems were subjected to 2000, 5000, and 10,000 psi pressures with 1 and 4 hr pressing durations. The temperatures used in hot pressing the various alloys were as follows: 6061 at 420, 490, 565°C; 2024 and 2219 at 420 and 490°C; 5052 at 420 and 565°C; 4343 at 490 and 565°C. It is noteworthy that the use of temperatures as high as 565°C was permitted in this study because BORSIC fiber was used. At these temperatures boron is more susceptible to degradation than BORSIC (Refs. 4.3,4).

The hot pressed panels had the dimensions of 1 in. x 5 in. and were approximately .030 in. thick. Each of these panels was cut into three 1/4 in. x 5 in. transverse tensile specimens to produce a total of 216 specimens for testing. The cutting was performed with a diamond cut off wheel and the specimens were tested in a parallel sided configuration. Strain gages were mounted on both sides of each of these specimens to compensate for any bending during modulus measurement. The specimens were aligned in grips by use of a 12.5X microscope and a specially designed alignment jig. This was done in such a way as to leave a 1 in. long gage length between grips. The gripped specimens were then aligned in a Timius-Olsen tensile tester and strained at a strain rate of 0.01 in. per minute.

Composites containing fiber volume fractions ranging from 13% to 50% were also prepared to determine transverse elastic modulus as a function of filament content. Filament content was varied by changing filament spacing and substrate foil thickness during plasma sprayed tape fabrication.

Measurements of the transverse elastic modulus at elevated temperature were performed on BORSIC-6061 and BORSIC-2024 composites containing 46% volume fraction 4.2 mil fiber. Two different techniques of measurement were used. The first method was to use elevated temperature strain gaging techniques and to tensile test the gaged specimens at temperature. The second method was a dynamic determination of the modulus that is frequently referred to as the "free-free beam" technique and relies on the measurement of the resonant vibrational frequencies of composite specimens excited at temperature. Test specimens of rectangular cross section were suspended from two asbestos chords inside a split tube furnace. These wires were each attached to a microphone, one of which acted as a driver that received its signal from a variable frequency audio oscillator, while the second was used as a pickup to measure the amplitude and frequency of induced vibration. Maxima of amplitude were detected at the resonant frequencies of the composite bars tested. These frequencies were then used to calculate the elastic moduli (Refs. 4.5-9).

To determine composite response to compression loading in the transverse direction, specimens containing 46% BORSIC fiber in a 6061 matrix were fabricated by hot press diffusion bonding 40 layers of plasma sprayed tape. Two strain gages were bonded on opposite sides of each specimen to produce a stress-strain curve and to determine if any bending was taking place. Specimens were tested at room temperature at a strain rate of 0.01 in. per minute.



## Results and Discussion

The results of the tests performed on specimens hot press diffusion bonded under the range of conditions described in the Experimental Method section indicated that, for all cases, the elastic modulus did depend on the bonding parameters used. Increasing either the temperature or pressure of bonding resulted in higher transverse moduli for all the matrix-fiber combinations studied. The length of time allotted for bonding (either 1 or 4 hrs), however, had little effect on the resultant composite modulus. For the composites having matrices of 6061, 5052/56 or 4343 the best hot pressing conditions were found to be 565°C and 10,000 psi. For the 2024 and 2219 matrices, 490°C and 10,000 psi were best. Composites containing 50% BORSIC fiber and the above matrices bonded under the above conditions exhibited transverse elastic moduli of  $20 \times 10^6$  psi. This value is in substantial agreement with the theoretical predictions of Chen and Lin (Ref. 4.10) and Adams and Doner (Ref. 4.11) for a BORSIC-aluminum composite containing 50% fiber arranged in a hexagonal array. Other combinations of temperature and pressure were also found to produce fully consolidated composites having moduli equal to or nearly equal to the ideal value. The ranges of these bonding conditions are presented in Table IV-III for each composite system studied.

As composites were bonded at temperatures and pressures less than those given above, the transverse modulus was found to decrease. This decrease was found to be associated with the presence of voids in these composites as measured by a sink-float technique. For bonding pressures and temperatures lower than those described above and in Table IV-III, void contents in excess of 3% by volume were detected. These voids, present in the matrix, lower the elastic modulus considerably (Refs. 4.1,2).

The variation of composite transverse elastic modulus with BORSIC fiber content is presented in Fig. 4.5. The modulus increases with increasing volume fraction fiber, however, as pointed out by others (Refs. 4.10-14), a simple "rule of mixtures" approach that disregards filament packing array is not applicable to an analysis of transverse properties. Unlike the longitudinal elastic modulus, the transverse Young's modulus is sensitive to the filament distribution in the composite. Microstructural examination of the specimens tested in this investigation indicate that filament packing is best described in terms of a nearly hexagonal array and the data obtained agree best with a theoretical analysis based on this type of fiber distribution.

The results of transverse elastic modulus determinations at elevated temperature indicate that the modulus decreases with increasing test temperature and at 600°F the modulus is 10-20% less than the room temperature value. Figure 4.6 presents the data for both methods of modulus determination used. This decrease in modulus is due, in a large measure, to the decrease in modulus experienced by the matrix material over this same temperature interval. This can be seen from the data shown in Fig. 4.6 of the elastic modulus of a typical plasma sprayed plus foil matrix material prepared by hot pressing and tested in tension at elevated temperature. At 600°F the modulus has reached the value of  $7 \times 10^6$  psi in agreement with the value expected for a wrought material of the

same composition (Ref. 4.15). This decrease in matrix modulus of 30% can cause a major portion of the decrease in composite modulus observed (Ref. 4.11). The elastic modulus of the BORSIC fiber is also decreasing with increasing temperature (Refs. 4.16,17); however, little data is available in the temperature region of 600°F to obtain a reliable value. The data of Metcalfe and Schmitz (Ref. 4.16) indicate an elastic modulus of  $50 \times 10^6$  psi for boron at approximately 600°F. Using this modulus for the BORSIC fiber and a modulus of  $7 \times 10^6$  psi for the matrix, the work of Adams and Doner (Ref. 4.11) would indicate that a modulus of approximately  $18 \times 10^6$  psi would be expected. This is in fairly good agreement with the values obtained as shown in the figure.

The transverse elastic modulus measured during compression testing at room temperature was found to be  $18 \times 10^6$  psi. The specimen tested contained 46% volume fraction 4.2 mil BORSIC fiber. Thus, the elastic modulus as measured in compression is in substantial agreement with that measured in tension.

#### 4.3 Transverse Tensile Strength of 4.2 Mil BORSIC-Aluminum

The transverse tensile strength of BORSIC-aluminum composites has become an important factor in their structural application. Although a unidirectional 50% volume fraction 4.2 mil BORSIC-aluminum composite can exhibit a longitudinal ultimate tensile strength in excess of 160,000 psi, its transverse strength is only one-tenth of this value. This is in contrast to the anisotropy of the modulus for which the ratio is less than two to one. A method for circumventing this strength problem has been to cross ply layers of composite to provide the axial strength of fibers in more than one direction. This, however, is not always a satisfactory solution to the strength problem because of the decrease in stress sustainable in the original 0° direction. The preferred solution would be one in which we can increase the transverse tensile strength of composites without compromising their substantial 0° properties. A major goal of this contract is to gain an understanding of why the transverse strength is so low and how it can be improved.

##### 4.3.1 The Effects of Processing Parameters and Heat Treatment

###### Experimental Method

The composite specimens manufactured under a range of hot pressing conditions and described in the section on transverse elastic modulus were also used to determine the dependence of transverse tensile strength on bonding conditions. The bonding procedure used and the method of tensile testing are the same as those described in the earlier section. In addition, subsequent to fabrication, several heat treatment procedures were used in an attempt to determine their effect on composite transverse strength. The heat treatment procedures were performed on composites having 2024 and 6061 aluminum matrices. The first heat treatment, designated T-6, is described in Table IV-I while the second heat treatment used is a modification of the T-6 procedure. This modified procedure subjects the composite to a liquid nitrogen environment (78°K) for 16 hrs after quenching from the solution anneal. The usual T-6 aging procedure is performed after removal from the liquid nitrogen.

## Results and Discussion

The tensile test data obtained have indicated that the transverse strength of the BORSIC-aluminum composites produced under a range of bonding conditions is dependent upon the temperature and pressures used during consolidation. This is primarily due to the dependence of matrix porosity on hot pressing parameters. The plasma sprayed aluminum alloys can contain as much as 10-15% porosity in the as-sprayed condition. If some of this porosity is permitted to remain after bonding, the strength of the matrix material will be severely reduced. Coble and Kingery (Ref. 4.2) have summarized a considerable amount of data illustrating the loss of strength metals exhibit with increasing void content. This effect of porosity, however, has been eliminated by hot pressing under the conditions of 10,000 psi pressure and temperatures of 565°C (for 4343, 6061, 5052) and 490°C (for 2024 and 2024-2219). Using these bonding parameters no matrix porosity could be detected by the sink-float method. These conditions provided the highest values of tensile strength over the range of processing conditions used and agree with the conditions found to produce the highest transverse modulus values described earlier.

Even at full densification, however, the composite transverse strengths fall short of what certain theories have predicted. Work by Chen and Lin (Ref. 4.10) has indicated that the transverse strength of a 50% volume fraction BORSIC-aluminum composite should be nearly equal to the strength of the matrix material for a hexagonal fiber array. A square fiber array of the same volume fraction should exhibit approximately 75% of the matrix strength. Recent work by D. Adams (Ref. 4.18), using an elastic-plastic solution for the stress state in a BORSIC-aluminum composite subjected to transverse normal tensile loading, also indicates that the transverse strengths on the order of those of the unreinforced matrix are to be expected. The data in Fig. 4.7 do not agree with these predictions. This figure presents the transverse ultimate tensile strength of the composites described above as a function of matrix strength. The values of matrix strength are those obtained using the techniques described earlier in this report. For the fully consolidated composites, the average 90° ultimate tensile strength values are approximately 13,000 psi despite the fact that the matrix strengths are all substantially above this level. In addition, over the range of matrix strengths shown in the figure (17,500-30,000) no increase in transverse composite strength was noted with increasing matrix strength. This will be discussed more fully in a later section of this report.

The fracture mode was also found to vary with hot pressing conditions. The use of pressures and temperatures insufficient to cause full matrix consolidation resulted in the fracture path occurring in the composite matrix. The resultant fracture surface did not exhibit any fiber failure. In contrast to this, in the case of the fully consolidated specimens, the fracture path was through both the matrix and the fiber. The fracture surface of these specimens was characterized by fiber splitting. A typical fracture surface is illustrated in Fig. 4.8. This figure illustrates that all the fibers in the plane of the fracture surface are split longitudinally. The plane of splitting passes through the core of each of the fibers. In Fig. 4.8 the cores are visible as white lines in the centers of each of the fractured fibers. No evidence of fiber-matrix debonding is evident in the figure. Radiographic examination of the remainder

of the same specimen revealed that no fiber splits occurred in regions removed from the fracture surface. This was common to other specimens, containing approximately 50% fiber, examined in a similar fashion and indicates that the fiber splitting accompanying transverse tensile failure is a very localized event, occurring only at the final fracture region for these composites. Composites tested having much smaller fiber contents did not all exhibit this localized fiber splitting.

Several transverse tensile specimens were fabricated and tensile tested using an 1100 aluminum matrix and 4.2 mil BORSIC reinforcing fiber. The fracture surface of these specimens, as shown in Fig. 4.9, is nearly free of fiber splitting. Matrix failure predominates. This, as will be discussed in a later section, is due to the low strength of the aluminum matrix and is in sharp contrast to the behavior illustrated by Fig. 4.8.

The heat treatment of both the 2024 and 6061 matrix composites has resulted in considerable improvement in transverse tensile strength. Composite specimens containing approximately 50% BORSIC fiber in a 2024 matrix heat treated to the T-6 condition exhibited transverse tensile strengths of approximately 21,500 psi. The T-6 heat treatment is described in Table IV-I. This ability to cause an increase in strength by heat treatment is consistent with earlier work performed in this laboratory (Ref. 4.19) and elsewhere (Ref. 4.20). For BORSIC-6061 both the T-6 heat treatment and the modified treatment that subjected the composite to a liquid nitrogen environment (78°K) were used. This latter heat treatment has been used by other investigators (Ref. 4.21) to modify the residual stresses in the matrix. Both of the above heat treatment procedures resulted in a composite transverse strength of approximately 20,000 psi for a 50% volume BORSIC-6061 composite. The liquid nitrogen step did not cause any marked change in composite properties.

Figure 4.10 illustrates the stress strain curves of BORSIC-6061 composites tested in the 90° direction in both the T-6 and F (as-fabricated) conditions. It is seen that the T-6 heat treatment not only changes the composite ultimate tensile strength but also alters the entire stress strain curve. The heat treated material exhibits a linear behavior nearly all the way to the point of fracture. The proportional limit of the heat treated specimens was approximately 18,000 psi while that of as-fabricated specimens occurred at approximately 4000-6000 psi.

Figure 4.10 also illustrates an important point in the behavior of as-fabricated composites. Two different types of stress-strain curves were generated for composite specimens that have been manufactured and processed under identical conditions. In general, the initial portions of the curves were similar, however, for some specimens tested, fracture occurred at a strain of approximately 0.012 while for others the strain to fracture was twice this amount. The specimens which fail at the larger strain exhibit a region of increasing strain under nearly constant stress and frequently fracture in a region directly under the

strain gages on the specimen surface. Thus, this phenomenon may be associated with the propagation of failure through the specimen. Curves similar to this second type (larger strain to failure) have been observed by others (Ref. 4.22) as reported by Adams (Ref. 4.18).

#### 4.3.2 Transverse Strength as a Function of Test Temperature and Matrix Strength

##### Experimental Method

Transverse tensile tests were performed at room temperature, 200°F, 400°F, and 600°F. The specimen configuration used was the same as that described in earlier sections and the composites tested had 2024 and 6061 matrices. Both the F and T-6 composite conditions were tested. All testing was done in air and the specimens were held at the test temperature for 30 minutes prior to testing.

Transverse compression tests were performed at both room temperature and at 600°F. The 6061 matrix composite in the F condition was the only type of specimen tested. Testing was carried out by compressing between flat carbide platens. The compression specimen ends were ground flat and parallel. No further specimen end preparation was used.

##### Results and Discussion

The results of the transverse tensile testing of 4.2 mil BORSIC-6061 and BORSIC-2024 composites is presented in Figs. 4.11,12. As discussed in a previous section, the T-6 heat treatment increases the transverse strength above that of the as-fabricated composite. This difference becomes smaller with increasing test temperature as the overaging of the heat treated material takes place. At room temperature the strengths of the 2024 and 6061 matrix composites are approximately equal. As the test temperature is increased the 2024 composite retains a higher strength level than the 6061. This is in agreement with the unreinforced matrix properties presented in Figs. 4.3,4 where the 2024 alloy exhibited higher elevated temperature strength than the 6061 material.

A comparison of the data obtained for composite transverse strength with the unreinforced matrix strength reveals that for both 6061 and 2024 matrix materials, the difference between matrix strength and composite strength decreases with increasing temperature. In the comparison of the 2024 matrix composites with the unreinforced alloy, the composite transverse strength in the F condition decreases only slightly with increasing temperature despite a large decrease in matrix strength. For the T-6 condition both the unreinforced matrix and composite exhibit large decreases in tensile strength with increasing temperature. The 6061 matrix composite exhibited a large decrease in strength with increasing temperature for both the F and T-6 conditions.

The fracture surfaces of the composites tested were examined to determine the mode of fracture. As discussed earlier, at room temperature all of the fibers in the composite fracture surface were split longitudinally. This changed, however, as the test temperature increased. With increasing temperature

of test, the fraction of fracture surface occupied by split fibers decreased. In the case of the 6061 matrix composites, at 600°F no fiber splitting was found to occur and instead the mode of fracture corresponded to that of matrix failure. None of the fracture surfaces studied exhibited evidence of fiber-matrix debonding as a primary mode of fracture.

A summary of the transverse tensile strength of 4.2 mil BORSIC fiber reinforced composites as a function of matrix strength is presented in Fig. 4.13. The data include five different matrices, two of which are in both as-fabricated and heat treated conditions, as well as data obtained over the test temperature range of 70-600°F. Three distinct regions of behavior are seen to occur and are depicted in Fig. 4.14.

Region I - The fracture surfaces of the failed composites exhibited only small amounts of split fibers. In this region the composite strength is approximately equal to the matrix strength. Thus, in this region the matrix fails at an applied composite stress below that necessary for fiber failure. The behavior of the 1100 matrix composites at room temperature and the 6061 matrix composites at elevated temperature are characteristic of this region. The fracture surface presented in Fig. 4.9 is typical of these composites.

Region II - In this region of matrix strength the composite transverse tensile strength is substantially independent of matrix strength. Fracture surfaces are characterized by the presence of large amounts of fiber splitting, Fig. 4.8. In this region the matrix strength is sufficient to cause loading of the fibers to their ultimate transverse strength prior to composite failure. Upon fiber failure, however, the remaining composite matrix material also fails due to overload. The remaining matrix does not have the load carrying capability to prevent total composite failure subsequent to fiber failure. Thus, the constancy and level of composite strength in Region II and the points of transition between Regions I and II, and II and III are controlled by the fiber transverse tensile strength. A higher transverse tensile strength fiber would raise the composite strength level of the Region II plateau and also raise the matrix strength levels of the transition points between regions. Examples of this will be presented in later sections of this report.

Region III - In Region III, as in Region II, matrix strength is sufficient to cause transverse fiber failure prior to composite failure, however, matrix strength is also high enough to prevent immediate overload failure. Thus, the composite strength is determined by the net section of load bearing matrix left, subsequent to fiber splitting, and the strength of this matrix. In the case of the heat treated composites, the presence and magnitude of residual stresses, no doubt, is also of importance. Fracture surfaces are typically similar to that shown in Fig. 4.8.

It should be noted that the data for the 5052/56 matrix composite was presented in Region II, not in Region III. This matrix material contains both a foil of 5052 aluminum with a tensile strength of 28,000 psi and the plasma sprayed material of 5056 with a tensile strength of 42,000 psi. After fiber splitting occurs the major portion of the load carrying matrix consists of the

weaker 5052 foil due to the fact that the foil (or tape) plys are aligned parallel to the transverse tensile axis. Thus, the residual effective matrix strength for this composite is actually 28,000 psi which puts it in Region II.

The transverse compression tests were performed on 6061 matrix composite specimens containing 46% BORSIC fiber. The room temperature transverse compression stress-strain curve is presented in Fig. 4.15. It is plotted with the axial compression stress-strain curve for the same material (Ref. 4.19). The elastic modulus is approximately equal to that exhibited during transverse tension; however, the maximum load carrying capability is considerably greater than that in tension. After approximately 6% strain, and at a stress of 37,900 psi, the load began to decrease with increasing strain. The cause of this decrease was the shear failure of the specimen as shown in Fig. 4.16. At 600°F the specimens failed by the same mechanism, however, the maximum stress was 9500 psi. One specimen compressed at room temperature to the point of rupture was used to examine the fracture surfaces produced. The fractured specimen is shown in scanning electron microscope photographs in Fig. 4.17. As can be seen in the figure, fiber splitting is once again characteristic of the fracture surface. Also visible in Fig. 4.17 is evidence of large amounts of shear deformation of the aluminum between the split fibers.

#### 4.3.3 Transverse Tensile Strength as a Function of Volume Fraction Fiber

##### Experimental Method

To determine the effects of varying the volume fraction fiber on transverse tensile strength, composites were manufactured containing from 13% to 46% 4.2 mil BORSIC. The matrix used was 2024 aluminum. To produce this variation in fiber content a range of filament winding spacings and several different 2024 foil thicknesses were used in conjunction with the usual plasma spray-diffusion bonding procedures. Specimen testing procedures were the same as those described in previous sections.

##### Results and Discussion

The results of the tests performed on 0-46% BORSIC-2024 composites are presented in Fig. 4.18. For both the as-fabricated condition and T-6 condition, when tested at room temperature, the tensile strength decreases with increasing volume fraction fiber. At 600°F, however, the transverse strength is substantially independent of fiber volume fraction. The values of ultimate tensile strength used for the unreinforced matrix were obtained by testing plasma sprayed plus foil material as described in the section on matrix properties.

The lines drawn in Fig. 4.18 from the two 70°F unreinforced matrix strength data points do not represent a fit to the composite data but instead are a result of calculations performed using a simple model. In this model, it was assumed that the fibers had been removed from the composite leaving a network of cylindrical holes. The composite strength was then calculated on the basis of the net minimum cross-sectional area remaining. Little difference in strength was found between the square or hexagonal hole arrays. In both

the as-fabricated and T-6 conditions, the composite strengths were found to be in excess of those calculated.

The difference between composite behavior at room temperature and at 600°F can be related to differences in fracture mode. At room temperature the fracture surfaces are characterized by longitudinal splitting of all the fibers in the fracture surface. Composite behavior at room temperature is similar to that described in Fig. 4.14 for Regions I and III. At the high volume fractions of fiber, in the F condition, the matrix is overloaded by local fiber failure as was described for Region II. Matrix load carrying capability is increased by decreasing fiber content and composite heat treatment so that increasing composite strength can be achieved, typical of Region III. At 600°F, however, the amount of fiber splitting is far less and in some cases no fiber splitting at all is found. The failure occurs completely through the matrix. For this latter case of matrix failure the observation that composite strength is independent of volume fraction fiber is consistent with the prediction of Chen and Lin (Ref. 4.10) and corresponds to Region I in the previous analysis. It is also clear that the predictions of Ref. 4.10 do not hold for the tests performed at room temperature. This is due to the fiber mode of failure being operative at room temperature. The prediction based on the assumption of matrix failure thus should only be used when this mode of failure is predominant.

#### 4.3.4 The Effects of Tensile Specimen Configuration and Edge Conditions on Transverse Strength

##### Experimental Method

To determine the effects of tensile specimen configuration on measured transverse tensile strength, a series of specimens was prepared having three different geometries. These configurations were: parallel sided, parallel sided with aluminum doublers bonded to the specimens in the gripping areas and finally parallel sided with reduced sections of one inch in length. All specimens were basically 0.25 in. wide and 0.030 in. thick with the reduced section of the one specimen type being 0.210 in. wide. All specimens tested were 50% 4.2 mil BORSIC in a 6061 aluminum matrix.

The dependence of transverse tensile strength on specimen volume was studied by varying both the specimen thickness and specimen gage length. The gage length was varied sevenfold and the thickness was varied ninefold. These composites contained a range of from 50 to 3500 fibers in their tested gage sections. Composites all contained approximately 50% 4.2 mil BORSIC in a 6061 matrix and all specimens were tested in the parallel sided configuration with bonded aluminum doublers.

The observation has been made that fiber splitting is an important mode of fracture for 4.2 mil BORSIC-aluminum specimens tested in transverse normal loading. This splitting of fibers occurs across the entire specimen gage section, from edge to edge. Because of this, an investigation was performed to determine the effects of composite edge condition on transverse tensile strength. Tensile specimens were prepared containing 40% 4.2 mil



BORSIC in a 2024-2219 matrix. These specimens were 0.25 in. wide and were cut from diffusion bonded panels using three different methods. The first method consisted of cutting with diamond abrasive wheel and the second method was cutting by electrodischarge machining (EDM). The third procedure consisted of cutting with a diamond abrasive wheel and then polishing the specimen edges to remove 0.012 in. from each cut edge. At least three specimens were tested in each of these conditions.

A fourth type of edge condition was also studied. This consisted of tensile testing transverse composites with the fiber ends of the specimens remaining unstressed. To accomplish this, specimens one inch wide were hot press diffusion bonded. The fiber ends of these panels were freed from the matrix by dissolving away at least 0.25 in. from each edge of the panel. This then left a central load carrying region of aluminum 4.2 mil BORSIC with long free fiber ends protruding from both edges. These specimens were then tensile tested using the usual procedures described previously.

#### Results and Discussion

The results of the tensile tests performed on the specimens having three different configurations indicated that the use of the aluminum doublers on parallel sided specimens was successful in localizing all the fractures within the specimen gage length and away from the grip edges. In the case of specimens with no doublers, the fracture always occurred at the grip edge; however, there was only a 5% difference in ultimate tensile strength between the two types of specimens, those with doublers having the higher values averaging 13,900 psi. The use of a small reduced section, however, caused a 16% decrease in ultimate tensile strength below the above-mentioned value. These specimens failed in the gage section and not at the machined radii so that the decrease in strength can be attributed to the extra machining operations involved in preparing the specimens. It was found that for all specimen configurations and failure locations, the fracture surface was characterized by split fibers. From the above, it was concluded that the best configuration is the parallel sided specimen with doublers to diminish the stress concentrations in the grip end region and thus provide fractures occurring in the gage section. The testing of specimens without doublers does not, however, cause any appreciable decrease in tensile strength and thus the stress concentrations caused by the grips being used are not excessive.

The effects of varying the volume of the gage section of transverse tensile specimen were found to be small. Despite a large variation in specimen volume (sixtyfold) no significant changes in transverse tensile strength were found to occur. The values measured for all specimens tested ranged from 11,300 psi to 15,400 psi; however, no trend with specimen volume was found. As has been stated previously in this report, only a few fibers fail at the point of composite failure in transverse tension. The smallest specimens tested (containing 70 fibers in their test section) apparently contain a sufficient number of sites for failure to prevent the observation of a higher strength due to decreased volume.

The results obtained using the three different cutting procedures are given below:

1. Specimen edges prepared by cutting with a diamond abrasive wheel were found to contain badly broken fiber ends. The fiber ends are evidently broken and not cut by the motion of the wheel. Tensile strength obtained from tested specimens averaged 12,500 psi. Figure 4.19 shows the condition the fiber edges are in after abrasive wheel cutting. The edges of the specimen have been etched back to reveal notched and cracked fiber ends.
2. Specimen edges prepared by electrodischarge machining (EDM) were found to also have broken fiber ends. The average tensile strength exhibited by three specimens was 13,300 psi.
3. Preparation using a cutting wheel and then polishing resulted in fiber ends that were more smooth and less damaged in appearance than either of the above techniques provided. The average tensile strength of these specimens was 11,700 psi.

For all of the specimens tested in these three edge conditions, the fracture surface was characterized by split fibers. The method of cutting or edge preparation for the three cases studied had little effect on either the transverse tensile strength or the mode of failure.

Figure 4.20 is a radiograph taken of a transverse tensile specimen after having been stressed to the point of fracture. The test was stopped prior to complete specimen failure to study the mode of fracture propagation. This specimen, the edges of which were cut with a diamond abrasive wheel, began to fail at one of its edges. The radiograph shows the propagation of the edge initiated crack through the specimen. The longitudinal splitting of fibers is visible at the crack tip.

Figure 4.21 illustrates the configuration of the specimens with the free fiber ends. The stress-strain curves obtained by tensile testing BORSIC-2024 composite specimens of this configuration are shown in Fig. 4.22. A stress-strain curve exhibited by the more conventional type of transverse tensile specimens having cut edges is also included in the figure for comparison. It is seen that the specimens with the free and cut configurations exhibit the same elastic modulus; however, the tensile strength and strains to fracture of these composites differ substantially. For the as-fabricated (F) condition, the "cut-edges" composite exhibits a transverse tensile strength of 15,000 psi while the "free-end" composite is capable of 19,000 psi. In the T-6 condition, the "free-end" composite fails at 36,000 psi, while the tensile strengths of "cut-edge" composites having the same matrix and undergoing the same heat treatment were found to be only 22,000-24,000 psi. Thus, when the fiber edges of these composites are unstressed, the transverse tensile strength increases substantially. Figure 4.23 illustrates this same point; however, in this case, the matrix material is a 5052/56 aluminum alloy combination. In this figure, once again, the elastic modulus of the two types of specimens is independent of condition; and the

tensile strength of the free-fiber-end composite is nearly 30,000 psi. Figure 4.23 also illustrates that two different types of composite behavior are found to occur for the cut-edge composites. The composite can fail with a fracture strain of only 0.06%, or it can exhibit a fracture strain of 0.12%. In both cases, the tensile strength was approximately 12,000 psi. This type of behavior was previously discussed and illustrated in Fig. 4.10.

Figure 4.24 illustrates the tensile strengths obtained by testing "free-fiber-end" 90° specimens. In the figure, the composite tensile strength is plotted as a function of the ultimate tensile strength of the unreinforced matrix. The lines drawn indicate the tensile strengths to be obtained if composite behavior agreed with the analysis of Chen and Lin (Ref. 4.10). Strengths expected for both square and hexagonal fiber arrays are drawn. This figure is in marked contrast to one having similar axes reported earlier in Fig. 4.7 for cut-edge composites. In that figure it was seen that composites having 2024, 6061, and 5052/56 matrices all exhibited the same transverse strength. For the data reported in Fig. 4.24 this is no longer the case. The transverse strength of the composites tested is not constant and is dependent on matrix strength. The composites having the 5052/56 matrix material exhibited tensile strengths of approximately 30,000 psi while those having a 6061 matrix failed at only 20,000 psi. For all of these composites, the fracture surfaces of the tested specimens exhibited some fiber splitting. However, the fiber splitting observed was substantially less than that reported in the other sections of this report when the specimen edges were in the cut condition. The fracture surfaces of free fiber end and cut edge specimens are compared in Fig. 4.25. The specimen with free fiber ends is characterized primarily by a matrix mode of failure while the cut edge specimen is characterized primarily by fiber splitting.

The specimens tested in the free end condition with a 2024 aluminum matrix were found to exhibit larger amounts of fiber splitting. This is probably why the composite tensile strengths reported in Fig. 4.24 for these specimens were not higher. An example of the importance of fiber splitting in the fracture of these specimens is found in the two data points reported for the BORSIC-2024 composites in the T-6 condition. The lower value of tensile strength of 25,850 psi was exhibited by a specimen that had all the fibers in its fracture surface split. In the case of the other specimen, however, only 50% of the fibers in the fracture surface were split and the composite tensile strength was 36,750 psi.

Several transverse tensile specimens were tested with fiber ends protruding less than 0.25 in. beyond the matrix edge. No change in fracture mode or tensile strength was noted from that of cut edge specimens. This was found to be due to the fact that fiber edge damage extended further than 0.25 in. from the fiber ends. In a similar manner, some specimens were found to exhibit fiber damage to greater than 0.25 in. so that matrix removal would have to extend much further into the specimens to provide increased performance.

#### 4.3.5 Dispersion Hardened Aluminum 4.2 Mil BORSIC Composites

One of the major advantages of metal matrix composites over polymeric matrix composites is the higher temperature performance capability of the metal matrices. In the case of the BORSIC-aluminum system, compatibility between fiber and matrix is sufficient to permit long term exposure and usage at above 600°F, the upper temperature limit for structural application of most aluminum alloys. At present, however, BORSIC-aluminum is not generally being considered for higher temperature applications due to the low levels of composite transverse strength and shear strength. Both of these quantities are being controlled by matrix properties. The following section will describe efforts to achieve an aluminum alloy matrix that will permit composite application at higher temperatures.

##### Experimental Method

Five aluminum alloys, other than those described in the earlier section of this report, have been used in an attempt at providing BORSIC-aluminum composites with superior elevated temperature transverse strength. The alloy systems include aluminum-iron alloys, the alloy designated 8001 and high aluminum oxide content (21% by weight) aluminum fabricated from Sintered Aluminum Powder (S.A.P.). The 8001 and aluminum-iron matrix composites were fabricated using only fiber and matrix powder. These composites were created by plasma spraying the powder onto the fibers to produce tape consisting of only plasma sprayed material and fiber. Plasma spraying was not used to fabricate the S.A.P. matrix composites. In this case the S.A.P. was in 2 mil thick foil form. Tapes were prepared by bonding fiber to the foil with polystyrene which is outgassed prior to diffusion bonding. The procedure for composite manufacture was basically the same as that described in other sections of this report. Sections of tapes of BORSIC-aluminum alloy were hot press diffusion bonded to produce composite specimens. In addition, fiberless specimens were manufactured and tested to determine base matrix properties.

The aluminum-iron alloy system was chosen as a likely candidate for high temperature applications because of the results obtained by powder metallurgy at Alcoa (Ref. 4.23). Excellent strength, creep and stress rupture properties at temperatures of up to 800°F have been obtained. The most commonly used alloy contains approximately 8% Fe and can exhibit a tensile strength of 10,000 psi at 800°F (Ref. 4.23). This is due to an extremely fine dispersion of  $\text{FeAl}_3$  generated in these materials by powder metallurgical techniques. The S.A.P. foil was also chosen for its proven outstanding elevated temperature properties.

The 8001 alloy (1.1%Ni, 0.6%Fe) is also a dispersion hardened matrix material and has superior corrosion resistance to the aluminum iron or aluminum copper alloys at elevated temperatures. Because of this latter property, 8001 alloy has found application in atomic reactors. The strength of wrought forms of this alloy, however, is quite low at elevated temperature (5000 psi at 600°F). Through the use of plasma spray techniques to generate a fine dispersion of intermetallics, it will be shown that higher strengths can be obtained.

## Results and Discussion

Fiberless matrix specimens of aluminum alloys containing 1.8, 5.2, and 7.4% Fe were fabricated by the plasma spray plus diffusion bonding procedure. These specimens were tensile tested at temperatures ranging from room temperature to 600°F. The specimens containing 5.2% Fe demonstrated higher tensile strengths than either of the other alloys. This was associated with a fine dispersion of  $\text{FeAl}_3$  distributed in the matrix as a result of plasma spraying and probably the rapid cooling from the liquid droplet form in this procedure. Experiments performed by Schiel and Masuda (Ref. 4.24) on the supercooling of aluminum iron alloys may explain the superior properties of the 5.2% Fe alloy. Although the eutectic point of this system occurs at approximately 2% Fe, rapid cooling through the eutectic produces a fine coupled eutectic structure at compositions having higher concentrations of Fe. The authors found that supercooling of 100°C causes this coupled region to occur at approximately 5% Fe while at higher and lower concentrations the structure is no longer coupled. At room temperature the unreinforced Al-5.2% Fe material exhibited an elastic modulus of  $10 \times 10^6$  psi, a tensile strength of 19,000 psi and a strain to fracture of 20%. At 600°F the tensile strength was 12,000 psi. Composites containing 46% 4.2 mil BORSIC fiber and a matrix of this same alloy were found to exhibit a room temperature transverse elastic modulus of approximately  $18 \times 10^6$  psi, a transverse tensile strength of 12,500 psi and a strain to fracture of 0.13%. At 600°F the transverse tensile strength was 9000 psi. The results of these tests have indicated that the plasma spray plus diffusion bonding procedures used are not yet capable of causing the aluminum iron system to achieve the level of strength obtained using powder metallurgical techniques. In the powder metallurgical procedure the material is fabricated by compaction and extrusion. The extrusion procedure, not applicable to the composites described herein, provides a microstructure that is even finer than the one obtained by plasma spraying.

Specimens of 8001 aluminum alloy (1.1%Ni, 0.5%Fe) were prepared by plasma spraying plus hot pressing. This alloy also contains a precipitate, which is extremely stable at high temperatures (800°F), due to its insolubility in the aluminum matrix. In the absence of any fiber reinforcement the tensile strength of this material at 70°F, 400°F, and 600°F is 20,000 psi, 18,000 psi, and 12,500 psi respectively. These values can be compared with the strength obtained for extruded rod of the same alloy: 20,000 psi, 12,000 psi, and 5400 psi respectively (Ref. 4.25). This comparison reveals that the plasma sprayed material, probably due to the finely dispersed microstructure developed by plasma spraying, has markedly superior strength at elevated temperature as compared with the wrought material. Composite strengths obtained, however, were not as high. Specimens containing approximately 50% 4.2 mil BORSIC failed at 6000 psi at 600°F.

Figure 4.26 is a typical photomicrograph of the cross section of the BORSIC-SAP composites. The resultant transverse tensile strengths of 4.2 mil BORSIC-SAP are given in Fig. 4.27. At 70°F, 300°F, and 600°F, the composite fracture surfaces are primarily characterized by fiber splitting. At 900°F level the matrix is weaker than the fibers and composite failure occurs by matrix shear fracture. The strength level achieved at 600°F with the SAP is higher than that obtained with 6061 (5000 psi), 8001 (6000 psi), or Al-Fe

(9000 psi) matrix composites tested previously under this program. Only the 2024-T6 matrix has achieved higher strength levels over the entire temperature range of up to 600°F. In the F condition, however, the 2024 matrix is also weaker than the SAP at elevated temperature. The SAP matrix is stronger after long-time exposure at the high temperatures compared to the 2024-T6 at temperatures of 600°F and above due to the rapid overaging of the 2024 and the stability of the SAP. This matrix is the best of the dispersion hardened systems tested under this program. The transverse strain to failure of the sintered aluminum powder matrix composites is less than that of the other matrix alloy composites. At 70°F the strains to failure measured were 0.056% and 0.088%. This low level of ductility makes these composites extremely sensitive to eccentric loading during testing.

Tensile specimens were also tested with the fibers aligned parallel to the tensile axis. These tests were performed to insure that no fiber degradation was taking place during diffusion bonding at the above-mentioned conditions. The average tensile strength of specimens containing 52% BORSIC was 168,000 psi. This strength level agrees well with those obtained for other 4.2 mil BORSIC-aluminum matrix composites and indicates that no fiber degradation is taking place when the SAP matrix is used.

#### 4.3.6 Transverse Fiber Properties

The fracture of 4.2 mil BORSIC-aluminum transverse tensile and compression specimens is associated with the failure of the reinforcing BORSIC fibers as described in the composite transverse strength results section. Failure of fibers, at a composite stress level of 10,000-20,000 psi, is difficult to reconcile with axial fiber strengths on the order 400,000 psi. This observed behavior is inconsistent with calculated fiber stress concentration factors, on the order of 1.5 to 3.0 (Ref. 4.18), operating during transverse loading and suggests that fiber strength is much lower in the transverse direction than the axial direction. To better understand the failure of these composites, a test is required which can determine the transverse tensile strength of the anisotropic fibers. Unfortunately, it is not feasible to pull the BORSIC fiber in a direction perpendicular to its axis. Therefore, the test used to measure tensile strength is actually a diametral compression test in which the material fails in tension (Refs. 4.26-33). This test permits tensile stresses to be placed on brittle materials without the problems of traction gripping or the introduction of loading eccentricities.

#### Experimental Method

The diametral compression test is performed by loading a right circular cylinder in compression diametrically between two flat platens. Under this loading configuration tensile stresses are produced along the diameter connecting the two loading regions in a direction normal to the compressive axis. For the test to be a valid tensile test the specimen must fail along the diametral plane that includes the two lines of contact between specimen and loading platens. In the ideal case of line contact between platens and specimen, the tensile stresses  $\sigma$  generated on the loaded diameter are uniform and calculable using the expression:

$$\sigma = \frac{2 P}{\pi D l}$$

where P equals the applied load, D equals the cylinder diameter and l is the cylinder length. Unfortunately, for this ideal case there are compressive and shear stresses of extremely large magnitude developed at the contact loading surfaces which can cause material failure of an undesired nature. In the boron fiber, however, due to the residual stress pattern failure is initiated from centrally located cracks.

The diametral compression test was used on 4.2 mil and 5.7 mil diameter BORSIC and 5.6 mil boron fibers by loading 0.5 in. long segments of fiber in compression between smooth tungsten carbide platens. Alignment was provided by a specially constructed jig which could be placed under the crosshead of a Tinius-Olsen tensile testing machine. The load was applied at 0.01 in. per minute and was found to increase in a linear manner with time until the loaded fiber suddenly fractured causing a single abrupt drop in load. The maximum load observed was that used to calculate a tensile stress assumed to be responsible for failure. As with many high strength brittle materials, failure was usually accompanied by shattering of the entire specimen.

#### Results and Discussion

Figure 4.28 presents the strength distribution of 78 4.2 mil BORSIC fiber specimens tested in diametral compression. The distribution is skewed sharply to the lower strength with a mode of 30,000 psi. The main significance of these data is that fibers can fail at the low strength levels indicated in the figure. These values are far less than the tensile strengths of BORSIC fibers tested in the axial direction (400,000-500,000 psi) and indicate that the strength of these fibers is anisotropic.

Figure 4.29 is a photograph of a fragment of 4.2 mil BORSIC fiber that was fractured during this series of tests. The fracture surface is along a diametral plane and very similar to that observed on fibers split in 90° composite tensile tests. This lends support to the analogy between the diametral compression test and the failure of fibers in the transverse tensile test.

One possible reason for the anisotropy of strength of 4.2 mil BORSIC fibers may be attributable to the existence of fiber flaws in orientations capable of reducing transverse strength. Such flaws have been observed in boron fibers (Ref. 4.34) and can be seen in the polished cross sections of BORSIC fibers. These flaws have been postulated to be the result of interfacial voids at the tungsten-boron interface of these fibers and the generation of residual stress patterns during fiber manufacture (Ref. 4.34).

Figure 4.30 illustrates the effects such flaws or cracks would have on the performance of fibers tested in diametral compression. A compression load P is applied to the fiber generating a tensile stress  $\sigma$  at right angles to the applied load. A crack positioned as shown in the figure will cause the fiber to fail at a stress  $\sigma_0$ . The magnitude of this stress would depend on the

length of the crack and the crack tip radius as described by Griffith's classical analysis. As the crack is rotated by an angle  $\theta$  ( $0 \leq \theta \leq 90^\circ$ ) the stress  $\sigma$  must increase to cause failure of the fiber as described by the expression  $\sigma_0/\cos \theta$ . Only the term  $\cos \theta$  enters into this expression because in a circular cross sectional fiber, as the plane of the flaw is rotated, the cross sectional area remains constant. A constant crack length and a uniform stress field in the cylindrical fiber are assumed. During diametral compression testing the angle of  $\theta$  has equal probabilities of having any value between 0 and  $90^\circ$  with respect to the compression axis. Using the stress values and numbers of fibers fractured at each stress in Fig. 4.28, partitioning these fibers into 16 populations and associating a value of  $\theta$  with each of these populations, the value of  $\sigma_0$  can be obtained using the formula  $\sigma_0 = \sigma \cos \theta$  for each partitioned group. Thus, it is assumed that the five highest values of  $\sigma$  measured resulted from the diametral compression of fibers having a value of  $\theta$  between  $90^\circ$  and  $84.37^\circ$ . The average value of  $87.1^\circ$  was used for  $\theta$  in this partitioned group and the cosine of this angle was multiplied by the average value of  $\sigma$  measured for this group of five values to obtain  $\sigma_0$ . This was repeated for all the other groups of fibers and Fig. 4.30 presents the values of  $\sigma_0$  obtained. This figure shows that, using the model of a fiber flaw reduces the data of Fig. 4.28 to a relatively narrow range of  $\sigma_0$ , i.e. the stress necessary to fracture the fiber when  $\theta = 0$ . The variation in  $\sigma_0$  obtained is probably a result of variation in the flaw size in the fibers tested. The values shown in the figure would indicate that the largest flaw observed would be 16.5 times as large as the smallest. This result is obtained by assuming  $\sigma_0$  is inversely proportional to the square root of flaw size.

The results of the diametral compression of the large diameter boron and BORSIC fibers are presented in Figs. 4.31,32. The tensile stress at fiber fracture was calculated using the equation presented above. Both fibers exhibit strength distributions markedly different from that for 4.2 mil BORSIC. In the former case, no fibers failed at stresses below 140,000 psi, while in the latter case, the majority of the fibers failed below this stress level. The mode for the distribution of the large diameter boron fiber is 330,000 psi while that of the 4.2 mil BORSIC was found to be 30,000 psi. The transverse tensile strength of the large diameter BORSIC is also considerably higher than that of the smaller fiber, however, it is lower than the strength of the 5.6 mil boron. In addition, the distributions of transverse fiber strengths for the large diameter fibers are more nearly "normal" than is that characteristic of the 4.2 mil fiber. Thus, it is likely that the radial flaw model of fiber failure described above is not controlling the transverse fiber fracture of the large diameter fibers since the presence of a flaw would not be represented by a normal distribution of strength.

The large diameter boron and BORSIC fibers are produced in a manner similar to that used in the past to produce 4.0 mil fiber. The boron is deposited onto a 0.5 mil diameter tungsten substrate to produce a fiber of approximately 5.5 to 5.6 mils in diameter. As a result of this increase in fiber diameter, the ratio of boron to tungsten in the fiber is approximately one-half that characteristic of the 4.0 mil fiber. This has caused a decrease in fiber density and cost. The large diameter BORSIC fiber is produced by depositing an approximately 0.1 mil thick coating of SiC on the boron fiber. A cross section of the resultant large diameter BORSIC fiber is presented in Fig. 4.33.



The larger ratio of boron to tungsten for the large diameter fibers may be of importance in both the axial and transverse tensile strengths of the fiber. Wawner (Ref. 4.26) has pointed out that the removal of boride core of a boron fiber caused a marked increase in fiber strength. Similarly, Adler (Ref. 4.27) has shown, on the basis of the magnitude of residual stresses developed due to core reaction during fiber fabrication, that the transverse splitting tendency of boron fibers should decrease with increasing fiber diameter.

#### 4.3.7 BORSIC-Aluminum-Stainless Steel Composites

##### Experimental Method

Specimens were prepared with stainless steel fiber reinforcement at right angles to the 4.2 mil BORSIC fiber axis. These specimens were prepared by hot press diffusion bonding plasma sprayed tapes of AFC-77 stainless steel fiber with tapes of BORSIC-6061 aluminum. The stainless steel fiber tapes were made by winding 0.002 in. diameter fiber onto a mandrel covered with 0.001 in. thick 6061 alloy foil and plasma spraying a coating of the same alloy. The amount of stainless steel fiber in the resultant composite could be adjusted to any desired level by controlling the number of stainless steel reinforced layers hot pressed into the composite. The stainless steel fibers used had an as-drawn strength of 463,000 psi.

##### Results and Discussion

Composites containing 6% volume fraction 0.002 in. diameter AFC-77 stainless steel fibers oriented at 90° to 46% volume fraction BORSIC fiber in a 6061 matrix were tested. The tensile strength of these composites was 41,000 psi at room temperature when tested parallel to the stainless steel fiber axis. The elastic modulus for this same orientation was  $23 \times 10^6$  psi and the strain to fracture 1.14%. Figure 4.34 illustrates an interesting feature of these composites. The figure is a radiograph of a steel reinforced 4.2 mil BORSIC-aluminum specimen that has been tensile tested along the steel fiber axis. Many of the BORSIC fibers in the area radiographed have split longitudinally along their axes. This area is not near the composite fracture surface and thus indicates that the presence of the stainless steel fibers permits fiber splitting without crack propagation to a greater extent than that detected in composites without the steel wires. Transverse tensile tests were also performed at 400°F, 600°F, and 900°F on these composites. The results of these tests are presented in Fig. 4.35. The values of ultimate tensile strength obtained offer significant improvement over those currently attainable in 4.2 mil BORSIC-aluminum. This is particularly true at the elevated temperatures where the excellent high temperature properties of the AFC-77 wires are of importance. Tensile test results have been obtained by testing BORSIC-aluminum stainless steel composites in a direction parallel to the BORSIC fibers. Composites containing 40% by volume 4.2 mil BORSIC fiber parallel to the tensile axis and 6% steel fiber transverse to the tensile axis failed at a stress of 126,000 psi (average of six tests). This ultimate tensile strength would indicate no significant loss of composite strength in the BORSIC fiber direction due to the addition of the steel fibers.

The addition of the steel fibers also increases the energy necessary to fracture a composite specimen in impact. This was demonstrated by fabricating a full sized Charpy impact specimen containing 5.5% steel fiber, 42% 4.2 mil BORSIC and 52.5% 6061 aluminum. The steel fiber was oriented perpendicular to the machined notch (along the major dimension of the specimen), and the BORSIC fiber was oriented in the plane of the notch and parallel to the notch root. The impact energy needed to fracture this specimen was 4.5 ft/lb. As will be noted from the fracture results discussed in a later section of this report, this impact energy is approximately four times the energy necessary to fracture a BORSIC aluminum specimen of the same orientation.

#### 4.3.8 BORSIC-Aluminum-Titanium Composites

##### Experimental Method

Titanium was added to the composites for reinforcement in the transverse direction by replacing the aluminum foils with titanium foils. The manufacturing process consisted of winding a layer of fiber onto a titanium alloy foil substrate and plasma spraying with 6061 aluminum. The resultant tapes were then hot press diffusion bonded to form multilayer composites. Titanium alloys used Ti-6Al-4V, Ti-13V-11Cr-3Al, and Ti-11.5Mo-6Zr-4.5Sn alloy referred to as Beta III (produced by Crucible Steel). Both of these recently-incorporated alloys are heat treatable and of the beta type. The former can be strengthened after a solution treatment by the precipitation of fine particles of  $TiCr_2$  plus alpha phase to a level of up to 215,000 psi, and the Beta III alloy can be strengthened by the precipitation of alpha phase producing a structure that combines high strength levels with weldability, excellent cold formability, and excellent fracture toughness. This last property makes Beta III an extremely desirable addition to BORSIC-aluminum composites.

##### Results and Discussion

The use of the titanium foils in place of aluminum foils has been successful in producing large increases in the transverse tensile strength without causing any major penalties in the axial properties. Composites containing 50% volume fraction BORSIC, 20% (Ti-13V-11Cr-3Al) and 30% 6061 aluminum alloy were found to exhibit transverse strengths averaging 40,000 psi and longitudinal strengths of 150,000 psi. Specimens containing 21% volume fraction Beta III titanium, 44% BORSIC, and 35% 6061 aluminum provided transverse ultimate tensile strengths of 53,000 psi and axial strengths of 163,000 psi. The transverse fracture strains of these composites were approximately 0.8%, which is a considerable increase over the fracture strains of 0.15% for unreinforced BORSIC-aluminum composites. This work confirms earlier investigations using Ti-6Al-4V and C.P. Ti foils as lamellar reinforcement to improve transverse properties.

Figure 4.36 is a radiograph of a specimen of BORSIC-aluminum titanium subsequent to tensile testing in a direction  $90^\circ$  to the fiber axis. The region radiographed is not near the composite fracture surface, however, fibers are split longitudinally. As in the case of the BORSIC-aluminum steel fiber composites, the titanium reinforcing foils permit fiber splitting to occur without composite failure.

#### 4.4 Transverse Tensile Properties of 5.6 Mil Fiber Reinforced Composites

##### Experimental Method

Composite specimens uniaxially reinforced with 5.6 mil boron and 5.7 mil BORSIC were prepared for transverse tensile testing. The specimens were cut from composite panels with a diamond abrasive wheel. Specimen configuration and test procedures are the same as those described previously in this report. The specimens were parallel sided and 0.250 in. wide with a 1.0 in. long gage length and doublers cemented to the gripping areas.

##### Results and Discussion

The transverse tensile strengths of 6061-F, 6061-T6, 2024-F, and 2024-T6 matrix composites reinforced with large diameter boron fiber are presented in Table IV-IV. A typical stress-strain curve for a composite in the T-6 condition is given in Fig. 4.37. The data indicate significantly higher transverse tensile strengths than those obtained previously with either 4.2 mil BORSIC or 4.0 mil boron. Composite strengths increase with increasing matrix strength and are, over the range investigated, independent of volume fraction fiber. Figure 4.38 presents a typical fracture surface indicating the primary mode of failure to be matrix rupture, very little fiber splitting is present. Fiber splitting is noted to occur at the cut edges of the specimen. This is a result of damage introduced during specimen cutting with a diamond abrasive wheel. This damage, although detracting from the total composite strength, does not cause fiber splitting to propagate across the entire specimen width as was shown to be the case for 4.2 mil diameter fiber.

The transverse tensile strength of 5.6 mil boron-2024-T6 composites was determined as a function of test temperature. The data are presented in Fig. 4.39. Included in the figure are data previously reported herein for 4.2 mil BORSIC-2024-T6 composites. The transverse strength of the large diameter fiber composites is considerably greater than that of the 4.2 BORSIC fiber composites at both 70°F and 400°F. At 600°F both composites failed at the same stress level. This equality of strength at the higher temperature is due to the fact that both composites are now failing primarily by matrix rupture and thus would be expected to exhibit the same strength, independent of fiber diameter.

The transverse tensile properties of 5.7 mil BORSIC-aluminum are presented in Table IV-V. These data include composite matrices of 6061, 2024, 5052/56 and 1100 aluminum. Figure 4.40 indicates the dependence of transverse tensile strength on matrix tensile strength. This dependence is clearly different from that previously presented in Fig. 4.13 for the dependence of 4.2 mil BORSIC-aluminum transverse strength on matrix strength. Figure 4.40 includes the theoretical prediction of Chen and Lin (Ref. 4.10) for both hexagonal and square arrays of fiber. Since all the composites tested with 5.7 mil BORSIC failed primarily by matrix rupture, this agreement was expected. A typical fracture surface is given in Fig. 4.41. It is clear that some fiber splitting has occurred predominantly due to composite edge damage during cutting. It is the variation of the amount of this edge damage and splitting which causes significant variation in composite strength at the higher matrix strength levels.

Larger observed amounts of splitting are associated with lower strengths. Large amounts of dimpling of the aluminum plasma spray and foil indicate significant amounts of local plastic deformation taking place during failure. Only slight indications of fiber-matrix debonding occurred.

Figures 4.42, 43 contain typical stress strain curves for transverse tensile testing of 5.7 mil BORSIC 6061-T6 and 1100 aluminum. Outstanding features of these curves are the high tensile strength of the former and the exceptionally large strain to failure of the latter. The transverse tensile strain to failure was observed to increase with increasing matrix ductility and decreasing volume fraction fiber. The highest strain to failure, approximately 0.6% for 54% fiber reinforcement, was obtained for the 1100 matrix aluminum composites. This level of failure strain is of particular significance because it is approximately equal to the composite axial tensile failure strain. Thus, the 1100 matrix composite is not anisotropic in its failure strain, a point that may have appreciable significance in applications where cross ply layups are used.

The variation of composite transverse tensile strength with volume fraction fiber is presented in Fig. 4.44. The data, for a 6061 matrix system, indicate that composite strength is substantially independent of matrix strength. Variations in composite strength do occur, as was pointed out earlier, due to variations in split fiber degree as a result of edge damage. The highest value of strength obtained was 44,000 psi for a composite tested in the T-0 condition. This is higher than the strength usually obtained for heat treated foil plus plasma spray matrices. It is, however, approximately equal to that obtained for wrought 6061-T6 material and may thus just reflect variations in efficiency of composite heat treatment. Dependence on volume fraction fiber is far different from that exhibited by 4.2 mil fiber composites where composite strength increased with decreasing fiber content. The above described independence of strength with fiber content has been predicted (Ref. 4.11).

The dependence of transverse elastic modulus on volume fraction fiber is presented in Fig. 4.45. This relationship is similar to that exhibited by 4.2 mil BORSIC reinforced composites and agreement with theoretical prediction is excellent.

The dependence of composite transverse tensile strength on test temperature is presented in Fig. 4.46 for 6061 matrix composites. At all test temperatures the composite strength is very nearly equal to the matrix strength as given in Fig. 4.47. Matrix failure was observed at all temperatures.

The composite transverse tensile strengths obtained using several different types of boron and BORSIC fibers as well as silicon carbide fiber are presented in Fig. 4.48. All of these composites were fabricated at United Aircraft Research Laboratories using 2024 aluminum alloy plasma sprayed tapes. The comparison of strengths reveals that several different fibers can provide composite strengths in excess of 40,000 psi. These high strength composites exhibited only small amounts of fiber splitting. Fibers that did undergo considerable fiber splitting, 4.0 mil boron and 4.2 mil BORSIC, provided considerably weaker composites.

#### 4.5 Titanium Matrix Composites

BORSIC fiber reinforced titanium matrix composites have been fabricated and tested during this program because of their significance for application with long time exposures at temperatures in excess of 500°F. These composites will be shown to have significant advantages over monolithic titanium in terms of both axial and transverse elastic modulus as well as axial tensile strength. On a specific (property divided by material density) basis these advantages will be even greater.

##### Experimental Method

Composite fabrication was carried out using polystyrene (fugitive binder) bonded tapes and the hot press diffusion bonding procedure. Tapes were fabricated by winding the fiber over titanium foil and spraying with a polystyrene-xylene mixture which hardened to bond fiber and foil together. Diffusion bonding was performed in a two stage process. The fugitive binder was removed by holding the composite "lay up" at 450°C for 30 minutes. The second stage of the procedure was the diffusion bonding of the composites for 30-60 minutes at elevated temperature, 750-870°C, at pressures of from 10-15 x 10<sup>3</sup> psi. The diffusion bonding was performed in vacuum of approximately 5 x 10<sup>-6</sup> torr.

The materials used in composite fabrication included both 4.2 mil and 5.7 mil diameter BORSIC fiber. Matrices of commercial purity (75A) titanium, Ti-6Al-4V and Beta III titanium were used. The Beta III titanium is a Crucible Steel alloy having a composition of 11.5% Mo, 6.0% Zr, 4.5 % Sn and is noted for its high strength, superior fracture toughness and excellent cold formability.

Unidirectionally reinforced tensile specimens were prepared and tested at both 0° and 90° to the fiber axis. The specimens were parallel sided. Aluminum doublers were bonded onto the specimens for gripping, leaving 1.0 in. to 1.5 in. long gage lengths. Specimen mounted extensometers and strain gages were used to measure modulus and strain to failure. Tests performed at elevated temperature, as well as those performed at room temperature, were in air with 20 minutes at temperature prior to testing allotted for system thermal equilibrium to be achieved.

Measurements of elastic modulus were made at elevated temperature using the free-free beam technique previously described in section 4.2.

##### Results and Discussion

The results of the tensile testing of 4.2 mil BORSIC reinforced specimens are presented in Table IV-VI. Mechanical data as well as hot pressing temperature are given for each specimen. The hot pressing parameters given for each composite system were chosen after several hot pressings had been performed under varied conditions to establish the best pressing conditions. Axial tensile strengths of up to 180,000 psi were achieved with axial elastic moduli in excess of twice those of the monolithic titanium alloys. Transverse tensile strengths were considerably lower, approximately 31,000 psi. This low transverse strength was associated with large amounts of fiber splitting on the

composite fracture surfaces. As was shown in the case of aluminum matrix composites, this mode of fiber failure can severely limit composite strength.

Both axial and transverse elastic moduli were higher than those of the unreinforced titanium matrices. The axial composite moduli agree well with rule of mixtures predictions based on constituent material's moduli of  $58 \times 10^6$  psi for BORSIC,  $11 \times 10^6$  psi for full annealed and furnace cooled Beta III titanium (Ref. 4.28), and  $15 \times 10^6$  psi for commercially pure titanium. Transverse elastic moduli also agree well with theoretical predictions (Refs. 4.10,11) and, due to the low elastic modulus of the Beta III matrix, are nearly equal to those obtained for aluminum-BORSIC composites as presented in section 4.2. The comparison of titanium-BORSIC composite elastic moduli with monolithic titanium moduli is further increased in favor of the composites when these properties are compared on a specific or modulus over density basis. The density of titanium containing 50% by volume BORSIC is 20% less than the density of the matrix alone.

The axial elastic modulus of Beta III-BORSIC composites was determined as a function of test temperature by the free-free beam technique. The data, presented in Fig. 4.49, indicate that the modulus decreases from a value of  $35 \times 10^6$  psi at  $70^\circ\text{F}$  to  $31 \times 10^6$  psi at  $1200^\circ\text{F}$ . The composite elastic modulus is much less sensitive to temperature than most monolithic titanium alloys.

The tensile test data for composites fabricated using 5.7 mil BORSIC are presented in Table IV-VII. Only the Ti-6Al-4V matrix was used due to a lack of Beta III alloy foil of the thickness needed to produce composites with nearly 50% fiber content. Both the axial and transverse composite strengths are superior to those obtained with the 4.2 mil fiber. The axial strengths were, in every case but one, superior to that of the unreinforced matrix. The one exception, bonded at  $750^\circ\text{C}$ , was lower in strength due to the presence of large amounts of fiber breakage in the composite after fabrication. The bonding temperature was too low to permit the titanium to distribute the hot press load uniformly throughout the composite. Pressing at the higher temperatures alleviated this problem.

The transverse tensile strength of the 5.7 mil BORSIC composites is superior to that of the 4.2 mil fiber composites due to the lack of fiber splitting in the larger diameter fiber specimens. The composite mode of failure was altered to one consisting primarily of matrix and fiber-matrix interfacial rupture. These modes of failure predominated over the entire temperature range investigated,  $70$ - $1000^\circ\text{F}$ . The transverse composite tensile strength at  $1000^\circ\text{F}$  was still up to 33,000 psi.

The axial and transverse composite tensile fracture strains noted in Table IV-VII are approximately 0.5% and 0.38% respectively. The lack of a major difference between these values (for BORSIC-aluminum the difference is nearly a factor of two for most matrix alloys) may be of importance if cross ply composite configurations are desired. A large transverse failure strain can prevent  $90^\circ$  ply failure prior to total composite failure.

The transverse elastic modulus of the 5.7 mil fiber composites was greater than that reported in Table IV-VI for 4.2 mil fiber composites. This difference is not due, however, to the change in fiber diameter but rather to an accompanying change in matrix composition. The Ti6/4 matrix, used for the larger fiber composites, has a modulus of approximately  $16 \times 10^6$  psi as compared to that reported previously for the Beta III alloy,  $11 \times 10^6$  psi.

A Charpy impact specimen of Ti-6Al-4V containing 59% 5.7 mil BORSIC was impact tested at room temperature. The impact strength of this specimen was 436 in.-lbs/in.<sup>2</sup>.

#### 4.6 Conclusions

1. The transverse elastic modulus of BORSIC-aluminum composites is sensitive to the degree of composite consolidation and bonding and thus can be used as a measure for determining the integrity of these composites.

2. The dependence of transverse elastic modulus on constituent material properties and composite morphology is well described by existing formulations. These include the work of Chen and Lin, Adams and Tsai, and Adams and Doner.

3. The transverse tensile strength and transverse tensile failure strain of BORSIC-aluminum composites can be severely limited by low fiber transverse tensile strength.

4. The 5.6 mil boron and 5.7 mil BORSIC fibers have a significantly higher transverse tensile strength than 4.0 mil boron and 4.2 mil BORSIC. These higher fiber strengths have resulted in higher composite transverse strengths and failure strains for the large diameter fiber containing composites.

5. BORSIC-aluminum composites, having heat treatable aluminum alloy matrices can be significantly strengthened in the transverse orientation by heat treatment.

6. The dependence of the transverse tensile strength of BORSIC and boron aluminum composites on constituent material properties and composite structure is well described by the analysis of Chen and Lin, when longitudinal fiber splitting is not taking place. In the presence of fiber splitting, the composite strength can be calculated on the basis of a reduction in effective composite cross sectional area due to fiber failure.

7. Composite and fiber edge condition can severely effect the strength of transverse tensile specimens.

8. Radiographic techniques, which reveal the condition of the boron fiber core, provide a useful nondestructive inspection method for the examination of boron aluminum composite condition.

9. The addition of transverse reinforcements such as stainless steel fibers and titanium foils increase composite transverse strength significantly.

10. Dispersion hardened aluminum matrices such as sintered aluminum powder provide BORSIC-aluminum composites with superior elevated temperature strength and microstructural stability.

11. BORSIC reinforced titanium matrix composites exhibit elastic moduli and strength significantly superior to those of monolithic titanium alloys.



#### SECTION IV - REFERENCES

1. J. K. Mackenzie, "The Elastic Constants of a Solid Containing Spherical Poles", Proc. Roy. Soc., 63B, 2, 1950.
2. R. L. Coble and W. D. Kingery, "Effect of Porosity on Physical Properties of Sintered Alumina", J. Am. Cer. Soc., Vol. 39, p. 377, 1956.
3. E. M. Breinan and K. G. Kreider, "Axial Creep and Stress Rupture of Boron Aluminum Composites", Metallurgical Trans., Vol. 1, Jan. 1970.
4. M. Basche, F. Galasso, and R. Fanti, "Preparation and Properties of Silicon Carbide Coated Fibers", Fiber Science and Technology, Vol. 1, p. 19, 1968.
5. D. Hartog, Mechanical Vibration, McGraw Hill, 1956.
6. S. Spinner and R. Valore, J. of Research of the National Bureau of Std., Vol. 6, p. 459, 1958.
7. S. Spinner, Reichard and Tefft, J. of Research of the National Bureau of Std., Vol. 64A, p. 147, 1960.
8. S. Spinner and G. W. Cleek, J. of App. Phys., Vol. 31, p. 1407, 1960.
9. H. J. Stokes, J. of Scientific Inst., Vol. 37, p. 117, 1960.
10. P. E. Chen and J. M. Lin, "Transverse Properties of Fibrous Composites", Materials Research and Standards, p. 29, August 1969.
11. D. F. Adams and D. R. Doner, "Transverse Normal Loading of a Unidirectional Composite", J. Composite Materials, Vol. 1, p. 152, 1967.
12. D. Adams, S. Tsai, J. Comp. Materials, 368, 1969.
13. A. Zecca, D. Hay, J. Comp. Materials, 556, 1970.
14. J. Ashton, J. Halpin and P. Petit, "Primer on Composite Materials Analysis", Technomic Press, 1969.
15. K. R. Van Horn, "Aluminum", American Society for Metals, Vol. 2, 1967.
16. A. Metcalfe and G. Schmitz, Gas Turbine Conference, Cleveland, March 1969.
17. E. Ellison and D. Boon, J. of Less Common Metals, Vol. 13, p. 103, 1967.
18. D. Adams, "Inelastic Analysis of a Unidirectional Composite Subjected to Transverse Normal Loading", J. Com. Materials, Vol. 4, p. 310, 1970.
19. K. Kreider and M. Marciano, "Mechanical Properties of BORSIC-Aluminum Composites", Trans. AIME, Vol. 243, p. 1279, 1969.

#### SECTION IV - REFERENCES (Cont'd)

20. J. Cristian and J. D. Forest, "Development and Application of High Matrix Strength Al-Boron", ASM Tech. Report No. P9-55.2.
21. I. Toth, "Tensile and Fatigue Behavior of Boron Reinforced Aluminum Composites", Presented at Spring 1970 AIME Meeting.
22. C. W. Rogers, AFML Contract AF33(615)-527, Seventh Quarterly Report, March 1968.
23. R. J. Towner, "Atomized Powder Alloys of Aluminum", Metals Progress, p. 70, May 1968.
24. E. Schiel and Y. Masuda, "Über das eutektische Gefüge von Al-Cu und Al-Fe Legierungen bei starken Unterkühlungen", Aluminum, p. 51, Feb. 1955.
25. P. L. Mehr, Private Correspondence, Alcoa Research Laboratories, New Kensington, Pa.
26. F. E. Wawner, Modern Composite Materials, edited by Broutman and Crock, Addison-Wesley, 1967.
27. R. Adler and Hammond, App. Phys. Letters 14 354, 1969.
28. V. Peterson, et al, AIAA Paper No. 68-976, and Crucible Steel Data Sheet.



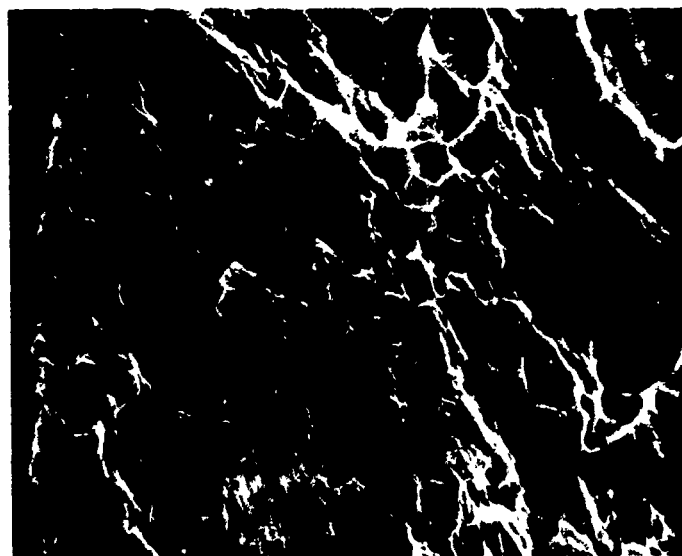
Reproduced from  
best available copy.

100X



350X

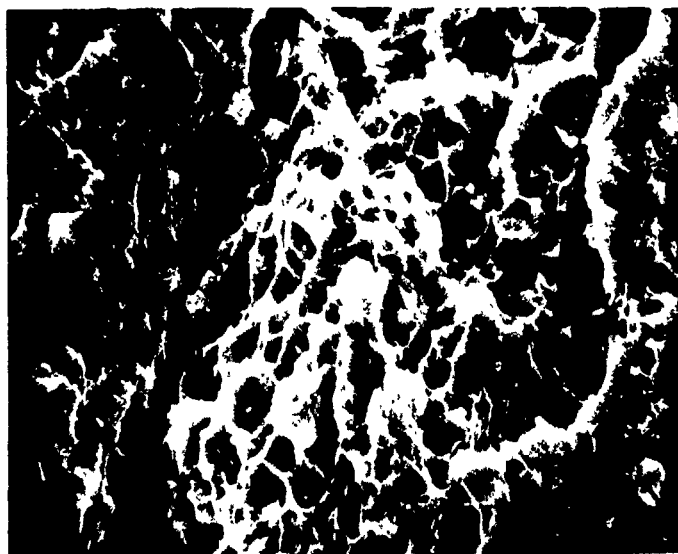
FIGURE 4-1 ALUMINUM - 7% Si PLASMA SPRAYED AND FOIL MATRIX MATERIAL



a. 6061 MATRIX

1500X

FOIL  $\longleftrightarrow$  PLASMA SPRAY



b. 2024 MATRIX

1500X

FIGURE 4-2. ALUMINUM ALLOY MATRIX FRACTURE SURFACE

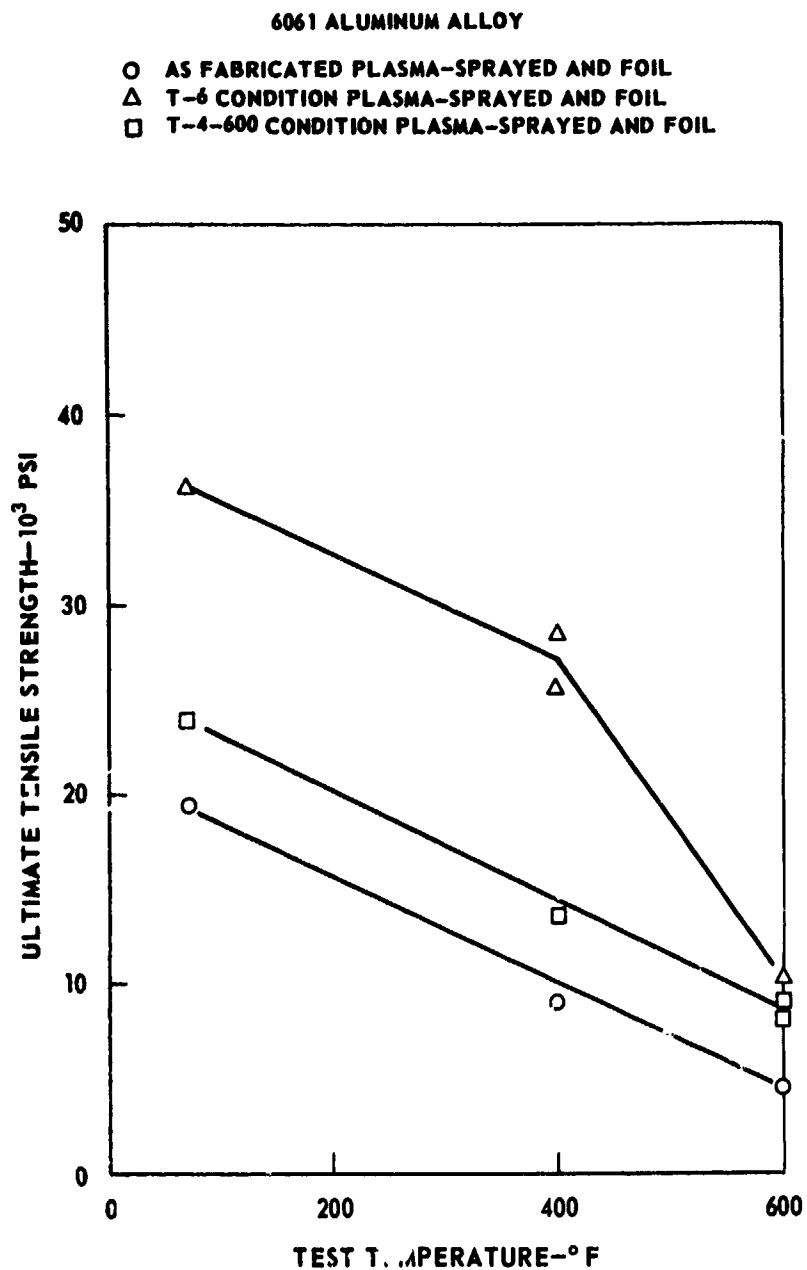


FIGURE 4-3. ULTIMATE TENSILE STRENGTH OF 6061 MATRIX AS  
A FUNCTION OF TEMPERATURE

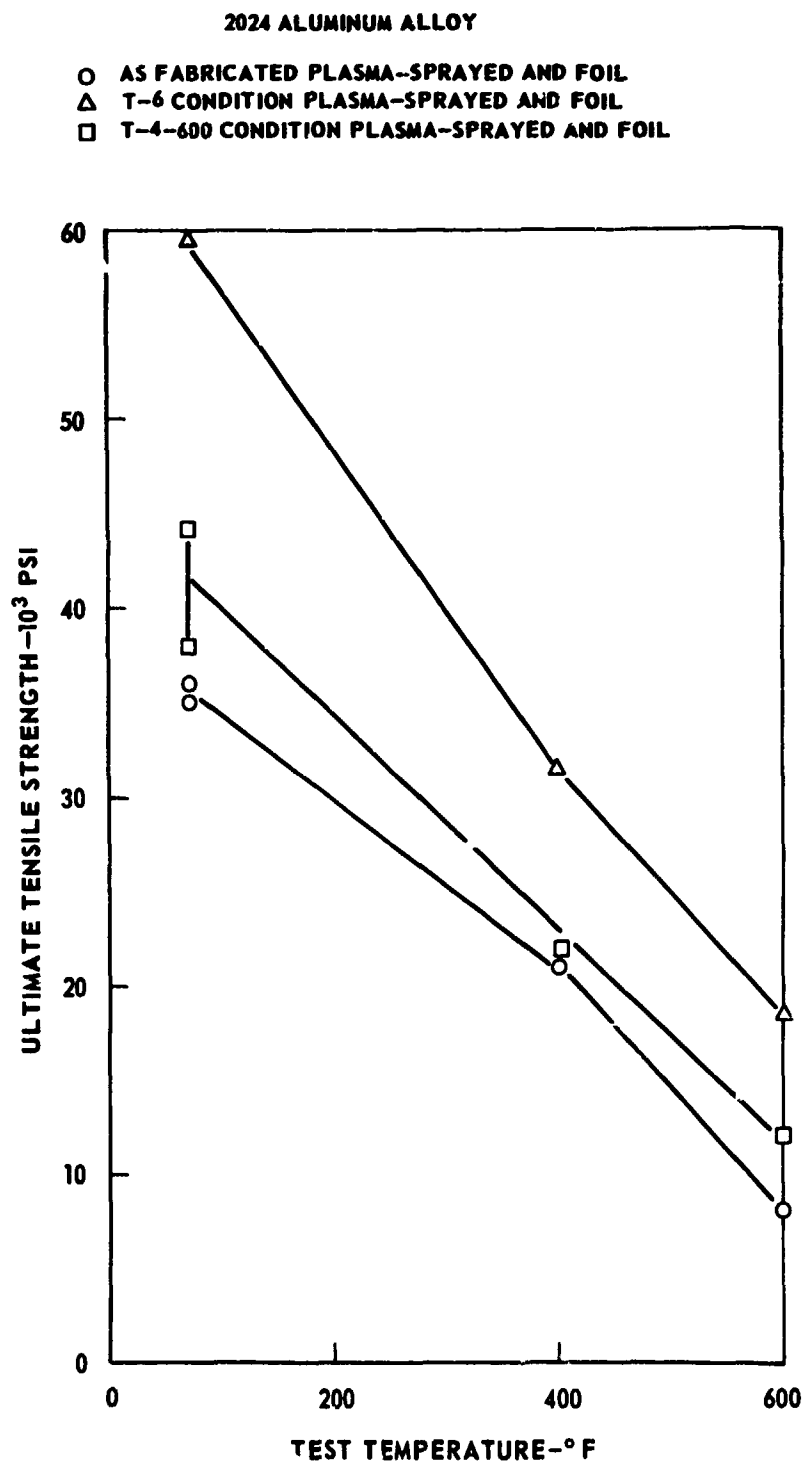


FIGURE 4-4. ULTIMATE TENSILE STRENGTH OF 2024 MATRIX AS A FUNCTION OF TEMPERATURE

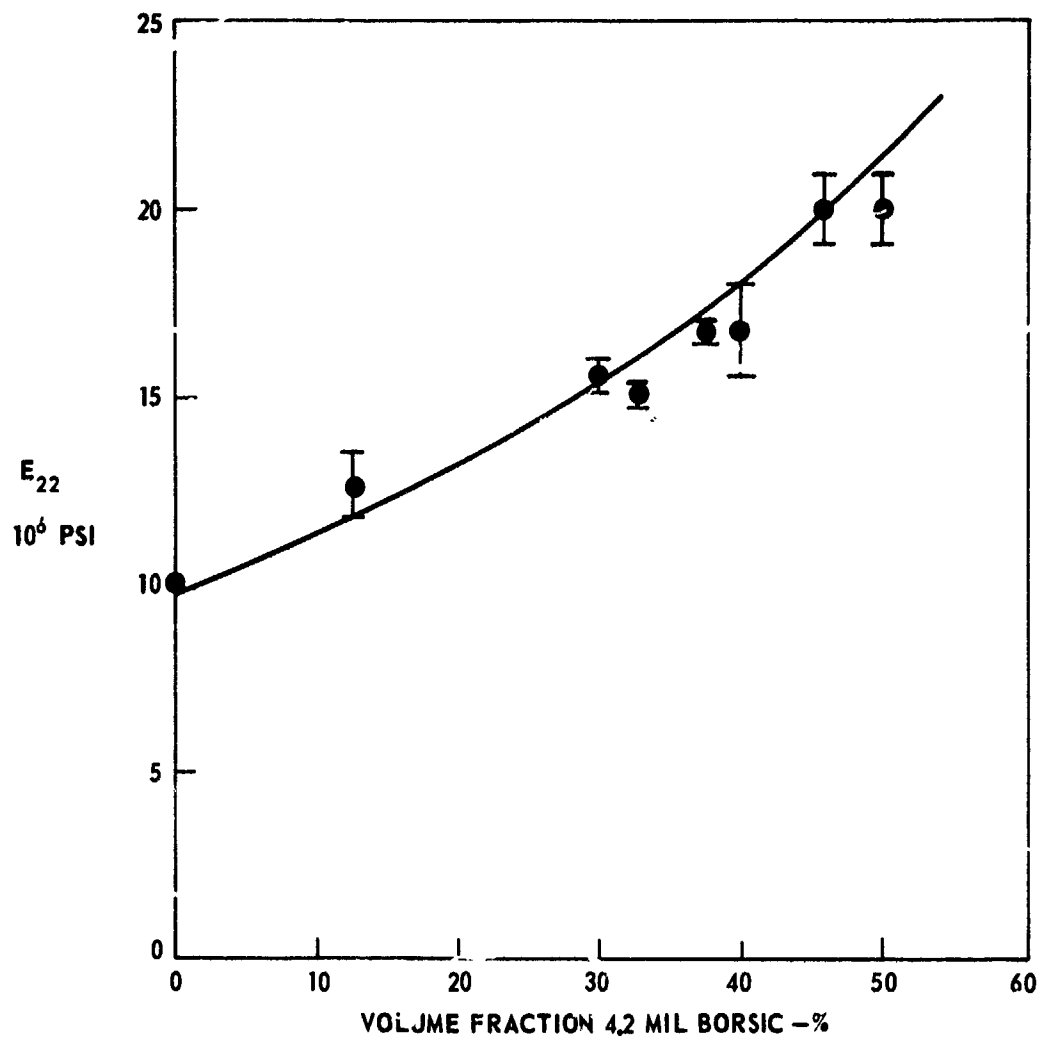


FIGURE 4-5. COMPOSITE TRANSVERSE ELASTIC MODULUS

- 46% 4.2 mil, BORSIC - 6061 DYNAMIC MODULUS DETERMINATION
- 46% 4.2 mil, BORSIC - 6061 TENSILE TEST MODULUS DETERMINATION
- × 46% 4.2 mil, BORSIC - 2024 TENSILE TEST MODULUS DETERMINATION
- △ 2024-2219 MATRIX MATERIAL - NO FIBER

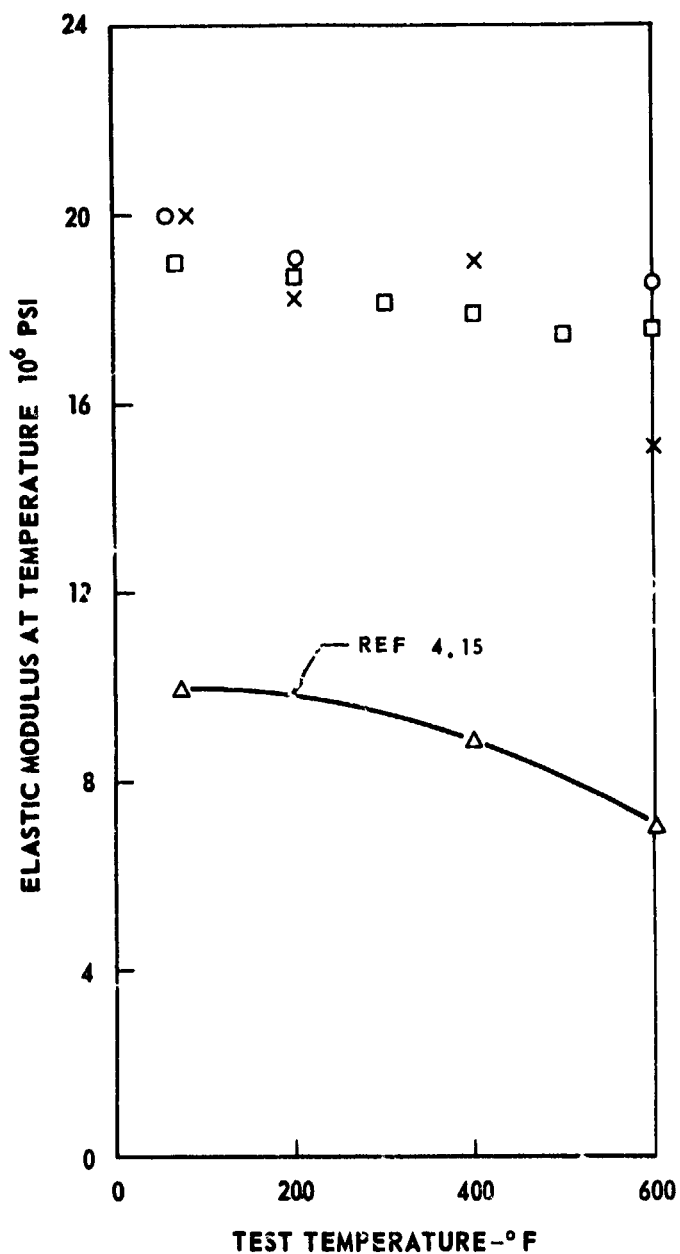


FIGURE 4-6. TRANSVERSE MODULUS AS A FUNCTION OF TEMPERATURE



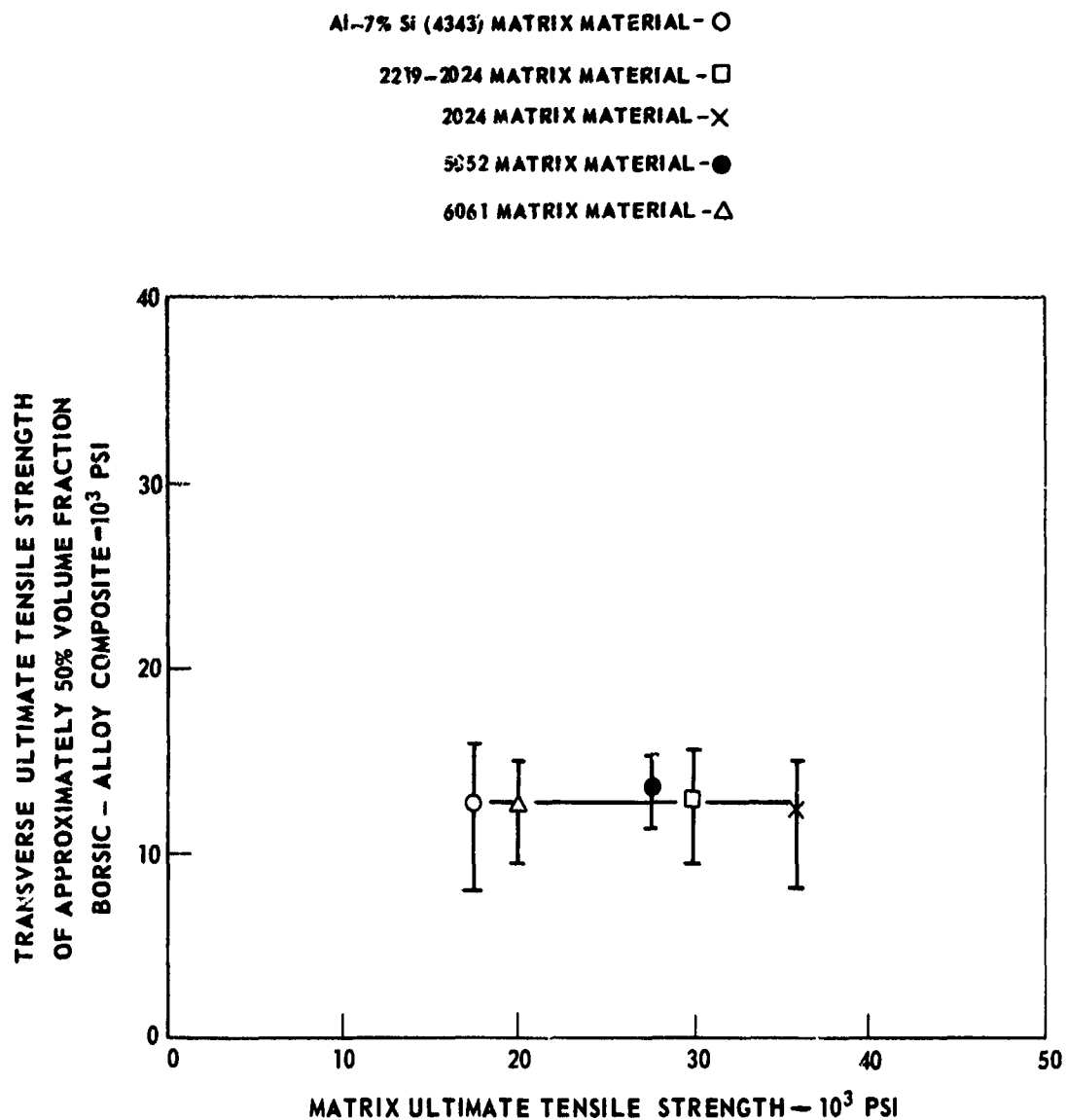


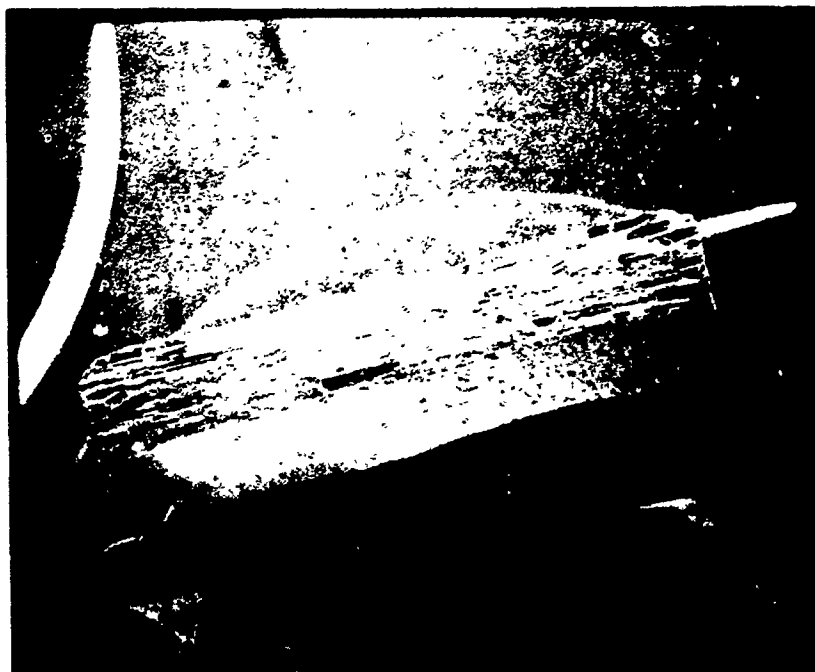
FIGURE 1-7. TRANSVERSE STRENGTH AS A FUNCTION OF MATRIX STRENGTH  
FOR 4.2 MIL BORSIC-ALUMINUM



Reproduced from  
best available copy.

36X

FIGURE 4-8. FRACTURE SURFACE OF A 50 % VOLUME FRACTION 4.2 MIL BORSIC®  
- 6061 COMPOSITE 90° TENSILE SPECIMEN



12X

Reproduced from  
best available copy.



50X

FIGURE 4-9 TRANSVERSE TENSILE FRACTURE OF 4.2 mil BORSIC - 1100

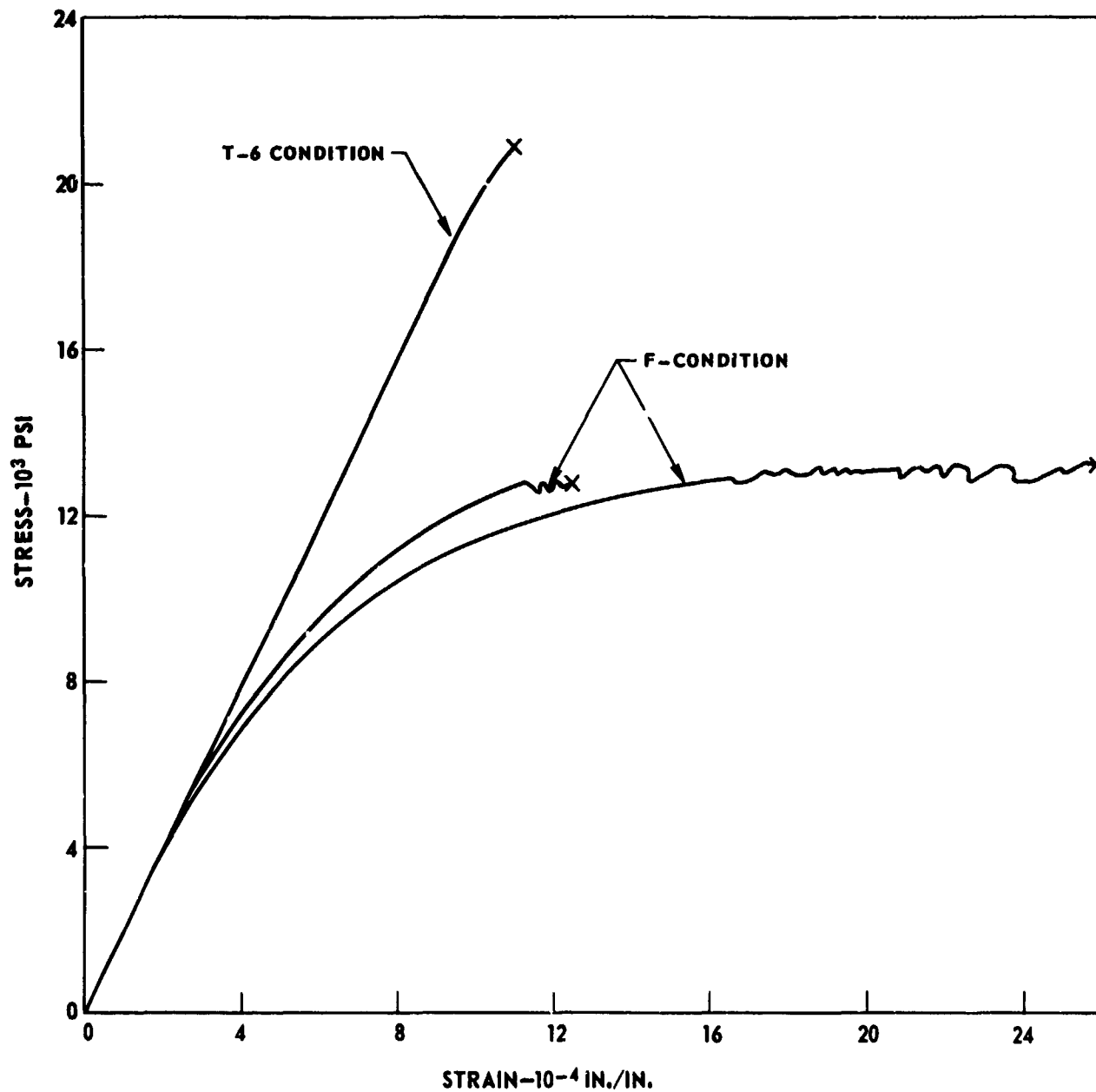


FIGURE 4-10. 46 v/o 4.2 MIL BORSIC - 6061 ALUMINUM 90° TENSILE STRESS STRAIN CURVES

## 46% VOL. FRACTION BORSIC - 6061 AL ALLOY

○ AS FABRICATED CONDITION  
△ T-6 CONDITION

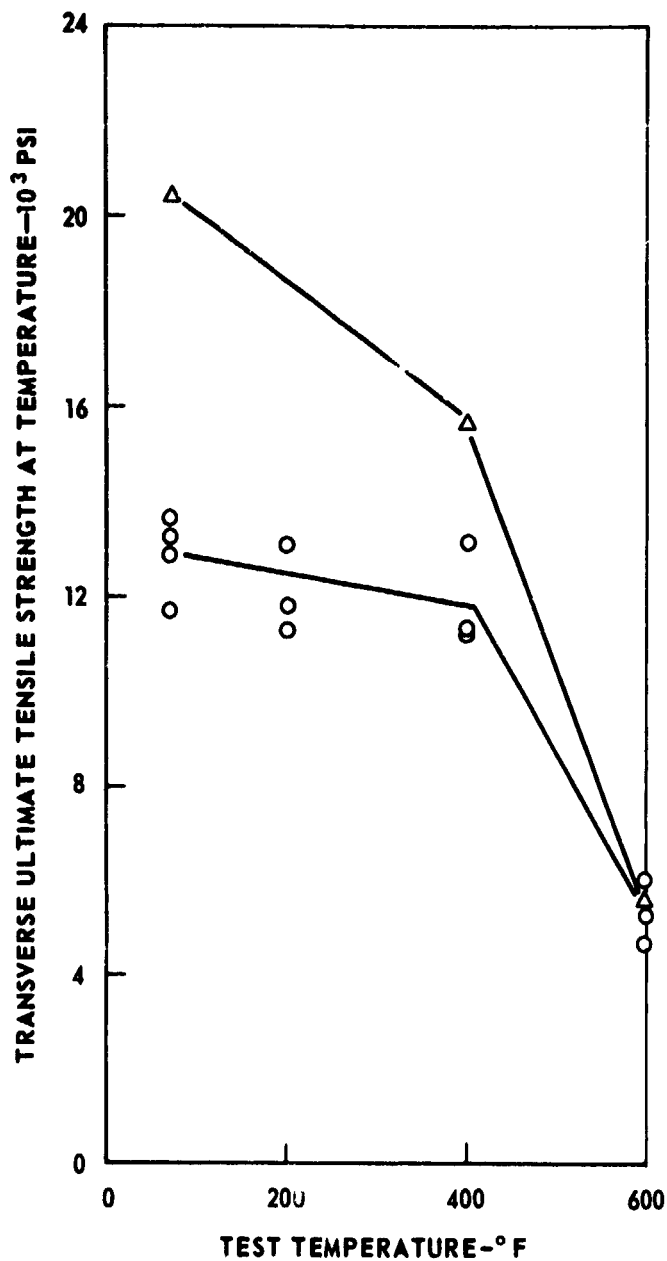


FIGURE 4-11 TRANSVERSE TENSILE STRENGTH OF 4.2 MIL BORSIC-6061 ALUMINUM AS A FUNCTION OF TEST TEMPERATURE

## 46% VOL. FRACTION BORSIC - 2024 AL ALLOY

○ - AS FABRICATED CONDITION

△ - T-6 CONDITION

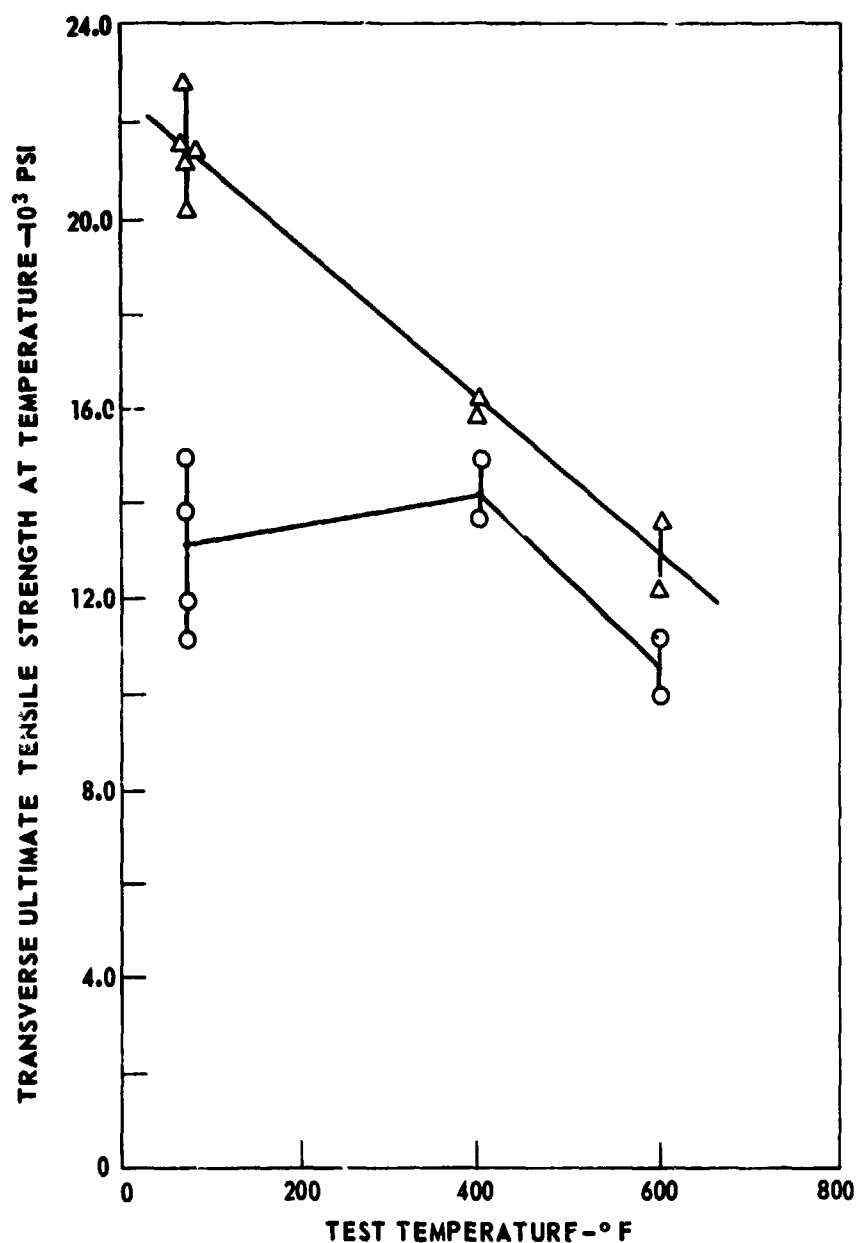


FIGURE 4-12. TRANSVERSE TENSILE STRENGTH OF 4.2 MIL BORSIC-2024 ALUMINUM AS A FUNCTION OF TEST TEMPERATURE

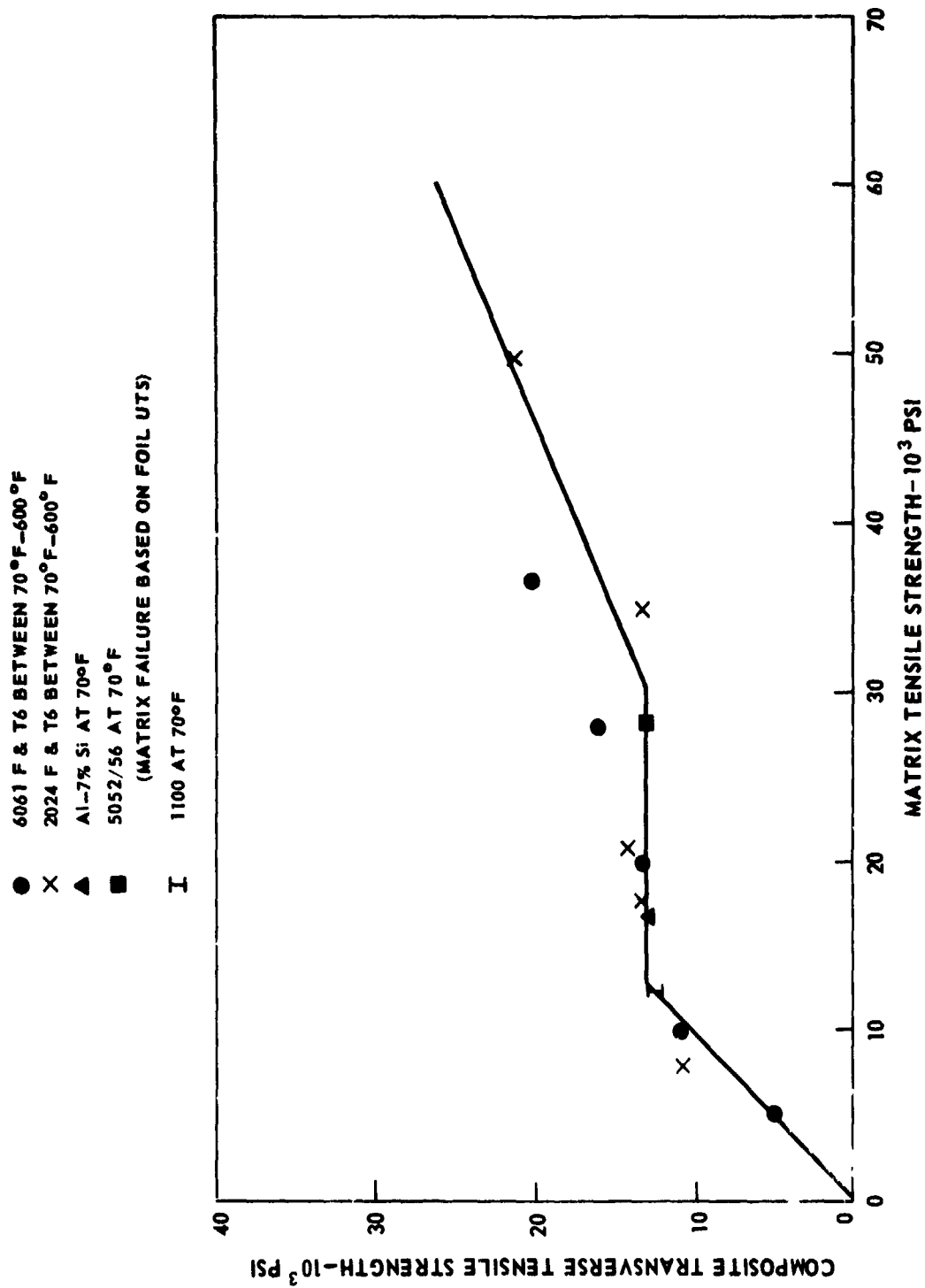


FIGURE 4-13. TRANSVERSE TENSILE STRENGTH OF 50% BY VOLUME 4.2 MIL BORSIC-ALUMINUM

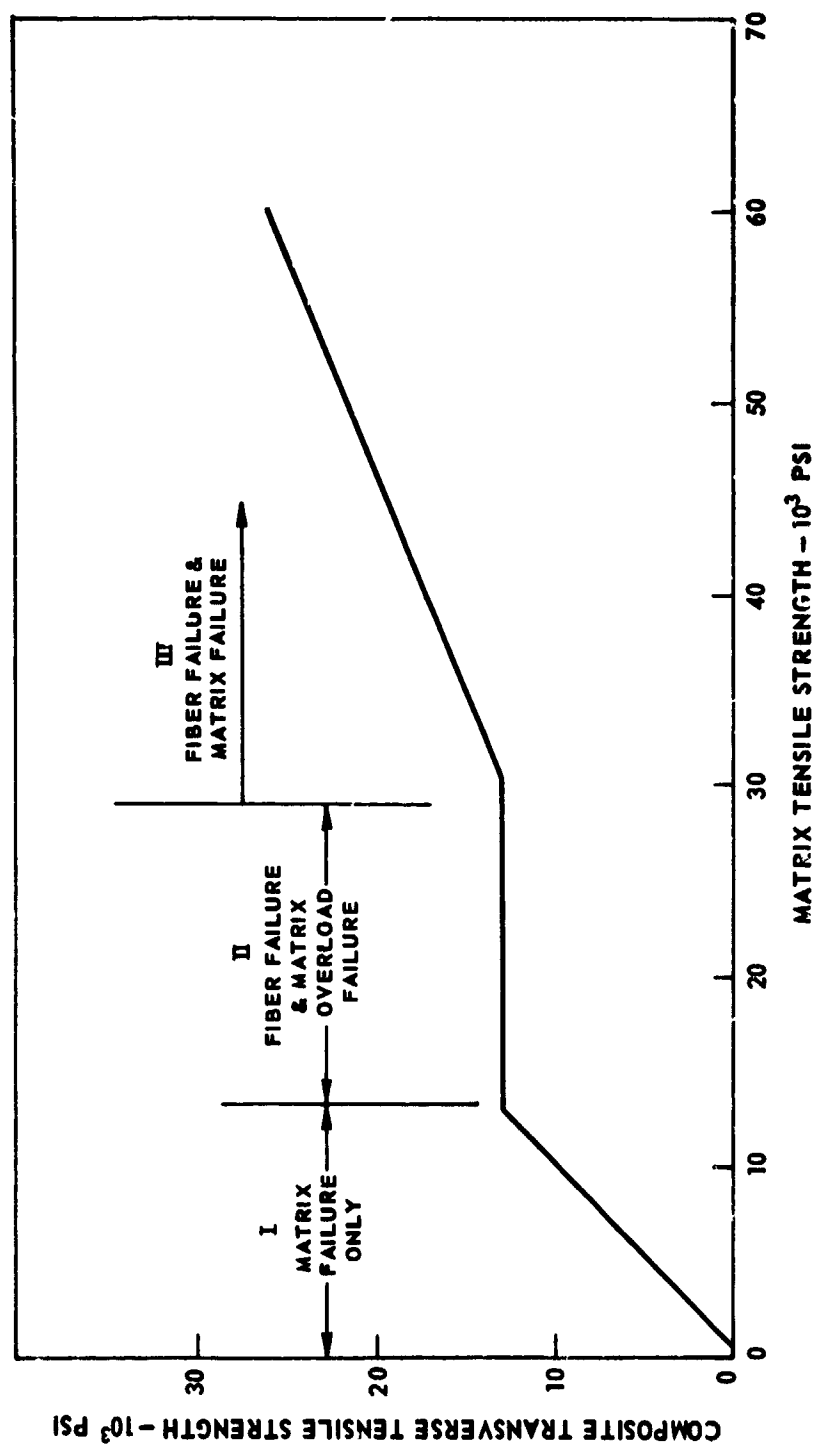


FIGURE 4-14. TRANSVERSE TENSILE STRENGTH OF 50% BY VOLUME 4.2 MIL BORSIC-ALUMINUM



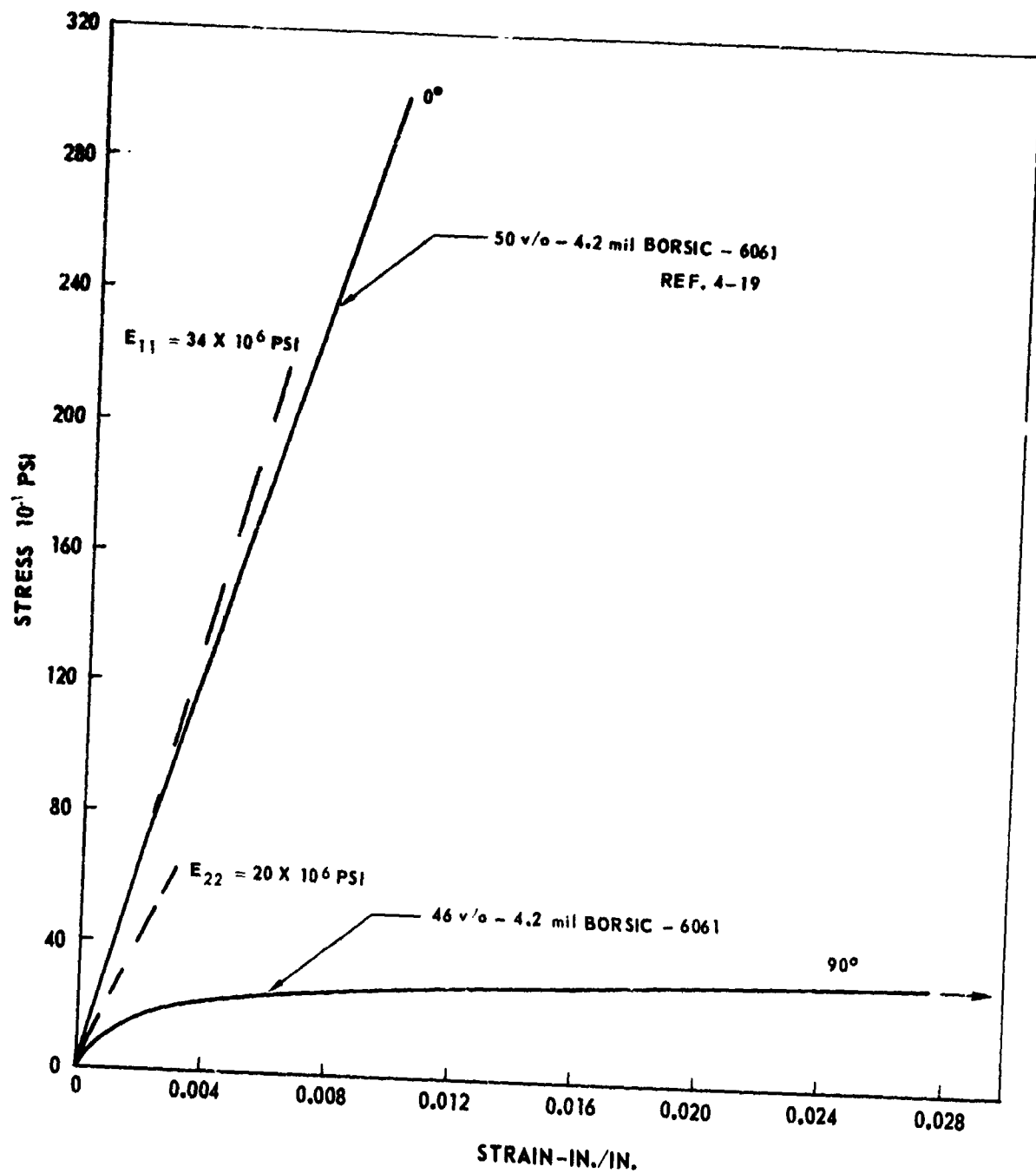
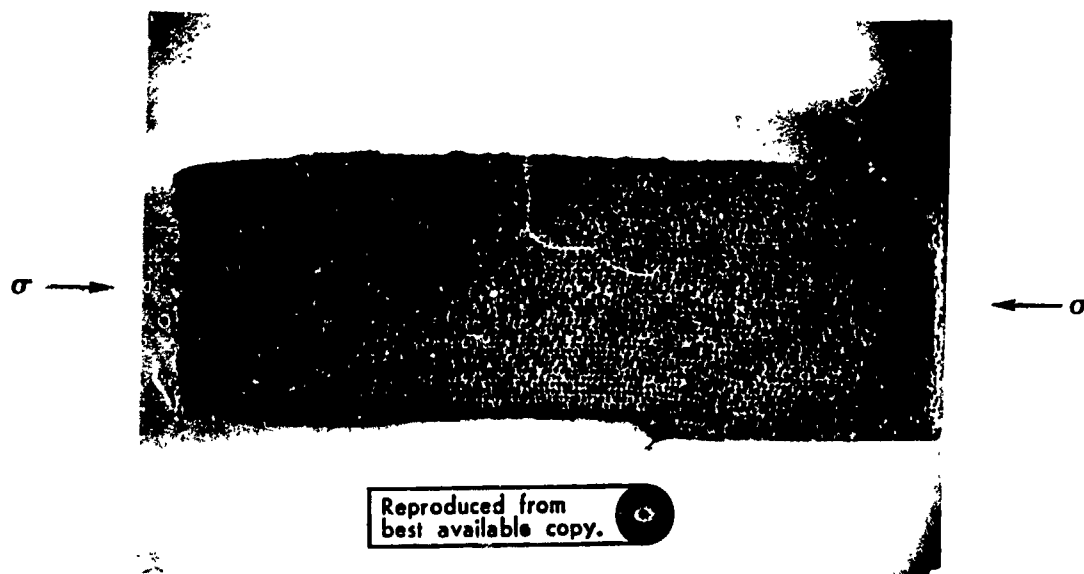


FIGURE 4-15. COMPRESSIVE STRESS STRAIN CURVES FOR AXIAL AND 90° FIBER REINFORCEMENT



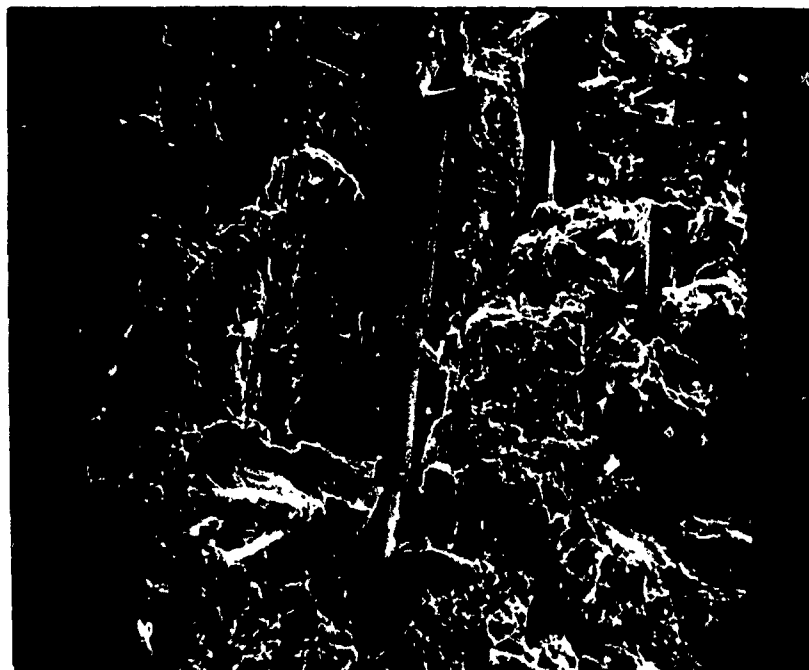
6X

FIGURE 4-16. TRANSVERSE COMPRESSION SPECIMEN OF BORSIC-6061  
ALUMINUM AFTER COMPLETION OF TEST



Reproduced from  
best available copy.

250 $\mu$



50 $\mu$

FIGURE 4-17. FRACTURE SURFACE OF A TRANSVERSE COMPRESSION SPECIMEN

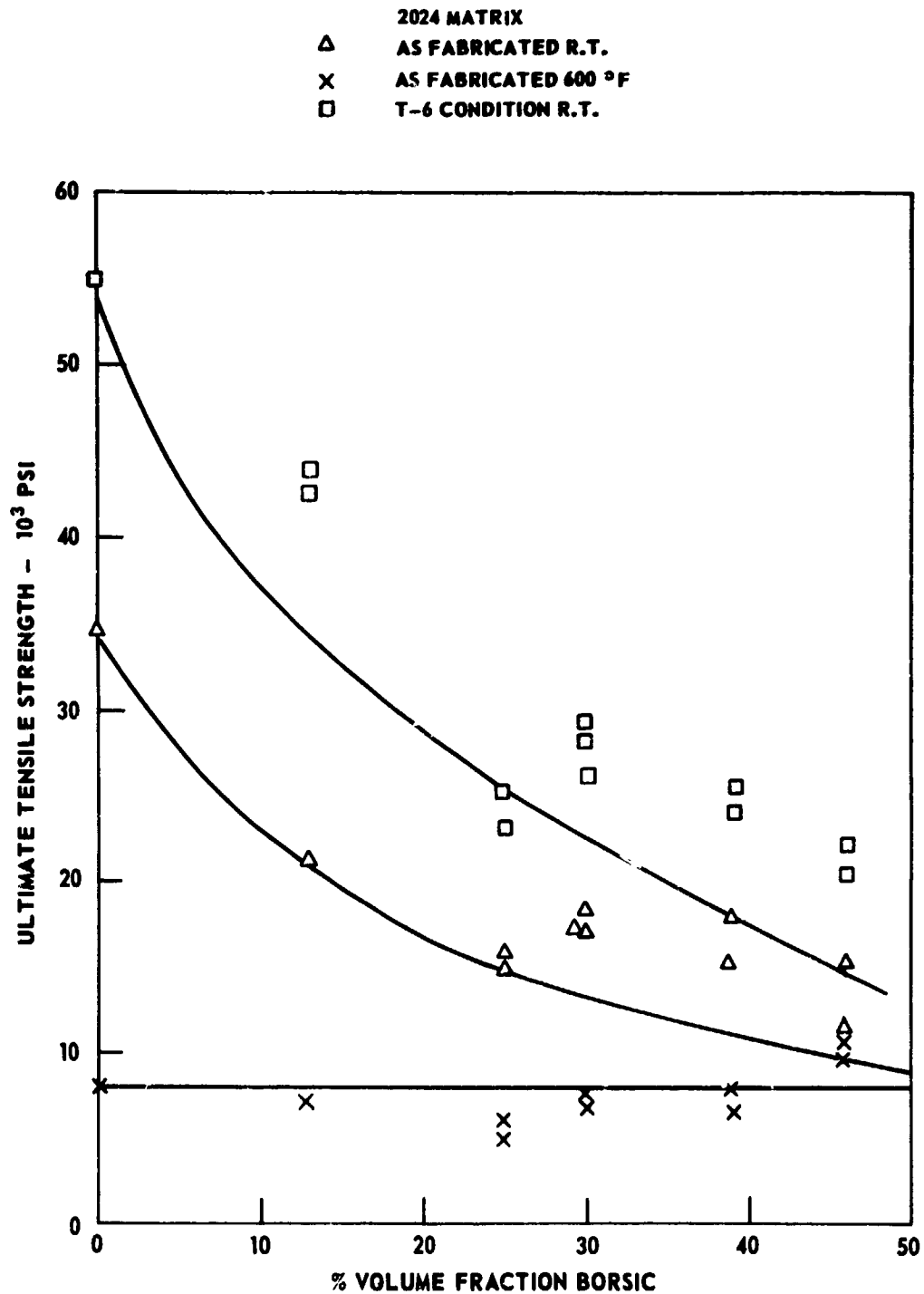
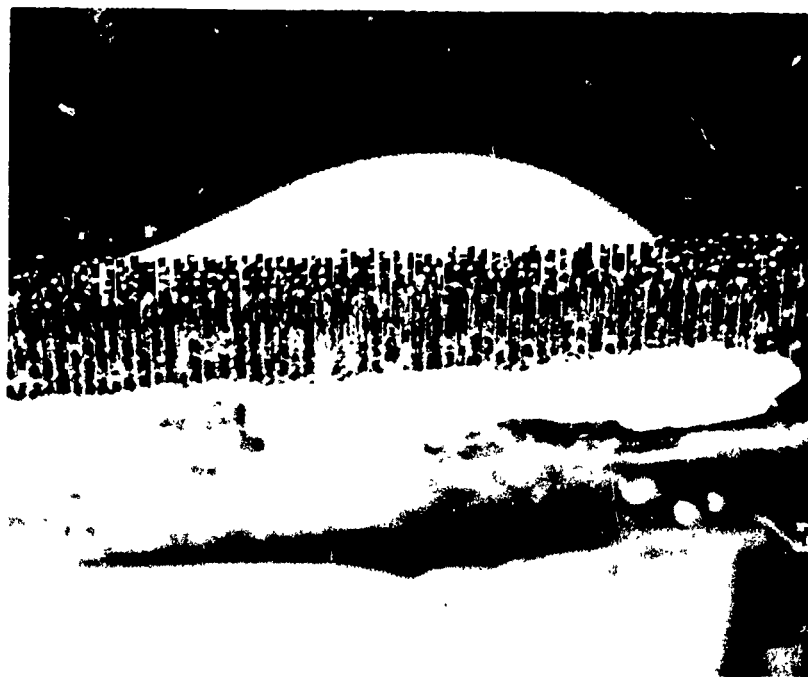


FIGURE 4-18. TRANSVERSE TENSILE STRENGTH AS A FUNCTION OF VOLUME FRACTION 4.2 MIL BORSIC FIBER



10X

Reproduced from  
best available copy.



CUT FIBERS

30X

FIGURE 4-19. 4.2 MIL BORSIC<sup>®</sup> FIBERS CUT BY A DIAMOND ABRASIVE  
CUTOFF WHEEL AND MATRIX

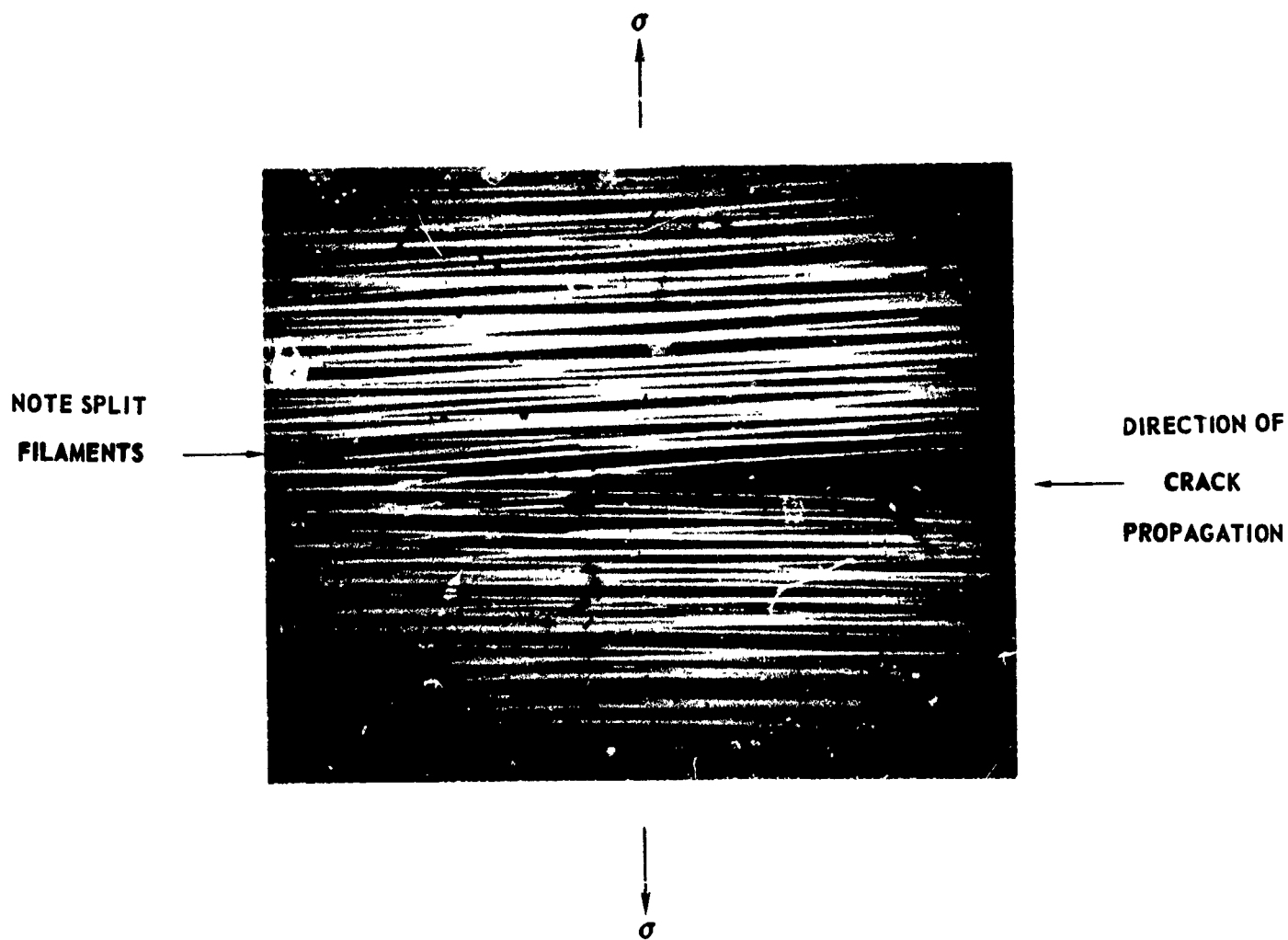
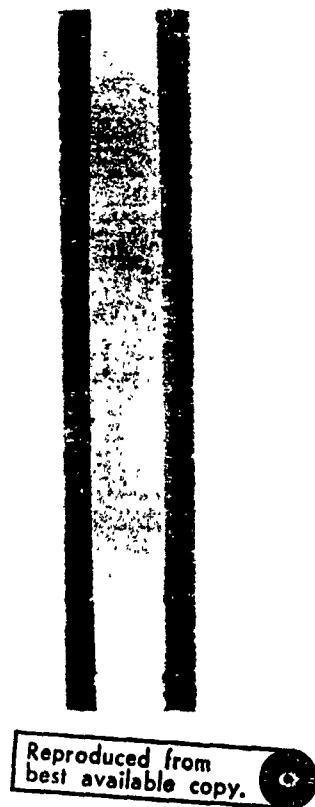


FIGURE 4-20. RADIOGRAPH OF CRACK TIP IN 4.2 MIL BORSIC-6061  
TRANSVERSE TENSILE SPECIMEN



Reproduced from  
best available copy.

FIGURE 4-21. 90° 4.2 MIL BORSIC-AL TENSILE SPECIMEN WITH FREE FIBER ENDS

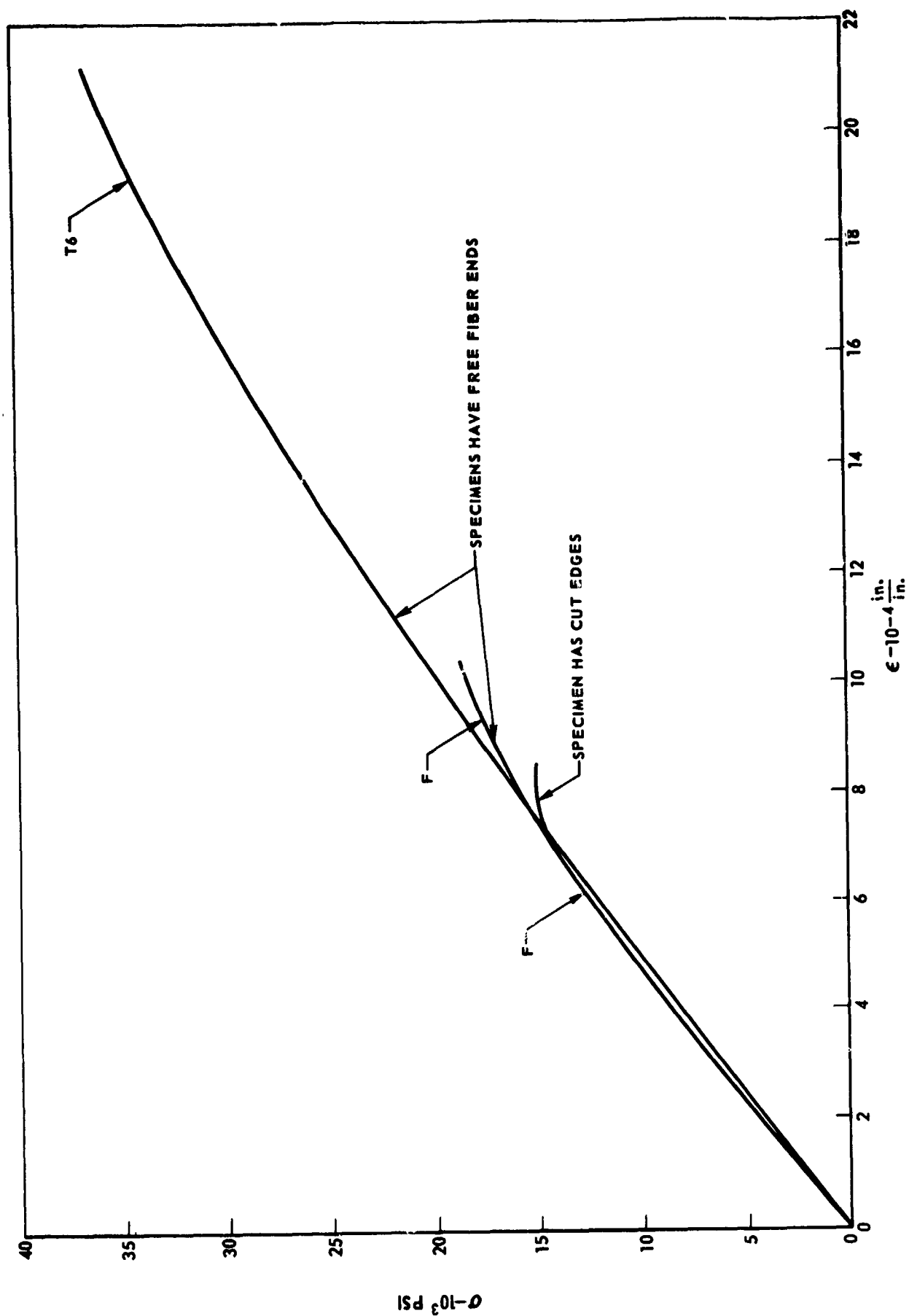


FIGURE 4-22. TRANSVERSE TENSILE TEST 46V/O 4.2 MIL BORSIC-2024 AL ALLOY



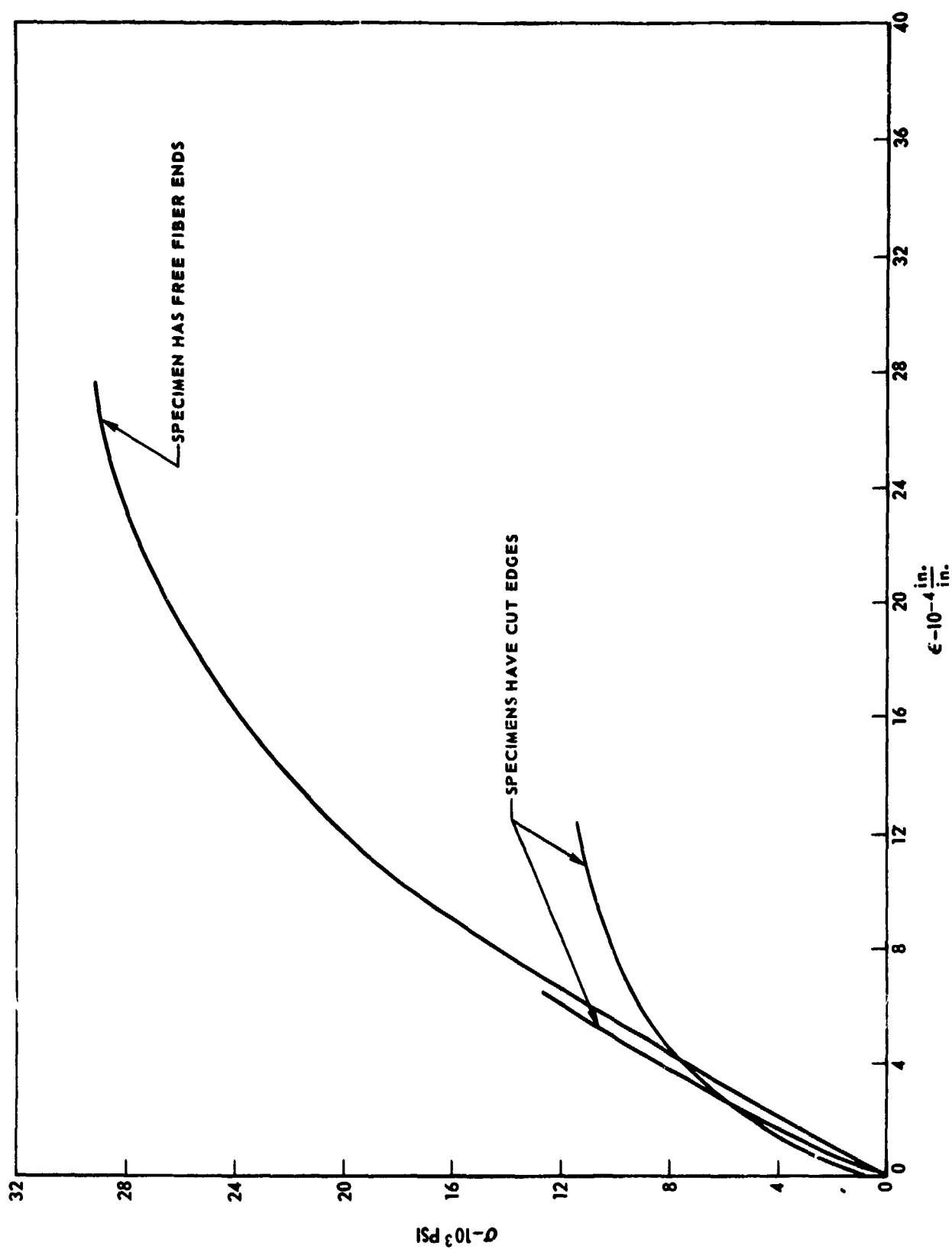


FIGURE 4-23. TRANSVERSE TENSILE TEST 46V/O 4.2 MIL BORSIC-5052/56 AL ALLOY

SPECIMENS HAVE FREE FIBER EDGES

MATRIX ALLOY

- = 5052/56
- X = 2024F
- O = 2024T6
- △ = 6061F

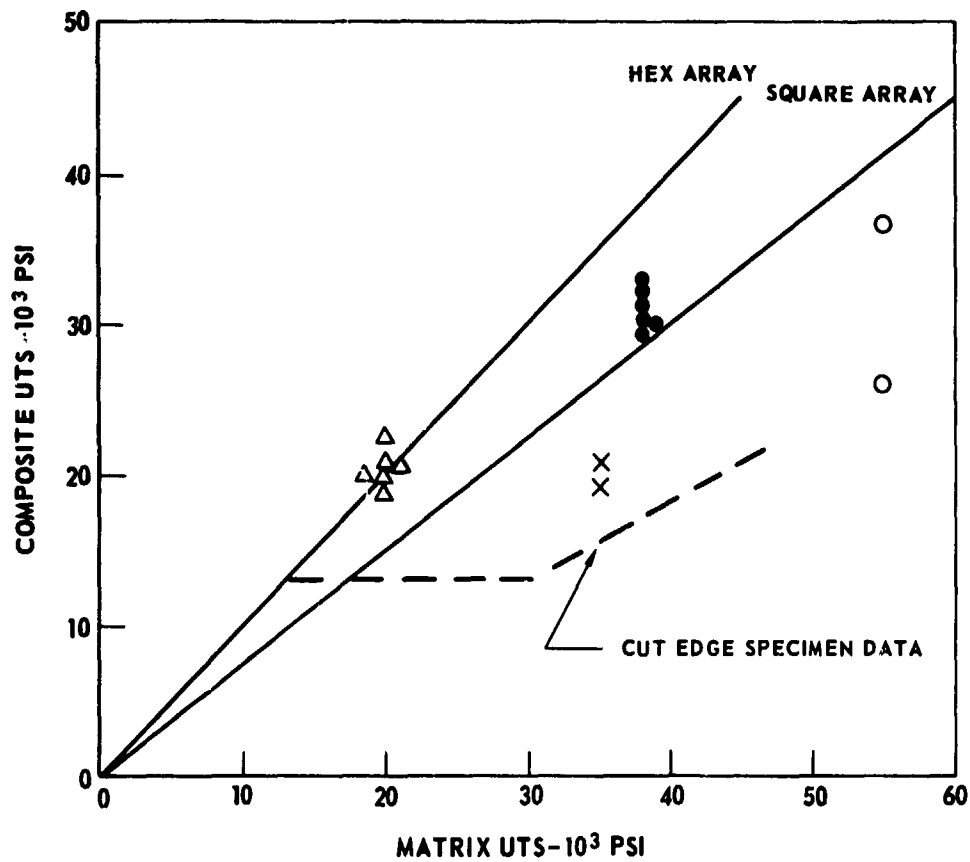
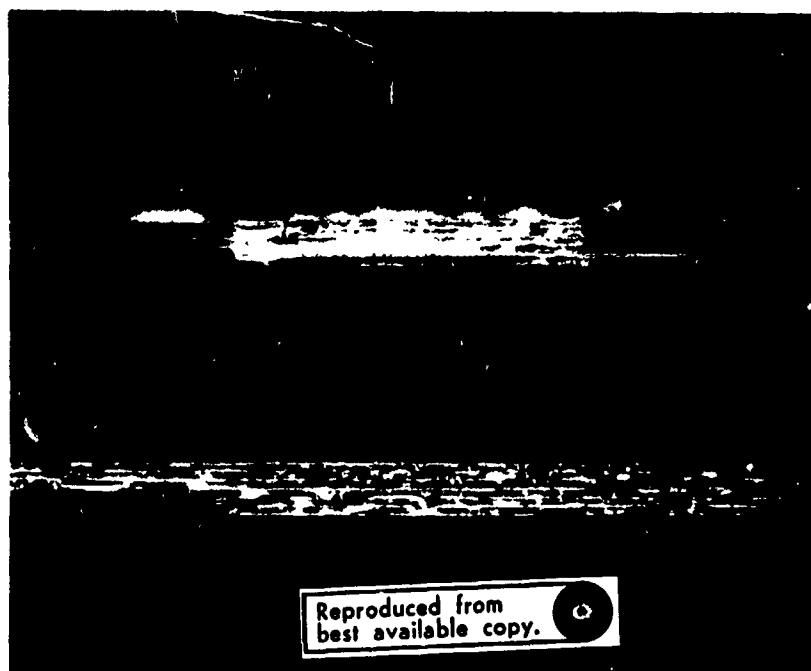
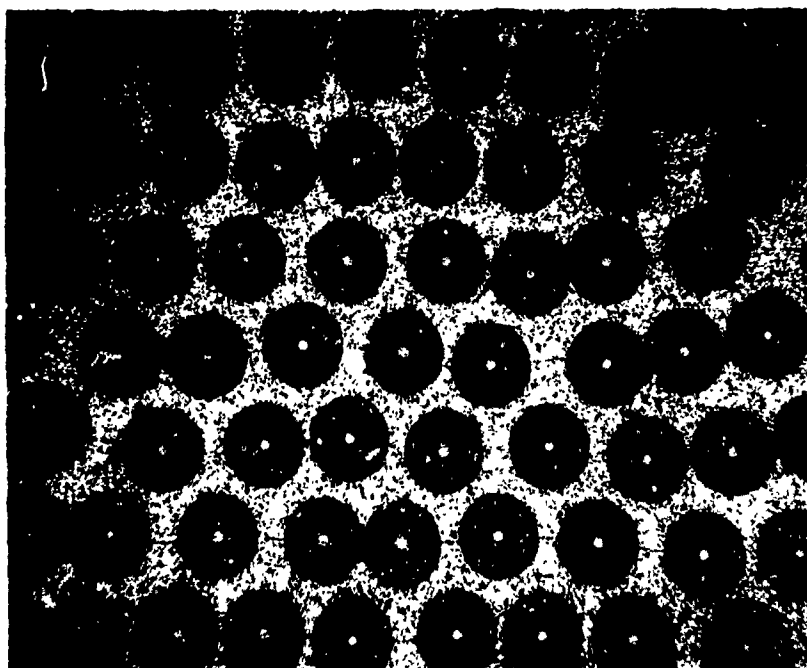


FIGURE 4-24. TRANSVERSE TENSILE STRENGTH OF 46 V/O 4.2 MIL BORSIC-ALUMINUM



8X

FIGURE 4-25. FRACTURE SURFACES OF FREE FIBER END (TOP)  
AND CUT EDGE (BOTTOM)  
SPECIMENS OF 50 V/O-4.2 MIL BORSIC-5052/56



100X

FIGURE 4-26. 51 V/O 4.2 MIL BORSIC - S.A.P.

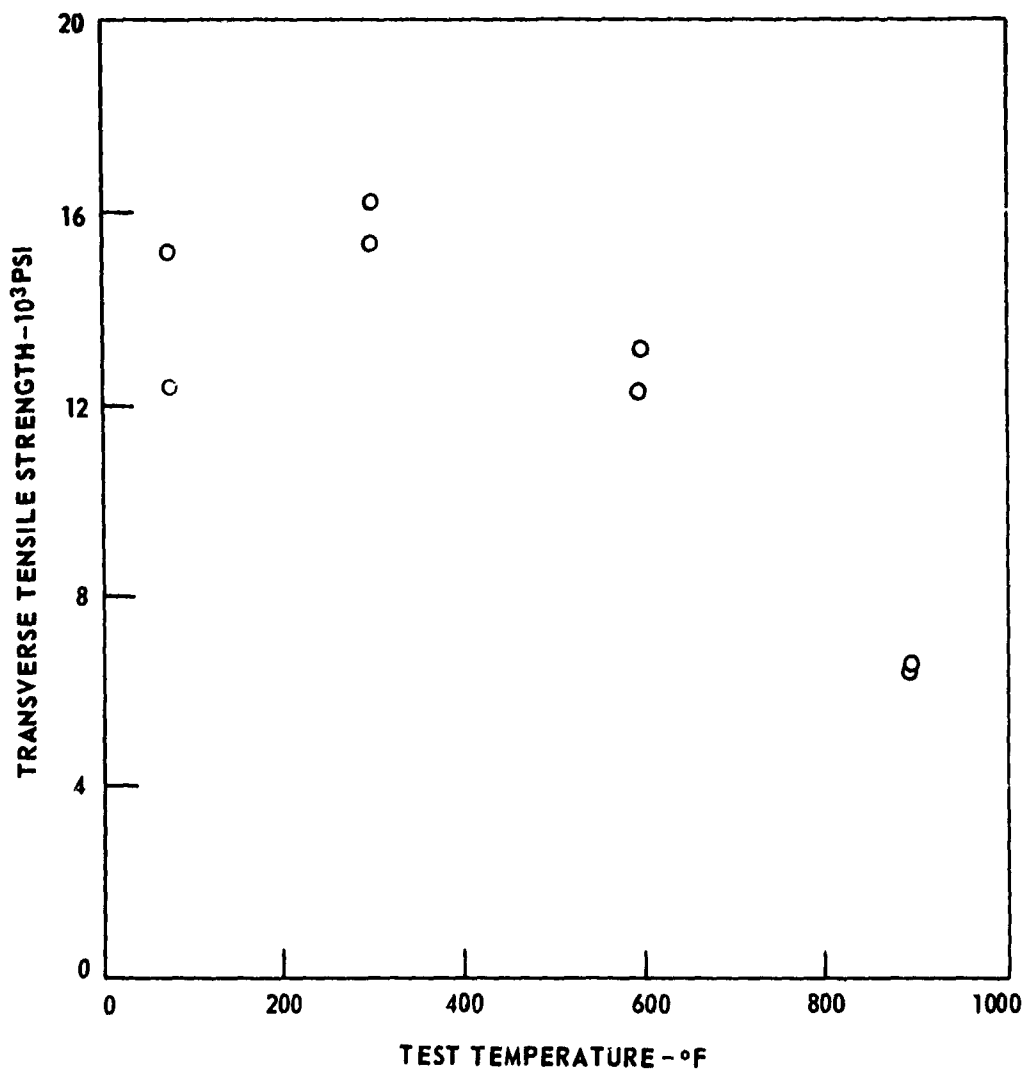


FIGURE 4-27. TRANSVERSE TENSILE STRENGTH OF 51 v/o 4.2 MIL BORSIC-S.A.P.

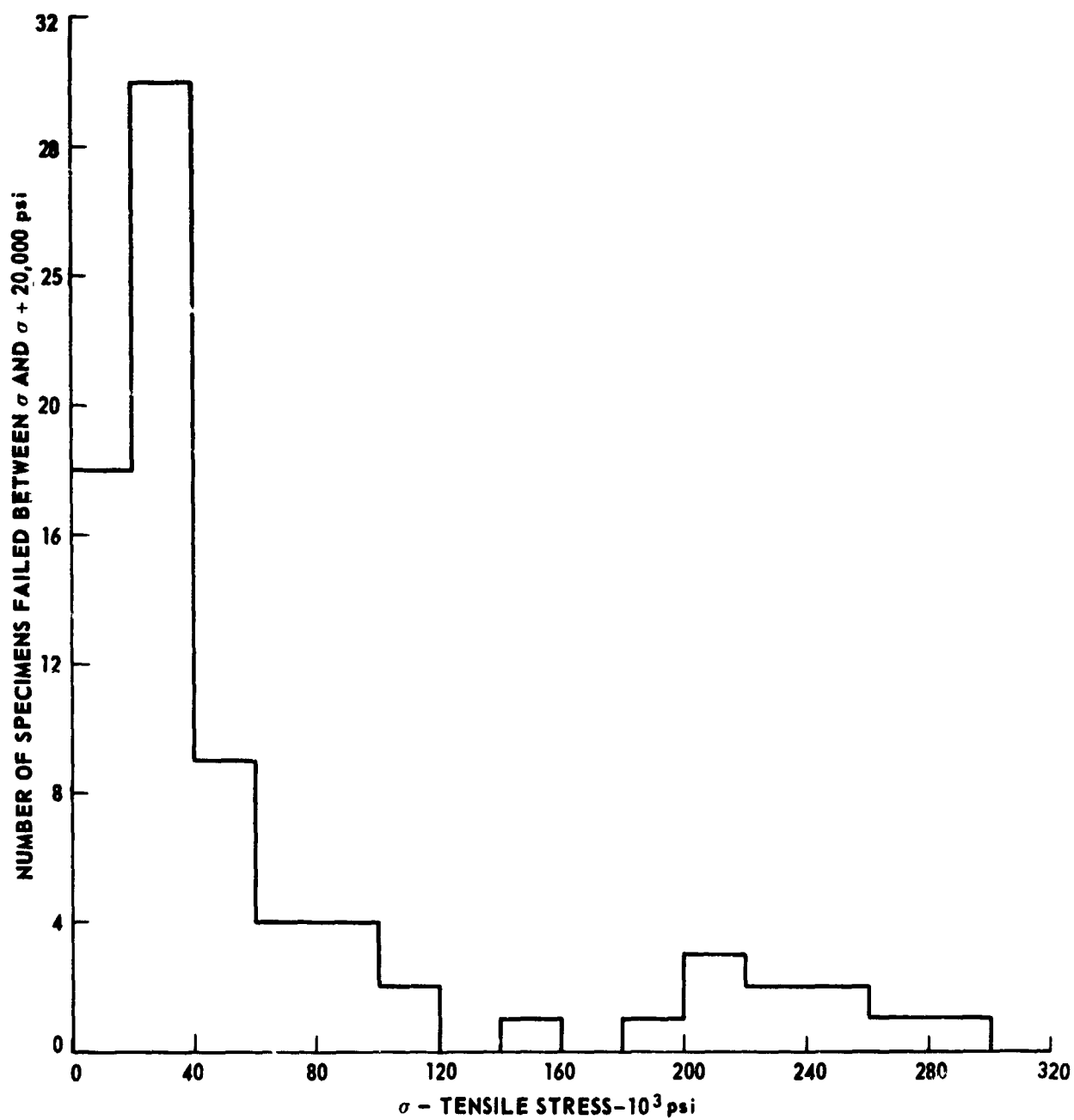


FIGURE 4-28. STRENGTH DISTRIBUTION OF 4.2 MIL BORSIC FIBER TESTED IN DIAMETRAL COMPRESSION



Reproduced from  
best available copy.

50μ

FIGURE 4-29. FRAGMENTS OF A BORSIC FIBER FRACTURED UNDER DIAMETRAL COMPRESSION

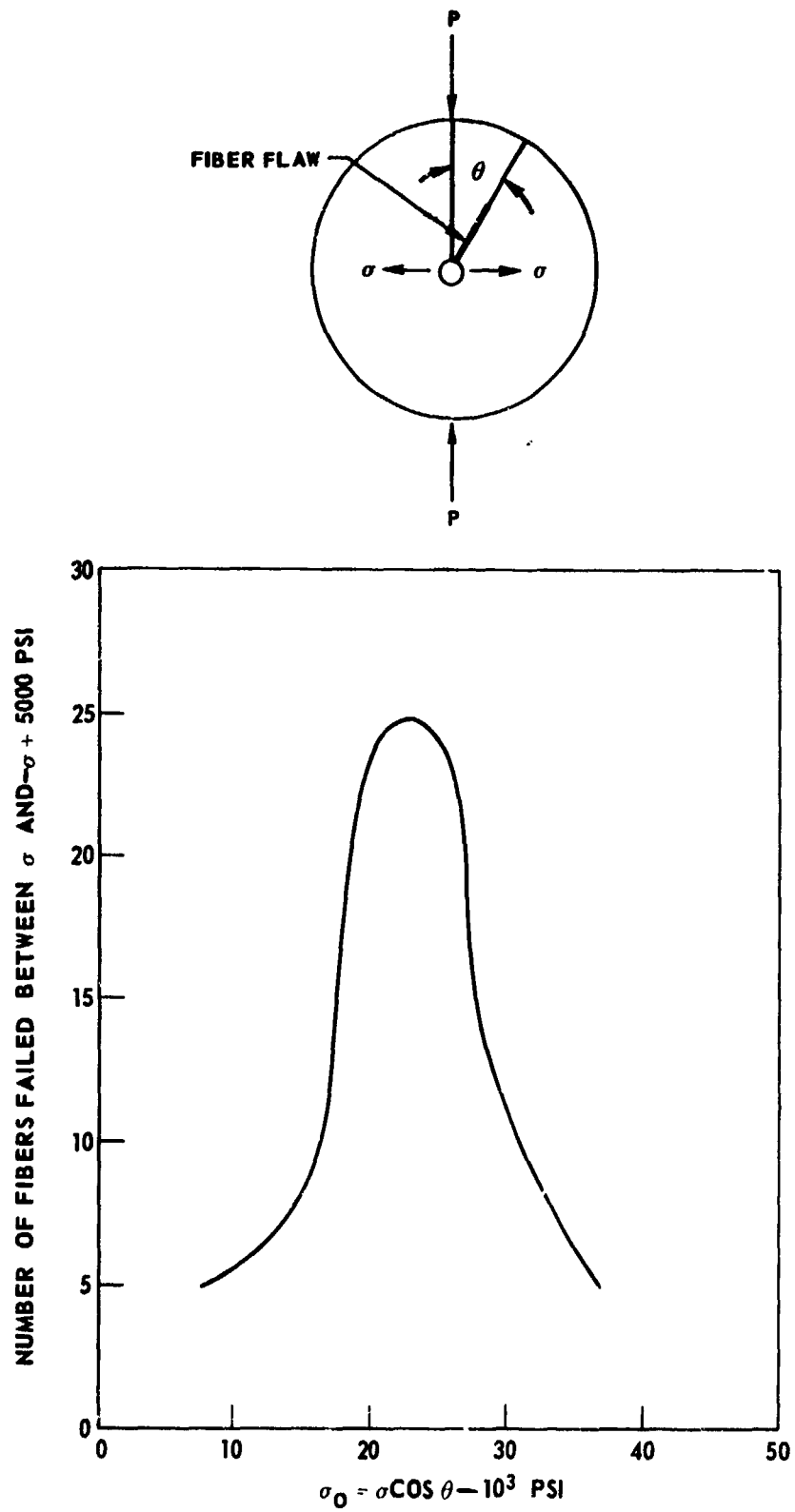


FIGURE 4-30. FIBER FRACTURE USING THE FIBER FLAW MODEL



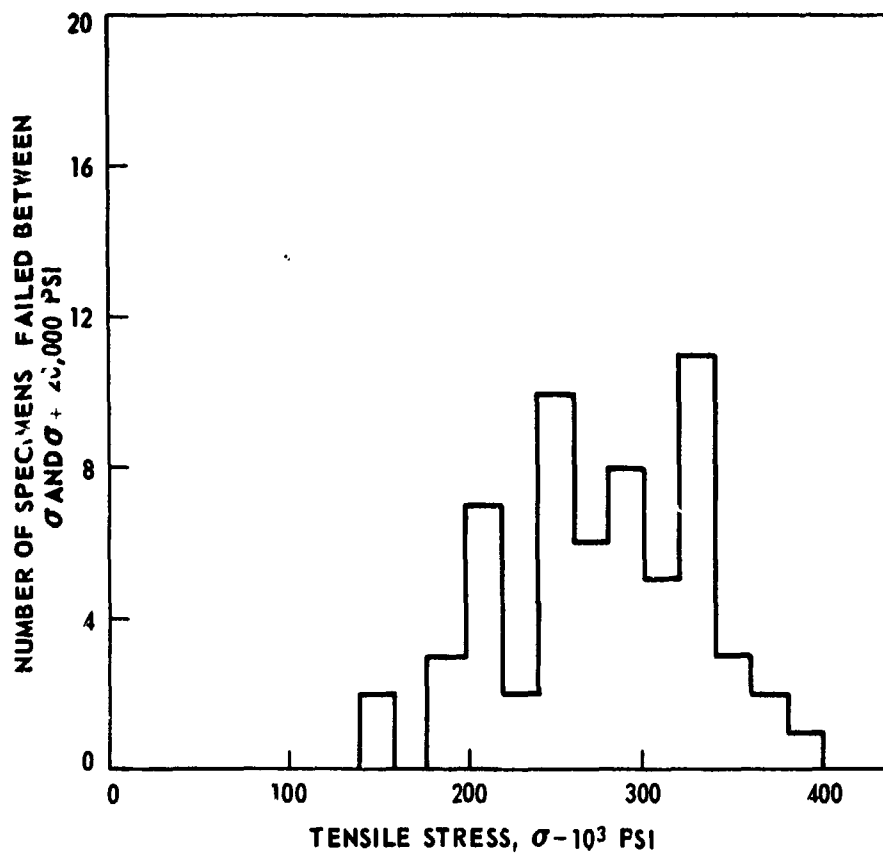


FIGURE 4-31. STRENGTH DISTRIBUTION OF 5.6 MIL BORON FIBER TESTED IN DIAMETRAL COMPRESSION

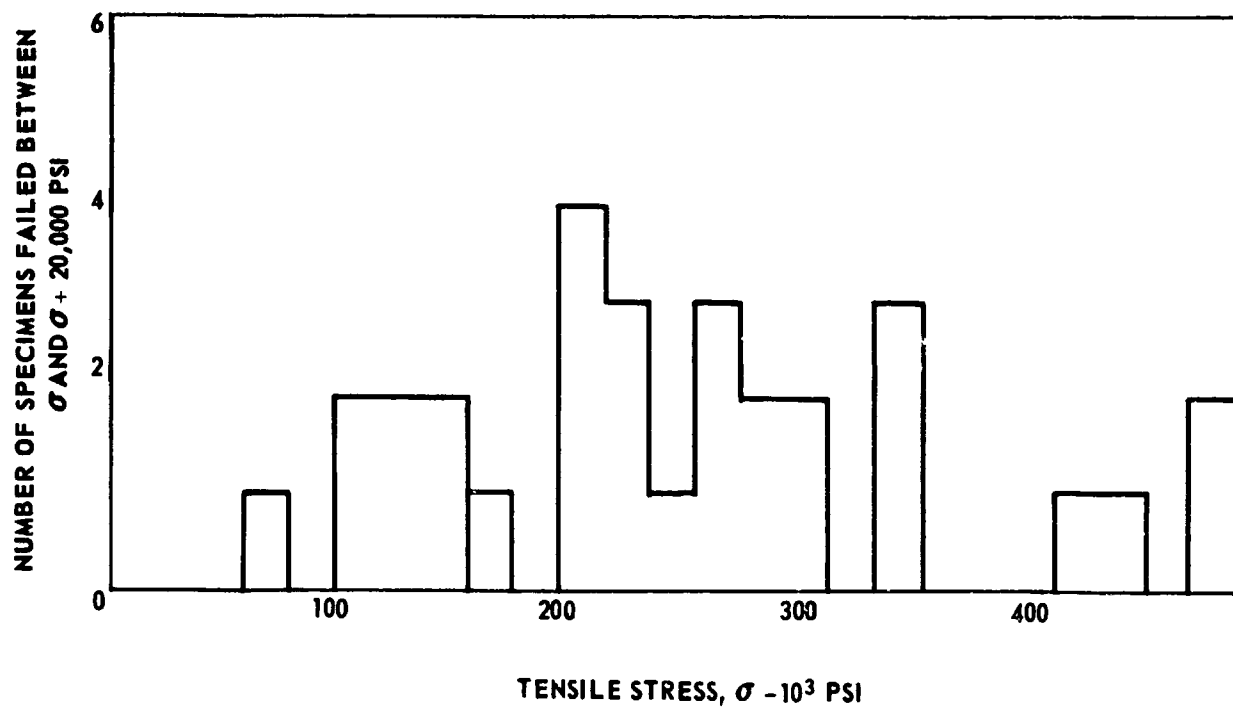
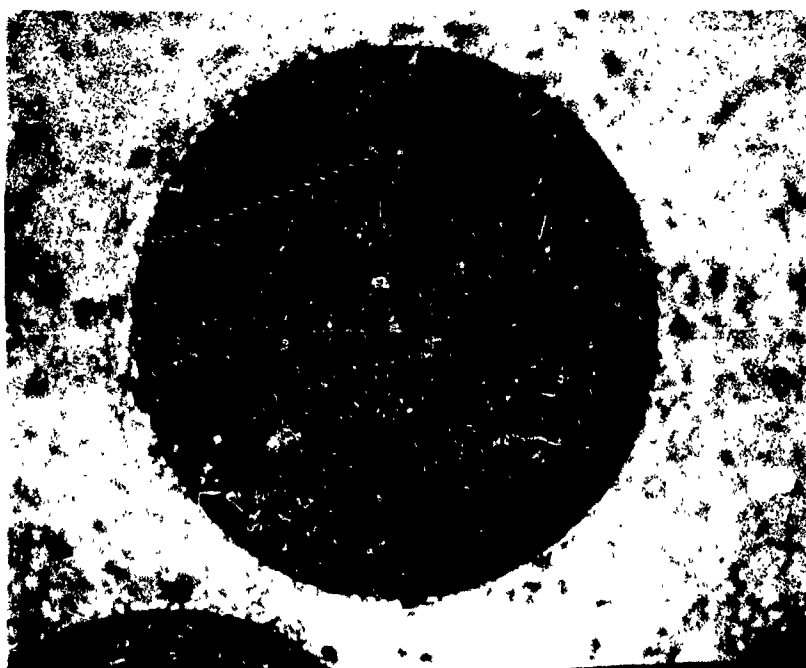


FIGURE 4-32. STRENGTH DISTRIBUTION OF 5.7 MIL BORSIC FIBER TESTED  
IN DIAMETRAL COMPRESSION



Reproduced from  
best available copy.

500X

FIGURE 4-33. 5.7 MIL DIAMETER BORSIC FIBER

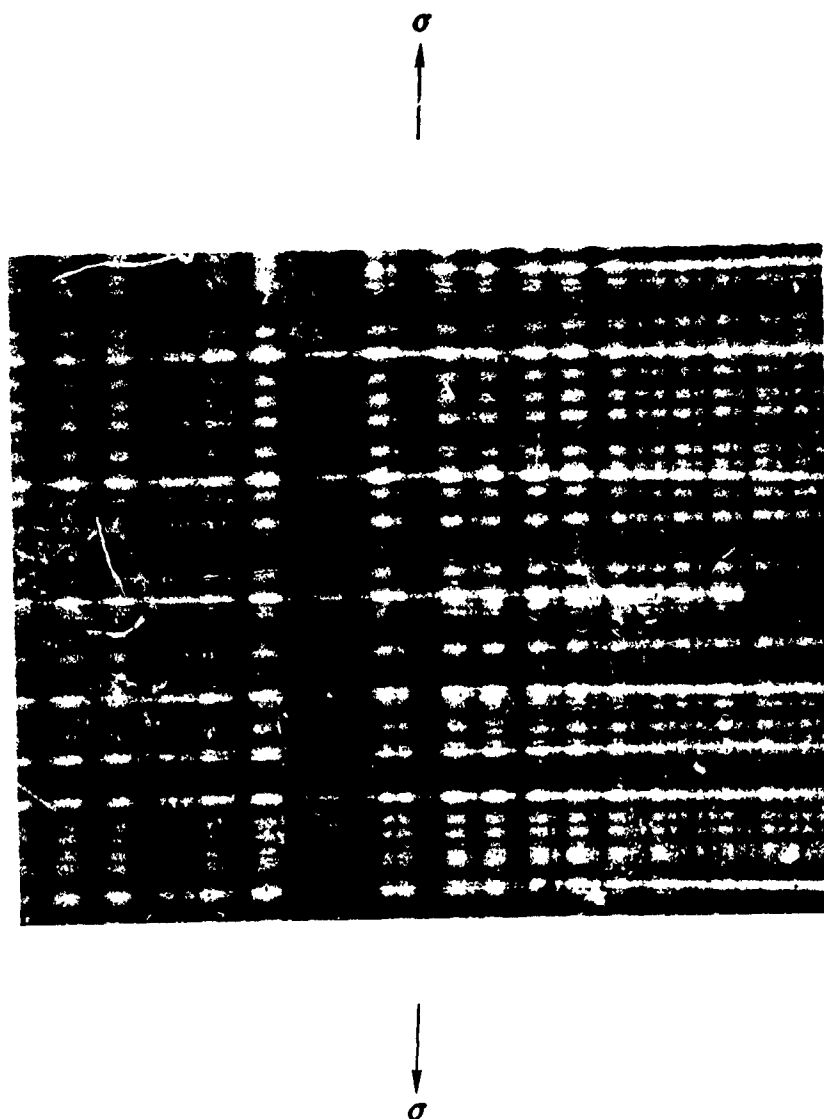


FIGURE 4-34. RADIOGRAPH OF 4.2 MIL BORSIC-6061-AFC-77 TENSILE SPECIMEN

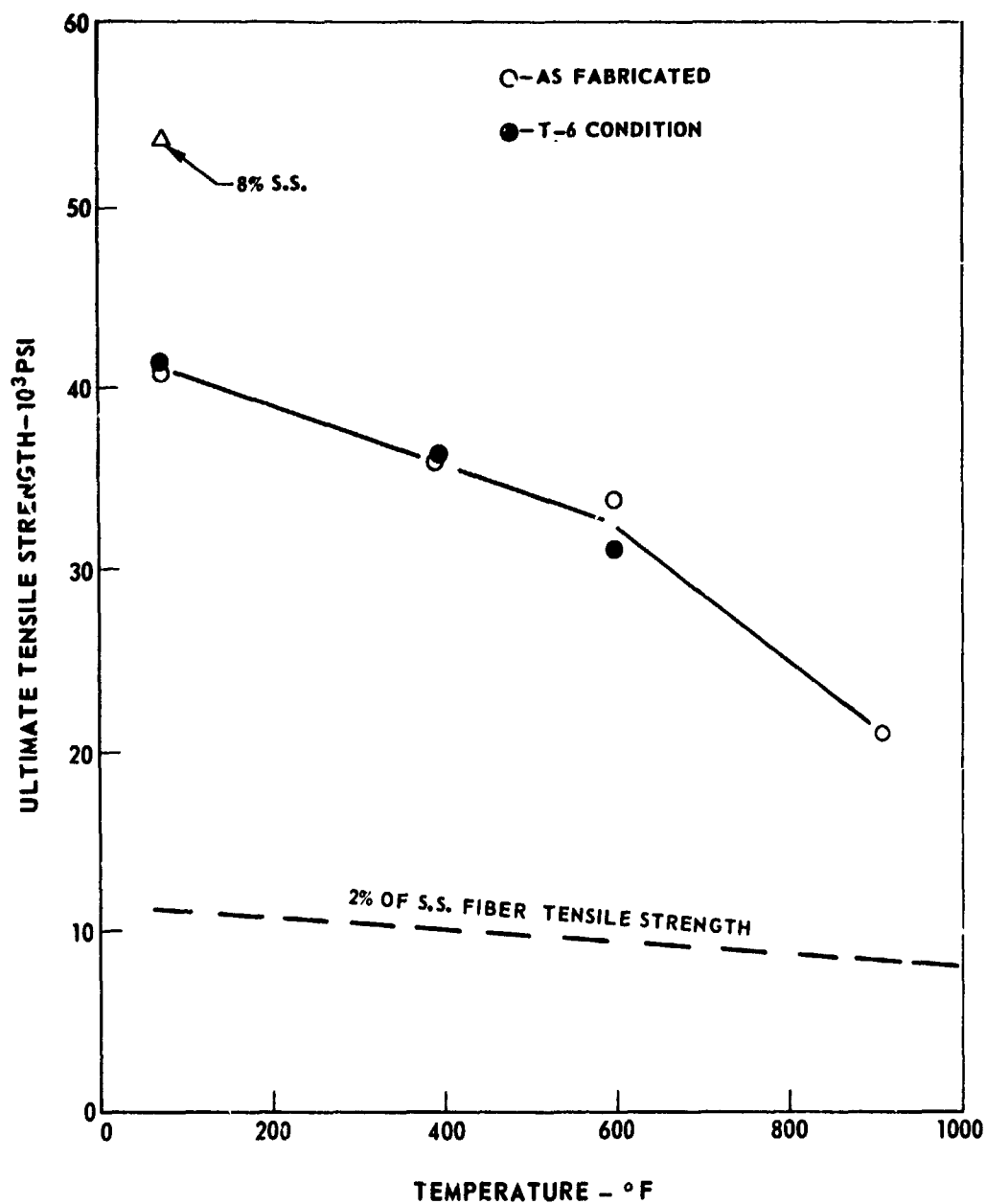


FIG. 4-35, TRANSVERSE 47% - 4.2 MIL BORSIC - 6061 - AXIAL - 6% - S. S.  
TESTED IN THE AXIAL DIRECTION

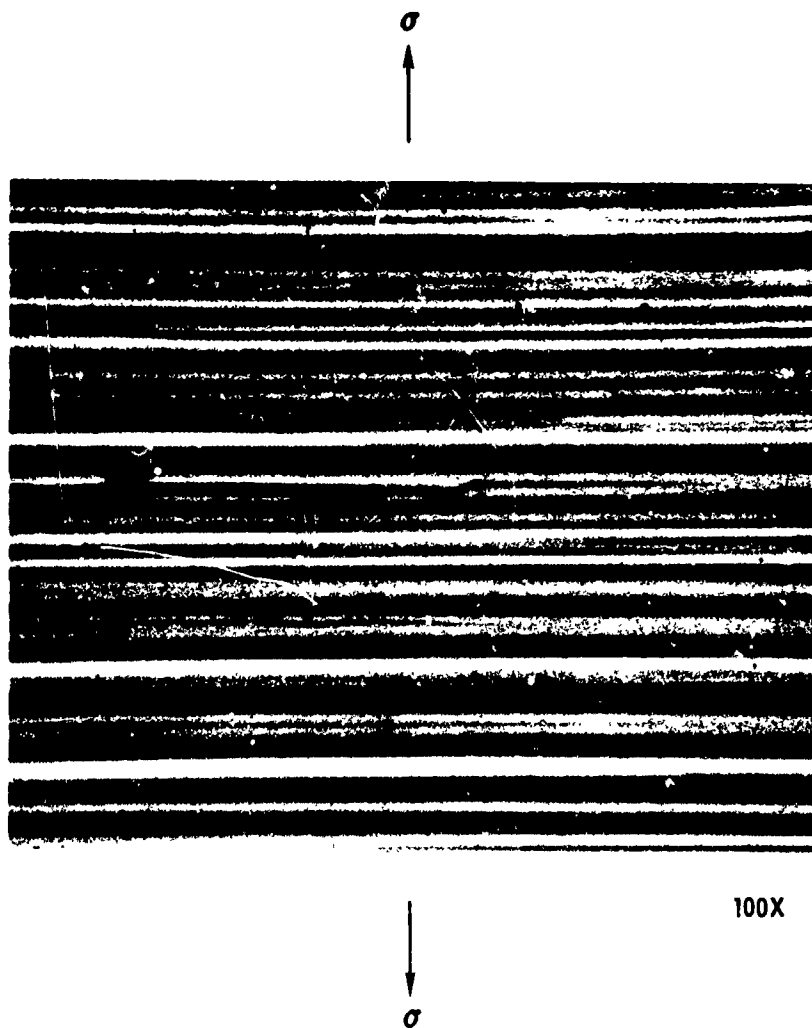


FIGURE 4-36. RADIOGRAPH OF 45 v/o - 4.2 MIL BORSIC-35 v/o -6061  
-20% -Ti-6/4 TENSILE SPECIMEN

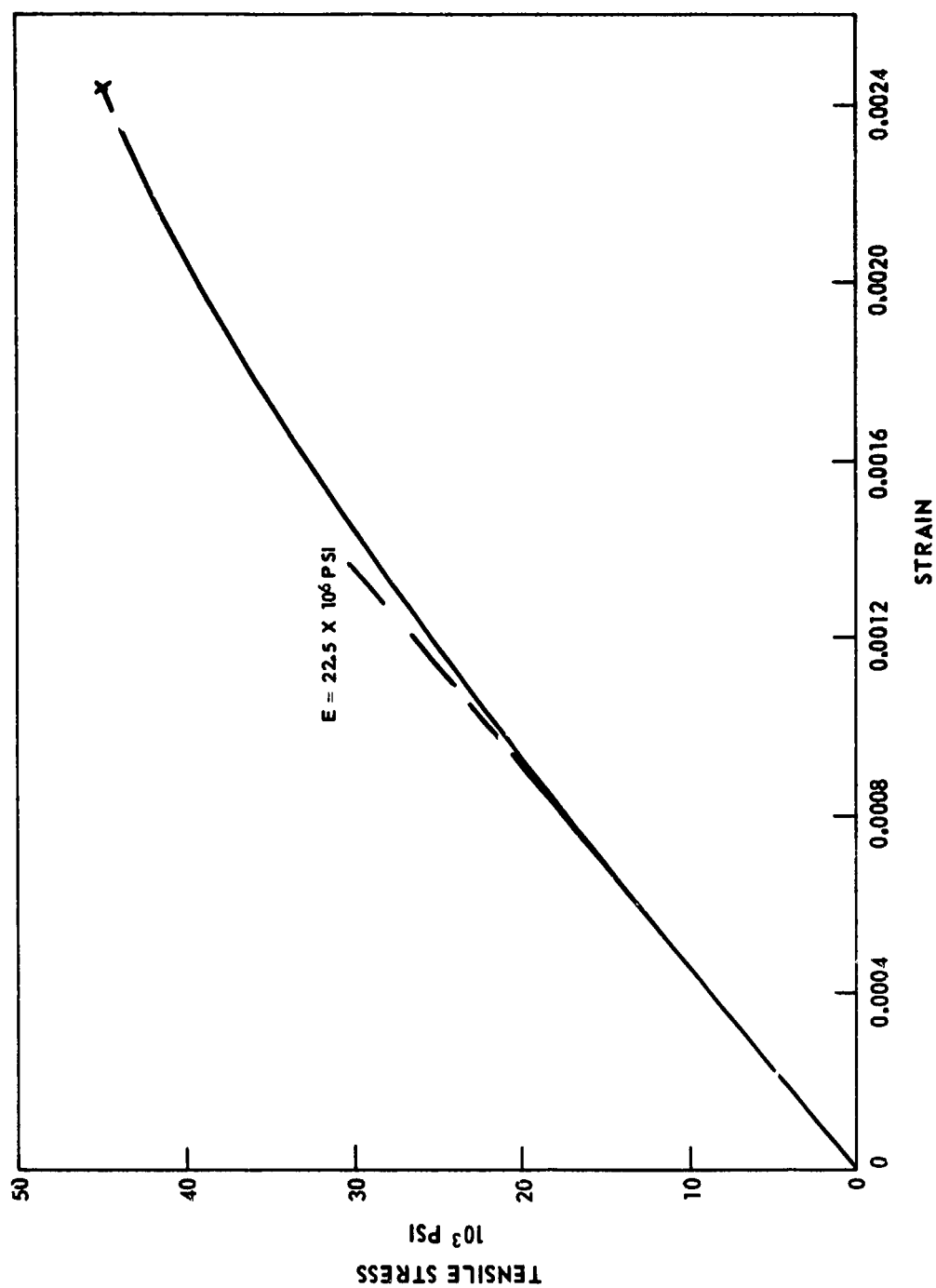


FIGURE 4-37. TRANSVERSE TENSILE STRESS-STRAIN CURVE FOR 55 v/o-5.6 MIL BORON  
2024-T6 COMPOSITE TESTED AT 70°F



52% LARGE DIAMETER BORON - 2024 T6

FIGURE 4-38. COMPOSITE TRANSVERSE TENSION FRACTURE SURFACE



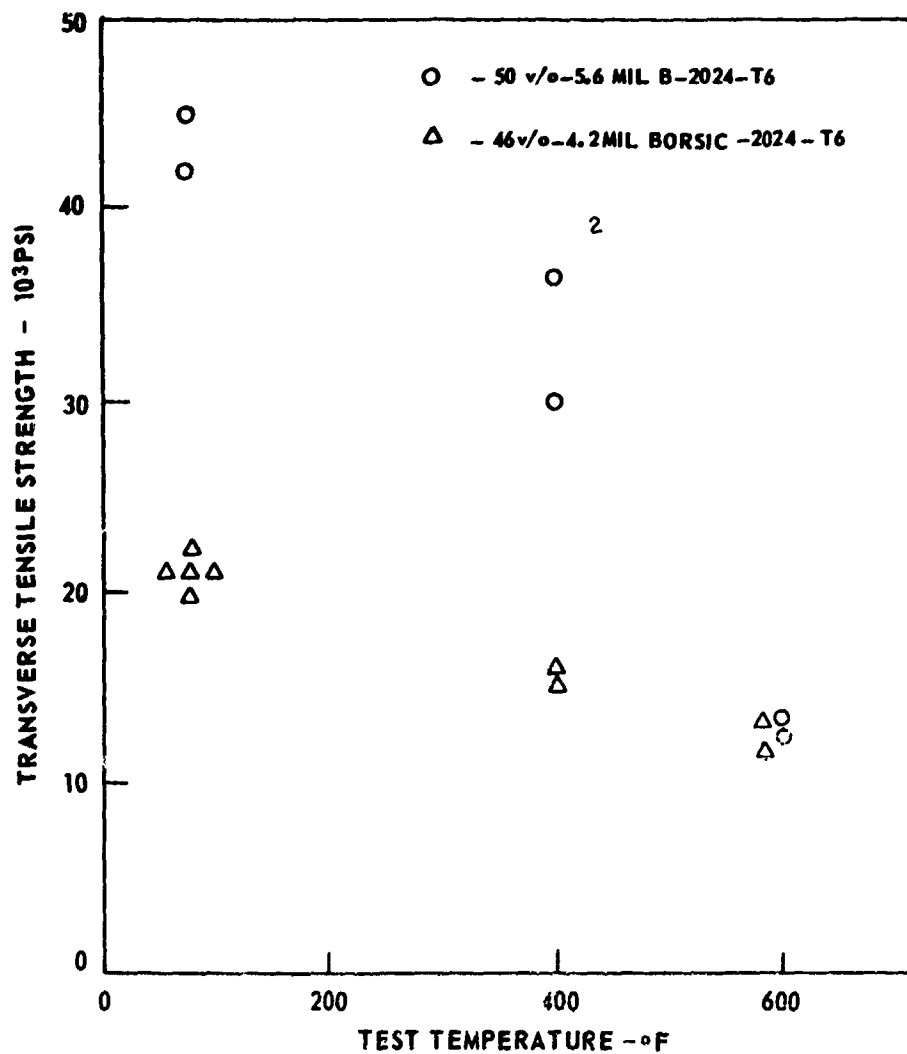


FIGURE 4-39. TRANSVERSE TENSILE STRENGTH AS A FUNCTION OF TEST TEMPERATURE

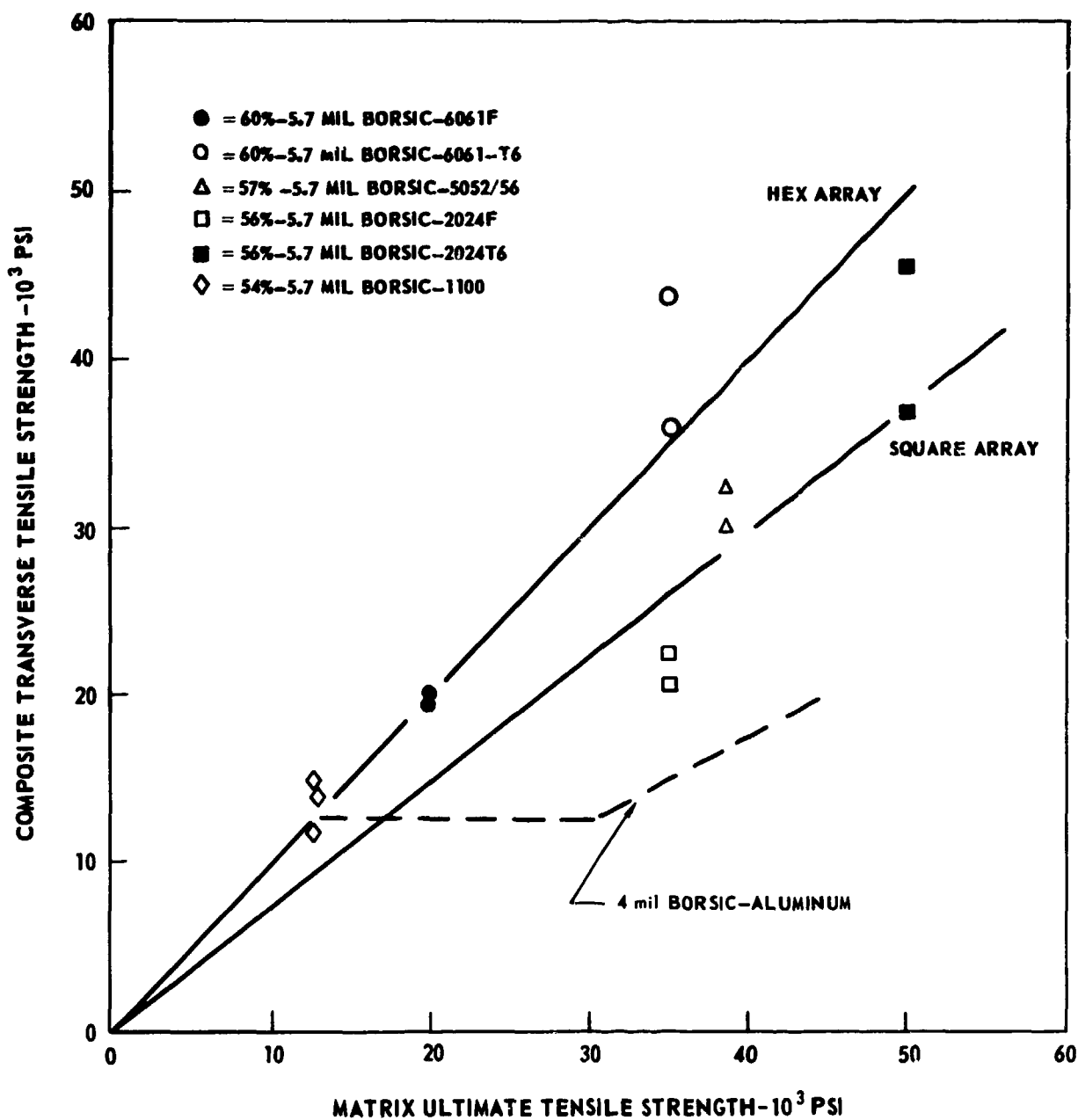
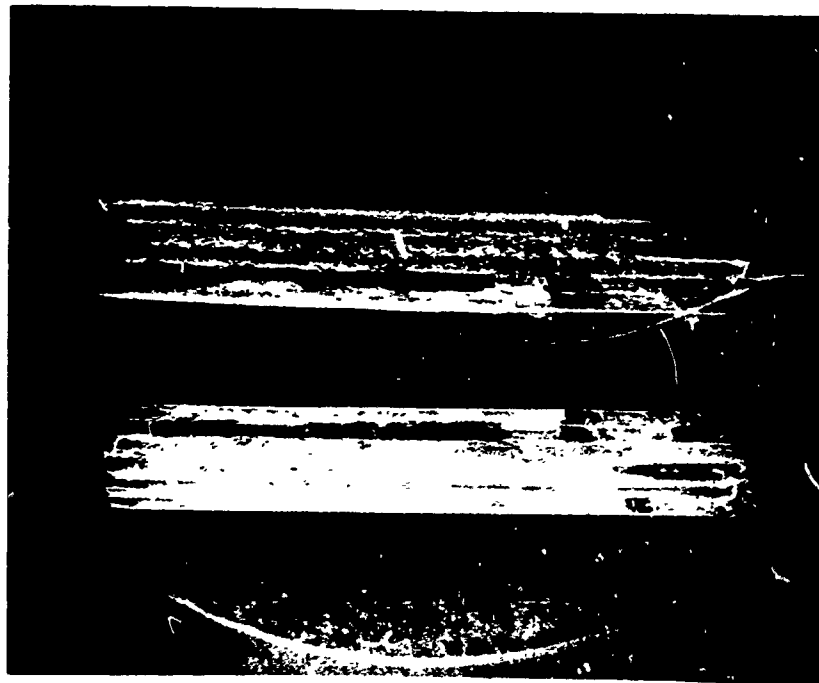
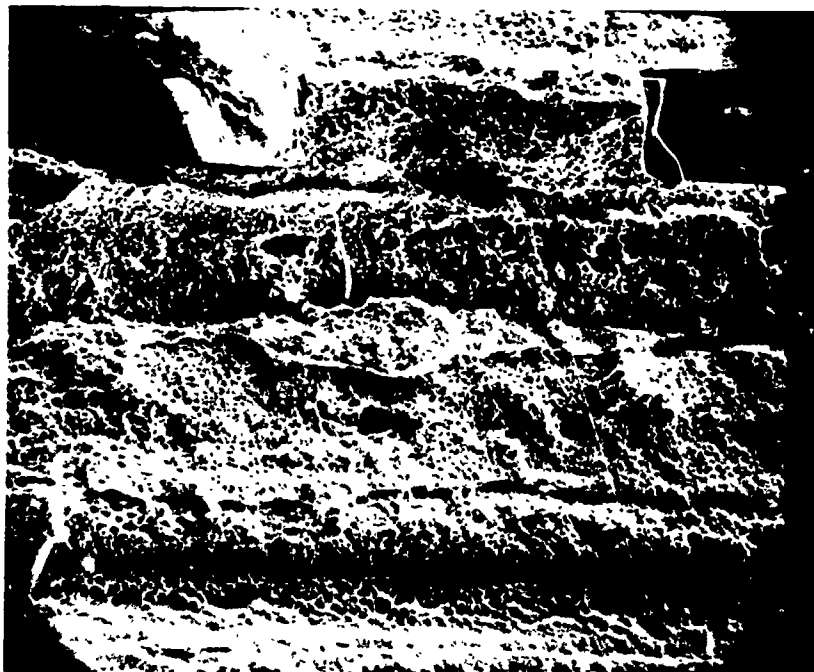


FIGURE 4-40.COMPOSITE TRANSVERSE UTS AS A FUNCTION OF MATRIX UTS



Reproduced from  
best available copy.

1000 μ



100 μ

FIGURE 4-41. TRANSVERSE TENSILE FRACTURE SURFACE OF 56 v/o-5.7 MIL BORSIC-2024

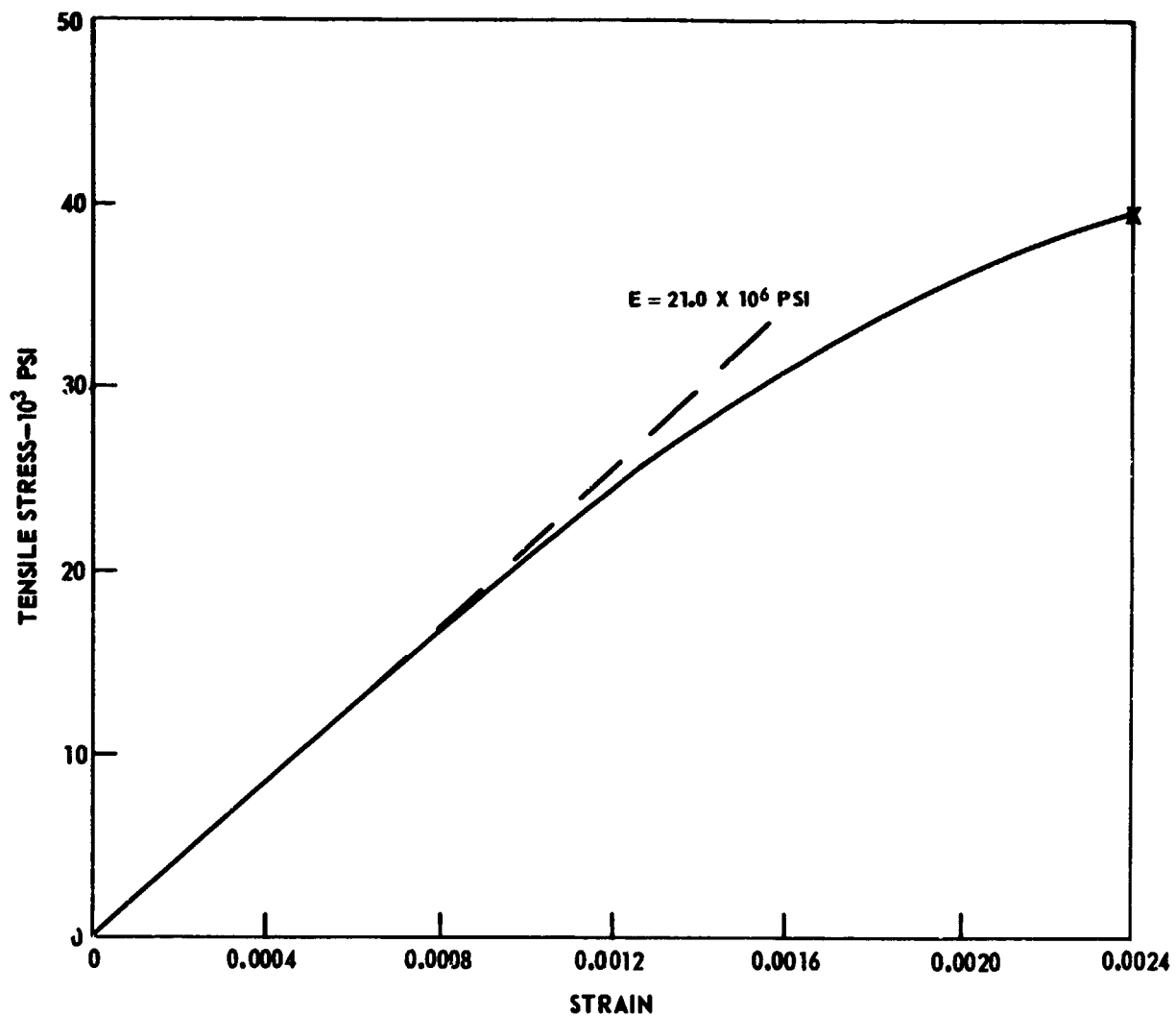


FIGURE 4-42. TRANSVERSE TENSILE STRESS-STRAIN CURVE FOR 52 v/o-5.7 MIL BORSIC 6061-T6 COMPOSITE TESTED AT 70°F

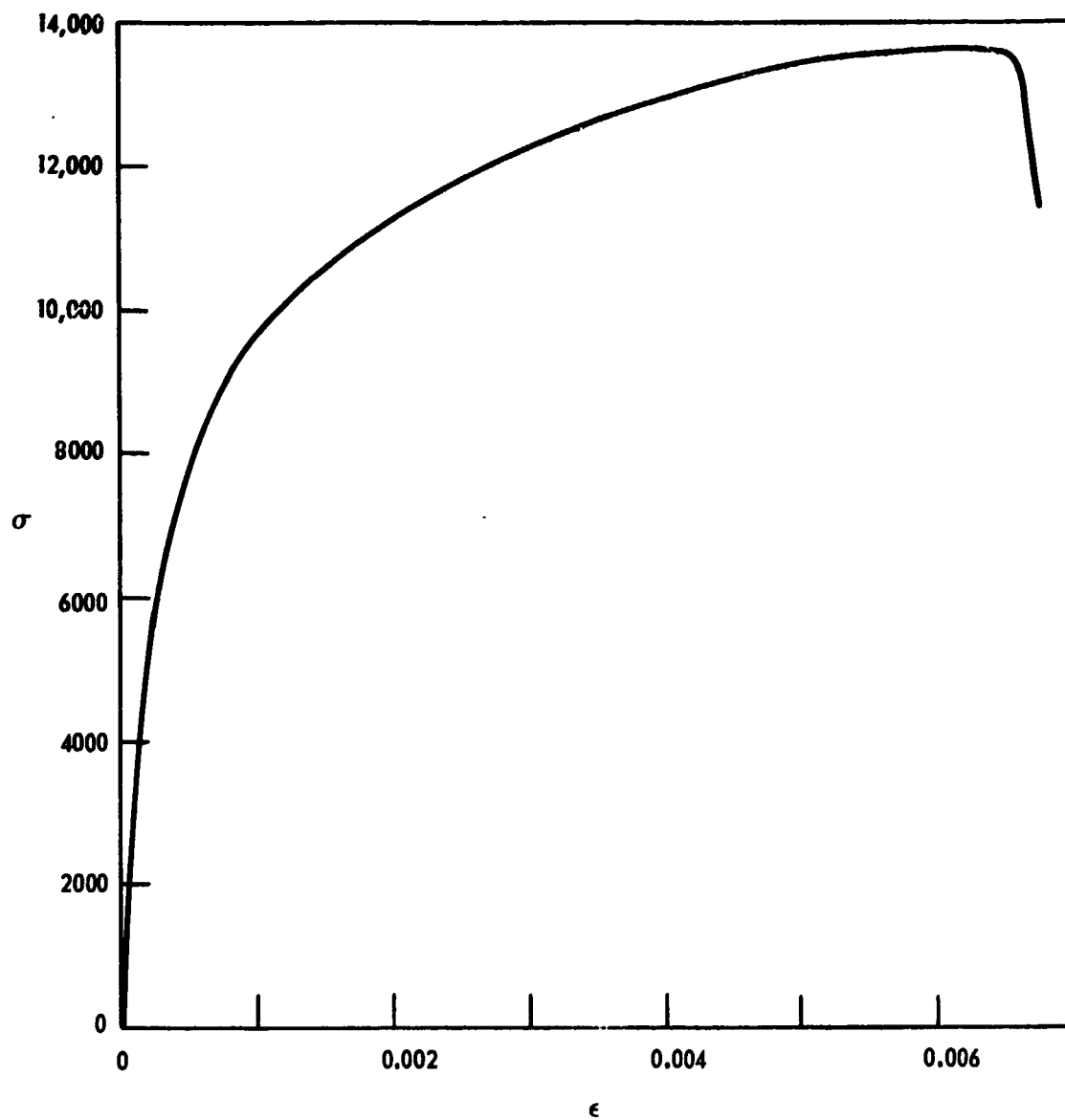


FIGURE 4-43. TRANSVERSE TENSILE STRESS-STRAIN CURVE FOR 54 v/o-5.7 BORSIC-1100

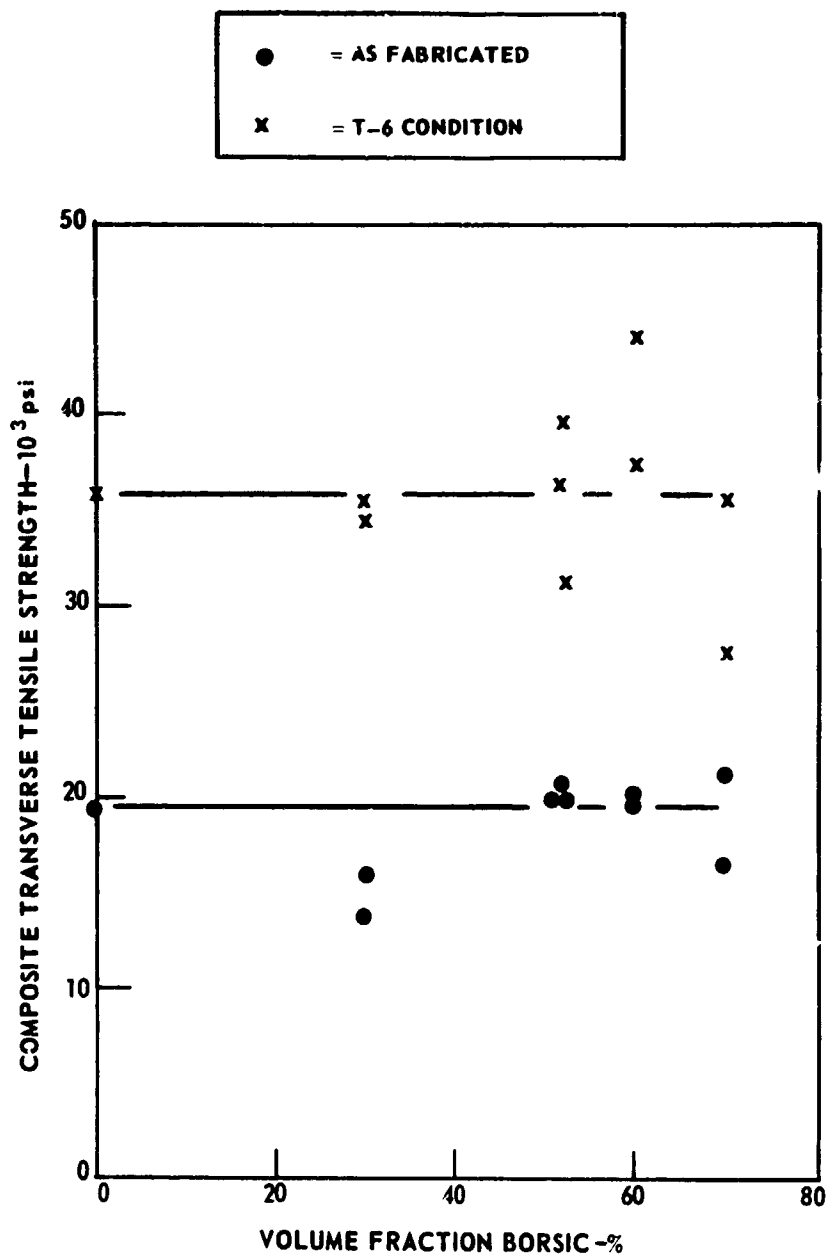


FIGURE 4-44. TRANSVERSE TENSILE STRENGTH OF 5.7 MIL BORSIC-6061

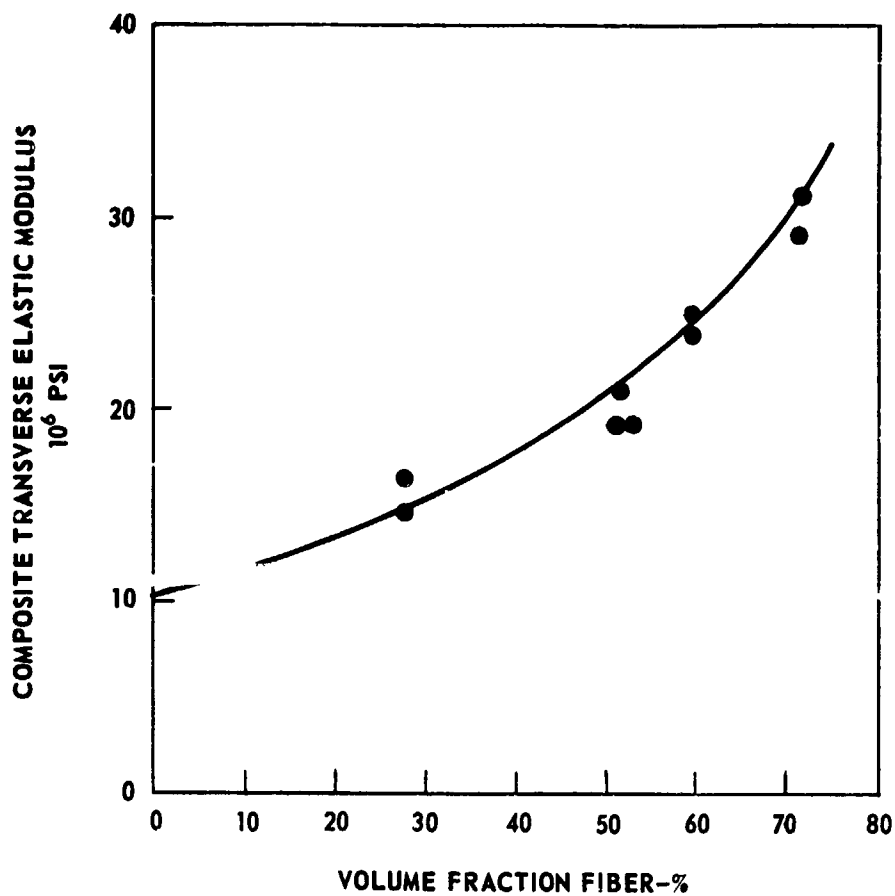


FIGURE 4-45. TRANSVERSE TENSILE ELASTIC MODULUS FOR 5.7 MIL BORSIC-6061 ALUMINUM COMPOSITES

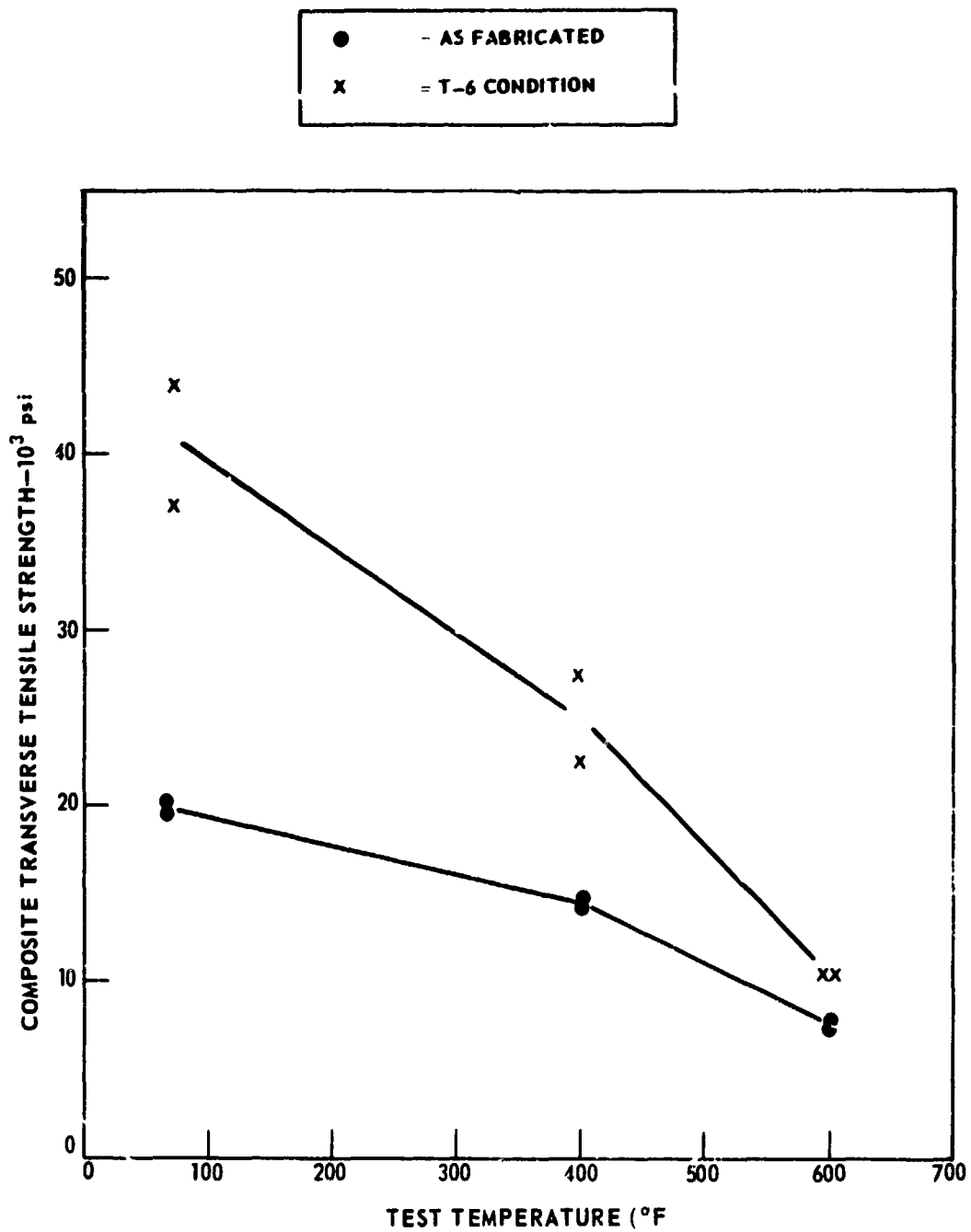


FIGURE 4-46. TRANSVERSE TENSILE STRENGTH OF 60 v/o-5.7 MIL BORSIC-6061



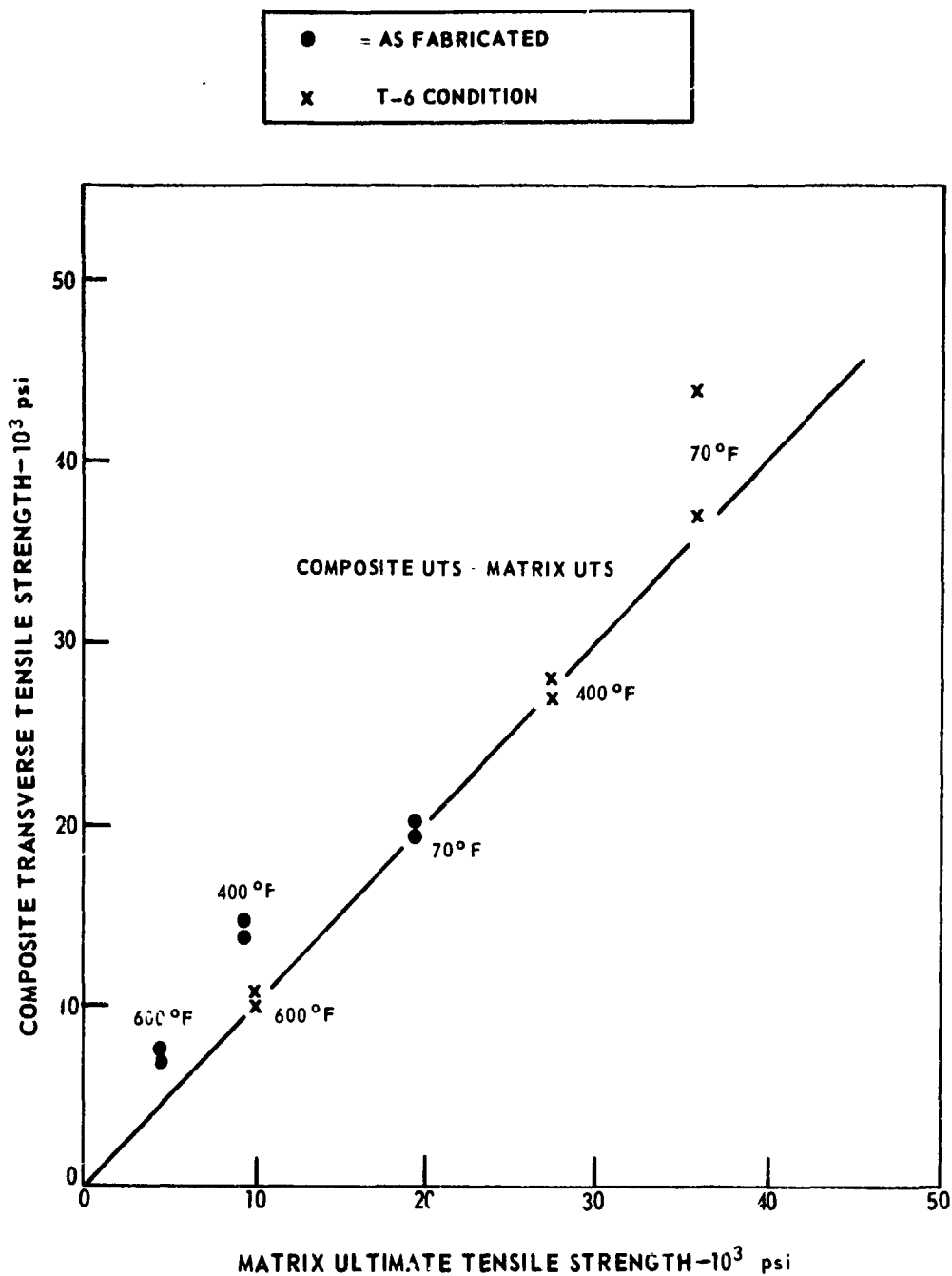


FIGURE 4-47. COMPOSITE TRANSVERSE UTS AS A FUNCTION OF MATRIX UTS FOR 60 v/o-5.7 MIL BORSIC-6061

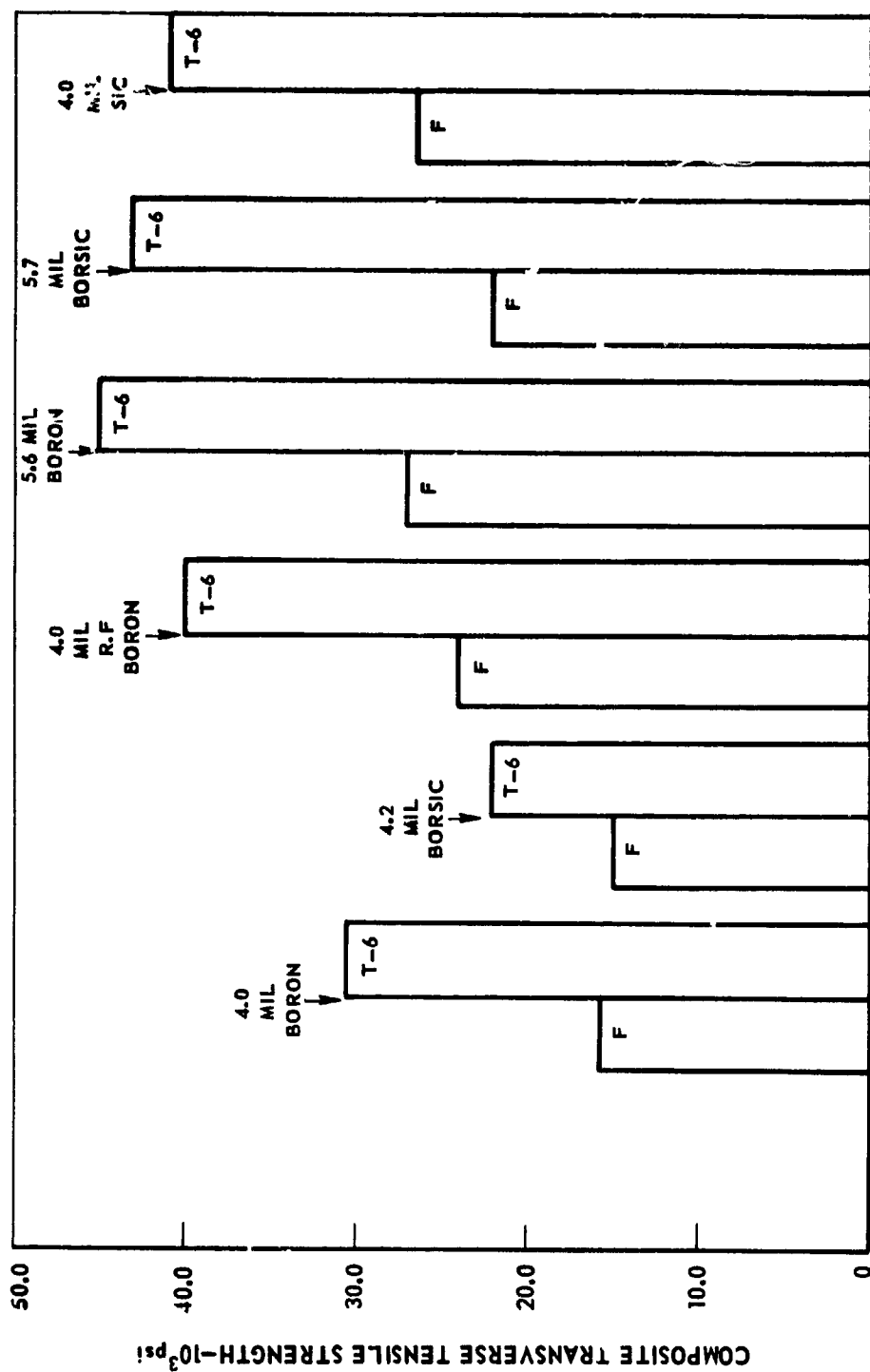
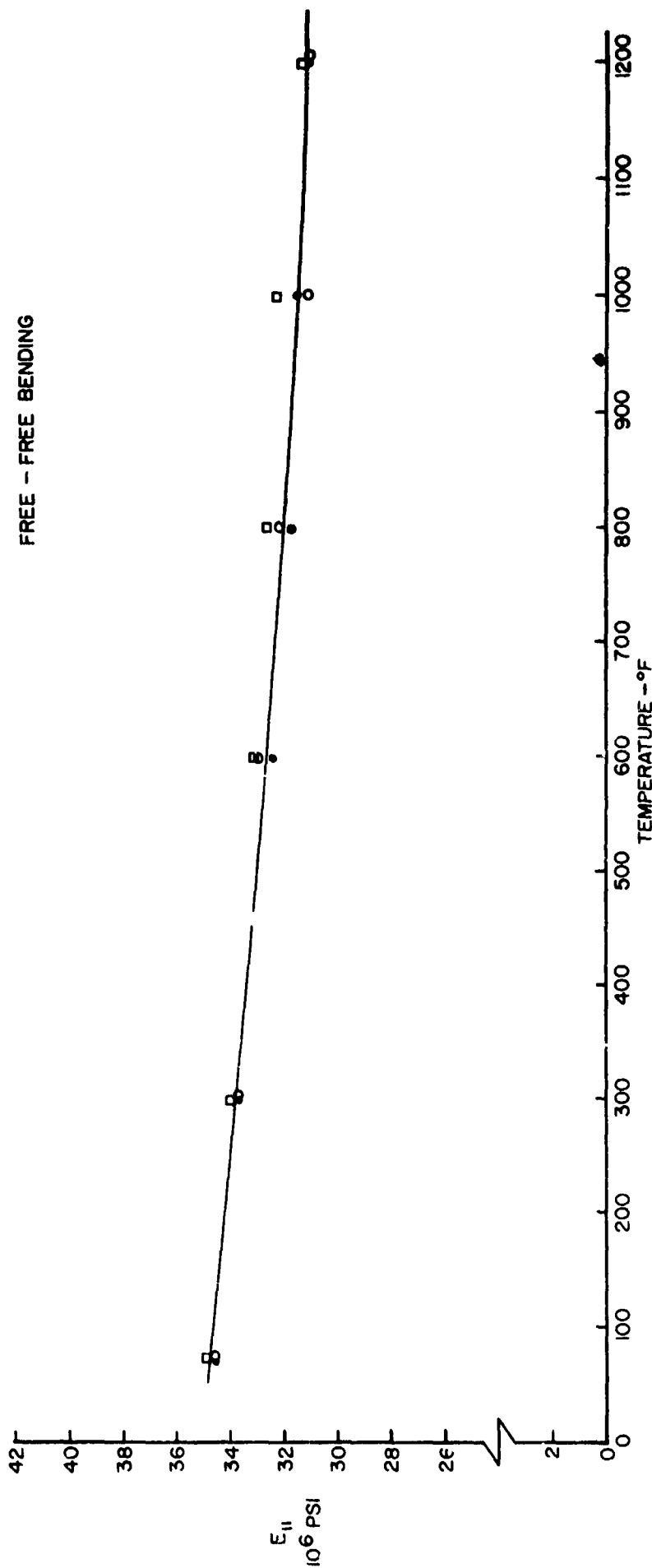


FIGURE 4-48. TRANSVERSE TENSILE STRENGTH OF 2024 ALUMINUM MATRIX COMPOSITES AS A FUNCTION OF FIBER TYPE (40-50% FIBER CONTENT)



**FIGURE 4-49. DYNAMIC MODULUS,  $E_{11}$ , AS A FUNCTION OF TEMPERATURE FOR 50 PERCENT BY VOLUME BORON + BETA III TITANIUM COMPOSITE MATERIAL**

Table IV-I

## Heat Treatment Procedures

<u>Matrix and Condition</u>	<u>Fiber Type</u>	<u>Solution Temp. and Time</u>	<u>Water Quench</u>	<u>Aging Temp. and Time</u>
6061 T6	BORSIC	40 min @ 985°F	yes	18 hrs @ 320°F
	Boron	40 min @ 920°F	yes	18 hrs @ 320°F
6061 T-4-600	BORSIC	40 min @ 985°F	yes	1 hr @ 600°F
	Boron	40 min @ 920°F	yes	1 hr @ 600°F
2024 T6	BORSIC	40 min @ 920°F	yes	16 hrs @ 375°F
	Boron	40 min @ 920°F	yes	16 hrs @ 375°F
2024 T-4-600	BORSIC	40 min @ 920°F	yes	1 hr @ 600°F
	Boron	40 min @ 920°F	yes	1 hr @ 600°F

Table IV-II

Experimentally Determined Properties of Plasma  
Sprayed Material with Foil

<u>Alloy</u>	<u>Elastic Modulus 10<sup>6</sup> psi</u>	<u>Yield Stress at 0.2% Offset 10<sup>3</sup> psi</u>	<u>Ultimate Tensile Strength 10<sup>3</sup> psi</u>	<u>Strain to Fracture (1 in. gage length)</u>
6061	10.2	11.2	19.6	16%
2024	10.4	18.6	35.0	13%
1100-1145	9.1	6.2	12.5	20%
Al-7% Si	10.5	9.4	17.5	23%
2219 (no foil)	9.6	14.4	27.6	12%
5052/56	9.8	19.5	38.6	13%

Typical Properties of Wrought Material  
in the Annealed Condition\*

<u>Alloy</u>	<u>Yield Stress 10<sup>3</sup> psi</u>	<u>Ultimate Tensile Strength 10<sup>3</sup> psi</u>	<u>Strain to Fracture (2 in. gage length)</u>
6061	8.0	18.0	25%
2024	11.0	27.0	20%
1100	5.0	13.0	35%
2219	10.0	25.0	20%
5052	13.0	28.0	25%
5056	22.0	42.0	35%

\*"Aluminum, Vol. 1 Properties, Physical Metallurgy and Phase Diagrams"  
Ed. by Kent R. Van Horn, 1967.

Table IV-III

Diffusion Bonding Conditions Capable of Producing  
Fully Consolidated 50% BORSIC-Matrix Composites

<u>Matrix Alloy</u>	<u>Range of Pressure (10<sup>3</sup> psi)</u>	<u>Temperature (°C)</u>
6061	2 to 10	565°
	5 to 10	490°
	10	420°
2024	5 to 10	490°
5052/56	2 to 10	565°
	10	420°
Al-7% Si	2 to 10	565°
	5 to 10	490°

Table IV-IV

## Transverse Tensile Properties of 5.6 mil B-Al

<u>Matrix</u>	<u>v/o Boron</u>	<u>UTS (10<sup>3</sup> psi)</u>	<u>Elastic Modulus (10<sup>6</sup> psi)</u>	<u>Strain to Failure (%)</u>
2024F	45	27.0		
	45	27.2		
	45	26.2		
2024-T6	45	48.0		
	45	48.7		
	45	38.2		
2024-T6	55	41.9	21.0	0.23
		45.0	22.5	0.24
2024F	66	26.0		
		27.3		
6061F	50	18.9		
	50	19.0		
	50	18.3		
6061-T6	50	34.8		
	50	37.4		
	50	41.7		

Table IV-V

## Transverse Tensile Properties of 5.7 mil BORSIC-Al

<u>Matrix</u>	<u>v/o Fiber</u>	<u>UTS 10<sup>3</sup> psi</u>	<u>Elastic Modulus 10<sup>6</sup> psi</u>	<u>Strain to Fracture %</u>
6061-F	30	16.0 14.0	15.0	0.45
6061-T6	30	35.1 34.6	15.5	0.31
6061-F	52	19.3 20.5 19.3		
6061-T6	52	31.2 36.6 39.8	18.9 19.0 21.0	0.19 0.23 0.24
6061-F	60	19.9 19.7	24.0	0.26
6061-T6	60	44.0 37.2		0.23
6061-F	70	16.8 21.2 18.8	32.3	0.29
6061-T6	70	35.4 27.6	29.2	0.14
2024-F	56	22.4 20.8	22.8	0.171
2024-T6	56	46.0 37.1	24.7	0.202
5052/56	57	30.4 32.6	25.8	0.308 0.50
1100	54	13.6 13.8 11.7	21.8 23.2	0.68 0.52 0.60



Table IV-VI

## 4.2 Mil BORSIC-Titanium Composites

<u>Matrix Alloy</u>	<u>Volume Fraction Fiber (%)</u>	<u>Orientation</u>	<u>Bonding Temperature</u>	<u>Elastic Modulus (psi)</u>	<u>Ultimate Tensile Strength (psi)</u>
CP Ti	47	0°	800°C	37 x 10 <sup>6</sup>	146,000
	48	0°	800°C	31 x 10 <sup>6</sup>	123,000
	38	0°	750°C	35 x 10 <sup>6</sup>	99,000 99,000
Ti 6/4	30	0°	750°C		139,000
	30	0°	800°C		146,000
	47	0°	800°C		144,000
	46	0°	800°C		154,000
	46	0°	800°C		153,000
	46	0°	800°C		172,000
Beta III	48	0°	800°C	38 x 10 <sup>6</sup>	179,500
		0°			162,000
	46	90°	800°C	22 x 10 <sup>6</sup>	30,600
		90°		22 x 10 <sup>6</sup>	31,000
	50	0°	800°C	34 x 10 <sup>6</sup>	146,000
		0°		33 x 10 <sup>6</sup>	126,000
				35 x 10 <sup>6</sup>	129,000
	50	90°	800°C	22 x 10 <sup>6</sup>	31,000
				22 x 10 <sup>6</sup>	31,000

Table IV-VII

## 5.7 Mil BORSIC-Titanium Composites

<u>Matrix Alloy</u>	<u>Volume Fraction Fiber %</u>	<u>Orientation</u>	<u>Bonding Temperature</u>	<u>Elastic Modulus psi</u>	<u>Ultimate Tensile Strength psi</u>	<u>Failure Strain %</u>
Ti6/4	0	--	As Rcvd.		160,000	8.0
Ti6/4	0	--	800°C		166,000	7.0
Ti6/4	23	0°	800°C		174,000 191,000	
Ti6/4	23	90°	800°C		47,500 48,300	
Ti6/4	45	0°	750°C		133,000 133,000	
Ti6/4	43	0°	870°C	33 x 10 <sup>6</sup>	180,000 186,000 176,000	0.52
Ti6/4	40	90°	870°C	29 x 10 <sup>6</sup> 31 x 10 <sup>6</sup>	54,000 56,000 48,000	0.46 0.28
Ti6/4	40	90°	870°C	27 x 10 <sup>6</sup> 28 x 10 <sup>6</sup>	54,000 49,500	0.42 0.34
		90°	870°C	Tested at 600°F	42,000 41,200	
		90°	870°C	Tested at 1000°F	33,200 24,200	

## OFF-AXIS BEHAVIOR

### SUMMARY

The elastic constants of 50 v/o 4.2 mil BORSIC + 6061-F aluminum were determined at 70°F. For the 4.2 mil BORSIC material  $E_{11} = 33.8 \times 10^6$  psi,  $E_{22} = 20.5 \times 10^6$  psi,  $G_{12} = 8.15 \times 10^6$  psi and  $\nu_{12} = 0.24$ . The engineering constants of 63% 5.7 mil BORSIC plus 6061-T6 aluminum are  $E_{11} = 43.7 \times 10^6$  psi,  $E_{22} = 28.3 \times 10^6$  psi,  $G_{12} = 11.1 \times 10^6$  psi, and  $\nu_{12} = 0.24$ . These results compare well with the micromechanical predictions available in the literature.

The variations of elastic constants with angle to the fiber direction are in good agreement with the transformation equations. The amount of shear coupling is small compared to the more orthotropic polymeric composite systems such as boron + epoxy. The maximum normal and coupled shear fracture strains are exhibited near 30° (1.2%) and 10° (>2%) to the filament direction in 4.2 mil BORSIC + 6061-F material.

The strength of both materials is well predicted by the maximum distortional energy theory (without artificially pinning the curve at an intermediate angle). The fracture surfaces of the 4.2 mil BORSIC + 6061-F material are characterized by fiber rupture at low angles (0°, 2°, 5°) and by fiber splitting and matrix shear at intermediate and high angles (10°, 30°, 45°, 60°, 80°, 90°). In the 5.7 mil BORSIC + 6061-T6 material fiber splitting was nearly absent as a result of the higher transverse strength of the large diameter fiber.

The use of sonic velocity measurements to calculate the off-axis modulus, ( $E_{11}(\theta) = 1/S_{11}(\theta)$ ) of fiber reinforced composite materials can result in significant error if a relationship of the form  $E_{11} = .826 \rho V^2$  is employed. Stiffness in the orthogonal directions are underestimated and intermediate angle stiffnesses are overestimated resulting in greatly overestimated values of shear modulus. Extensional wave velocities measured as a function of angle to the filament orientation are within 4% of the values predicted by the analysis which includes shear coupling effects by Reuter.

## V. OFF-AXIS BEHAVIOR

Although the anisotropy of fiber-reinforced composites is well recognized, greatest attention has been given to the measurement of mechanical properties in unidirection parallel to the aligned filaments. The elastic properties of off-axis composites have been calculated using the transformation equations of anisotropic elasticity theory. Several analyses of strength as a function of angle have also been published; these have been briefly reviewed by Tsai (Refs. 5.1,2).

The most common theories are the following:

### 1. Maximum Stress

$$\begin{aligned}\sigma_i &\leq X/\cos^2 \theta \\ &\leq Y/\sin^2 \theta \\ &\leq S/\sin \theta \cos \theta\end{aligned}\quad (5.1)$$

### 2. Maximum Strain

$$\begin{aligned}\sigma_i &\leq X/(\cos^2 \theta - \nu_{12} \sin^2 \theta) \\ &\leq Y/(\sin^2 \theta - \nu_{21} \cos^2 \theta) \\ &\leq S/\sin \theta \cos \theta\end{aligned}\quad (5.2)$$

### 3. Maximum Work Theory

$$\frac{1}{\sigma_i^2} = \frac{\cos^4 \theta}{X^2} + \left[ \frac{1}{S^2} - \frac{1}{X^2} \right] \cos^2 \theta \sin^2 \theta + \frac{\sin^4 \theta}{Y^2} \quad (5.3)$$

where  $X$  = composite strength parallel to the fibers  
 $Y$  = composite strength perpendicular to the fibers  
 $S$  = shear strength.

The maximum stress and maximum strain theories assume that three independently operating failure modes occur which depend on orientation:

1. Fiber tensile failure is expected at low angles.
2. Matrix shear failure is expected at intermediate angles.
3. Matrix plane strain tensile failure is expected at angles close to  $90^\circ$ .

The maximum work theory considers strength interactions and assumes that failure will occur when the distortional energy exceeds a critical level.

All of these relationships are based on phenomenological approaches that use the theory of elasticity to predict initial failure or yield conditions of the material without specific reference to the mechanisms of deformation and fracture.

The off-axis behavior of 10 layer unidirectional 4.2 mil BORSIC plus 50% by volume 6061-F aluminum matrix composite material was investigated in two ways: using ordinary tensile testing at seven orientations with respect to the fiber axis and by measurements of sonic velocity.

In addition, samples of 63% by volume 5.7 mil BORSIC plus 6061-T6 aluminum composite materials were also evaluated using tensile tests.

## 5.1 Tensile Tests

### Experimental Method

Six inch long unidirectional panels were fabricated with the following filament orientations: 0°, 2°, 5°, 10°, 30°, 45°, 60°, 80°, and 90°. Straight-sided "IITRI" tensile specimens from these panels were then machined. An EDM tool was constructed for a six inch long reduced gage specimen that might be more suitable for low angle tests than the IITRI design; specimens of this geometry were also machined and prepared for testing.

It had been established (Refs. 5.3-7) that the testing technique used for measuring off-axis properties was extremely important because of the sensitivity of the test specimen to end effects such as constraint and moments applied by the gripping. Under the influence of an off-axis load the shear coupling compliance  $S_{16}$  causes a rectangular specimen to distort into a parallelogram; if this distortion is restricted as a result of rigid clamping at the specimen ends, a nonuniform stress state is induced in the material. The following procedures were adopted to minimize this testing problem:

1. Adhesively bonded aluminum doubler material was employed in grip attachment areas. This layer was sufficiently strong in shear to transfer longitudinal load into the specimen and sufficiently compliant to minimize transverse interaction between the deforming specimen and relatively massive fixturing.
2. Testing was performed using a fixture that permitted specimen rotation in order to accommodate shear coupling distortion (Fig. 5.1). The rotation axis was positioned close to the restraint boundary so as to minimize the effective moment arm acting on the specimen.
3. The ratio of test specimen gage length to width ( $l/w$ ) was 10 to 1 or greater to reduce the ratio of bending moment to tensile load.

Tests were conducted in an Instron Tensile machine. Rosette strain gage instrumentation was needed to determine the state of stress in an off-axis test. Separate studies by L. E. Dardi have shown that strain rate effects can be important in room temperature tests of  $\pm 45^\circ$  BORSIC-aluminum. Therefore, continuous load-strain recording equipment was used to monitor rosette strain gage instrumentation on all specimens (Fig. 5.2). The strain rate in all tests was 0.005 in./in./min.

A diagram of the coordinate system employed in this study is given in Fig. 5.3; where  $x, y$  are the load axes and 1, 2 are the orthotropic axes. Two rosette orientations were employed in the off-axis testing; these are depicted in Fig. 5.4. The results were interpreted in the following way:

In two dimensions, any linear strain can be expressed by the following relationship:

$$\epsilon_{\theta} = \epsilon_x m^2 + \epsilon_y n^2 + \gamma_{xy} mn \quad (5.4)$$

where  $\epsilon_{\theta}$  = linear strain in gage direction  
 $x, y$  = reference coordinate system  
 $m, n$  =  $\cos \theta$ ;  $\sin \theta$

Therefore, in the case of Configuration I:

$$\begin{aligned} \text{for } \theta = 0^\circ; \epsilon_0 &= \epsilon_x \\ \theta = 90^\circ; \epsilon_{90} &= \epsilon_y \\ \theta = 45^\circ; \epsilon_{45} &= \epsilon_x/2 + \epsilon_y/2 + \gamma_{xy}/2 \end{aligned} \quad (5.5)$$

$$\text{and } \gamma_{xy} = 2 \epsilon_{45} - \epsilon_0 - \epsilon_{90}$$

In the case of Configuration II:

$$\begin{aligned} \text{for } \theta = 0^\circ; \epsilon_0 &= \epsilon_x \\ \theta = 270^\circ; \epsilon_{-90} &= \epsilon_y \\ \theta = 315^\circ; \epsilon_{-45} &= \epsilon_x/2 + \epsilon_y/2 - \gamma_{xy}/2 \end{aligned} \quad (5.6)$$

$$\text{and } \gamma_{xy} = -(2 \epsilon_{-45} - \epsilon_0 - \epsilon_{-90})$$

Thus, in an orthotropic material, it is necessary to distinguish between these configurations in order to obtain the proper sign of shear strain.

The compliance coefficients  $S_{11}$ ,  $S_{12}$ , and  $S_{16}$  were determined by measuring the ratios of strain to applied stress. The constitutive relations for an orthotropic bar in plane stress can be written:

$$\begin{aligned} \epsilon_x &= S_{11} \sigma_x + S_{12} \sigma_y + S_{16} \tau_{xy} \\ \epsilon_y &= S_{12} \sigma_x + S_{22} \sigma_y + S_{26} \tau_{xy} \\ \gamma_{xy} &= S_{16} \sigma_x + S_{26} \sigma_y + S_{66} \tau_{xy} \end{aligned} \quad (5.7)$$

where the  $S_{ij}$  are the compliance coefficients with respect to the  $x, y$  coordinate system (Fig. 5.3). Therefore, under uniaxial tension, where  $\sigma_y = \tau_{xy} = 0$ ,

$$\begin{aligned} S_{11} &= \epsilon_x / \sigma_x \\ S_{12} &= \epsilon_y / \sigma_x \\ S_{16} &= \gamma_{xy} / \sigma_x \end{aligned} \quad (5.8)$$

Consistency among the experimental results was checked using the transformation equations (Refs. 5.8).

$$\begin{aligned}
S_{11} &= \frac{m^4}{E_{11}} + \frac{n^4}{E_{22}} + \left[ \frac{1}{G_{12}} - \frac{2\nu_{12}}{E_{11}} \right] m^2 n^2 \\
S_{12} &= \left[ \frac{1}{E_{11}} + \frac{1}{E_{22}} - \frac{1}{G_{12}} \right] m^2 n^2 - \frac{\nu_{12}}{E_{11}} (m^4 + n^4) \\
S_{16} &= \left[ \frac{1}{G_{12}} - \frac{2\nu_{12}}{E_{11}} - \frac{2}{E_{11}} \right] m^3 n - \left[ \frac{1}{G_{12}} - \frac{2\nu_{12}}{E_{11}} - \frac{2}{E_{22}} \right] n^3 m \\
S_{66} &= 4 \left[ \frac{1}{E_{11}} + \frac{1}{E_{22}} + \frac{2\nu_{12}}{E_{11}} \right] m^2 n^2 + \frac{1}{G_{12}} (m^2 - n^2)^2
\end{aligned} \tag{5.9}$$

where:  $m; n = \cos \alpha ; \sin \alpha$

In addition, a computerized least squares analysis was conducted using the transformation equations and measured values of  $E_{11}$ ,  $E_{22}$ , and  $\nu_{12}$  to determine the value of  $G_{12}$  that best fit the experimentally determined levels of  $S_{12}$ .

### Results and Discussion

#### Elastic Properties

The results of all tests with both the 50 v/o 4.2 mil fiber composites and the 63 v/o 5.7 mil fiber composites are listed in Tables V-I and V-II, respectively. The compliance coefficients,  $S_{11}$ ,  $S_{12}$ , and  $S_{16}$ , are given as a function of angle to the filament direction in Figs. 5.5-5.10. The solid lines in these figures represent theoretical levels obtained from the transformation equations (Ref. 5.8).

The experimentally determined values used in the calculation were  $E_{11} = 33.8 \times 10^6$  psi,  $E_{22} = 20.7 \times 10^6$  psi, and  $\nu_{12} = 0.24$  in the case of the 50 v/o 4.2 mil BCRSIC composites and  $E_{11} = 43.7 \times 10^6$  psi,  $E_{22} = 28.3 \times 10^6$  psi, and  $\nu_{12} = 0.24$  for the 63 v/o 5.7 mil fiber composite material.  $G_{12}$  was obtained using a least squares analysis; the results shown in Figs. 5.5-5.7 (4.2 mil) correspond to  $G_{12} = 8.15 \times 10^6$  psi and those in Figs. 5.8-5.10 (5.7 mil) correspond to  $G_{12} = 11.1 \times 10^6$  psi. Agreement between theory and experiment is very good at all angles.

In Table V-III these levels of  $G_{12}$  as well as the other engineering constants are compared with the values predicted by several common micro-mechanical analyses. Excellent agreement between theory and experiment was obtained. The greatest disparity (+7.8%) is found for  $G_{12}$  in the 63 v/o 5.7 mil BORSIC material.

In the case of the 50% 4.2 mil BORSIC + 6061-F material  $S_{11}$  increases nearly monotonically from  $2.96 \times 10^{-8}$  in<sup>2</sup>/lb at  $\alpha = 0^\circ$  ( $E_{11} = 33.8 \times 10^6$  psi) to  $4.88 \times 10^{-8}$  in<sup>2</sup>/lb at  $\alpha = 90^\circ$  ( $E_{22} = 20.5 \times 10^6$  psi) as given in Fig. 5.5. The ratio of  $S_{11}$  at  $\alpha = 65^\circ$  (near maximum) to that at  $\alpha = 90^\circ$  is approximately 1.01 as determined using the transformation equations with  $G_{12} = 8.15 \times 10^6$  psi. The absence of a pronounced maximum in  $S_{11}$  (or minimum in  $E_x$ ) is due to the high shear modulus of the aluminum matrix. The impact of varying  $G_{12}$  at constant  $E_{11}$ ,  $E_{22}$ , and  $\nu_{12}$  can be seen in Figs. 5.11-5.13.  $S_{12}$  is symmetrical about  $45^\circ$  (Fig. 5.6). The average value measured at  $\alpha = 0^\circ$  is  $-0.70 \times 10^{-8}$  in<sup>2</sup>/lb and at  $\alpha = 90^\circ$  is  $-0.74 \times 10^{-8}$  in<sup>2</sup>/lb ( $\nu_{12} = 0.24$ ); at  $\alpha = 45^\circ$ ,  $S_{12} = -1.56 \times 10^{-8}$  in<sup>2</sup>/lb.

$S_{16}$  is zero at  $\alpha = 0^\circ$ , and rises to a maximum positive value of approximately  $1.17 \times 10^{-8}$  in<sup>2</sup>/lb near  $\alpha = 30^\circ$  (Fig. 5.7). At angles greater than  $65^\circ$ ,  $S_{16}$  becomes slightly negative and then rises to zero at  $\alpha = 90^\circ$ . Thus, in the elastic range the BORSIC fibers rotate away from the axis of applied load when the loading angle is less than  $65^\circ$  but greater than  $0^\circ$ , and rotate toward the load axis at higher angles. This behavior is similar to that reported for boron-epoxy (Ref. 5.9). The elastic behavior of the 5.7 mil BORSIC + 6061-T6 material is similar to that of the 4.2 mil BORSIC material and will not be discussed in detail. The results of these tests indicate that the amount of shear coupling in BORSIC-aluminum is small. The material is much less orthotropic than polymeric matrix composites such as boron-epoxy.

### Strength Properties

Typical stress-strain curves for 50 v/o 4.2 mil BORSIC + 6061-F aluminum and 63 v/o 5.7 mil BORSIC + 6061-T6 aluminum materials are given in Figs. 5.14-5.17. The maximum normal fracture strain (1.2%) of the 4.2 mil BORSIC + 6061 system is found at  $30^\circ$ . At  $0^\circ$  the longitudinal fracture strain of the filament limits the strain of the composite, whereas at  $90^\circ$  the fracture strain of 4.2 mil material is determined by the transverse strain capability of the fiber (splitting). The  $0^\circ$  and  $90^\circ$  normal fracture strains of 5.7 mil material are determined by the strength of the fibers and the matrix, respectively. These effects are discussed in greater detail in the Transverse Properties section of this report.

The maximum coupled ultimate shear strain occurs near  $10^\circ$  ( $> 2.0\%$ ) for 50 v/o 4.2 mil BORSIC + 6061-F material. Insufficient tests were conducted to determine the angle of maximum ultimate shear strain for 63 v/o 5.7 mil BORSIC + 6061-T6 material. The largest values obtained at  $45^\circ$  averaged 1.3% compared to approximately 0.6% for the 4.2 mil BORSIC system at the same angle.

The tensile strength of both materials is given as a function of angle in Figs. 5.18-5.19. Calculated strengths using the maximum stress, Eq. (5.1), maximum strain, Eq. (5.2), and maximum work theory, Eq. (5.3) are also plotted in Figs. 5.18-5.19. For 4.2 mil BORSIC + 6061-F material average experimentally determined strengths at  $0^\circ$  and  $90^\circ$  were used for X and Y. The value of S (shear strength) employed was  $14.0 \times 10^3$  psi as determined in other experimental work at United Aircraft Corporation by K. M. Prewo.



In the case of the 5.7 mil + 6061-T6 material, X and Y were experimentally determined and S was obtained in the following way. Since 90° failure occurred without fiber splitting and the results of the transverse property investigation indicated that under this condition transverse composite strength equals the matrix strength, the UTS of the matrix was found to be 32.2 ksi. Assuming that the ratio of shear to tensile strength of the in situ matrix material was similar to that of wrought aluminum alloy, a value of 22.2 ksi was obtained as given in Table V-IV.

Experimental strengths are equal to or slightly higher than those predicted by the maximum distortional energy criterion and slightly lower than levels expected with the maximum stress criterion; (a somewhat greater disparity exists with the maximum strain criterion). Furthermore, composite strength at 2° and 5° is less than that at 0° as expected by the maximum work criterion, whereas a slight increase is predicted by the maximum stress and maximum strain criteria. Thus, the maximum distortional energy criterion appears to be most appropriate for BORSIC/6061 aluminum. The filament orientation in all specimens was confirmed and found to be within one-half degree of the nominal value. At a given angle, the strengths measured using straight-sided specimens were similar to those obtained with reduced gage section samples.

#### Fractography

The fracture surfaces of 4.2 BORSIC/6061-F composites at 0°, 2°, and 5° were irregular and nearly transverse to the loading axis (Fig. 5.20). Samples tested at 10° exhibited an irregular fracture path with alternating segments of matrix shear and zones of fiber fracture, Fig. 5.21; the overall path was oriented at approximately 30° to 40° from the loading axis. The fracture of 30° material occurred along a plane parallel to the filaments at 30° to the loading axis, Fig. 5.21. Failure occurred by matrix shear and a relatively small amount of fiber splitting.

Six 45° specimens were evaluated with the rotating grips used above and two were tested in rigid grips. The strengths of these specimens were found to be independent of gripping arrangement. The fracture of 45° material tested in the rotating grips occurred at approximately 45° to the loading axis by matrix shear and extensive fiber splitting, Fig. 5.22. The samples tested in the rigid grips displayed similar features but also exhibited a jogged region of fiber fracture near the specimen mid line (Fig. 5.22). This may have been the result of grip restraint as the crack opened and propagated across the sample. The general similarity of the measured strengths with and without the rotating grips indicate the minor anisotropy of boron aluminum compared to resin composites.

The fracture of the 60° and 80° material occurred along a plane parallel to the filaments at 60° and 80°, respectively to the loading axis, Fig. 5.23. Failure occurred in both specimens primarily by fiber splitting.

The 90° (transverse) specimen fractured in a plane nearly perpendicular to the loading axis, Fig. 5.24. Extensive fiber splitting occurred.

Fracture surface features of the 63 v/o 5.7 mil BORSIC + 6061-T6 material were similar to those of the 4.2 mil material at 0° but fundamentally different at 10°, 30°, 45°, and 90°. Fiber splitting was nearly absent from all specimens and confined almost entirely to regions adjacent to machined surfaces. Views of 10°, 30°, and 45° fractures are given in Fig. 5.25. A transverse photomicrograph of this material is given in Fig. 5.26.

## 5.2 Sonic Velocity Measurements

### Experimental Method

One inch diameter wafers of BORSIC plus 50% by volume 6061-F aluminum alloy matrix were prepared by electrodischarge machining of hot press diffusion bonded laminates of plasma sprayed monolayer tapes. The sonic velocity across the diameters of two wafers was measured as a function of angle from the filament orientation using the apparatus shown in Fig. 5.27.

A Hewlett Packard Model 214A pulse generator provided a triggering signal for an Arenberg Model PG 650C pulsed oscillator and Tektronic type 556 oscilloscope. A one cycle, 1 MHz, signal was emitted by the pulsed oscillator which activated a damped Bronson Z-701-C 1 MHz transducer. The wave was detected by an undamped transducer positioned on the opposite edge of the specimen. The signal was then conditioned by an Arenberg Model PA-620 preamplifier and an Arenberg Model LFA-550 low frequency amplifier, and displayed on the oscilloscope.

Sonic velocities in the composite disc were calculated using the distance between the transducers and measurements of time obtained with the oscilloscope. The latter were calibrated using aluminum bar stock of known dimensions and sonic velocity.

### Results and Discussion

Sonic velocity measurements were made at ten angles relative to the filament orientation. The results expressed as material density times the square of sonic velocity are given in Fig. 5.28. Young's modulus ( $1/S_{11}$ ) was determined from these measurements using the following relationship (Ref. 5.10):

$$E = \rho V_E^2 \left[ \frac{(1 + \nu)(1 - 2\nu)}{(1 - \nu)} \right] \quad (5.9)$$

where  $E$  = elastic modulus  
 $V_E$  = velocity of sound  
 $\rho$  = material mass density  
 $\nu$  = Poisson's ratio

This expression results from an analysis of extensional wave propagation in elastic isotropic homogeneous plates. BORSIC/aluminum is neither homogeneous nor isotropic, and Poisson's ratio is an elastic constant that varies with the angle of orientation relative to the direction of filament alignment. However, this relationship had been applied to determine composite material moduli using a

constant Poisson's ratio of 0.23 by Zurbrick (Ref. 5.10). Therefore, if  $\nu = 0.23$

$$E = \rho V_E^2 (0.863) \quad (5.10)$$

Using Eq. (5.10) longitudinal and transverse moduli of  $32 \times 10^6$  to  $33 \times 10^6$  psi and  $18 \times 10^6$  to  $20 \times 10^6$  psi, respectively are obtained. These values are close to but slightly below results established by tensile testing, which are  $33.8 \times 10^6$  psi and  $20.5 \times 10^6$  psi respectively.

The accuracy of moduli obtained in this way for off-angles such as  $45^\circ$  ( $22 \times 10^6$  to  $23 \times 10^6$  psi) can be assessed in two ways. Direct comparison with the results of mechanical tests at  $45^\circ$  ( $21.5 \times 10^6$  psi) indicates they are approximately 5% too high. In addition, an indirect assessment can be made using the functional relationship between modulus and angle due to Tsai (Ref. 5.8):

$$\frac{1}{E} = \frac{m^4}{E_L} + \left( \frac{1}{G_{LT}} - \frac{2\nu_{LT}}{E_L} \right) m^2 n^2 + \frac{n^4}{E_T} \quad (5.11)$$

where  $E$  = Young's modulus  
 $m = \cos \theta$   
 $n = \sin \theta$   
 $E_L$  = longitudinal modulus  
 $E_T$  = transverse modulus  
 $G_{LT}$  = shear modulus  
 $\nu_{LT}$  = major Poisson's ratio

Using  $E_L = 32.5 \times 10^6$  psi,  $E_T = 19.0 \times 10^6$  psi,  $\nu_{LT} = 0.23$  and fitting Eq. (5.11) to the values of off-axis modulus, one obtains a value of  $G_{LT}$  of approximately  $9 \times 10^6$  psi. This value is approximately 10% higher than the value obtained using mechanical tests,  $8.15 \times 10^6$  psi.

In BORSIC-aluminum these disparities are of a similar order as the uncertainty in measurements and resulting values may be useful. However, much greater errors arise with polymeric matrix composites such as boron-polyimide (Ref. 5.11). Off-axis moduli determined using the assumption that  $E$  (or  $1/S_{11}$ ) is directly related to  $\rho V_E^2$  by Eq. (5.10) lead to values of shear moduli higher than those measured by other tests.

Reuter gives an analysis of wave propagation in an orthotropic plate in plane stress leading to the following relationships (Ref. 5.12):

$$v_{E-S}^2 = \frac{2}{\rho \{ (L+N) - [(L-N)^2 + 4M^2]^{1/2} \}} \quad (5.12)$$

$$v_{S-E} = \frac{2}{\rho \{ (L+N) + [(L-N)^2 + 4M^2]^{1/2} \}} \quad (5.13)$$

where  $V_{E-S}$  = extension-shear wave velocity  
 $V_{S-E}$  = shear-extension wave velocity  
 $L = S_{66} - S_{26}^2/S_{22}$   
 $M = S_{16} - S_{12}S_{22}$   
 $N = S_{11} - S_{12}^2/S_{22}$   
 $S_{ij}$  = compliance coefficients

For the special cases of longitudinal and transverse orientations, these expressions reduce to the following:

$$E_{11} = \rho V_E^2 (1 - E_{22}/E_{11} \nu_{12}^2), \quad \theta = 0^\circ \quad (5.14)$$

$$E_{22} = \rho V_E^2 (1 - E_{22}/E_{11} \nu_{12}^2), \quad \theta = 90^\circ \quad (5.15)$$

$$G_{12} = \rho V_S^2 \quad \theta = 0^\circ \text{ or } \theta = 90^\circ \quad (5.16)$$

Equations (5.12) and (5.13) indicate that  $E_{11}$  and  $E_{22}$  are not simply proportional to density times the square of the proper wave velocity as in Eq. (5.9).

The ratio of  $0.863 \rho V_E^2$  to  $E$  was calculated as a function of angle using Eqs. (5.11) and (5.12) and is given in Fig. 5.29. The results show that  $E (1/S_{11})$  is underestimated at low and high angles and overestimated at intermediate orientations ( $25^\circ$  to  $50^\circ$ ). The combined effect results in a larger overestimate of  $G_{12}$ . In addition, the assumption that the direction of energy propagation is coincident with transducer orientation which was used to calculate the sonic velocity is not valid at all angles in fiber reinforced composites because the wavefront is not spherical and wave interference effects can arise (Ref. 5.13). Thus, considerable attention must be given to experimental technique, particularly in more orthotropic systems.

Theoretical values of  $\rho V_E^2$  are given with the experimental data in Fig. 5.29. Experimental values are approximately 8% higher than the theoretical level (Reuter) at  $0^\circ$  which represents the greatest point of disparity. Since  $\rho$  can be accurately determined, the greatest disparity in  $V_E$  is approximately 4%.

### 5.3 Conclusions

1. Off-axis tensile testing of BORSIC + 6061 aluminum can be used to determine elastic and strength properties as a function of orientation without significant complications due to system orthotropy.
2. The elastic constants of BORSIC + 6061 are within 8% of the values predicted by micromechanical analyses and the variation of elastic properties with angle is consistent with expectation based on the transformation equations.
3. The ultimate strength of BORSIC + 6061 composite material as a function of angle is well represented by the maximum distortional energy failure criterion.

4. The extensional wave velocity,  $V_E$ , measured in BORSIC + 6061 as a function of angle to the filament direction are within 4% of the values predicted by the Reuter analysis which includes shear coupling effects.

5. Off-axis BORSIC + 6061 elastic moduli determined using the assumption by Zurbrick that  $E (1/S_{11})$  is directly proportional to  $\rho V_E^2$  lead to values of  $G_{12}$  that are approximately 10% higher than those determined by other methods. The error would be greater in the case of more orthotropic composite systems.

## SECTION V - REFERENCES

1. S. W. Tsai, "Strength Theories of Filamentary Structures, Fundamental Aspects of Fiber Reinforced Composites", Interscience Publishers, 1968.
2. V. D. Azzi and S. W. Tsai, Exp. Mech., 1965.
3. N. J. Pagano and J. C. Halpin, J. Composite Materials, Vol. 2, p. 18, 1968.
4. R. R. Rizzo, J. Composite Materials, Vol. 3, p. 202, 1969.
5. E. Wu and R. Thomas, J. Composite Materials, Vol. 2, p. 523, 1968.
6. G. L. Richards, T. P. Airhart, and J. E. Ashton, J. C mposite Materials, Vol. 3, p. 586, 1969.
7. J. E. Ashton, J. C. Halpin, and P. H. Petit, Primer on Composite Materials: Analysis, Technomic Publishing Co., p. 98, 1969.
8. S. W. Tsai, "Mechanics of Composite Materials Part II: Theoretical Aspects", Technical Report AFML-TR-66-149, Nov. 1966.
9. N. J. Pagano, "The Importance of Signs of Shear Stress and Shear Strain in Composites", J. Composite Materials, Vol. 3, p. 166, 1969.
10. J. R. Zurbrick, "Development of Nondestructive Tests for Predicting Elastic Properties and Component Volume Fractions in Reinforced Plastic Composite Materials", Contract F33615-67-C-1285, Tech. Report, AFML-TR-68-233, Sept. 1968.
11. L. E. Dardi and F. J. Vicki, Pratt & Whitney Aircraft, Unpublished work.
12. R. C. Reuter, J. Comp. Materials, Vol. 4, p. 129, Jan. 1970.
13. Private Communication, Prof. Pao, Cornell University.
14. R. Hill, "Theory of Mechanical Properties of Fiber-Strengthened Materials: I. Elastic Behavior", J. Mech. Phys. Solids, Vol. 12, p. 199, 1964.
15. J. J. Hermans, "The Elastic Properties of Fiber-Reinforced Materials When the Fibers are Aligned", Koninklijke Nederlandse Akademik Van Wetenschappen, Amsterdam Proceedings, Series B, Vol. 70, No. 1, p. 1, 1967.
16. A. R. Zecca and D. R. Hay, "Elastic Properties of Metal-Matrix Composites", J. Composite Materials, Vol. 4, p. 566, 1970.
17. J. C. Halpin and S. W. Tsai, "Environmental Factors in Composite Materials Design", AFML-TR-67-423.

SECTION V - REFERENCES (Cont'd)

18. Hashim and B. W. Rosen, "The Elastic Moduli of Fiber-Reinforced Materials", J. of Applied Mechanics, p. 223, June 1964.
19. K. R. Van Horn, ed., Aluminum, Vol. 1, Properties, Physical Metallurgy, and Phase Diagrams, American Society for Metals, Metals Park, Ohio, 1967.



FIGURE 5-1  
OFF-AXIS SPECIMEN IN ROTATING GRIDS



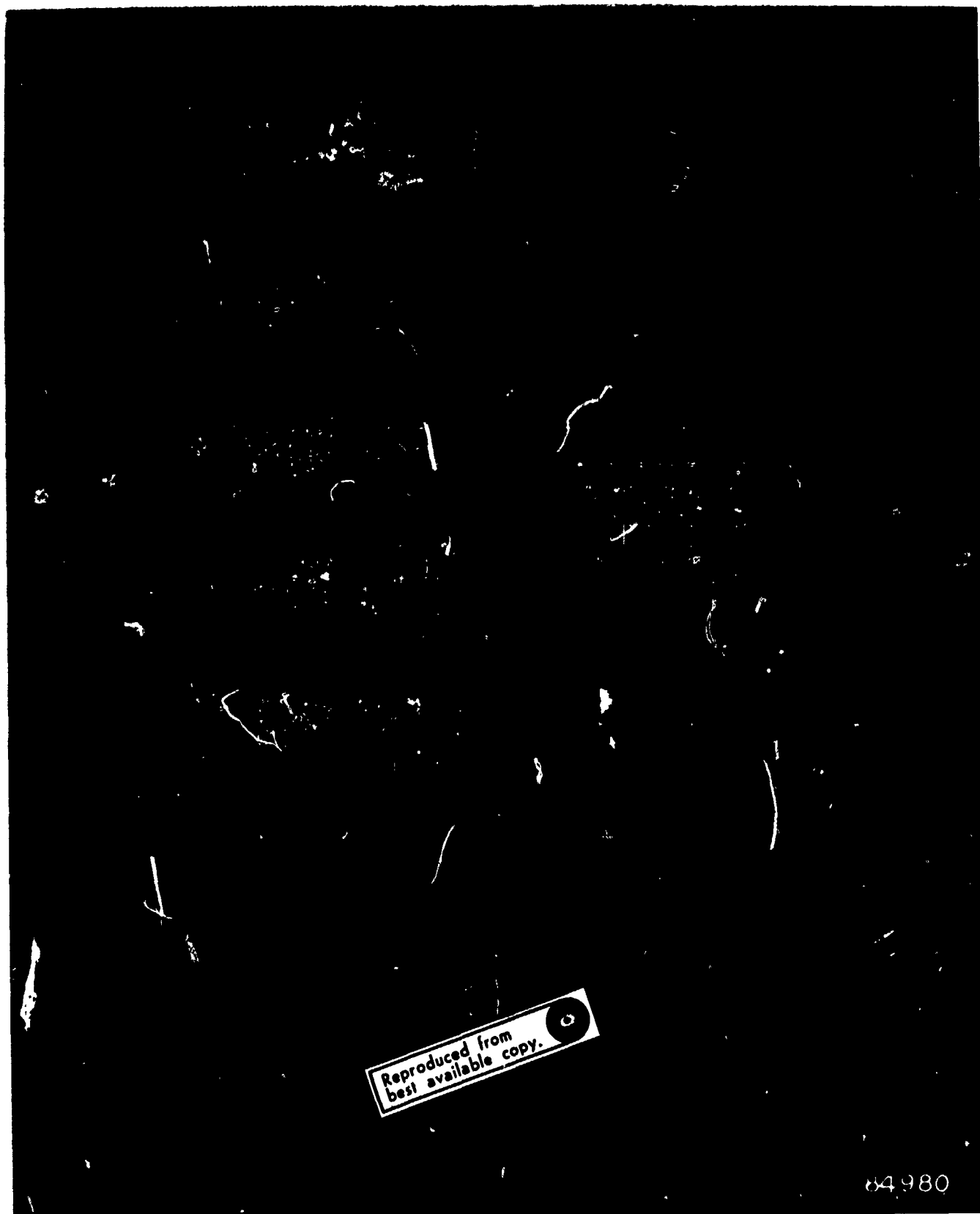


FIGURE 5-2  
CONTINUOUS LOAD-STRAIN RECORDING INSTRUMENTATION

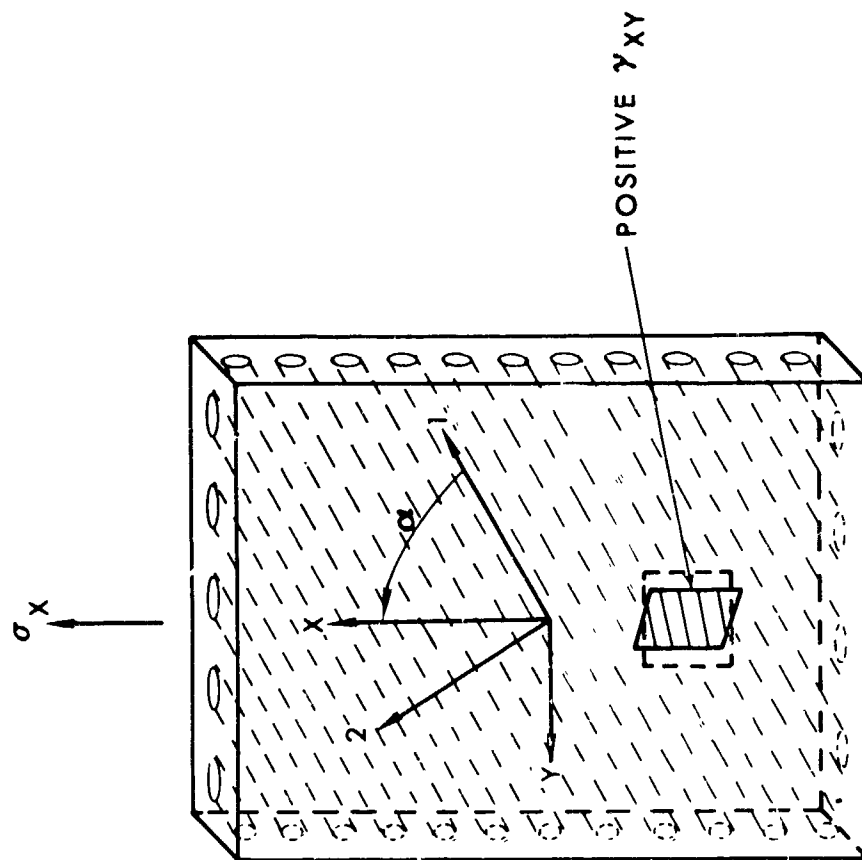
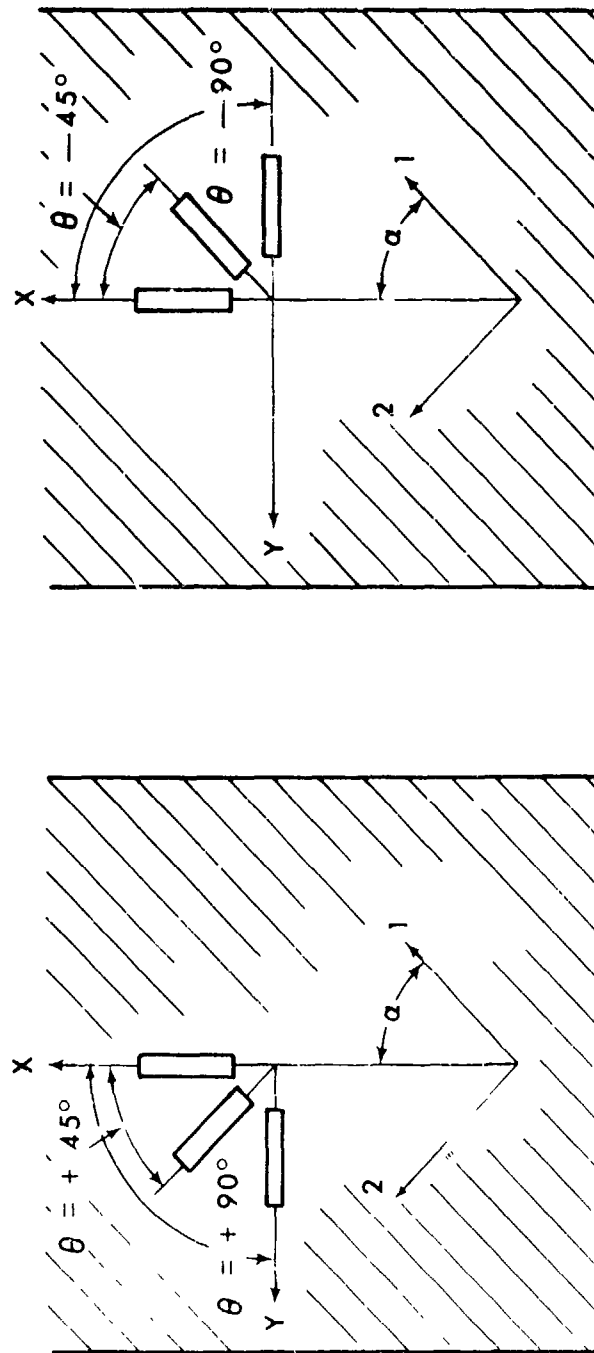


FIGURE 5-3  
COORDINATE SYSTEM FOR OFF-AXIS UNIAXIAL TENSION TESTS  
WITH ORTHOTROPIC AXES 1, 2 AND LOAD AXES X, Y



CONFIGURATION I

CONFIGURATION II

FIGURE 5-4  
ROSETTE STRAIN GAGE CONFIGURATIONS USED  
IN OFF-AXIS TENSION TESTS

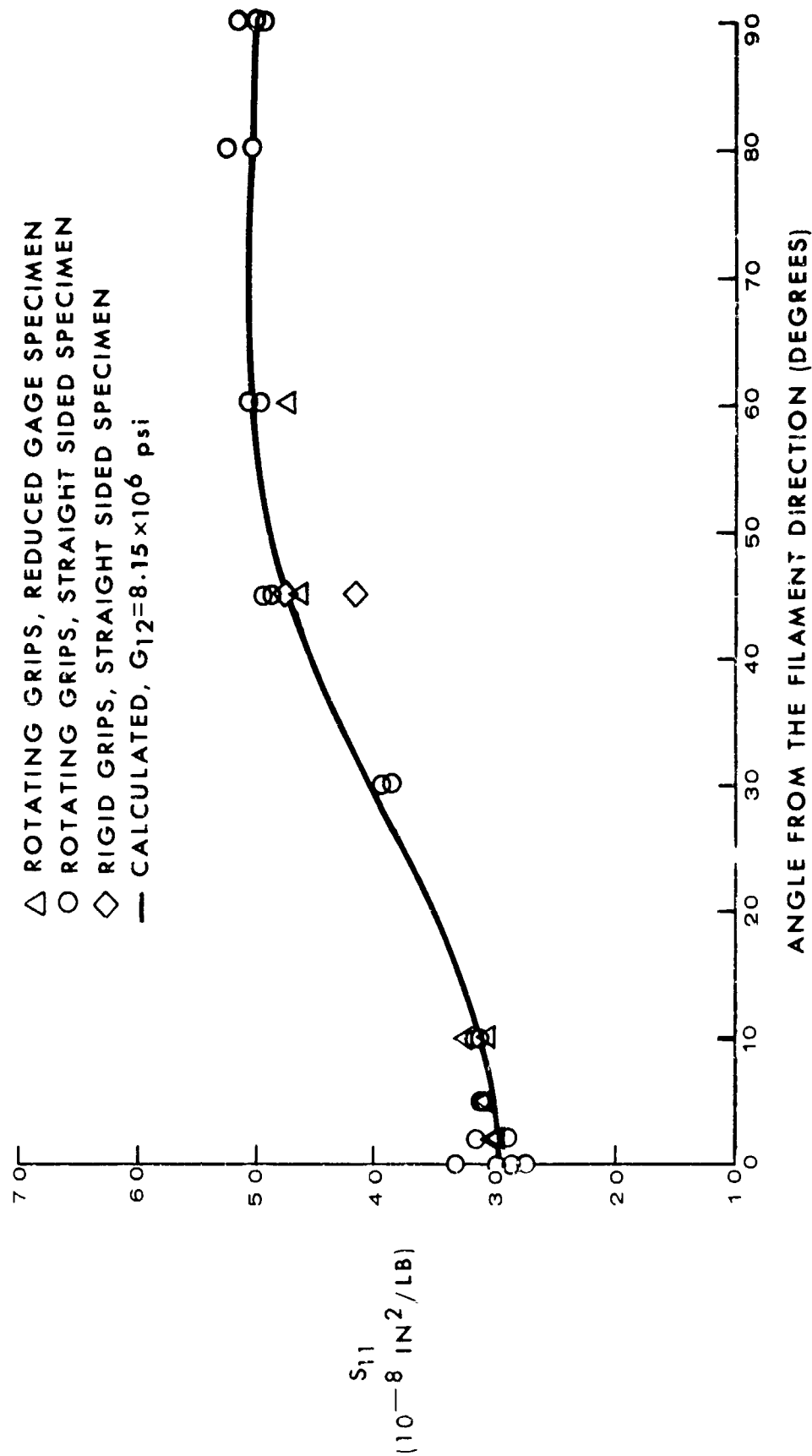


FIGURE 5-5

$S_{11}$  OF UNIDIRECTIONAL 4.2 mil BORSIC -6061F ALUMINUM  
 AS A FUNCTION OF ANGLE FROM THE FILAMENT DIRECTION

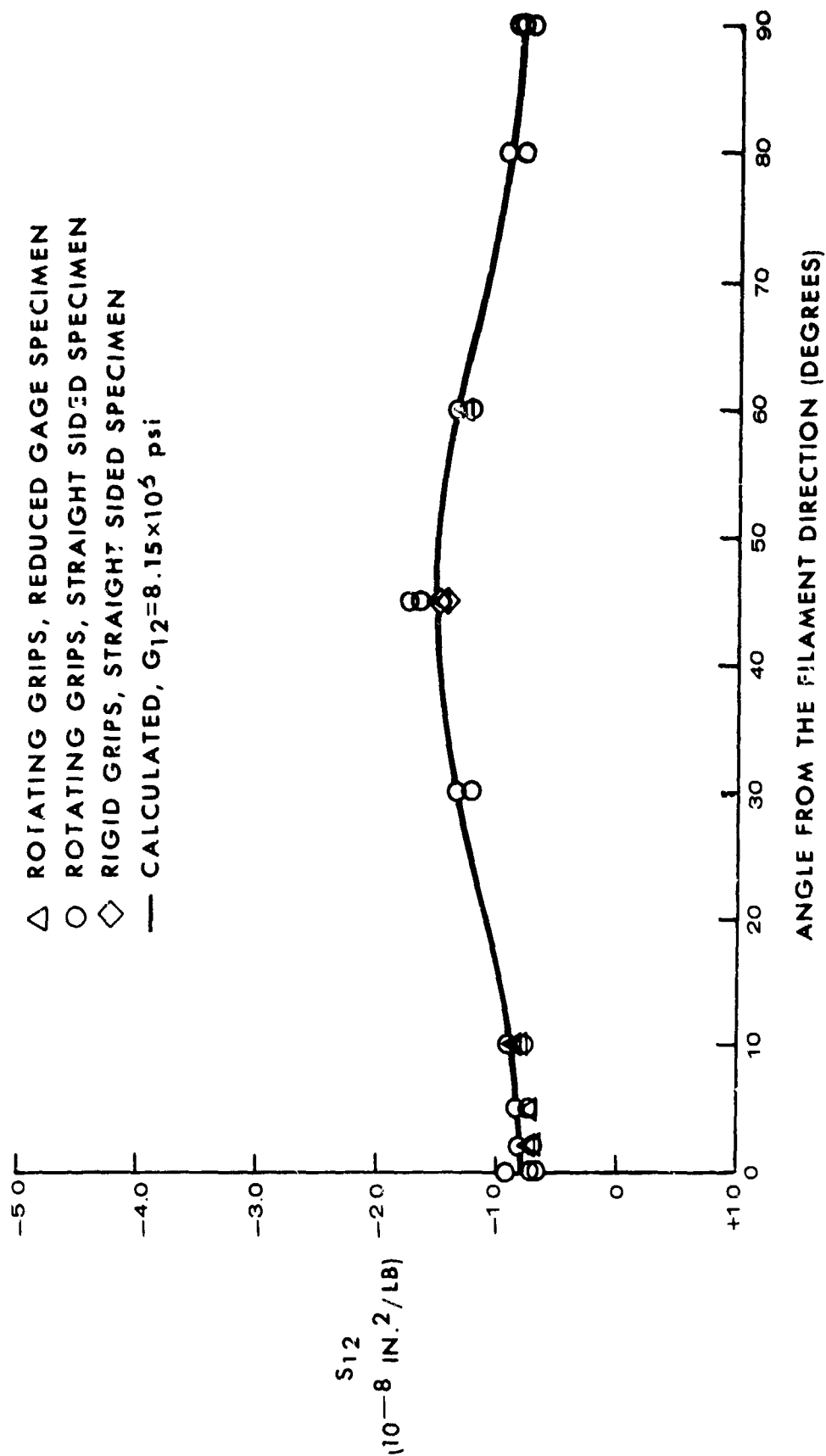


FIGURE 5-6

$S_{12}$  OF UNIDIRECTIONAL 4.2mil BORSIC -6061F ALUMINUM AS A FUNCTION  
 OF ANGLE FROM THE FILAMENT DIRECTION

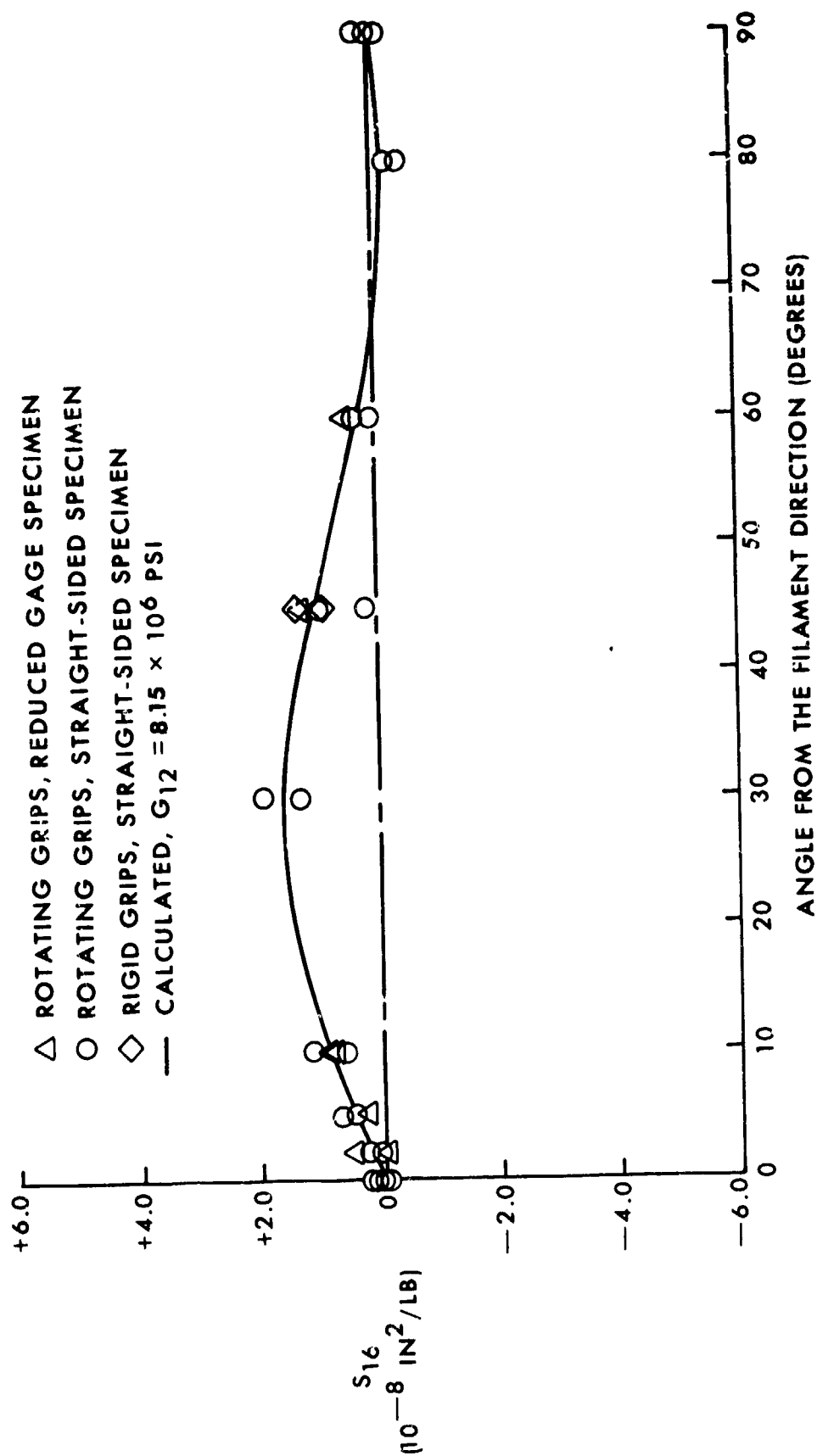
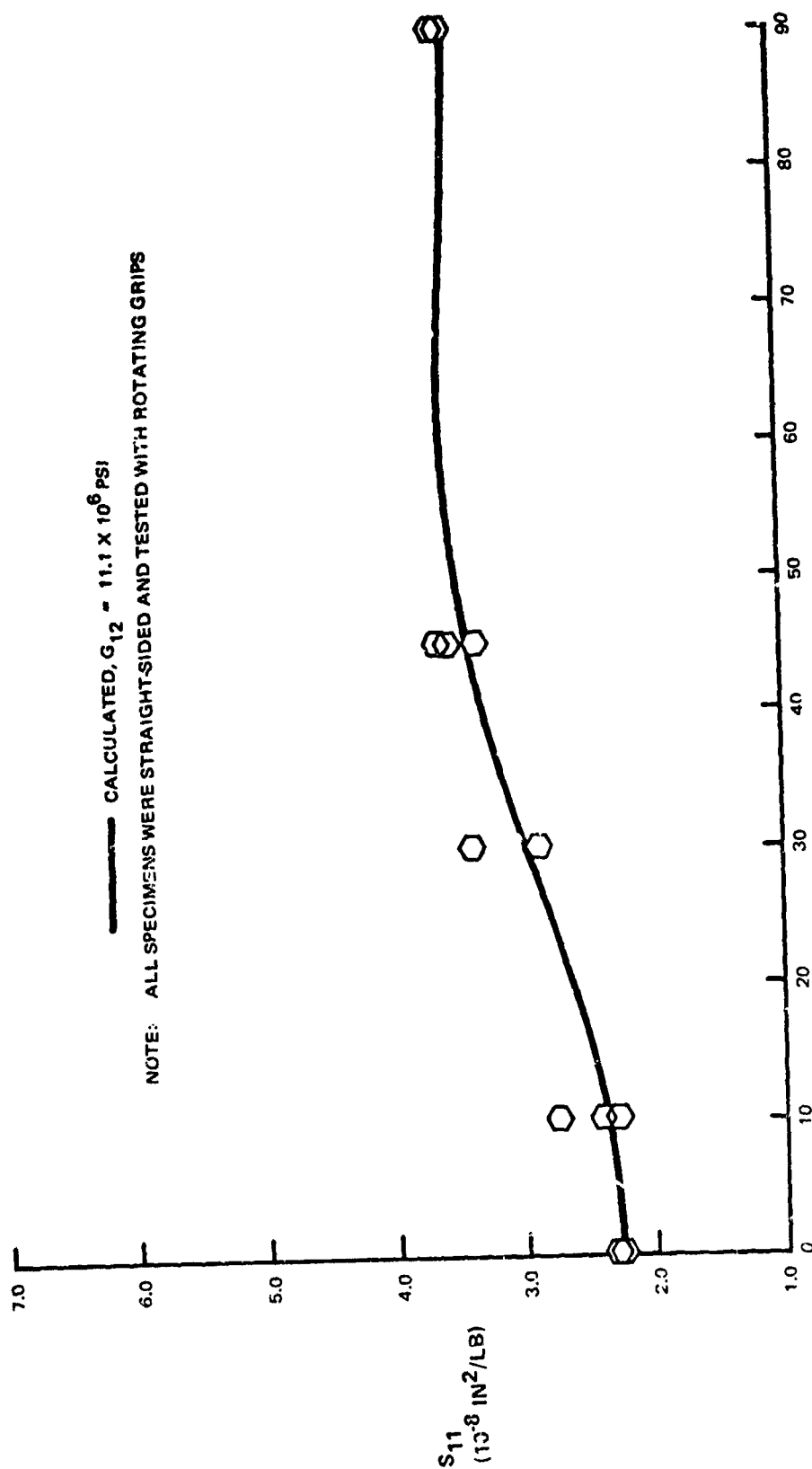


FIGURE 5-7

$S_{16}$  OF UNIDIRECTIONAL 4.2 MIL BORSIC -6061F ALUMINUM AS A FUNCTION  
 OF ANGLE FROM THE FILAMENT DIRECTION



ANGLE FROM THE FILAMENT DIRECTION (DEGREES)

FIGURE 5-8  
 $S_{11}$  OF UNIDIRECTIONAL 5.7 MIL BORSIC + 6061-T6 ALUMINUM  $\mu$  AS A FUNCTION  
 OF ANGLE FROM THE FILAMENT DIRECTION

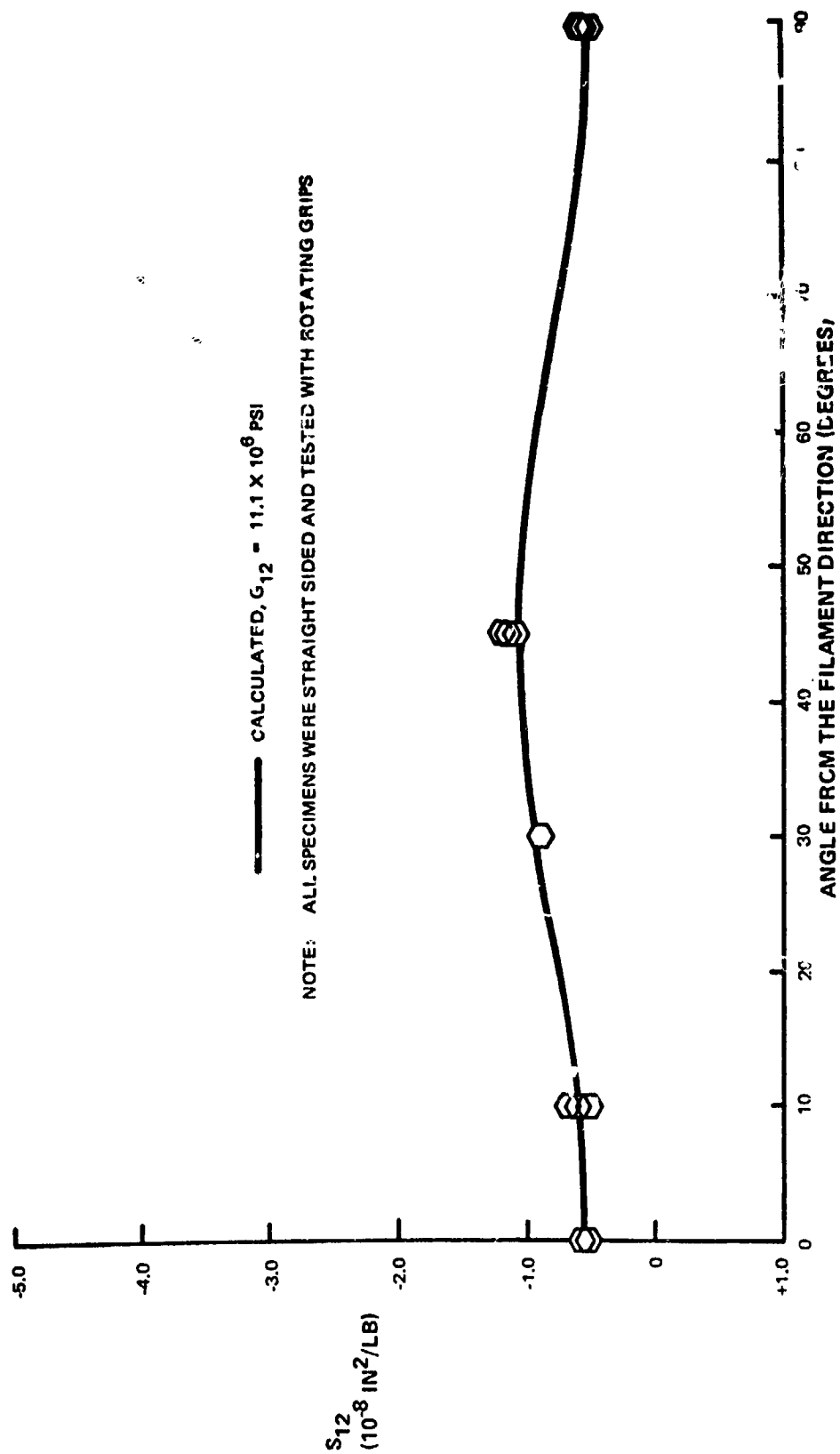


FIGURE 5-9  
 $S_{12}$  OF UNIDIRECTIONAL 5.7 MIL BORSIC + 6061-T5 ALUMINUM AS A FUNCTION  
 OF ANGLE FROM THE FILAMENT DIRECTION



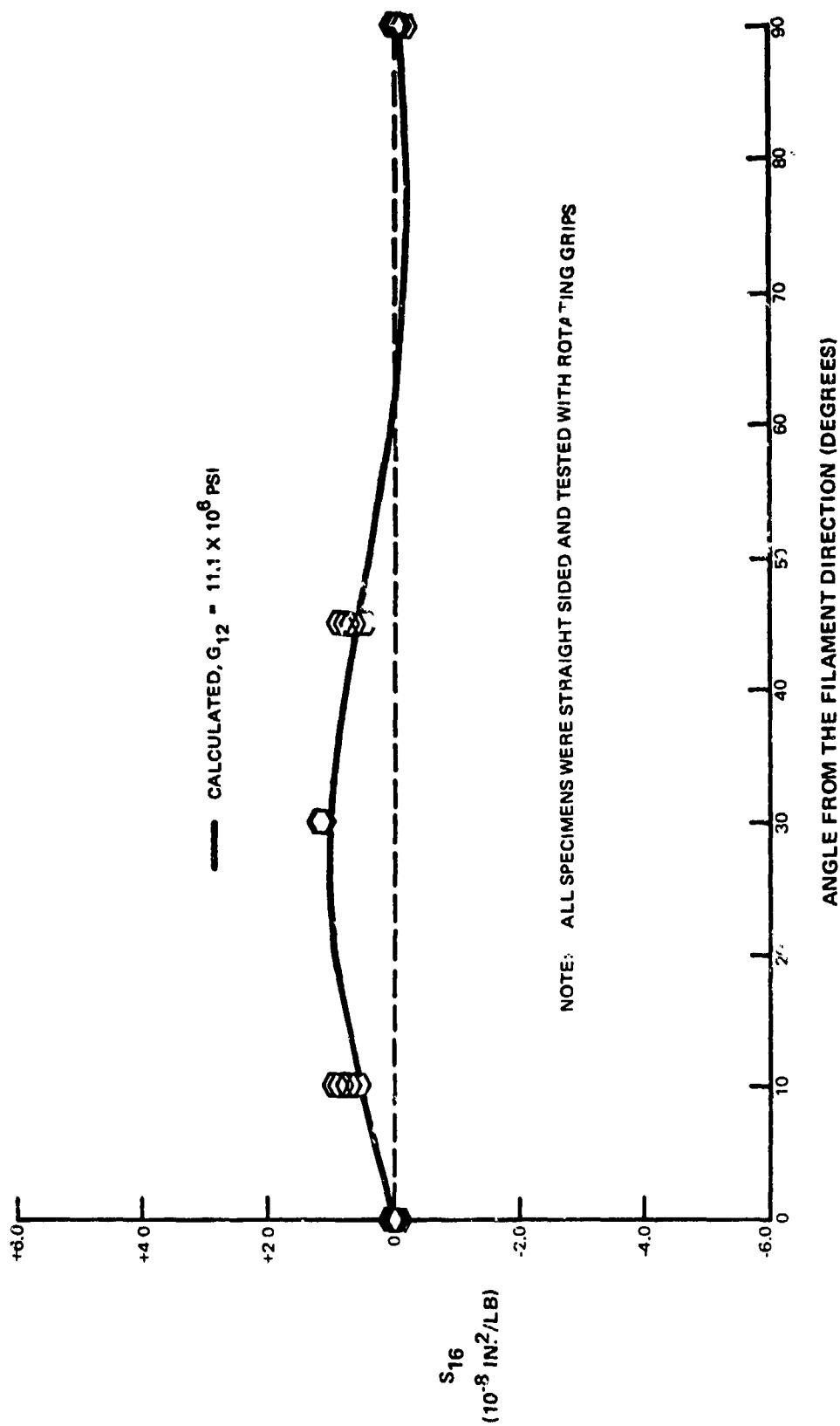


FIGURE 5-10  
 $S_{16}$  OF UNIDIRECTIONAL 5.7 MIL BORSIC + 6061-T6 ALUMINUM AS A FUNCTION  
 OF ANGLE FROM THE FILAMENT DIRECTION

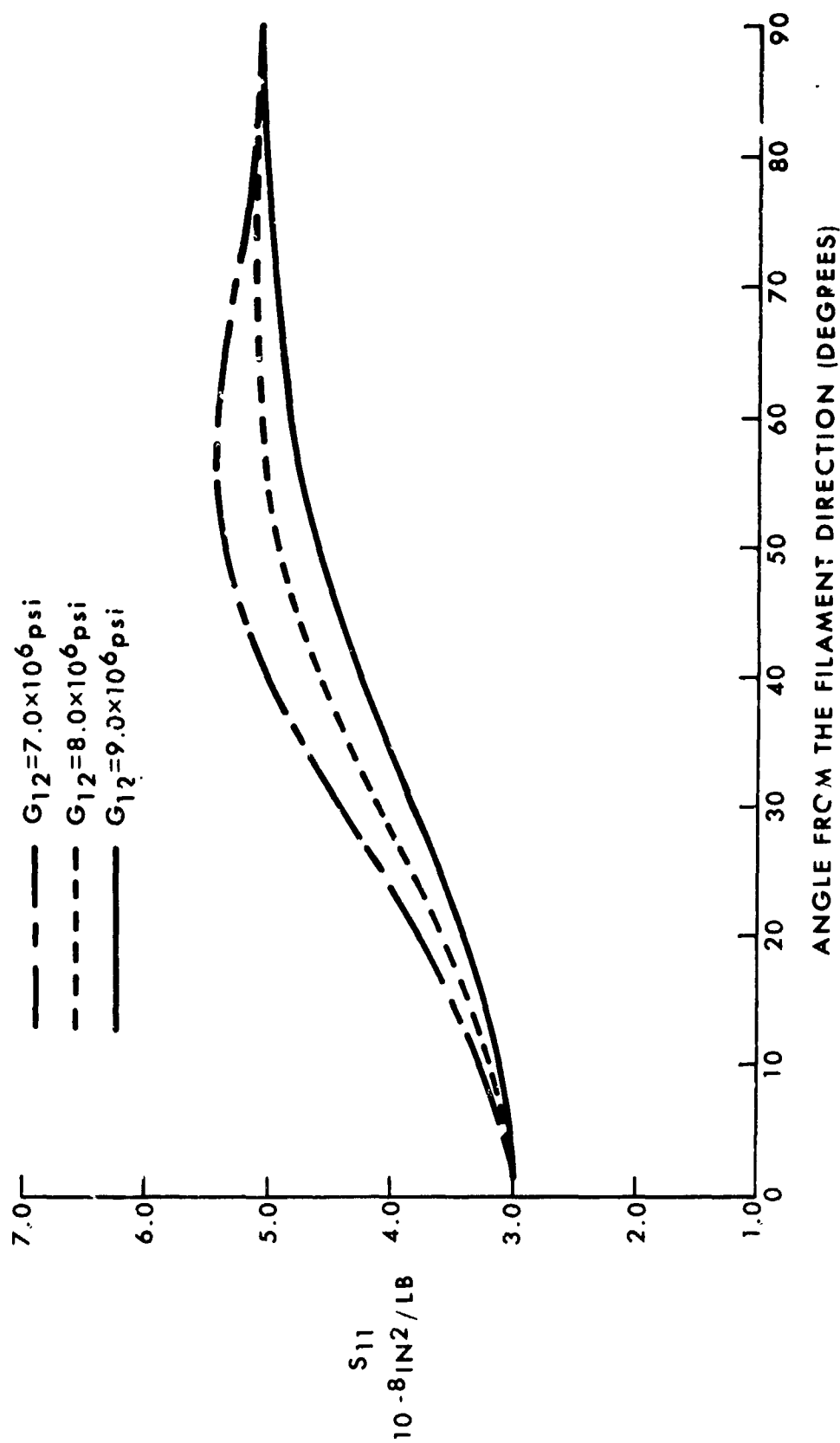


FIGURE 5-11

THEORETICAL  $S_{11}$  VALUES FOR UNIDIRECTIONAL BORSIC-6061F ALUMINUM  
AS A FUNCTION OF ANGLE FROM THE FILAMENT DIRECTION

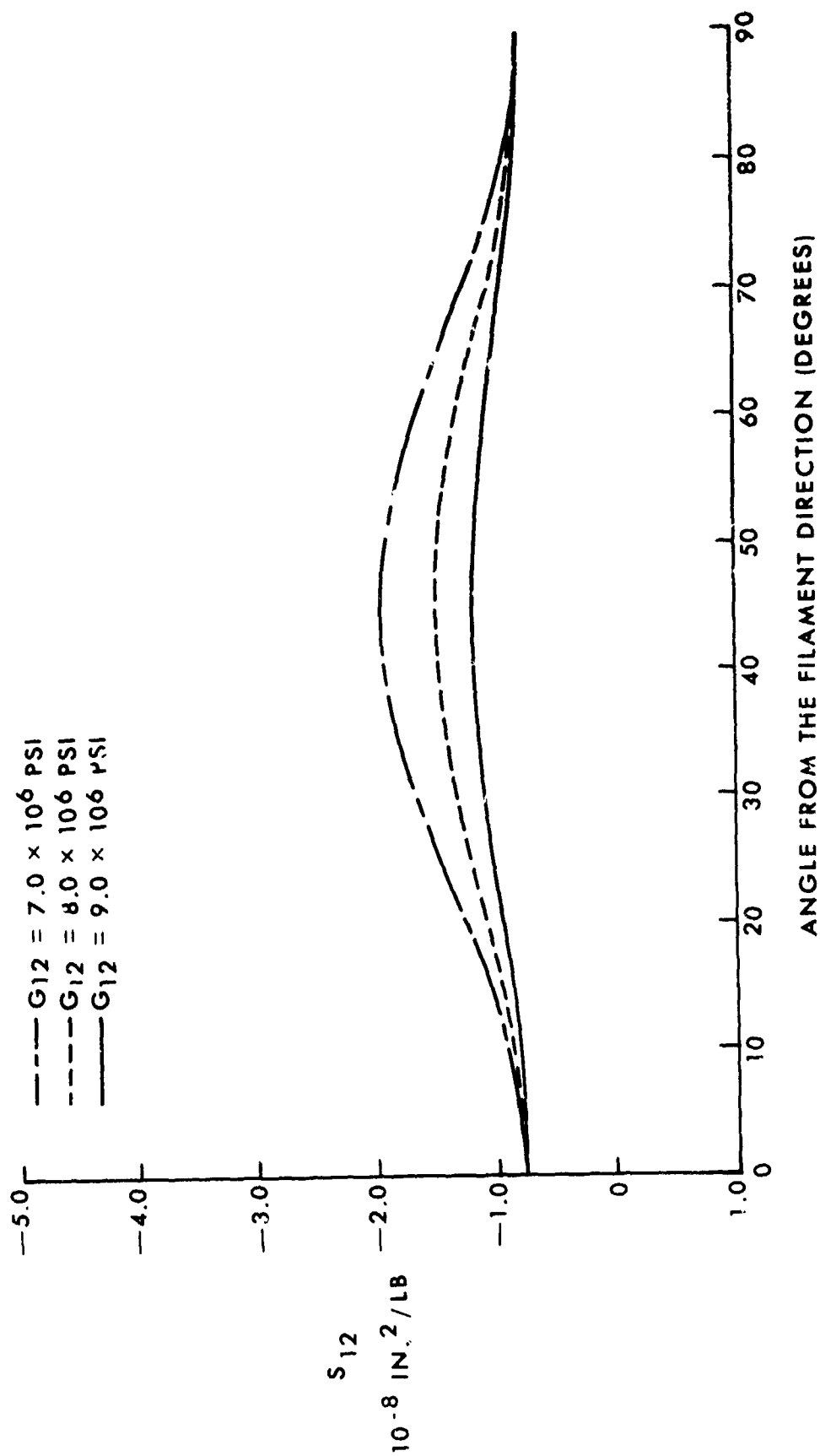


FIGURE 5-12

THEORETICAL  $S_{12}$  VALUES FOR UNIDIRECTIONAL BORSIC-6061F ALUMINUM  
AS A FUNCTION OF ANGLE FROM THE FILAMENT DIRECTION

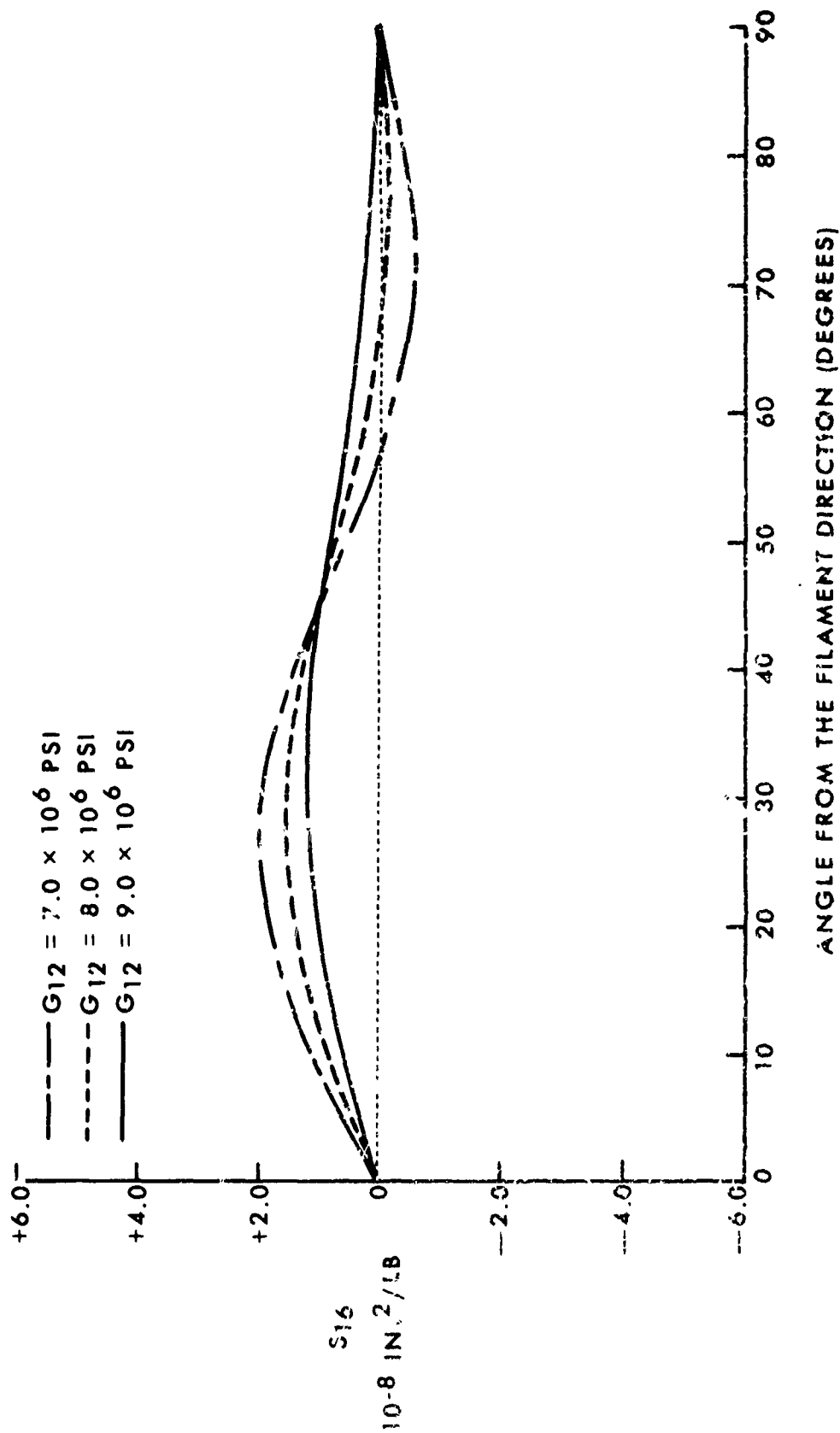


FIGURE 5-13

THEORETICAL  $S_{16}$  VALUES FOR UNIDIRECTIONAL BORSIC-6061F  
ALUMINUM AS A FUNCTION OF ANGLE FROM THE FILAMENT DIRECTION

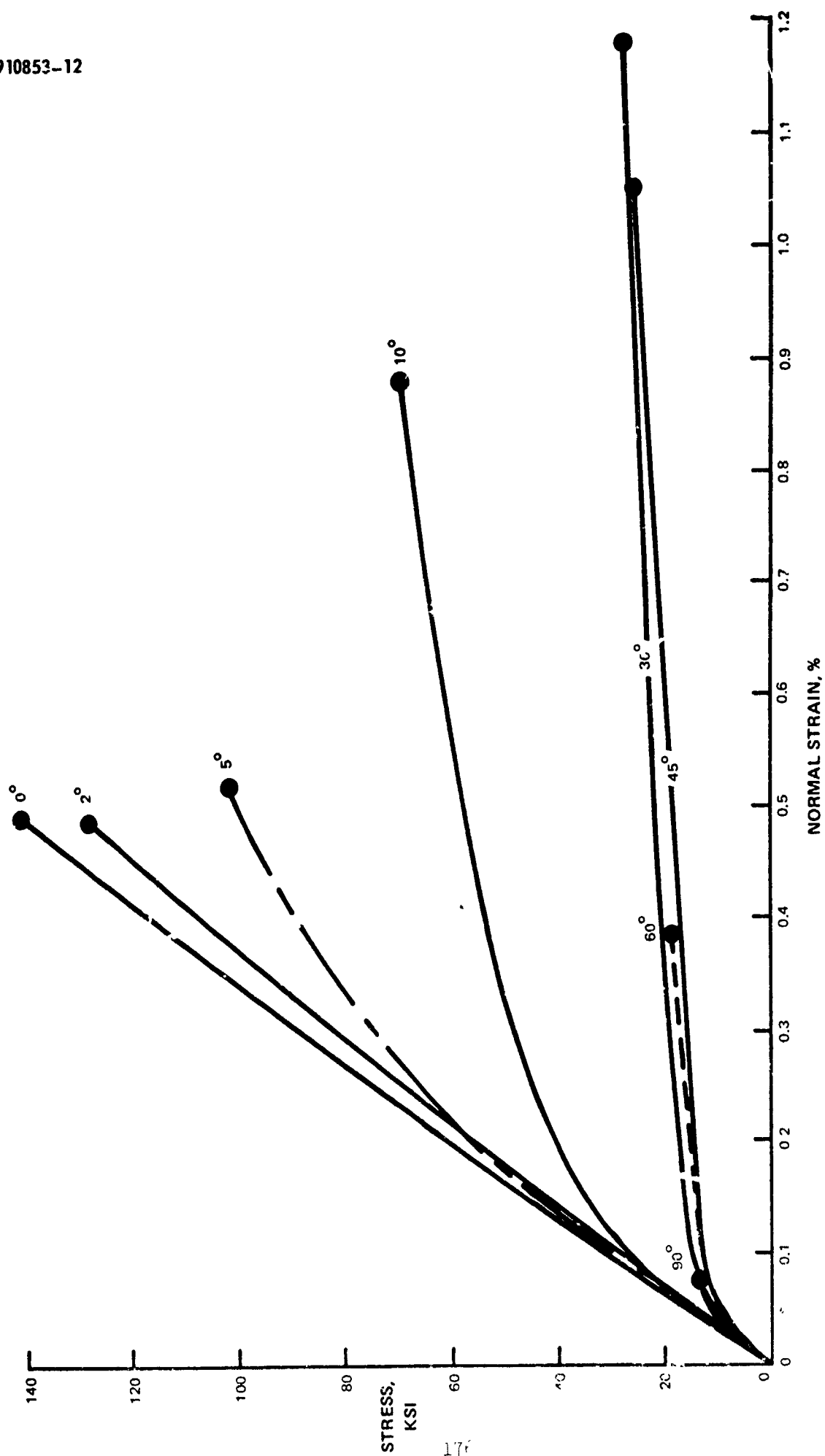
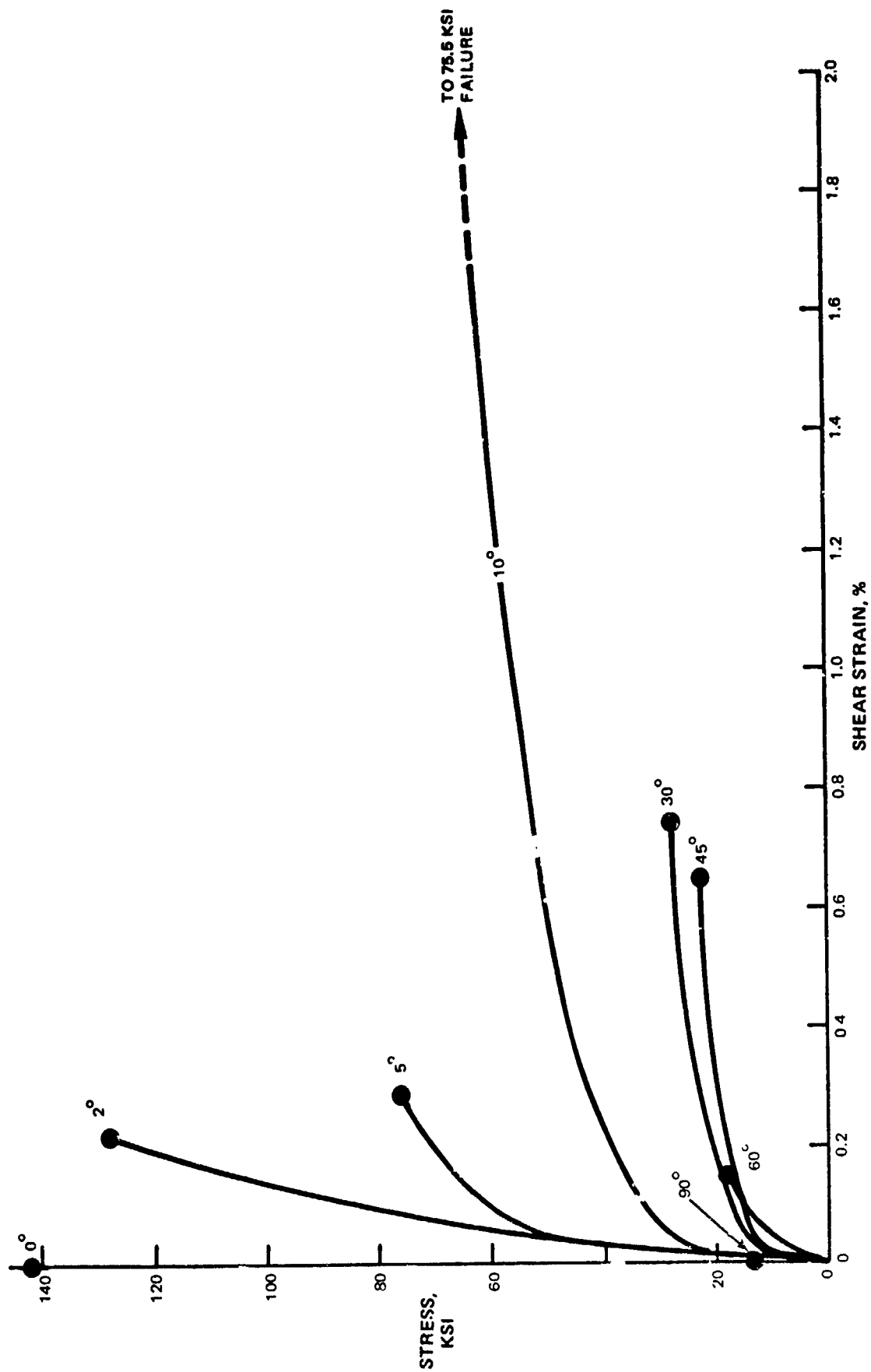
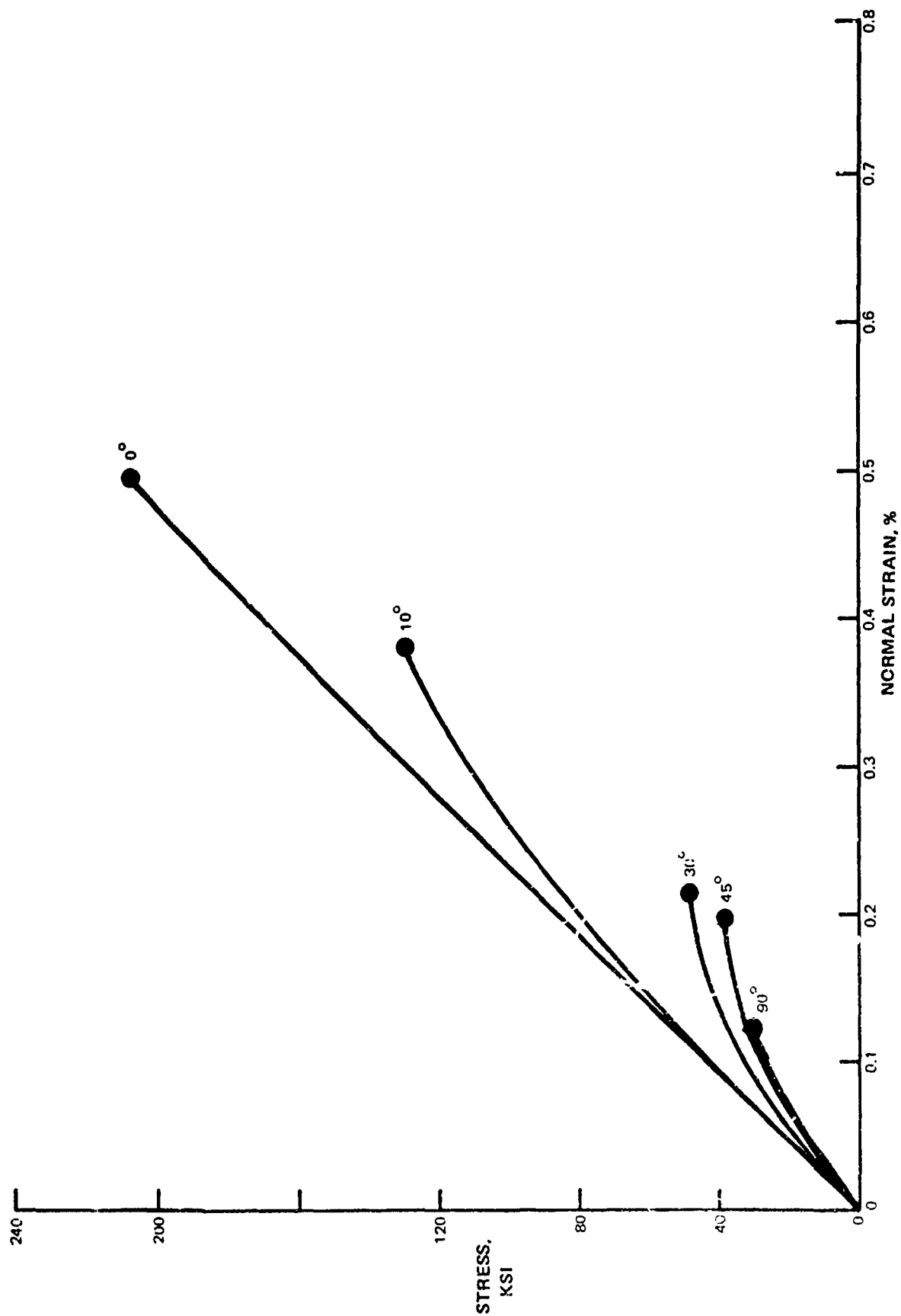


FIGURE 5-14  
STRESS - NORMAL STRAIN CURVES FOR 50 V/O 4.2 MIL BORSIC + 6061F ALUMINUM

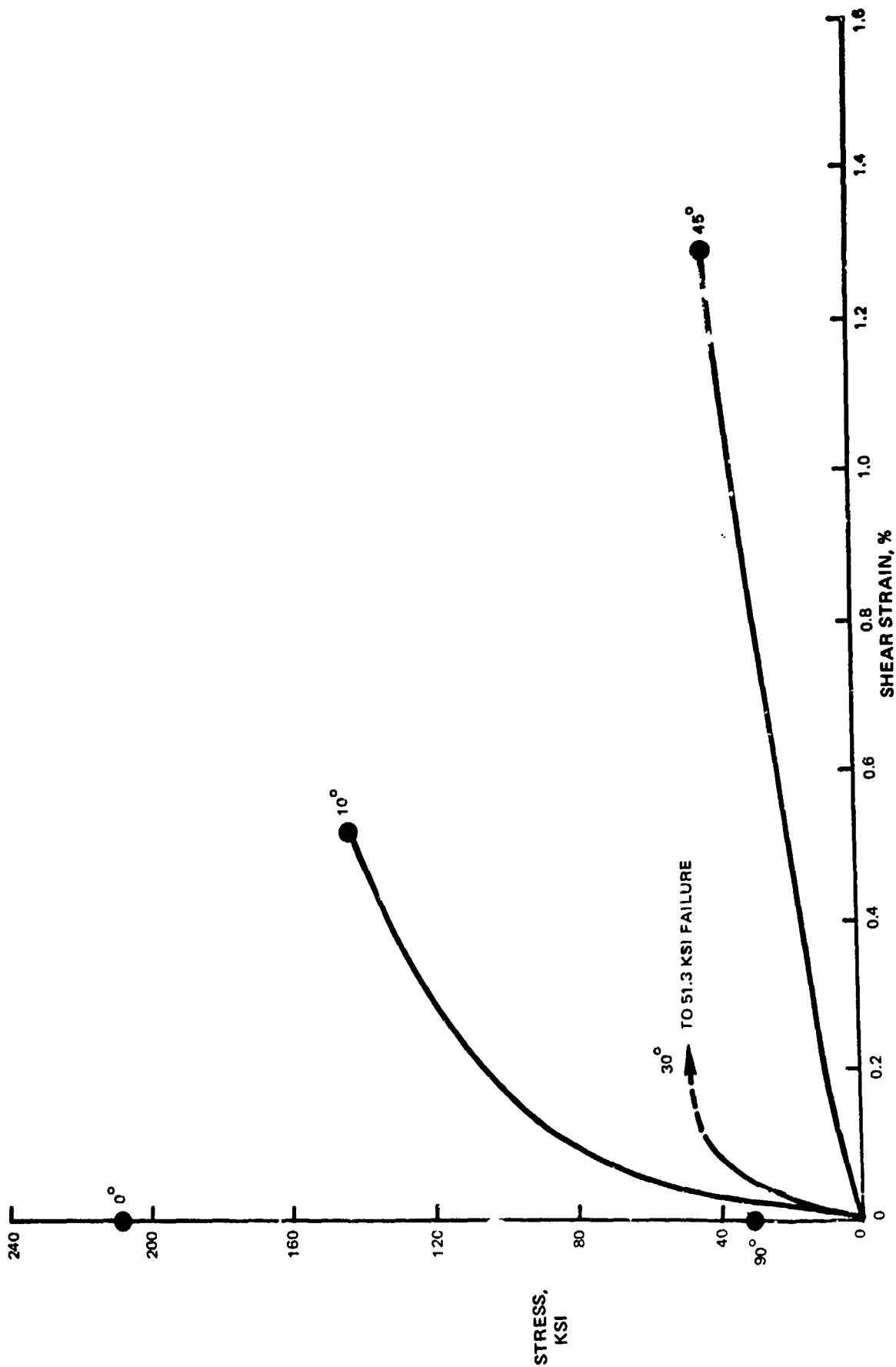


STRESS - SHEAR STRAIN CURVES FOR 50 V/0 4.2 MIL BORSIC + 6061F ALUMINUM  
FIGURE 5-15



STRESS - NORMAL STRAIN CURVES FOR 63 V/O 5.7 MIL BORSIC + 6061-T6 ALUMINUM

FIGURE 5-16



STRESS - SHEAR STRAIN CURVES FOR 63 v/o 5.7 MIL BORNIC + 6061-T6 ALUMINUM  
FIGURE 5-17



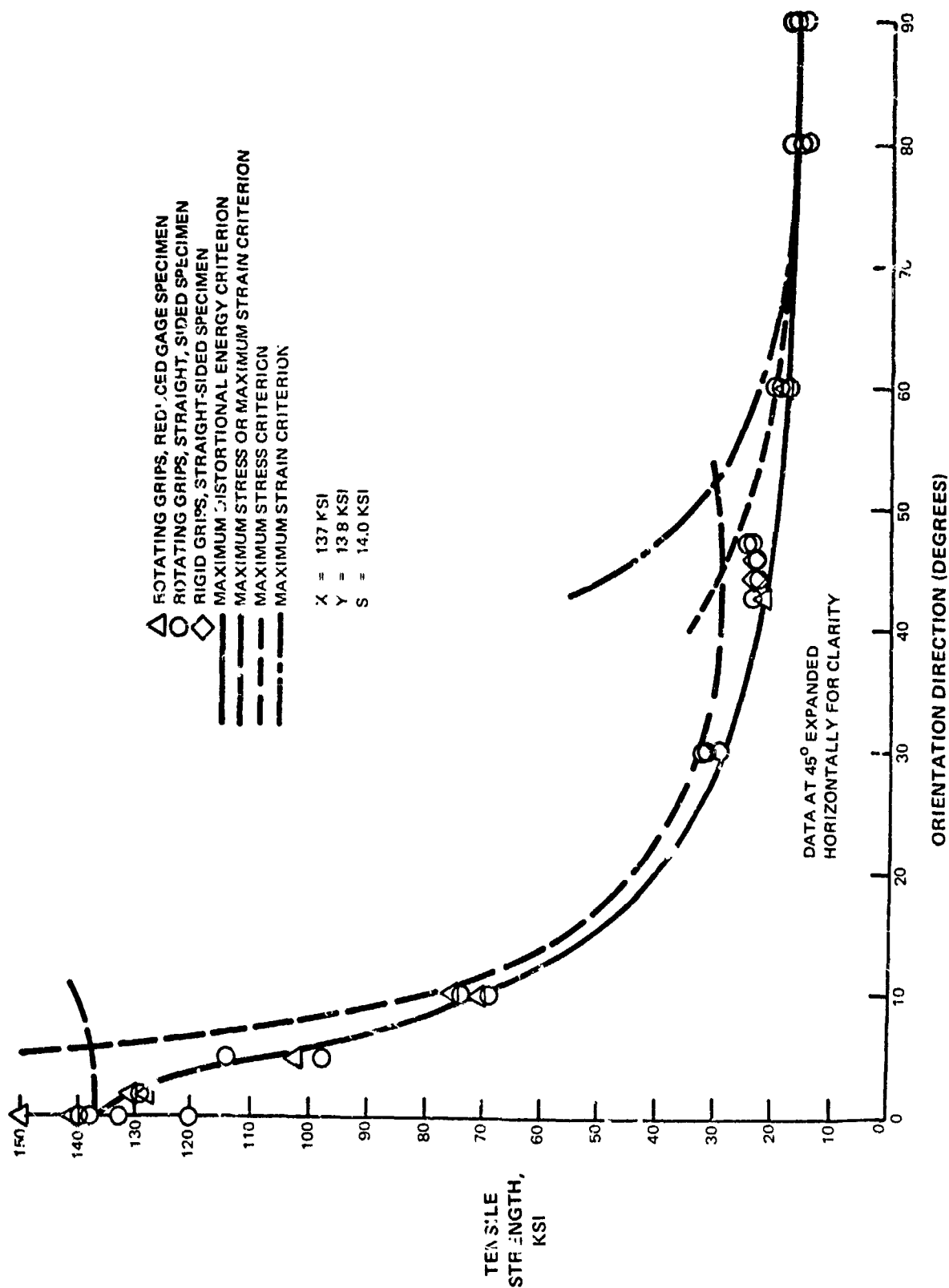


FIGURE 5-18  
OFF-AXIS TENSILE STRENGTH OF 4.2 MIL BORSIC + 6061F ALUMINUM

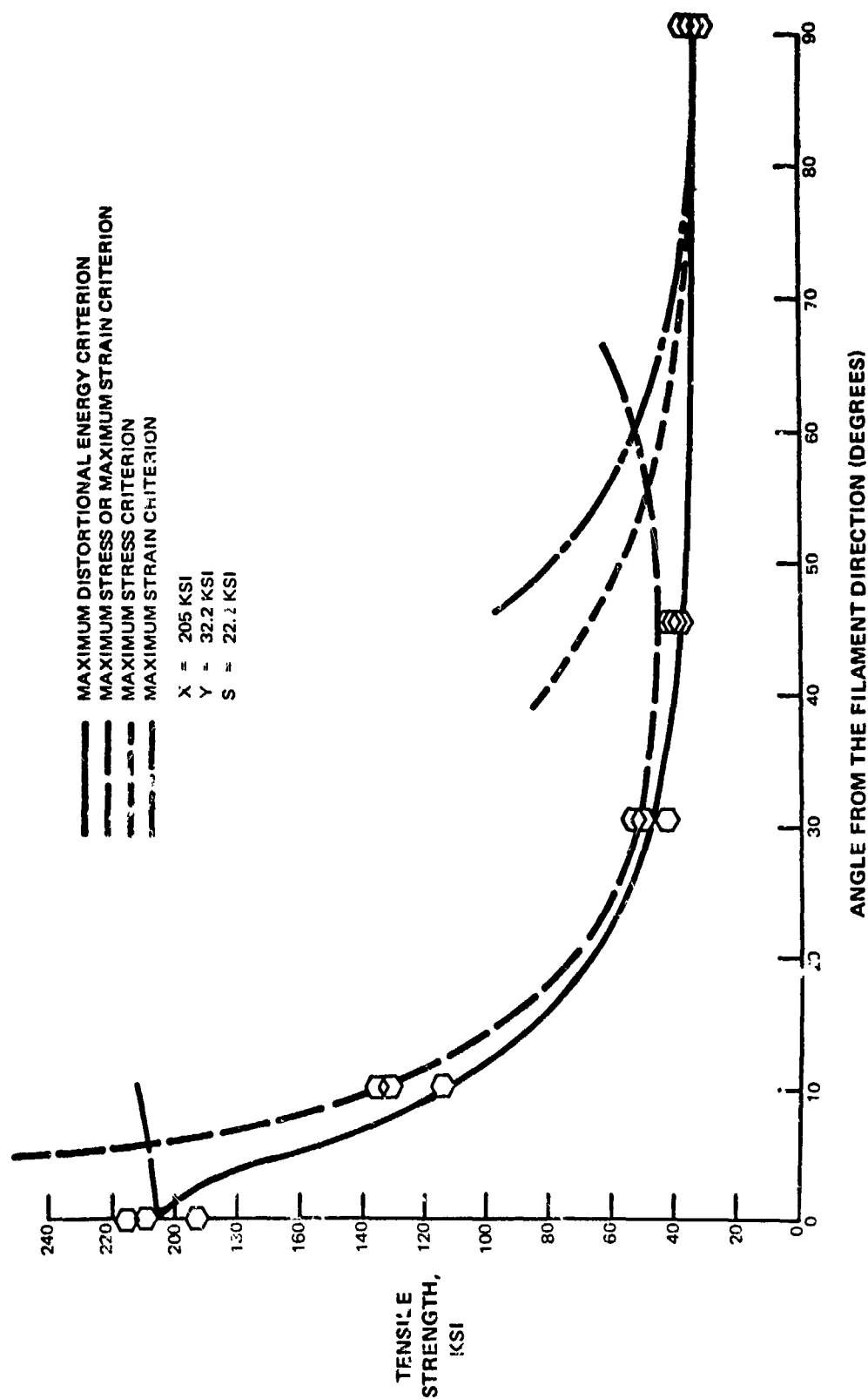
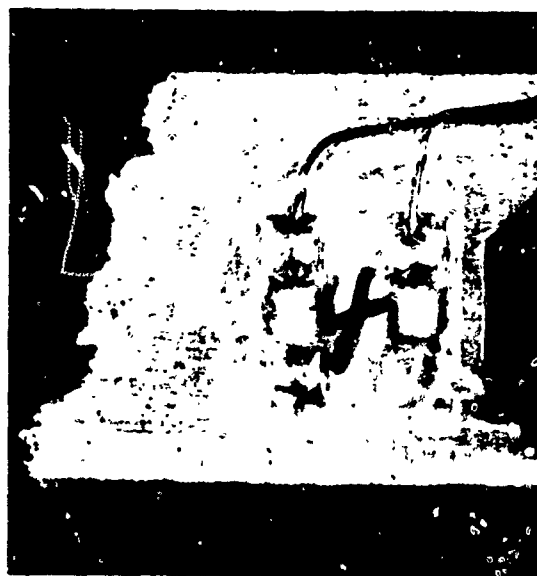


FIGURE 5-19

OFF-AXIS TENSILE STRENGTH OF 5.7 MIL BORSIC + 6061-T6 ALUMINUM



Reproduced from  
best available copy.

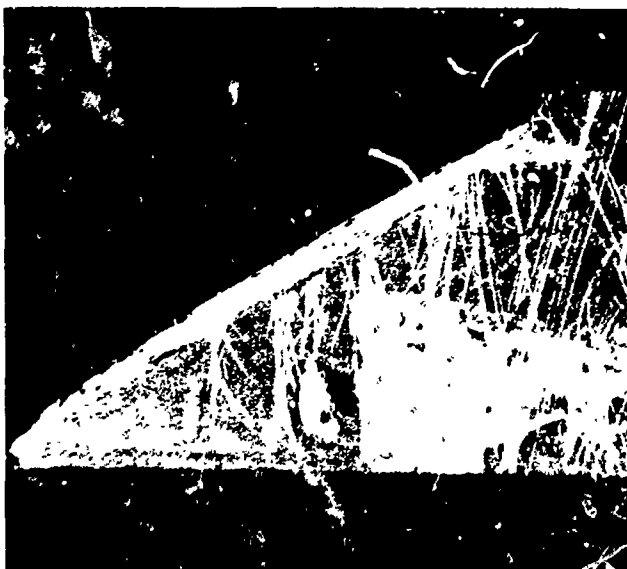


5°

2°

0°

FIGURE 5-20  
END AND SIDE VIEWS OF FRACTURED 0.2, AND 5 DEGREE OFF-AXIS 50 v/c 4.2 MIL  
BORSIC 6061-F ALUMINUM TENSILE SPECIMENS



Reproduced from  
best available copy.



30°

10°

FIGURE 5-21  
END AND SIDE VIEWS OF FRACTURED 10 AND 30 DEGREE OFF AXIS 0.2 MIL BCRSIC  
+ 6061F ALUMINUM TENSILE SPECIMENS



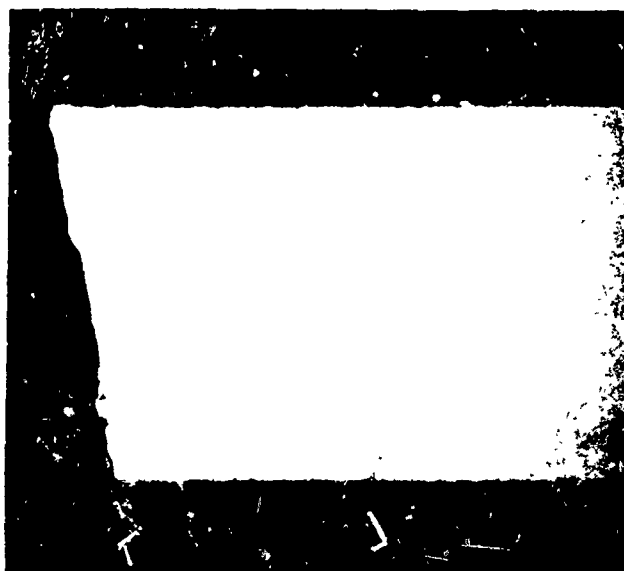
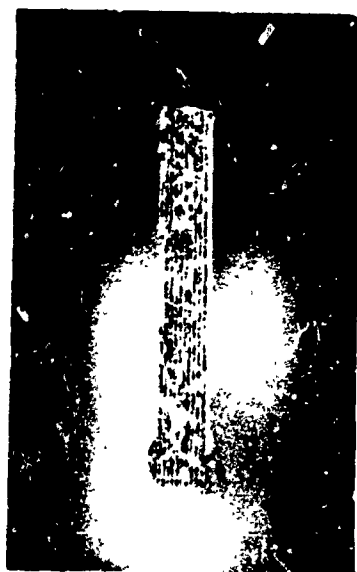
45° (RIGID GRIP)

Reproduced from  
best available copy.



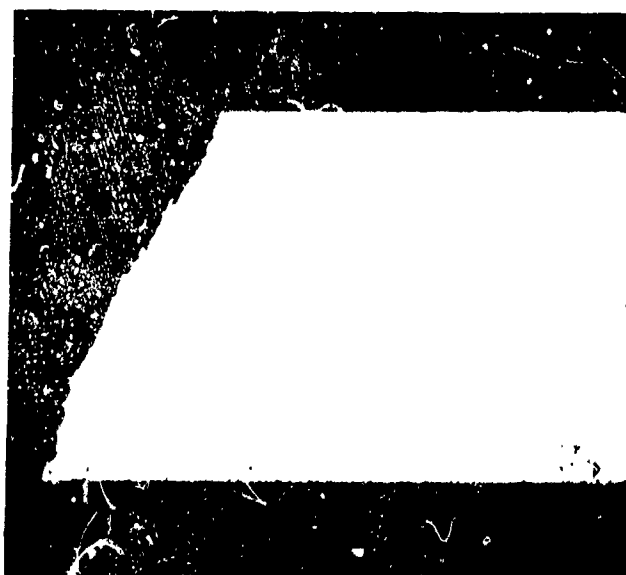
45° (ROTATING GRIP)

FIGURE 5-22  
END AND SIDE VIEWS OF FRACTURED 45 DEGREE OFF-AXIS 4.2 MIL BORSIC<sup>®</sup> + 6061F  
ALUMINUM TENSILE SPECIMENS TESTED IN ROTATING AND RIGID GRIPS



80°

Reproduced from  
best available copy.



60°

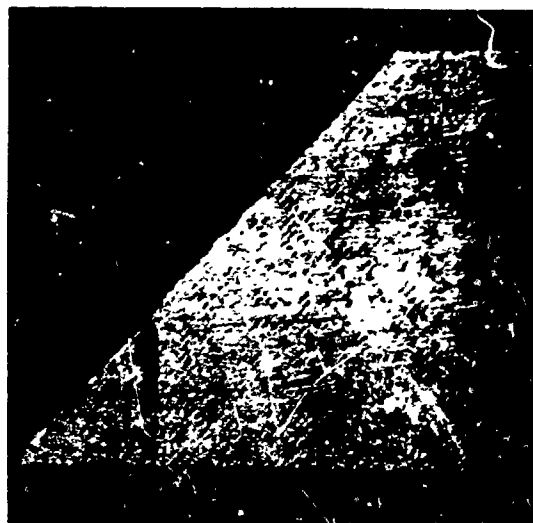
FIGURE 5-23  
END AND SIDE VIEWS OF FRACTURED 60 AND 80 DEGREE OFF-AXIS 4.2 MIL.  
BOFSC® 6061F ALUMINUM TENSILE SPECIMENS



Reproduced from  
best available copy.



FIGURE 5-24  
END AND SIDE VIEW OF FRACTURED 90 DEGREE OFF-AXIS  
4.2 MIL BORSIC<sup>®</sup> + 6061 F ALUMINUM TENSILE SPECIMEN



45°

30°

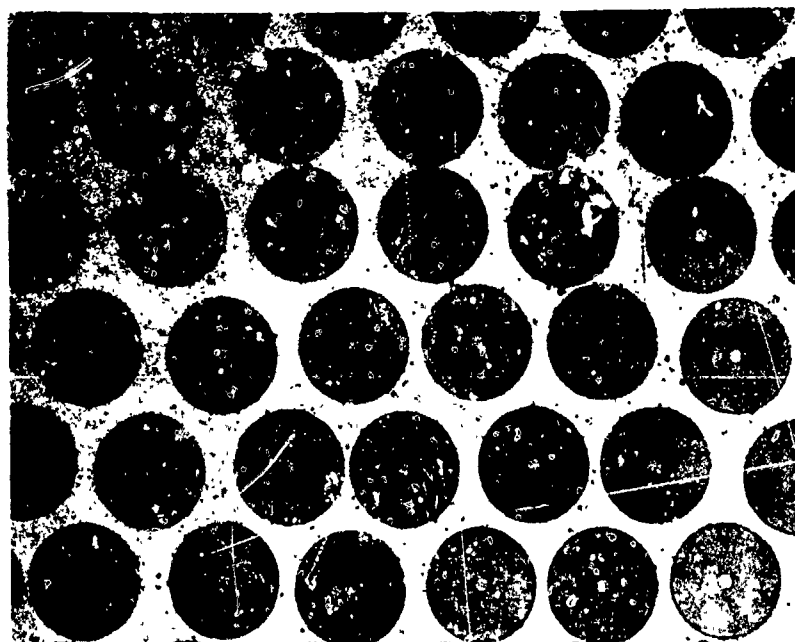
10°

Reproduced from  
best available copy.



FIGURE 5-25  
END AND SIDE VIEWS OF FRACTURED 10°, 30°, AND 45° OFF-AXIS 63 V/O  
5.7 MIL BORSIC + 6061-F ALUMINUM TENSILE SPECIMENS





MAG: 100X

FIGURE 5-26  
TRANSVERSE SECTION OF 5.7 MIL BORSIC<sup>®</sup> + 6061-T6 COMPOSITE MATERIAL

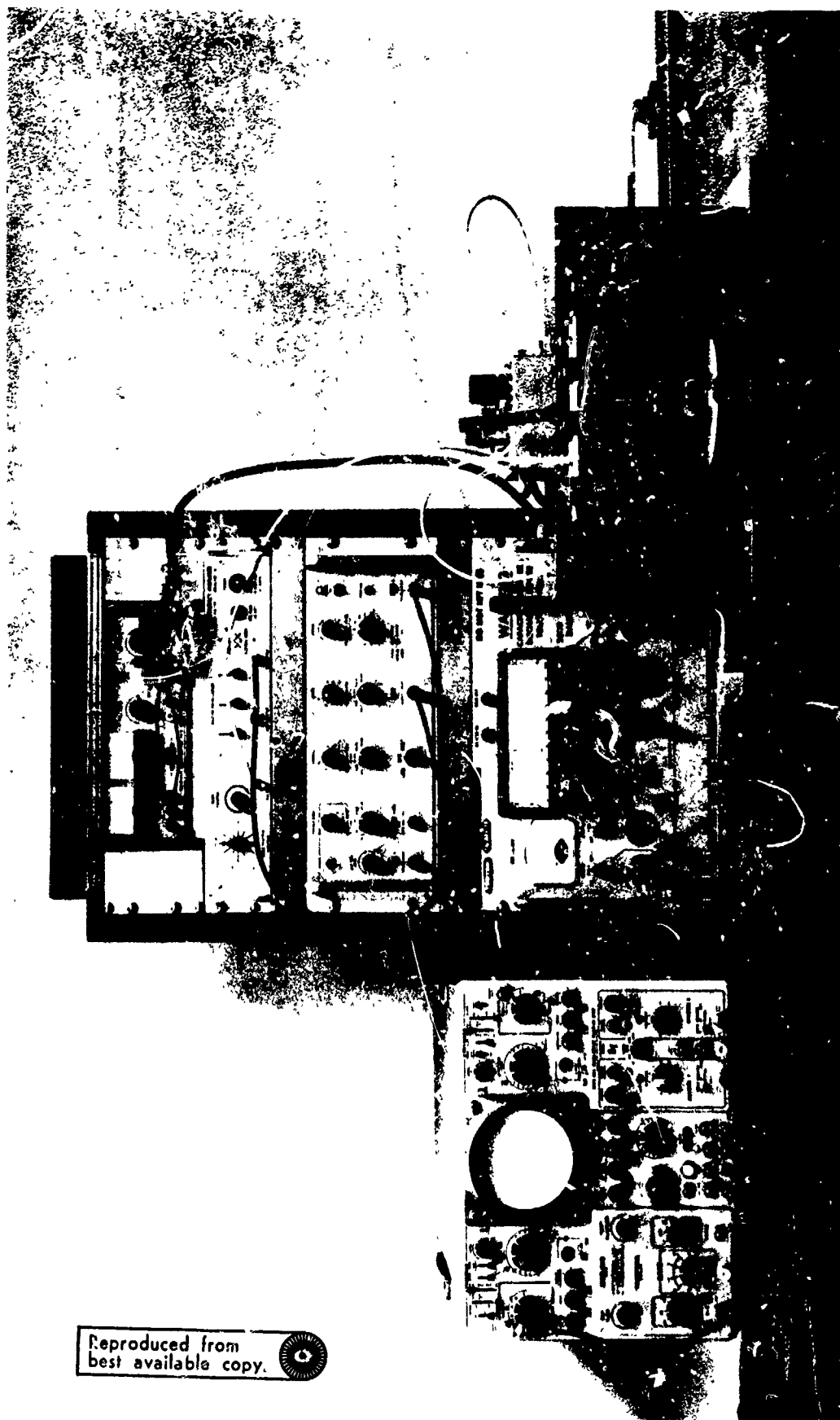


FIGURE 5-27  
ULTRASONIC VELOCITY MEASUREMENT SYSTEM

Reproduced from  
best available copy.



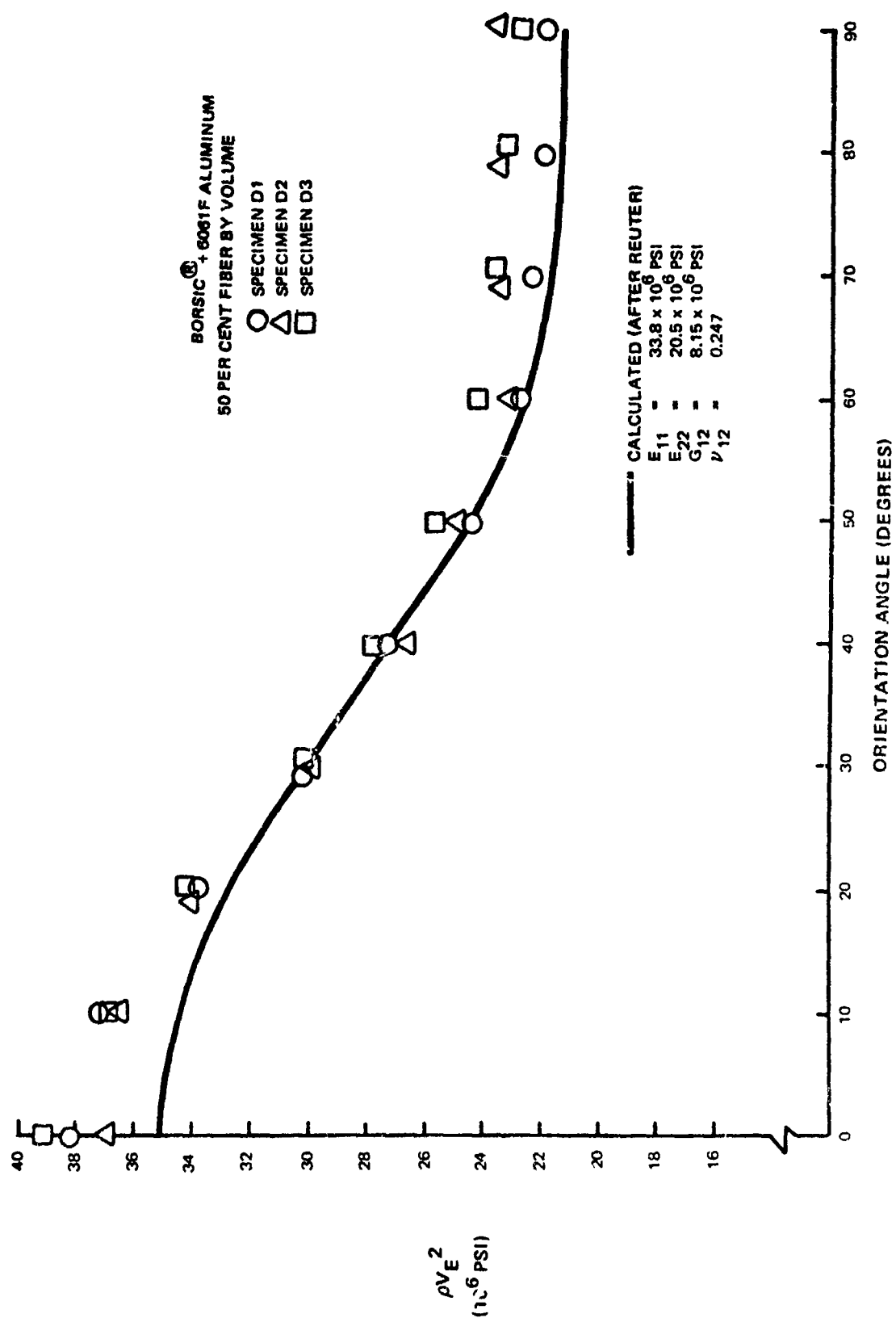


FIGURE 5-28  
DENSITY TIMES THE SQUARE OF SONIC VELOCITY AS A FUNCTION OF ANGLE  
RELATIVE TO THE FILAMENT ORIENTATION

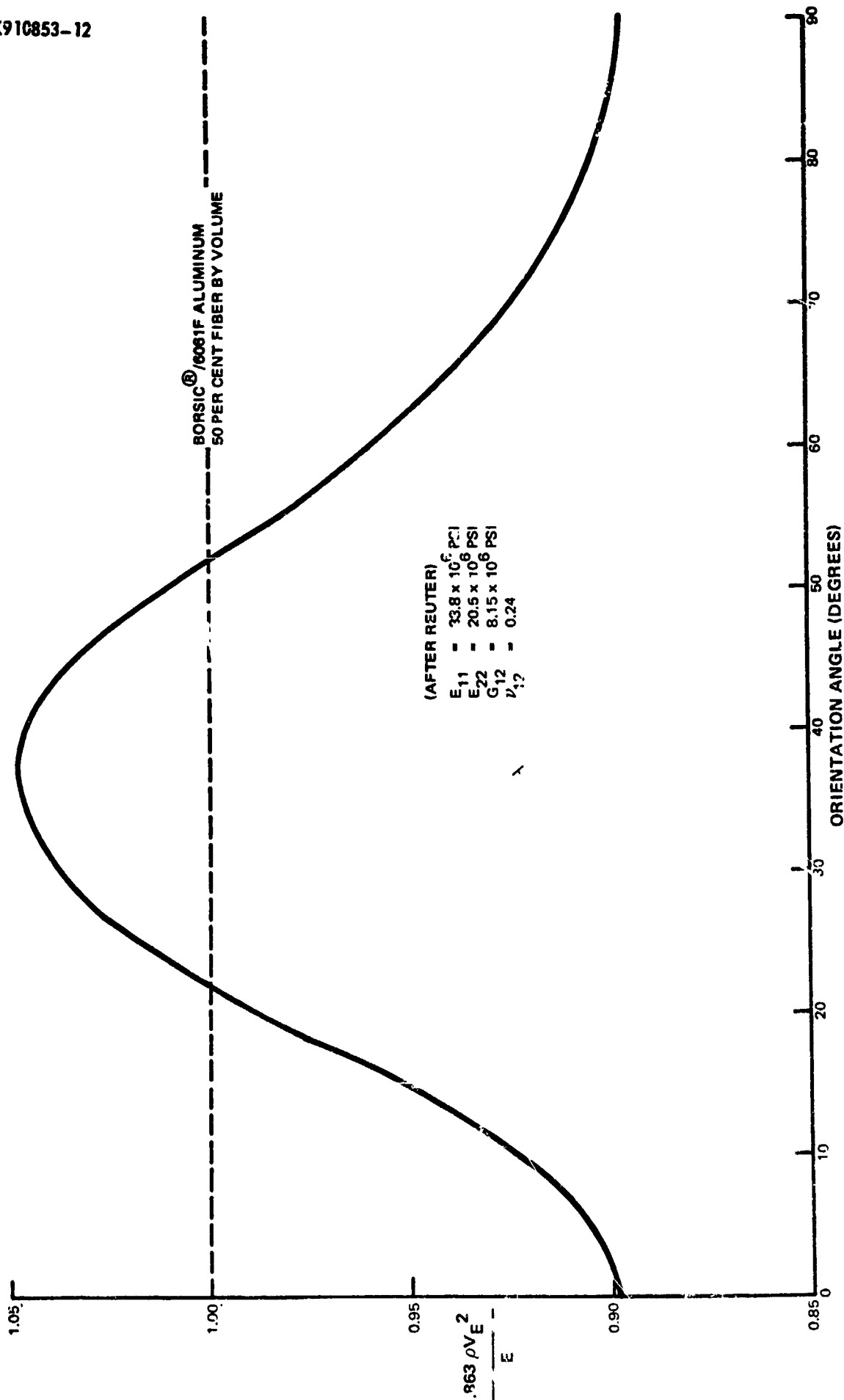


FIGURE 5-29  
RATIO OF DENSITY TIMES THE SQUARE OF SONIC VELOCITY TO ELASTIC  
MODULUS AS A FUNCTION OF ANGLE RELATIVE TO THE FILAMENT ORIENTATION

Table V-I

## Results of 4.2 Mil EORSIC + 6061-F Off-Axis Tests

Specimen Number	Fiber Orient (Degrees)	UTS (ksi)	Compliance Coefficients		
			$S_{11}$ ( $10^{-8}$ in <sup>2</sup> /lb)	$S_{12}$ ( $10^{-8}$ in <sup>2</sup> /lb)	$S_{16}$ ( $10^{-8}$ in <sup>2</sup> /lb)
OA1	0	121	2.86	-0.69	0.08
OA2	0	133	2.99	-0.77	0.01
OA3	0	140	2.74	-0.72	0.11
OA4	0	138	3.36	-0.89	-0.16
OX1***	0	141	2.98	--	--
OX2	0	150	2.82	-0.44	-0.15
		Avg.: 137	2.96	-0.70	-0.11
		Calc*: 137	2.96	-0.70	0.00
OA5	2	129	2.91	-0.65	0.23
OA6**	2	---	3.16	-0.80	0.00
OA7	2	131	3.02	-0.72	-0.01
OA8	2	128	3.05	-0.73	0.46
		Avg.: 129	3.04	-0.73	0.17
		Calc.: 130	2.96	-0.73	0.17
OA9	5	114	3.09	-0.63	0.44
OA10	5	97.7	3.09	-0.73	0.60
OA11	5	102	3.10	-0.73	0.26
		Avg.: 101	3.09	-0.76	0.46
		Calc.: 105	3.00	-0.75	0.42
OA12	10	68.7	3.31	-0.79	0.59
OA13	10	73.9	3.04	-0.85	1.18
OA14	10	75.1	3.10	-0.81	0.79
OA15	10	70.5	3.25	-0.83	0.84
		Avg.: 72.1	3.18	-0.82	0.85
		Calc.: 70.3	3.10	-0.82	0.81
OA16	30	31.1	3.85	-1.20	1.99
OA17	30	28.2	3.95	-1.34	1.29
OX3	30	30.9	3.84	-0.97	0.93
		Avg.: 30.1	3.88	-1.17	1.41
		Calc.: 27.7	4.00	-1.17	1.47

Table V-I (Cont'd)

Specimen Number	Fiber Orient (Degrees)	UTS (ksi)	Compliance Coefficients		
			$S_{11}$ ( $10^{-8}$ in <sup>2</sup> /lb)	$S_{12}$ ( $10^{-8}$ in <sup>2</sup> /lb)	$S_{16}$ ( $10^{-8}$ in <sup>2</sup> /lb)
OA18***	45	21.4	--	--	--
OA19	45	22.2	4.94	-1.71	0.96
OA20	45	21.8	4.80	-1.65	0.17
OA21	45	20.5	4.64	-1.49	1.31
OA22****	45	22.5	4.15	-1.44	1.33
OA23****	45	22.4	4.76	-1.50	0.85
OX4	45	22.5	4.62	-1.57	1.41
OX5***	45	23.1	--	--	--
		Avg.:	22.0	4.65	-1.56
		Calc.:	19.7	4.66	-1.47
					0.99
					0.96
OA24	60	16.0	5.03	-1.36	0.35
OA25	60	17.5	4.94	-1.24	0.08
OA26	60	16.1	4.74	-1.24	0.49
		18.1	4.87	-1.24	-0.06
		Avg.:	16.9	4.90	-1.27
		Calc.:	16.0	4.96	-1.29
					0.21
					0.19
OA27	80	13.0	4.86	-0.80	-0.28
OA28	80	12.9	5.22	-0.92	-0.48
OX6	80	15.1	4.79	-0.70	-0.10
		Avg.:	13.7	4.96	-0.84
		Calc.:	14.0	4.91	-0.82
					-0.29
					-0.15
OA29	90	12.6	4.97	-0.80	-0.06
OA30	90	14.2	4.92	-0.72	0.25
OA31	90	14.5	5.20	-0.78	-0.13
OX7	90	13.7	4.44	-0.65	-0.14
		Avg.:	13.8	4.88	-0.74
		Calc.:	13.8	4.88	-0.73
					-0.02
					0.00

\*UTS calculated using maximum work theory with  $X = 137$  ksi,  $Y = 13.8$  ksi;  
 $S = 14.0$  ksi; compliance coefficients calculated using the transformation  
equations with  $E_{11} = 33.8 \times 10^6$  psi;  $E_{22} = 20.5 \times 10^6$  psi;  $G_{12} = .15$  psi;  
and  $\nu_{12} = 0.24$ .

\*\*Doubblers detached before failure

\*\*\*Strain gage failure

\*\*\*\*Rigid grips used

Table V-II

## Results of 5.7 Mil BORSIC + 6061-T6 Off-Axis Tests

Specimen Number	Fiber Orient (Degrees)	UTS (ksi)	$S_{11}$ ( $10^{-8}$ in <sup>2</sup> /lb)	$S_{12}$ ( $10^{-8}$ in <sup>2</sup> /lb)	$S_{16}$ ( $10^{-8}$ in <sup>2</sup> /lb)
F 1	0	214	2.31	-0.54	-0.06
F 2**	0	192	--	--	--
F 3	0	208	2.28	-0.56	-0.05
		Avg.: 205	2.29	-0.55	-0.05
		Calc*: 205	2.29	-0.55	0.0
F 4	10	113	2.43	-0.57	0.82
F 5	10	134	2.29	-0.59	0.92
F 6	10	129	2.75	-0.69	0.60
		Avg.: 128	2.49	-0.62	0.78
		Calc.: 111	2.39	-0.61	0.55
F 7**	30	40.1	3.40	--	--
F 8	30	48.4	2.87	-0.90	1.14
F 9**	30	51.3	--	--	--
		Avg.: 49.4	3.13	-0.90	1.14
		Calc.: 47.2	2.99	-0.94	0.99
F 10	45	38.9	3.57	-1.18	0.74
F 11	45	39.1	3.36	-1.12	0.83
F 12	45	39.2	3.66	-1.15	0.49
		Avg.: 39.1	3.53	-1.15	0.69
		Calc.: 36.6	3.43	-1.07	0.62
F 13	90	34.9	3.50	-0.54	-0.15
F 14	90	31.2	3.53	-0.58	-0.08
F 15	90	30.5	3.55	-0.58	-0.01
		Avg.: 32.2	3.53	-0.57	-0.08
		Calc: 32.2	3.53	-0.57	0.0

\*UTS calculated using maximum work theory with  $X = 20.5$  ksi,  $Y = 32.2$  ksi,  $S = 22.2$  ksi; compliance coefficients calculated using the transformation equations with  $E_{11} = 43.7 \times 10^6$  psi,  $E_{22} = 28.3 \times 10^6$  psi,  $G_{12} = 11.1 \times 10^6$  psi,  $\nu_{12} = 0.24$ .

\*\*Strain gage failure

Table V-III  
Micromechanical Elastic Predictions for BORSIC + 6061 Aluminum

Elastic Constant	Theoretical Method*	50 v/o 4.2 mil Fiber			63 v/o 5.7 mil Fiber		
		Calc.	Measured	Percent Disparity	Calc.	Measured	Percent Disparity
$E_{11}$ ( $10^6$ psi)	Rule-of-Mixtures	33.5	33.8	+0.9	40.9	43.7	+ 6.9
$E_{22}$ ( $10^6$ psi)	Hill (Ref. 5.14) and Hermans (Ref. 5.15) cited by Ref. 5.16	20.5	20.5	0	25.6	28.3	+10.5
$G_{12}$ ( $10^6$ psi)	Halpin-Tsai** (Ref. 5.17) and Hasin and Rosen (Ref. 5.18)	8.15	8.15	0	10.3	11.1	+ 7.8
$\nu_{12}$	Rule-of-Mixtures	0.24	0.24	0	0.24	0.24	00
$\nu_{21}$	Maxwell's Reciprocity	0.14	0.15	+7.1	0.15	0.16	+ 6.7

\*Calculated using the following constituent properties:

$$\begin{array}{l}
 E_M = 10.0 \times 10^6 \text{ psi} \\
 G_M = 3.75 \times 10^6 \text{ psi} \\
 \nu_M = 0.33 \\
 E_F (4.2 \text{ mil}) = 57 \times 10^6 \text{ psi} \\
 G_F (4.2 \text{ mil}) = 25 \times 10^6 \text{ psi} \\
 \nu_F (4.2 \text{ mil}) = 0.14 \\
 E_F (5.7 \text{ mil}) = 59 \times 10^6 \text{ psi} \\
 G_F (5.7 \text{ mil}) = 25 \times 10^6 \text{ psi} \\
 \nu_F (5.7 \text{ mil}) = 0.18
 \end{array}$$

\*\*Using  $\delta = 1.0$



Table V-IV

## Strength of 6061 Aluminum Alloy

<u>Material</u>	<u>Temperature</u>	<u>UTS (ksi)</u>	<u>Shear Strength (ksi)</u>	<u>Shear Strength UTS</u>
6061* (wrought)	0	18	12	0.67
	T4, T451	35	24	0.69
	T6, T651	45	30	0.67
6061 matrix (plasma sprayed + hot pressed)	T6	32.2	22.2	0.69

\*After Van Horn (Ref. 5.19)

## FATIGUE FAILURE MECHANISMS

### SUMMARY

The low cycle fatigue of unidirectional and cross ply reinforced BORSIC-aluminum composites has been explored to determine the mechanisms of failure. Both 4.2 mil and 5.7 mil BORSIC fiber was used in a 6061 aluminum alloy matrix. As was found in the case of transverse tensile properties, the lack of splitting of the large diameter fiber has facilitated a significant improvement in composite performance. The importance of matrix ductility in isolating and blunting composite crack tips during fatigue has been demonstrated. Also, the nature of crack tip extension by progressive fiber failure has been illustrated. The crack tip blunting during fatigue, and not during quasi static tensile failure, is markedly different from the behavior of structural metals. This fatigue crack blunting tendency is of considerable importance for the future development of composite systems.

It has been demonstrated that cross ply specimens of 5.7 mil BORSIC-6061, tested at  $45^\circ$  to the fiber axes, exhibit static and low cycle fatigue strains to failure in excess of 10%.

Radiographic techniques have been used to show the extent and location of fiber damage in BORSIC-aluminum. The final plane of composite failure can be detected by this technique prior to final instability. The use of acoustic emission and residual stress measurement have also been useful in assessing composite damage.

## VI. FATIGUE FAILURE MECHANISMS

Many of the structural applications involving composite materials require that performance be under oscillating load conditions. These conditions may include combinations of axial static and fatigue loading. The purpose of this investigation of the fatigue of BORSIC-aluminum was to explore fatigue failure mechanisms and to provide, through the understanding of these mechanisms, improved materials for future applications. Although S-N diagrams are presented, these diagrams are not proposed as design information for applications, instead, these curves are intended to present a general overview of specimen performance in fatigue.

### 6.1 Fatigue of Axially Reinforced Specimens

#### Experimental Method

Axially reinforced fatigue specimens were fabricated using a 6061 aluminum alloy matrix and 4.2 mil diameter BORSIC fibers. Hot pressing parameters were 10,000 psi at 565°C. Each fatigue specimen was five inches long and was tested with a one inch gage length. Specimens with machined reduced gage sections and parallel sided specimens were both tested. The reduced section specimens were 0.210 inch wide in the gage section and 0.250 inch wide at the grip area while the parallel sided specimens were fully 0.250 inch wide along the entire specimen length, Fig. 6.1a. All specimens had doublers of aluminum foil (0.010 inch thick) bonded on in the grip region. It should be noted that no significant difference in performance was observed between specimen configurations and that no longitudinal splitting of the axially reinforced specimens at the machined shoulders of the reduced section was observed in fatigue testing. Fatigue testing was performed using a Tinius-Olsen tensile testing machine at loading rates of from five to ten cycles per minute. Loading of all specimens was performed such that the minimum load applied in each cycle was 10% of the maximum load, Fig. 6.1b. This corresponds to an "A ratio" (ratio of alternating stress to mean stress) of 0.82. All applied loads were tensile and strain gages were used to monitor specimen deformation. The use of only tensile stresses and non-zero minimum stresses assured an absence of effects due to bending (sometimes encountered when compressive stresses are applied) and maintained initial alignment of the testing system.

Several specimens were tensile tested in a testing machine mounted on an X-ray unit to permit radiographic observation of BORSIC fibers under stress. Fiber condition can be readily examined during a tensile test by this technique because of the large absorption coefficient of the tungsten rich cores of the BORSIC fibers as compared to the absorption coefficients of the boron, silicon carbide and aluminum composite components. The BORSIC-aluminum specimens were irradiated by X-rays with a high resolution film placed in contact with the specimens. The fiber cores appear on the film, a negative after development, as distinct white lines while all other components appear much darker. Almost every individual fiber in a composite can be resolved for even high volume fractions of fiber because the boride core is only 0.0005 in. in diameter and thus

little overlap of images occurs. The specimen test procedure involved a succession of steps of specimen loading and irradiation, while at load, to obtain fiber condition in the composites as a function of applied load.

Acoustic emission of several specimens was monitored using a small transducer mounted on the specimen surfaces during testing. The signal of this transducer was amplified and recorded during tension and fatigue testing. This signal was then later "replayed" and analyzed in conjunction with the stress history of the tested specimen. This acoustic detection system was found to detect also the deformation of aluminum matrix specimens.

Three methods were used to determine the condition of the matrix as a function of fatigue life. These were: metallographic observation, hardness indentation and X-ray residual stress measurement. The last of these was performed using a diffractometer and X-ray technique described elsewhere (Ref. 6.1). A calibration of this technique was obtained using the four point bend loading of 6061 aluminum in the X-ray machine with the specimen surface tangent to the focusing circle. Strain gage measurements, used to determine surface strain were compared with X-ray measurements of strain to calibrate the residual stress measurements made on fatigued composites. It should be noted that only changes in material condition near specimen surfaces can be detected using this technique.

### Results and Discussion

Axially reinforced composite specimens containing 4.2 mil BORSIC were fabricated at 48% and 38%, by volume, fiber. The results of the fatigue testing of these specimens are given in Fig. 6.2. The average tensile strength of the 48% BORSIC specimens was  $143 \times 10^3$  psi and that of the 38% fiber composites  $101 \times 10^3$  psi. These strengths are, on the average, approximately 12% lower than those expected for 4.2 mil BORSIC-6061 composites based on previous results obtained for similar material (Refs. 6.2,3). This lower strength was due to somewhat lower overall strength of the fiber used in these composites as compared to that used in the above referenced reports. Average fiber strengths ranged from  $350-450 \times 10^3$  psi for the present composites. Failure (specimen fracture constituted failure) at  $10^4$  cycles occurred at a maximum stress of approximately  $125 \times 10^3$  psi and  $90 \times 10^3$  psi for the 48% and 38% BORSIC composites respectively. This provides a ratio of stress at  $10^4$  cycles to ultimate tensile strength of approximately 0.88 for both composites investigated. Similar results have been obtained in the past for the tension tension low cycle fatigue of boron reinforced 2024 aluminum (Ref. 6.4). The 2024 matrix composites, containing 45% by volume of 4.0 mil boron and tested at an "r ratio" of approximately 1.0, exhibited a ratio of approximately 0.82 of stress at  $10^4$  cycles to ultimate tensile strength. This similarity in result is particularly interesting because of the considerable differences between the composites described herein and those referenced. The 2024 matrix of the boron reinforced composites consisted entirely of plasma sprayed material. No foils were used. Composite strength was, however, similar to that tested during this program, i.e. 110,000 psi for 41% boron fiber. Toth (Ref. 6.5) has reported slightly lower ratios of  $10^4$  cycle stress to

tensile strength for 4.0 mil boron reinforced 6061 matrix composites. These composites were fabricated using only aluminum foils and fiber, no plasma sprayed material, and tested in tension-tension fatigue at 1500 cpm with an "A ratio" of 1.0.

The results obtained in this investigation indicate that composite axial fatigue strength can be increased, for a given composite system, by increasing volume fraction fiber reinforcement. This is in agreement with other observations (Ref. 6.6) made for boron-aluminum. Both axial tensile strength and fatigue performance were found to increase to maintain a nearly constant ratio of stress at  $10^4$  cycles failure to ultimate tensile strength. The effects of matrix and fiber on composite fatigue behavior have not been quantitatively separated in this investigation, however, results of the fatigue testing of boron fiber by Salkind and Patarini (Ref. 6.7), indicate that boron fibers may be susceptible to fatigue damage. It is interesting to note that their data indicate a fatigue strength at  $10^4$  cycles of 0.89 of the average fiber tensile strength. Unfortunately, this result may not be applicable to the presently reported axial fatigue data due to the use of a rotating beam wire tester for the accumulation of data. This type of test generates a nonuniform axial fiber stress pattern having its maxima at the fiber surface. Thus, fiber fracture in this test was probably nucleated at the fiber surface. This is not necessarily the case for all fibers tested in axial tension, particularly because of the residual axial compressive stresses present at the fiber surface as a result of fabrication procedures. More recent results of Shimmin (Ref. 6.8) indicate that boron fibers tested in axial fatigue are not susceptible to fatigue damage. Further tests performed on both boron and BORSIC fibers are needed to clearly establish the nature of the fatigue properties of these fibers.

The roles of fiber and matrix in composite fatigue behavior can be more clearly uncovered by examining the performance of several specimens by acoustic and radiographic techniques. This will be described in the next paragraphs.

Axial 6061 matrix specimens containing 50% by volume BORSIC fiber were radiographed to record fiber condition prior to fatigue testing. The radiographs taken indicated that fibers in the composites were well aligned parallel to the specimen axis and predominantly undamaged. Some small amounts of damage were noted, in the region of machined fillets, Fig. 6.3a and randomly in the gage length of the specimen as depicted in Fig. 6.4a. Residual stress measurements, made by X-ray technique on the same composites, indicated matrix residual stresses near the specimen surface of approximately +2000 psi in tension parallel to the fiber axis for the as-fabricated condition. This stress level was increased to +13,000 psi by the T-6 quench and age heat treatment. These matrix tensile stresses are a result of the mismatch between fiber and matrix coefficients of thermal expansion and are offset by equal axial compressive stresses in the fibers for a 50% composite. The increase in fiber compressive residual stress with heat treatment is a major reason for the increase in T-6 BORSIC-aluminum axial tensile strength. A composite strength increase of 14,000 psi was obtained by T-6 heat treatment for the specimens on which the residual stress measurements were made.

Fatigue testing was performed on the above described as-fabricated specimens. A considerable amount of acoustic emission was detected from each specimen during the first tensile cycle of fatigue. Ensuing cycles, however, caused smaller amounts of emission. Only when the maximum tensile stress was raised above that previously applied to the specimen did the level of acoustic emission once again increase. The emission was characterized by a series of distinct and separate high frequency and high amplitude events accompanied by a less distinct lower amplitude background. The former effect was associated with fiber fracture while the latter was due to matrix deformation. Figures 6.3a and 6.3b indicate some of the fiber damage occurring in the fatigued specimens. Fiber breakage has taken place in the region of some preexisting damage and propagated into the specimen. The preexisting fiber damage and ensuing fiber breakage with fatigue cycles has served to cause a local region of stress enhancement. Other evidence of fiber breakage during fatigue was found throughout the bulk of the specimen, Fig. 6.4b. This breakage appeared to occur randomly and not be associated with preexistent specimen flaws. Breaks did not necessarily occur on a well defined plane perpendicular to the applied stress axis. Instead, the fiber fracture axial positions varied. This was also observed in the notched fatigue specimens which are described below. Such behavior is expected due to the variation of fiber strength with position along fiber length and the load transfer capabilities of the matrix (Ref. 6.9-12).

Matrix residual stress state, measured by X-ray technique, was found to change with fatigue cycling. After 10 cycles of axial fatigue between  $10^4$  and  $10^5$  psi the matrix residual stress was measured to be -11,000 psi compression in the fiber axis direction. This level of stress decreased in magnitude to -8000 psi by cycling the specimen between the same stress limits for an additional 90 cycles. The above observations can be explained by noting that the matrix, initially in residual tension, yields during the first application of axial tensile stress to the composite. Upon composite unloading the matrix must go into compression to accommodate the total imposed change in stress and strain. The residual compressive matrix stress is balanced by tensile stresses in the fibers. Thus, although the composite and fibers are undergoing tension-tension fatigue cycling, the matrix can be undergoing tension-compression fatigue.

Two fatigue specimens containing 38%-4.2 BORSIC were fatigued for 10,000 and 11,400 cycles and then tensile tested to determine the effects of fatigue damage on composite tensile strength. The maximum fatigue stress levels applied were 66,500 psi and 75,000 psi respectively. Radiographic observation revealed that the fatigue damage of fibers occurred in each of these specimens prior to composite failure, however, final composite tensile strengths were 120,000 psi and 110,000 psi respectively. These strengths are approximately equal to those obtained by tensile testing unfatigued specimens. Although the specimens have been fatigued for greater than  $10^4$  cycles, the fiber breakage and composite damage induced by this history is apparently no more severe than that incurred by a tensile specimen, during the progress of a simple tensile test, prior to fracture.

Radiographic examination of the fracture surfaces of fatigued specimens revealed that the reinforcing fibers do not cleave or separate at a single point, Fig. 6.5, but that they shatter during failure in a manner typical of high strength brittle materials. The fracture of fibers, as presented in Figs. 6.3 and 6.4, during fatigue damage prior to final composite failure is also characterized by this same shattering and thus is not just associated with the advance of a crack front through the composite.

## 6.2 Fatigue of Center Notched Specimens

### Experimental Method

Uniaxially reinforced specimens were tested in simple axial tension and fatigue with notches machined in the central portions of the gage sections. These specimens were approximately 0.83 in. wide and 5 in. long. The specimens were parallel sided with 1.25 in. long doublers placed in the grip areas leaving 3.50 in. long gage sections. Notches were machined into these specimens by electrodischarge machining. The notches were slits having a length of 0.10 in. and a width of 0.005 in. The notch tip root radii were larger than 0.0025. These specimens were examined radiographically during mechanical testing by the procedures described in the Experimental Method of section 6.1.

### Results and Discussion

Center notched specimens were tested in both simple tension and fatigue. The tensile test results obtained are presented in Table VI-I for both the 30% and 56% by volume 5.7 mil BORSIC fiber reinforced specimens. Tensile test ultimate tensile strength data indicated that the center notches caused a decrease in net section tensile strength at specimen failure. Unnotched specimens containing 30% and 56% fiber failed at 112,000 psi and 195,000 psi respectively. The net section fracture stress of similar specimens with EDM slots was reduced to 73,000 psi and 156,000 psi, based on net section, yielding ratios of notched to unnotched strength of 0.65 (30% fiber) and 0.80 (56% fiber). The fractured specimens are presented in Fig. 6.5 for the higher strength composite. Both of the specimens shown exhibited fairly rough fracture surfaces. The center notched specimen's surface was somewhat less irregular due to the ability of the notch to define the region of failure. The notched specimen exhibited longitudinal splits normal to the primary fracture surface after failure. These splits were most pronounced, and visible in Fig. 6.6, at the edges of the preexisting notch and also occurred in the region above and below the plane of the original notch. They were not found to occur elsewhere in the specimen or in the unnotched tensile specimen indicating their association with failure and the complex stress state at the notch.

The behavior of notched tensile specimens during tensile loading was recorded radiographically. The radiographs shown in Figs. 6.7 and 6.8 were taken at the edges of a hole in a specimen prior to and after fracture respectively. The radiographs in Fig. 6.7 were taken at 96% of ultimate tensile fracture load of the specimen. The regions of damage shown were at the circumferential positions on the hole diameter perpendicular to the applied tensile stress. Fiber fracture was first found to occur at 87% of the fracture stress of the specimen.

Fibers first failed at the very edge of the hole and, as the applied stress increased, failed progressively further from the hole. Fracture did not occur in just one position for each fiber; fibers frequently exhibited multiple failures. Fiber fracture also did not follow a simple planar path. The "jagged" nature of the path is due to the combined effects of load transfer in the matrix and the distribution of weak spots in the fiber. Jogs on the order of 0.015 in. - 0.030 in. were typical. The final fracture of the specimen followed this pre-defined jogged plane very closely, Fig. 6.8. The radiographic technique clearly shows the specimen condition in the region of failure just prior to tensile instability.

The morphology of individual fiber core breaks, as shown in Fig. 6.7, indicates that fiber fracture is probably initiated at the fiber surface. This observation is due to the multiple or shattered nature of each break. The angles of the outer edges of these breaks to the tensile axis suggest that the fracture radiated out from a surface flaw in a manner similar to the fracture of glass rods. The segmented appearance of the fracture thus being due to the crack division characteristic of high velocity failure in brittle materials.

Several axially reinforced center notched specimens containing 56% fiber were fatigued prior to final tensile testing to determine the effects of cyclic stress on composite structure and residual strength. Radiographs, taken at the notch tips of one of these specimens after cycling between 135,000 psi and 13,500 psi for 1347 cycles, are presented in Fig. 6.9. The fiber damage shown was not present in the as-prepared specimen. The fiber damage extends to one fiber spacing beyond the machined notch. Only a few randomly spaced fiber breaks were found to occur elsewhere on the specimen. Further cycling of the specimen to a total of 3800 cycles at the above given stress level did not cause any further fiber fracture to extend from the notch. Instead, large longitudinal matrix shear splits were observed to develop in the specimen. These originated at the outer edges of the damaged areas shown in Fig. 6.9 and extended for up to 0.5 in. from the notch plane. The specimen was tensile tested to failure after completion of the 3800 cycles. Figure 6.10 is a photograph of the fractured specimen indicating that the previously noted shear planes effectively blunted and isolated the machined flaw from the remainder of the specimen. The net section fracture stress of this specimen was 188,000 psi, indicating a ratio of notched to unnotched strength of 0.96. This is compared to a ratio of 0.8 for a notched, but not prefatigued, specimen. This is quite different from the behavior of many high strength monolithic materials where fatigue at low stress levels tends to sharpen machined notch tips.

Figure 6.11 is a photograph, taken in the scanning electron microscope, of the surface of the electrodischarge machined notch. The fibers which were shown as fractured in Fig. 6.9 are shown to be present attached to the machined surface. The large shear walls have isolated this plateau. Figure 6.12a is characteristic of the morphology of these shear walls. Large amounts of deformation of the aluminum matrix have taken place with the direction of shear parallel to the composite fiber axis. Figure 6.12b is a SEM photo taken of the specimen fracture surface removed from the notch area. Some fiber pullout is observed. This occurs primarily by the pull out of small groups of fibers with secondary pull out of individual fibers from these groups.



As indicated in Table VI-I, other center notched specimens were also fatigued prior to tensile failure. In each case the specimens exhibited shear failure at the notch tips. After the designated number of cycles each specimen was tensile tested. The resultant fracture regions are shown in Fig. 6.13. Comparison of these fractures and net UTS values with those in Fig. 6.10 indicates that the observed composite strength increases with increasing effectiveness of the shear splits to isolate the center notch from the remainder of the specimen.

### 6.3 Transverse Tensile Fatigue

#### Experimental Method

Transverse tensile specimens were fabricated using 4.2 mil and 5.7 mil diameter BORSIC fibers in 6061 aluminum. These specimens were prepared and tested in a manner similar to that described previously for the axially reinforced fatigue specimens. Several specimens of 5.7 BORSIC were heat treated to the T-6 condition (sol. @ 985°F, quench and age at 320°F) prior to testing.

#### Results and Discussion

The results of the low cycle fatigue testing of the 4.2 mil BORSIC reinforced 90° composites are presented in Fig. 6.14. The ultimate tensile strength of the specimen tested was 14,600 psi, and the stress at 10,000 cycles was approximately 11,500 psi. In every case it was observed that the specimen fracture surfaces were characterized by split fibers; however, those specimens that failed after 116, 1170, and 7565 cycles also exhibited some degree of matrix failure not observed with those specimens that failed after far fewer cycles. This indicates that the matrix is undergoing some weakening during the fatigue test that caused it to become the site of fracture initiation after many cycles of deformation. The fact that the matrix is accumulating fatigue damage is further substantiated by the observation that under constant stress amplitude the total plastic strain of the specimen increases with increasing number of cycles. The amount of plastic strain increment with each cycle decreasing as the number of cycles increases. Although the total composite specimen strain at the point of failure is on the order of 0.1% strain, the strain exhibited by the aluminum matrix is several times this value in localized regions of the composite due to the small contributions of the BORSIC fibers to composite extensions. It is these regions of high matrix strain that probably act as the nucleation sites of fracture after many cycles of loading. Hardness indentation measurements made in these regions did not reveal changes in hardness due to fatigue cycling. Any variations in aluminum due to cycling were overshadowed by the proximity of the BORSIC fibers which caused large changes in hardness with position between fibers.

Considerable improvement in fatigue properties was achieved through the use of 5.7 mil BORSIC fiber. The data is presented in Fig. 6.15 for both T-6 heat treated and as-fabricated specimens. The average ultimate tensile strengths of these specimens were approximately 40,000 and 20,000 psi respectively. Despite the much higher strength of the as-fabricated 5.7 mil fiber specimens, as compared to the 4.2 mil fiber specimens, the stress required to cause failure at  $10^4$  cycles was nearly the same.

Two specimens, one each in the F and T-6 conditions, were fatigued to  $10^4$  cycles without failure and then tensile tested. The stress applied to the F, as-fabricated specimen was nearly equal to the failure stress at  $10^4$  cycles. Despite this severe cyclic history the ultimate tensile strength was equal to that of unfatigued material. A similar result was found for the T-6 heat treated specimen. In this case the applied fatigue stress was approximately 80% of the  $10^4$  cycle failure stress. This lack of degradation of residual composite strength indicates that the major portion of the fatigue life of these specimens is associated with straining of the aluminum rather than propagation of cracks in the material. Crack formation and propagation occurs in the very late stages of the fatigue history.

#### 6.4 Fatigue of Cross Ply Composites

##### Experimental Method

4.2 Mil and 5.7 mil BORSIC cross ply specimens ( $0^\circ/90^\circ$ ) were prepared and tested at  $0^\circ$  to a principle axis and  $45^\circ$  to both principle axes. These cross ply specimens were bonded at a pressure of 5000 psi to avoid fiber breakage at the crossing points of fibers. This breakage, although not severe, was noted to occur when bonding at the higher pressure of 10,000 psi. The lower pressure was sufficient to cause full consolidation of the composites. Fatigue testing procedures were similar to those described in the previous sections.

##### Results and Discussion

The results of the fatigue testing of 4.2 mil BORSIC fiber reinforced cross ply composites are presented in Fig. 6.16. Data obtained for composites tested at both  $0^\circ$  and  $45^\circ$  to one of the principle fiber axes are shown. For both of the composite types represented, the fracture surfaces were predominantly characterized by fiber splitting. In the case of the  $0^\circ/90^\circ$  test configuration, all of the fibers in the fracture surfaces of the  $90^\circ$  plies were split along their length. Evidence of fiber splitting was found to occur also at regions removed from the fracture surface. Figure 6.17 is a radiograph of such a region showing the presence of fiber splits normal to the applied composite tensile stress. Failure of the  $90^\circ$  plies occurs removed from the primary fracture due to the limited failure strain of these plies (0.15%) as compared to the failure strain of the axial lamellae (0.5%). The failure strain of the overall composite was found to be approximately equal to that of the  $0^\circ$  plies. The tensile strength of these composites, 71,000 psi, corresponds closely to that calculated by using a simple rule of mixtures approximation of the contribution of axial and transverse plies to the total composite strength. The former contributes approximately 65,000 psi and the latter contributes 7000 psi to arrive at a total of 72,000 psi which agrees with the strength observed. It is interesting to note that, although the failure of the  $0^\circ$  plies controls composite failure, the ratio of failure stress at  $10^4$  cycles to ultimate tensile strength of these specimens was 0.95 which is somewhat higher than the similar ratio of 0.88 for axially reinforced specimens.

The fracture surface of a 4.2 mil BORSIC  $+45^\circ$  specimen is shown in Fig. 6.18. The fracture surface was characterized by a jagged appearance consisting of alternating regions of longitudinally split and axially failed fibers. The axially failed fibers exhibited fracture surfaces typical of those observed in the fracture of uniaxially reinforced  $0^\circ$  specimens. Some fiber fractures exhibited a large amount of shattering while others were of the classical cup-cone configuration. As can be seen in Fig. 6.18, several of the fibers failed in a combined mode of axial tensile failure and transverse splitting. The longitudinally split fibers exhibited fracture surfaces that were always rough on one-half of the surface due to "river patterns" associated with the renucleation of fracture when crossing the fiber core, and smooth on the other half. The failure strain of the unfatigued specimens was approximately 0.8% indicating little deformation of the aluminum matrix even in this orientation in which matrix shear could be substantiated. This matrix contribution can be realized if the fibers are prevented from splitting, as will be shown later in the case of 5.7 mil BORSIC reinforced composites. The tensile fracture stress of the  $+45^\circ$  4.2 mil BORSIC specimens (18,000 psi) was approximately equal to that of the uniaxially reinforced off-axis specimens (20,000 psi). The failure strains of these composites were also approximately equal, 0.8% and 1% respectively. From this similarity in performance it can be observed that the maximum distortional energy criterion, (Ref. 6.14) which accurately describes the locus of failure stress with filament angle to tensile axis for unidirectionally reinforced specimens, also applies to the present cross ply configuration.

The performance of the  $0^\circ/90^\circ$  5.7 mil BORSIC composites differed from that described above for the 4.2 mil fiber composites in that fiber splitting was not a major characteristic of the specimen fracture surfaces. This is shown in Fig. 6.19 and is in agreement with the previously described performance of transverse tensile specimens. The tensile stress strain curve of a 5.7 mil cross ply specimen is presented in Fig. 6.20. Two elastic moduli are noted in the figure. The primary elastic modulus corresponds to the stress-strain region in which both the  $90^\circ$  and  $0^\circ$  plies are behaving elastically. The observed value of  $27 \times 10^6$  psi is in fair agreement with an anticipated value of approximately  $30 \times 10^6$  psi based on a rule of mixtures approximation for the contributions of the  $0^\circ$  ( $18 \times 10^6$  psi) and  $90^\circ$  ( $12 \times 10^6$  psi) plies. At a composite strain of 0.03%, a second straight line portion of the stress strain curve was observed with a modulus of  $17 \times 10^6$  psi. In this region the  $90^\circ$  plies have already yielded and the  $0^\circ$  plies are still behaving elastically. The point of transition between the primary and secondary linear regions and the point of final departure from the secondary linear region are effected not only by the stress-strain characteristics of the two different ply orientations but also by the residual stress state left in the composite after fabrication. The thermal expansion coefficient of the  $90^\circ$  plies is approximately three times that of the  $0^\circ$  plies (Ref. 6.15). Thus it would be expected that the  $90^\circ$  plies would be left in residual tension and the  $0^\circ$  plies in compression as a result of the "cool down" from the hot-pressing conditions.

The fatigue performance of the  $0^\circ/90^\circ$  composites is shown in Fig. 6.21. Both as-fabricated and T-6 heat treated specimens were tested and little difference in performance was found. This is in contrast to the fact that uniaxially reinforced composite strength can be increased in both transverse and axial directions by T-6 heat treatment. No decrease in strength due to heat treatment, however, was noted as has been reported previously by other investigators (Ref. 6.17). The lack of improved strength due to heat treatment is likely due to a complicated residual stress state developed in the cross ply composite as a result of the rapid quench used and the differences in coefficient of thermal expansion between plies cited above and the difference in this quantity between fiber and matrix. Quenching would leave the matrix in biaxial tension for this biaxial lay up and thus severely reduce its strain capability. This would particularly decrease the effectiveness of the  $90^\circ$  plies and thus negate strength increases due to precipitation hardening of the matrix.

One  $0^\circ/90^\circ$  specimen of 5.7 mil BORSIC-6061 was fatigued for  $10^4$  cycles, at 90% of the stress necessary to cause failure at that number of cycles, and then tensile tested. No degradation in composite strength was observed to take place due to the fatigue history. This agrees with the similar observations made with uniaxially reinforced composites tested at both  $0^\circ$  and  $90^\circ$  to the fiber axis. Once again, the damage introduced during the first major portion of the fatigue history is not more severe than that introduced during the simple tensile test prior to ultimate failure.

Figure 6.22 is a radiograph taken of a crack tip in a 5.7 mil cross ply specimen. This crack tip is a secondary fracture which branched off from the primary crack plane and was stopped suddenly by the unloading of the specimen as a result of the primary fracture. The grid formed by the cross plied fiber cores acts as a high resolution strain gage system in which the displacements of the fibers and intersection points describe the displacement field at the crack tip. This displacement field was observed to extend out normal to the crack plane and coincided with the region over which axial fiber fracture could be observed. It was also observed that fractured fibers occurred ahead of the observable crack.

The stress-strain performance of 5.7 mil BORSIC cross ply specimens tested at  $45^\circ$  to the principle fiber axes is presented in Fig. 6.23. Curves developed for both as-fabricated and prefatigued specimens are shown. The large strain to failure of the as-fabricated specimens tested is the outstanding feature of their performance. Strains in excess of 10% were found to occur. This large elongation was due to the fact that the 5.7 mil fibers did not split during testing, thus permitting the aluminum matrix to undergo large amounts of deformation. This deformation was accompanied by a reduction in specimen width and a rotation of the fiber axes toward the tensile axis. No appreciable reduction in specimen thickness was measured. The total fiber rotation was typically on the order of  $8^\circ$ . At fracture the fibers were approximately  $37^\circ$  to the tensile axis. A typical fracture surface of this type of specimen is shown in Fig. 6.24. It is observed that matrix failure and fiber tensile failure are the predominant fracture surface features. A higher magnification view of the same specimen is shown in Fig. 6.25.

The tensile performance of both as-fabricated and T-6 heat treated +45° specimens was determined. The heat treatment did not cause an appreciable increase in composite strength, however, it did cause a significant decrease in composite ductility. The fracture strain of the T-6 heat treated composites was only approximately 1% as compared to greater than 10% in the as-fabricated (F) condition. The fracture mode of the T-6 composites is still one of matrix failure and tensile fiber failure. No significant amounts of longitudinal fiber splitting were observed. The observed decrease in ductility may be the reason for the lack of strength increase. As seen in Fig. 6.23, approximately 60% of the composite strength, in the F condition, is developed after composite yielding. The large deformation taking place permits significant matrix work hardening to take place and rotation of the fibers toward the tensile axis. This latter factor can also cause an increase in composite strength (Ref. 6.14). The T-6 heat treated composite material does not undergo either of these processes and thus must develop its strength within 1% of composite elongation. This is accomplished primarily by the increase in matrix yield strength due to heat treatment.

Fatigue cycling of both F and T-6 heat treated +45° composites indicated that these composites were not very sensitive to tension-tension fatigue over the  $10^4$  cycle range. It was found that cycling at approximately 80% of the UTS of the F and T-6 composites for 15,000 and 6000 cycles respectively did not cause decrease in residual composite strength. The data are presented in Table VI-II. The major effect of the cycling was to cause a decrease in residual strain to failure of the composites cycled. This is shown in Fig. 6.23 for the as-fabricated specimen that had been cycled for 15,000 cycles prior to final tensile testing. The specimen had strained to approximately 9% during the 15,000 cycles and thus, by straining an additional 1.5% in tension after fatigue, exhibited its full failure strain prior to rupture. The values of stress calculated for the stress strain curves presented in Fig. 6.23 are based on the original as-fabricated dimensions of the specimens tested. The curves are thus "engineering" and not "true" stress-strain curves. Normally, for BORSIC-aluminum composites, the difference between these two types of stress measurements (true stress is calculated using instantaneous cross sectional areas) is insignificant due to the small strain capability of the composite. In this case this is not true. The fracture stresses of the as-fabricated and fatigued specimens represented in Fig. 6.23 are raised to 35,200 psi and 38,400 psi from 31,600 psi and 34,300 psi respectively by using the final composite cross sectional area at failure as a basis by calculation.

## 6.5

### Conclusions

1. The methods of acoustic emission, residual stress measurement and radiography have been useful in characterizing the changes in structural integrity of BORSIC-aluminum specimens during mechanical testing. The plane of final composite failure prior to final rupture can be defined by radiography.

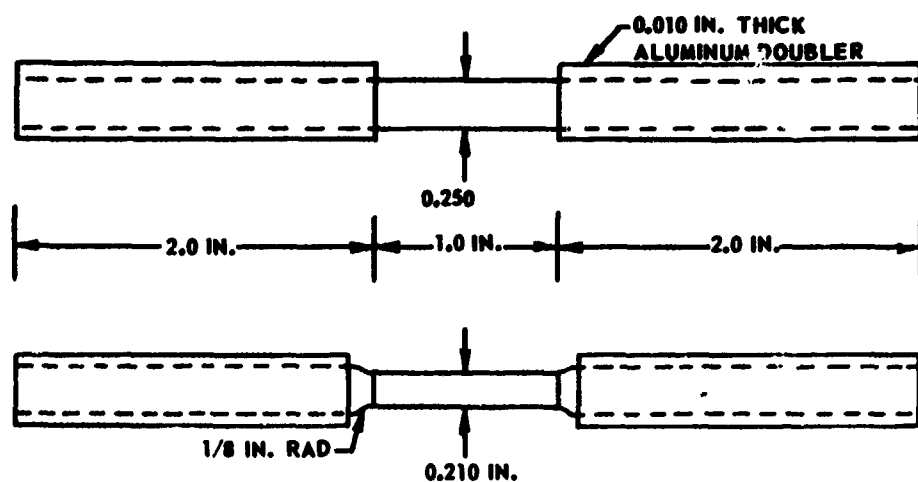
2. Axial tension-tension low cycle fatigue of unidirectionally reinforced BORSIC-aluminum is characterized by progressive failure of BORSIC fibers in regions of preexisting localized specimen damage and stress concentrations and the failure of fibers throughout the bulk of the specimen. Regions of significant amounts of fiber damage define the final plane of failure for the specimen.

3. Shear of the aluminum matrix parallel to the fiber axis in unidirectionally reinforced composites can prevent the progression of a crack across a specimen. Unlike the behavior of many monolithic materials, crack blunting can occur during the fatigue of notched specimens.

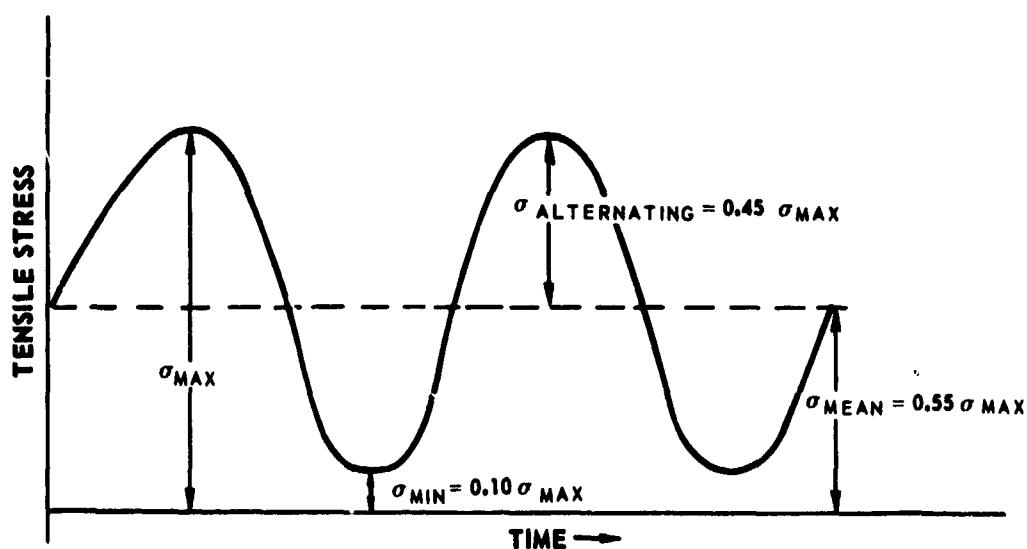
4. The elimination of longitudinal fiber splitting, by the use of 5.7 mil fiber rather than 4.2 mil fiber significantly increased the static and fatigue performance of cross ply BORSIC-aluminum composites and has dramatically increased the total elongation to fracture.

## SECTION VI - REFERENCES

1. B. D. Cullity, "Elements of X-ray Diffraction", Addison-Wesley, 1959.
2. K. G. Kreider, et al, "Plasma Sprayed Metal Matrix Fiber Reinforced Composites", AFML-TR-68-119.
3. K. G. Kreider and M. Marciano, "Mechanical Properties of BORSIC-Aluminum Composites", Trans. AIME, 245, 1279, 1969.
4. K. G. Kreider and G. R. Leverant, "Boron Fiber Metal Matrix Composites by Plasma Spraying", AFML-TR-66-219.
5. I. J. Toth, "Time Dependent Mechanical Behavior of Metal Matrix Composites", Air Force Tech. Report AFML-TR-71-102.
6. I. J. Toth, "The Time Dependent Mechanical Behavior of Composite Materials", AFML-TR-70-174.
7. M. Salkind and V. Patarini, Trans. AIME, Vol. 239, 1268, 1967.
8. K. D. Shimmin, Unpublished result as referred to by Toth in Refs. 5 and 6 above.
9. D. M. Schuster and E. Scala, AIAA Jl. 6, 527, 1968.
10. C. Zweben, AIAA Jl. 6, 2325, 1968.
11. C. Zweben and W. Rosen, AIAA Paper No. 69-123, 1969.
12. C. Zweben, J. Comp. Mats. 3, 713, 1969.
13. C. A. Berg, Fib. Sci. & Tech., Vol. 3, 295, 1971.
14. S. Tsai, "Strength Theories of Filamentary Structures" in Fundamental Aspects of Fiber Reinforced Materials, Interscience Publishers, 1968.
15. V. Patarini and K. Kreider, Met. Trans. 1, 3431, 1970.



(a) FATIGUE SPECIMEN CONFIGURATIONS



(b) FATIGUE STRESS - CYCLE PROCEDURE

FIGURE 6.1 EXPERIMENTAL METHOD IN FATIGUE TESTING



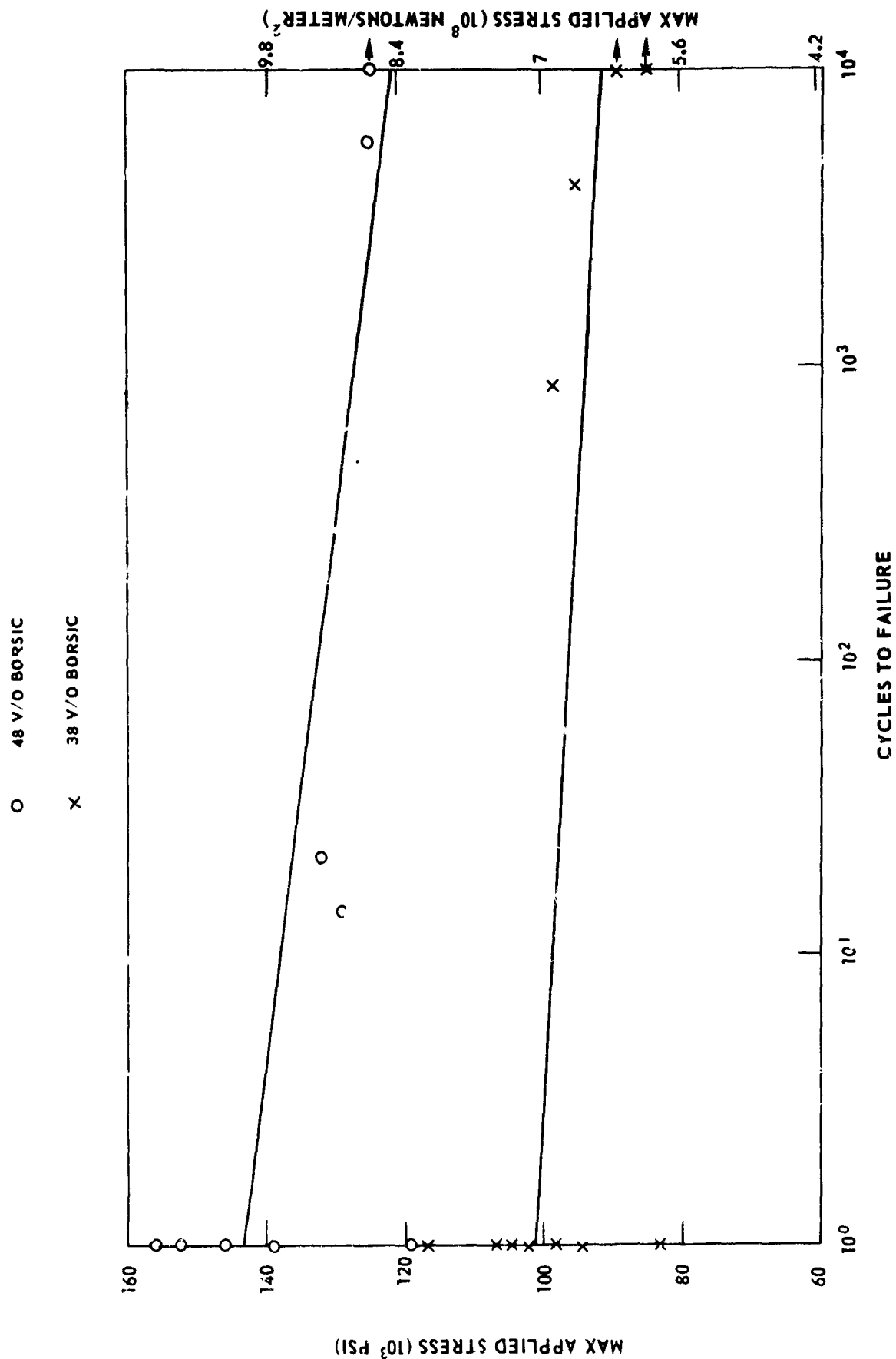
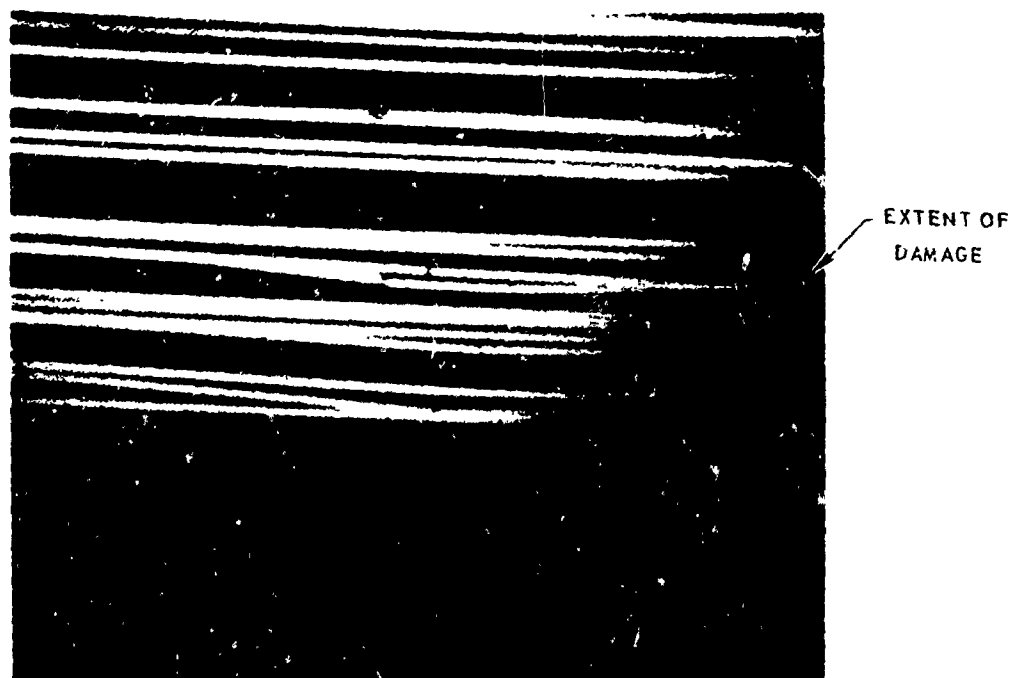
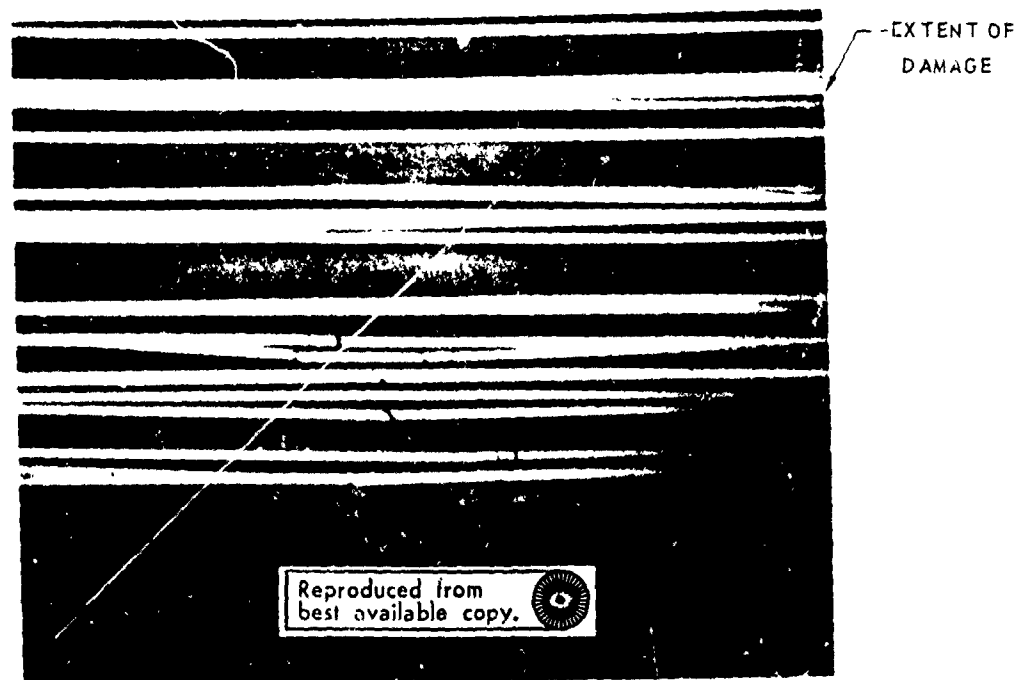


FIGURE 6-2. AXIAL TENSION - TENSION LOW CYCLE FATIGUE OF 4.2 MIL BORSIC - 6061F ALUMINUM

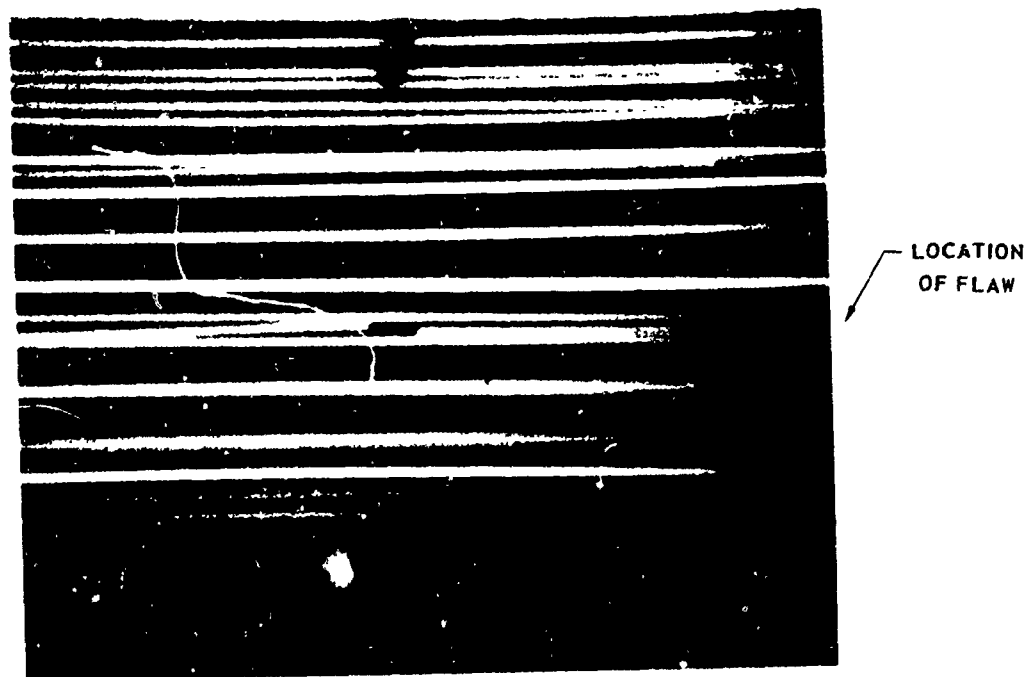


(a) PRIOR TO TEST

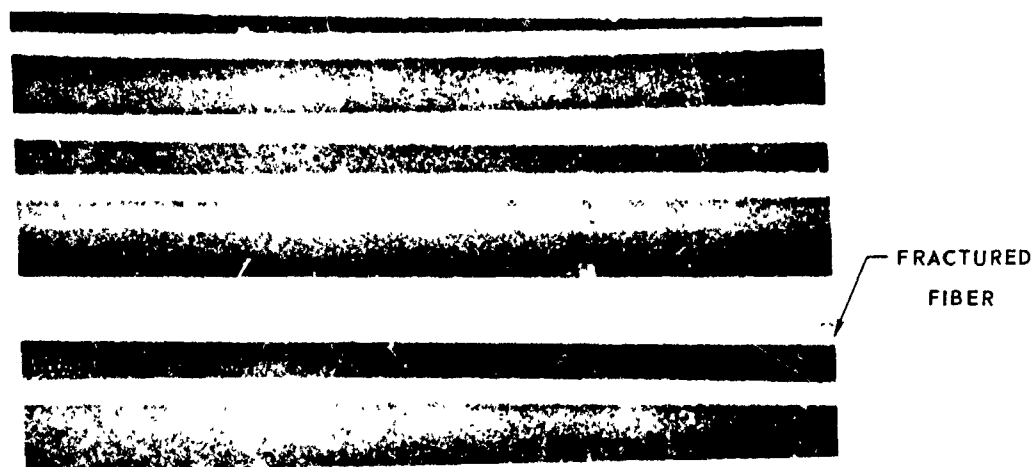


(b) AFTER FATIGUE TESTING

FIGURE 6-3 REGION OF AXIAL - 50 v o - 4.2 MIL BORSIC-6061 FATIGUE SPECIMEN



(a) FLAW EXISTING PRIOR TO TESTING PHOTOGRAPHED AFTER FATIGUE TEST



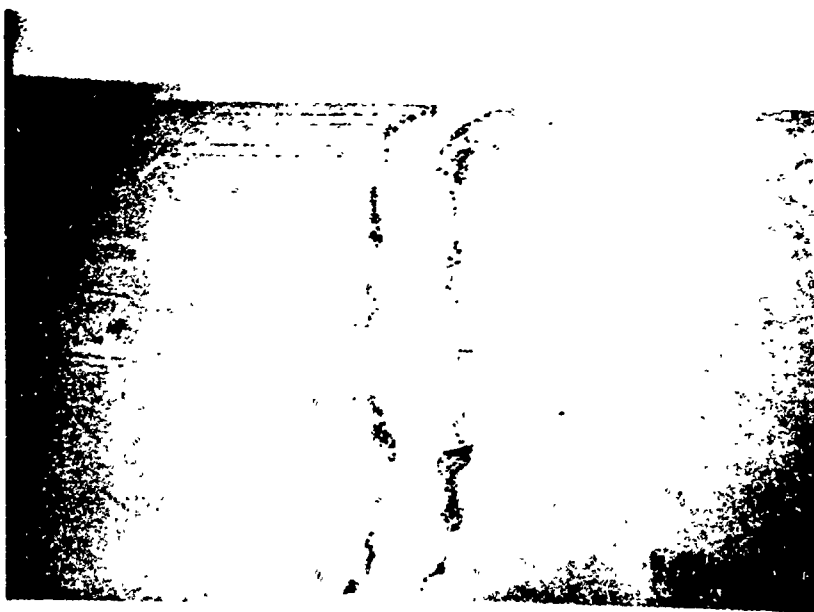
(b) FIBER FRACTURE DURING FATIGUE

FIGURE 6 - 4. AXIAL 50% - 4.2 MIL BORSIC-6061 FATIGUE SPECIMEN AFTER FATIGUE TESTING



50X

FIGURE 6-5. RADIOGRAPH TAKEN AT THE FRACTURE SURFACE OF A  $0^0$  -  
50 v/o - 4.2 MIL BORSIC-6061- ALUMINUM COMPOSITE  
UNNOTCHED LOW CYCLE FATIGUE SPECIMEN



b) NOTCHED NET UTS 156,000 PSI

Reproduced from  
best available copy.



a) UNNOTCHED NET UTS 195,000 PSI

FIGURE 6-6. 56 V'0-5.7 BORSIC - 6061 TENSILE SPECIMENS

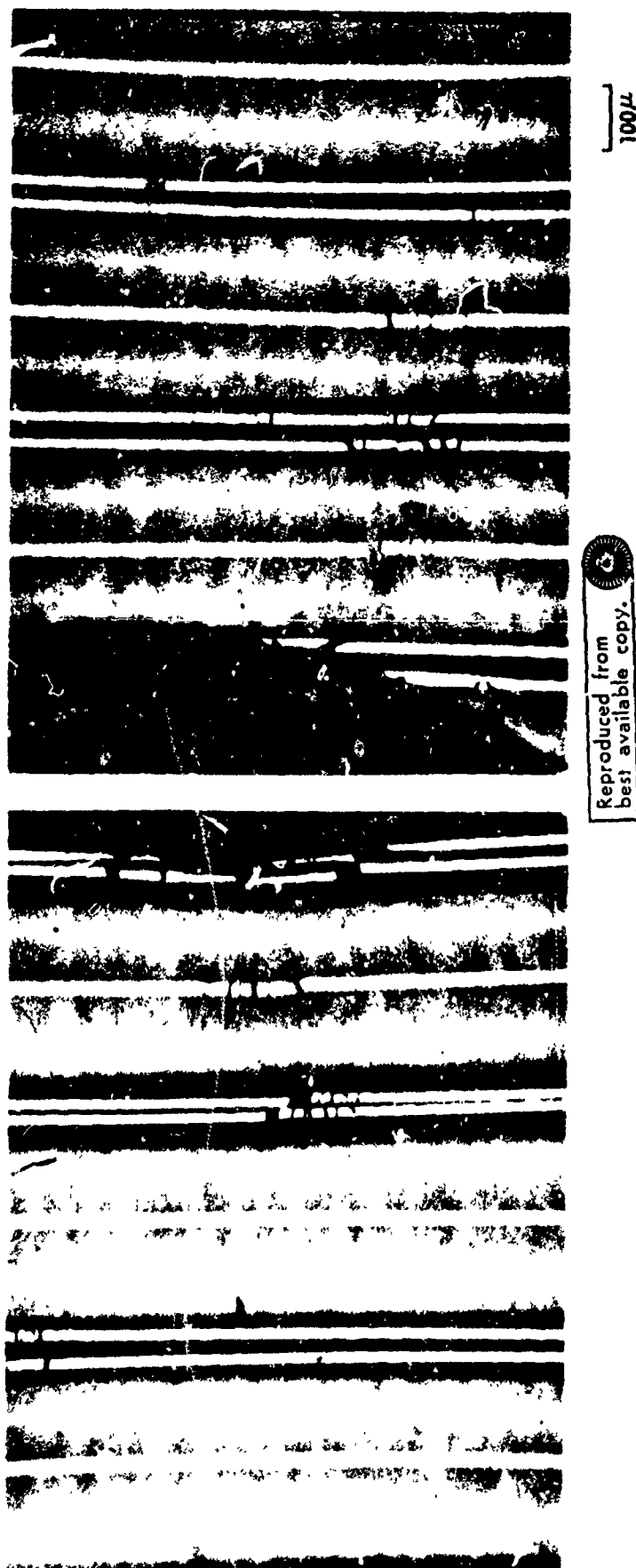


FIGURE 5-7. PROGRESSIVE FIBER FAILURE AT THE EDGES OF NOTCH IN 30 v/o - 5.7 MIL BORSIC - 6061  
TENSILE SPECIMEN LOADED TO 96% OF THE ULTIMATE FRACTURE LOAD



100μ

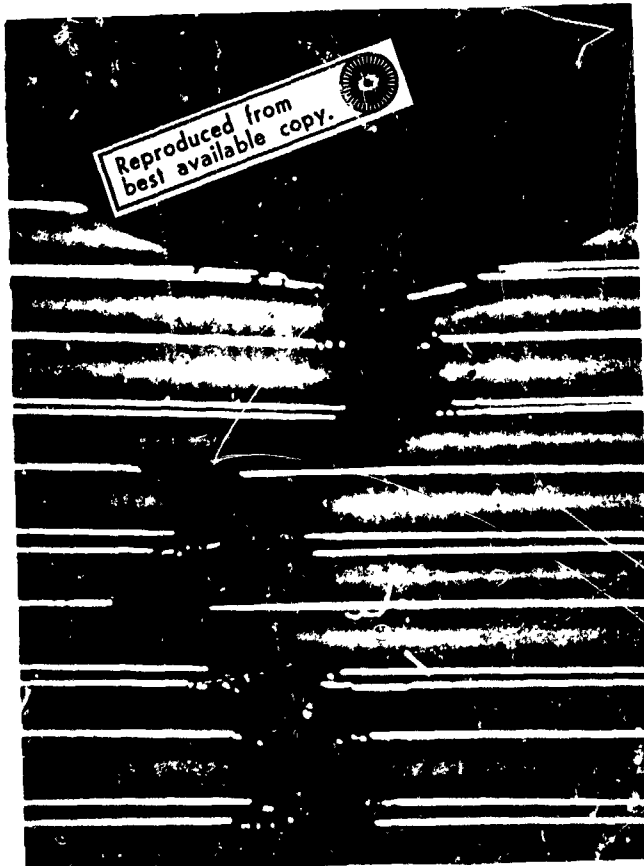


FIGURE 6-8. NOTCH EDGES AFTER TENSILE FAILURE  
FOR SAME SPECIMEN AS FIGURE 6 - 7

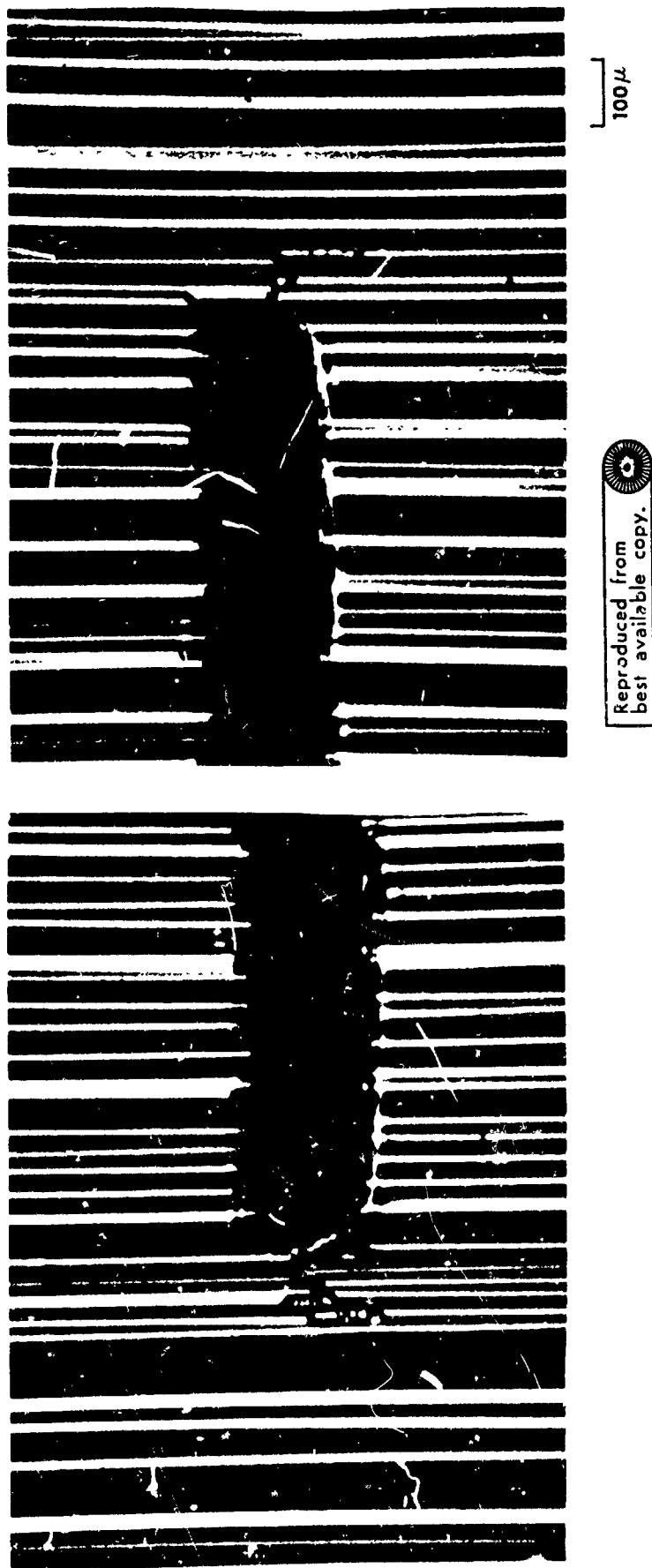


FIGURE 6-9. NOTCH TIPS OF 56V/O - 5.7 MIL BORSIC - 6061 - FATIGUE SPECIMEN AFTER 1347 CYCLES





Reproduced from  
best available copy.



2000 $\mu$

FIGURE 6-10. FRACTURED CENTER NOTCHED FATIGUE SPECIMEN  
NET UTS = 188,000 PSI  
SAME SPECIMEN AS FIGURE 6 - 9

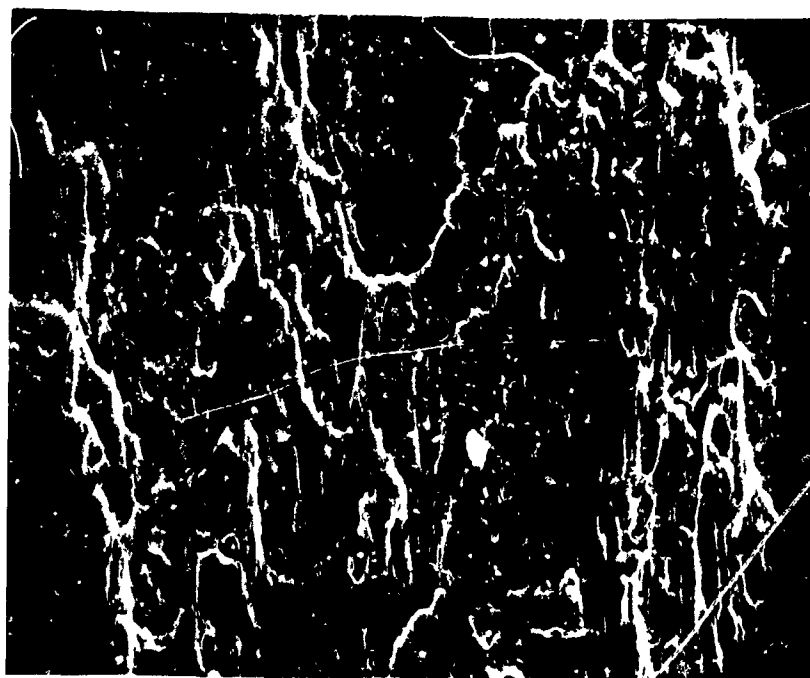


Reproduced from  
best available copy.



500  $\mu$

FIGURE 6-11. NOTCH REGION OF FRACTURED FATIGUE SPECIMEN  
SAME SPECIMEN AS FIGURE 6 - 9



(a) SHEAR FAILURE ON SHEAR WALLS

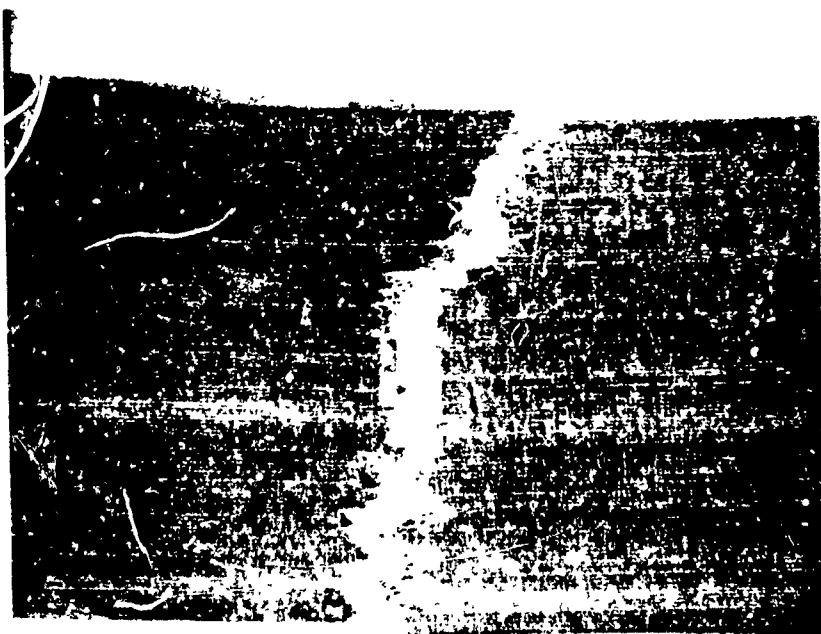
15  $\mu$



(b) TENSILE FAILURE AWAY FROM NOTCH

500  $\mu$

FIGURE 6-12. FRACTURE SURFACE OF CENTER NOTCHED FATIGUE SPECIMEN  
SAME SPECIMEN AS FIGURE 6 - 9



(b) 5176 CYCLES    NET UTS = 135,000 PSI

Reproduced from  
best available copy.



3.5X



(a) 10,000 CYCLES    NET UTS = 171,000 PSI

FIGURE 6-13. FRACTURED SPECIMENS AFTER FATIGUE CYCLING

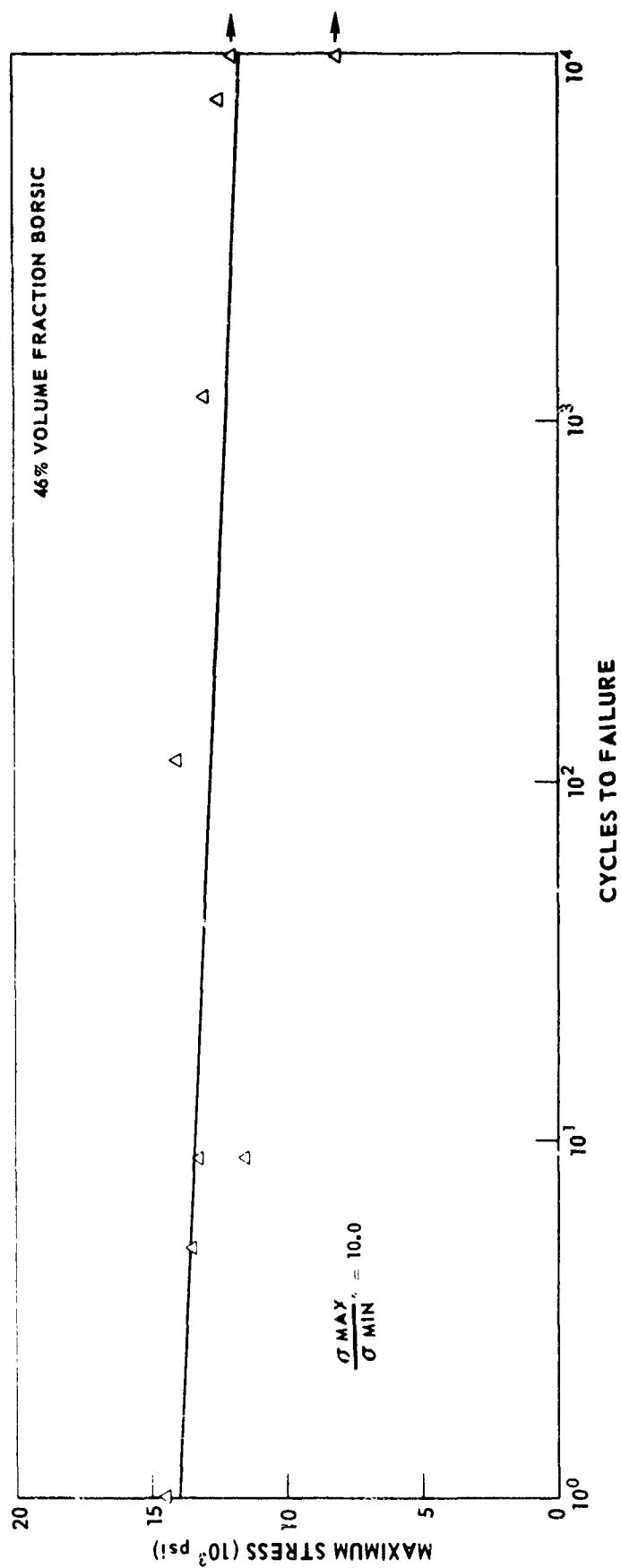


FIGURE 6-14. TRANSVERSE TENSION-TENSION LOW CYCLE FATIGUE OF 4.2 MIL BORSIC-6061 ALUMINUM

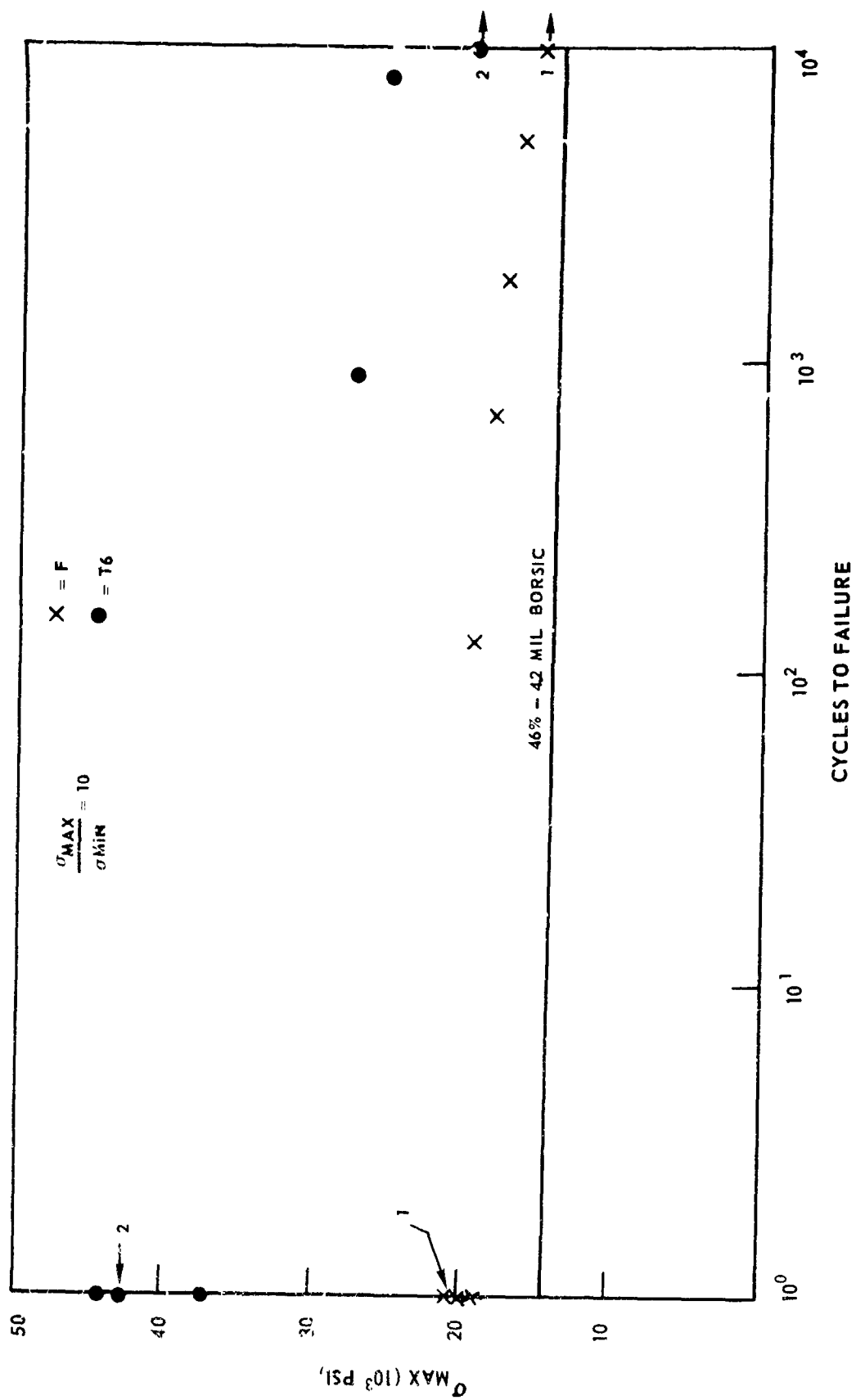


FIGURE 6-15. TRANSVERSE TENSION - TENSION LOW CYCLE FATIGUE OF 57% 5.7 BORNIC-6061 ALUMINUM

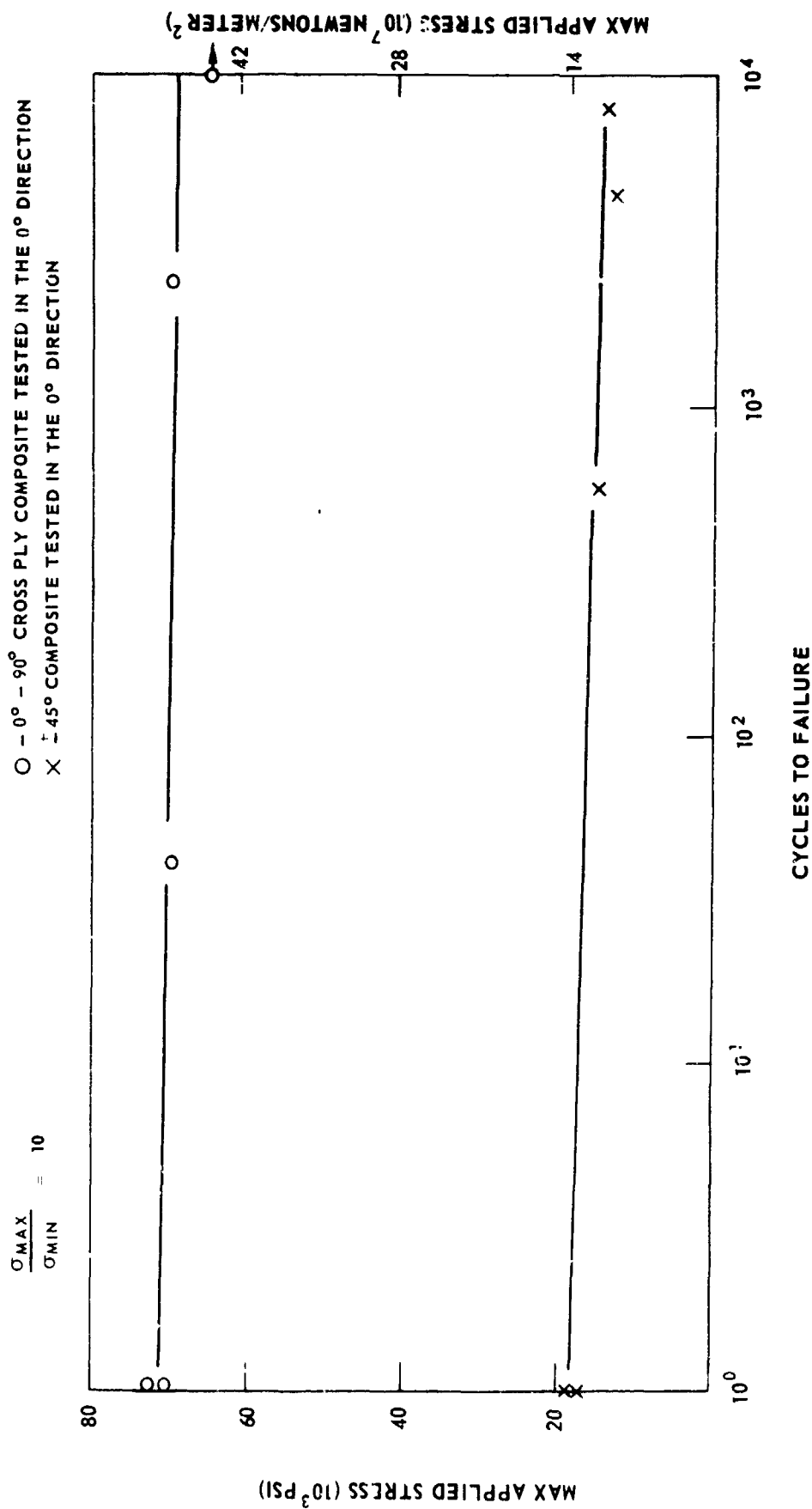


FIGURE 6-16 TENSION - TENSION LOW CYCLE FATIGUE OF 44 V/O 4.2 MIL BORSIC - 6061 ALUMINUM

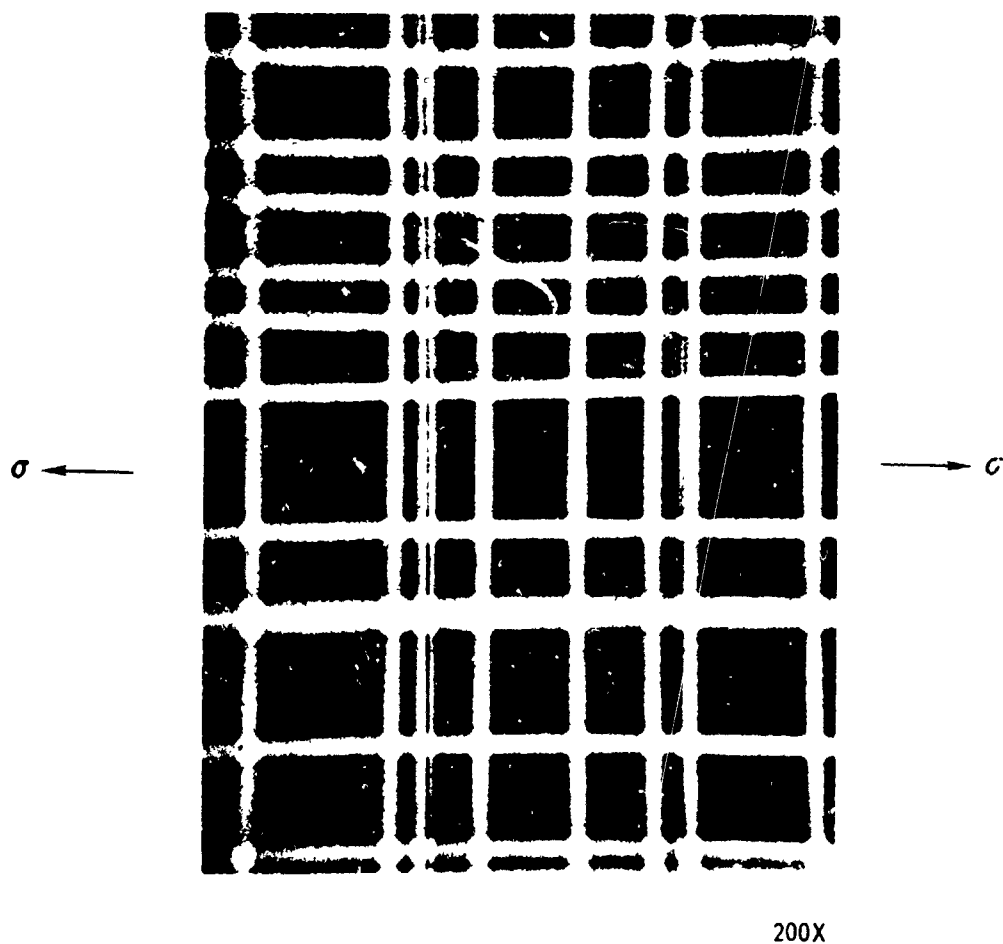


FIGURE 6 - 17. RADIOGRAPH OF FATIGUED CROSS PLY 4.2 MIL BORSIC - 6061 COMPOSITE



Reproduced from  
best available copy.

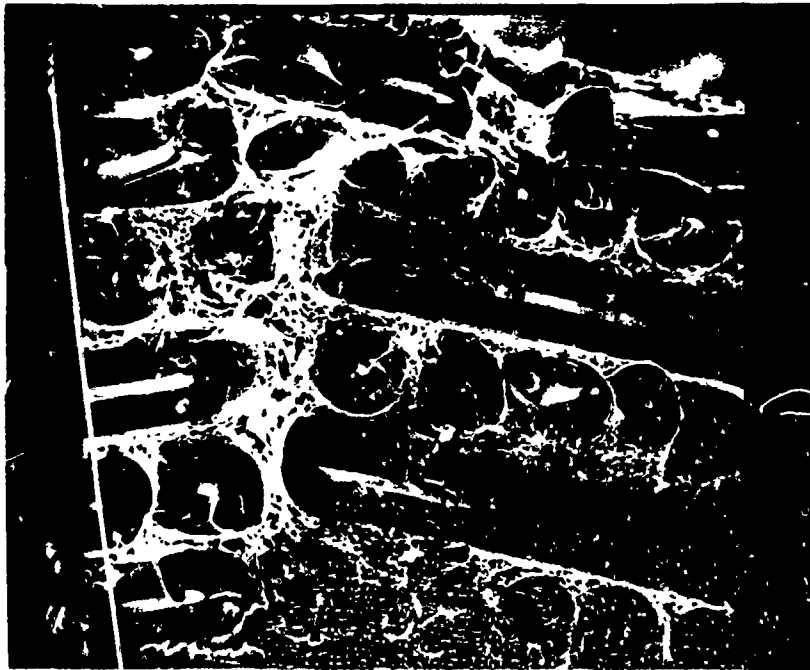


FIGURE 6-13 FRACTURE SURFACE OF  $\pm 45^\circ$  - 4.2 MIL  
BORSIC-6061 FATIGUE SPECIMEN



FIGURE 6-19. FRACTURE SURFACE OF  $0^{\circ} 90^{\circ}$ -5.7 MIL BORSIC-6061  
FATIGUE SPECIMEN

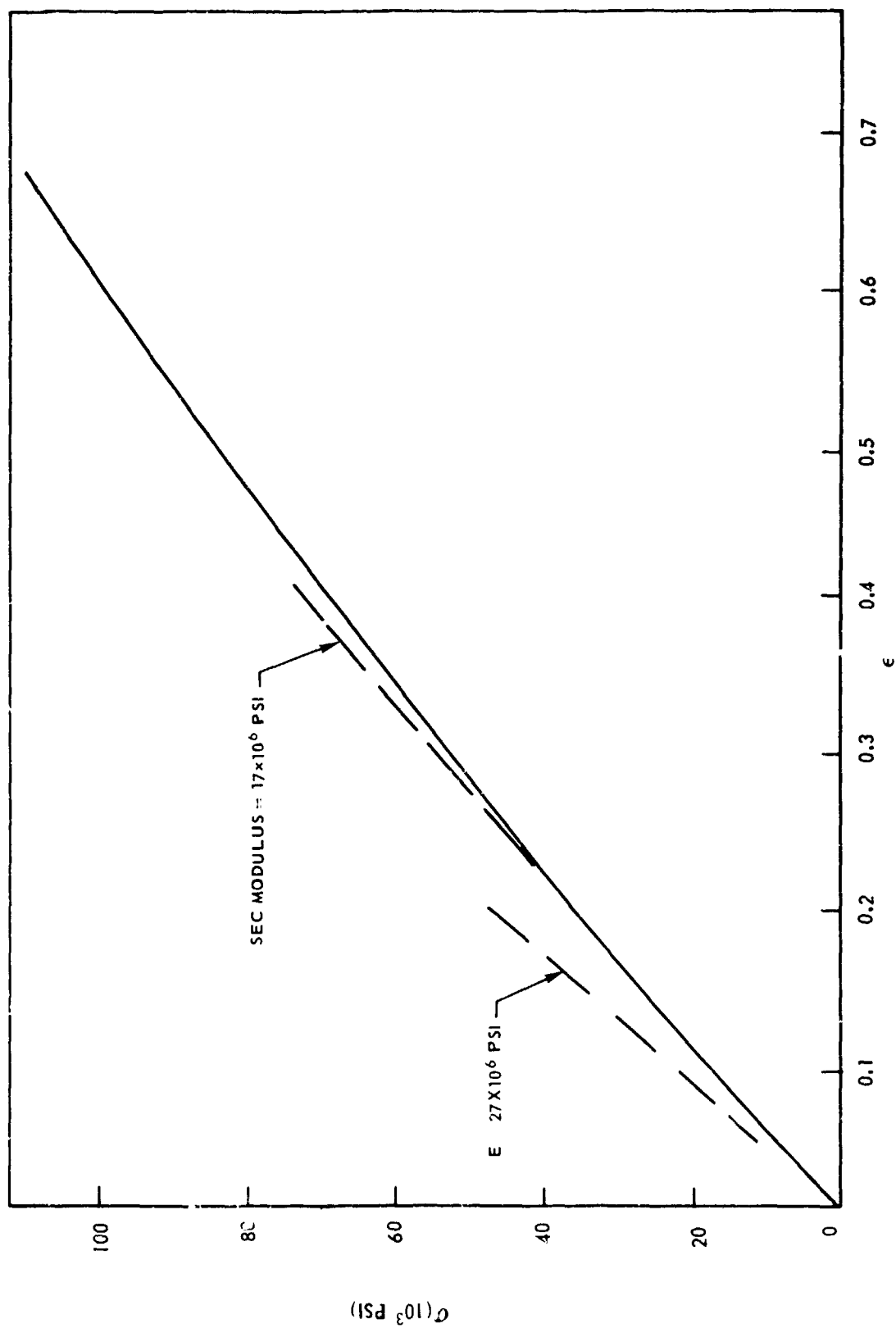


FIGURE 5-20. TENSILE STRESS STRAIN CURVE FOR 0°/90° 57V/o-5.7 BORSIC-6061

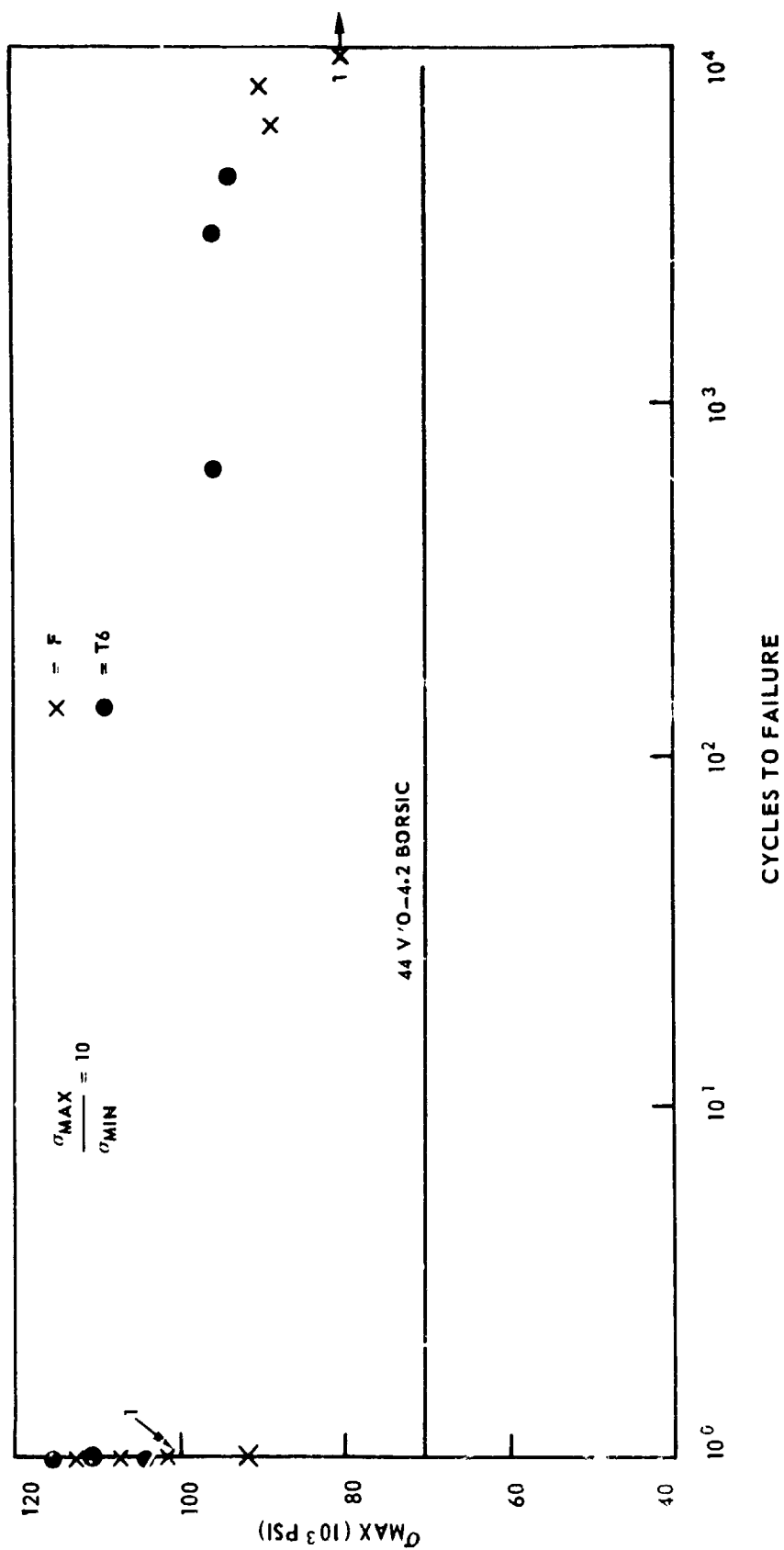


FIGURE 6-21. TENSION - TENSION LOW CYCLE FATIGUE OF 0°/90° 57 v/o -5.7 BORSIC-6061

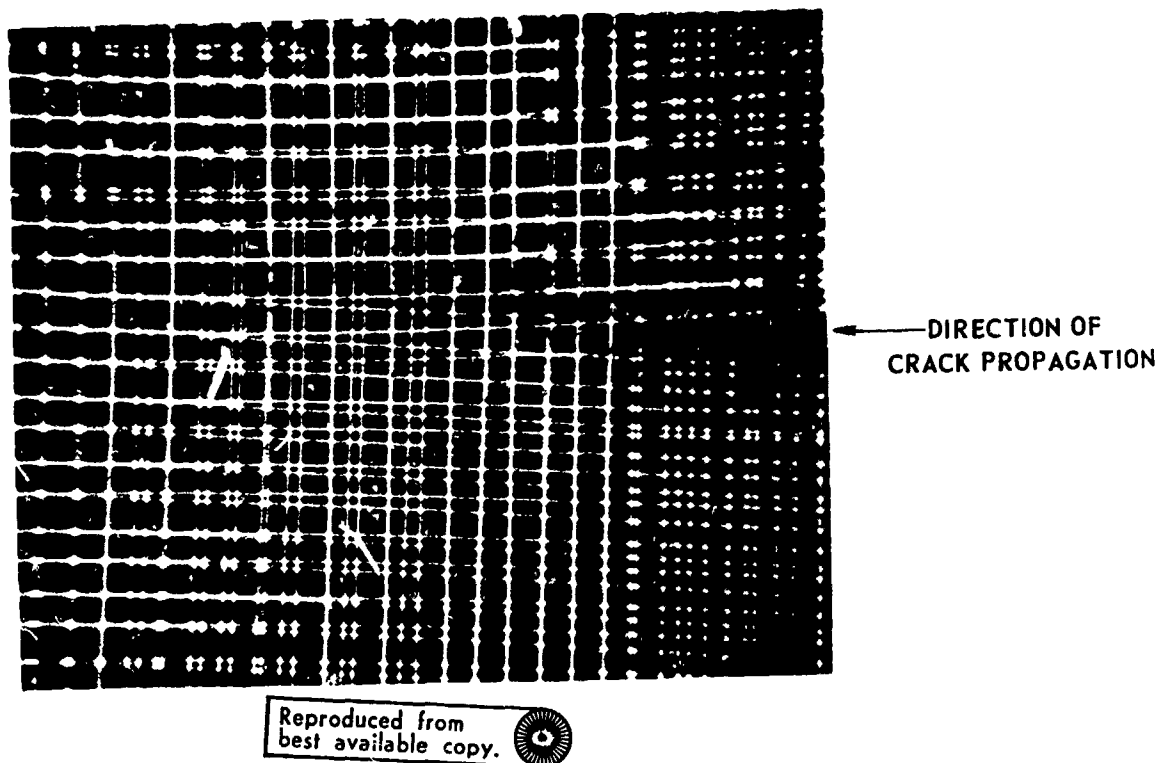
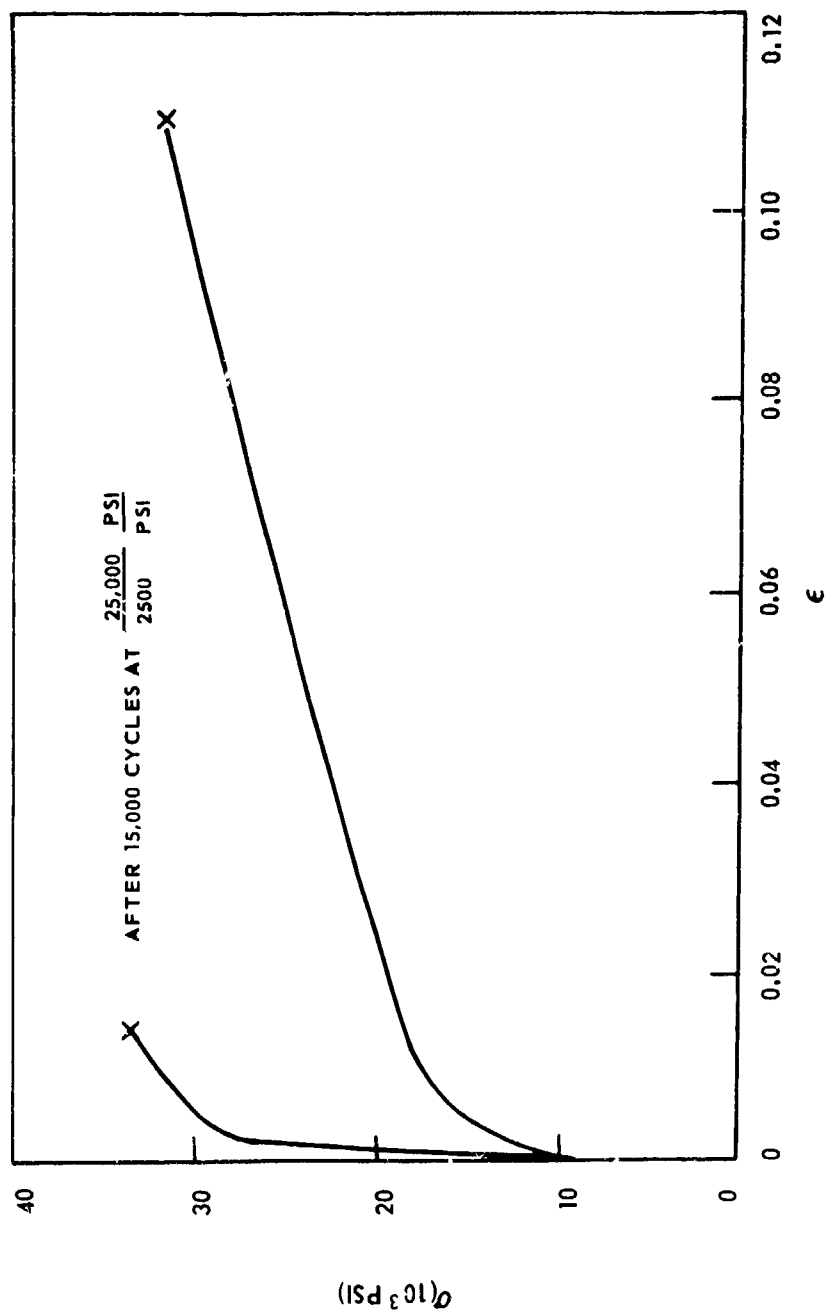


FIGURE 6-22 RADIOGRAPH OF CRACK TIP  
IN 0° 90°-57 v/o - 5.7 MIL BORSIC - 6061

FIGURE 6-23. TENSILE STRESS STRAIN CURVE FOR  $\pm 45^\circ$  BORNIC-6061

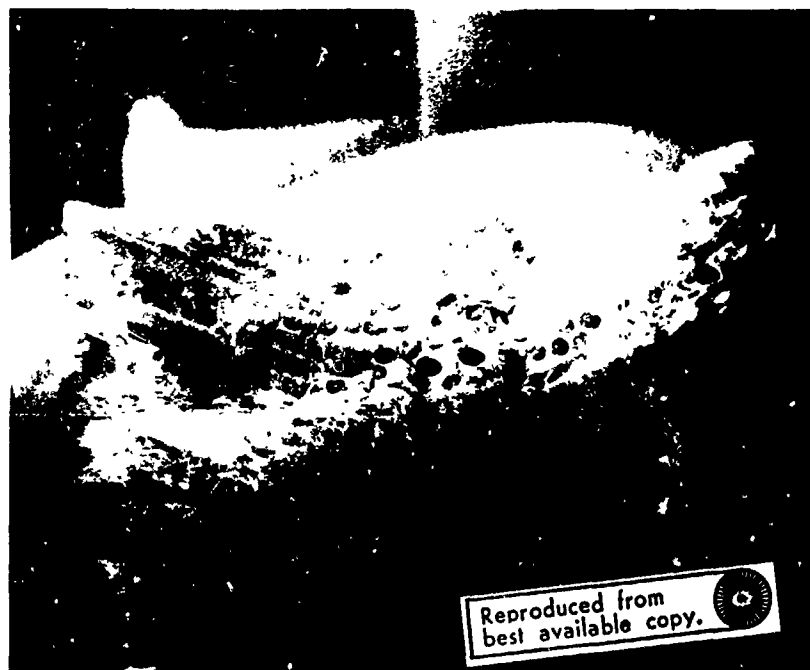


FIGURE 6-24. FRACTURE SURFACE OF  $\pm 45^\circ$  5.7 BORSIC  
6061 FATIGUE SPECIMEN



Reproduced from  
best available copy.



FIGURE 6 - 25. FIBER FRACTURE IN A  $\pm 45^\circ$  - 57 v/o  
5.7 MIL BORSIC - 6061 FATIGUE SPECIMEN



significantly lower, no load fluctuations are observed, and abrupt failure does not occur. In addition, the unloading curve displays a long "tail" extending to deflections that are high relative to those at maximum load.

#### Notched Flexural Strength

Notched flexural strengths of both longitudinally and transversely reinforced materials were determined using beam theory; the results are given in Fig. 7.17. The behavior of these specimens can be accounted for in the following way.

The ratio of notched to unnotched tensile strength for 50% 4.2 mil BORSIC + 6061-F material in the presence of large flaws is approximately 0.53 (85 ksi/160 ksi), Fig. 8.3. The flexural strength of this composite is 225 ksi, Fig. 3.8, which is approximately 1.40 times the tensile strength. In addition, the tensile strengths of 50%, 41%, 32%, 4.2 mil BORSIC + 6061-F are 160 ksi, 131 ksi, and 102 ksi respectively (Ref. 7.7).

Assuming that:

1. The ratio of notched to unnotched strength in the presence of a large flaw is the same in bending as in tension (0.53);
2. The notched to unnotched strength ratio is independent of fiber content (0.53);
3. The ratio of flexural strength to tensile strength is independent of fiber content (1.40);

the following notched flexural strengths are calculated: 119 ksi at 50%; 97 ksi at 41%; and 76 ksi at 32%. The measured values agree closely: 116 ksi at 50%, 85 ksi at 41% (single test), and 78 ksi at 32%, Fig. 7.17.

The notched to unnotched tensile strength ratio for transversely reinforced 4.2 mil BORSIC + 6061-F composite material is approximately 1.00; net tensile strength is unaffected by the crack, Fig. 8.17. In addition, the transverse tensile strength of 4.2 mil BORSIC + 6061-F is nearly independent of fiber content at approximately 15 ksi, Figs. 3.13, 4.7, and 4.13.

Assuming that:

1. The net fracture stress in bending is unaffected by the notch as in the case of tension;
2. The ratio of flexural strength to tensile strength is the same for transversely reinforced material as for longitudinally reinforced material; then a notched strength of approximately 21 ksi is expected for all three fiber contents. Measured values range from 18.9 ksi to 28.0 ksi and are approximately 30% higher at 50% than at 32%, Fig. 7.17. Agreement with the calculation is reasonable but not as close as for the longitudinally reinforced material.

Table VI-II

Tensile Properties of 57%-5.7 mil BORSIC-6061 Cross Ply  
Composites Tested at 45° to the Fiber Axes

<u>Composite Condition</u>	<u>Ultimate Tensile Strength</u> 10 <sup>3</sup> psi	<u>Strain to Failure</u> %
F (As Fabricated)	38.6	10.2
"	37.6	13.8
" Prefatigued 15,000 cycles at 25,000 psi	34.3	10.1
"	33.9	10.6
"	31.6	10.0
"	30.0	13.0
T-6 (Heat Treated)	38.6	1.6
" Prefatigued 6000 cycles at 6000 psi	34.0	1.2
"	34.3	1.6
"	39.7	--

## NOTCH BEND FRACTURE

### SUMMARY

The fracture behavior of BORSIC + aluminum composites has been investigated using Charpy impact tests and slow bend tests of Charpy "V" notch specimens in several orientations and fiber volume fractions. The energy per unit area of longitudinally reinforced material was found to increase with fiber volume percentage. The impact energy of transversely reinforced BORSIC + aluminum is nearly independent of volume fraction fiber and approximately one-third to one-fifth that of longitudinally reinforced material. The energy per unit area of  $\pm 45^\circ$  orientations are intermediate to longitudinally and transversely reinforced materials.

Potentially significant mechanisms of energy absorption were discussed and it was found that the impact energy per unit area,  $G$  in.-lb/in.<sup>2</sup> could be expressed in terms of the fiber diameter,  $d_f$ , fiber strength,  $\sigma_f$ , volume fraction fiber,  $V_f$ , and matrix shear yield strength by the relationship:

$$G = 26 + 8.5 \times 10^{-3} \frac{\sigma_f^2 d_f V_f}{\tau_m}$$

Interrupted slow bend tests were employed to investigate deformation in the specimens. An important mechanism of energy absorption proved to be matrix plastic strain. This was confirmed in tests of Charpy specimens with reduced thickness at constant notch dimensions which exhibited a nearly linear decrease in energy per unit area due to the decrease in shear stress with span to depth ratio.

Extensive fractography was conducted using both scanning electron and conventional light microscopy. Three regions, differing in degrees of filament bundle protrusion, characterized the fracture surfaces of longitudinally reinforced material. The fracture surfaces of transversely reinforced 4.2 mil BORSIC + aluminum materials exhibit extensive fiber splitting, whereas transversely reinforced 0.7 mil BORSIC + aluminum composites do not exhibit significant splitting.

## VII. NOTCHED BEND FRACTURE

Composite materials containing relatively high volume fractions of BORSIC or other brittle high modulus reinforcements exhibit nearly elastic behavior and a limited strain capability when loaded in the direction of fiber alignment. This occurs in the reinforcement direction because high modulus filaments carry the bulk of the load and largely determine the longitudinal strain to failure. At intermediate to large angles from the fiber direction the properties of the matrix and the transverse properties of the fiber become important but the matrix plastic strain is constrained by the rigid fibers. In addition, transverse splitting of weak fibers can diminish the plastic elongation by further concentration of the strain field. The effects of constituent properties on the deformation and fracture behavior of sound composites has been discussed in sections IV and V of this report. This investigation was concerned with composite behavior in the presence of large flaws under flexural loadings.

### 7.1 Charpy Impact Tests

#### Experimental Method

The intent of the first series of experiments was to measure the gross energy associated with fracture as a function of volume percent fiber, matrix properties, and composite anisotropy. Full size notched Charpy specimens of 30 v/o, 40 v/o, and 50 v/o 4.2 mil BORSIC + 6061-F, 50 v/o 4.2 mil BORSIC + 6061-T6, 63 v/o 5.7 mil BORSIC + 6061-F, 50 v/o 4.2 mil BORSIC + 2024-F, and 50 v/o 4.2 mil BORSIC + 5052/56-F were prepared with three crack plane orientations.

Since unidirectional BORSIC/aluminum can be considered transversely isotropic, the specimen geometries are referred to as types "LT", "TL", "TT", where the first letter refers to the direction (longitudinal or transverse) normal to the nominal crack plane and the second letter denotes the direction of crack propagation.

Since the laminate designs of many composite structures contain  $+45^\circ$  plies to provide increased torsional stiffness, the impact behavior of this material is also of direct interest. Plasma-sprayed monolayer tapes were fabricated and vacuum hot press bonded into 80-layer 6 in. x 2 in.  $[(+45)_{40}]_T$  blocks of 50 v/o 4.2 mil BORSIC + 6061-F composite material. Full size notched Charpy specimens of two orientations were evaluated. The distinction between the two arises because the equivalent longitudinal and transverse laminate directions of  $+45^\circ$  material are distinct from the through-thickness or three direction of the laminate. In one case, coded "X", both the crack plane normal and crack propagation direction is directed along a  $+45^\circ$  laminate axis. In the second case, coded "Z", the crack plane normal is parallel to a  $+45^\circ$  laminate direction (1 or 2 axis) but the direction of crack propagation is through the laminate thickness perpendicular to the laminae (3 axis).

A final series of experiments involved tests with Charpy specimens of subsized width and thickness. Since significant plasticity effects accompany the fracture of BORSIC-aluminum, these experiments were aimed at determining the degree to which the apparent fracture energy measured in an impact test depends on sample size in given specimen orientation.

The bulk of this work was performed using material consolidated from plasma sprayed monolayer tapes. The microstructures of these materials were characterized by good fiber spacing, excellent bonding, and less than one percent voids, Fig. 7.1. In addition, impact tests were also performed using material fabricated from polystyrene bonded fiber and matrix foils. These were also well consolidated and bonded.

In all of these tests, measurements were taken of the loss of pendulum energy, in accordance with ASTM Standard A370-67 using a 24 ft-lb capacity machine. Pendulum velocity at impact was approximately 11 ft per second.

### Results and Discussion

#### Work of Fracture

The results of the Charpy "V" notch impact tests are listed in Table: VII-I and VII-II. The relationships of volume fraction fiber and specimen orientation to impact energy of 6061-F matrix composites are given in Fig. 7.2. The impact energy of longitudinally reinforced material (type LT) increases with volume fraction fiber and is approximately three times greater than the energies of the transversely reinforced materials (types TL and TT). The difference in energy between types TL and TT is approximately 10% and both of these energy levels remain nearly constant with volume fraction fiber.

Types TL and TT absorb substantially less energy than type LT because both are oriented such that the large longitudinal specimen stress loads the composite in the direction perpendicular to the fibers, whereas in the type LT specimens, the large longitudinal specimen stress is directed along the fiber direction and matrix shear stresses are higher. Both the tensile strength and fracture strain of BORSIC/aluminum are much lower in the transverse direction than in the longitudinal direction. In addition, since the crack in type LT is propagating in a plane normal to the filaments, every fiber in the composite must be broken. Energy is absorbed in type LT specimens by matrix shear in planes parallel to the filaments and by the process of "pulling out" subcritical fiber lengths on both sides of the fracture surface (Refs. 7.1,2).

The difference in energy between types TL and TT is small and may, in part, be associated with the orientation of active slip planes relative to the fiber direction (Ref. 7.3). Slip (plastic deformation) ahead of the advancing crack tip on planes oriented from  $45^\circ$  to  $90^\circ$  to the crack can take place with comparatively little fiber interaction in type TT specimens. In type TL, however, relatively little plastic deformation can occur without transferring load to the fibers since the  $45^\circ$  slip planes intersect the array of filaments. Thus, the relative volume of matrix material undergoing plastic deformation is larger

in type TT and this may produce the higher fracture energy values. If plane strain conditions are developed in this specimen, part of the difference might be attributed to the fact that type TL specimens experience an induced transverse specimen stress normal to the fibers while the transverse stress in type TT lies in the stronger direction (parallel to the fibers).

Neither type TT nor TL appears to exhibit a significant variation in work of fracture as a function of volume fraction fiber. Lower fracture work was expected as a result of decreased volume of the ductile phase. However, as is shown in Fig. 7.2, the impact energy is nearly independent of volume fraction fiber in a similar manner to the transverse tensile strength.

The 6061-T6 matrix composites exhibit fracture energies substantially lower than those of 6061-F matrix composites, Fig. 7.3. The energy is 40% lower in the LT orientation, 50% lower in the TL orientation, and 62% lower in the TT orientation. Similarly, the 2024-F matrix and 5052/5056-F matrix composites exhibit fracture energies less than one-half of those of the 6061-F matrix composites, Table VII-I.

The tensile strengths of these composite systems (longitudinal and transverse) and the elastic moduli of the matrices are very similar. Therefore, the variations in composite fracture behavior arise from differences in the in situ matrix strength and ductility.

Varying the width of the Charpy specimen does not affect the fracture energy of type LT 4.2 mil BORSIC + 6061-F material, Fig. 7.4. This suggests that the additional transverse constraint arising from increased width is insignificant in view of the constraint already on the matrix in the specimen. The width independence of energy could be of practical significance if the Charpy test were part of a quality control specification. Decreasing the width of a type TT specimen from 0.400 in. to 0.100 in. however, results in approximately a 50% decrease in measured energy. This may be due in part to filament damage during machining. Surfaces normal to the fiber orientation are particularly susceptible to machining damage since the fiber splits easily. Weakened filament can result in a reduced transverse strain (or stress) capability and the energy required to fracture the specimen would be lower.

Reducing the thickness of the Charpy specimen while maintaining constant notch dimensions results in a nearly linear decrease in measured energy per unit area, Fig. 7.5. This appears to be related to the decrease in the ratio of horizontal shear stress to tensile stress parallel to the fibers.  $\tau/\sigma$  is directly proportional to the depth to span ratio. This confirms that an important mechanism is matrix deformation in planes of "easy shear" parallel to the filaments.

The behavior of the two  $\pm 45^\circ$  laminate test configurations is consistent with this principle, Fig. 7.6. The type Z orientation exhibits approximately 50% more energy absorption than does type X. This difference arises because as the crack opens extensive matrix shear occurs in planes that are parallel to the plies (fibers) and normal to the crack plane. In the type X orientation all planes parallel to the advancing crack front intersect filaments and less plastic

deformation occurs. The preferred shear planes are oriented at  $45^\circ$  to the crack plane; these are parallel to one-half of the filaments and normal to the other half.

### Fractography

It was determined by optical fractographic examination that the fracture surface characteristics were similar for the various fiber volume fractions of the 4,2 mil + 6061-F system. Detailed examination of the fracture surfaces was made by scanning electron microscopy on composites containing volume fractions of 0.50. The results of this examination are discussed below.

A photograph of a typical LT fracture is presented in Fig. 7.7. The machined notch lies on the right, fracture has progressed from right to left in Fig. 7.7 (left) along a surface roughly normal to the filaments. At least three kinds of fiber breaks are evident. Filaments exhibiting little or no protrusion from the matrix usually fragment into wafer-like sections, while filaments protruding significantly from the surface tend to exhibit a conical fracture surface. In addition, a very small number of both conical and wafered are longitudinally split. No matrix delamination or fiber matrix interfacial failure is observed. The type LT fracture surface can be characterized by three regions:

1. Region I: An area extending from 2 to 10 fiber layers (0.010 in. to 0.050 in.) adjacent to the notch with relatively long protruding fibers, each with a "sheath" of aluminum matrix, and holes or cavities that correspond to protruding fibers on the mating surface. These protrusions typically contain from 1 to 5 filaments and extend from 0.025 in. to 0.060 in. from the nominal fracture plane in the case of 6061-F matrix material.

2. Region II: An Area extending over approximately two-thirds of the reduced section where fiber bundles of up to several hundred filaments have been pulled out (or are protruding) from the nominal fracture surface. These areas usually exhibit markings on the matrix fracture surface where the bundles have been pulled out, Fig. 7.7 (right). Within a given bundle, the plane of matrix shear rupture or the local fracture surface is typically less than 0.001 in. from the ends of fractured filaments.

3. Region III: A shelf extending from 12 to 20 fiber layers (0.060 in. to 0.100 in.) from the back surface of the specimen that is nearly flat. The areas of bundle pull out characterizing region II are totally absent. The extent of this region remains nearly constant with changes in either the width or thickness of the specimen, Figs. 7.8 and 7.9 (left).

Region I results from the extensive longitudinal matrix shear near the crack tip that occurs during loading prior to unstable crack growth. Region II is produced by matrix shear rupture along planes linking positions where filaments are broken ahead of the advancing crack. The crack can turn and run longitudinally for short distances, resulting in areas of fiber bundle protrusion (Ref. 7.3). Region III, the shelf, appears to be a result of fiber

damage in the specimen under the loading nose which is subjected to contact stresses. This effect will be discussed in the slow bend section of this report.

A typical type TL fracture is shown in Fig. 7.10 (left). The notch is at the bottom of the photograph and the crack has propagated upward. In this orientation the composite is loaded in a transverse direction and the crack propagates longitudinally with respect to the fibers. Under these conditions nearly all the filaments exposed on the fracture are longitudinally split. The crack does not simply split all the fibers in a single plane and propagate across the specimen; frequent deviations to adjacent layers of fibers both in the direction of propagation and more often, across the specimen width, are observed.

Longitudinal splitting usually occurs along a plane roughly bisecting the filament, exposing the tungsten boride core. However, splitting can also occur within the SiC coating or between the boron fiber and the SiC coating as shown in Fig. 7.10 (right). On the left is a filament split through the core; on the right is a region of SiC coating material displaying a smooth but cracked fracture surface suggestive of cleavage failure. Between the two is an area of aluminum matrix that has failed in shear rupture.

A typical type TT failure is shown in Fig. 7.11 (left). The notch lies on the lower left of this photograph; the crack has propagated toward the upper right of the figure in a direction roughly normal to the filaments under the influence of an applied stress transverse to the fibers. The fracture appearance is very similar to that of a type TL specimen. Nearly all the fibers are longitudinally split and the fracture is not flat. The largest irregularities occur in the direction of propagation; less frequent deviations to adjacent fiber layers are found across the specimen width. A closer view of a split filament appears in Fig. 7.11 (right). Typically, on one side of the core the fracture surface appears very smooth while on the opposite side it is comparatively rough. The orientation of the fracture (rough-smooth) was found to be random with respect to the direction of crack propagation.

The fracture surfaces of the 4.2 mil BORSIC + 6061-T6, 8 mil boron + 6061-F, 5.6 mil BORSIC + 6061-F, 4.2 mil BORSIC + 2024-F and 4.2 mil BORSIC + 5052/5056-F systems are similar to those of the 4.2 mil BORSIC + 6061-F system just described. However, the type LT fractures of the 6061-T6, 2024-F and 5052/5056-F matrix system exhibit protrusion lengths in both zone I and zone II that are less than one-half of those of 4.2 mil BORSIC + 6061-F material. This is expected as a result of higher matrix yield strength and shorter critical load transfer length. In the case of the 8 mil boron + 6061-F system the protrusion lengths were greater, Fig. 7.12.

Fracture of the  $+45^\circ$  4.2 mil BORSIC + 6061-F composite material occurred in a surface approximately normal to the specimen at the reduced section. Regardless of the direction of crack propagation the fracture surface exhibited a  $+45^\circ$  saw tooth character parallel to the original laminae (1-2 plane), Fig. 7.13. This reflects the preferred shear planes described previously.



The impact energy of BORSIC + aluminum is more than an order of magnitude greater than monolithic ceramics such as alumina (less than 0.1 ft-lb, Ref. 7.4) even in a transverse orientation, but is approximately five times lower than common structural alloys such as Ti-6Al-4V (15-20 ft-lbs, Ref. 7.5) as shown in Fig. 7.14.

## 7.2 Slow Bend Tests

### Experimental Method

Slow bend tests were conducted using a 60,000 lb Baldwin hydraulic tensile machine and a three point fixture identical to the one used in the impact tests. A deflection rate of 0.050 in. per minute was employed. Continuous load-deflection curves were obtained using the outputs from an LVDT deflectometer and the load cell. Slow bend tests were either interrupted prior to failure to permit metallographic observations of crack extension, or loaded to fracture to determine the maximum load and the integrated area under the load deflection curve.

### Results and Discussion

#### Load-Deflection Response

A typical load-deflection curve for 6061 matrix type axially reinforced type LT specimens, Charpy "V" notch tested in slow bending is given in Fig. 7.15. The applied load needed to maintain a constant deflection rate (0.050 in./min) increases smoothly until near maximum load. The curve initially displays a positive second derivative probably as a result of compressive yielding at the loading noses and seating of the deflectometer. A fairly large, almost linear region follows until the interlaminar shear stress reaches approximately  $5 \times 10^3$  to  $8 \times 10^3$  ksi and yielding is observed. Fluctuations are observed near maximum load. Abrupt failure does not occur until the specimen has been deflected well beyond the point of maximum load. When failure does occur, the recording equipment employed here does not respond quickly enough to monitor the curve. Figure 7.15 contains a dashed line constructed parallel to the curve generated when the apparatus is once more able to measure the unloading curve. The area under the curve was taken using this line as a boundary. The behavior of type LT 2024 matrix composites is similar to this except that observed deflections beyond maximum load are small, less than those of 6061-F matrix material.

It should be noted from Fig. 7.15 that the specimen exhibits considerable plastic deflection prior to unstable crack growth. The energy absorbed is not simply the elastic energy required to load the specimen to its breaking load as reported for glass-polyester (Ref. 7.6).

A typical load-deflection curve of a transversely reinforced composite appears in Fig. 7.16. Behavior of specimen in the other transverse orientation, type TT, is nearly identical to that of type "L". These curves exhibit loading behavior similar to that of type LT material. However, the maximum loads are

significantly lower, no load fluctuations are observed, and abrupt failure does not occur. In addition, the unloading curve displays a long "tail" extending to deflections that are high relative to those at maximum load.

#### Notched Flexural Strength

Notched flexural strengths of both longitudinally and transversely reinforced materials were determined using beam theory; the results are given in Fig. 7.17. The behavior of these specimens can be accounted for in the following way.

The ratio of notched to unnotched tensile strength for 50% 4.2 mil BORSIC + 6061-F material in the presence of large flaws is approximately 0.53 (85 ksi/160 ksi), Fig. 8.3. The flexural strength of this composite is 225 ksi, Fig. 3.8, which is approximately 1.40 times the tensile strength. In addition, the tensile strengths of 50%, 41%, 32%, 4.2 mil BORSIC + 6061-F are 160 ksi, 131 ksi, and 102 ksi respectively (Ref. 7.7).

Assuming that:

1. The ratio of notched to unnotched strength in the presence of a large flaw is the same in bending as in tension (0.53);
2. The notched to unnotched strength ratio is independent of fiber content (0.53);
3. The ratio of flexural strength to tensile strength is independent of fiber content (1.40);

the following notched flexural strengths are calculated: 119 ksi at 50%; 97 ksi at 41%; and 76 ksi at 32%. The measured values agree closely: 116 ksi at 50%, 85 ksi at 41% (single test), and 78 ksi at 32%, Fig. 7.17.

The notched to unnotched tensile strength ratio for transversely reinforced 4.2 mil BORSIC + 6061-F composite material is approximately 1.00; net tensile strength is unaffected by the crack, Fig. 8.17. In addition, the transverse tensile strength of 4.2 mil BORSIC + 6061-F is nearly independent of fiber content at approximately 15 ksi, Figs. 3.13, 4.7, and 4.13.

Assuming that:

1. The net fracture stress in bending is unaffected by the notch as in the case of tension;
2. The ratio of flexural strength to tensile strength is the same for transversely reinforced material as for longitudinally reinforced material; then a notched strength of approximately 21 ksi is expected for all three fiber contents. Measured values range from 18.9 ksi to 28.0 ksi and are approximately 30% higher at 50% than at 32%, Fig. 7.17. Agreement with the calculation is reasonable but not as close as for the longitudinally reinforced material.

### Work of Fracture

The energy to fracture the slow bend specimens was determined by integrating under the load-deflection curves. Results for type LT BOPSI<sup>®</sup> + 6061-F material compare closely with energies obtained in impact tests, Fig. 7.18. The greatest disparity was found at 32 v/o fiber, 25%; at 50 v/o fiber the results were nearly the same. Tests on 2024 matrix composites with 50 v/o fiber also resulted in substantially the same energy levels: 185 and 169 in.-lb/in.<sup>2</sup> in slow bend tests compared to 180 and 166 in.-lb/in.<sup>2</sup> in impact tests.

Results for the type TL and TT specimens are given in Fig. 7.19. Observed slow bend energy levels are only one-quarter to two-thirds of the energies measured in impact tests. This effect may be related to the different strain rates characterizing the two tests. The ultimate strength of 1100-0 aluminum for example increases from 11 ksi to approximately 17 ksi as the strain rate is increased from  $10^{-6}$  to  $10^3$  (Ref. 7.8). In addition, multiaxial stress can have an appreciable effect on strain rate sensitivity (Ref. 7.9). The impact energies could be higher than the slow bend values because annealed 6061 alloy is a relatively low yield strength material and the effect of increased strength is to increase the work of matrix rupture, Fig. 7.20. The maximum disparities in all three orientations are found at the lowest fiber volume percents (highest matrix fraction).

### Interrupted Tests

Photographs of a type LT slow bend test specimen interrupted prior to maximum load (at point A in Fig. 7.15) are given in Fig. 7.21. Extensive general matrix slip is evident on the polished surfaces both at the notch tip and under the loading nose. Little plastic deformation has occurred near mid thickness. In addition, the filaments in the region under the loading nose are broken in several fiber layers. This most likely caused the previously mentioned zone III on the fracture surfaces of broken specimens.

A type LT specimen interrupted after maximum load but before unstable crack propagation (at point B in Fig. 7.15) is shown in Fig. 7.22. Extensive matrix shear has occurred throughout the entire reduced section. A large number of fiber fractures are evident with the highest density of breaks near the notch tip. It should be noted that these surface fibers were undoubtedly weakened by the polishing operation; filaments within the specimen may not exhibit this degree of multiple fracture.

Surface views of a type TL specimen test that was interrupted after maximum load was reached (at point A in Fig. 7.16) are shown in Fig. 7.23. Longitudinal splitting is evident in filaments below the notch. The specimen has not yet sustained gross deflections and separated. Extensive slip parallel to the fibers has also occurred, Fig. 7.23 (right).

Similar views of a type TT specimen appear in Fig. 7.24. The surface is characterized by extensive fiber splitting and zones of intense matrix shear linking split filaments.

### 7.3 Notched Bend Analysis

There are three potentially significant mechanisms of energy absorption in BORSIC + aluminum composites associated with crack initiation and propagation:

1.  $U_\gamma$ , Energy to create new fiber surface area
2.  $U_E$ , Elastic energy needed to load up the fibers
3.  $U_P$ , Plastic work in the matrix.

Fiber-matrix debonding and matrix-matrix delamination are not observed in properly fabricated plasma sprayed composites and are therefore not included above. These sources of energy absorption are discussed in the following sections.

#### Fiber Fracture Surface Energy

This contribution to the observed fracture work is small as demonstrated below. The surface energy of boron fiber can be approximated as being slightly higher than ceramics such as  $MgO$  or  $SiO_2$  glass but less than that of beryllium, or 1200-1600 ergs/cm<sup>2</sup> ( $6-9 \times 10^{-3}$  in.-lb/in.<sup>2</sup>) (Ref. 7.12). The fiber fracture surface energy contribution to the toughness of a 50% by volume fiber composite is therefore small:  $6-9 \times 10^{-3}$  in.-lb/in.<sup>2</sup>. Even if one increases this value by a factor of 50 (Ref. 7.12) to account for probable local plasticity effects in the filament, and also by a factor of 10 to allow for the possibility of multiple breaks in each fiber, the resulting contribution is only 5 in.-lb/in.<sup>2</sup>, compared to experimental values of over 300 in.-lb/in.<sup>2</sup> for the composite in the LT orientation and over 75 in.-lb/in.<sup>2</sup> for 6061-F matrix material in transversely reinforced orientations.

#### Fiber Elastic Energy

An important parameter in fracture tests is the quantity of elastic energy stored in the specimen since this represents a source of potential energy available to perform the work of fracture. In advanced composite systems such as BORSIC + aluminum this elastic energy is largely contained in the filaments. Significant amounts of elastic energy are needed to initiate fracture in these materials since matrix or interfacial effects isolate the filaments from stress singularities and fracture does not occur at extremely low levels of applied stress.

Since the stress distribution throughout a notched ductile matrix composite has not been established, an estimate of the elastic energy in the BORSIC + aluminum specimens considered in this investigation is given below and compared to measured values of fracture work.

One may consider a rectangular bar notched at the center subjected to three-point bending so as to load the material below the notch in tension. It is assumed that simple beam theory can be applied, that behavior is elastic,

and that the beam modulus in tension equals that in compression. It is further assumed that there is no stress concentration effect associated with the notch and that the depth of the notch simply reduces the height of material under stress.

The maximum total elastic energy in the specimen at peak load is then given by:

$$U = AL \sigma_c^2 / 18E$$

where  $U$  = total energy in specimen  
 $A$  = cross-sectional area  
 $L$  = length between supports (1.57 in. for Charpy fixture)  
 $\sigma_c$  = fracture stress  
 $E$  = elastic modulus along the axis of the beam.

If this energy were consumed in creating the fracture surface of area  $A$ , the measured work per unit area,  $U_E$ , would then be:

$$U_E = L \sigma^2 / 18E \quad (7.1)$$

Equation (7.1) represents an upper bound on the elastic energy since stress concentration effects at the notch result in lower stress levels throughout the beam at failure compared to the unnotched geometry.

Using the notched flexural strengths determined previously and assuming rule-of-mixtures moduli, one obtains the levels of elastic energy listed in Table VII-III. Also given in Table VII-III are elastic energy values determined from the area under the elastic triangle of several slow bend tests. The elastic energy contribution is approximately 0.29 to 0.34 of the total fracture work measured for type LT specimens. This amount of elastic energy is better represented by the expression:

$$U_E = L \sigma_c^2 / 25E_c \quad (7.2)$$

In the case of type TL and TT specimens the elastic energy estimate is approximately 2 in.-lb/in.<sup>2</sup>. Since the total absorbed energy is much more than the maximum elastic energy the fracture is not abrupt and plastic energy is absorbed after maximum load is passed (Figs. 7.15, 7.16).

Equation (7.2) can be conveniently written in terms of constituent properties using rule-of-mixtures expressions for composite modulus and strength and neglecting the matrix contributions:

$$\sigma_c \approx V_f \sigma_f \quad (7.3)$$

$$E_c \approx V_f E_f \quad (7.4)$$

Therefore:

$$U_E \approx L/25 V_f \sigma_f^2 / E_f \quad (7.5)$$

### Matrix Plastic Work

Matrix plastic work contributions could arise from the several mechanisms including the following:

1. Matrix rupture in zones linking filament fractures as the specimen separates,
2. Shear around the circumference of fibers or fiber bundles as they are "pulled out" during specimen separation,
3. Shear in plastic zones near the flaw tip in planes at 45° to 90° from the crack plane,
4. Horizontal shear throughout the specimen volume in planes parallel to the fibers.

These contributions are not necessarily independent, though a given element of matrix can deform as a result of different mechanisms at varying stages of the loading and fracture process.

The energy to rupture zones of matrix between filament breaks, mechanism 1 above, is proportional to the volume of matrix material failed,  $V_R$ , and the energy per unit volume,  $U_M$ , needed to fracture the matrix:

$$U_R = V_R U_M \quad (7.6)$$

$U_M$  can be conveniently obtained from the area under the true stress-strain curve.

$$U_M = \int_0^{\epsilon_f} \sigma d\epsilon \approx \left[ \left( \frac{\sigma_u + \sigma_{ys}}{2} \right) \epsilon_f \right] \approx \left( \frac{\sigma_u + \sigma_{ys}}{2} \right) \left[ \ln \left( \frac{1}{1-RA} \right) \right] \quad (7.7)$$

where  $\epsilon_f$  = true fraction strain  
 $\sigma_{ys}$  = matrix yield strength  
 $\sigma_u$  = matrix ultimate strength  
RA = reduction of area.

$V_R$  can be estimated using a simple two dimensional model. The inter-fiber matrix thickness,  $\lambda$ , and the fiber diameter,  $d$ , are related to the volume fraction fiber,  $V_f$ , by the relationship:

$$V_f = d/\lambda + d \quad (7.8)$$

and  $\lambda = d (1-V_f)/V_f$

In addition, if it is assumed that matrix rupture occurs over diamond shaped elements between filaments arising from  $45^\circ$  shear, then

$$V_R/A = \lambda^2/2 \quad 1/\lambda+d \quad (7.9)$$

Substituting

$$U_R = d^2(1-V_f)^2/2 V_f^2 (V_f/d) U_M = d/2 (1-V_f)^2/V_f U_M \quad (7.10)$$

For 4.2 mil BORSIC + 6061-F,  $U_M = 9.8 \times 10^3$  in.-lb/in.<sup>2</sup>, Eq. (7.7) and  $d = 4.1 \times 10^{-3}$  in.; therefore:

$$U_R = 1.9 \text{ in.-lb/in.}^2 \text{ for } 50 \text{ v/o}$$

$$U_R = 6.3 \text{ in.-lb/in.}^2 \text{ for } 30 \text{ v/o}$$

These energies are very small relative to the measured work of fracture. In addition the impact strength of BORSIC + aluminum increases with a decrease in volume percent of the ductile phase rather than decreasing as indicated by Eq. (7.10) and this energy contribution can be neglected.

Kelly (Ref. 7.1) has advanced an expression for the maximum work required for fiber pullout, mechanism 2 above, assuming all filaments are of critical length and that the critical length can be calculated from the shear log single fiber inclusion analysis:

$$U_{PO} = V_f d_f \sigma_f^2 / 24 \tau_m \quad (7.11)$$

This expression is not directly applicable for calculating the pull out energy in BORSIC + aluminum since the model was developed primarily for composites which exhibit interfacial failure and individual fiber pull out. However, the functional dependence of energy on constituent properties may apply to the case of bundle shear at pullout lengths shorter than  $l_c$ . Note that the dependence on  $V_f$  and  $\sigma_f^2$  is identical to that in Eq. (7.5) for the elastic energy at maximum load. Since the fractography studies indicate little individual fiber pullout the energy absorbed for this mechanism is probably much smaller than calculated in Eq. (7.11).

The amount of plastic deformation for mechanisms 3, crack tip shear, and 4, horizontal shear can be calculated to be:

1.  $V_S$  is proportional to a power of composite strength,  $\sigma_c$ , since this determines the maximum load and deflection,
2.  $V_S$  is proportional to a function,  $F$ , which relates the level of average shear stress in the sample to the maximum load,
3.  $V_S$  is inversely proportional to the shear yield strength of the matrix,  $\tau_m$ , since this determines how much of the strain is plastic,

4.  $V_S$  is proportional to the volume fraction matrix,  $V_M$ , since this determines the volume of the deforming constituent.

In the elastic case, the shear function,  $F$ , is proportional to the depth to span ratio,  $h/L$ . Therefore, if:

$$V_S = K (\sigma_c) / \tau_m V_m (h/L) \quad (7.12)$$

If composite strength is approximated by  $V_f \sigma_f$  one obtains:

$$V_S = \frac{\text{const } V_f^n (1-V_f) \sigma_f^2 (h/L)}{\tau_m} \quad (7.13)$$

This expression is zero when  $V_f = 0$ , rises to maximum at  $V_f = n/n + 1$ , and goes to zero at  $V_f = 1$ . Thus, if  $n = 1$  these contributions from matrix shear are maximum at fifty percent fiber and reduced by sixteen percent at thirty percent fiber. If  $n = 2$ , the maximum is found at sixty-six percent filament and the dependence of work on  $\sigma_f$  and  $\tau_m$  is identical to that in Eq. (7.11).

Experimentally determined type LT impact energies are given as a function of Kelly's pullout parameter, Eq. (7.11),  $V_f d_f \sigma_f^2 / 24 \tau$ , in Fig. 7.25. The correlation coefficient of the least squares line shown is 0.977 compared to a level of 0.708 required for 99.9% confidence. These results indicate that the dependence of impact energy on constituent properties given in Eqs. (7.5) (7.11) and (7.13) (with  $n = 2$ ) are appropriate. The impact energy of type LT BORSIC + aluminum composites can be given by the expression:

$$G \text{ (in.-lb/in.}^2\text{)} = 25.7 + 8.46 \times 10^{-3} \frac{\sigma_f^2 V_f d_f}{\tau_m} \quad (7.14)$$

The magnitude of the total measured energy, which includes shear contributions and may include unrecovered elastic energy, is approximately twenty to twenty-five percent of that suggested by the pullout relation, Eq. (7.11). This confirms the fractographic observations discussed earlier. It should be noted that the strength of the filament in various materials was not directly measured. Instead, relative fiber strength was obtained by dividing average longitudinal tensile strength by the volume fraction fiber, Table VII-IV. This represents the average filament stress on the fiber at composite tensile fracture ignoring matrix contributions. The results of this calculation, Table VII-IV, indicate strengths of 320 ksi, 331 ksi, and 280 ksi for 4.2 mil, 5.7 mil, and 8.0 mil fibers, respectively.

#### 7.4 Conclusions

1. The energy absorbed during impact tests of BORSIC + aluminum arises from matrix shear primarily in planes parallel to the filaments and as a result of unrecovered elastic energy in the specimen.



2. Impact energy per unit area,  $G$  (in.-lb/in.<sup>2</sup>) of longitudinally reinforced material can be expressed in terms of the fiber diameter,  $d_f$ , fiber strength,  $\sigma_f$ , volume fraction fiber,  $V_f$ , and matrix shear yield strength by the empirical relationship:

$$G = 26 + 8.5 \times 10^{-3} \sigma_f^2 d_f V_f / \tau_m$$

3. Reducing the thickness of the type LT Charpy specimen at constant notch dimensions results in a nearly linear decrease in measured energy per unit area due to the decrease in horizontal shear stress with depth to span ratios.

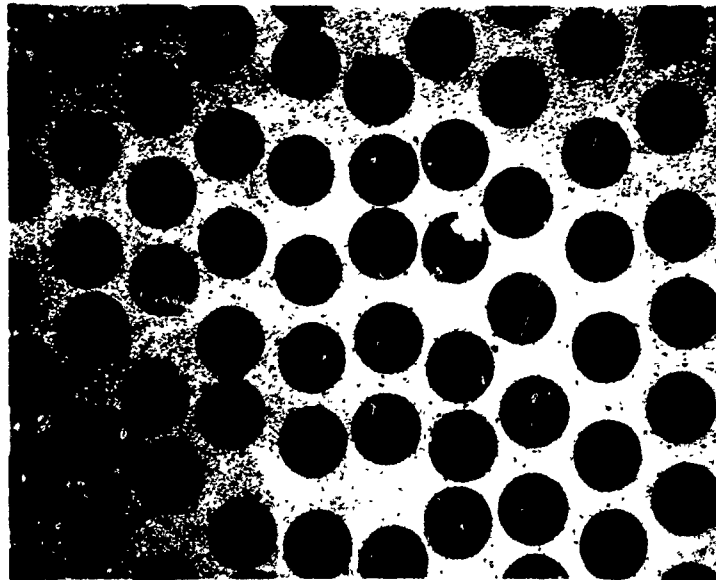
4. Reducing the width of the type LT Charpy specimen at constant notch dimensions and height has no significant effect on fracture energy per unit area.

5. Slow bend load-deflection curves of longitudinally reinforced BORSIC + aluminum display considerable plastic deformation prior to unstable crack growth; transversely reinforced material also deforms plastically.

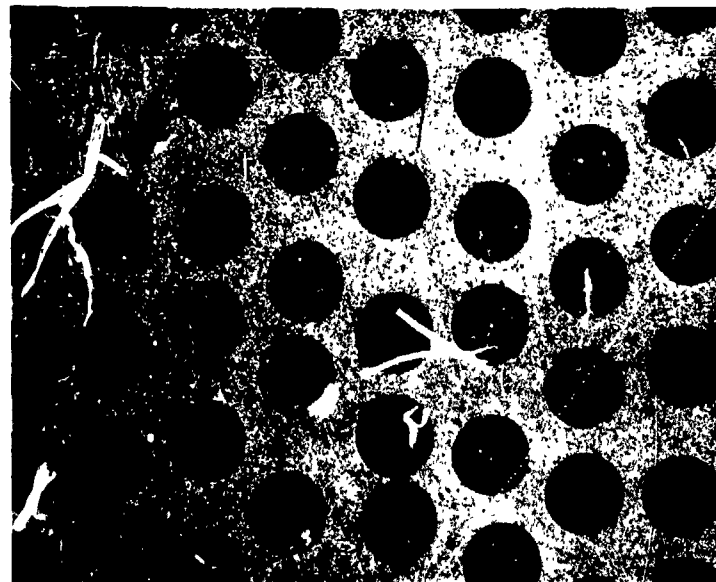
6. Longitudinally reinforced materials exhibit fracture surfaces characterized by three regions of differing degrees of filament bundle protrusion. The fracture surfaces of transversely reinforced materials containing 4.2 mil BORSIC exhibit extensive fiber splitting largely along diametral planes whereas those containing 5.7 mil BORSIC do not exhibit significant splitting.

## SECTION VII - REFERENCES

1. A. Kelly, Strong Solids, Clarendon Press, 1966.
2. J. Cook and J. E. Gordon, Proc. Royal Soc. A., Vol. 282, p. 508-520, 1964.
3. M. J. Salkind and F. D. George, Trans. AIME, Vol. 242, p. 1237-1247, 1968.
4. J. F. Lynch, C. G. Ruderer, and W. H. Duckworth, ed., Engineering Properties of Selected Ceramic Materials, American Ceramic Society, Columbus, Ohio, 1966.
5. D. L. Ruckle, Pratt & Whitney Aircraft, unpublished work.
6. W. Spath and M. E. Rosner, Impact Testing of Materials, Gordon and Breach, New York, 1961.
7. K. G. Kreider, R. D. Schile, E. M. Breinan, M. A. Marciano, "Plasma Sprayed Metal Matrix Fiber Reinforced Composites", AFML-TR-68-119, July, 1968.
8. S. R. Bodner, "Strain Rate Effects in Dynamic Loading of Structures", in Behavior of Materials under Dynamic Loading Rates, p. 93, ASME, 1965.
9. E. A. Ripperger, "Dynamic Plastic Behavior of Aluminum, Copper and Iron", in Behavior of Materials under Dynamic Loading, N. J. Huffington, Jr. Ed., p. 62, ASME, 1965.
10. J. G. Kaufman and M. Holt, "Fracture Characteristics of Aluminum Alloys", Alcoa Research Laboratories.
11. B. L. Averbach, "Some Physical Aspects of Fracture" in Fracture, Vol. 1, H. Liebowitz, ed., Academic Press, 1968.

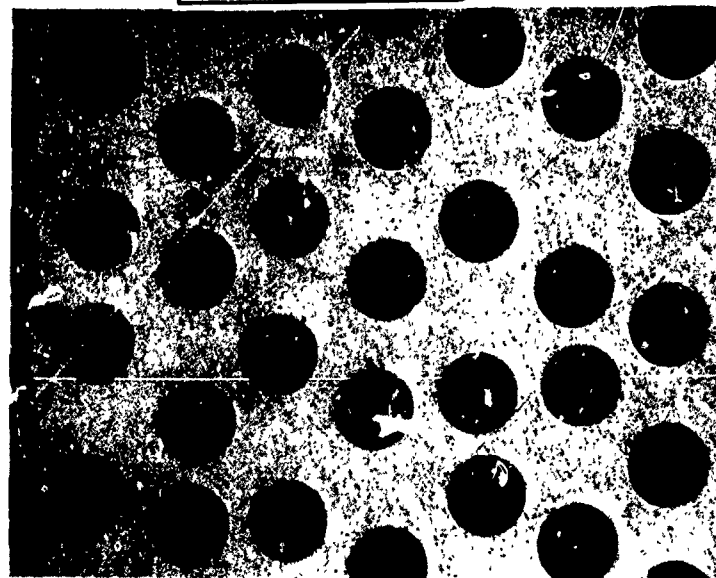


50 v/o



41 v/o

Reproduced from  
best available copy.



32 v/o

MAG 100X

FIGURE 7-1  
MICROSTRUCTURES OF 4.2 MIL BORSIC®  
+6061-F ALUMINUM COMPOSITE MATERIAL

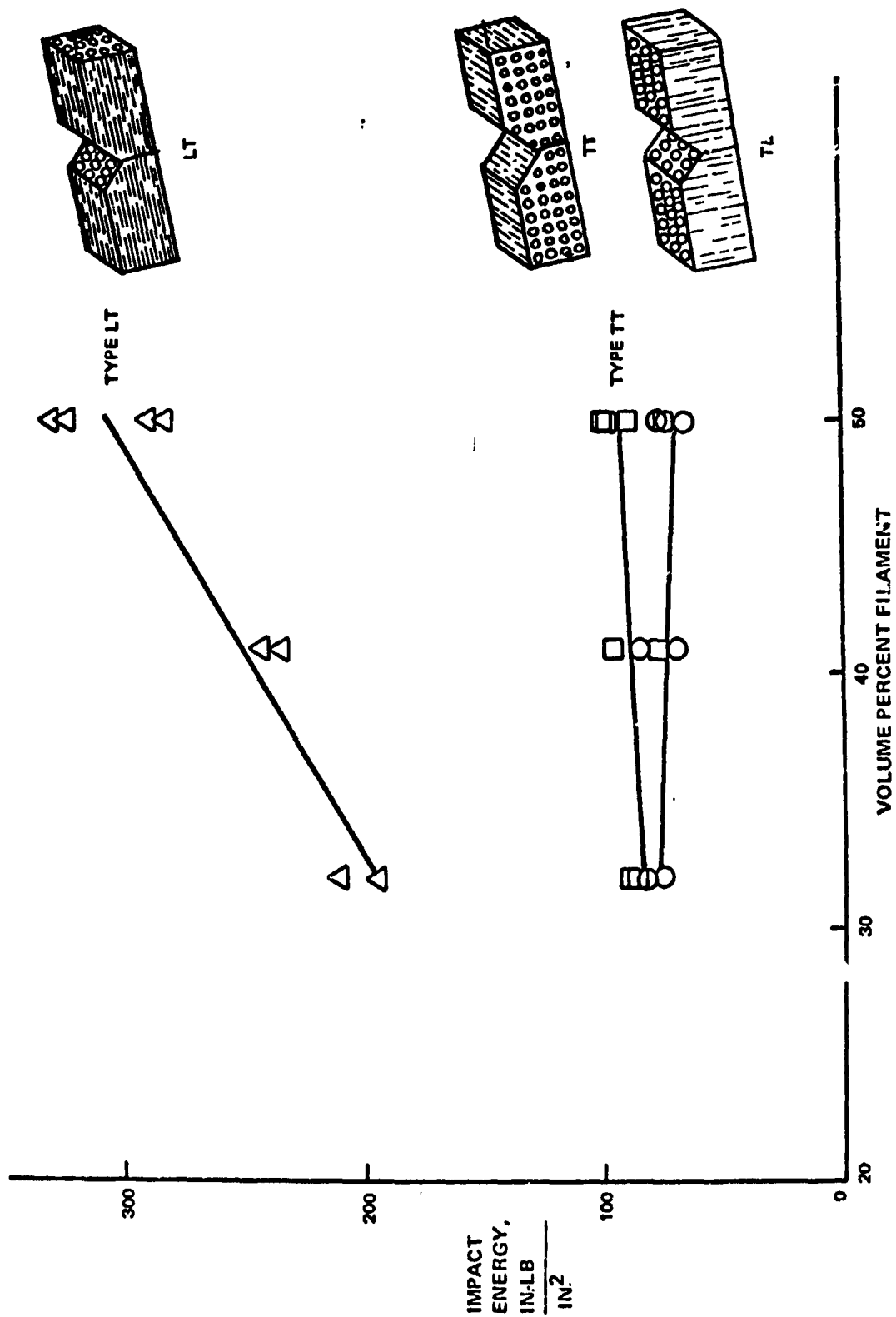


FIGURE 7-2  
IMPACT ENERGY PER UNIT AREA FOR 4.2 MIL BORSIC + G061F ALUMINUM  
FULL SIZE CHARPY "V" NOTCH SPECIMENS

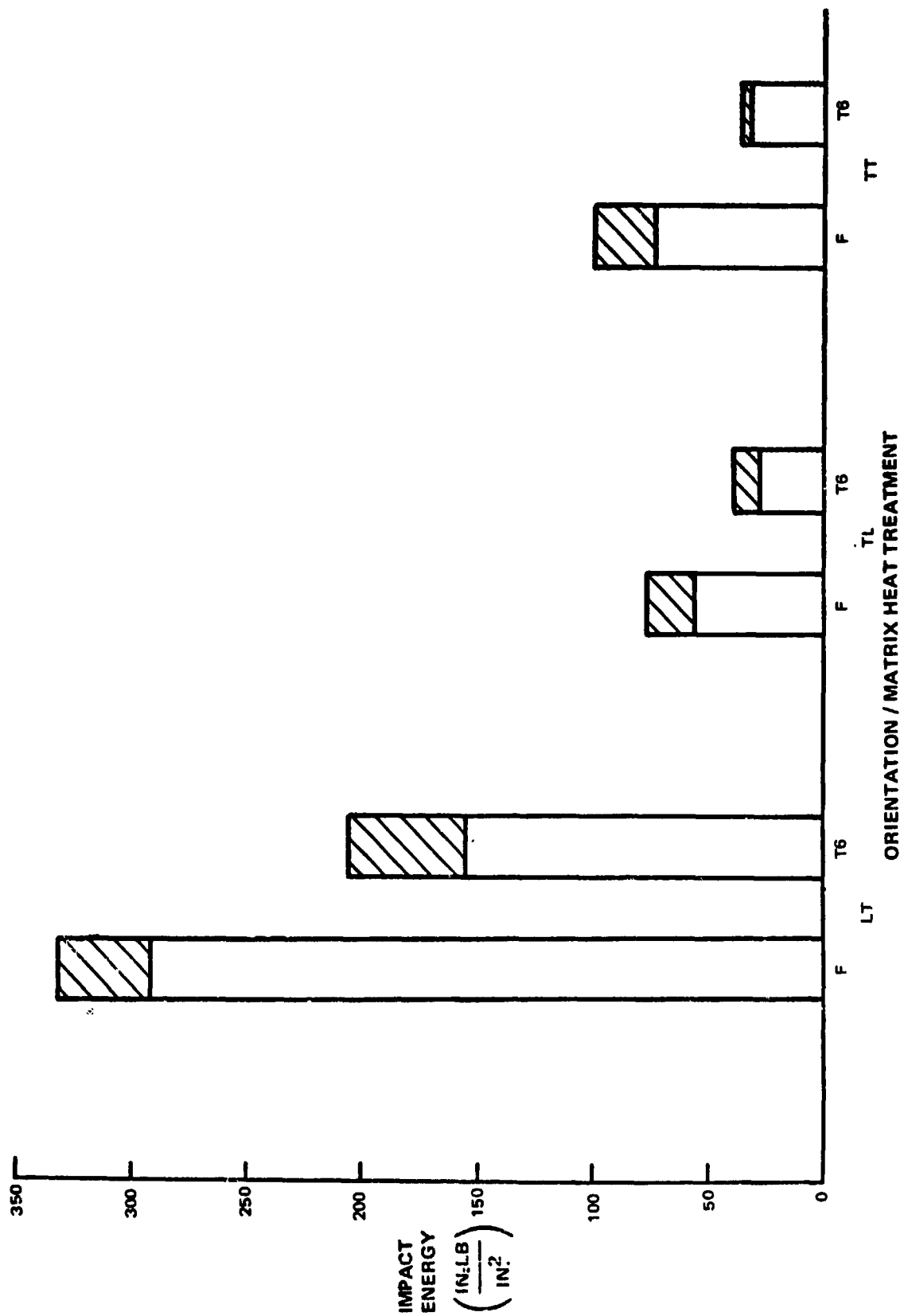


FIGURE 7-3

EFFECT OF HEAT TREATMENT ON THE IMPACT ENERGY PER UNIT AREA FOR 50 v/o BORSIC +  
 6061 ALUMINUM (FULL SIZE CHARPY "V" NOTCH SPECIMENS)

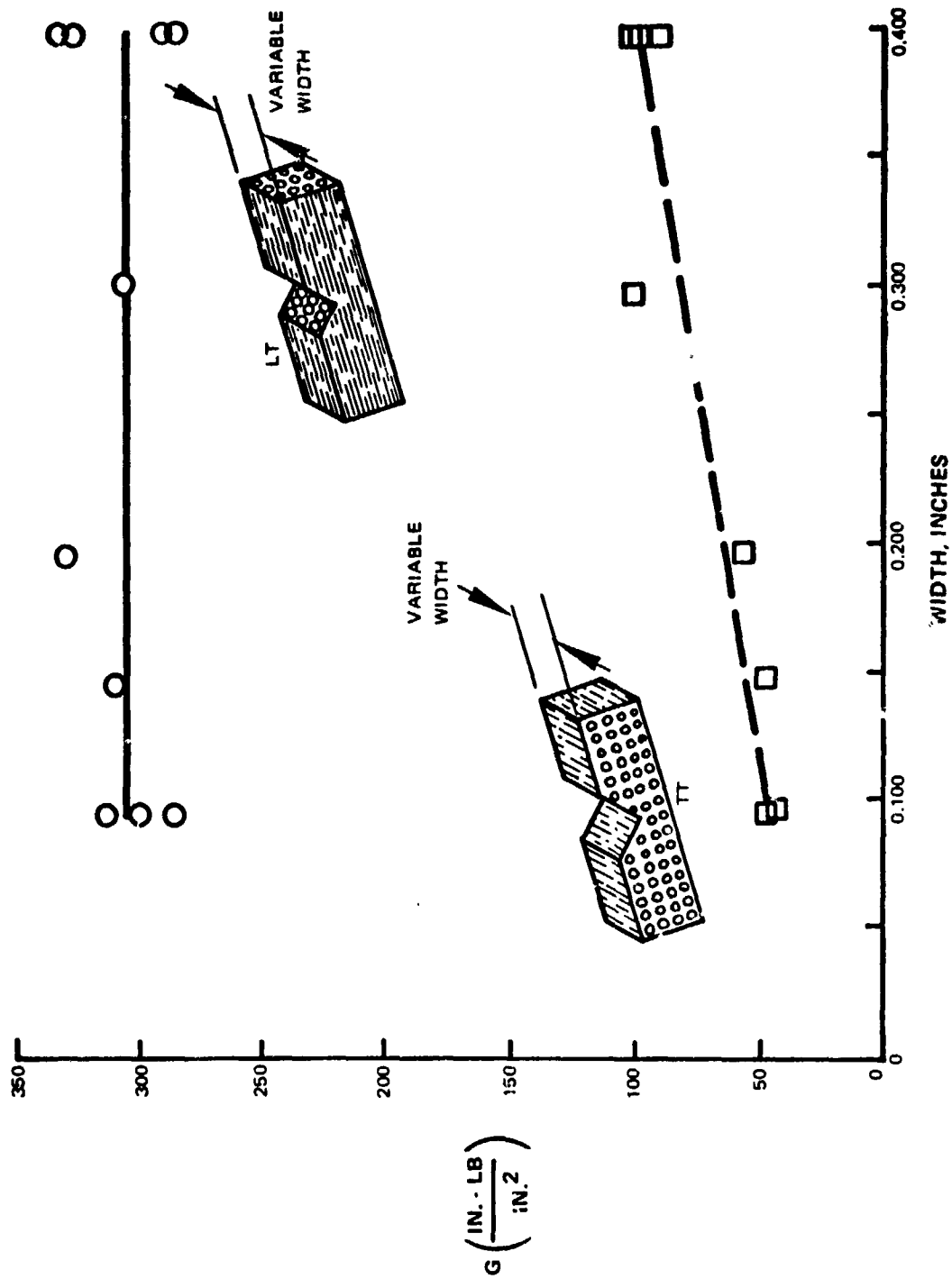


FIGURE 7-4

EFFECT OF WIDTH ON THE IMPACT-ENERGY PER UNIT AREA FOR 4.2 MIL BORSIC +  
6061-F ALUMINUM CHARPY "V" NOTCH SPECIMENS

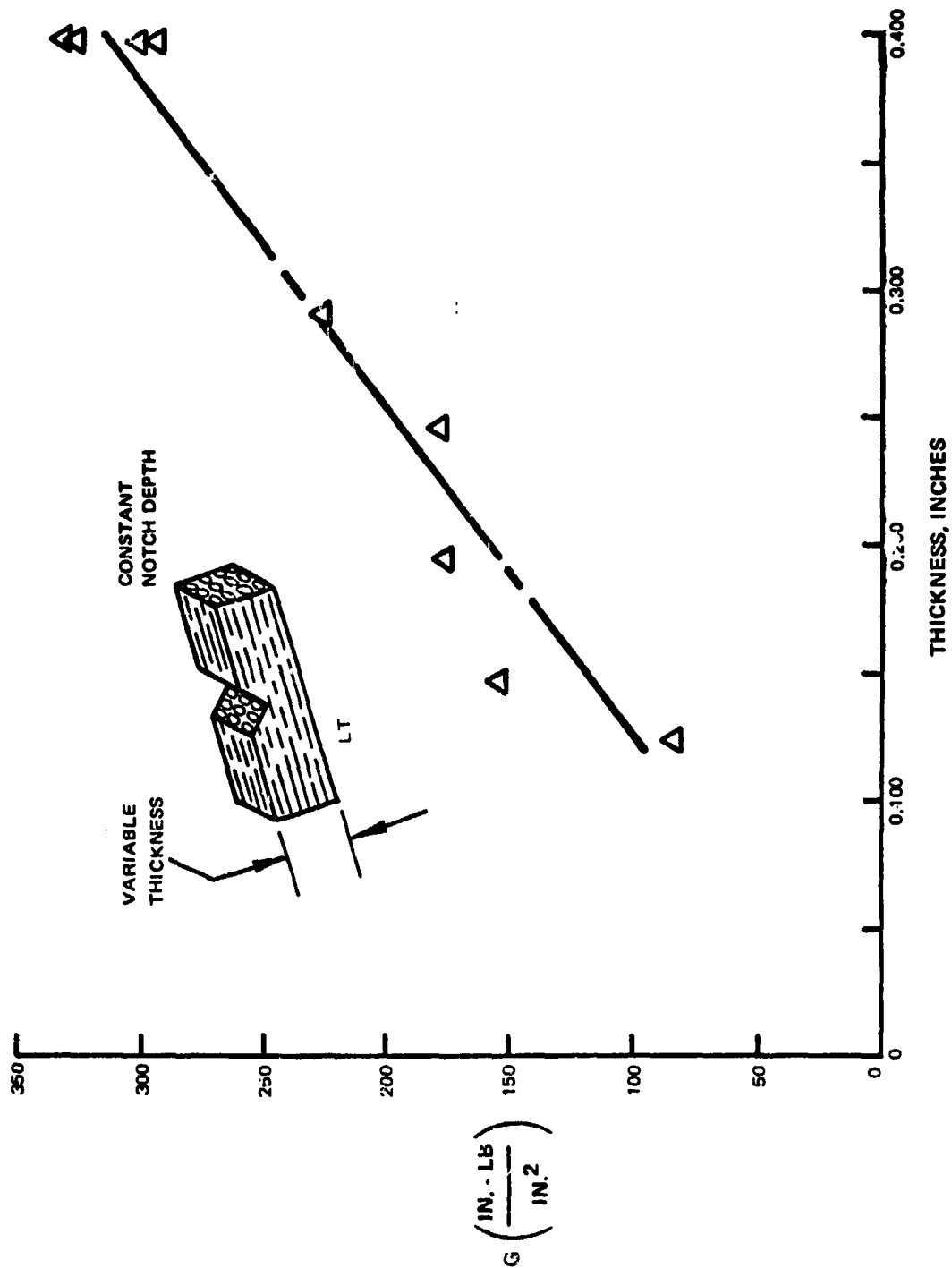


FIGURE 7-5  
EFFECT OF THICKNESS ON THE IMPACT ENERGY PER UNIT  
AREA FOR 4.2 MIL BORSIC + 6061-F ALUMINUM CHARPY  
1/4" NOTCH SPECIMENS

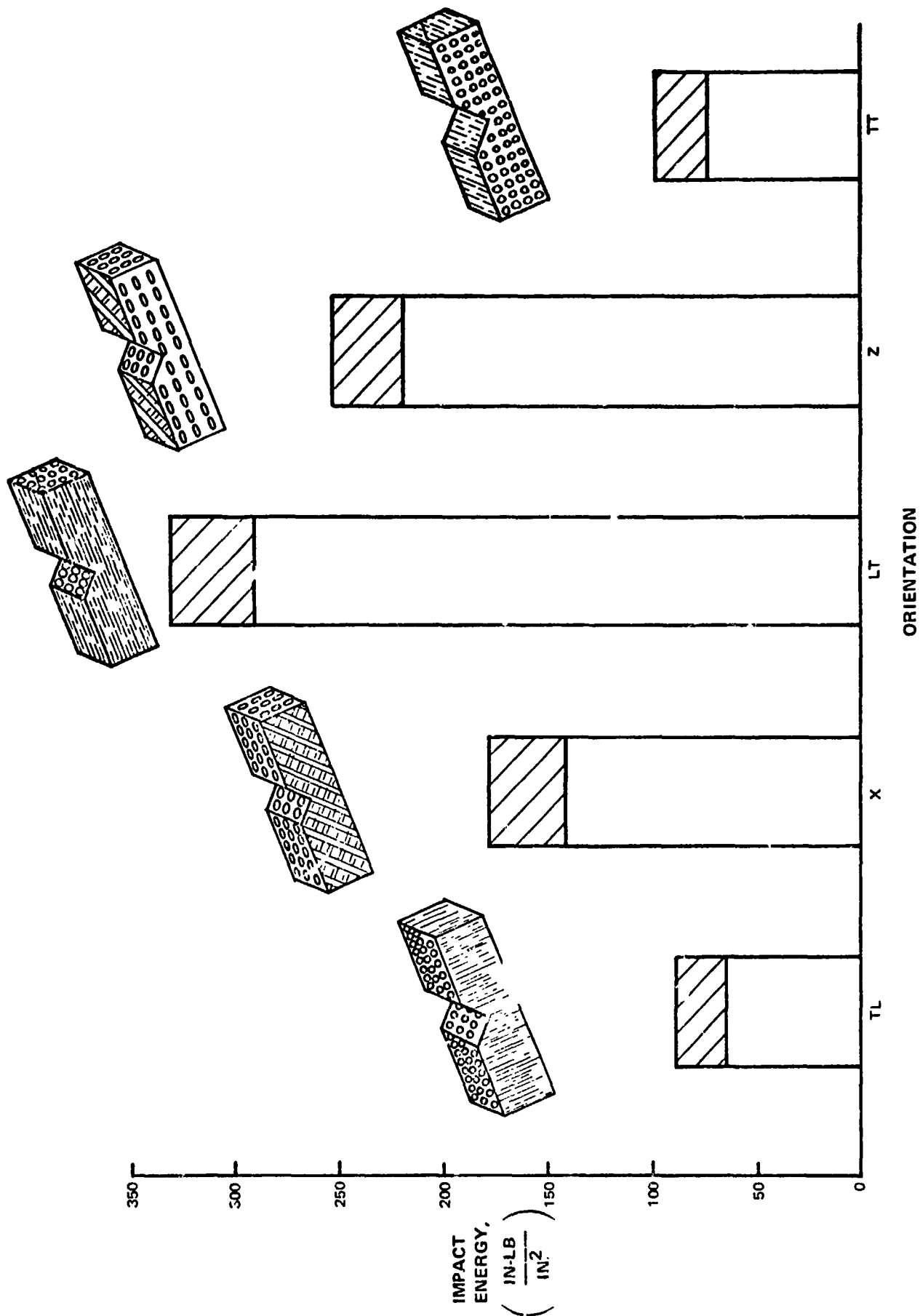


FIGURE 7-6

EFFECT OF ORIENTATION ON IMPACT ENERGY PER UNIT AREA FOR 4.2 MIL BORSIC + 6061F ALUMINUM FULL SIZE CHARPY "V" NOTCH SPECIMENS





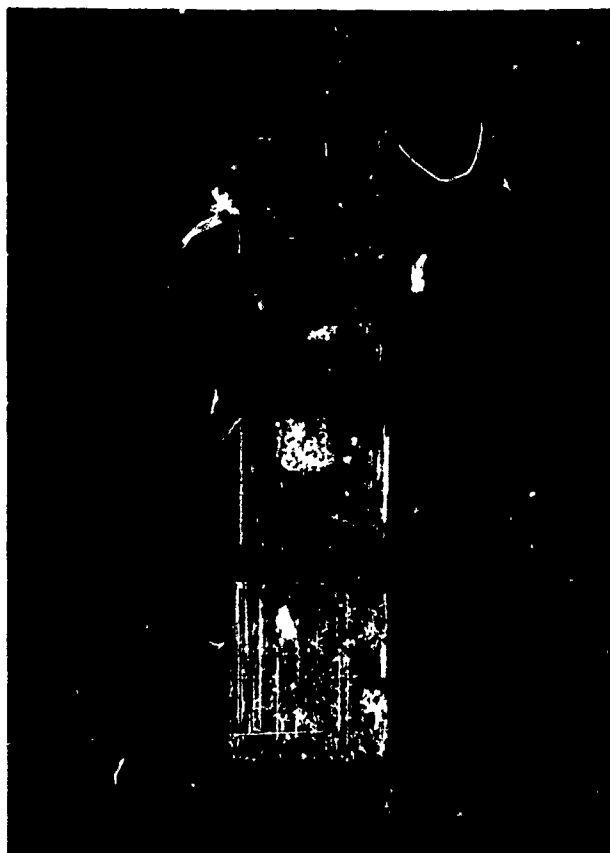
MAG: 100X

Reproduced from  
best available copy.

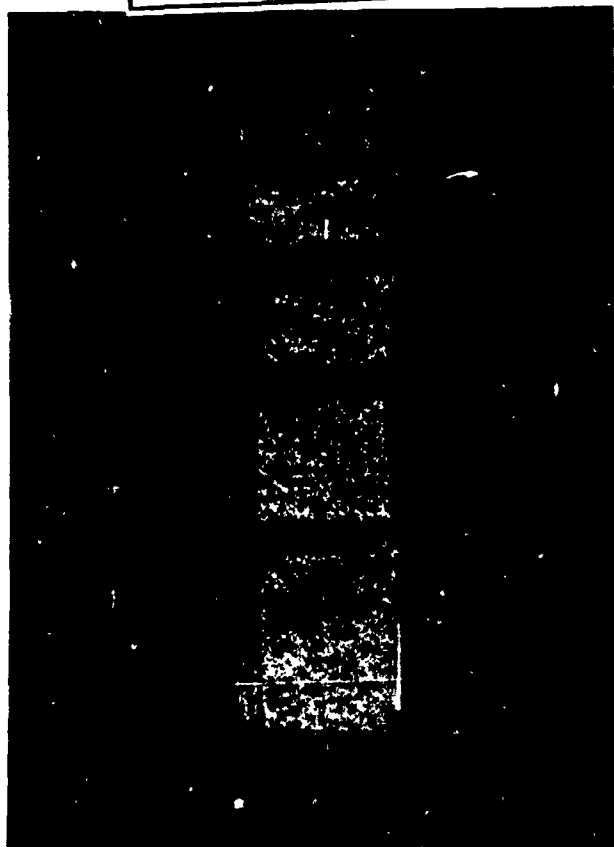


MAG: 15X

FIGURE 7-7  
SCANNING ELECTRON FRACTOGRAPH OF TYPE LT 50 v/o 4.2 MIL BORSIC®+6061-F  
ALUMINUM IMPACT SPECIMEN



Reproduced from  
best available copy.



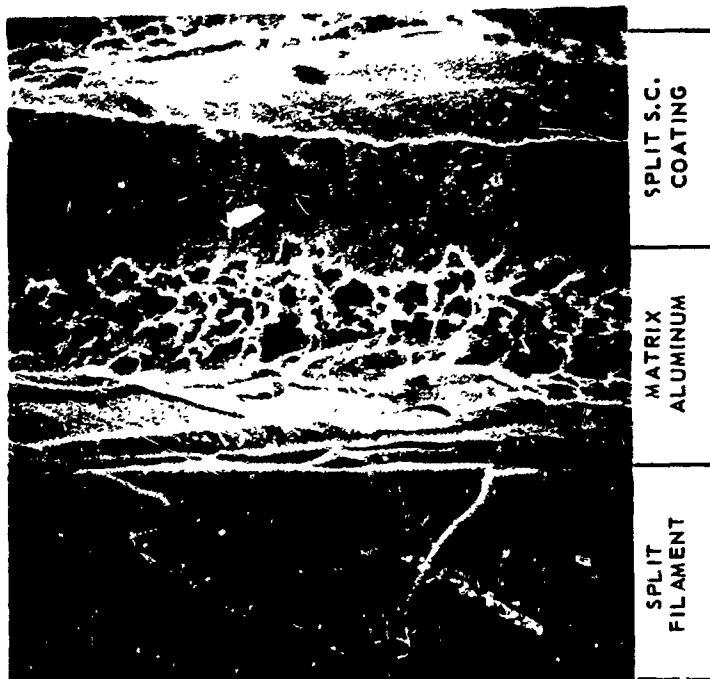
TYPE TT

MAG: 2X

TYPE LT

MAG: 2X

FIGURE 7-9  
CHARPY IMPACT FRACTURE SURFACES OF 4.2 MIL BORSIC® + 6061-F  
CONSTANT THICKNESS AND NOTCH DEPTH—VARIABLE WIDTH

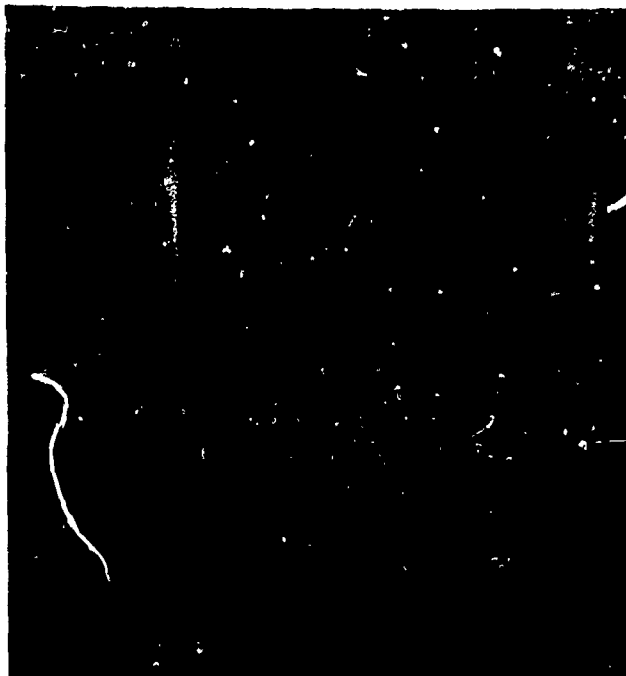


Reproduced from  
best available copy.



MAG: 15X

FIGURE 7-10  
SCANNING ELECTRON FRACTOGRAPH OF TYPE TL 5C v/o 4.2 MIL BORSIC + 6061-F  
ALUMINUM IMPACT SPECIMEN



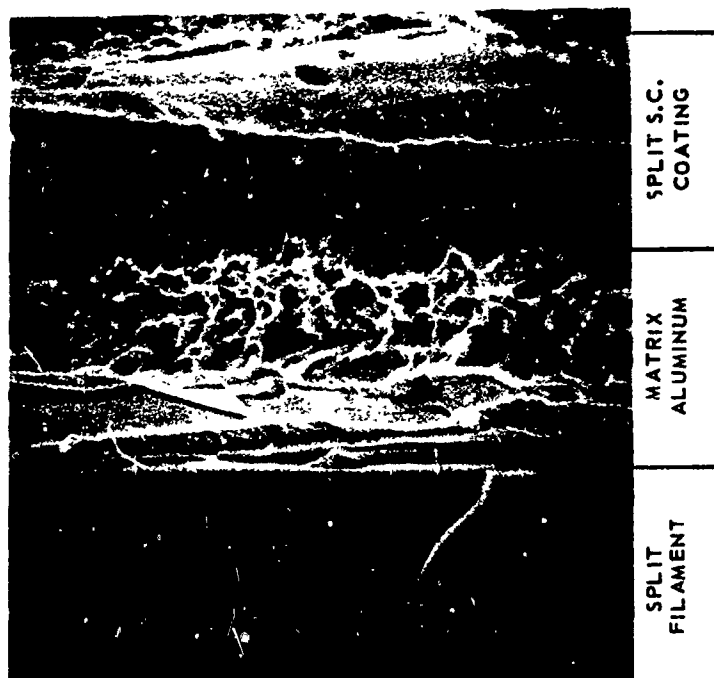
MAG: 850X

Reproduced from  
best available copy.



MAG: 15X

FIGURE 7-11  
SCANNING ELECTRON FRACTOGRAPH OF TYPE TT 50 v/o 4.2 MIL 80RSIC®  
+6061-F ALUMINUM IMPACT SPECIMEN



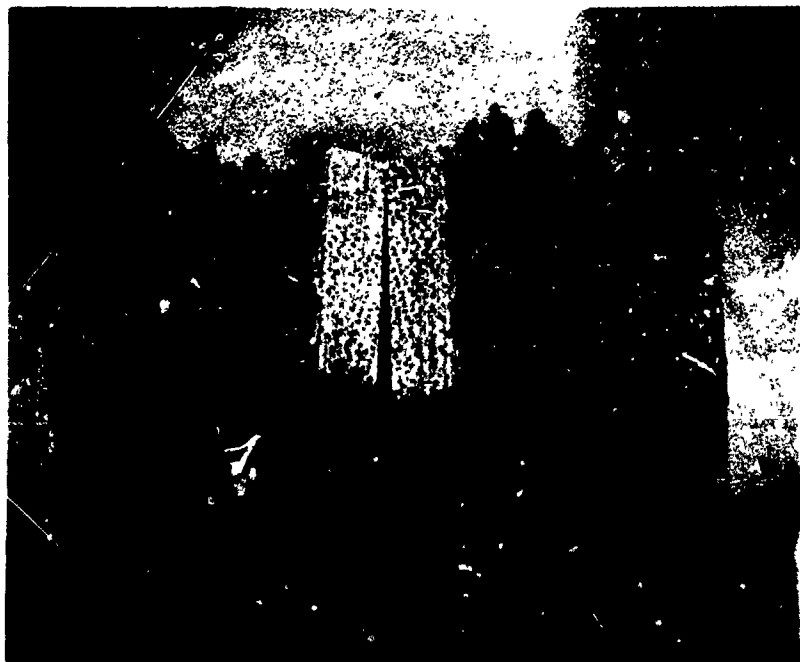
Reproduced from  
best available copy.

6



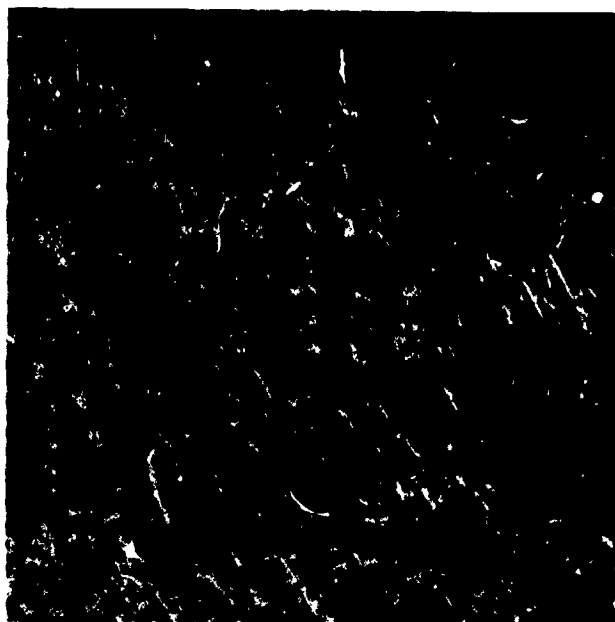
MAG: 15X

FIGURE 7-10  
SCANNING ELECTRON FRACTOGRAPH OF TYPE TL 50 V/O 4.2 MIL BORSIC + 6061-F  
ALUMINUM IMPACT SPECIMEN

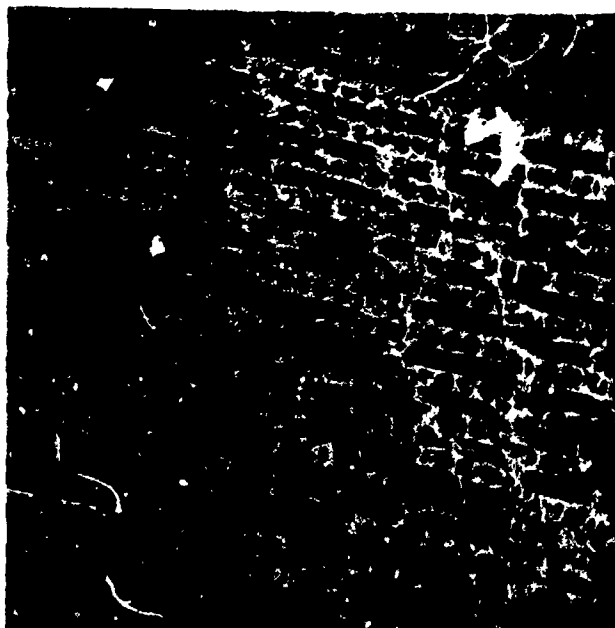


MAG: 4.5X

**FIGURE 7-12**  
**FRACTOGRAPH OF TYPE LT 63 V/O 8.0 MIL BORON + 6061-F ALUMINUM**  
**IMPACT SPECIMEN**



MAG: 20X  
TYPE X



MAG: 20X  
TYPE Z

Reproduced from  
best available copy.

FIGURE 7-13  
SCANNING ELECTRON FRACTOGRAPHS OF 50 v/o 4.2 MIL BORSIC® ±45°  
ALUMINUM ±45 DEGREE LAMINATES

K910853-12

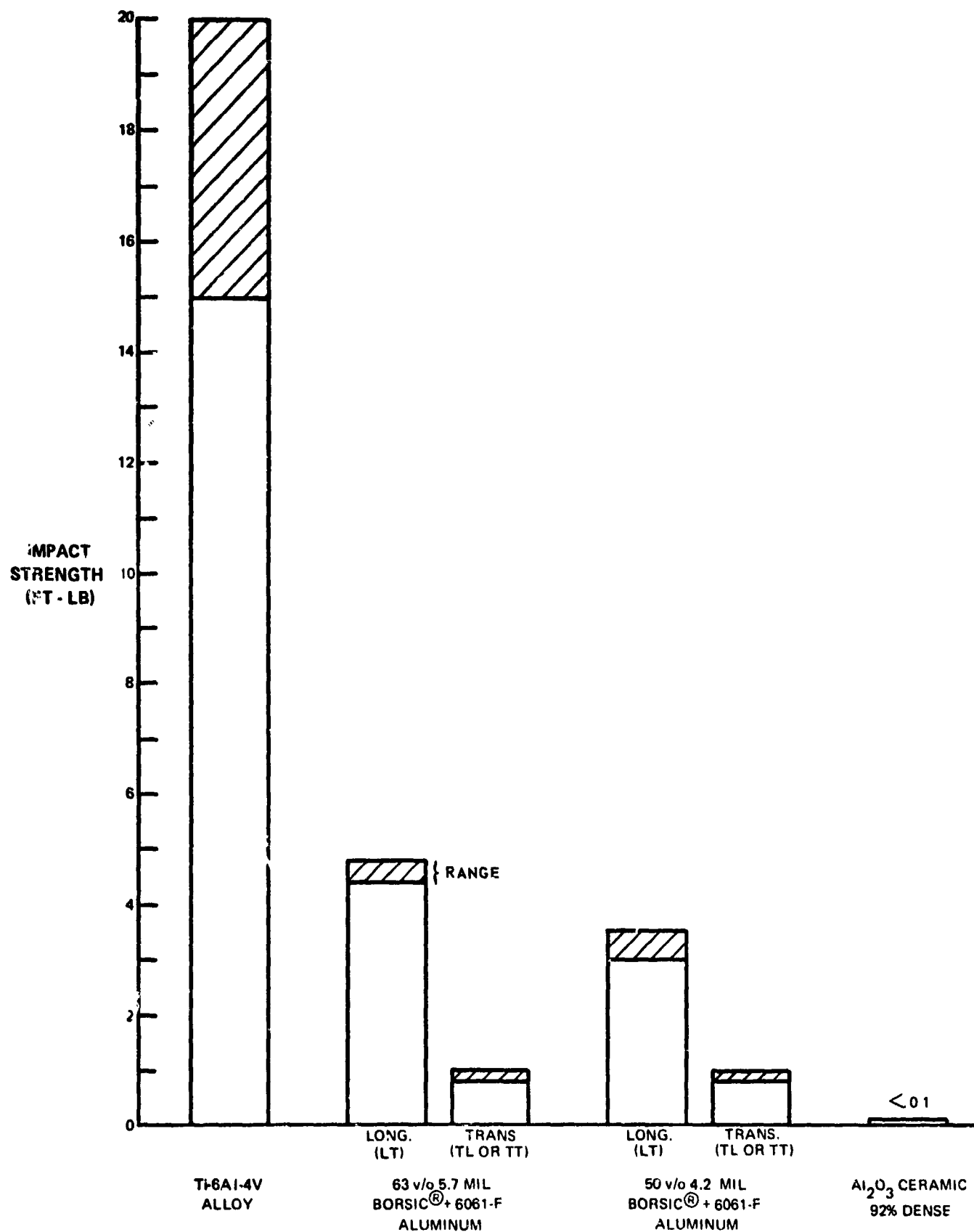


FIGURE 7-14

CHARPY IMPACT STRENGTH OF SELECTED MATERIALS



K910853-12

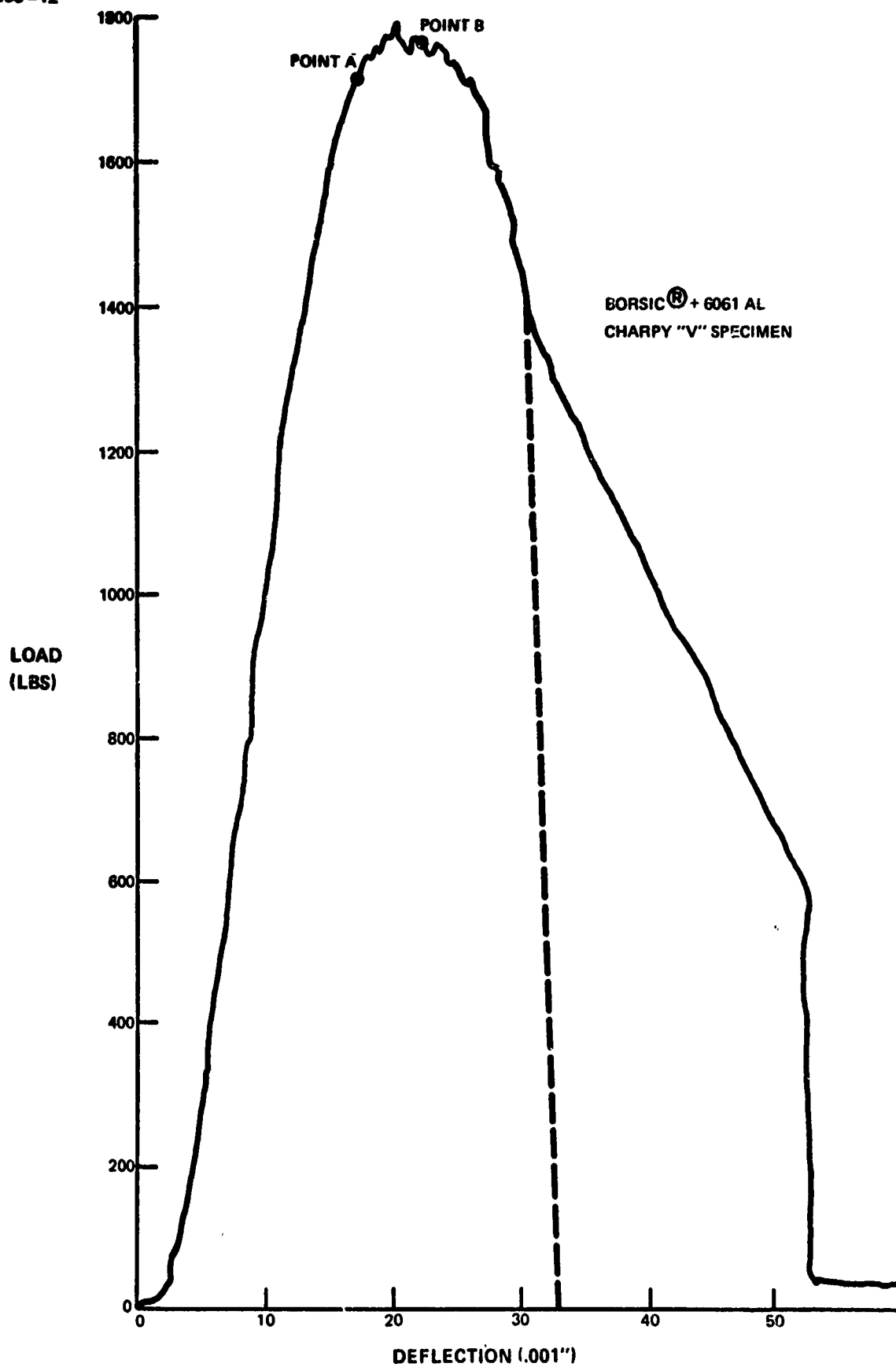


FIGURE 7-15  
TYPICAL LOAD-DEFLECTION CURVE FOR TYPE LT 4.2 MIL BORSIC® + 6061 AL SLOW BEND TEST

K910853-12

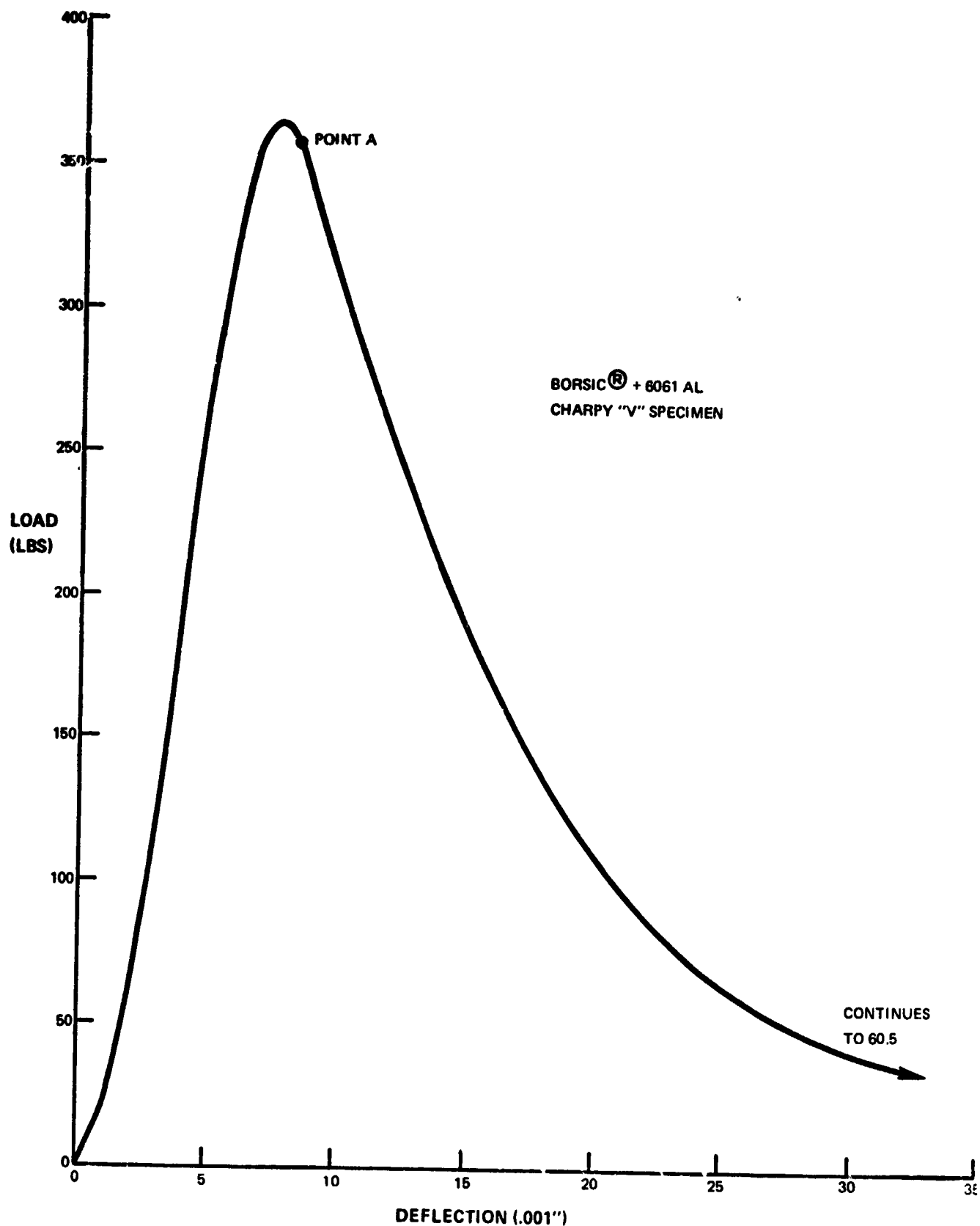
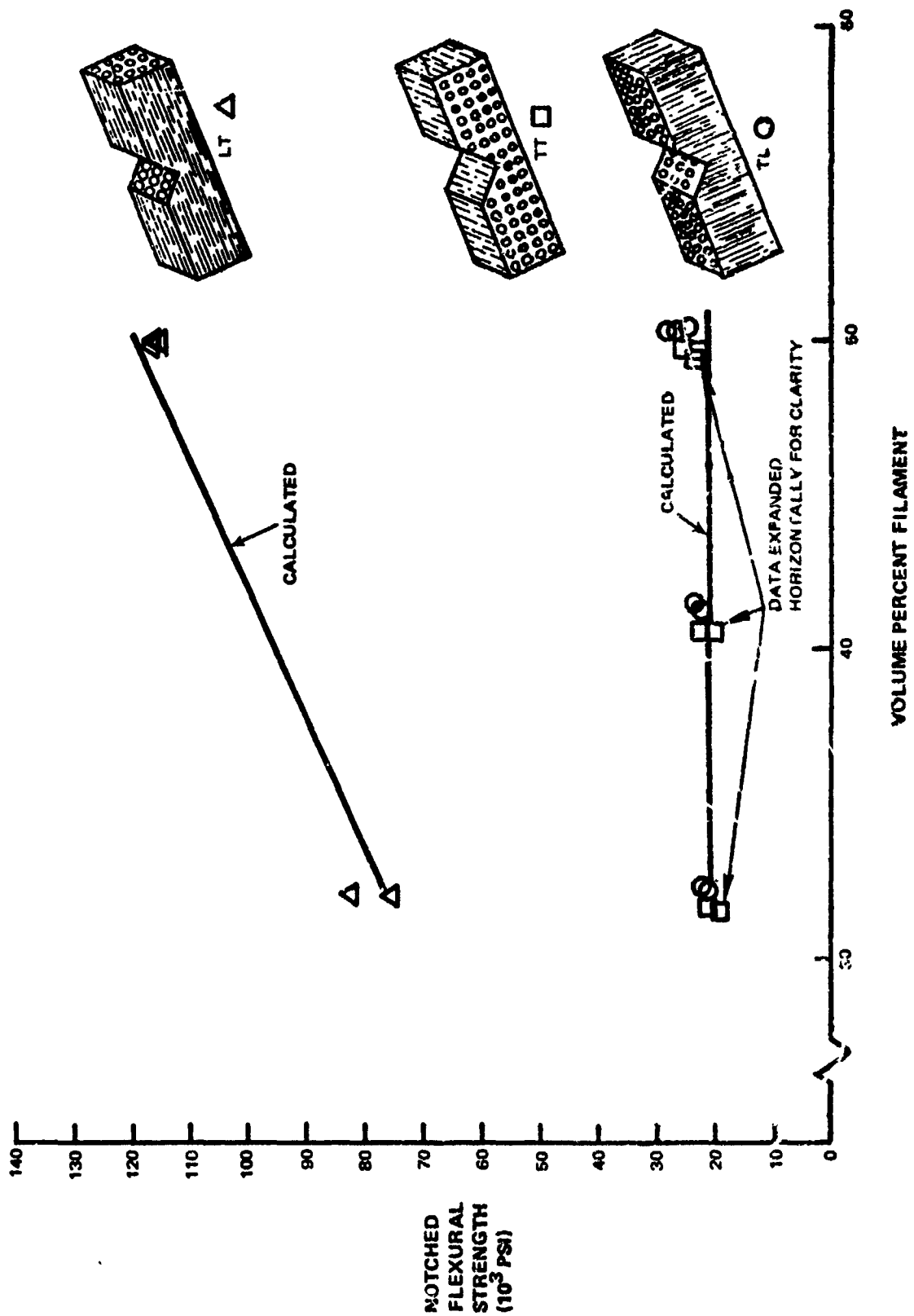


FIGURE 7-16  
TYPICAL LOAD-DEFLECTION CURVE FOR TYPE TL AND TYPE TT  
4.2 MIL BORSIC® + 6061 AL SLOW BEND TEST



VOLUME PERCENT FILAMENT

FIGURE 7-17

EFFECT OF VOLUME PERCENT FILAMENT ON THE  
NOTCHED FLEXURAL STRENGTH OF 4.2 MIL BORSIC® + 6061F ALUMINUM

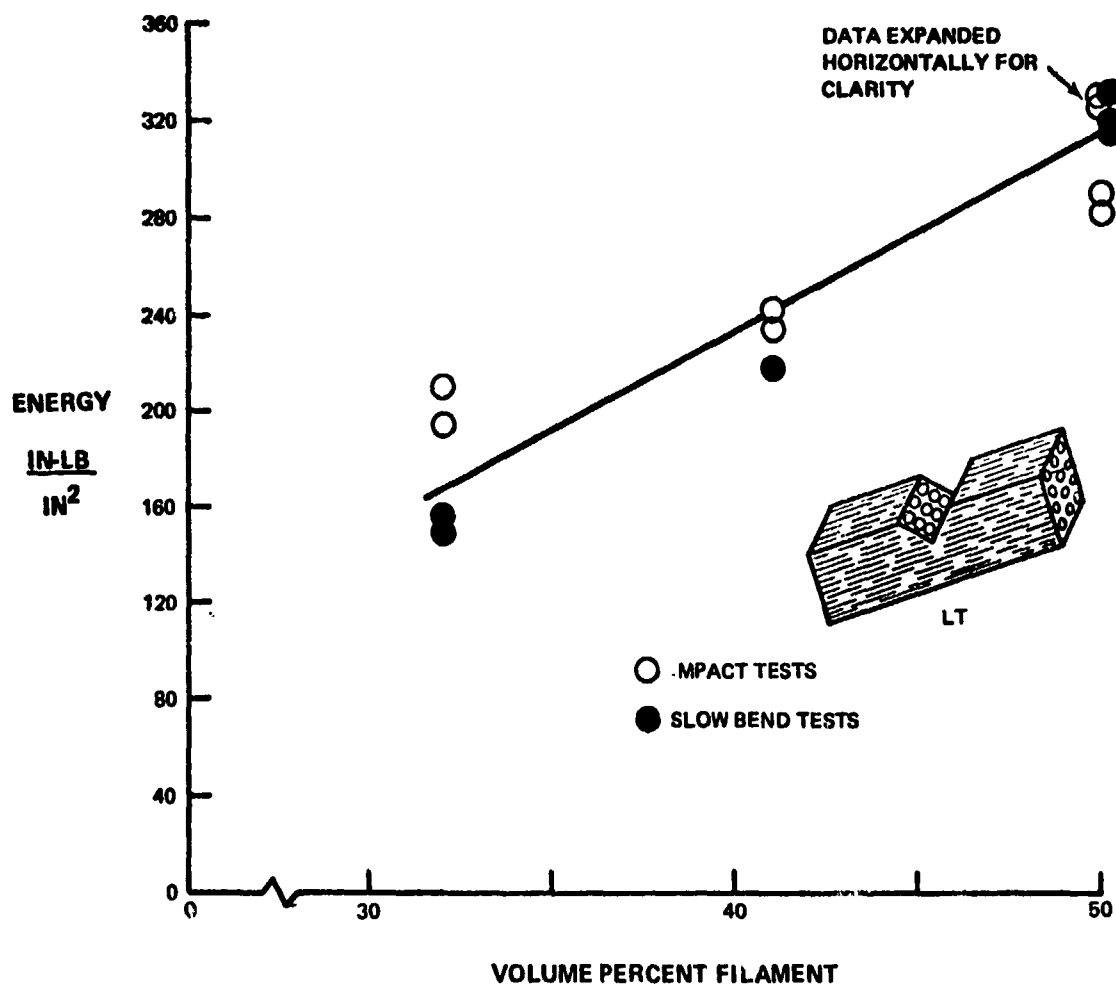


FIGURE 7-18  
VARIATION OF IMPACT AND SLOW BEND FRACTURE ENERGY WITH VOLUME PERCENT  
FIBER FOR AXIALLY REINFORCED 4.2 MIL BORSIC® + 6061F ALUMINUM COMPOSITES

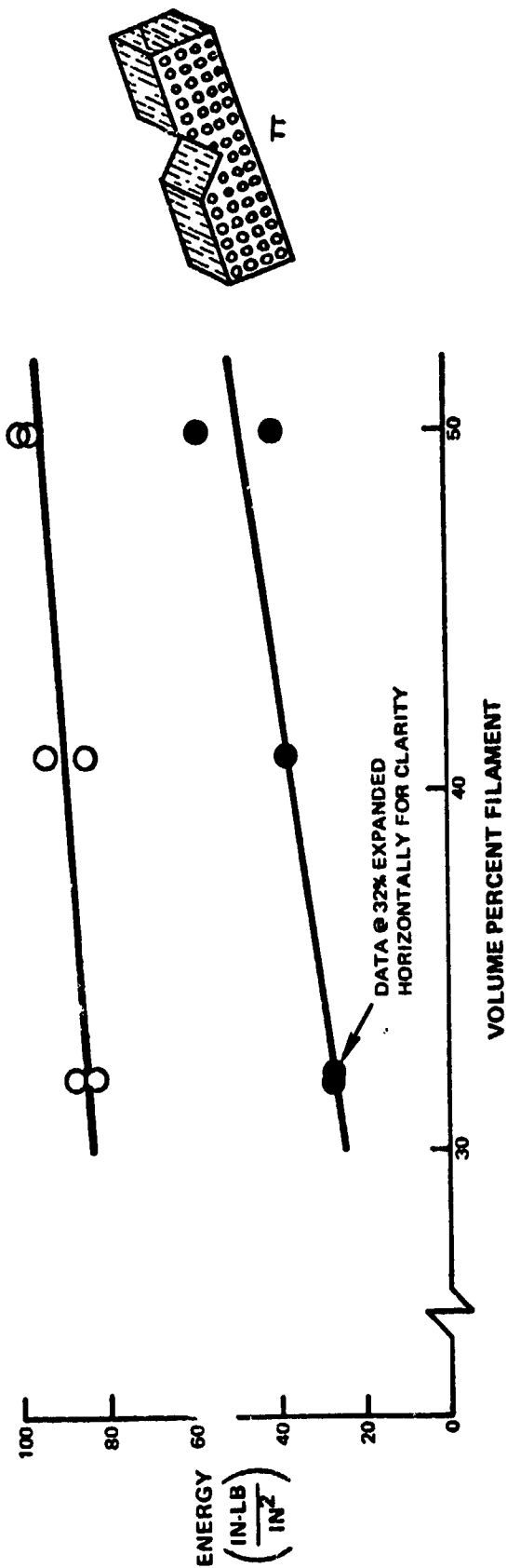
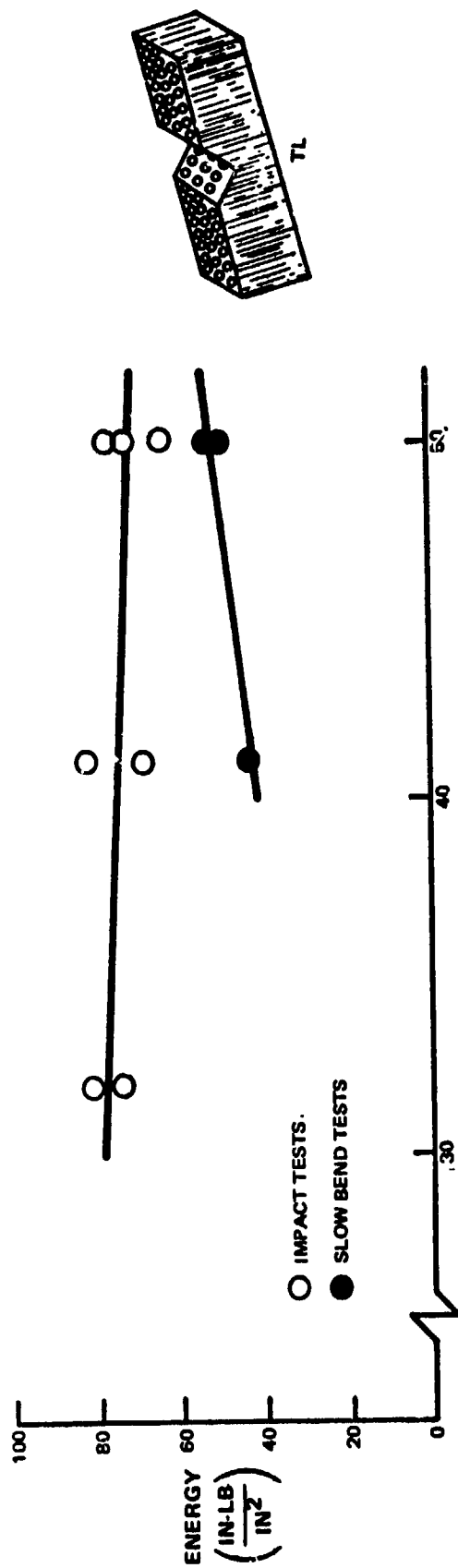


FIGURE 7-19  
VARIATION OF IMPACT AND SLOW BEND FRACTURE ENERGY WITH VOLUME PERCENT  
FIBER FOR TRANSVERSELY REINFORCED 4.2 MIL BORSIC® + 6061F ALUMINUM COMPOSITES

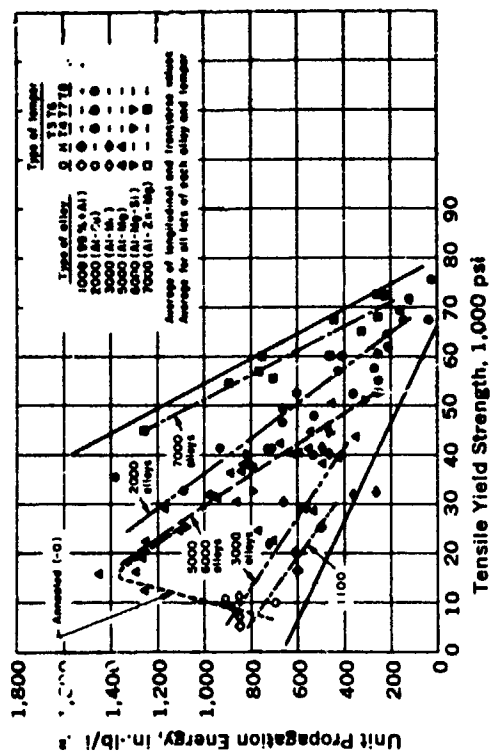
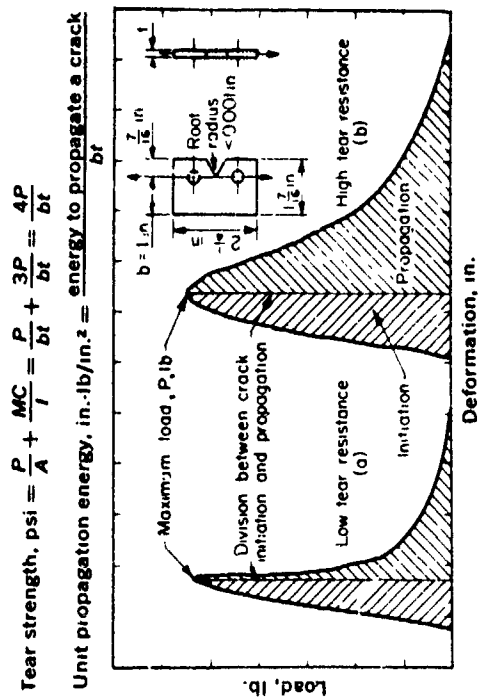
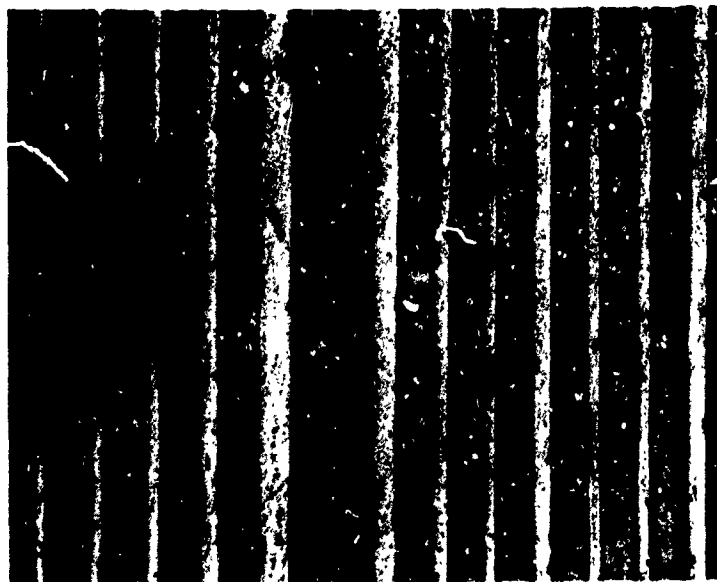


FIGURE 7-20



KAHN TEAR-TEST SPECIMENS AND REPRESENTATION OF LOAD-DEFORMATION CURVES (LEFT) AND UNIT PROPOGATION ENERGY vs. TENSILE YIELD STRENGTH OF 0.063 IN. ALUMINUM ALLOY SHEET (RIGHT) (AFTER KAUFMAN AND HOLT)

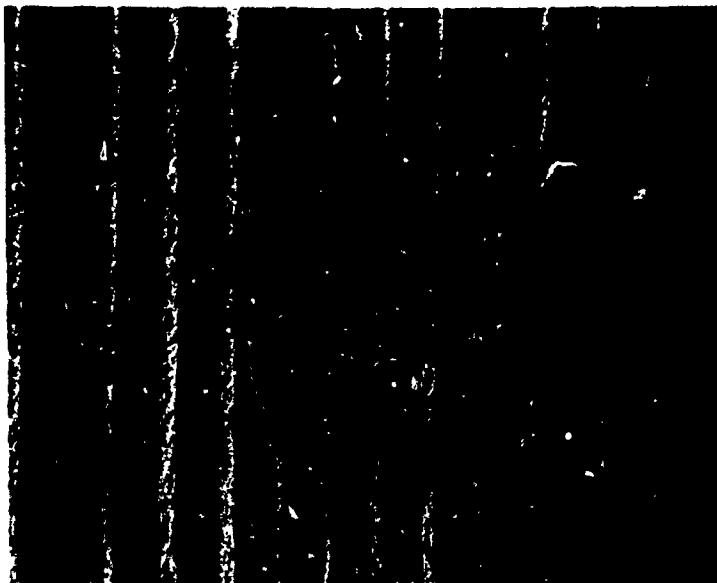


NOTCH ROOT

Reproduced from  
best available copy.



MID-THICKNESS  
UNDER NOTCH

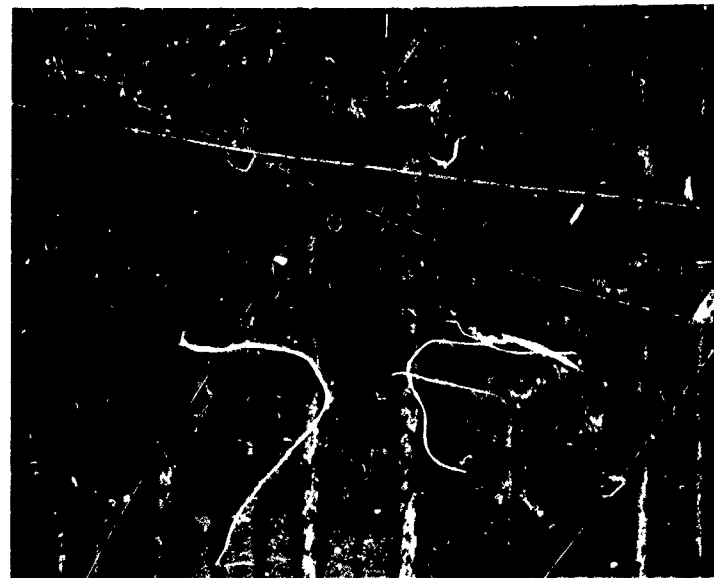


REGION UNDER  
LOADING NOSE

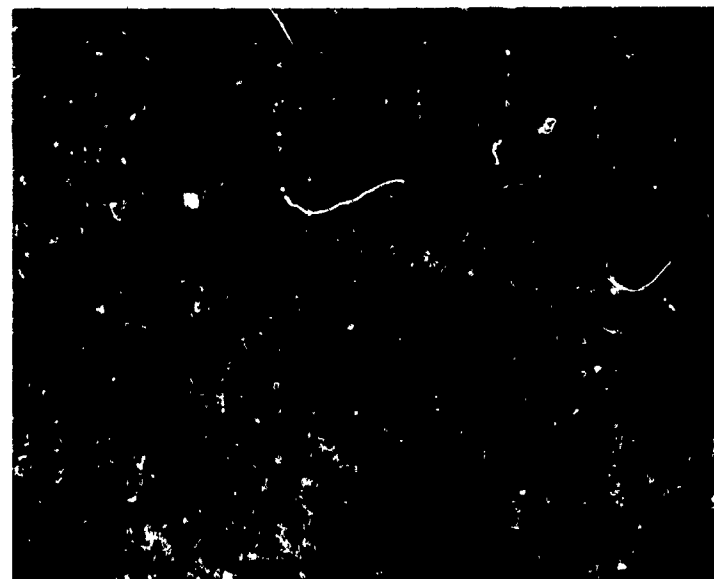
MAG 50 X

FIGURE 7-21

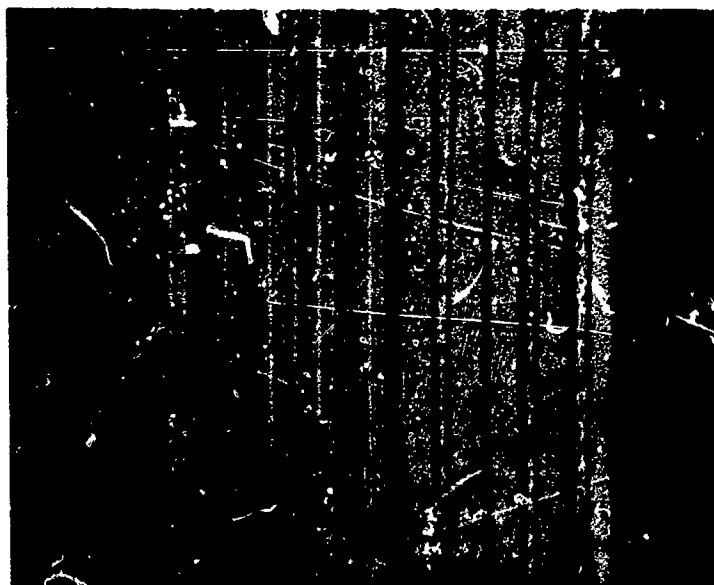
PHOTOMICROGRAPHS OF INTERRUPTED THREE POINT BEND TEST OF TYPE LT 41 v/o  
4.2 MIL 80 RSIC® + 6061-F ALUMINUM .  
(SPECIMEN POLISHED PRIOR TO TEST AND LOADED TO POINT A IN FIGURE 7-15)



NOTCH ROOT



MID-THICKNESS UNDER NOTCH



REGION UNDER LOADING NOSE

MAG 50X

FIGURE 7-22  
PHOTOMICROGRAPHS OF INTERRUPTED THREE POINT BEND TEST OF TYPE LT 50 v/o 4.2 MIL  
BORSIC® + 6061-F ALUMINUM. (SPECIMEN POLISHED PRIOR TO TEST AND LOADED  
TO POINT B IN FIGURE 7-15)





MAG: 250X

Reproduced from  
best available copy.



MAG: 50X

FIGURE 7-23  
PHOTOMICROGRAPHS OF INTERRUPTED THREE POINT BEND TEST OF TYPE TL 41 v/o 4.2 MIL  
BORSIC® + 6061-F ALUMINUM (SPECIMEN POLISHED PRIOR TO TEST AND LOADED  
TO POINT A IN FIGURE 7-16 )



MAG: 250X

Reproduced from  
best available copy.



MAG: 50X

FIGURE 7-24  
PHOTOMICROGRAPHS OF INTERRUPTED THREE POINT BEND TEST OF TYPE TT 50 v/s 4.2 MIL  
BORSIC® + 6061-F ALUMINUM (SPECIMEN POLISHED PRIOR TO TEST AND LOADED  
TO POINT A IN FIGURE 7-16)

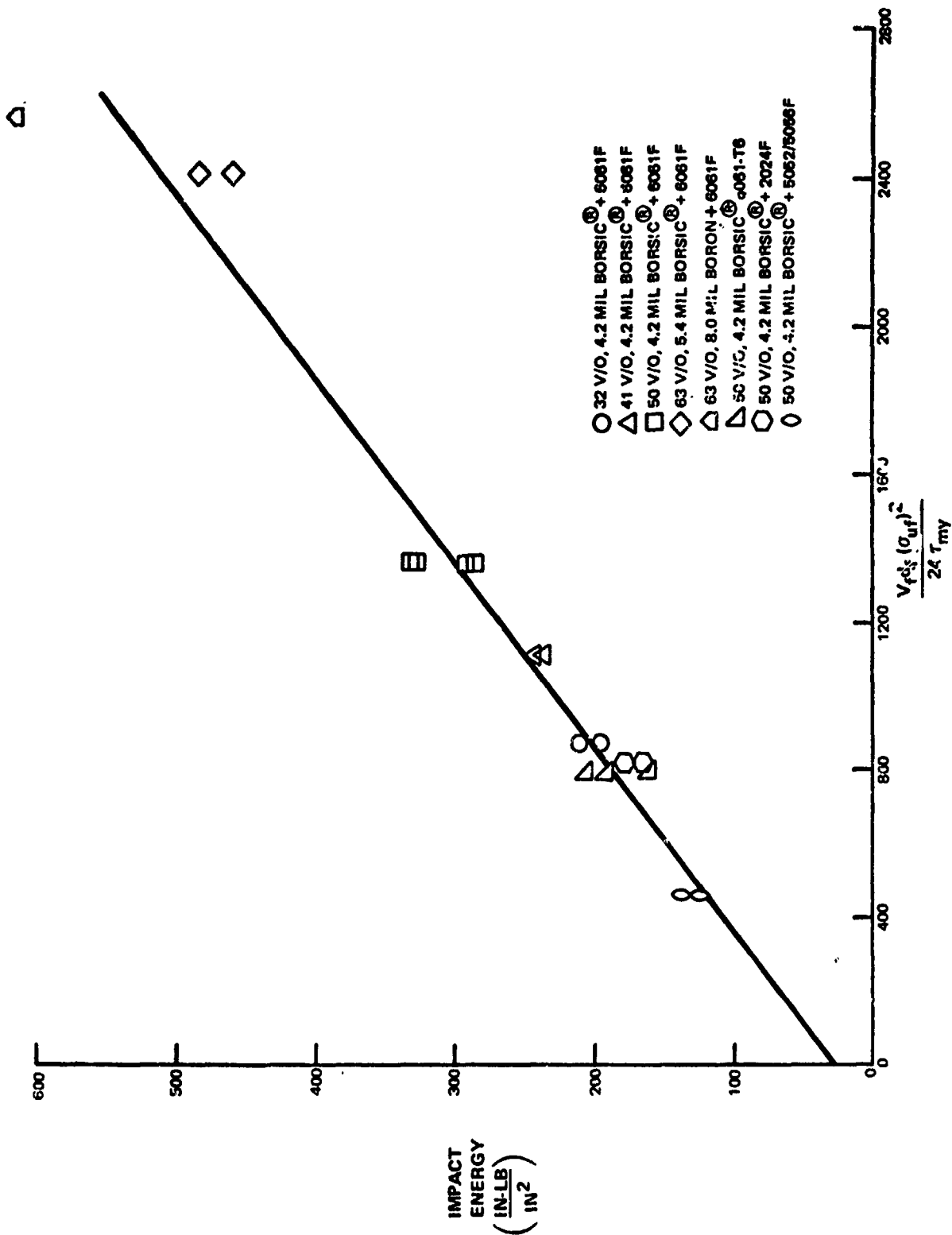


FIGURE 7-25  
VARIATION OF IMPACT ENERGY PER UNIT AREA WITH THE PARAMETER  $\frac{V_f d_t (\sigma_{uf})^2}{24 \tau_{my}}$  FOR BORSIC<sup>®</sup> + ALUMINUM AND BORON + ALUMINUM COMPOSITES

Table VII-I

Impact Energy Per Unit Area for Plasma Sprayed  
BORSIC + Aluminum Composites

(Full size Charpy "V" notch specimens)\*

<u>Matrix Alloy</u>	<u>Fiber</u>	<u>Nominal Fiber v/o</u>	<u>Orientation/Energy (in.-lb/in.<sup>2</sup>)</u>				
			<u>TL</u>	<u>X</u>	<u>LT</u>	<u>Z</u>	<u>TT</u>
6061-F	4.2 mil BORSIC	32	81.9		195		88.3
			<u>74.8</u>		<u>211</u>		<u>84.3</u>
			<u>78.3</u>		<u>203</u>		<u>86.3</u>
	4.2 mil BORSIC	41	68.8		236		94.9
			<u>83.3</u>		<u>213</u>		<u>75.2</u>
			<u>76.1</u>		<u>240</u>		<u>85.1</u>
	4.2 mil BORSIC	50			284		73.0
			73.2	141	292	219	99.3
			65.1	143	327	219	97.9
			<u>76.9</u>	<u>179</u>	<u>332</u>	<u>253</u>	<u>89.1</u>
			<u>71.4</u>	<u>154</u>	<u>309</u>	<u>230</u>	<u>89.8</u>
	5.7 mil BORSIC	63			460		
			73.6		<u>483</u>		86.9
					<u>471</u>		
	3.0 mil Boron	63			615		
6061-T6	4.2 mil BORSIC	50	39.7		160		36.7
			28.1		192		32.4
			<u>38.6</u>		<u>206</u>		<u>32.6</u>
			<u>35.5</u>		<u>186</u>		<u>33.9</u>
2024-F	4.2 mil BORSIC	50	28.5		180		40.6
			<u>35.5</u>		<u>166</u>		<u>28.8</u>
			<u>32.0</u>		<u>173</u>		<u>34.7</u>
5052 foil/ 5056	4.2 mil BORSIC	50			124		
					<u>138</u>		
					<u>131</u>		

\*Specimen width is .395 ± .003 in.; specimen thickness is .395 ± .003 in.

Table VII-II

Impact Energy per Unit Area for Nominal 50 v/o 4.2 Mil  
BORSIC Fiber + Aluminum

(Sub-size Charpy "V" notch specimens, constant notch depth)

<u>Matrix Alloy</u>	<u>Orientation</u>	<u>Width (in.)</u>	<u>Thickness (in.)</u>	<u>Energy (in.-lb/in.<sup>2</sup>)</u>
6061-F (plasma sprayed)	LT	.275	.376	307
		.194	.375	330
		.144	.377	310
		.094	.370	315
		.094	.370	300
		.094	.369	<u>287</u>
				301
		.375	.289	226
		.371	.245	178
		.377	.195	176
		.375	.146	154
		.370	.124	83.1
	TT	.295	.374	99.8
		.196	.374	55.2
		.147	.375	46.0
		.096	.371	42.7
		.095	.372	<u>46.0</u>
				44.0
6061-F (foil)	TL	.316	.395	79.6
		.321	.394	62.5
		.318	.395	<u>71.3</u>
				71.1
	LT	.317	.392	215
		.317	.395	181
		.317	.393	<u>178</u>
				198

Table VII-II (Cont'd)

<u>Matrix Alloy</u>	<u>Orientation</u>	<u>Width (in.)</u>	<u>Thickness (in.)</u>	<u>Energy (in.-lb/in.<sup>2</sup>)</u>
6061-F (foil)	TT	.394	.318	78.1
		.394	.320	69.1
		.391	.319	<u>85.1</u> 77.1
2024-F (foil)	TL	.316	.396	56.4
		.316	.393	52.7
		.315	.392	<u>53.4</u> 54.2
	LT	.314	.393	160
		.318	.396	143
		.315	.395	<u>144</u> 149
	TT	.393	.316	59.5
		.392	.317	80.0
		.390	.317	<u>76.3</u> 71.9

Table VII-III

Slow Bend Fracture Work for Type LT  
BORSIC + 6061-F Specimens

<u>v/o Fiber</u>	<u>Total Energy</u> <u>(in.-lb/in.<sup>2</sup>)</u>	<u>Elastic Energy</u>		
		<u>Estimated</u> <u><math>\sigma_{2L}/18E</math></u> <u>(in.-lb/in.<sup>2</sup>)</u>	<u>Measured</u> <u>(in.-lb/in.<sup>2</sup>)</u>	<u><math>\sigma_{2L}/25E</math></u> <u>(in.-lb/in.<sup>2</sup>)</u>
50	318	131	92	94
	322	131	102	94
41	218	101	75	73
32	157	70	52	50
	149	70	45	50

Table VII-IV

## Strength of Filaments in Impact Specimens

<u>Material</u>	<u>Fiber</u>	<u>Average Tensile UTS (10<sup>3</sup> psi)</u>	<u>Fiber Strength (10<sup>3</sup> psi)</u>
4.2 mil BORSIC + 6061-F <sup>(1)</sup> (Ref.)	50	160	320
	41	131	320
	32	102	<u>319</u>
			Ave. 320
5.7 mil BORSIC + 6061-T6 <sup>(2)</sup>	61	206 <sup>(3)</sup>	338
	63	205 <sup>(4)</sup>	<u>325</u>
			Ave. 331
8.0 mil boron + 6061-F (Ref.)	50	140	<u>280</u>
			Ave. 280

(1) Actual fiber diameter is  $4.1 \times 10^{-3}$  in.

(2) Actual fiber diameter is  $5.4 \times 10^{-3}$  in.

(3) Results of environmental investigation, Section III

(4) Results of off-axis investigation, Section V



## NOTCH TENSILE FRACTURE

### SUMMARY

BORSIC aluminum and BORSIC titanium center notched specimens were evaluated in uniaxial tension. The fracture strength of longitudinally reinforced 50 v/o 4.2 mil BORSIC + 6061-F and 50 v/o 4.2 mil BORSIC + 2024-F was empirically found to be given by the following expressions:

$$\sigma_{\text{gross}} = 52 (2c)^{-0.27} \text{ ksi} \quad 2c > 0.025$$

$$\sigma_{\text{net}} = \sigma_{\text{UTS}} \quad 2c < 0.025$$

where  $2c$  = crack length

$$\sigma_{\text{gross}} = (1 - 2c/w) \sigma_{\text{net}} \quad (w = 2 \text{ in.})$$

Notched BORSIC + aluminum was found to exhibit significant longitudinal matrix shear prior to fracture which causes notch blunting. These composites have a propensity for longitudinal shear fracture which reduces the notch sensitivity.

The behavior of notched longitudinally reinforced 50 v/o 4.2 mil BORSIC + Beta III titanium is similar to that of 4.2 mil BORSIC + aluminum. Longitudinal splits were not observed with this material.

The net fracture strengths of transversely reinforced 50 v/o 4.2 mil BORSIC + 6061-F and 63 v/o 5.7 mil BORSIC + 6061-F were found to be equal on a net section area basis to that of unnotched material. The transverse net strength of the 4.2 mil BORSIC material is governed by the transverse strength of the fibers.

## VIII. NOTCH TENSILE FRACTURE

The overall goals of this investigation are to determine whether the fracture of BORSIC + aluminum can be successfully treated within the framework of existing linear elastic fracture mechanics, to assess the significance of fracture work, to examine the mechanisms of fracture, and to study the effect of constituent properties and composite geometry on material behavior. An understanding of these factors is needed to facilitate future material property improvements as well as to provide confidence in material applications.

The method of approach used was to determine the response of flawed unidirectional composite material to symmetric uniaxial loading in a direction normal to the flaw orientation. Center-notched specimens, measuring 6 in. overall and 2 in. wide, containing initial flaw sizes ranging from 0.02 in. to 0.80 in. were used. This particular specimen was initially chosen in order to obtain the analytical simplicity of the center notch geometry at a sufficient width so that finite width corrections might be ignored in a first order analysis. Loading was accomplished through 1 in. compliant doublers (rather than pinholes) in a manner similar to current composite material tensile testing practice, Fig. 8.1. An alignment fixture was employed to ensure proper positioning of the specimens. Strain gage measurements on smooth specimens indicated that the maximum strain disparity across the specimen and between opposite faces was less than one percent.

The bulk of this work was performed using 50 v/o 4.2 mil BORSIC + 6061-F material. Three specimen thicknesses (nominal 0.050 in., 0.100 in., and 0.150 in.) and two types of notch geometry (center notch and center circular hole) were examined. In addition, a limited number of tests were performed with center-notched 4.2 mil BORSIC + 2024-F, 4.2 mil BORSIC + 6061-T6, 4.2 mil BORSIC + 2024-T6, 5.7 mil BORSIC + 6061-F, 4.2 mil BORSIC + Beta III titanium, and HMG-50 graphite + BP-907 epoxy.

Notches were usually introduced into the BORSIC + aluminum and BORSIC + titanium samples by first electrodischarge machining (EDM) slots perpendicular to the specimen edge and then extending them using 0.005 in. diameter diamond coated rocket wire. However, the flaws in a number of specimens were prepared with tip radii of 0.004 in. entirely by EDM techniques. No differences in response were observed between the two populations. The notches in the graphite + epoxy material were introduced by drilling 0.010 in. diameter holes in the center of the specimens and extending them with the 0.005 in. diameter abrasive wire.

### 8.1 Longitudinal Reinforcement

In these series of experiments, the filaments were parallel to the load axis and normal to the flaw. Fiber alignment was within  $0^{\circ}30'$  as determined by X-ray radiographic techniques. Test results are listed in Tables VIII-I, II, III, IV, V and discussed in greater detail in the following sections.

### 8.1.1 BORSIC + Aluminum Composites

#### Fracture Strength

The effect of flaw length on the net fracture strength of 50 v/o 4.2 mil BORSIC composites with 6061-F (17 tests) and 2024-F (10 tests) matrix materials is given in Fig. 8.2. The dependence is characterized by three regions:

1. Region I: The fracture strength of specimens with very short flaws (less than 0.025 to 0.030 in.) is much like the ultimate tensile strength of unnotched material. Notch weakening is not observed.

2. Region II: Net fracture strength decreases with increased flaw size up to flaw lengths of approximately 0.3 in.

3. Region III: Notch strength remains nearly constant at approximately 85 ksi for flaw lengths greater than 0.3 in. This represents a notched to unnotched strength ratio of approximately 0.53. At flaw length: greater than 0.6 in. ( $2c/W > 0.3$ ) net fracture stress appears to increase, probably as a result of finite width effects.

The fracture strengths of the 2024-F matrix and 6061-F matrix composites are nearly equal. A similar result was observed with regard to the maximum load carrying capability of the notched bend tests. These observations contrast sharply with the results of the impact and slow bend tests in which the fracture energies measured in the BORSIC/6061-F system were approximately twice those demonstrated by the BORSIC/2024-F material. Thus, energy measured in impact tests is not simply related to composite static strength in the presence of a flaw.

The gross fracture strength of 4.2 mil BORSIC + 6061-F and 4.2 mil BORSIC + 2024-F is well represented by a straight line on log-log coordinates. Net fracture strength,  $\sigma_G$ , and net fracture stress are related by crack length,  $2c$ , and specimen width,  $w$ , by the relationship:

$$\sigma_G = (1-2c/w) \sigma_N \quad (8.1)$$

Since  $w$  equals 2 in. for the bulk of these tests, gross and net stress are within 5% for  $2c \leq 0.1$ . A computerized least squares analysis of the data established that one could write with 99.9% confidence:

$$\sigma_G = 52.0 (2c)^{-0.27} \text{ ksi} \quad (8.2)$$

$$0.80 > 2c > .025$$

$$\sigma_N = \sigma_{UTS} \quad (8.3)$$

$$2c < 0.025$$

The fracture strengths of 6061-F matrix composites in 0.100 in. and 0.150 in. thicknesses are nearly equal to those at 0.050 in. No effects of thickness due to either changes in constraint or variations in material properties were observed, Fig. 8.3.

The net fracture strength of 4.2 mil BORSIC + 6061-F containing 0.125 in. radius circular holes is given in Fig. 8.4 (3 tests). These specimens failed at 102 ksi to 106 ksi. These results are nearly 25% higher than the average strength exhibited in the presence of center slots (0.0023 in. tip radius) but fall within the overall strength band. The results of Adsit and Witzell (Ref. 8.12) for 0.070 in. diameter holes appear to be consistent with the present determinations.

This relative insensitivity of fracture strength to notch tip radius was further examined using two specimens with tip radii of 0.005 in. In Table VIII-VI the test results from these specimens are compared with those from the 0.0023 in. radius samples used in the bulk of this work. Fracture strengths with the more blunt flaws are actually slightly lower than those measured with 0.0023 in. radius flaws of the same length. However, this difference is not significant compared to the range of strengths measured in all tests.

This insensitivity of fracture strength to crack tip radius and to flaw size above 0.3 in. indicates that matrix yielding occurs at the crack tip. This behavior would be expected on the basis of the low yield strength of 6061-F material (11.2 ksi). In addition, the observed ratio of notched to unnotched strength (approximately 0.5) is much higher than would be expected on the basis of theoretical elastic stress concentration factors if plastic effects did not occur. (For example, the  $K_t$  of an 0.3 in. flaw with 0.0023 in. tip radius is approximately 28; this effect will be discussed later in greater detail.)

Test results with center-notched 4.2 mil BORSIC + 6061-T6, 4.2 mil BORSIC + 2024-T6, and 5.7 mil BORSIC + 6061-F composites suggest a similar dependence of strength on flaw size as with 4.2 mil BORSIC + 6061-F material, Fig. 8.5. These composites exhibit higher notched strengths, which may largely reflect their higher tensile strengths. A notched to unnotched strength ratio of 0.5 to 0.6 is observed in the presence of large flaws, which is also similar to that of 4.2 mil BORSIC + 6061-F material. To a confidence of 90% the strength for 5.7 mil BORSIC + 6061-F is given by:

$$\sigma_G = 87.3 (2c)^{-0.16} \quad 2c < 0.17$$

#### Load-Deflection Response

Continuous records of applied load versus the displacement of gage points located on opposite sides of the flaws were obtained for several specimens of 4.2 mil BORSIC + 6061-F aluminum composite material. These load-displacement curves exhibit three stages: an elastic range, followed by a large smooth nonlinear range, and finally a region with extensive fluctuations, Fig. 8.6.

To investigate whether the fluctuations or "pop-ins" reflected slow crack growth, one composite specimen test was interrupted prior to failure at a point on the load-displacement curve subsequent to initiation of the

irregularities. Based on the fracture stresses exhibited by specimens tested to failure, the load level at the point of test interruption was approximately 90% of the ultimate capacity. There were no cracks on the specimen surface either colinear with the original flaw or in the longitudinal direction. (None had been observed during visual observations, using a cathetometer, of over thirty tests.) The matrix material around the crack was then dissolved with acid in order to observe filament condition. Many fibers in the first layer ahead of the crack tip were broken; however, other fibers were undamaged. These results were confirmed in a series of experiments using X-ray radiography, as discussed in Section VI. Thus, despite the extensive amount of nonlinear behavior, the crack only grew approximately 0.005 in. at each tip. It appears that the crack opening displacement (COD) in B + Al is not directly proportional to the amount of crack extension, at least in the direction colinear with the original flaw. Significant shear deformation occurs in the specimens on planes parallel to the filaments near the flaw tip. Specimen compliance then increases without crack extension.

Several 4.2 mil BORSIC + 6061-F specimens were loaded that had been sprayed with stresscoat. A typical crack pattern appears in Fig. 8.7. The cracking behavior is determined by the magnitudes of the principal stresses in the coating. These cracks form perpendicular to the greatest principal stress, parallel to the smaller principal stress, and represent stress trajectories or isostatics (Ref. 8.13). In addition, the crack density is proportional to the stress level.

Several observations can be drawn from Fig. 8.7.

1. The highest stress in the sample occurs at the notch tip. The specimen edge also appears to be a region of significant stress concentration, perhaps as a result of flaws introduced during machining.
2. The curvature of the cracks suggests that significant stress concentration ahead of the flaw persists to distances of approximately 0.050 to 0.070 in.
3. The shielded zones above and below the flaw appear more elliptical or elongated in the longitudinal direction compared with those in isotropic materials.
4. The difference in crack density above and below the flaw in regions far removed from the flaw suggests there was a small amount of axial grip misalignment during this particular test.

#### Fractography

The fracture path exhibited by the BORSIC + aluminum systems, though extremely irregular, tended to be approximately coplanar with the original flaw. The heat treated sample fractures were more planar than those of as-fabricated material, perhaps as a result of shorter critical load transfer lengths. In addition to the main fracture surface, every specimen that was

evaluated displayed longitudinal splits. These splits originated at points behind the flaw tip, often at the point of changing crack height of the EDM slot. Visual examinations revealed that the topography of the main fracture surface was similar to that exhibited by longitudinal tensile specimens. Fracture surface features of regions directly ahead of the machined flaw did not appear different from those of areas nearer the specimen edge, Fig. 8.8.

A side view of a fractured 4.2 mil BORSIC + 2024-F specimen and an X-ray radiograph of a region near the tip of the original flaw in another specimen of the same type appear in Fig. 8.9. The change in contrast around the region of crack extension in the conventional photograph arises because "stresscoat" has broken away from this area during specimen failure.

The fiber image produced in the X-ray micrograph is due to the 0.0005 in. diameter tungsten boride core of the filament. Several features are notable:

1. There is considerable fiber (core) breakage below the fracture surface. This may be damage that occurred prior to gross crack extension or far more likely be the result of reverberations after specimen separation.
2. There is comparatively little fiber damage below the crack section introduced by EDM machining.
3. The region of longitudinal splitting contains many split filaments and exhibits a permanent transverse displacement relative to surrounding material. This suggests that the region was subjected to significant transverse tensile stress at some time during the test. High shear stresses could also be involved.
4. The area where the stresscoat broke away from the sample terminates along the longitudinal splits. It has remained on the sample in those areas remote from the fracture and in the shielded areas above and below the original flaw.

Two BORSIC + aluminum specimens failed near the doublers rather than at the flaw. One specimen contained a 0.020 in. flaw, Fig. 8.10; in the other it measured 0.050 in. Thus in Region I or early in Region II, the stress concentration associated with gripping the specimen can be of the same magnitude as the stress concentration associated with the flaw.

To investigate the matrix plasticity effects around flaws, several specimens were held at constant load and their surfaces were examined using standard replicating techniques. A Cr shadowed replica of a 4.2 mil BORSIC + 6061-F sample containing a 0.125 in. radius circular hole that was interrupted at less than  $10^3$  psi below its fracture stress is shown in Fig. 8.11. On the left is a crack that has initiated, run longitudinally, and then been arrested. The dark vertical bands around the hole circumference are zones of plastic deformation in the matrix. It could be easily observed visually that the hole was elliptical in shape at this load.

A conventional photograph of this same region after fracture is given in Fig. 8.12. The arrested crack has propagated in Fig. 8.12 across the specimen. In addition, the regions of longitudinal shear seen in Fig. 8.11 coincide exactly with the short splits around the circumference of the hole. These separations most likely result in part from reverberations in the specimen on fracture. Similar observations on center-notched specimens established that the longitudinal splits (Figs. 8.8, 8.9) occur on a region very near the longitudinal matrix deformation.

#### 8.1.2 BORSIC + Titanium Composites

##### Fracture Strength

Four fracture tests were conducted using 50 v/o 4.2 mil BORSIC + Beta III titanium composite material using crack lengths of 0.049 in. to 0.168 in., Fig. 8.13. The tensile strength of this material, which had been determined previous to this investigation (Ref. 8.14), typically ranged from 163 ksi to 168 ksi, Table VIII-VII. The results in Fig. 8.13 appear to suggest that the notch sensitivity of BORSIC + Beta III is less than that of BORSIC + aluminum since the notched to unnotched strength ratio is 0.74 for the largest flaw tested and the variation of net fracture stress with flaw size is less. However, the results fall within the BORSIC + aluminum band and additional tests are required to draw a confident comparison.

##### Fractography

Fracture surface features were similar to those of BORSIC + aluminum except no longitudinal splits were observed, Fig. 8.14. This is a result of the higher shear strength of the titanium alloy.

The specimen with the shortest flaw, 0.049 in., failed at the grips at a net fracture stress similar to the other three tests, Fig. 8.15. Similar behavior has been noted with BORSIC + aluminum, Fig. 8.10. Thus, the effective stress concentration in fibers ahead of the notch is of a similar magnitude to the stress concentration due to gripping despite the high shear strength of the matrix.

#### 8.1.3 HMG-50 + BP 907 Composites

##### Fracture Strength

Six fracture tests were performed of 50 v/o HMG-50 graphite + BP 907 epoxy composite material in order to provide comparison of the boron aluminum with a polymeric matrix system. The behavior of these specimens was markedly different than that of the metal matrix systems; longitudinal splits (cracks) formed at the crack tips prior to failure and fracture occurred at the grips rather than at the reduced section.

The tensile strength of HMG-50 + BP 907 which had been previously determined (Ref. 8.15), ranges from 68 ksi to 110 ksi, with an average of 98 ksi. The net fracture strength measured in the present tests ranged from

64 ksi to 96 ksi, Fig. 8.13. The material was not significantly weakened by the notch beyond that due to the loss in cross section and

$$\sigma_N \approx \sigma_{UTS} \quad 2c < 0.6 \quad (8.4)$$

### Fractography

The failed specimens were characterized by longitudinal splits at regions other than at the crack tip and very large permanent crack openings, Fig. 8.16. (The flaw shown was initially 0.005 in. high.) Material behind the flaw remained attached to the grip sections. The crack path runs from the specimen edge along the grip boundary, longitudinally to the crack tip, across the flaw, longitudinally to the grip, and across the specimen once again.

Optical examination of the fracture surfaces at high magnification indicated that the longitudinal splits propagated preferentially at the fiber-matrix interface. The features of the transverse components of the fracture were similar to those characterizing longitudinal tensile failures.

## 8.2 Transverse Reinforcement

### Experimental Method

These experiments were conducted with the flaws parallel to the fiber direction using 6061-F matrix composites. Test procedures and alignment standards were identical to those used for longitudinally reinforced material. Two materials were investigated: 50 v/o 4.2 mil BCRIC + 6061-F and 63 v/o 5.7 mil BORSIC + 6061-F.

### Results and Discussion

Results of the fracture tests are given in Fig. 8.17 and Table VIII-IX. The flawed specimens of both materials exhibited a net fracture stress independent of flaw length which was similar to the levels encountered in measurements of transverse tensile strength: 12 ksi to 18 ksi in the case of 4.2 mil BORSIC material and 17 ksi to 26 ksi in the case of the 5.7 mil BORSIC composites. Thus, the observed fracture strength is:

$$\sigma_{NET} \approx \sigma_{UTS} \quad 2c < 0.6 \quad (8.5)$$

The center-notched transversely reinforced (type TL) specimens fractured along surfaces nearly coplanar with the original flaws. A typical failed 4.2 mil BORSIC + 6061-F specimen is shown in Fig. 8.18. The sample exhibits a 45° slanted fracture surface. The specimen edge "rotations" relative to the original 90° flaw were invariably in the opposite sense (clockwise and counterclockwise). A region of extensive fiber splitting lies directly ahead of the original flaw. Regions of fracture surface outward from the center exhibited varying degrees of splitting from specimen to specimen. The 5.7 mil BORSIC + 6061-F displayed similar features except that fiber splitting was minimal and restricted to a small area at the original notch tips.



The percentages of split fibers appearing on fracture surfaces of 4.2 mil BORSIC material in regions removed from the original flaws were measured as described in Section III. The variation of fracture strength with percent split fibers is shown in Fig. 8.19 for the same population of specimens that appeared in Fig. 8.17 as well as for those appearing in Fig. 3.14. The excellent correlation obtained reinforces the earlier observation that transverse strength is governed by the transverse strength of the fibers.

### 8.3 Analysis

#### 8.3.1 Fracture Mechanics

It was mentioned in the introduction to section VIII that for homogeneous elastic orthotropic materials the Griffith-Irwin fracture criterion is applicable if the flaw is oriented along one of the principal directions of elastic symmetry and propagation is colinear with the original flaw (Refs. 8.1-11).

The Griffith-Irwin expression is a thermodynamic one arising from equating the elastic energy release associated with incremental crack extension to the energy required to create new surface or perform local plastic work. The critical stress system criterion is derived by describing the stress field ahead of the crack with elastic stress field equations that contain a  $C^{-1/2}$  type singularity. This stress criterion is characterized by the stress intensity factor  $K$ ; for the opening mode one can write (Ref. 8.16):

$$G = \pi K^2 \sqrt{\frac{A_{11} A_{22}}{2}} \left[ \sqrt{\frac{A_{22}}{A_{11}}} + \frac{2 A_{12} + A_{66}}{2 A_{11}} \right]^{1/2} \quad (8.6)$$

and

$$K = \sigma_F C^{1/2} \quad (8.7)$$

This implies that for a given material

$$\sigma_F^2 C = \text{const} \quad (8.8)$$

where  $\sigma_F$  = gross fracture stress  
 $C$  = half crack length at the onset of unstable crack extension  
 $A_{ij}$  = elastic constants  
 $G$  = crack extension force or energy per unit area of crack extension.

The results of all longitudinally reinforced center-notched tension tests of 4.2 mil BORSIC + 6061-F and 4.2 mil BORSIC + 2024-F are given in Fig. 8.20, where gross fracture strength is presented as a function of flaw size. The data is well characterized by a linear fit on log-log coordinates exhibiting a slope of -0.27. A slope of -0.50 would be expected from the Griffith-Irwin relationship of linear elastic fracture mechanics.

Original flaw lengths were used in Fig. 8.20 since acid digestion experiment had showed that little fiber breakage had occurred ahead of the flaw at loads very close to failure, and because visual observations of many tests indicated that fracture occurred abruptly without prior crack extension on the specimen surface. On a net stress basis the data are not described by a straight line on log-log coordinates. Application of the Irwin "tangent formula" for finite width correction (Ref. 8.1) causes a negligible change which is in the direction of poorer agreement. As a result, if standard linear elastic fracture mechanics are used to characterize fracture of BORSIC + 6061-F aluminum a "critical stress intensity" would emerge that is a function of crack length despite "valid" test conditions (Ref. 8.12). A similar difficulty would arise for transversely reinforced material, Fig. 8.17, since  $\sigma_N = \text{const.}$  in this orientation.

### 8.3.2 Flaw Stress Field

The fracture process is governed by the state of stress around the crack tip and in isotropic homogeneous materials the longitudinal stress normal to the flaw is the significant variable (Ref. 8.1). Fracture mechanics provide unique and single-valued relationships among stress, strain and energy when plasticity effects are small. Implicit in this treatment is the assumption that there is sufficient stress generated (or sufficient local work is performed) at the crack tip or point of singularity to break atomic bonds.

The inhomogeneity and strength anisotropy of BORSIC + aluminum and many other fiber reinforced materials complicates this situation. The elastic stress field at the boundary and directly ahead of an elliptical crack, oriented in directions of elastic symmetry, in a semi-infinite plate under uniaxial tension is given in Figs. 8.21-8.23. The analysis of Savin (Ref. 8.18) was employed to calculate, as a function of position: (1) the ratio of longitudinal normal stress to the applied tensile stress,  $K_{xx}$ ; (2) the ratio of longitudinal shear stress to the applied tensile stress,  $K_{xy}$ ; and (3) the ratio of normal transverse stress to the applied tensile stress,  $K_{yy}$ , an elliptical crack of length 0.100 in. and 0.030 tip radius in BORSIC + aluminum was analyzed.

$K_{xx}$  is maximum at the crack tip and decays ahead of the flaw more slowly than  $1/\sqrt{r}$ , Fig. 8.21.  $K_{xy}$  is maximum (-0.99) slightly behind the crack tip with a sign of shear strain consistent with the actual displacements, Fig. 8.22.  $K_{yy}$  is zero at the crack tip and attains local maxima both ahead of and behind (0.55) the tip of the notch, Fig. 8.23. The root radius used here is an estimate of what is likely to be the minimum effective value, one-half the critical load transfer length, and a  $2c$  of 0.100 in. was chosen as being typical of the crack lengths evaluated in this program.

On the basis of these stress concentration factors and the longitudinal strength (160 ksi), transverse strength (15 ksi) and shear strength (15 ksi) of BORSIC + 6061-F aluminum, one would expect:

1. Shear yielding at 15.1 ksi (15/0.99)

2. Transverse tensile failure at 27.2 ksi (15/0.55)
3. Longitudinal failure at 38 ksi (160/4.21).

The measured gross fracture strength of this material with a 0.100 in. flaw is over 100 ksi, rather than 38 ksi because failure by shear yielding occurs first and this relieves the stress concentration. Regardless of how sharp an initial flaw, one assumes (or how low a net section stress is implied) sufficient local fiber displacement to cause fracture is not generated because extensive shear deformation occurs behind flaw tip, and the "excess load" arising from the discontinuity is supported by a larger volume of material. Evidence of tip blunting and shear displacements observed in this material have been discussed previously. Although significant stress concentrations can be developed over a volume of material with dimensions related to the critical load transfer length, fracture cannot occur at low nominal stresses as a result of a stress singularity.

Since 6061-F is not elastic to failure one would expect shear yielding at stresses below 15 ksi and this is observed, Fig. 8.6.

### 8.3.3 Notch Blunting Indices

A list of maximum stress concentration factors for BORSIC + Al, BORSIC + Ti, and graphite + epoxy is given in Table VIII-X. One can define a longitudinal shear index  $I_{xy}$  by the following expression:

$$I_{xy} \equiv K_{xx}/X \cdot S/|K_{xy}| \quad (8.9)$$

where  $K_{ij}$  = stress concentration factors  
 $S$  = shear strength  
 $X$  = longitudinal tensile strength

This represents the fraction of the applied stress for tensile failure at which shear failure occurs. A similar index can be written for transverse failure.

$I_{xy}$  for isotropic materials is always greater than one and this effect cannot apply. For BORSIC + aluminum,  $I_{xy}$  is approximately 0.4 (elastic) at a crack length of 0.100 in. and  $I_{xy}$  decreases for sharper cracks. The material will yield but not break and a degree of notch sensitivity remains.

For graphite + epoxy  $I_{xy}$  is approximately 0.7 at a flaw length of 0.100 in. Since graphite + epoxy is nearly elastic to failure, the material will split near the notch tip and eliminate the effect of stress concentration Fig. 8.13.

For BORSIC + titanium  $I_{xy}$  is probably greater than one, but  $I_{yy}$  can be less than one. This may have caused the relative notch insensitivity observed, Fig. 8.13.

#### 8.3.4 System Comparisons

The notch strength (toughness) of the composite systems evaluated in this work are compared to several common isotropic materials in Fig. 8.24. The gross fracture strength of the isotropic materials was calculated using the Irwin tangent formula (Ref. 8.1) uncorrected for plastic zone and the following data:

1.  $K_{IC} \approx 50 \text{ ksi } V_m$  for Ti-6Al-4V (Ref. 8.19)
2.  $G_C = 340 \text{ in.-lb/in.}^2$  for 2024-T3 aluminum (Ref. 8.20)
3.  $G_C = 0.04 \text{ in.-lb/in.}^2$  for soda lime glass (Refs. 8.20,21).

Also shown is a hypothetical system of 160 ksi strength that is unaffected by the notch:

$$\sigma_F = \sigma_{UTS} (1 - 2c/w)$$

The composite systems are weaker in the presence of flaws than the constant net stress upper bound. However, they are comparable to or somewhat stronger than Ti-6Al-4V alloy and clearly superior to 2024-T3 (or glass which is more than an order of magnitude less flaw resistant than the other systems).

#### 8.4 Conclusions

1. Linear elastic fracture mechanics does not provide a valid framework for predicting the fracture strength of BORSIC + 6061 Al, BORSIC + 2024 Al, BORSIC + Beta III Ti, or graphite + epoxy as a result of notch blunting effects that arise from inhomogeneity and anisotropy of strength.
2. The failure strength of these composite materials is governed by the level of strain generated in filaments ahead of the crack or in the reduced section in the presence of notch blunting effects.
3. The energy measured in an impact or slow bend test is not simply related to the strength of these systems in the presence of a flaw.
4. The notch strengths of longitudinally reinforced BORSIC + aluminum, BORSIC + Beta III titanium, and graphite + epoxy are comparable to or somewhat higher than Ti-6Al-4V alloy and clearly superior to 2024-T3 aluminum alloy.

## SECTION VIII - REFERENCES

1. A. S. Tetelman and A. J. McEvily, Jr., Fracture of Structural Materials, John Wiley and Sons, 1967.
2. E. M. Wu, J. Applied Mech., Vol. 34, p. 967-974, 1967.
3. E. M. Wu, "Application of Fracture Mechanics to Orthotropic Plates", Univ. of Illinois, TAM Report 248, Naval Research Laboratory, Contract No. Nonr 2947(02)X, 1963.
4. E. M. Wu and R. C. Reuter, "Crack Extension in Fiberglass Reinforced Plastics", Univ. of Illinois, TAM Report 275, Bureau of Naval Weapons, NOW-64-0178-d, 1965.
5. E. M. Wu, "A Fracture Criterion for Orthotropic Plates Under the Influence of Compression and Shear", Univ. of Illinois, TAM Report 283, Bureau of Naval Weapons, Contract No. NOW-0204-d, 1965.
6. G. R. Irwin, "Analytical Aspects of Crack Stress Field Problems", Univ. of Illinois, TAM Report No. 213, March 1962.
7. E. M. Wu, "Discontinuous Mode of Crack Extension in Unidirectional Composites", Univ. of Illinois, TAM Report No. 309, 1968.
8. E. M. Wu, "Fracture Mechanics of Anisotropic Plates", S.W. Tsai, et al, Composite Materials Workshop, Technomic Publishing Co., p. 20-43, 1968.
9. G. C. Sih, et al, Int. J. Fracture Mech., Vol. 3, p. 189-203, 1965.
10. P. C. Paris and G. C. Sih, "Stress Analysis of Cracks", ASTM STP 381, p. 30-83, 1965.
11. D. D. Ang and M. L. Williams, J. Applied Mech., Vol. 28, No. 3, p. 278-372, 1961.
12. N. R. Adsit and W. E. Witzell, "Fracture Toughness of Aluminum-Boron Composites", SAMPE, p. 391, 1969.
13. J. W. Dally and W. F. Riley, Experimental Stress Analysis, McGraw-Hill Book Company, New York, 1965.
14. L. E. Dardi and L. J. Pionke, Pratt & Whitney Aircraft, Unpublished work.
15. L. E. Dardi and J. C. Preston, Jr., Pratt & Whitney Aircraft, Unpublished work.
16. G. C. Sih, P. C. Paris, and G. R. Irwin, "On Cracks in Rectilinearly Anisotropic Bodies", Intl. J. of Fracture Mechanics, Vol. 1, No. 3, p. 189-203, 1965.

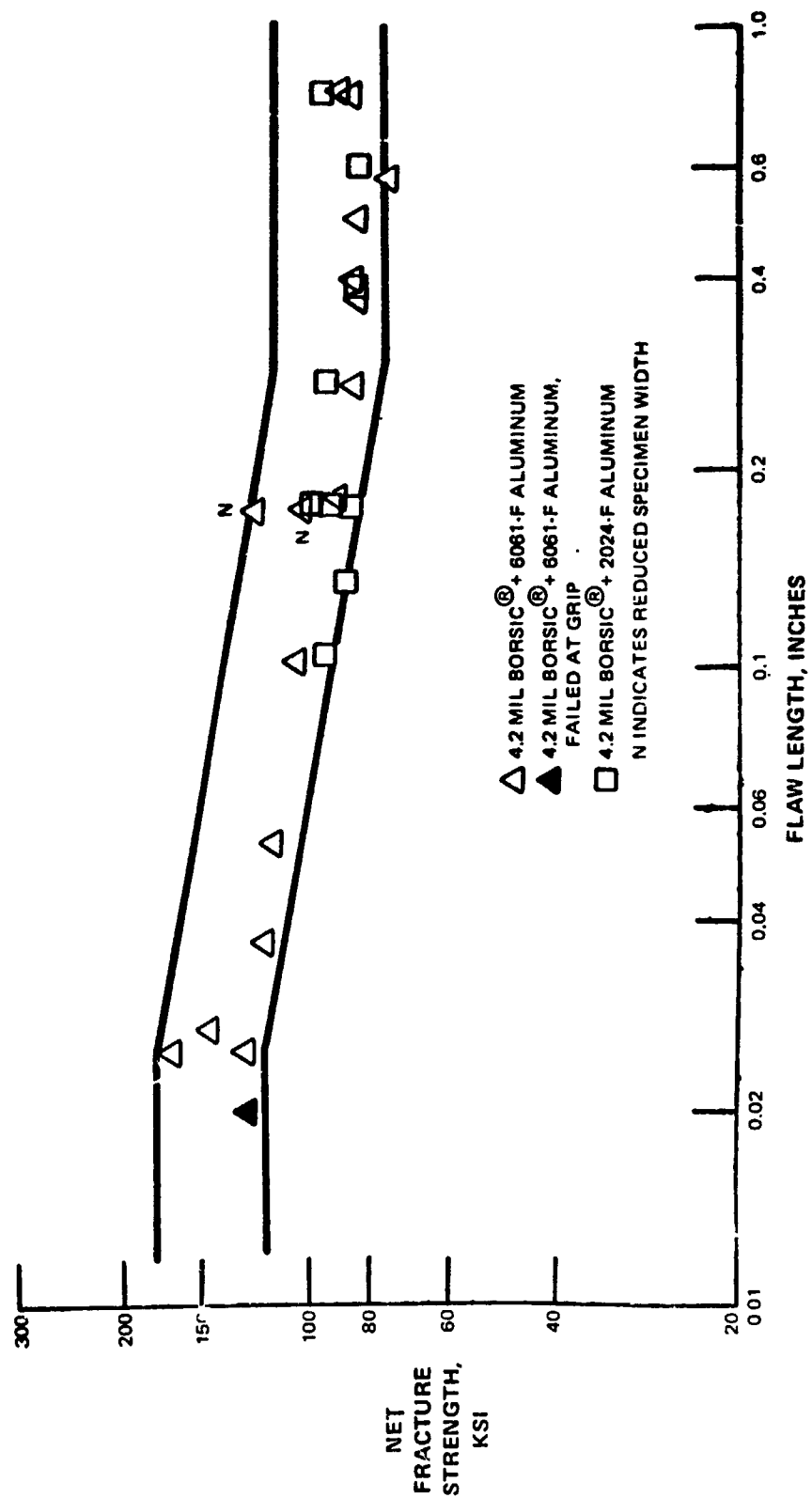
SECTION VIII - REFERENCES (Cont'd)

17. E. F. Olster and R. C. Jones, "Toughening Mechanisms in Fiber Reinforced Metal Matrix Composites", Report R70-75, Department of Civil Engineering, Massachusetts Institute of Technology, Cambridge, Mass., Nov. 1970.
18. G. N. Savin, Stress Concentration Factors Around Holes, Translated by W. Johnson and E. Gros, Pergamon Press, London, 1961.
19. D. L. Ruckle, Pratt & Whitney Aircraft, Unpublished work.
20. N. H. Polakowski, E. J. Ripling, Strength and Structure of Engineering Materials, Prentice-Hall, Inc., Englewood Cliffs, New Jersey, p. 416, 1966.
21. "1971 Materials Selector", Materials Engineering, Vol. 72, No. 6, p. 312, 1970.



MAG: 0.34 X

FIGURE 8-1  
CENTER-NOTCHED TENSILE SPECIMEN IN LOADING FIXTURE





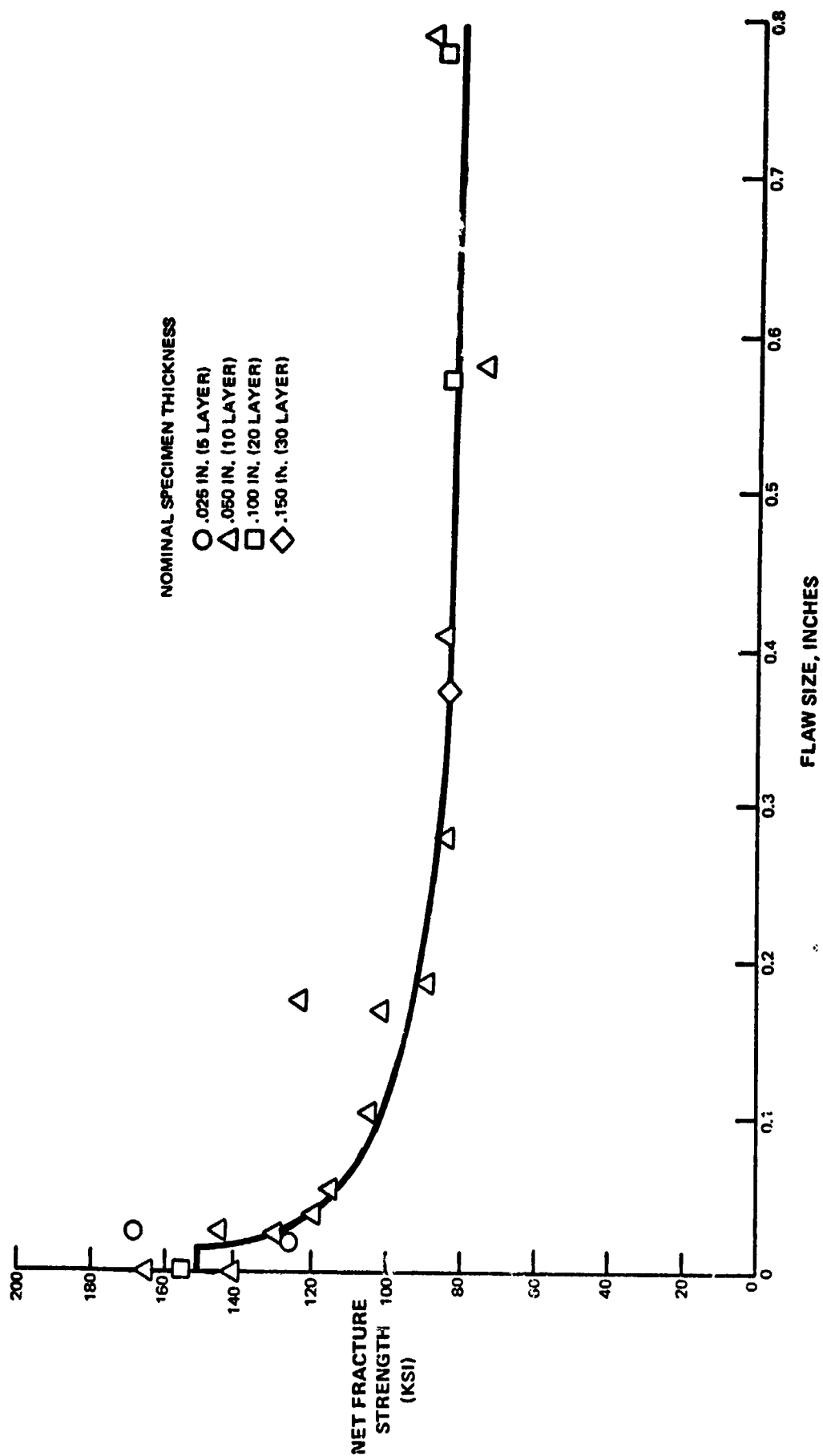


FIGURE 8-3

VARIATION OF NET FRACTURE STRENGTH WITH FLAW SIZE  
AS A FUNCTION OF SPECIMEN THICKNESS FOR 4.2 MIL BORSIC +  
6061-F ALUMINUM COMPOSITES

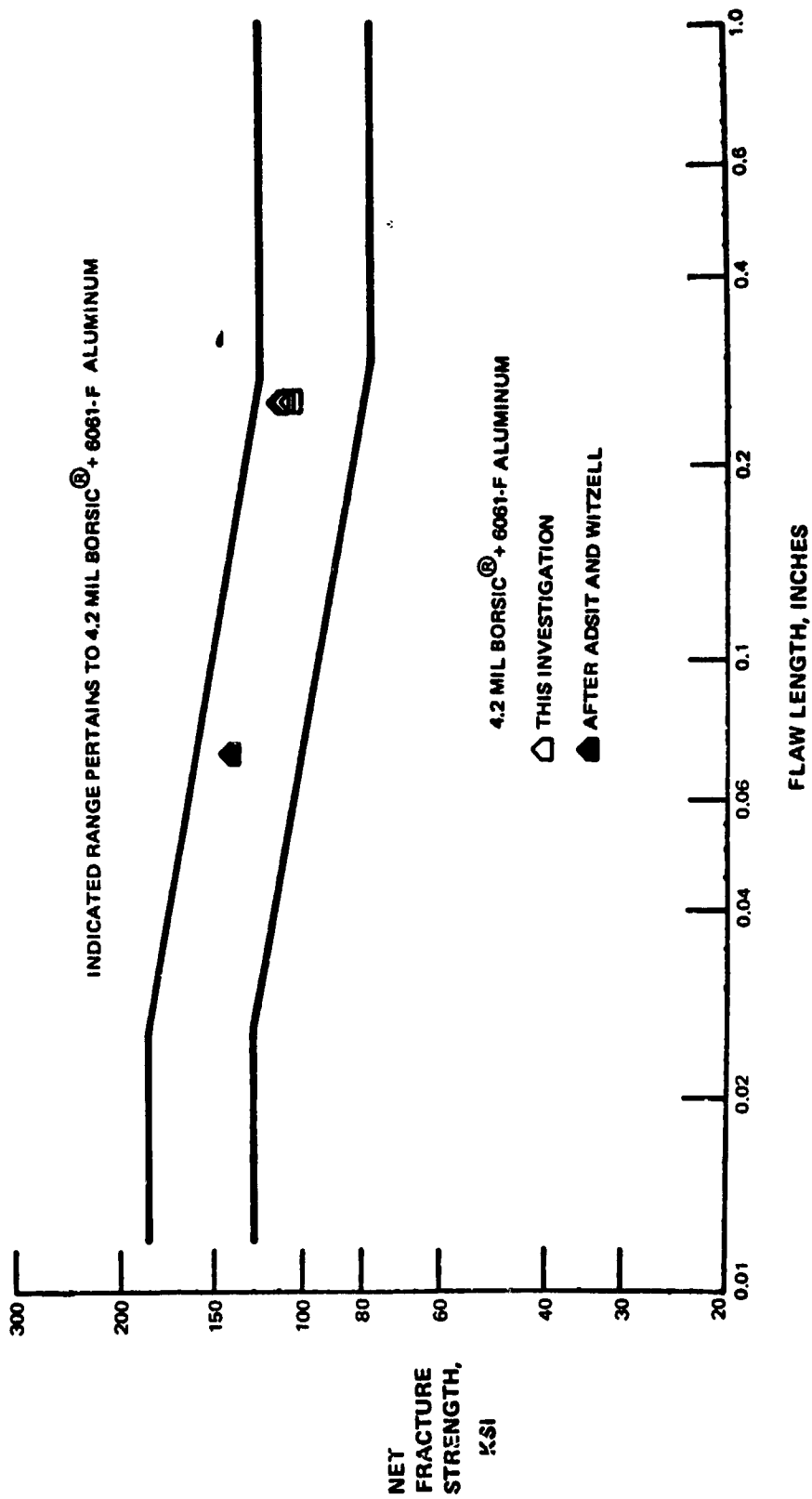


FIGURE 8-4  
NET FRACTURE STRENGTH OF 4.2 MIL BORSIC + 6061-F ALUMINUM  
WITH CENTER CIRCULAR HOLES

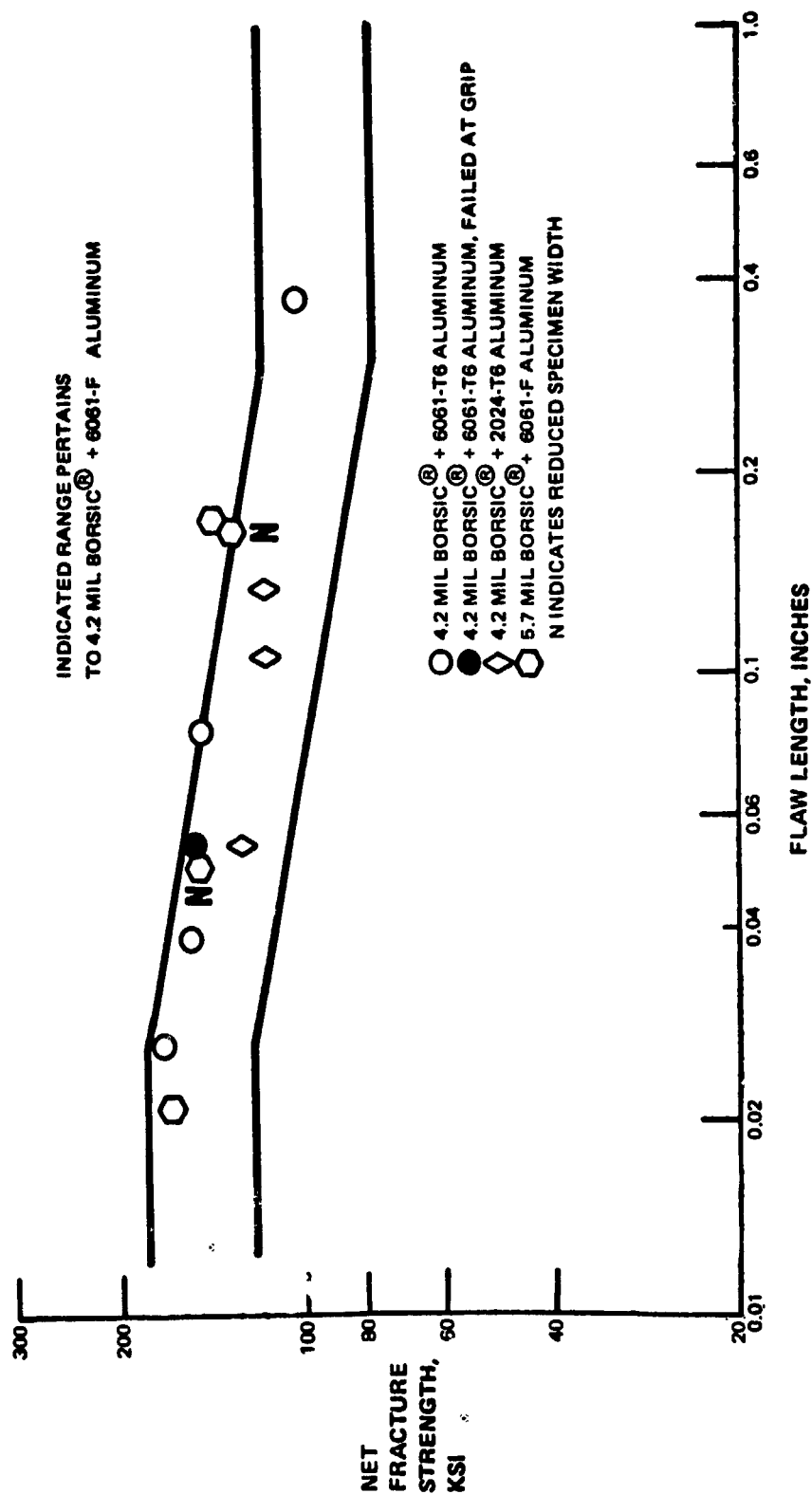


FIGURE 8-5  
NET FRACTURE STRENGTH OF NOTCHED HEAT TREATED 4.2 MIL  
BORSIC + ALUMINUM

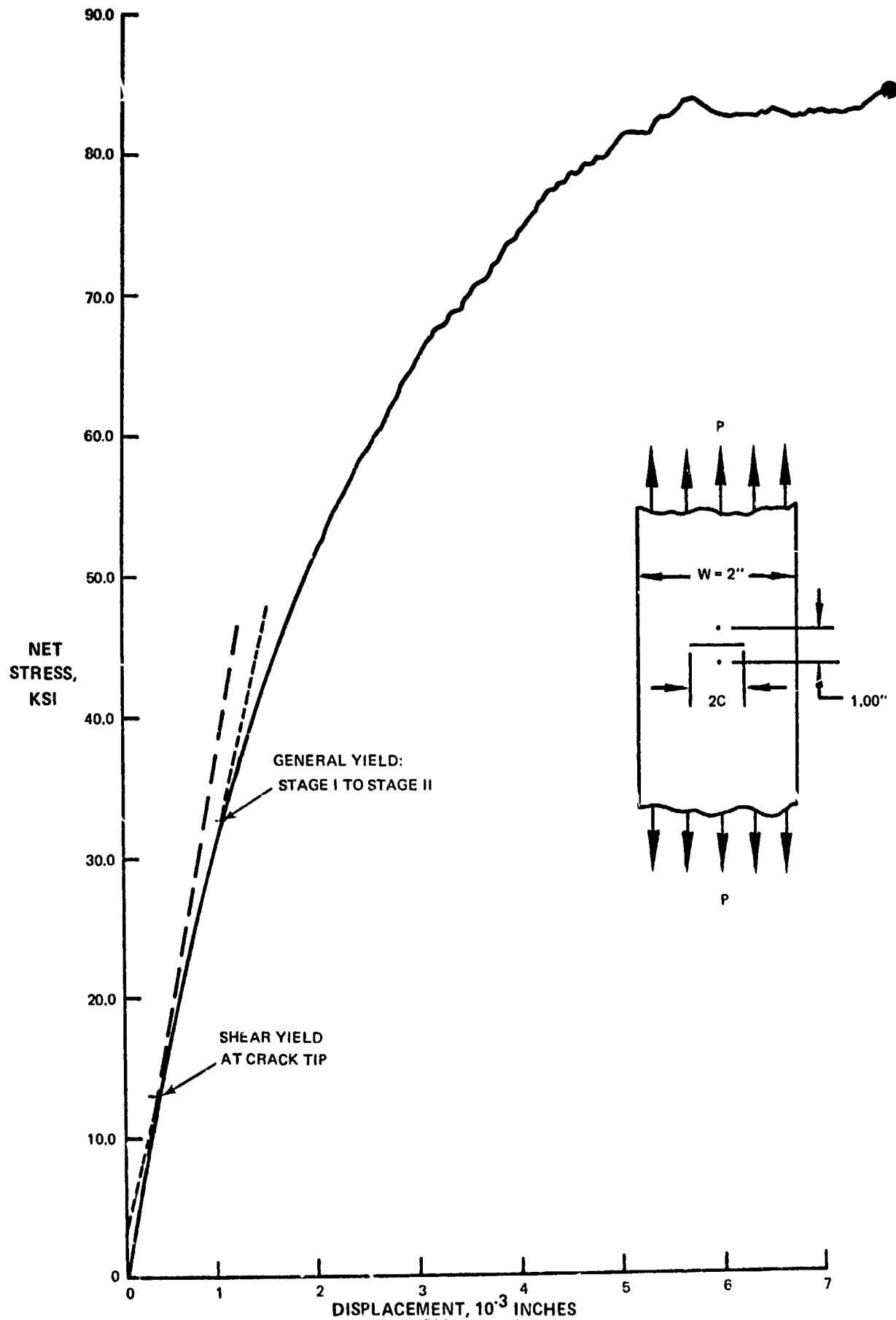
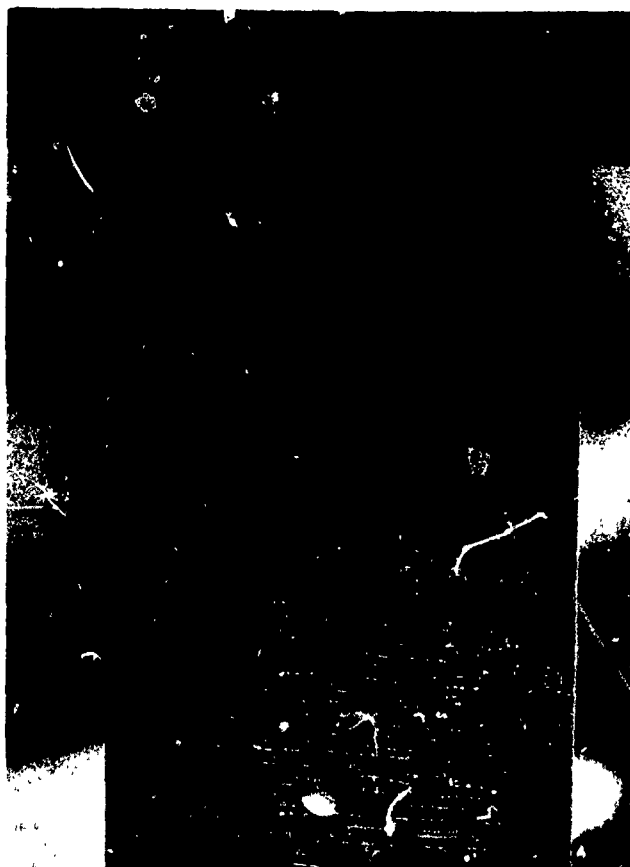


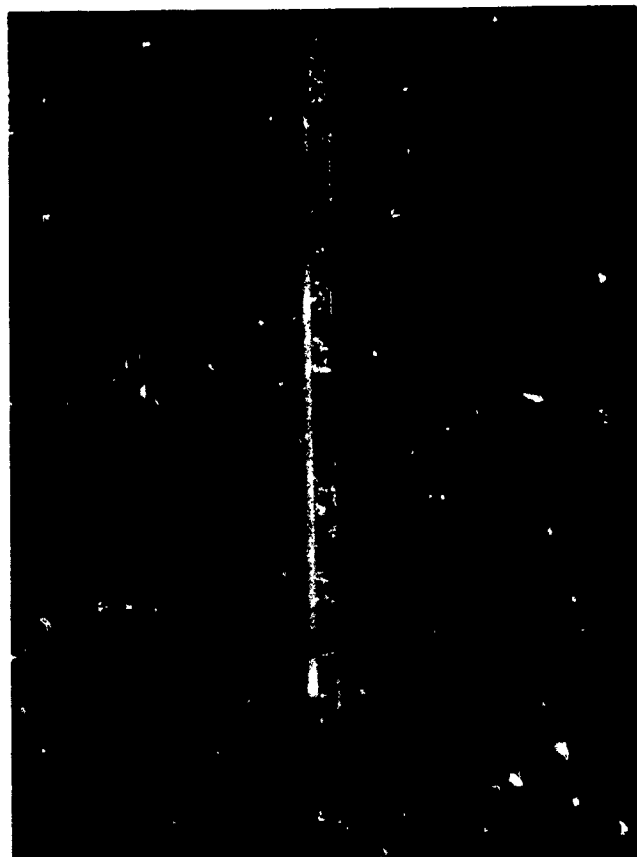
FIGURE 8-6  
TYPICAL STRESS-DISPLACEMENT CURVE FOR 4.2 MIL BORSIC + 6061-F ALUMINUM  
CENTER NOTCH SPECIMEN UNDER UNIAXIAL TENSION



Reproduced from  
best available copy.

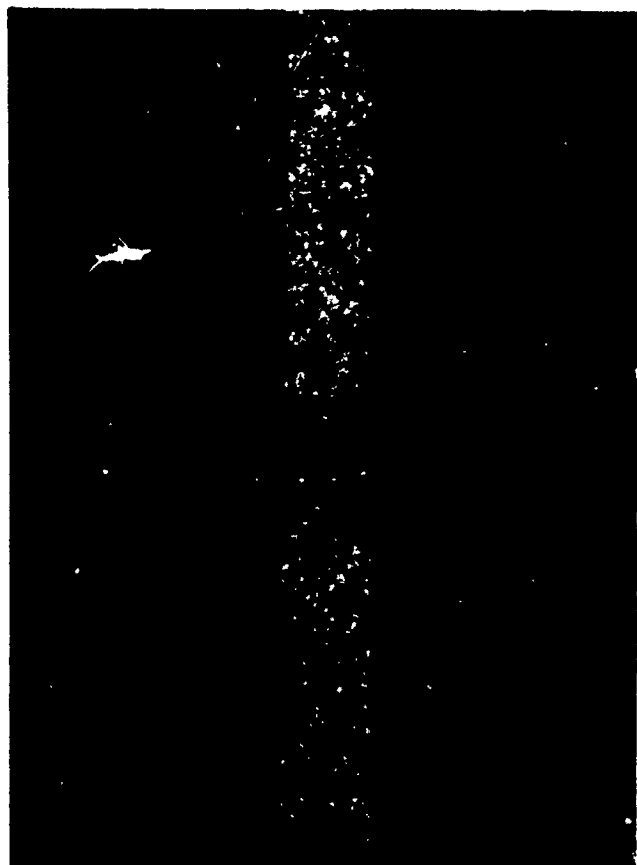
MAG: 1.8 X

**FIGURE 8-7**  
**VIEW OF STRESS-COAT CRACK PATTERN ON AN AXIALLY REINFORCED (TYPE LT)**  
**50 v/o 4.2 MIL BORSIC® + 2024-F ALUMINUM CENTER-NOTCHED TENSILE SPECIMEN**



MAG: 2X

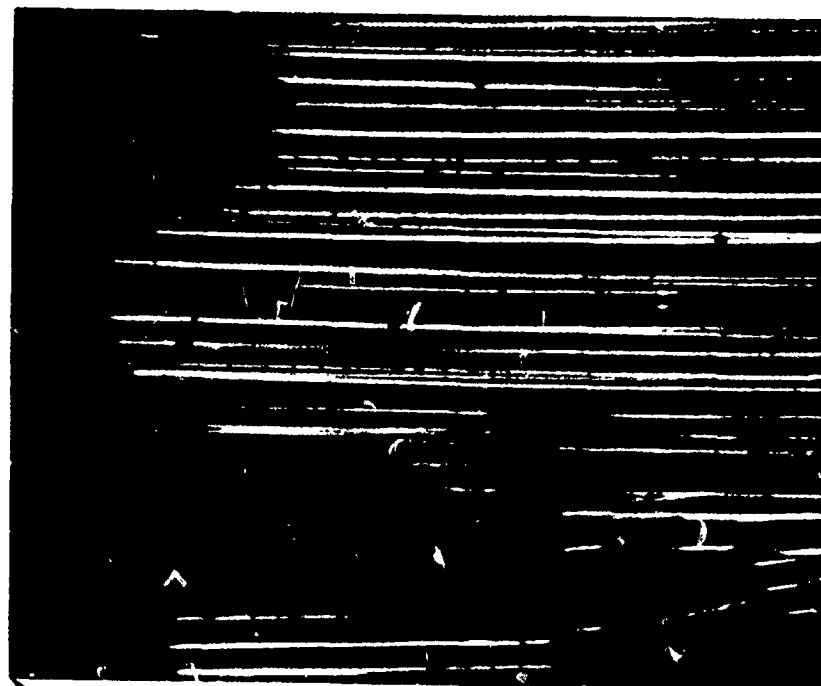
Reproduced from  
best available copy.



MAG: 10X

FIGURE 8-8

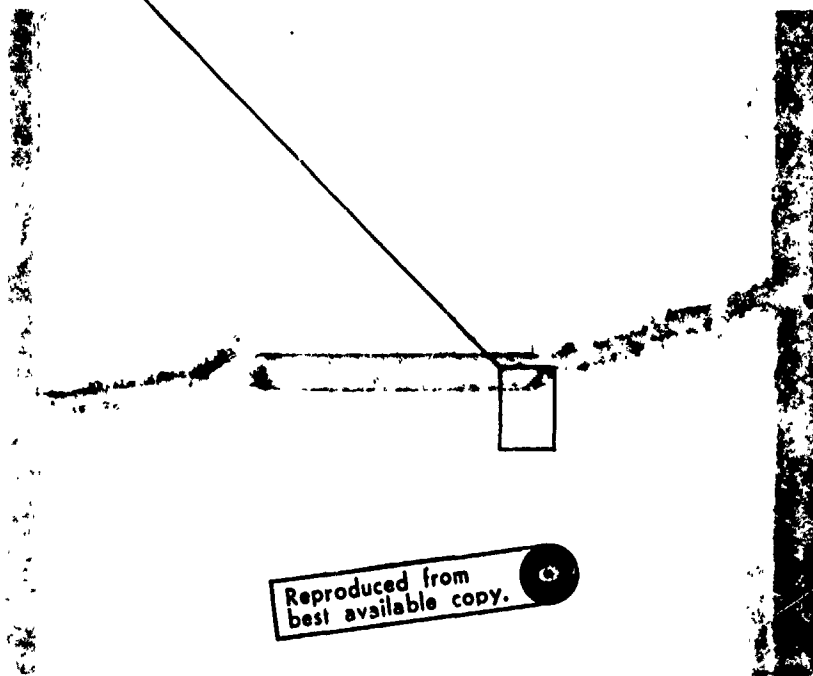
FRACTURE SURFACE OF 50 V/O 4.2 MIL BORSIC<sup>®</sup> + 6061-F ALUMINUM  
CL. NOTCHED TENSILE SPECIMEN



MAG: 50 X

FIGURE 8-9

SIDE VIEW OF FRACTURED AXIALLY REINFORCED (TYPE LT) 4.2 MIL BORSIC + 2024-F ALUMINUM  
ALLOY CENTER NOTCHED TENSILE SPECIMEN (LEFT) AND X-RAY RADIOGRAPH OF REGION NEAR  
ORIGINAL CRACK TIP (RIGHT)



MAG: 2 X

Reproduced from  
best available copy.

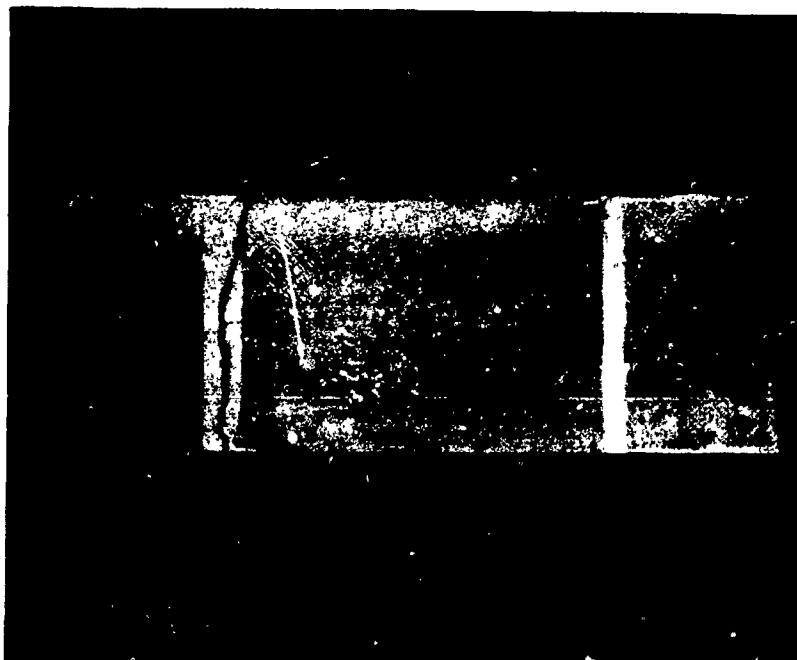


FIGURE 8-10  
FRACTURED 4.2 MIL BORSIC<sup>®</sup> + 6061 ALUMINUM  
CENTER NOTCHED SPECIMEN





FIGURE 8-11

Cr SHADOWED REPLICA AROUND CIRCULAR HOLE IN 4.2 MIL 6061F ALUMINUM  
AT 99 PERCENT OF FRACTURE STRESS

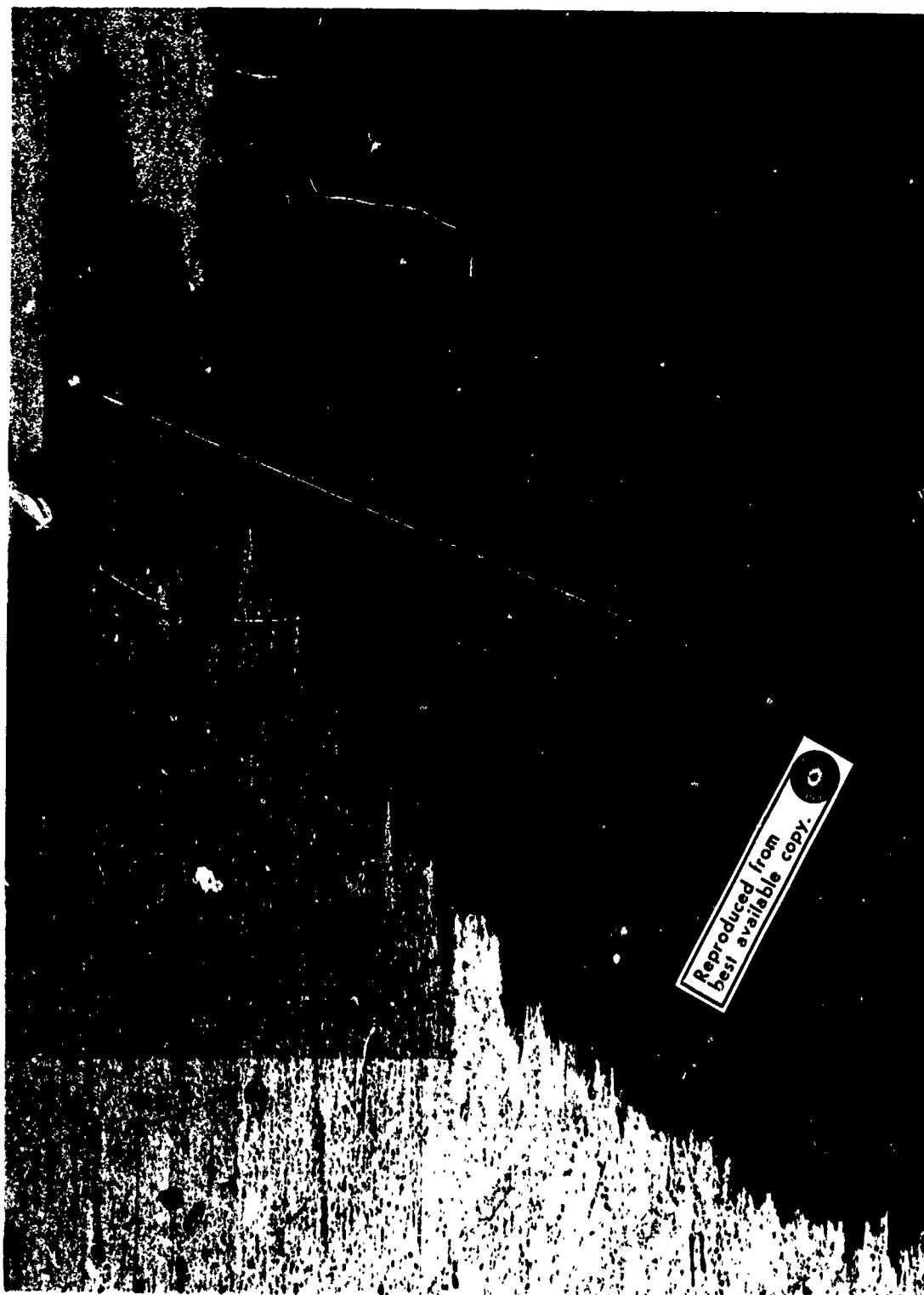


FIGURE 8-12

FRACTURED 4.2 MIL BORSIC + 6061-F ALUMINUM SPECIMEN CONTAINING A CIRCULAR HOLE

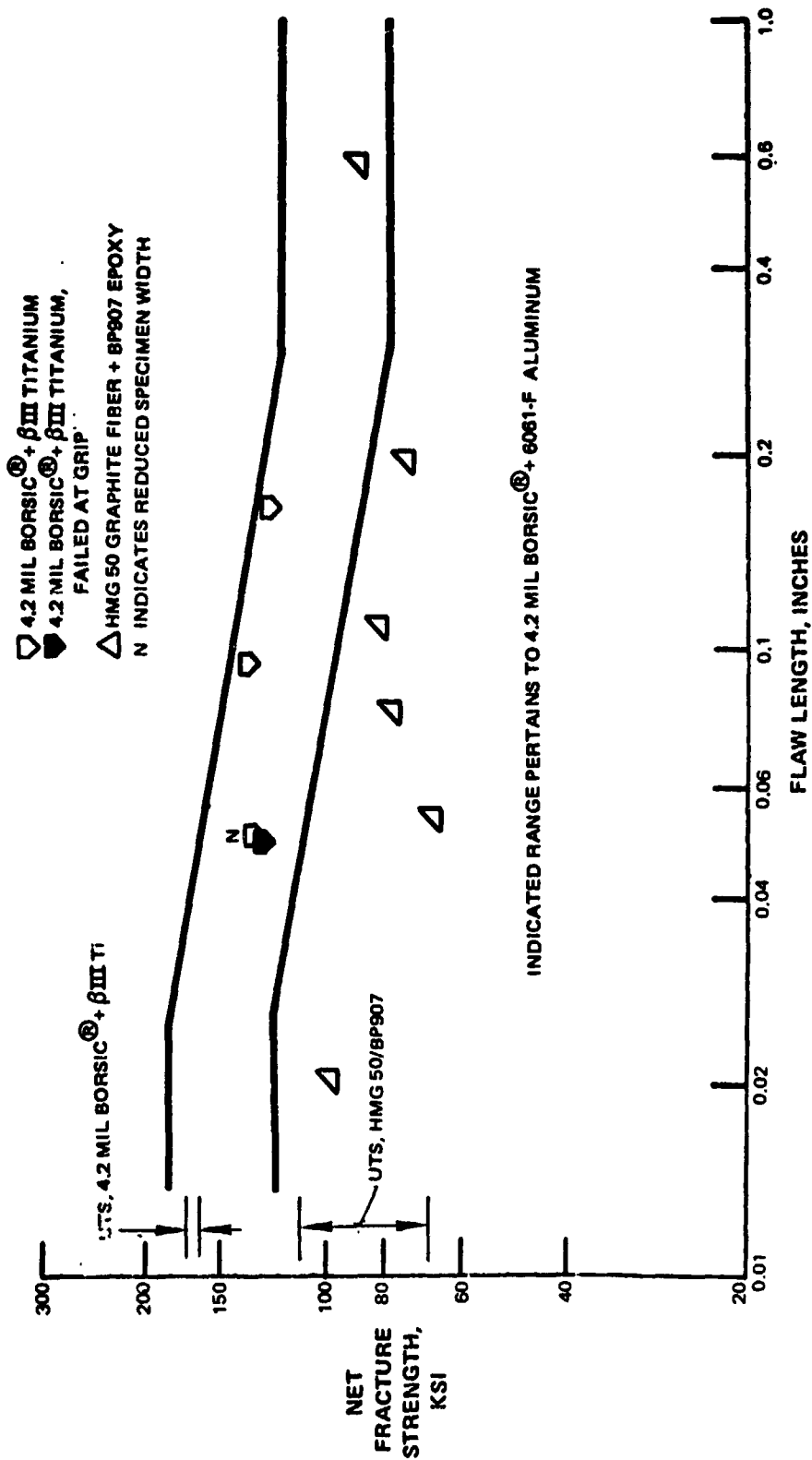
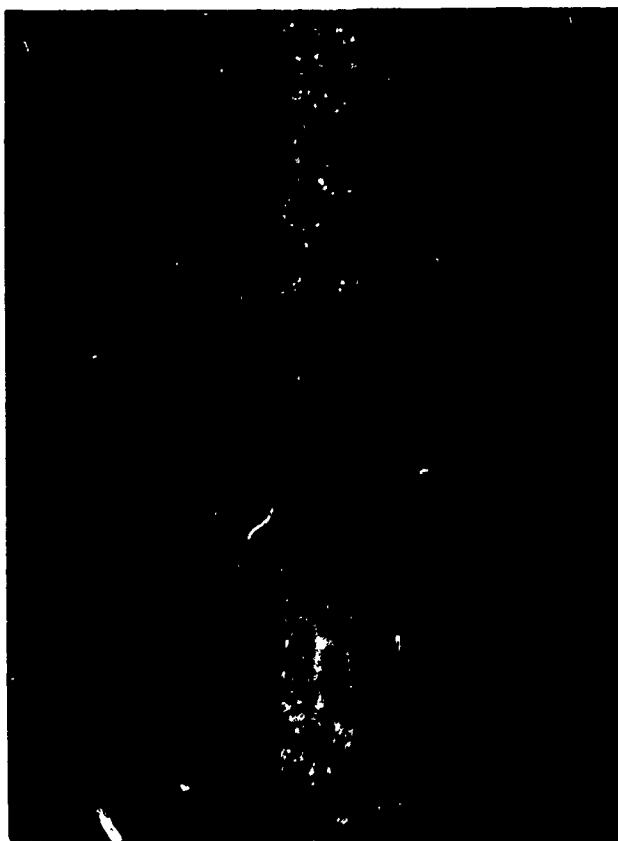
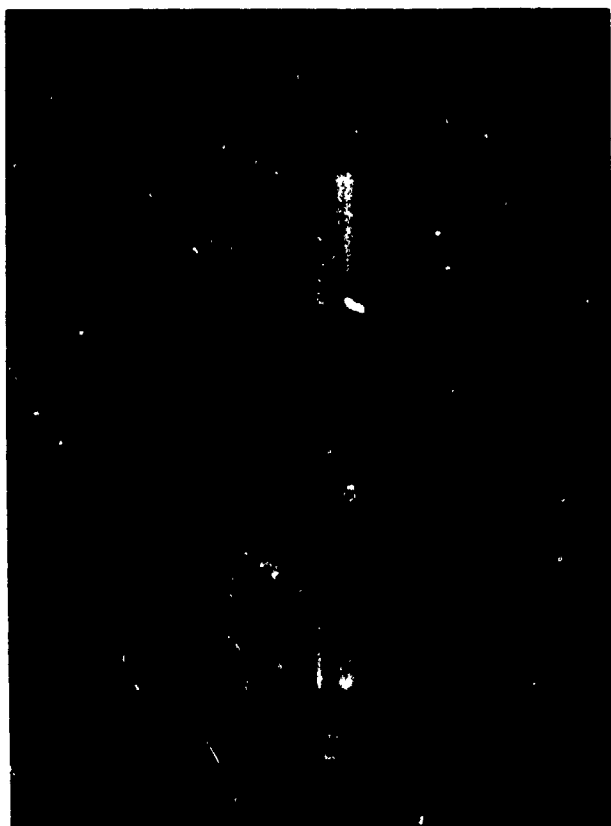


FIGURE 8-13  
NET FRACTURE STRENGTH OF CENTER NOTCHED 4.2 MIL  
BORSIC + TITANIUM AND GRAPHITE + EPOXY



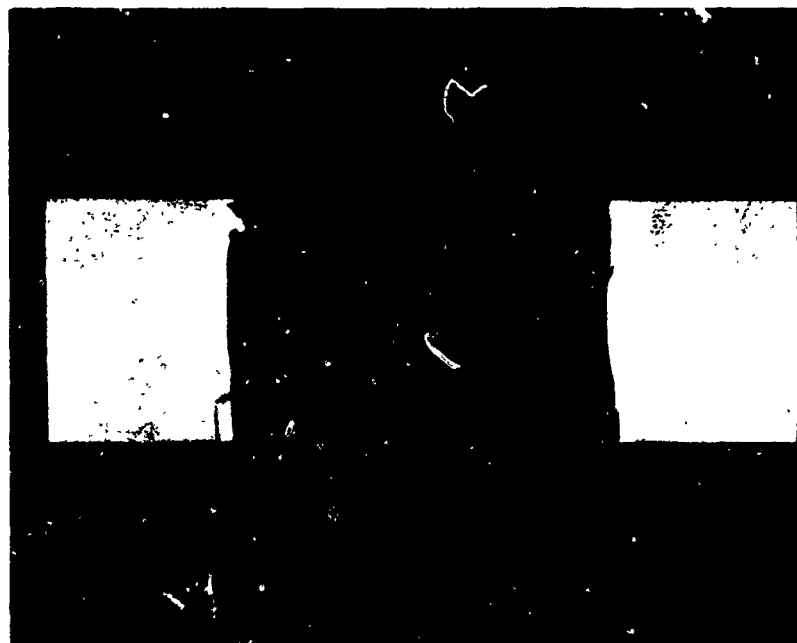
MAG: 10X

Reproduced from  
best available copy.



MAG: 2X

FIGURE 8-14  
FRACTURE SURFACE OF 50 v/o 4.2 MIL BORSIC® + BETA III  
TITANIUM CENTER-NOTCHED TENSILE SPECIMEN.



Reproduced from  
best available copy.

FIGURE 8-15  
FRACTURED 4.2 MIL BORSIC + BETA III TITANIUM CENTER NOTCHED SPECIMEN



MAG: 0.75X



MAG: 5X

Reproduced from  
best available copy.

FIGURE 8-16  
VIEW OF FRACTURED LONGITUDINALLY REINFORCED (TYPE LT) 50 v/o  
HMG-50 GRAPHITE + BP-907 EPOXY CENTER NOTCHED TENSILE SPECIMEN

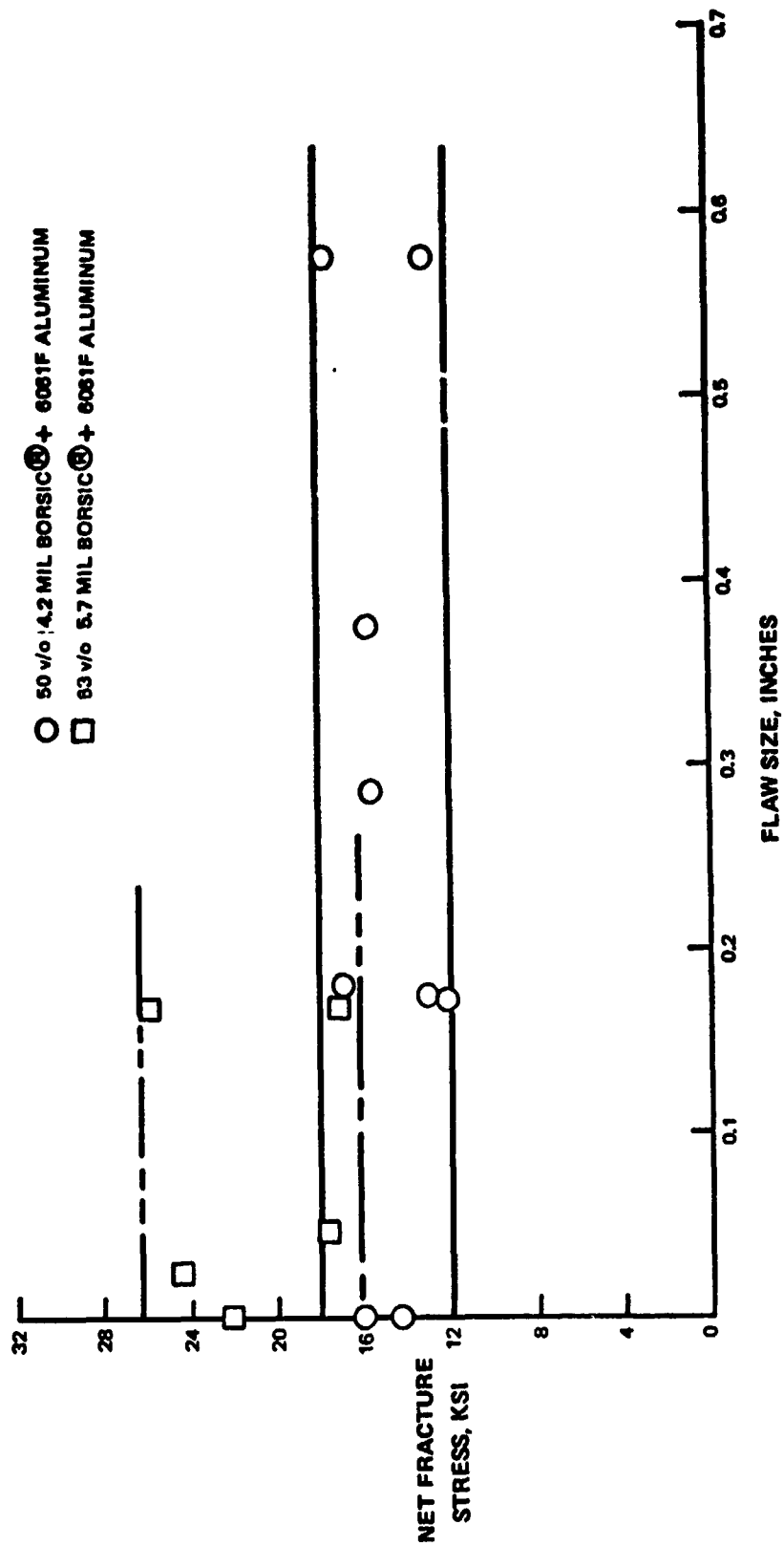


FIGURE 8-17

NET FRACTURE STRESS AS A FUNCTION OF INITIAL FLAW  
LENGTH FOR BORSIC® + 6031F ALUMINUM COMPOSITE MATERIAL



MAG: 2 X

**FIGURE 8-18**  
**FRACTURE SURFACE OF A TYPICAL TRANSVERSELY REINFORCED (TYPE TL) 50 v/o 4.2 MIL**  
**BORSIC®+ 6061-F ALUMINUM CENTER-NOTCHED TENSILE SPECIMEN**



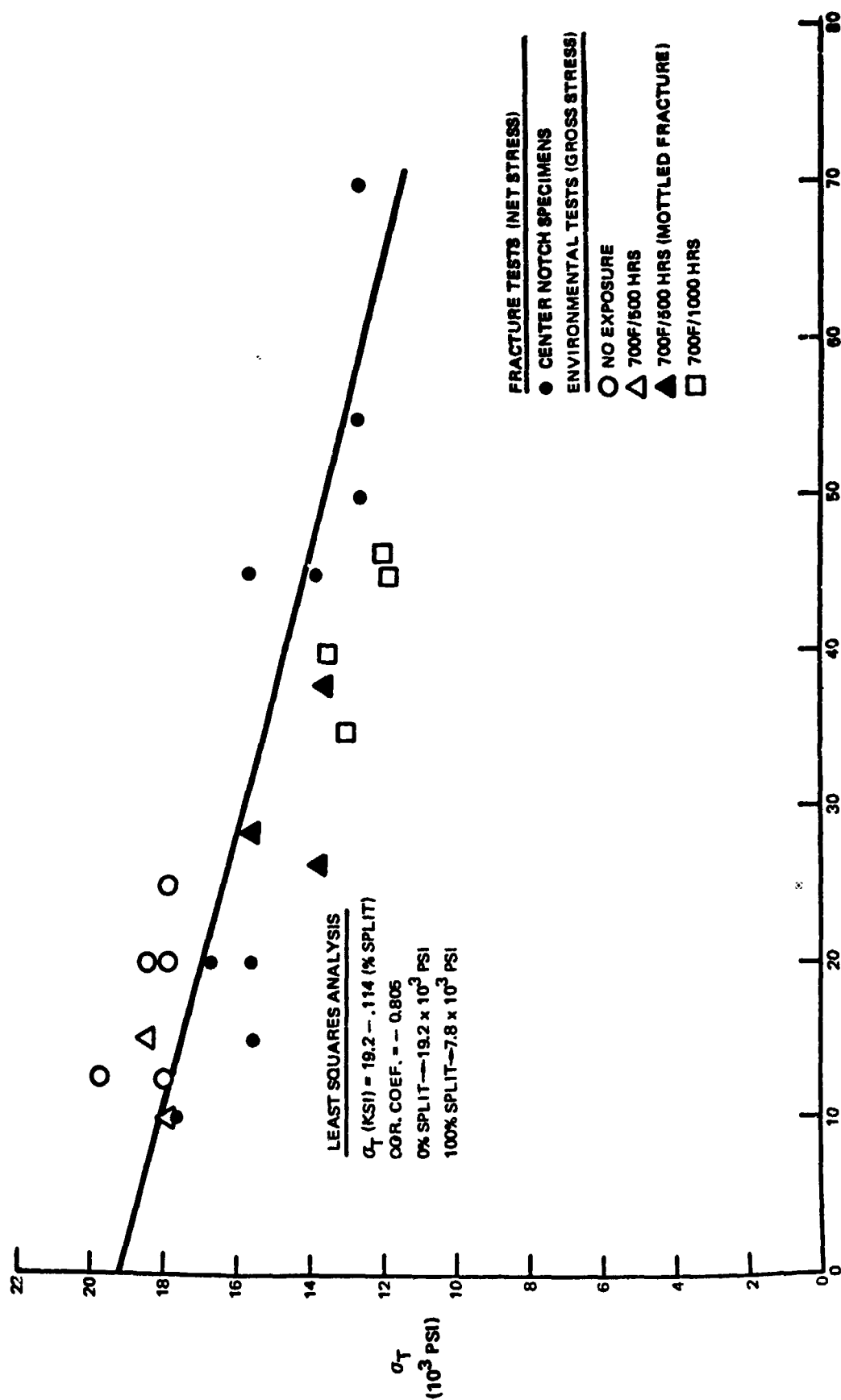
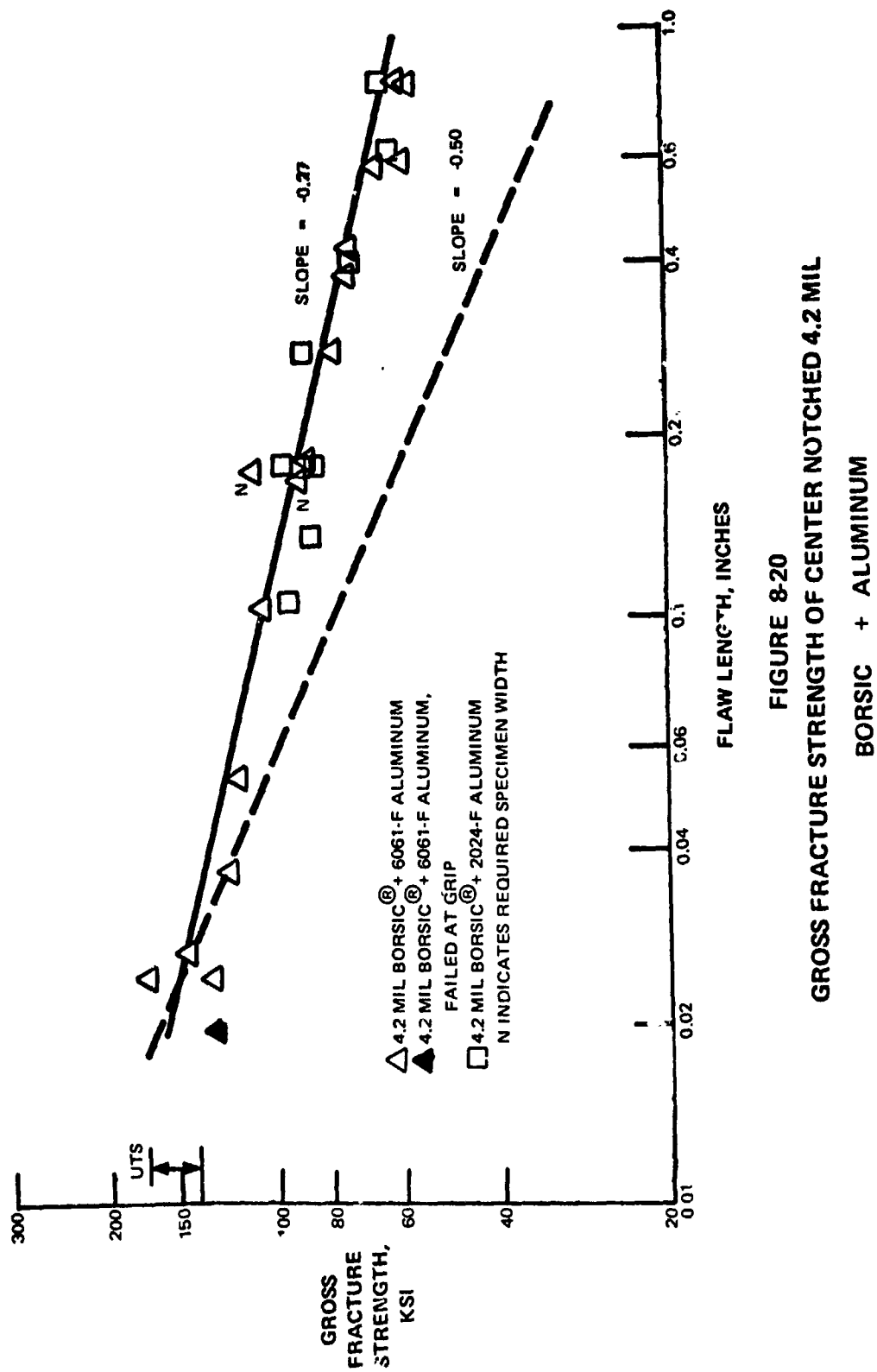


FIGURE 8-19

VARIATION OF TRANSVERSE STRENGTH WITH  
 PERCENT SPLIT FIBERS ON THE FRACTURE SURFACE OF  
 50v/o 4.2 MIL BORSIC + 6061-F ALUMINUM COMPOSITE MATERIAL



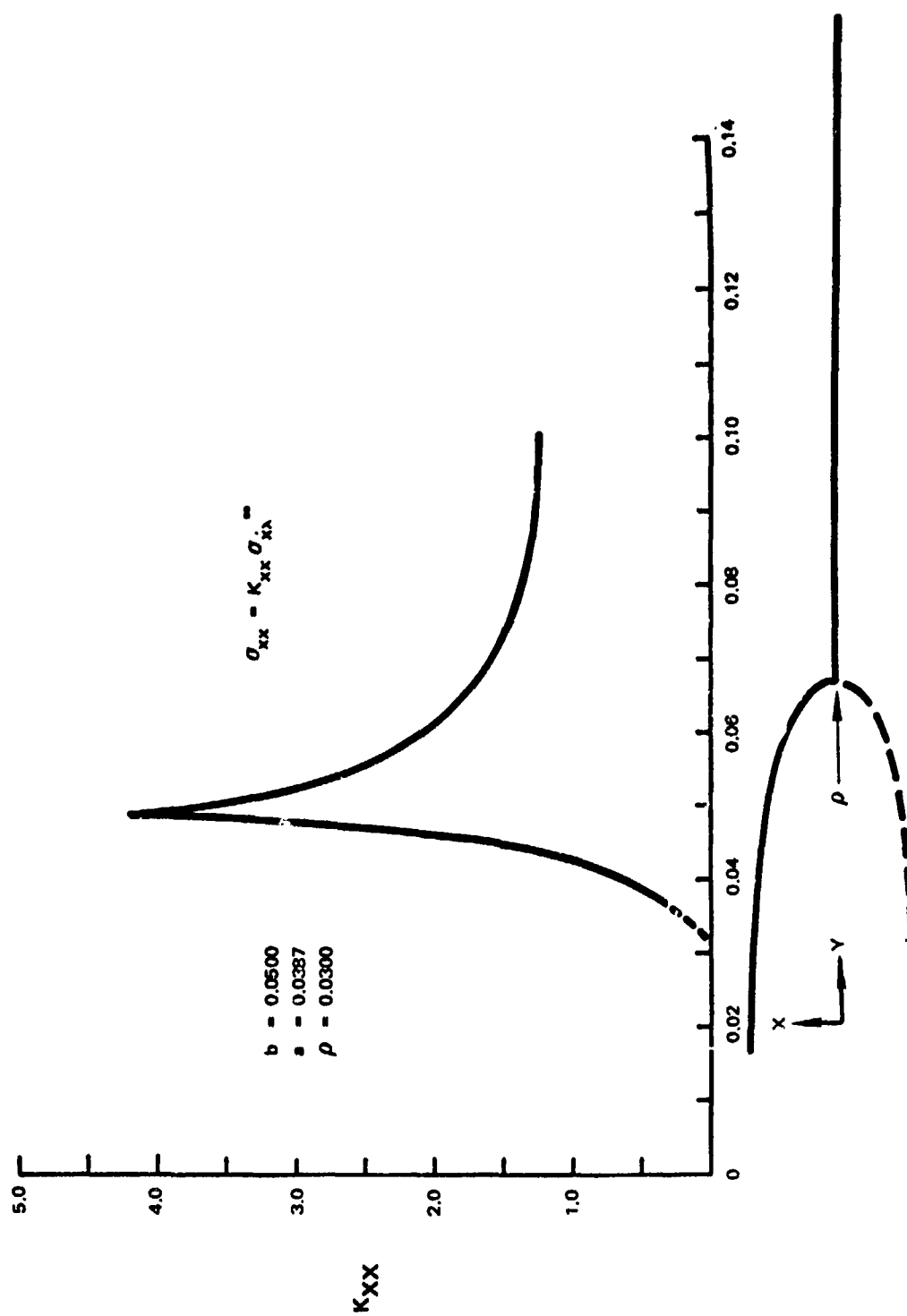


FIGURE 8-21  
 ELASTIC LONGITUDINAL STRESS CONCENTRATION FACTOR FOR 50 v/o  
 4.2 MIL BORSIC + 6061-T ALUMINUM UNDER UNIAXIAL LONGITUDINAL  
 TENSION

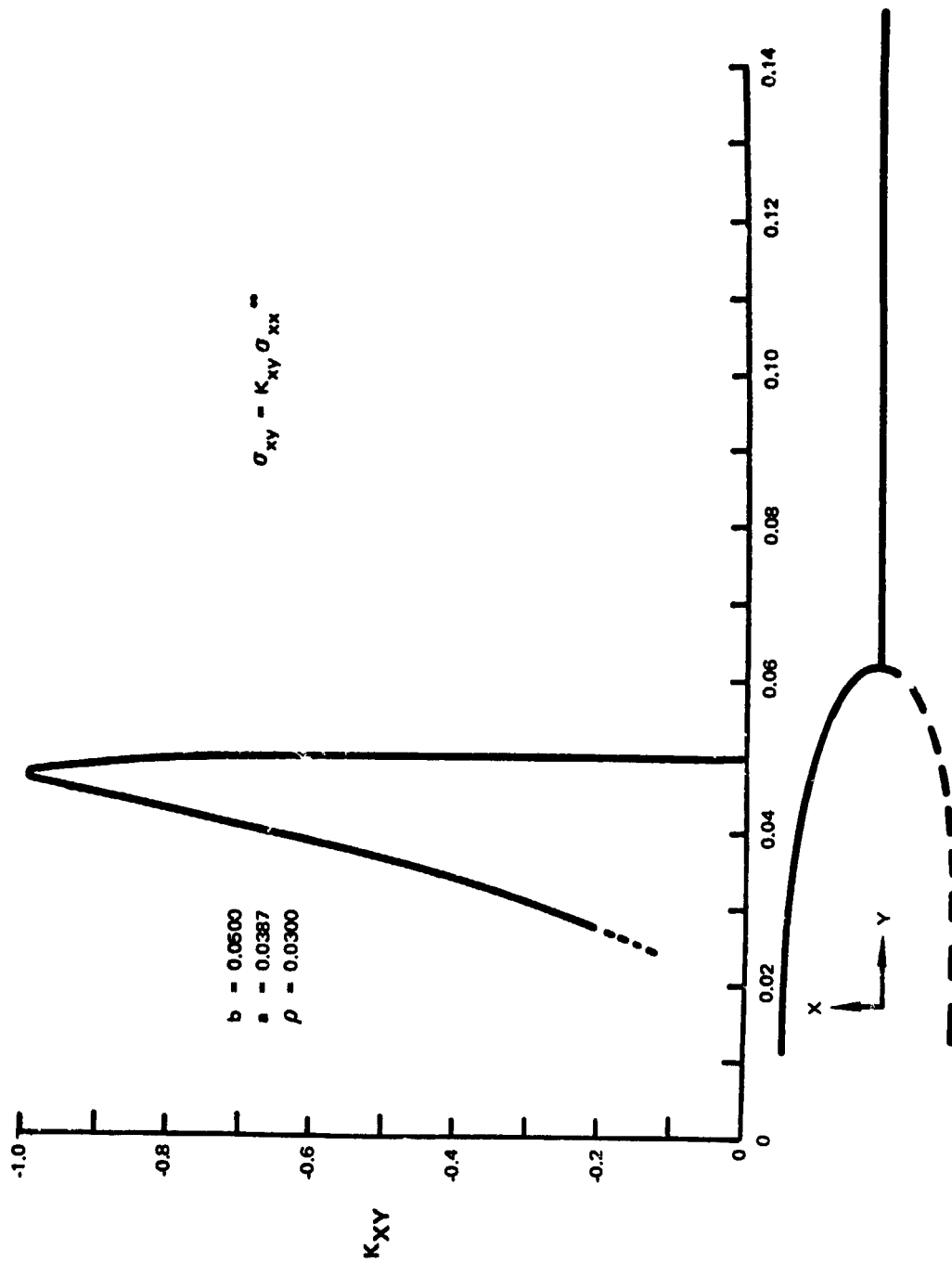
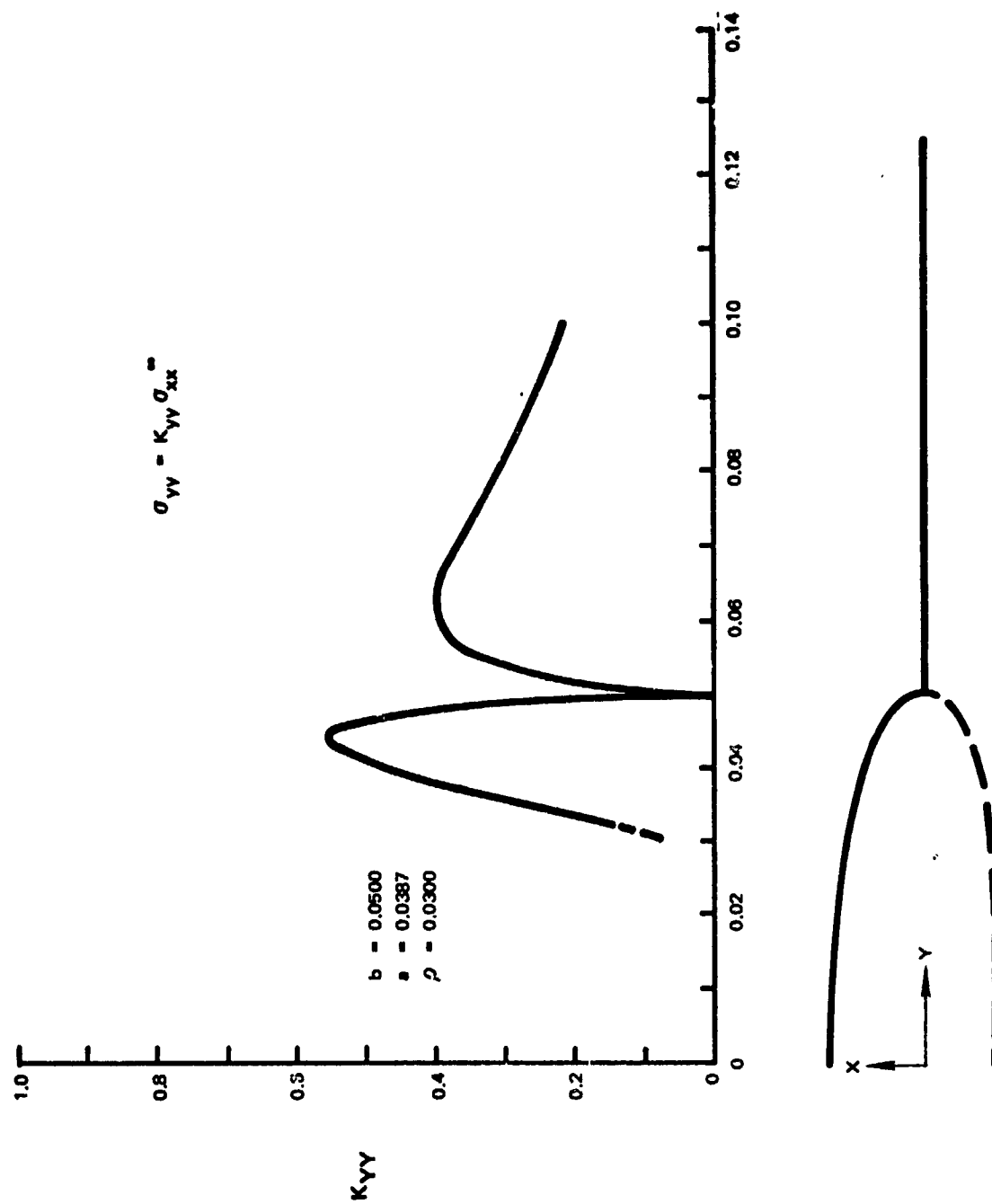


FIGURE 8-22

ELASTIC SHEAR STRESS CONCENTRATION FACTOR FOR 50V/o 4.2 MIL  
BORSIC + 6061-F ALUMINUM UNDER UNIAXIAL LONGITUDINAL TENSION



**FIGURE 8-23**  
**ELASTIC TRANSVERSE STRESS CONCENTRATION FACTOR FOR 50 v/o**  
**4.2 MIL BORSIC + 6061-F ALUMINUM UNDER UNIAXIAL LONGITUDINAL**  
**TENSION**

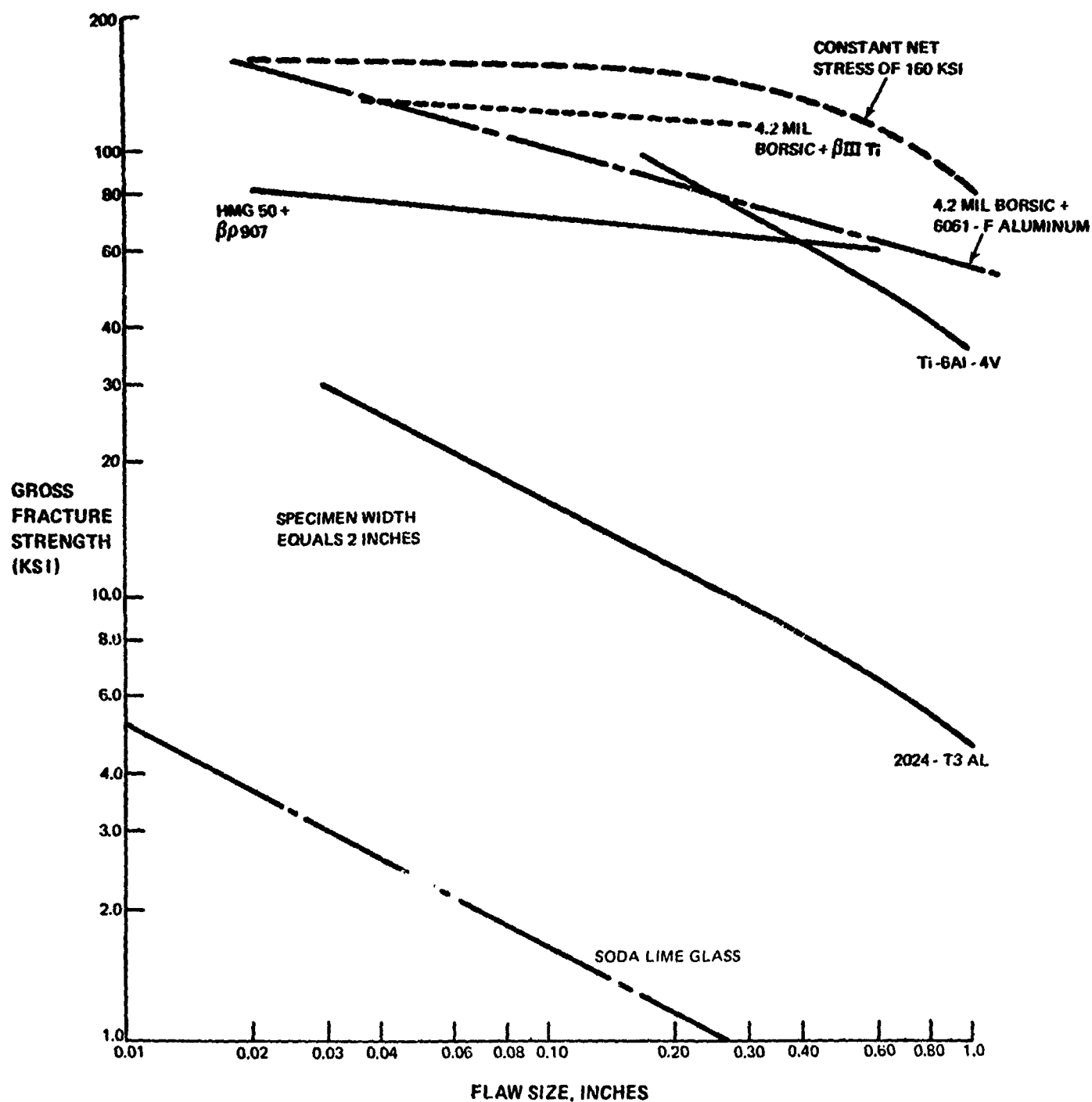


FIGURE 8-24  
VARIATION OF GROSS FRACTURE STRENGTH WITH  
FLAW SIZE FOR SELECTED MATERIALS

Table VIII-I

**Fracture Strength of Longitudinally  
Reinforced Center Notched BORSIC + Aluminum Composites**

<u>Spec. Type</u>	<u>Width (in.)</u>	<u>Thick. (in.)</u>	<u>Initial Flaw Length (in.)</u>	<u>Ult. Load (lbs)</u>	<u>Gross Fracture Stress (ksi)</u>	<u>Net Fracture Stress (ksi)</u>
S	1.996	0.0483	0	14,900	155	155
S	1.997	0.0502	0	13,900	139	139
S	1.936	0.0232	0.020	5,610*	125*	126*
S	2.020	0.0252	0.025	8,450	166	168
S	1.936	0.0480	0.025	11,820	127	129
S	2.019	0.0535	0.027	14,600	143	145
S	2.020	0.0535	0.037	12,600	117	119
S	2.026	0.0540	0.053	12,200	112	115
S	2.018	0.0539	0.102	10,800	99.3	105
S	0.949	0.0467	0.167	3,750	84.5	103
S	0.967	0.0467	0.175	4,580	101	124
S	2.012	0.0506	0.178	7,450**	73.2**	80.3**
S	2.015	0.0485	0.185	7,950	81.3	89.6
S	2.015	0.0492	0.278	7,200	72.6	84.3
S	2.000	0.1516	0.372	20,625	68.0	83.6
S	2.018	0.0522	0.408	7,150	67.9	85.1
S	2.019	0.0967	0.570	11,700	59.9	83.5
S	2.019	0.0504	0.580	16,000	53.5	75.3
S	2.017	0.0968	0.780	10,200	52.3	85.2
S	1.996	0.0483	0.790	5,200	53.8	89.1
FS	2.002	0.0429	0	18,120	211	211
FS	2.005	0.0426	0.021	13,820	162	164
FS	0.989	0.0433	0.049	5,900	138	145
FS	0.984	0.0433	0.165	4,575	107	129
FS	2.001	0.0430	0.168	10,870	126	138
T	2.008	0.0501	0	16,600	165	165
T	2.013	0.0497	0	13,900	139	139
T	1.978	0.0490	0.105	8,600	88.8	93.7
T	1.987	0.0491	0.135	7,940	81.4	87.3
T	2.012	0.0478	0.178	7,500	78.0	85.5
T	2.014	0.0464	0.178	7,750	82.9	91.1
T	1.999	0.0485	0.278	7,800	80.5	93.4
T	1.998	0.0477	0.392	6,400	67.2	83.5
T	2.012	0.0460	0.575	5,100	55.1	77.2
T	1.998	0.0486	0.602	5,500	56.6	81.1
T	1.997	0.0472	0.788	5,400	57.3	94.6

S Specimens are 4.2 mil BORSIC + 6061F matrix

T Specimens are 4.2 mil BORSIC + 2024F matrix

FS Specimens are 5.7 mil BORSIC + 6061F matrix

\* Failed at grip

\*\* Interrupted test

Table VIII-II

Fracture Strength of Longitudinally Reinforced  
50 Percent by Volume 4.2 mil BORSIC + 6061-F  
Aluminum Composites with Center Circular Holes

<u>Width</u> <u>(in.)</u>	<u>Thick.</u> <u>(in.)</u>	<u>Initial</u> <u>Flaw</u> <u>Length</u> <u>(in.)</u>	<u>Ult.</u> <u>Load</u> <u>(lbs)</u>	<u>Gross</u> <u>Fracture</u> <u>Stress</u> <u>(ksi)</u>	<u>Net</u> <u>Fracture</u> <u>Stress</u> <u>(ksi)</u>
2.025	0.0486	0.247	8900	90.4	103
2.028	0.0511	0.252	9640	93.0	106
1.936	0.0328	0.254	5610	88.4	102



Table VIII-III

Fracture Strength of Longitudinally Reinforced Heat  
Treated Center Notched 50 Percent by Volume  
4.2 mil BORSIC + Aluminum Composites

Spec. Type	Width (in.)	Thick. (in.)	Initial Flaw Length (in.)	Ult. Load (lbs)	Gross Fracture Stress (ksi)	Net Fracture Stress (ksi)
ST	2.028	0.0503	0.026	16,800	165	167
ST	2.032	0.0542	0.038	16,400	149	152
ST	2.023	0.0546	0.053	15,900*	144*	148*
ST	2.025	0.0482	0.078	13,780	141	147
ST	2.023	0.0539	0.102	11,800	108	114
ST	2.024	0.0968	0.271	13,050	66.6	76.9
ST	2.024	0.0519	0.367	8,600	81.9	100
TT	1.975	0.0514	0.054	11,300	111	114
TT	1.980	0.0469	0.104	10,000	108	114
TT	1.975	0.0466	0.131	9,760	96.7	114

ST specimens are 6061-T6; TT are 2024-T6

\*Failed at grip

Table VIII-IV

Fracture Strength of Longitudinally Reinforced Center  
 Notched 50 Percent by Volume 4.2 mil  
 BORSIC + Beta III Titanium Composites

<u>Width (in.)</u>	<u>Thick. (in.)</u>	<u>Initial Flaw Length (in.)</u>	<u>Ultimate Load (lbs)</u>	<u>Gross Fracture Stress (ksi)</u>	<u>Net Fracture Stress (ksi)</u>
1.860	0.0427	0	13,420	169	169
1.805	0.0418	0.049	9,080*	120*	124*
0.947	0.0449	0.051	5,160	121	128
1.850	0.0410	0.094	9,480	125	132
1.679	0.0420	0.168	7,740	110	122

\*Failed at grips

Table VIII-V

Fracture Strength of Longitudinally Reinforced Center  
Notched 50 Percent by Volume HMG-50  
Graphite + BP-907 Epoxy Composites

<u>Width</u> <u>(in.)</u>	<u>Thick.</u> <u>(in.)</u>	<u>Initial</u> <u>Flaw</u> <u>Length</u> <u>(in.)</u>	<u>Ultimate</u> <u>Load</u> <u>(lbs)</u>	<u>Gross</u> <u>Fracture</u> <u>Strength</u> <u>(ksi)</u>	<u>Fracture</u> <u>Strength</u> <u>(ksi)</u>
2.001	0.0682	0	11,205	83.2	83.2
1.992	0.0720	0	15,630	109	109
2.000	0.0690	0.021	13,160	95.4	96.4
2.000	0.0712	0.054	8,900	62.5	64.2
1.979	0.0704	0.080	10,890	75.1	78.2
2.000	0.0671	0.109	10,080	75.1	79.4
1.998	0.0753	0.199	9,700	64.5	71.6
1.979	0.0701	0.595	8,160	59.0	84.3

Table VIII-VI

Net Fracture Strength of 4.2 mil 50 Percent  
by Volume Type LT EORSIC + Aluminum Composites

<u>Specimen Number</u>	<u>Matrix Alloy</u>	<u>Crack Length (in.)</u>	<u>Tip Radius (in.)</u>	<u>Fracture Strength (ksi)</u>
P4	6061	0.570	0.0023	83.5
P9	6061	0.580	0.0023	75.3
T4	2024	0.602	0.0023	81.1
T9	2024	0.575	0.005	77.2
T5	2024	0.788	0.0023	94.6
P5	6061	0.790	0.0023	89.1
P10	6061	0.780	0.005	85.2

Table VIII-VII

Longitudinal Tensile Properties of 50 Volume  
Percent 4.2 mil BORSIC + Beta III Titanium

<u>Specimen</u>	<u>Width (in.)</u>	<u>Thickness (in.)</u>	<u>UTS (ksi)</u>	<u><math>E_{11}</math> (<math>10^6</math> psi)</u>	<u><math>\nu_{12}</math></u>
H-1	0.399	0.044	168	36.5	0.26
H-2	0.401	0.044	164	32.6	0.25
H-3	0.400	0.044	167	33.5	0.26
H-4	0.401	0.039	192	37.0	0.26
F-2	0.398	0.048	163	33.6	0.25

Table VIII-VIIF

Longitudinal Tensile Properties of  
HMG-50 Graphite + BP-907 Epoxy Composites

<u>Specimen</u>	<u>Width</u> <u>(in)</u>	<u>Thickness</u> <u>(in)</u>	<u>UTS</u> <u>(ksi)</u>	<u>F<sub>11</sub></u> <u>(10<sup>6</sup> psi)</u>
BD-1	0.201	0.110	98.3	20.0
BD-2	0.203	0.112	102	21.5
BD-3	0.199	0.111	109	25.2
BD-4	0.201	0.108	105	20.5
CS-1	0.200	0.101	67.0	28.4
CS-2	0.198	0.098	95.5	29.4
CS-3	0.197	0.103	110	27.2
CS-4	0.201	0.099	90.1	30.0

Table VIII-IX

Fracture Strength of Transversely Reinforced  
Center Notched BORSIC + 6061-F Aluminum Composites

<u>Spec. Type</u>	<u>Width (in.)</u>	<u>Thick. (in.)</u>	<u>Initial Flaw Length (in.)</u>	<u>Ult. Load (lbs)</u>	<u>Gross Fracture Stress (ksi)</u>	<u>Net Fracture Stress (ksi)</u>
SP	1.995	0.0519	0	1480	14.3	14.3
SP	1.994	0.0512	0	1640	16.1	16.1
SP	1.996	0.0516	0.172	1150	11.2	12.2
SP	1.992	0.0516	0.175	1230	12.0	13.1
SP	1.991	0.0511	0.180	1560	15.3	16.9
SP	1.989	0.0509	0.285	1360	13.4	15.7
SP	1.996	0.0510	0.375	1310	12.9	15.8
SP	1.997	0.0506	0.575	1270	12.6	17.7
SP	2.005	0.0512	0.575	970	9.4	13.2
FS	1.998	0.0426	0	1890	22.2	22.2
FS	1.973	0.0432	0.025	2060	24.2	24.5
FS	0.978	0.0424	0.046	705	17.0	17.8
FS	0.969	0.0424	0.168	580	14.1	17.1
FS	1.963	0.0429	0.168	2000	23.75	25.9

Table VIII-X

Elastic Stress Concentration Factors for  
0.100 Inch Elliptical Flaws in Fiber  
Reinforced Composite Systems

<u>System</u>	<u>Tip Radius</u>	<u>Max SCF</u>		
		<u>K<sub>xx</sub></u>	<u>K<sub>xy</sub></u>	<u>K<sub>yy</sub></u>
BORSIC + Beta III Titanium	0.0025	11.58	-2.99	1.91
BORSIC + Aluminum	0.0025	12.13	-2.97	1.81
HMG-50 Graphite + BP-907 Epoxy	0.0025	28.39	-2.67	0.73
BORSIC + Beta III Titanium	0.005	8.49	-2.17	1.36
BORSIC + Aluminum	0.030	4.21	-0.99	0.55
HMG-50 Graphite + BP-907 Epoxy	0.003	26.01	-2.44	0.67
BORSIC + Aluminum	0.050	3.49	-0.81	0.44